PROCEEDINGS OF THE SEVENTEENTH WORKSHOP ON GENERAL RELATIVITY AND GRAVITATION in JAPAN

Noyari Conference Hall, Nagoya University,
Higashiyama Campus, Nagoya, Japan
December 3–7, 2007

Edited by
Yasusada Nambu, Eiji Mituda
Misao Sasaki

PREFACE

The seventeenth workshop on General Relativity and Gravitation in Japan was held at Noyori Conference Hall, Nagoya University, located in the Higashiyama Campus from 3 December to 7 December 2007. The main purpose of this workshop was to review the latest progress in the field of general relativity, gravitation and general relativistic astrophysics as well as to promote interaction between researchers working in these fields.

The workshop was organized as an international conference and composed of 12 invited talks 89 contributed short talks (50 oral presentations and 39 poster presentations). Among them, 19 were presented by the researchers from overseas. All the talks were given in English. The workshop was attended by about 170 researchers. We appreciate very much all the participants for their contribution to the workshop.

We would like to thank Ms. K. Yokota and Ms. N. Takahashi, the secretaries at the Kyoto University, for their devoted transaction for various official works. We are also grateful to the graduate students of the gravitational theory group in the Department of Physics, Nagoya University for their cooperation in management of the workshop. The workshop was financially supported in part by Grants-in-Aid for Sscientific Research(B) No.17340075 and Grant-in-Aid for Creative Scientific Research No.19GS0219.

Y. Nambu and E. Mitsuda April 2008

Organizing Committees

E. Mitsuda, Y. Nambu (Local comittees; Nagoya University)
H. Asada (Hirosaki University) T. Chiba (Nihon University)
A. Hosoya (Tokyo Institute of Technology) K. Ioka (KEK)
H. Ishihara (Osaka City University) Y. Kojima (Hiroshima University) H. Kodama (KEK)
K. Maeda (Waseda University) S. Mukohyama (University of Tokyo)
K. Nakao (Osaka City University) T. Nakamura (Kyoto University)
K. Oohara (Niigata University) M. Sasaki (YITP) M. Shibata (University of Tokyo)
T. Shiromizu (Tokyo Institute of Technology) N. Sugiyama (Nagoya University)
J. Soda (Kyoto University) T. Tanaka (Kyoto University)
J. Yokoyama (University of Tokyo)

Table of Contents

Invited talks

Oral Presentation

Poster Presentation

Can $F(R)$-gravity be a viable model: the universal unification scenario for inflation, dark energy and dark matter

Shin'ichi Nojiri[1] and Sergei D. Odintsov[2]

[1] *Department of Physics, Nagoya University, Nagoya 464–8602, Japan*
[2] *Instituciò Catalana de Recerca i Estudis Avançats (ICREA) and Institut de Ciencies de l'Espai (IEEC-CSIC), Campus UAB, Facultat de Ciencies, Torre C5-Par-2a pl, E-08193 Bellaterra (Barcelona), Spain*

Abstract

We review on the viability of $F(R)$-gravity. We show that recent cosmic acceleration, radiation/matter-dominated epoch and inflation could be realized in the framework of $F(R)$-gravity in the unified way. For some classes of $F(R)$-gravity, the correction to the Newton law is extremely small and there is no so-called matter instability (the very heavy positive mass for additional scalar degree of freedom is generated). The reconstruction program in modified gravity is also reviewed and it is demonstrated that *any* time-evolution of the universe expansion could be realized in $F(R)$-gravity. Special attention is paid to modified gravity which unifies inflation with cosmic acceleration and passes local tests. It turns out that such a theory may describe also dark matter.

1 Introduction

Recent astrophysical observations indicate that the accelerating expansion of the universe has started about five billion years ago and the present universe is flat. This implies the existence of dark energy, that is, unknown component in the universe.

Usually the evolution of the universe can be described by the FRW equation:

$$\frac{3}{\kappa^2}H^2 = \rho \ . \tag{1}$$

Here the spatial part of the universe is assumed to be flat. We denote the Hubble rate by H, which is defined in terms of the scale factor a by

$$H \equiv \frac{\dot{a}}{a} \ . \tag{2}$$

In (1), ρ expresses the energy density of the usual matter, dark matter, and dark energy. The dark energy could be cosmological constant and/or a matter with 'equation of state (EoS)' parameter w, which is less than $-1/3$ and is defined by

$$w \equiv \frac{p}{\rho} < -1/3 \ . \tag{3}$$

Instead of including unknown exotic matter or energy, one may consider the modification of gravity, which corresponds to the change of the l.h.s. in (1).

An example of such modified gravity pretending to describe dark energy could be the scalar-Einstein-Gauss-Bonnet gravity [1], whose action is given by

$$S = \int d^4x\sqrt{-g}\left\{\frac{1}{2\kappa^2}R - \frac{1}{2}\partial_\mu\phi\partial^\mu\phi - V(\phi) + f(\phi)\mathcal{G}\right\} \ . \tag{4}$$

Here $\mathcal{G}$ is Gauss-Bonnet invariant:

$$\mathcal{G} \equiv R^2 - 4R_{\mu\nu}R^{\mu\nu} + R_{\mu\nu\rho\sigma}R^{\mu\nu\rho\sigma} \ . \tag{5}$$

[1] E-mail:nojiri@phys.nagoya-u.ac.jp
[2] E-mail:odintsov@ieec.uab.es, also at Lab. Fundam. Study, Tomsk State Pedagogical University, Tomsk

Another example is so-called $F(R)$-gravity (for a review, see [2]). In $F(R)$-gravity models, the scalar curvature R in the Einstein-Hilbert action

$$S_{\rm EH} = \int d^4x\sqrt{-g}R \ , \tag{6}$$

is replaced by a proper function of the scalar curvature:

$$S_{F(R)} = \int d^4x\sqrt{-g}F(R) \ . \tag{7}$$

Recently, an interesting realistic theory has been proposed in [3], where $F(R)$ is given by

$$F(R) = \frac{1}{2\kappa^2}\left(R + f_{HS}(R)\right) \ , \quad f_{HS}(R) = -\frac{m^2 c_1 \left(R/m^2\right)^n}{c_2\left(R/m^2\right)^n + 1} \ . \tag{8}$$

In this model, R is large even in the present universe, and $f_{HS}(R)$ could be expanded by the inverse power series of R:

$$f_{HS}(R) \sim -\frac{m^2c_1}{c_2} + \frac{m^2c_1}{c_2^2}\left(\frac{R}{m^2}\right)^{-n} + \cdots \ , \tag{9}$$

Then there appears an effective cosmological constant $\Lambda_{\rm eff}$ as $\Lambda_{\rm eff} = m^2c_1/c_2$, which generates the accelerating expansion in the present universe

In the HS-model (8), there occurs a flat spacetime solution, where $R = 0$, since the following condition is satisfied:

$$\lim_{R\to 0} f_{HS}(R) = 0 \ . \tag{10}$$

An interesting point in the HS model is that several cosmological conditions could be satisfied.

In the next section, we review on the general properties of $F(R)$-gravity. After some versions of $F(R)$-gravity were proposed as a model of the dark energy, there appeared several criticisms/viability criteria, which we review in Section 3. It is shown how the critique of modified gravity may be removed for realistic models. In Section 4, we propose models [4] and [5], which unify the early-time inflation and the recent cosmic acceleration and pass several cosmological constraints. Reconstruction program for $F(R)$-gravity is reviewed in Section 5. The partial reconstruction scenario is proposed. Section six is devoted to the description of dark matter in terms of viable modified gravity where composite scalar particle from $F(R)$ gravity plays the role of dark particle. Some summary and outlook is given in the last section.

2 General properties of $F(R)$-gravity

In this section, the general properties of the $F(R)$-gravity are reviewed. For general $F(R)$-gravity, one can define an effective equation of state (EoS) parameter. The FRW equations in Einstein gravity coupled with perfect fluid are:

$$\rho = \frac{3}{\kappa^2}H^2 \ , \quad p = -\frac{1}{\kappa^2}\left(3H^2 + 2\dot H\right) \ . \tag{11}$$

For modified gravities, one may define an effective EoS parameter as follows:

$$w_{\rm eff} = -1 - \frac{2\dot H}{3H^2} \ . \tag{12}$$

The equation of motion for modified gravity is given by

$$\frac{1}{2}g_{\mu\nu}F(R) - R_{\mu\nu}F'(R) - g_{\mu\nu}\Box F'(R) + \nabla_\mu\nabla_\nu F'(R) = -\frac{\kappa^2}{2}T_{(m)\mu\nu} \ . \tag{13}$$

By assuming spatially flat FRW universe,

$$ds^2 = -dt^2 + a(t)^2\sum_{i=1,2,3}\left(dx^i\right)^2 \ , \tag{14}$$

the FRW-like equation follows:

$$0=-\frac{F(R)}{2}+3\left(H^2+\dot H\right)F'(R)-18\left(4H^2\dot H+H\ddot H\right)F''(R)+\kappa^2\rho_{(m)} \tag{15}$$

There may be several (often exact) solutions of (15). Without any matter, assuming that the Ricci tensor could be covariantly constant, that is, $R_{\mu\nu}\propto g_{\mu\nu}$, Eq.(13) reduces to the algebraic equation:

$$0=F(R)-2RF(R)\ . \tag{16}$$

If Eq.(16) has a solution, the Schwarzschild (or Kerr) - (anti-)de Sitter space is an exact vacuum solution (see[6] and refs. therein).

When $F(R)$ behaves as $F(R)\propto R^m$ and there is no matter, there appears the following solution:

$$H\sim\frac{-\frac{(m-1)(2m-1)}{m-2}}{t}\ , \tag{17}$$

which gives the following effective EoS parameter:

$$w_{\mathrm{eff}}=-\frac{6m^2-7m-1}{3(m-1)(2m-1)}\ . \tag{18}$$

When $F(R)\propto R^m$ again but if the matter with a constant EoS parameter w is included, one may get the following solution:

$$H\sim\frac{\frac{2m}{3(w+1)}}{t}\ , \tag{19}$$

and the effective EoS parameter is given by

$$w_{\mathrm{eff}}=-1+\frac{w+1}{m}\ . \tag{20}$$

This shows that modified gravity may describe early/late-time universe acceleration.

3 Criticism of $F(R)$-gravity

Just after the $F(R)$-models were proposed as models of the dark energy, there appeared several works [7, 8] (and more recently in [9, 10]) criticizing such theories.

First of all, we comment on the claim in [7]. Note that one can rewrite $F(R)$-gravity in the scalar-tensor form. By introducing the auxiliary field A, we rewrite the action (7) of the $F(R)$-gravity in the following form:

$$S=\frac{1}{\kappa^2}\int d^4x\sqrt{-g}\left\{F'(A)\left(R-A\right)+F(A)\right\}\ . \tag{21}$$

By the variation over A, one obtains $A=R$. Substituting $A=R$ into the action (21), one can reproduce the action in (7). Furthermore, we rescale the metric in the following way (conformal transformation):

$$g_{\mu\nu}\to \mathrm{e}^{\sigma}g_{\mu\nu}\ ,\quad \sigma=-\ln F'(A)\ . \tag{22}$$

Hence, the Einstein frame action is obtained:

$$\begin{aligned} S_E &= \frac{1}{\kappa^2}\int d^4x\sqrt{-g}\left(R-\frac{3}{2}g^{\rho\sigma}\partial_\rho\sigma\partial_\sigma\sigma-V(\sigma)\right)\ , \\ V(\sigma) &= \mathrm{e}^{\sigma}g\left(\mathrm{e}^{-\sigma}\right)-\mathrm{e}^{2\sigma}f\left(g\left(\mathrm{e}^{-\sigma}\right)\right)=\frac{A}{F'(A)}-\frac{F(A)}{F'(A)^2} \end{aligned} \tag{23}$$

Here $g\left(\mathrm{e}^{-\sigma}\right)$ is given by solving the equation $\sigma=-\ln\left(1+f'(A)\right)=\ln F'(A)$ as $A=g\left(\mathrm{e}^{-\sigma}\right)$. Due to the scale transformation (22), there appears a coupling of the scalar field σ with usual matter. The mass of σ is given by

$$m_\sigma^2\equiv\frac{1}{2}\frac{d^2V(\sigma)}{d\sigma^2}=\frac{1}{2}\left\{\frac{A}{F'(A)}-\frac{4F(A)}{\left(F'(A)\right)^2}+\frac{1}{F''(A)}\right\}\ . \tag{24}$$

Unless m_σ is very large, there appears the large correction to the Newton law. Naively, one expects the order of the mass m_σ could be that of the Hubble rate, that is, $m_\sigma \sim H \sim 10^{-33}\,\mathrm{eV}$, which is very light and the correction could be very large, which is the claim in [7].

We should note, however, that the mass m_σ depends on the detailed form of $F(R)$ in general [11]. Moreover, the mass m_σ depends on the curvature. The curvature on the earth R_{earth} is much larger than the average curvature R_{solar} in the solar system and R_{solar} is also much larger than the average curvature in the unverse, whose order is given by the square of the Hubble rate H^2, that is, $R_{\mathrm{earth}} \gg R_{\mathrm{solar}} \gg H^2$. Then if the mass becomes large when the curvature is large, the correction to the Newton law could be small. Such a mechanism is called the Chameleon mechanism and proposed for the scalar-tensor theory in [12]. In fact, the HS model [3] has this property and the correction to the Newton law can be very small on the earth or in the solar system. In the HS model, the mass m_σ is given by (see also [13])

$$m_\sigma^2 \sim \frac{m^2 c_2^2}{2n(n+1)c_1} \left(\frac{R}{m^2}\right)^{n+2} . \tag{25}$$

Here the order of the mass-dimensional parameter m^2 could be $m^2 \sim 10^{-64}\,\mathrm{eV}^2$. Then in solar system, where $R \sim 10^{-61}\,\mathrm{eV}^2$, the mass is given by $m_\sigma^2 \sim 10^{-58+3n}\,\mathrm{eV}^2$ and in the air on the earth, where $R \sim 10^{-50}\,\mathrm{eV}^2$, $m_\sigma^2 \sim 10^{-36+14n}\,\mathrm{eV}^2$. The order of the radius of the earth is $10^7\,\mathrm{m} \sim \left(10^{-14}\,\mathrm{eV}\right)^{-1}$. Therefore the scalar field σ could be heavy enough if $n \gg 1$ and the correction to the Newton law is not observed being extremely small. On the other hand, in the air on the earth, if we choose $n = 10$, for example, one gets the mass is extremely large:

$$m_\sigma \sim 10^{43}\,\mathrm{GeV} \sim 10^{29} \times M_{\mathrm{Planck}} . \tag{26}$$

Here M_{Planck} is the Planck mass. Hence, the Newton law correction should be extremely small.

Let us discuss the matter instability proposed in [8], which may appear when the energy density or the curvature is large compared with the average one in the universe, as is the case inside of the planet. Multiplying $g^{\mu\nu}$ with Eq.(13), one obtains

$$\Box R + \frac{F^{(3)}(R)}{F^{(2)}(R)}\nabla_\rho R \nabla^\rho R + \frac{F'(R)R}{3F^{(2)}(R)} - \frac{2F(R)}{3F^{(2)}(R)} = \frac{\kappa^2}{6F^{(2)}(R)}T . \tag{27}$$

Here T is the trace of the matter energy-momentum tensor: $T \equiv T^{\ \rho}_{(m)\rho}$. We also denote $d^nF(R)/dR^n$ by $F^{(n)}(R)$. Let us now consider the perturbation from the solution of the Einstein gravity. We denote the scalar curvature solution given by the matter density in the Einstein gravity by $R_b \sim (\kappa^2/2)\rho > 0$ and separate the scalar curvature R into the sum of R_b and the perturbed part R_p as $R = R_b + R_p$ ($|R_p| \ll |R_b|$). Then Eq.(27) leads to the perturbed equation:

$$\begin{aligned} 0 \ =\ & \Box R_b + \frac{F^{(3)}(R_b)}{F^{(2)}(R_b)}\nabla_\rho R_b \nabla^\rho R_b + \frac{F'(R_b)R_b}{3F^{(2)}(R_b)} \\ & - \frac{2F(R_b)}{3F^{(2)}(R_b)} - \frac{R_b}{3F^{(2)}(R_b)} + \Box R_p + 2\frac{F^{(3)}(R_b)}{F^{(2)}(R_b)}\nabla_\rho R_b \nabla^\rho R_p + U(R_b)R_p . \end{aligned} \tag{28}$$

Here $U(R_b)$ is given by

$$\begin{aligned} U(R_b) \ \equiv\ & \left(\frac{F^{(4)}(R_b)}{F^{(2)}(R_b)} - \frac{F^{(3)}(R_b)^2}{F^{(2)}(R_b)^2}\right)\nabla_\rho R_b \nabla^\rho R_b + \frac{R_b}{3} \\ & - \frac{F^{(1)}(R_b)F^{(3)}(R_b)R_b}{3F^{(2)}(R_b)^2} - \frac{F^{(1)}(R_b)}{3F^{(2)}(R_b)} + \frac{2F(R_b)F^{(3)}(R_b)}{3F^{(2)}(R_b)^2} - \frac{F^{(3)}(R_b)R_b}{3F^{(2)}(R_b)^2} \end{aligned} \tag{29}$$

It is convinient to consider the case that R_b and R_p are uniform, that is, they do not depend on the spatial coordinate. Hence, the d'Alembertian can be replaced with the second derivative with respect to the time coordinate: $\Box R_p \to -\partial_t^2 R_p$ and Eq.(29) has the following structure:

$$0 = -\partial_t^2 R_p + U(R_b)R_p + \mathrm{const.} . \tag{30}$$

Then if $U(R_b) > 0$, R_p becomes exponentially large with time t: $R_p \sim e^{\sqrt{U(R_b)}t}$ and the system becomes unstable. In the $1/R$-model [14], since the order of mass parameter m_μ is

$$\mu^{-1} \sim 10^{18}\text{sec} \sim \left(10^{-33}\text{eV}\right)^{-1} \ , \tag{31}$$

one finds

$$\begin{aligned} U(R_b) &= -R_b + \frac{R_b^3}{6\mu^4} \sim \frac{R_0^3}{\mu^4} \sim \left(10^{-26}\text{sec}\right)^{-2} \left(\frac{\rho_m}{\text{g}\,\text{cm}^{-3}}\right)^3 \ , \\ R_b &\sim \left(10^3\text{sec}\right)^{-2} \left(\frac{\rho_m}{\text{g}\,\text{cm}^{-3}}\right) \end{aligned} \tag{32}$$

Hence, the model is unstable and it would decay in 10^{-26} sec (for planet size). On the other hand, in $1/R + R^2$-model [11], we find

$$U(R_0) \sim \frac{R_0}{3} > 0 \ . \tag{33}$$

Then the system could be unstable again but the decay time is $\sim 1,000$ sec, that is, macroscopic. In HS model [3], $U(R_b)$ is negative[13]:

$$U(R_0) \sim -\frac{(n+2)m^2 c_2^2}{c_1 n(n+1)} < 0 \ . \tag{34}$$

Therefore, there is no matter instability[13].

Let us discuss the critical claim against modified gravity in [9, 10]. As shown in (16), as an exact solution, there appears de Sitter-Schwarzschild spacetime in $F(R)$-gravity. The claim in [9, 10] is that the solution does not match onto the stellar interior solution. Since it is difficult to construct explicit solution describing the stellar configuration even in the Einstein gravity, we now proceed in the following way: First, we separate $F(R)$ into the sum of the Einstein-Hilbert part and other part as $F(R) = R + f(R)$. Then Eq.(13) has the following form:

$$\begin{aligned} &\frac{1}{2}g_{\mu\nu}R - R_{\mu\nu} - \frac{1}{2}g_{\mu\nu}\Lambda + \frac{\kappa^2}{2}T_{(m)\mu\nu} \\ &= -\frac{1}{2}g_{\mu\nu}\left(f(R) + \Lambda\right) + R_{\mu\nu}f'(R) + g_{\mu\nu}\Box f'(R) - \nabla_\mu\nabla_\nu f'(R) \ . \end{aligned} \tag{35}$$

Here $-\Lambda$ is the value of $f(R)$ in the present universe, that is, Λ is the effective cosmological constant: $\Lambda = -f(R_0)$. We now treat the r.h.s. in (35) as a perturbation. Then the last two derivative terms in (35) could be dangerous since there could be jump in the value of the scalar curvature R on the surface of stellar configuration. Of course, the density on the surface could change in a finite width Δ as in Figure 1 and the derivatives should be finite and the magnitude could be given by

$$\partial_\mu \sim \frac{1}{\Delta} \ . \tag{36}$$

One now assumes the order of the derivative could be the order of the Compton length of proton:

$$\partial_\mu \sim m_p \sim 1\,\text{GeV} \sim 10^9\,\text{eV} \tag{37}$$

Here m_p is the mass of proton. It is also assumed

$$R \sim R_e \sim 10^{-47}\,\text{eV}^2 \ , \tag{38}$$

that is, the order of the scalar curvature R is given by the order of it inside the earth.

In case of the $1/R$ model [14], one gets

$$\Box f'(R) \sim \nabla_\mu\nabla_\nu f'(R) \sim \frac{m_p^2\mu^4}{R^2} \sim 10^{-20}\,\text{eV}^2 \gg R_e \ . \tag{39}$$

Then the perturbative part could be much larger than unperturbative part in (35), say, $R \sim R_e \sim 10^{-47}\,\text{eV}^2$. Therefore, the perturbative expansion could be inconsistent.

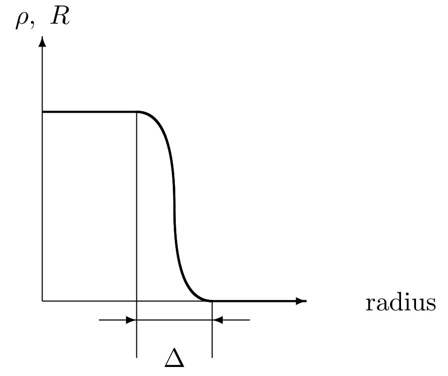

Figure 1: Typical behavior of R and ρ near the surface of the stellar configuration.

In case of the model [3], however, we find

$$\Box f'(R) \sim \nabla_\mu \nabla_\nu f'(R) \sim \frac{m_p^2 \Lambda}{m^2} \left(\frac{R}{m^2} \right)^{-n-1} \sim 10^{-3-17n}\, \mathrm{eV}^2 \ . \tag{40}$$

Then if $n > 2$, we find $\Box f'(R)$, $\nabla_\mu \nabla_\nu f'(R) \ll R_e$ and therefore the perturbative expansion could be consistent. This indicates that such modified gravity model may pass the above test. Thus, it is demonstrated that some versions of modified gravity may easily pass above tests.

4 Unifying inflation and late-time acceleration

In this section, we consider an extension of the HS model [3] to unify the early-time inflation and late-time acceleration, following proposals [4, 5].

In order to construct such models, we impose the following conditions:

- Condition that inflation occurs:
$$\lim_{R\to\infty} f(R) = -\Lambda_i \ . \tag{41}$$
Here Λ_i is an effective early-time cosmological constant.
Instead of (41) one may impose the following condition
$$\lim_{R\to\infty} f(R) = \alpha R^m \ . \tag{42}$$
Here m and α are positive constants. Then as shown in (19), the scale factor $a(t)$ evolves as
$$a(t) \propto t^{h_0} \ , \quad h_0 \equiv \frac{2m}{3(w+1)} \ , \tag{43}$$
and $w_{\mathrm{eff}} = -1 + 2/3h_0$. Here w is the matter EoS parameter, which could correspond to dust or radiation. We assume $m \gg 1$ so that $\dot{H}/H^2 \gg 1$.
- The condition that there is flat spacetime solution is given as
$$f(0) = 0 \tag{44}$$
- The condition that late-time acceleration occurs should be
$$f(R_0) = -2\tilde{R}_0 \ , \quad f'(R_0) \sim 0 \ . \tag{45}$$
Here R_0 is the current curvature of the universe and we assume $R_0 > \tilde{R}_0$. Due to the condition (45), $f(R)$ becomes almost constant in the present universe and plays the role of the effective small cosmological constant: $\Lambda_l \sim -f(R_0) = 2\tilde{R}_0$.

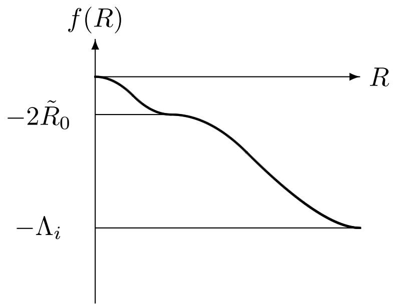

Figure 2: The typical behavior of $f(R)$ which satisfies the conditions (41), (44), and (45).

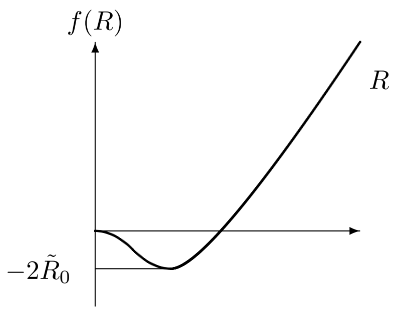

Figure 3: The typical behavior of $f(R)$ which satisfies the conditions (42), (44), and (45).

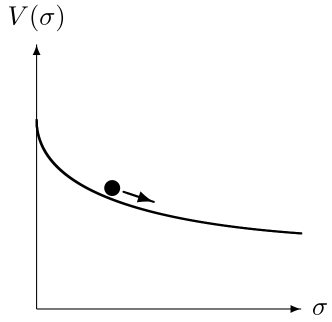

Figure 4: The potential in the inflationary epoch.

The typical behavior of $f(R)$ which satisfies the conditions (41), (44), and (45) is given in Figure 2 and the behavior of $f(R)$ satisfying (41), (42), and (45) is given in Figure 1.

Some examples may be of interest. An example which satisfies the conditions (41), (44), and (45) is given by the following action[4]:

$$f(R) = -\frac{(R-R_0)^{2n+1} + R_0^{2n+1}}{f_0 + f_1\left\{(R-R_0)^{2n+1} + R_0^{2n+1}\right\}} \ . \tag{46}$$

Here n is a positive integer. The conditions (42) and (45) require

$$\frac{R_0^{2n+1}}{f_0 + f_1 R_0^{2n+1}} = 2\tilde{R}_0 \ , \quad \frac{1}{f_1} = \Lambda_i \ . \tag{47}$$

One can now investigate how the exit from the inflation could be realized in the model (46). It is easier to consider this problem in the scalar-tensor form (Einstein frame) in (23). In the inflationary epoch, when the curvature $R = A$ is large, $f(R)$ has the following form:

$$f(R) \sim -\frac{1}{f_1} + \frac{f_0}{f_1^2 R^{2n+1}} \ . \tag{48}$$

Hence, one gets

$$\sigma \sim \frac{(2n+1)f_0}{f_1^2 A^{2n+2}} \ , \tag{49}$$

and

$$V(\sigma) \sim \frac{1}{f_1} - \frac{2(n+1)f_0}{f_1^2}\left(\frac{f_1^2\sigma}{(2n+1)f_0}\right)^{\frac{2n+1}{2n+2}} \ . \tag{50}$$

Note that the scalar field σ is dimensionless now. Let us check the condition for the slow roll, $|V'/V| \ll 1$. Since

$$\frac{V'(\sigma)}{V(\sigma)} \sim -f_1\left(\frac{f_1^2\sigma}{(2n+1)f_0}\right)^{-\frac{1}{2n+2}} \ , \tag{51}$$

if we start with $\sigma \sim 1$, one finds

$$\frac{V'(\sigma)}{V(\sigma)} \sim -\left(\frac{R_0}{\Lambda_i}\right)^{\frac{2n}{2n+1}} \ , \tag{52}$$

which is very small and the slow roll condition is satisfied.

Thus, the value of the scalar field σ increases very slowly as in Figure 4 and the scalar curvature R becomes smaller. When σ becomes large enough and R becomes small enough, the inflation could stop.

Another possibility to achieve the exit from the inflation is to add small non-local term to gravitational action.

We now consider another example, where $f(R)$ satisfies the conditions (42), (44), and (45) [5]:

$$f(R) = \frac{\alpha R^{2n} - \beta R^n}{1 + \gamma R^n} \ . \tag{53}$$

Here α, β, and γ are positive constants and n is a positive integer. When the curvature is large ($R \to \infty$), $f(R)$ behaves as

$$f(R) \to \frac{\alpha}{\gamma} R^n \ . \tag{54}$$

To achieve the exit from the inflation, more terms could be added in the action. Since the derivative of $f(R)$ is given by

$$f'(R) = \frac{nR^{n-1}\left(\alpha\gamma R^{2n} - 2\alpha R^n - \beta\right)}{\left(1 + \gamma R^n\right)^2} \ , \tag{55}$$

we find the curvature R_0 in the present universe, which satisfies the condition $f'(R_0) = 0$, is given by

$$R_0 = \left\{ \frac{1}{\gamma} \left(1 + \sqrt{1 + \frac{\beta\gamma}{\alpha}} \right) \right\}^{1/n} \ , \tag{56}$$

and

$$f(R_0) \sim -2\tilde{R}_0 = \frac{\alpha}{\gamma^2} \left(1 + \frac{\left(1 - \beta\gamma/\alpha\right)\sqrt{1 + \beta\gamma/\alpha}}{2 + \sqrt{1 + \beta\gamma/\alpha}} \right) \ . \tag{57}$$

Let us check if we can choose parameters to reproduce realistic cosmological evolution. As a working hypothesis, we assume $\beta\gamma/\alpha \gg 1$, then

$$R_0 \sim \left(\beta/\alpha\gamma\right)^{1/2n} \ , \quad f(R_0) = -2\tilde{R}_0 \sim -\beta/\gamma \tag{58}$$

We also assume $f(R_I) \sim (\alpha/\gamma)R_I^n \sim R_I$. Here R_I is the curvature in the inflationary epoch. As a result, one obtains

$$\alpha \sim 2\tilde{R}_0 R_0^{-2n}, \ \beta \sim 4\tilde{R}_0^2 R_0^{-2n} R_I^{n-1}, \ \gamma \sim 2\tilde{R}_0 R_0^{-2n} R_I^{n-1}. \tag{59}$$

Hence, we can confirm the assumption $\beta\gamma/\alpha \gg 1$ if $n > 1$ as

$$\frac{\beta\gamma}{\alpha} \sim 4\tilde{R}_0^2 R_0^{-2n} R_I^{2n-2} \sim 10^{228(n-1)} \gg 1 \ . \tag{60}$$

Thus, we presented modified gravity models which unify early-time inflation and late-time acceleration. One should stress that the above models (46) and (53) satisfy the cosmological constraints/local tests in the same way as in the HS model [3].

5 Reconstruction of $F(R)$-gravity

In this section, it is shown how we can construct $F(R)$ model realizing *any* given cosmology (including inflation, matter-dominated epoch, *etc*) using technique of ref.[15]. The general $F(R)$-gravity action with general matter is given as:

$$S = \int d^4x \sqrt{-g} \left\{ F(R) + \mathcal{L}_{\mathrm{matter}} \right\} \ . \tag{61}$$

The action (61) can be rewritten by using proper functions $P(\phi)$ and $Q(\phi)$ of a scalar field ϕ:

$$S = \int d^4x \sqrt{-g} \left\{ P(\phi)R + Q(\phi) + \mathcal{L}_{\mathrm{matter}} \right\} \ . \tag{62}$$

Since the scalar field ϕ has no kinetic term, one may regard ϕ as an auxiliary scalar field. By the variation over ϕ, we obtain

$$0 = P'(\phi)R + Q'(\phi) \ , \tag{63}$$

which could be solved with respect to ϕ as $\phi = \phi(R)$. By substituting $\phi = \phi(R)$ into the action (62), we obtain the action of $F(R)$-gravity where

$$F(R) = P(\phi(R))R + Q(\phi(R)) \ . \tag{64}$$

By the variation of the action (62) with respect to $g_{\mu\nu}$, the equation of motion follows:

$$0 = -\frac{1}{2}g_{\mu\nu}\left\{P(\phi)R + Q(\phi)\right\} - R_{\mu\nu}P(\phi) + \nabla_\mu\nabla_\nu P(\phi) - g_{\mu\nu}\nabla^2 P(\phi) + \frac{1}{2}T_{\mu\nu} \tag{65}$$

In FRW universe (14), Eq.(65) has the following form:

$$\begin{aligned} 0 &= -6H^2P(\phi) - Q(\phi) - 6H\frac{dP(\phi(t))}{dt} + \rho \\ 0 &= \left(4\dot{H} + 6H^2\right)P(\phi) + Q(\phi) + 2\frac{d^2P(\phi(t))}{dt} + 4H\frac{dP(\phi(t))}{dt} + p \end{aligned} \tag{66}$$

By combining the two equations in (66) and deleting $Q(\phi)$, we obtain

$$0 = 2\frac{d^2P(\phi(t))}{dt^2} - 2H\frac{dP(\phi(t))}{dt} + 4\dot{H}P(\phi) + p + \rho \ . \tag{67}$$

Since one can redefine ϕ properly as $\phi = \phi(\varphi)$, we may choose ϕ to be a time coordinate: $\phi = t$. Then assuming ρ, p could be given by the corresponding sum of matter with a constant EoS parameters w_i and writing the scale factor $a(t)$ as $a = a_0 \mathrm{e}^{g(t)}$ (a_0 : constant), we obtain the second rank differential equation:

$$0 = 2\frac{d^2P(\phi)}{d\phi^2} - 2g'(\phi)\frac{dP(\phi))}{d\phi} + 4g''(\phi)P(\phi) + \sum_i \left(1 + w_i\right)\rho_{i0}a_0^{-3(1+w_i)}\mathrm{e}^{-3(1+w_i)g(\phi)} \ . \tag{68}$$

If one can solve Eq.(68), with respect to $P(\phi)$, one can also find the form of $Q(\phi)$ by using (66) as

$$Q(\phi) = -6\left(g'(\phi)\right)^2 P(\phi) - 6g'(\phi)\frac{dP(\phi)}{d\phi} + \sum_i \rho_{i0}a_0^{-3(1+w_i)}\mathrm{e}^{-3(1+w_i)g(\phi)} \ . \tag{69}$$

Thus, it follows that any given cosmology can be realized by some specific $F(R)$-gravity.

We now consider the cases that (68) can be solved exactly. A first example is given by

$$g'(\phi) = g_0 + \frac{g_1}{\phi} \ . \tag{70}$$

For simplicity, we neglect the contribution from matter. Then Eq.(68) gives

$$0 = \frac{d^2P}{d\phi^2} - \left(g_0 + \frac{g_1}{\phi}\right)\frac{dP}{d\phi} - \frac{2g_1}{\phi^2}P \ . \tag{71}$$

The solution of (71) is given in terms of the Kummer functions or confluent hypergeometric functions:

$$P = z^\alpha F_K(\alpha, \gamma; z) \ , \quad z^{1-\gamma}F_K(\alpha - \gamma + 1, 2 - \gamma; z) \tag{72}$$

Here

$$\begin{aligned} & z \equiv g_0\phi \ , \quad \alpha \equiv \frac{1 + g_1 \pm \sqrt{g_1^2 + 10g_1 + 1}}{4} \ , \\ & \gamma \equiv 1 \pm \frac{\sqrt{g_1^2 + 10g_1 + 1}}{2} \ , \quad F_K(\alpha, \gamma; z) = \sum_{n=0}^{\infty} \frac{\alpha(\alpha+1)\cdots(\alpha+n-1)}{\gamma(\gamma+1)\cdots(\gamma+n-1)}\frac{z^n}{n!} \ . \end{aligned} \tag{73}$$

Eq.(70) gives the following Hubble rate:

$$H = g_0 + \frac{g_1}{t} \ . \tag{74}$$

Then when t is small, H behaves as

$$H \sim \frac{g_1}{t} \ , \tag{75}$$

which corresponds to the universe with matter whose EoS parameter is given by

$$w = -1 + \frac{2}{3g_1} \ . \tag{76}$$

On the other hand, when t is large, we find

$$H \to g_0 \ , \tag{77}$$

that is, the universe is asymptotically deSitter space.

We now show how we could reconstruct a model unifying the early-time inflation with late-time acceleration. In principle, one may consider $g(\phi)$ satisfying the following conditions:

- The condition for the inflation ($t = \phi \to 0$):

$$g''(0) = 0 \ , \tag{78}$$

  which shows that $H(0) = g'(0)$ is almost constant, which corresponds to the asymptotically deSitter space.

- The condition fot the late-time acceleration (at $t = \phi \sim t_0$):

$$g''(t_0) = 0 \ , \tag{79}$$

  which corresponds to the asymptotically deSitter space again.

An example could be

$$g'(\phi) = g_0 + g_1 \frac{\left(t_0^2 - \phi^2\right)^n - t_0^{2n}}{\left(t_0^2 - \phi^2\right)^n + c} \ . \tag{80}$$

Here g_0, g_1, and c are positive constants and n is positive integer greater than 1. Note that $g'(\phi)$ is a monotonically decreasing function of ϕ if $0 < \phi < t_0$ We also assume

$$0 < g_0 - \frac{g_1 t_0^{2n}}{c} \ll g_0 \ . \tag{81}$$

One should note that $g'(0) = g_0$ corresponds to the large Hubble rate in the inflationary epoch and $g'(t_0) = g_0 - \frac{g_1 t_0^{2n}}{c}$ to the small Hubble rate in the present universe. It is very difficult to solve (68) with (80), so we expand $g'(\phi)$ for small ϕ. For simplicity, we consider the case that $n = 2$ and no matter presents. Then

$$g(\phi) = g_0 - \frac{2g_1 t_0^2}{t_0^4 + c}\phi^2 + \mathcal{O}\left(\phi^4 \text{ or } g_1^2\right) \ . \tag{82}$$

Hence, one gets

$$\begin{aligned} P(\phi) \ &= \ P_0 + P_1 \mathrm{e}^{g_0\phi} - \frac{2g_1 t_0^2}{t_0^4 + c}\left[P_1 \left\{\frac{\phi^3}{3} - \frac{3\phi^2}{g_0} + \frac{6\phi}{g_0^2} - \frac{6}{g_0^4}\right\} \mathrm{e}^{g_0\phi} + \left\{\frac{2\phi^2}{g_0} + \frac{4\phi}{g_0^2}\right\} P_0 \right. \\ & \left. -\frac{P_2}{g_0}\mathrm{e}^{g_0\phi} - P_3\right] + \mathcal{O}\left(g_1^2\right) \ . \end{aligned} \tag{83}$$

Using boundary conditions we can specify different modified gravities which unify the early-time inflation with late-time acceleration. The important element of above reconstruction scheme is that it may be applied partially. For instance, one can start from the known model which passes local tests and describes the late-time acceleration. After that, the reconstruction method may be applied only at very small times (inflationary universe) to modify such a theory partially. As a result, we get the modified gravity with necessary early-time behavior and (or) vice-versa.

6 Dark Matter from $F(R)$-gravity

It is extremely interesting that dark matter could be explained in the framework of viable $F(R)$-gravity which was discussed in previous sections.

The previous considerations of $F(R)$-gravity suggest that it may play the role of gravitational alternative for dark energy. However, one can study $F(R)$-gravity as a model for dark matter. There have been proposed several scenarios to explain dark matter in the framework of $F(R)$-gravity. In most of such approaches[16], the MOND-like scenario or power-law gravity have been considered. In such scenarios, the field equations have been solved and the large-scale correction to the Newton law has been found and used as a source of dark matter.

There was, however, an observation [17] that the distribution of the matter is different from that of dark matter in a galaxy cluster. From this it has been believed that the dark matter can not be explained by the modification of the Newton law but dark matter should represent some (particles) matter.

It is known that $F(R)$-gravity contains a particle mode called 'scalaron', which explicitly appears when one rewrites $F(R)$-gravity in the the scalar-tensor form (23). In the Einstein gravity, when we quantize the fluctuations over the background metric, we obtain graviton, which is massless tensor particle. In case of $F(R)$-gravity, when one quantizes the fluctuations of the scalar field in the background metric, one gets the massive scalar particles in the addition to the graviton. Since the scalar particles in $F(R)$-gravity are massive, the pressure could be negligible and the strength of the interaction between such the scalar particles and usual matter should be that of the gravitational interaction order and therefore very small. Hence, such scalar particle could be a natural candidate for dark matter.

In the model [3] or our models (46) and (53), the mass of the effective scalar field depends on the curvature or energy density, in accord with so-called Chameleon mechanism. As our models (46) and (53) describe the early-time inflation as well as late-time acceleration, the 'scalaron' particles, that is, the scalar particles in $F(R)$-gravity, could be generated during the inflationary era. An interesting point is that the mass could change after the inflation due to Chameleon mechanism. Especially in the model (46), the mass decreases when the scalar curvature increases as shown in (49). Hence, in the inflationary era, when the curvature is large, one may consider the model where m_σ is large. After the inflationary epoch, the scalar particles, generated by the inflation, could lose their mass. Since the mass corresponds to the energy, the difference between the mass in the inflationary epoch and that after the inflation could be radiated as energy and could be converted into the matter and the radiation. This indicates that the reheating could be naturally realized in such model. Let the mass of σ in the inflationary epoch be m_I and that after inflation be m_A. Then for N particles, the radiated energy E_N may be estimated as

$$E = (m_I - m_A)\, N \ , \tag{84}$$

which could be converted into radiation, baryons and anti-baryons (and leptons). It is believed that the number of early-time baryons and anti-baryons is 10^{10} times of the number of baryons in the present universe. Since the density of the dark matter is almost five times of the density of the baryonic matter, we find

$$m_I > 10^{10} m_A \ . \tag{85}$$

In the solar system, one gets $A = R \sim 10^{-61}\,\mathrm{eV}^2$. Then if $n \gg 10 \sim 12$ and $\Lambda_i \sim 10^{20\sim 38}$, the order of the mass m_σ is given by

$$m_\sigma^2 \sim 10^{239\sim 295-10n}\,\mathrm{eV}^2 \ , \tag{86}$$

which is large enough so that σ could be Cold (non-relativistic) Dark Matter. On the other hand, in $1/R$-model, the corresponding mass is given by

$$m_{1/R}^2 \sim \frac{\mu^4}{R} \sim 10^{-51}\,\mathrm{eV}^2 \ . \tag{87}$$

Here μ is the parameter with dimension of mass and $\mu \sim 10^{-33}\,\mathrm{eV}$. The mass $m_{1/R}$ is very small and cannot be a Cold Dark Matter. The corresponding composite particles can be a Hot (relativistic) Dark Matter but Hot Dark Matter has been excluded due to difficulty to generate the universe structure formation.

In the inflationary era, the spacetime is approximated by the de Sitter space:

$$ds^2 = -dt^2 + \mathrm{e}^{2H_0 t} \sum_{i=1,2,3} \left(dx^i\right)^2 \ . \tag{88}$$

Then the scalar particle σ could be Fourier-transformed as

$$\sigma = \int d^3k \tilde{\sigma}(\mathbf{k}, t) \mathrm{e}^{-i\mathbf{k}\cdot\mathbf{x}} \ . \tag{89}$$

Hence, the number of the particles with $\mathbf{k}$ created during inflation is proportional to $\mathrm{e}^{\nu\pi}$. Here

$$\nu \equiv \sqrt{\frac{m_\sigma^2}{H_0^2} - \frac{9}{4}} \ . \tag{90}$$

Then if

$$\frac{m_\sigma^2}{H_0^2} > \frac{9}{4} \ , \tag{91}$$

sufficient number of the particles could be created.

In the original $f(R)$-frame (7), the scalar field σ appears as composite state. The equation of motion in $f(R)$-gravity contains fourth derivatives, which means the existence of the extra particle mode or composite state. In fact, the trace part of the equation of motion (13) has the following Klein-Gordon equation-like form:

$$3\nabla^2 f'(R) = R + 2f(R) - Rf'(R) - \kappa^2 T \, . \tag{92}$$

The above trace equation can be interpreted as an equation of motion for the non trivial 'scalaron' $f'(R)$. This means that the curvature itself propagates. In fact the scalar field σ in the scalar-tensor form of the theory can be given by 'scalaron', which is the combination of the scalar curvature in the original frame:

$$\sigma = -\ln\left(1 + f'(R)\right) \ . \tag{93}$$

Note that the 'scalaron' is different mode from graviton, which is massless and tensor.

Eq.(49) shows that the mass, which depends on the value of the scalar field σ, is given by

$$m_\sigma^2 \sim \frac{f_0}{f_1^2}\left(\frac{2n+1}{2n+2}\right)\left(\frac{f_1^2}{(2n+1)f_0}\right)^{\frac{2n+1}{2n+2}} \sigma^{-\frac{2n+3}{2n+2}} \ . \tag{94}$$

If the curvature becomes small, σ becomes large and m_σ^2 decreases. Then the scalar particles lose their masses after the inflation. The difference of the mass in the inflationary epoch and that after the inflation could be radiated as energy and can be converted into the matter and the radiation.

By substituting the expression of σ (49) into (94), one obtains

$$m_\sigma^2 \sim \frac{f_1^2 A^{2n+3}}{2(2n+1)(n+1)f_0} \ . \tag{95}$$

Note that A corresponds to the scalar curvature. Let denote the value of A in the inflationary epoch by A_I and that after the inflation by A_A. Then the condition (85) shows

$$\frac{m_I}{m_A} \sim \left(\frac{A_I}{A_A}\right)^{n+3/2} > 10^{10} \ . \tag{96}$$

For the model with $n = 2$, the condition (85) or (96) could be satisfied if $A_I/A_A > 10^3$, which seems to indicate that the reheating could be easily realized in such a model.

Now we check if the condition (91) could be satisfied. Note $H_0^2 \sim \Lambda_i$. Eq.(95) also indicates that in the inflationary era, where $A = R \sim \Lambda_i$, the magnitude of the mass is given by

$$m_\sigma^2 \sim \frac{\Lambda_i^{2n+1}}{R_0^{2n}} \ , \tag{97}$$

which is large enough and the condition (91) is satisfied. Here Eq.(47) is used. Thus, sufficient number of σ-particles could be created.

Let us consider the rotational curve of galaxy. As we will see the shift of the rotational curve does not occur due to correction to the Newton law between visible matter (baryon or intersteller gas) but due to invisible (dark) matter, and the Newton law itself is not modified.

Let the temperature of the dark matter be $T = 1/k\beta$ where k is the Boltzmann constant. First, we assume the mass m_σ of the scalar particle σ is constant. As the total mass of dark matter is much larger than that of baryonic matter and radiation, we neglect the contributions from the baryonic matter and radiation just for simplicity. We now work in Newtonian approximation and the system is spherically symmetric. Let the gravitational potential, which can be formed by the sum of the dark matter particles, be $V(r)$. Then the gravitational force is given by $\mathcal{F}(r) = -m dV(r)/dr$. If we denote the number density of the dark matter particles by $n(r)$, in the Newtonian approximation, by putting $\kappa^2 = 8\pi G$, one gets

$$\mathcal{F}(r) = -\frac{G m_\sigma^2}{r^2} \int_0^r 4\pi s^2 n(s) ds \tag{98}$$

and therefore $V(r)$ is given by

$$V(r) = 4\pi G m_\sigma \int^r \frac{ds}{s^2} \int_0^s u^2 n(u) du \ . \tag{99}$$

If one assumes the number density $n(r)$ of dark matter particles could obey the Boltzmann distribution, we find

$$n(r) = N_0 \mathrm{e}^{-\beta m_\sigma V(r)} \ . \tag{100}$$

Here N_0 is a constant, which can be determined by the normalization. Using (99) and (100) and deleting $n(r)$, the differential equation follows:

$$\left(r^2 V'(r)\right)' = 4\pi G m_\sigma N_0 r^2 \mathrm{e}^{-\beta m_\sigma V(r)} \ . \tag{101}$$

An exact solution of the above equation is given by

$$V(r) = \frac{2}{\beta m_\sigma} \ln\left(\frac{r}{r_0}\right) \ , \quad r_0^2 \equiv \frac{1}{2\pi G m_\sigma^2 N_0 \beta} \ . \tag{102}$$

As the general solution for the non-linear differential equation (101) is not known, we assume $V(r)$ could be given by (102). Then the rotational speed v of the stars in the galaxy could be determined by the balance of the gravitational force and the centrifugal force:

$$m_\star \frac{v^2}{r} = -\mathcal{F}(r) = m_\star V'(r) = \frac{2 m_\star}{\beta m_\sigma r} \ . \tag{103}$$

Here $m_\star$ is the mass of a star. Hence,

$$v^2 = \frac{2}{m_\sigma \beta} \ , \tag{104}$$

that is, v becomes a constant, which could be consistent with the observation.

For the dark matter particles from $f(R)$-gravity, the mass m_σ depends on the scalar curvature or the value of the background σ as in (94). The scalar curvature is determined by the energy density ρ (if pressure could be neglected as in usual baryonic matter and cold dark matter) and if we neglect the contribution from the baryonic matter, the energy density ρ is given by

$$\rho(r) = m_\sigma n(r) \ . \tag{105}$$

Therefore it follows

$$m_\sigma = m_\sigma\left(\rho(r)\right) = m_\sigma\left(m_\sigma n(r)\right) \ , \tag{106}$$

which could be solved with respect to m_σ:

$$m_\sigma = m_\sigma\left(n(r)\right) \ . \tag{107}$$

Furthermore by combining (100) and (107), one may solve m_σ with respect to $V(r)$ and N_0 as

$$m_\sigma = m_\sigma\left(N_0, V(r)\right) \ . \tag{108}$$

Then (98) could be modified as

$$\mathcal{F}(r) = -\frac{G m_\sigma\left(N_0, V(r)\right)}{r^2}\int_0^r 4\pi s^2 m_\sigma\left(N_0, V(r)\right) n(s) ds \tag{109}$$

which gives, instead of (101),

$$\left(r^2 V'(r)\right)' = 4\pi G m_\sigma\left(N_0, V(r)\right) N_0 r^2 \mathrm{e}^{-\beta m_\sigma(N_0, V(r))V(r)} \ . \tag{110}$$

Eq.(110) is rather complicated but at least numerically solvable.

For the model (46), if the curvature is large enough even around the galaxy, the mass m_σ is given by (95). The scalar curvature $A = R$ is proportional to the energy density (since the pressure could be neglected), $A \propto \rho$, and the energy density ρ is given by (105). Then

$$n(r) \sim \frac{1}{\kappa^2}\left\{\frac{2(n+1)(2n+1)f_0}{f_1^2}\right\}^{\frac{1}{2n+3}} \left(m_\sigma(r)\right)^{-\frac{2n+1}{2n+3}} \ . \tag{111}$$

Using (100), one also gets

$$V(r) = \frac{2n+1}{(2n+3)\beta m_\sigma(r)} \ln\frac{m_\sigma(r)}{m_0} \ , \quad m_0 \equiv \left(\kappa^2 N_0\right)^{-\frac{2n+3}{2n+1}}\left\{\frac{2(n+1)(2n+1)f_0}{f_1^2}\right\}^{\frac{1}{2n+1}} . \tag{112}$$

Here m_0 has mass dimension. By substituting (112) into (110), it follows

$$\begin{aligned} &\left(\frac{2n+1}{2n+3}\right)\frac{1}{\beta}\left\{r^2\left(1-\ln\frac{m_\sigma(r)}{m_0}\right)\frac{m_\sigma''(r)}{m_\sigma(r)^2} - r^2\left(3-2\ln\frac{m_\sigma(r)}{m_0}\right)\frac{\left(m_\sigma'(r)\right)^2}{m_\sigma(r)^3}\right. \\ &\left. +2r\left(1-\ln\frac{m_\sigma(r)}{m_0}\right)\frac{m_\sigma'(r)}{m_\sigma(r)^2}\right\} = \frac{1}{2}\left\{\frac{2(n+1)(2n+1)f_0}{f_1^2}\right\}^{\frac{1}{2n+3}} r^2\left(m_\sigma(r)\right)^{\frac{2}{2n+3}} \ . \end{aligned} \tag{113}$$

It is very difficult to find the exact solution of (113), although one may solve (113) numerically. Then we now consider the region where $m_\sigma \ll m_0$ but $\ln\left(m_\sigma/m_0\right)$ is slow varying function of r, compared with the power of r. In the region, we may treat $\ln\left(m_\sigma/m_0\right)$ as a large negative constant:

$$\ln\left(m_\sigma/m_0\right) \sim -C \ . \tag{114}$$

Then the following solution is obtained:

$$\begin{aligned} m_\sigma(r) &= m_0\left(\frac{r}{r_0}\right)^{-\frac{2(2n+3)}{2n+5}} \ , \\ r_0^2 &\equiv \frac{4(2n+1)(2n+9)C}{(2n+5)\beta}\left(\kappa^2 N_0\right)^{\frac{2n+5}{2n+1}}\left\{\frac{2(n+1)(2n+1)f_0}{f_1^2}\right\}^{-\frac{1}{2n+1}} \ . \end{aligned} \tag{115}$$

Note that r_0 can be real for any positive n. Eq.(112) shows that

$$V(r) = -\frac{2(2n+1)}{2n+5}\frac{1}{\beta m_0}\left(\frac{r}{r_0}\right)^{\frac{2(2n+3)}{2n+5}} \ln\frac{r}{r_0} \ . \tag{116}$$

Note that the potential (116) is obtained by assuming the Newton law by summing up the Newton potentials coming from the $f(R)$-dark matter particles ('scalaron') distributed around the galaxy. Eq.(115) indicates that the condition $m_\sigma \ll m_0$ requires $r \gg r_0$. Then by using the equation for the balance of the gravitational force and the centrifugal force, as in (103), we find

$$v \propto \left(\frac{r}{r_0}\right)^{\frac{2n+3)}{2n+5}} \ , \tag{117}$$

which is monotonically increasing function of r and the behavior is different from that in (104). If there is only usual baryonic matter without any dark matter, the velocity is the decreasing function of r, if there is also usual dark matter, as shown in (104), the velocity is almost constant, if dark matter originates from $f(R)$-gravity, as we consider here, there is a region where the velocity could be an *increasing* function of r. Of course, one should be more careful as these are qualitative considerations. The condition $m_\sigma \ll m_0$ requires $r \gg r_0$ but in the region faraway from galaxy, the scalar curvature becomes small and the approximation (95) could be broken. Anyway if there appears a region where velocity is the increasing function of r, this might be a signal of $f(R)$-gravity origin for dark matter. For more precise quantitative arguments, it is necessary to include the contribution from usual baryonic matter as well as to do numerical calculation. In any case, it seems very promising that composite particles from viable modified gravity which unifies inflation with late-time acceleration may play the role of dark matter.

7 Discussion

In summary, we reviewed $F(R)$-gravity and demonstrated that some versions of such theory are viable gravitational candidates for unification of early-time inflation and late-time cosmic acceleration. It is explicitly shown that the known critical arguments against such theory do not work for those models. In other words, the modified gravity under consideration may pass the local tests (Newton law is respected, the very heavy positive mass for additional scalar degree of freedom is generated). The reconstruction of modified $F(R)$ gravity is considered. It is demonstrated that such theory may be reconstructed for any given cosmology. Moreover, the partial reconstruction (at early universe) may be done for modified gravity which complies with local tests and dark energy bounds. This leads to some freedom in the choice of modified gravity for the unification of given inflationary era compatible with astrophysical bounds and dark energy epoch. As a final very promising result it is shown that modified gravity under consideration may qualitatively well describe dark matter, using the composite scalar particle from $F(R)$ theory and Chameleon scenario.

Thus, modified gravity remains viable cosmological theory which is realistic alternative to standard Einstein gravity. Moreover, it suggests the universal gravitational unification of inflation, cosmic acceleration and dark matter without the need to introduce any exotic matter. Moreover, it remains enough freedom in the formulation of such theory which is very positive fact, having in mind, coming soon precise observational data.

Acknowledgements

We are very indebted to the organizers of the workshop JGRG17(Japan) and VI Winter School on Theoretical Physics (Dubna, Russia) for the invitation to give the talks there. This work is supported in part by the Ministry of Education, Science, Sports and Culture of Japan under grant no.18549001 and 21st Century COE Program of Nagoya University provided by the Japan Society for the Promotion of Science (15COEG01) and in part by MEC (Spain) projects FIS2006-02842 and PIE2007-50/023 and by RFBR, grant 06-01-00609 (Russia).

References

[1] S. Nojiri, S. D. Odintsov, M. Sasaki, Phys. Rev. D **71** (2005) 123509 [arXiv:hep-th/0504052]; S. Nojiri, S. D. Odintsov, M. Sami, Phys. Rev. D **74** 046004 (2006) [arXiv:hep-th/0605039]; G. Cognola, E. Elizalde, S. Nojiri, S. D. Odintsov, S. Zerbini, Phys. Rev. D **75** 086002 (2007) [arXiv:hep-th/0611198].

[2] S. Nojiri and S. D. Odintsov, Int. J. Geom. Meth. Mod. Phys. **4**, 115 (2007) [arXiv:hep-th/0601213].

[3] W. Hu and I. Sawicki, Phys. Rev. D **76** (2007) 064004 [arXiv:0705.1158].

[4] S. Nojiri and S. D. Odintsov, Phys. Lett. B **657**, 238 (2007) [arXiv:0707.1941 [hep-th]].

[5] S. Nojiri and S. D. Odintsov, arXiv:0710.1738 [hep-th]; G. Cognola, E. Elizalde, S. Nojiri, S.D. Odintsov, L. Sebastiani and S. Zerbini, arXiv:0712.4017[hep-th].

[6] G. Cognola, E. Elizalde, S. Nojiri, S. D. Odintsov and S. Zerbini, JCAP **0502** (2005) 010 [arXiv:hep-th/0501096].

[7] T. Chiba, Phys. Lett. B **575** (2003) 1 [arXiv:astro-ph/0307338].

[8] A. D. Dolgov, M. Kawasaki, Phys. Lett. B **573** (2003) 1 [arXiv:astro-ph/0307285].

[9] A. L. Erickcek, T. L. Smith, M. Kamionkowski, Phys. Rev. D **74** (2006) 121501 [arXiv:astro-ph/0610483].

[10] T. Chiba, T. L. Smith, A. L. Erickcek, Phys. Rev. D **75** (2007) 124014 [arXiv:astro-ph/0611867].

[11] S. Nojiri, S. D. Odintsov, Phys. Rev. D **68** (2003) 123512 [arXiv:hep-th/0307288].

[12] J. Khoury and A. Weltman, Phys. Rev. D **69** (2004) 044026 [arXiv:astro-ph/0309411].

[13] S. Nojiri and S. D. Odintsov, Phys. Lett. B **652** (2007) 343 [arXiv:0706.1378[hep-th]].

[14] S. M. Carroll, V. Duvvuri, M. Trodden, M. S. Turner, Phys. Rev. D **70** (2004) 043528 [arXiv:astro-ph/0306438];
S. Capozziello, S. Carloni and A. Troisi, arXiv:astro-ph/0303041.

[15] S. Nojiri, S. D. Odintsov, Phys. Rev. D **74** (2006) 086005 [arXiv:hep-th/0608008]; hep-th 0611071.

[16] S. Capozziello, V. Cardone and A. Troisi, JCAP **0608** (2006) 001.

[17] D. Clowe, M. Bradac, A. H. Gonzalez, M. Markevitch, S. W. Randall, C. Jones, D. Zaritsky, arXiv:astro-ph/0608407;
http://today.slac.stanford.edu/feature/darkmatter.asp

Ghost condensation and gravity in Higgs phase

Shinji Mukohyama[1]

Department of Physics and Research Center for the Early Universe
The University of Tokyo, Tokyo 113-0033, Japan

Abstract

In this presentation I review basic properties of the simplest Higgs phase of gravity called ghost condensation, and discuss possible applications and observational bounds.

1 Introduction

Acceleration of the cosmic expansion today is one of the greatest mysteries in both cosmology and fundamental physics. Assuming that Einstein's general relativity is the genuine description of gravity all the way up to cosmological distance and time scales, the so called concordance cosmological model requires that about 70% of our universe should be some sort of energy with negative pressure, called dark energy. However, since the nature of gravity at cosmological scales has never been probed directly, we do not know whether the general relativity is really correct at such infrared (IR) scales. Therefore, it seems natural to consider modification of general relativity in IR as an alternative to dark energy. Dark energy, IR modification of gravity and their combination should be tested and distinguished by future observations and experiments.

From the theoretical point of view, however, IR modification of general relativity is not an easy subject. Most of the previous proposals are one way or another scalar-tensor theories of gravity, and are strongly constrained by e.g. solar system experiments [1] and the theoretical requirement that ghosts be absent [2, 3, 4]. The massive gravity theory [5] and the Dvali-Gabadadze-Porrati (DGP) brane model [6] are much more interesting IR modification of gravity, but they are known to have macroscopic UV scales [7, 8]. A UV scale of a theory is the scale at which the theory breaks down and loses its predictability. For example, the UV scale of the $4D$ general relativity is the Planck scale, at which quantum gravity effects are believed to become important. Since the Planck scale is microscopic, the general relativity maintains its predictability at essentially all scales we can directly probe. On the other hand, in the massive gravity theory and the DGP brane model, the UV scale is macroscopic. For example, if the scale of IR modification is the Hubble scale today or longer then the UV scale would be $\sim 1,000km$ or longer. At the UV scale an extra degree of freedom, which is coupled to matter, becomes strongly coupled and its quantum effects cannot be ignored. This itself does not immediately exclude those theories, but means that we need UV completion in order to predict what we think we know about gravity within $\sim 1,000km$. Since this issue is originated from the IR modification and the extra degree of freedom cannot be decoupled from matter, it is not clear whether the physics in IR is insensitive to unknown properties of the UV completion. In particular, there is no guarantee that properties of the IR modification of gravity will persist even qualitatively when the theories are UV completed in a way that they give correct predictions about gravity at scales between $\sim 1,000km$ and $\sim 0.1mm$.

Ghost condensation is an analogue of the Higgs mechanism in general relativity and modifies gravity in IR in a way that avoids the macroscopic UV scale [9] [2]. In ghost condensation the theory is expanded around a background without ghost and the low energy effective theory has a universal structure determined solely by the symmetry breaking pattern. While the Higgs mechanism in a gauge theory spontaneously breaks gauge symmetry, the ghost condensation spontaneously breaks a part of Lorentz symmetry since this is the symmetry relevant to gravity. In a gauge theory the Higgs mechanism makes it possible to give a mass term to the gauge boson and to modify the force law in a theoretically controllable way. Similarly, the ghost condensation gives a "mass term" to the scalar sector of gravity and

---

[1]E-mail: mukoyama@phys.s.u-tokyo.ac.jp

[2]See e.g.[10, 11, 12, 13, 14, 15, 16] for other related proposals.

modifies gravitational force in the linearized level even in Minkowski and de Sitter spacetimes. The Higgs phase of gravity provided by the ghost condensation is simplest in the sense that the number of Nambu-Goldstone bosons associated with spontaneous Lorentz breaking is just one and that only the scalar sector is essentially modified.

2 Ghost Condensation

The ghost condensation can be pedagogically explained by comparison with the usual Higgs mechanism as in the table shown below. First, the order parameter for ghost condensation is the vacuum expectation value (vev) of the derivative $\partial_\mu\phi$ of a scalar field ϕ, while the order parameter for Higgs mechanism is the vev of a scalar field Φ itself. Second, both have instabilities in their symmetric phases: a tachyonic instability around $\Phi = 0$ for Higgs mechanism and a ghost instability around $\partial_\mu\phi = 0$ for ghost condensation. In both cases, because of the instabilities, the system should deviate from the symmetric phase and the order parameter should obtain a non-vanishing vev. Third, there are stable point where small fluctuations do not contain tachyons nor ghosts. For Higgs mechanism, such a point is characterized by the vev of the order parameter satisfying $V' = 0$ and $V'' > 0$. On the other hand, for ghost condensation a stable point is characterized by $P' = 0$ and $P'' > 0$. Fourth, while the usual Higgs mechanism breaks usual gauge symmetry and changes gauge force law, the ghost condensation spontaneously breaks a part of Lorentz symmetry (the time translation symmetry) and changes linearized gravity force law even in Minkowski background. Finally, generated corrections to the standard Gauss-law potential is Yukawa-type for Higgs mechanism but oscillating for ghost condensation.

	Higgs mechanism	***Ghost condensate***
Order Parameter	$\langle \Phi \rangle$ 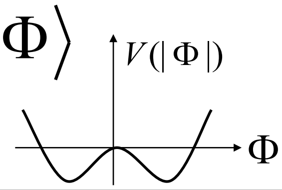	$\langle \partial_\mu \phi \rangle$ 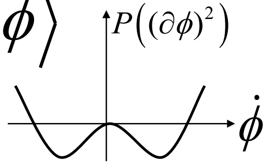
Instability	Tachyon $-m^2\Phi^2$	Ghost $-\dot{\phi}^2$
Condensate	V'=0, V''>0	P'=0, P''>0
Spontaneous breaking	Gauge symmetry	Lorentz symmetry
Modifying	Gauge force	Gravity
New potential	Yukawa-type	Oscillating

At this point one might wonder if the system really reach a configuration where $P' = 0$ and $P'' > 0$. Actually, it is easy to show that this is the case. For simplicity let us consider a Lagrangian $L_\phi = P(-(\partial\phi)^2)$ in the expanding FRW background with P of the form shown in the upper right part of the table. We assume the shift symmetry, the symmetry under the constant shift $\phi \to \phi + c$ of the scalar field. This symmetry prevents potential terms of ϕ from being generated. The equation of motion for ϕ is simply $\partial_t[a^3 P'\dot{\phi}] = 0$, where a is the scale factor of the universe. This means that $a^3 P'\dot{\phi}$ is constant and that

$$P'\dot{\phi} \propto a^{-3} \to 0 \quad (a \to \infty) \tag{1}$$

as the universe expands. We have two choices: $P' = 0$ or $\dot{\phi} = 0$, namely one of the two bottoms of the function P or the top of the hill between them. Obviously, we cannot take the latter choice since it is a ghosty background and anyway unstable. Thus, we are automatically driven to $P' = 0$ by the expansion of the universe. In this sense the background with $P' = 0$ is an attractor.

Having shown that the ghost condensate is an attractor, let us construct a low energy effective field theory around this background. For this purpose let us consider a small fluctuation around the background with $P' = 0$. For $\phi = M^2 t + \pi$, the quadratic action for π coming from the Lagrangian P is $\int d^4x[(P'(M^4)+M^4P''(M^4))\dot{\pi}^2 - P'(M^4)(\nabla\pi)^2]$. By setting $P'(M^4) = 0$ we obtain the time kinetic term $M^4P''(M^4)\dot{\pi}^2$ with the correct sign. Unless the function P is fine-tuned, P'' is non-zero at $P' = 0$. This means that the coefficient of the time kinetic term is non-vanishing and, thus, we do not have the strong coupling issue which the massive gravity and the DGP brane model are facing with. On the other hand, the coefficient of $(\nabla\pi)^2$ vanishes at $P' = 0$ and the simple Lagrangian P does not give us a spatial kinetic term for π. However, this does not mean that there is no spatial kinetic term in the low energy EFT for π. This just says that the leading spatial kinetic term is not contained in P and that we should look for the leading term in different parts. Indeed, other terms like $\tilde{P}((\partial\phi)^2)Q(\Box\phi)$ do contain spatial kinetic terms for π but the spatial-derivative expansion starts with the fourth derivative: $(\nabla^2\pi)^2 + \cdots$. If there is a non-vanishing second-order spatial kinetic term $(\nabla\pi)^2$ then it can be included in P by redefinition and the redefined P' goes to zero by the expansion of the universe as shown above. Namely, the expansion of the universe ensures that the spatial-derivative expansion starts from $(\nabla^2\pi)^2 + \cdots$. Combining this spatial kinetic term with the previously obtained time kinetic term and properly normalizing π, we obtain the low energy effective action of the form

$$M^4 \int d^4x \left[\frac{1}{2}\dot{\pi}^2 - \frac{\alpha}{M^2}(\nabla^2\pi)^2 + \cdots \right], \tag{2}$$

where α is a dimensionless parameter of order unity [3]. One might worry that other (nonlinear) terms in effective theory such as $\dot{\pi}(\nabla\pi)^2$ might mess up the effective action. In fact, it turns out that all such terms are irrelevant at low energy [9]. An important fact to show this is that the scaling dimension of π is not the same as its mass dimension 1 but is 1/4, reflecting the situation that the Lorentz symmetry is broken spontaneously. Moreover, it is also straightforward to show that all spurious modes associates with higher time derivative terms such as $(\ddot{\phi})^2$ have frequency above the cutoff M and, thus, should be ignored. In this sense, we are assuming the existence of a UV completion but not assuming any properties of it. Finally, it must be noted that the effective action of the form (2) is stable against radiative corrections. Indeed, the only would-be more relevant term in the effective theory is the usual spatial kinetic term $(\nabla\pi)^2$, but its coefficient P' is driven to an extremely small value by the expansion of the universe even if it is radiatively generated.

The effective action (2) would imply the low energy dispersion relation for π is $\omega^2 \simeq \alpha k^4/M^2$. However, since the background spontaneously breaks Lorentz invariance, π couples to gravity in the linearized level even in Minkowski or de Sitter background. Hence, mixing with gravity introduces an order M^2/M_{pl}^2 correction to the dispersion relation. As a result the dispersion relation in the presence of gravity is $\omega^2 \simeq \alpha k^4/M^2 - \alpha M^2k^2/2M_{pl}^2$. This dispersion relation leads to IR modification of gravity due to Jean's instability. Note that there is no ghost around the stable background $P' = 0$ and the Jeans's instability is nothing to do with a ghost.

In the above we have expanded a general Lagrangian consistent with the shift symmetry around the stable background in order to construct the low energy EFT. This is the most straightforward approach. An alternative, more powerful way is to use the symmetry breaking pattern. In this approach, we actually do not need to specify a concrete way of the spontaneous symmetry breaking. In this sense, the ghost around $\dot{\phi} = 0$ has nothing to do with the construction of the EFT around $P' = 0$. Indeed, it is suffice to assume the symmetry breaking pattern, namely from the full 4-dimensional Lorentz symmetry to the 3-dimensional spatial diffeomorphism [9].

Here, let us briefly review this approach based on the symmetry breaking pattern. This leads to the exactly same conclusion as above, but is more universal and can be applied to any situations as far as the symmetry breaking pattern is the same. We assume that (i) the 4-dimensional Lorentz symmetry

[3] With this normalization, π has the dimension of length.

is spontaneously broken down to a 3-dimensional spatial diffeomorphism and that (ii) the background spacetime metric is maximally symmetric, either Minkowski or de Sitter. With the assumption (i), we are left with the 3-dimensional spatial diffeomorphism $\vec{x} \to \vec{x}'(t, \vec{x})$. Our strategy here is to write down the most general action invariant under this residual symmetry. After that, the action for the Nambu-Goldstone (NG) boson π is obtained by undoing the unitary gauge.

For simplicity let us consider the Minkowski background plus perturbation: $g_{\mu\nu} = \eta_{\mu\nu} + h_{\mu\nu}$. The infinitesimal gauge transformation is $\delta h_{\mu\nu} = \partial_\mu \xi_\nu + \partial_\nu \xi_\mu$, where ξ^μ is a 4-vector representing the gauge freedom. Under the residual gauge transformation ξ^i $(i = 1, 2, 3)$, the metric perturbation transforms as

$$\delta h_{00} = 0, \quad \delta h_{0i} = \partial_0 \xi_i, \quad \delta h_{ij} = \partial_i \xi_j + \partial_j \xi_i. \tag{3}$$

Now let us seek terms invariant under the residual gauge transformation. Those terms must begin at quadratic order since we assumed that the flat spacetime is a solution to the equation of motion. The leading term (without derivatives acted on the metric perturbations) is $\int dx^4 M^4 h_{00}^2$. This is indeed invariant under the residual gauge transformation (3). From this term, we can obtain the corresponding term in the effective action for the NG boson π. Since $h_{00} \to h_{00} + 2\partial_0 \xi_0$, by promoting the broken symmetry ξ^0 to a physical degree of freedom π, we obtain the term $\int dx^4 M^4 (h_{00} - 2\dot{\pi})^2$. This includes a time kinetic term for π as well as a mixing term. At this point we wonder if we can get the usual space kinetic term $(\vec{\nabla}\pi)^2$ or not. The only possibility would be from $(h_{0i})^2$ since $h_{0i} \to h_{0i} - \partial_i \pi$ under the broken symmetry transformation $\xi^0 = \pi$. However, this term is not invariant under the residual spatial diffeomorphism ξ^i and, thus, cannot enter the effective action. Actually, there are combinations invariant under the spatial diffeomorphism. They are made of the geometrical quantity called extrinsic curvature. The extrinsic curvature K_{ij} in the linear order is $K_{ij} = \partial_j h_{0j} + \partial_i h_{0j} - \partial_0 h_{ij}$ and transforms as a tensor under the spatial diffeomorphism. Thus, $\int dx^4 \tilde{M}^2 (K_i^i)^2$ and $\int dx^4 \bar{M}^2 K^{ij} K_{ij}$ are invariant under spatial diffeomorphism and can be used in the action. Since $K_{ij} \to K_{ij} - \partial_i \partial_j \pi$ under the broken symmetry $\xi^0 = \pi$, we obtain $\int dx^4 (\tilde{M}^2 + \bar{M}^2)(\vec{\nabla}^2 \pi)^2$. Combining these terms with the above time kinetic term and properly normalizing the definition of π and M, we obtain

$$L_{eff} = M^4 \left\{ \frac{1}{2} \left(\dot{\pi} - \frac{1}{2} h_{00} \right)^2 - \frac{\alpha}{M^2} (\vec{\nabla}^2 \pi)^2 + \cdots \right\}, \tag{4}$$

where α is a dimensionless constant of order unity. By setting $h_{00} = 0$, this completely agrees with (2), which was obtained by expanding the scalar field action explicitly around the stable background. Here, in deriving the effective action all we needed was the symmetry breaking pattern. Thus, the low energy EFT of the ghost condensation is universal and should hold as far as the symmetry breaking pattern is the same.

In ghost condensation the linearized gravitational potential is modified at the length scale r_c in the time scale t_c, where r_c and t_c are related to the scale of spontaneous Lorentz breaking M as

$$r_c \simeq \frac{M_{\rm Pl}}{M^2}, \quad t_c \simeq \frac{M_{\rm Pl}^2}{M^3}. \tag{5}$$

Note that r_c and t_c are much longer than $1/M$. The way gravity is modified is peculiar. At the time when a gravitational source is turned on, the potential is exactly the same as that in general relativity. After that, however, the standard form of the potential is modulated with oscillation in space and with exponential growth in time. This is an analogue of Jeans instability, but unlike the usual Jeans instability, it persists in the linearized level even in Minkowski background. The length scale r_c and the time scale t_c above are for the oscillation and the exponential growth, respectively. At the time $\sim t_c$, the modification part of the linear potential will have an appreciable peak only at the distance $\sim r_c$. At larger distances, it will take more time for excitations of the Nambu-Goldstone boson to propagate from the source and to modify the gravitational potential. At shorter distances, the modification is smaller than at the peak position because of the spatial oscillation with the boundary condition at the origin. The behavior explained here applies to Minkowski background, but in ref. [9] the modification of gravity in de Sitter spacetime was also analyzed. It was shown that the growing mode of the linear gravitational potential disappears when the Hubble expansion rate exceeds a critical value $H_c \sim 1/t_c$. Thus, the onset of the IR modification starts at the time when the Hubble expansion rate becomes as low as H_c.

If we take the $M/M_{\rm Pl} \to 0$ limit then the Higgs sector is completely decoupled from the gravity and the matter sectors and, thus, the general relativity is safely recovered. Therefore, cosmological and astrophysical considerations in general do not set a lower bound on the scale M of spontaneous Lorentz breaking, but provide upper bounds on M. If we trusted the linear approximation for all gravitational sources for all times then the requirement $H_c \lesssim H_0$ would give the bound $M \lesssim (M_{\rm Pl}^2 H_0)^{1/3} \simeq 10MeV$, where H_0 is the Hubble parameter today [9]. However, for virtually all interesting gravitational sources the nonlinear dynamics dominates in time scales shorter than the age of the universe. As a result the nonlinear dynamics cuts off the Jeans instability of the linear theory, and allows $M \lesssim 100GeV$ [17].

Note that the ghost condensate provides the second most symmetric class of backgrounds for the system of field theory plus gravity. The most symmetric class is of course maximally symmetric solutions: Minkowski, de Sitter and anti-de Sitter. The ghost condensate minimally breaks the maximal symmetry and introduces only one Nambu-Goldstone boson.

Because of the universality of the low energy EFT, it is worthwhile investigating properties of the Higgs phase of gravity, whether or not it leads to interesting physical phenomena. Actually, it turns out that the physics in the Higgs phase of gravity is extremely rich and intriguing. They include IR modification of gravity [9], a new spin-dependent force [18], a qualitatively different picture of inflationary de Sitter phase [19, 20], effects of moving sources [21, 22], nonlinear dynamics [23, 17], properties of black holes [24, 25, 26], implications to galaxy rotation curves [27, 28, 29], dark energy models [30, 31, 32, 33, 34], other classical dynamics [35, 36], attempts towards UV completion [37, 38, 39], and so on.

3 Possible Applications

Dark energy: In the usual Higgs mechanism, the cosmological constant (cc) would be negative in the broken phase if it is zero in the symmetric phase. Therefore, it seems difficult to imagine how the Higgs mechanism provides a source of dark energy. On the other hand, the situation is opposite with the ghost condensation: the cc would be positive in the broken phase if it is zero in the symmetric phase. Hence, while this by itself does not solve the cc problem, this can be a source of dark energy.

Dark matter: If we consider a small, positive deviation of P' from zero then the homogeneous part of the energy density is proportional to a^{-3} and behaves like dark matter. Inhomogeneous linear perturbations around the homogeneous deviation also behaves like dark matter. However, at this moment it is not clear whether we can replace dark matter with ghost condensate. We need to see if it clumps properly. Ref. [17] can be thought to be a step towards this direction.

Inflation: We can also consider inflation within the regime of the validity of the EFT with ghost condensation. In the very early universe where H is higher than the cutoff M, we do not have a good EFT describing the sector of ghost condensation. However, the contribution of this sector to the total energy density ρ_{tot} is naturally expected to be negligible: $\rho_{ghost} \sim M^4 \ll M_p^2 H^2 \simeq \rho_{tot}$. As the Hubble expansion rate decreases, the sector of ghost condensation enters the regime of validity of the EFT and the Hubble friction drives P' to zero. If we take into account quantum fluctuations then P' is not quite zero but is $\sim (H/M)^{5/2} \sim (\delta\rho/\rho)^2 \sim 10^{-10}$ in the end of ghost inflation. In this way, we have a consistent story, starting from the outside the regime of validity of the EFT and dynamically entering the regime of validity. All predictions of the ghost inflation are derived within the validity of the EFT, including the relatively low-H de Sitter phase, the scale invariant spectrum and the large non-Gaussianity [19].

Black hole: In ref. [25] we consider the question "what happens near a black hole?" A ghost condensate defines a hypersurface-orthogonal congruence of timelike curves, each of which has the tangent vector $u^\mu = -g^{\mu\nu}\partial_\nu\phi$. It is argued that the ghost condensate in this picture approximately corresponds to a congruence of geodesics and the accretion rate of the ghost condensate into a black hole should be negligible for a sufficiently large black hole. This argument is confirmed by a detailed calculation based on the perturbative expansion w.r.t. the higher spatial kinetic term. The essential reason for the smallness of the accretion rate is the same as that for the smallness of the tidal force acted on an extended object freely falling into a large black hole.

4 Bounds

In this section we consider the bounds on the symmetry breaking scale M. We argue that the nonlinear dynamics cuts off the Jeans instability of the linear theory, and allows $M \lesssim 100$ MeV [17].

4.1 Jeans Instability

For $M \gtrsim 10$ MeV, the Jeans instability time is shorter than the lifetime of the universe, and we must consider the effects of this instability. We have seen that the nonlinear effects dominate near interesting gravitational sources, but the linear dynamics still controls the behavior of the system for sufficiently weak ghostone amplitudes. In the linear regime, fluctuations with wavelength $\lambda \gtrsim L_{\rm J}$ grow on a time scale

$$\tau \sim T_{\rm J} \frac{\lambda}{L_{\rm J}}, \tag{6}$$

where

$$L_{\rm J} \sim \frac{M_{\rm Pl}}{M^2}, \qquad T_{\rm J} \sim \frac{M_{\rm Pl}^2}{M^3} \tag{7}$$

are the Jeans length and time scales. Wavelengths of order $L_{\rm J}$ become unstable first, and longer wavelengths take longer to grow. Since fluctuations on wavelength shorter than $L_{\rm J}$ are stable, we expect the minimum size of a positive or negative energy region to be $L_{\rm J}$. On the other hand, the maximum size is determined by requiring that the time scale τ above be shorter than the Hubble time. Hence, a positive or negative region can grow within the age of the universe if its size L is in the range

$$L_{\rm J} \lesssim L \lesssim L_{\rm max}, \tag{8}$$

where

$$L_{\rm max} \sim \frac{M}{M_{\rm Pl} H_0} \sim R_\odot \left(\frac{M}{100 \text{ GeV}} \right). \tag{9}$$

The unstable modes grow at least until nonlinear effects become important. This happens for $\pi \gtrsim \pi_{\rm c}$, where

$$\pi_{\rm c} \sim \frac{\lambda^2}{\tau}. \tag{10}$$

or equivalently $\Sigma \gtrsim \Sigma_{\rm c}$ with

$$\Sigma_{\rm c} \sim \frac{\pi_{\rm c}}{\tau} \sim \frac{\lambda^2}{\tau^2} \sim \frac{M^2}{M_{\rm Pl}^2}. \tag{11}$$

It is reasonable to assume that the nonlinear effects cut off the Jeans instability at this critical amplitude. This mechanism will fill the universe with regions of positive and negative ghostone field with amplitude of order $\pm\Sigma_{\rm c}$ and the size in the range (8). Since Σ is a conserved charge, there will be equal amounts of positive and negative Σ.

The sun's Newtonian potential triggers the Jeans instability of the ghost condensate and, thus, it is expected that there be a positive or negative region around the sun. This is justified if the 'aether' is efficiently dragged by the sun and we now argue that this is indeed the case. To do this, it is useful to work in the rest frame of the sun. Far from the sun, the aether is moving with constant velocity $v \sim 10^{-3}$, but near the sun the velocity field will be distorted by the presence of the sun. By using the fluid picture of the ghostone field, we estimate the effect on a fluid particle with speed v and impact parameter r. The fluid particle will be a distance of order r away for a time $\Delta t \sim r/v$, so the change in the particle velocity in the impulse approximation is

$$\Delta v \sim \frac{R_{\rm S}}{r^2} \cdot \frac{r}{v} \sim \frac{R_{\rm S}}{vr}, \tag{12}$$

where $R_{\rm S}$ is the Schwarzschild radius of the source. Thus, the change in the velocity of a fluid particle becomes comparable to or greater than the initial velocity if $r < r_{\rm drag}$, where

$$r_{\rm drag} \sim \frac{R_{\rm S}}{v^2}, \tag{13}$$

For our sun, $r_{\rm drag} \sim 10 R_\odot$, so the dragged region extends *outside* the solar radius.[4]

We require that the absolute value of the mass of the lump with the critical density ρ_c and the size $L_{\rm max}$ be at worst less than the solar mass:

$$\rho_c L_{\rm max}^3 \lesssim M_\odot. \tag{14}$$

This requirement gives the bound

$$M \lesssim 10^3 \text{ GeV}. \tag{15}$$

Since the high power of M (the l.h.s. $\propto M^9$) is involved in (14), a more stringent requirement on the mass of the lump will not substantially improve the bound.

4.2 Twinkling from Lensing

We have argued that if $M \gtrsim 10$ MeV, then the Jeans instability fills the universe with regions of positive and negative energy of size $L \gtrsim L_{\rm J} \sim M_{\rm Pl}/M^2$ with energy density $\rho_{\rm c} \sim M^6/M_{\rm Pl}^2$. This will happen everywhere, in particular in the voids between galaxies. Any light that travels to us from far away will therefore be lensed by these positive and negative regions. These positive and negative energy regions move, because the local rest frame of the lensing regions is different from that of our galaxy, so the result is that the observed luminosity of any point source will change with time. This is similar to the twinkling of the stars in the night sky caused by time dependent temperature differences in the atmosphere. In this subsection, we work out the bounds on the ghost condensate from this effect.

Suppose that the universe is filled with regions of positive and negative energy with size L and density $\rho_{\rm c}$. A light ray traveling through such a region will lens by an angle

$$\Delta\theta \sim \Phi \sim \frac{\rho_{\rm c} L^2}{M_{\rm Pl}^2} \sim \frac{M^6 L^2}{M_{\rm Pl}^4}. \tag{16}$$

If a light ray travels a distance $d \gg L$, then it will undergo $N \sim d/L$ uncorrelated lensing events, so the total angular deviation will be enhanced by a $N^{1/2}$ random walk factor:

$$\Delta\theta_{\rm tot} \sim \left(\frac{d}{L}\right)^{1/2} \frac{M^6 L^2}{M_{\rm Pl}^4}. \tag{17}$$

We see that the largest angular deviation comes from the largest L and largest d.

The size of L is limited by the time for the Jeans instability to form as in (8). If the source is the cosmic microwave background, then $d \sim H_0^{-1}$ and we obtain

$$\Delta\theta_{\rm CMB} \sim \frac{M^{15/2}}{M_{\rm Pl}^{11/2} H_0^2} \sim \left(\frac{M}{100 \text{ GeV}}\right)^{15/2}, \tag{18}$$

for the largest regions with the size $L \sim L_{max}$. The high power of M makes the precise experimental limit on $\Delta\theta_{\rm CMB}$ irrelevant, and we obtain the bound

$$M \lesssim 100 \text{ GeV}. \tag{19}$$

For $M \sim 100$ GeV, the size of the largest critical region is $L \sim 10^{12}$ cm, approximately the radius of the sun. The local velocity of these regions relative to our galaxy is of order 10^{-3}, so the time scale for one of these regions to cross the line of sight is of order a day, which is therefore the time scale of the variation.

If there is a distant astrophysical source that is observed to shine with very little time variation, it may give a competitive bound. But given the high power of M involved, it seems difficult to improve on this bound significantly.

[4]This radius is still much less than the orbital radius of Mercury.

4.3 Supernova time-delay

Gravitational lensing considered in the previous subsection induces a time-delay for light-rays coming from far distances. With this time-delay effect, observed supernovae should be older than they appear. Thus, this effect would change the estimate of dark energy by observation of Type Ia supernovae. Since the determination of the dark energy by supernovae observation is known to be consistent with the WMAP data, we require that the time-delay is sufficiently shorter than the total time:

$$\frac{\Delta t}{t} \sim (\Delta\theta)^2 \sim \frac{M^6 L_{\rm max}^2}{M_{\rm Pl}^4} \leq 1. \tag{20}$$

Note that the precise experimental limit on the $\Delta t/t$ is irrelevant because of the higher power of M involved in the l.h.s. From this we obtain the bound

$$M \lesssim 10^3 \text{ GeV}. \tag{21}$$

5 Summary

The usual Higgs mechanism gives a mass to a gauge boson in a theoretically controllable way by spontaneously breaking the gauge symmetry. Similarly, the ghost condensation gives a "mass" to the scalar-sector of gravity by spontaneously breaking a part of Lorentz symmetry, the invariance under time re-parameterization. It has been shown that the structure of low energy effective field theory of ghost condensation is determined by the symmetry breaking pattern and does not depend at all on the way the symmetry is broken. In this sense the low energy effective field theory of ghost condensation has nothing to do with ghost.

The theory of ghost condensation opens up a number of new avenues for attacking cosmological problems, including inflation, dark matter, dark energy and black holes. Finally, it has been argued that the theory is compatible with all current experimental observations if the scale of spontaneous Lorentz breaking is lower than ~ 100 MeV. Our current understanding of the dynamics of gravity in Higgs phase is very immature. Most of its properties still remain unexplored.

References

[1] C. M. Will, "Theory and experiment in gravitational physics," Cambridge, UK: Univ. Pr. (1993) 380 p.

[2] J. M. Cline, S. Jeon and G. D. Moore, "The phantom menaced: Constraints on low-energy effective ghosts," Phys. Rev. D **70**, 043543 (2004) [arXiv:hep-ph/0311312].

[3] A. De Felice, M. Hindmarsh and M. Trodden, "Ghosts, instabilities, and superluminal propagation in modified gravity models," JCAP **0608**, 005 (2006) [arXiv:astro-ph/0604154].

[4] G. Calcagni, B. de Carlos and A. De Felice, "Ghost conditions for Gauss-Bonnet cosmologies," Nucl. Phys. B **752**, 404 (2006) [arXiv:hep-th/0604201].

[5] M. Fierz and W. Pauli, "On relativistic wave equations for particles of arbitrary spin in an electromagnetic field," Proc. Roy. Soc. Lond. A **173**, 211 (1939).

[6] G. R. Dvali, G. Gabadadze and M. Porrati, "4D gravity on a brane in 5D Minkowski space," Phys. Lett. B **485**, 208 (2000) [arXiv:hep-th/0005016].

[7] N. Arkani-Hamed, H. Georgi and M. D. Schwartz, "Effective field theory for massive gravitons and gravity in theory space," Annals Phys. **305**, 96 (2003) [arXiv:hep-th/0210184].

[8] M. A. Luty, M. Porrati and R. Rattazzi, "Strong interactions and stability in the DGP model," JHEP **0309**, 029 (2003) [arXiv:hep-th/0303116].

[9] N. Arkani-Hamed, H. C. Cheng, M. A. Luty and S. Mukohyama, "Ghost condensation and a consistent infrared modification of gravity," JHEP **0405**, 074 (2004) [arXiv:hep-th/0312099].

[10] V. A. Rubakov, "Lorentz-violating graviton masses: Getting around ghosts, low strong coupling scale and VDVZ discontinuity," arXiv:hep-th/0407104.

[11] S. L. Dubovsky, "Phases of massive gravity," JHEP **0410**, 076 (2004) [arXiv:hep-th/0409124].

[12] B. Holdom, "Accelerated expansion and the Goldstone ghost," JHEP **0407**, 063 (2004) [arXiv:hep-th/0404109].

[13] R. Bluhm and V. A. Kostelecky, "Spontaneous Lorentz violation, Nambu-Goldstone modes, and gravity," Phys. Rev. D **71**, 065008 (2005) [arXiv:hep-th/0412320].

[14] R. Bluhm, "Nambu-Goldstone modes in gravitational theories with spontaneous Lorentz breaking," arXiv:hep-th/0607127.

[15] I. Kirsch, "A Higgs mechanism for gravity," Phys. Rev. D **72**, 024001 (2005) [arXiv:hep-th/0503024].

[16] H. C. Cheng, M. A. Luty, S. Mukohyama and J. Thaler, "Spontaneous Lorentz breaking at high energies," JHEP **0605**, 076 (2006) [arXiv:hep-th/0603010].

[17] N. Arkani-Hamed, H. C. Cheng, M. A. Luty, S. Mukohyama and T. Wiseman, "Dynamics of gravity in a Higgs phase," JHEP **0701**, 036 (2007) [arXiv:hep-ph/0507120].

[18] N. Arkani-Hamed, H. C. Cheng, M. Luty and J. Thaler, "Universal dynamics of spontaneous Lorentz violation and a new spin-dependent inverse-square law force," JHEP **0507**, 029 (2005) [arXiv:hep-ph/0407034].

[19] N. Arkani-Hamed, P. Creminelli, S. Mukohyama and M. Zaldarriaga, "Ghost Inflation," JCAP **0404**, 001 (2004) [arXiv:hep-th/0312100].

[20] L. Senatore, "Tilted ghost inflation," Phys. Rev. D **71**, 043512 (2005) [arXiv:astro-ph/0406187].

[21] S. L. Dubovsky, "Star tracks in the ghost condensate," JCAP **0407**, 009 (2004) [arXiv:hep-ph/0403308].

[22] M. Peloso and L. Sorbo, "Moving sources in a ghost condensate," Phys. Lett. B **593**, 25 (2004) [arXiv:hep-th/0404005].

[23] D. Krotov, C. Rebbi, V. A. Rubakov and V. Zakharov, "Holes in the ghost condensate," Phys. Rev. D **71**, 045014 (2005) [arXiv:hep-ph/0407081].

[24] A. V. Frolov, "Accretion of ghost condensate by black holes," Phys. Rev. D **70**, 061501 (2004) [arXiv:hep-th/0404216].

[25] S. Mukohyama, "Black holes in the ghost condensate," Phys. Rev. D **71**, 104019 (2005) [arXiv:hep-th/0502189].

[26] S. L. Dubovsky and S. M. Sibiryakov, "Spontaneous breaking of Lorentz invariance, black holes and perpetuum mobile of the 2nd kind," Phys. Lett. B **638**, 509 (2006) [arXiv:hep-th/0603158].

[27] V. V. Kiselev, "Ghost condensate model of flat rotation curves," arXiv:gr-qc/0406086.

[28] V. V. Kiselev, "Ghost condensate model of flat rotation curves," arXiv:gr-qc/0507126.

[29] V. V. Kiselev and D. I. Yudin, "Gravitational lensing due to dark matter modelled by vector field," Class. Quant. Grav. **23**, 7417 (2006) [arXiv:gr-qc/0603128].

[30] F. Piazza and S. Tsujikawa, "Dilatonic ghost condensate as dark energy," JCAP **0407**, 004 (2004) [arXiv:hep-th/0405054].

[31] A. Krause and S. P. Ng, "Ghost cosmology: Exact solutions, transitions between standard cosmologies and ghost dark energy / matter evolution," Int. J. Mod. Phys. A **21**, 1091 (2006) [arXiv:hep-th/0409241].

[32] C. de Rham and A. J. Tolley, JCAP **0607**, 004 (2006) [arXiv:hep-th/0605122].

[33] P. Creminelli, M. A. Luty, A. Nicolis and L. Senatore, "Starting the universe: Stable violation of the null energy condition and non-standard cosmologies," JHEP **0612**, 080 (2006) [arXiv:hep-th/0606090].

[34] S. Mukohyama, "Accelerating universe and cosmological perturbation in the ghost condensate," JCAP **0610**, 011 (2006) [arXiv:hep-th/0607181].

[35] A. Anisimov and A. Vikman, "A comment on the classical stability of the ghost condensate," JCAP **0504**, 009 (2005) [arXiv:hep-ph/0411089].

[36] R. B. Mann and J. J. Oh, "Ghost condensation in the brane-world," arXiv:hep-th/0504172.

[37] M. L. Graesser, I. Low and M. B. Wise, "Towards a high energy theory for the Higgs phase of gravity," Phys. Rev. D **72**, 115016 (2005) [arXiv:hep-th/0509180].

[38] D. O'Connell, "Regulator dependence of the proposed UV completion of the ghost condensate," Phys. Lett. B **643**, 379 (2006) [arXiv:hep-th/0602240].

[39] S. Mukohyama, "Towards a Higgs phase of gravity in string theory," JHEP **0705**, 048 (2007) [arXiv:hep-th/0610254].

A new gravitational wave background from the Big Bang

Juan García-Bellido[1] and Daniel G. Figueroa[2]

Instituto de Física Teórica CSIC-UAM,
Universidad Autónoma de Madrid,
Cantoblanco 28049 Madrid, Spain

Abstract

The reheating of the universe after hybrid inflation proceeds through the nucleation and subsequent collision of large concentrations of energy density in the form of bubble-like structures moving at relativistic speeds. This generates a significant fraction of energy in the form of a stochastic background of gravitational waves, whose time evolution is determined by the successive stages of reheating: First, tachyonic preheating makes the amplitude of gravity waves grow exponentially fast. Second, bubble collisions add a new burst of gravitational radiation. Third, turbulent motions finally sets the end of gravitational waves production. From then on, these waves propagate unimpeded to us. We find that the fraction of energy density today in these primordial gravitational waves could be significant for GUT-scale models of inflation, although well beyond the frequency range sensitivity of gravitational wave observatories like LIGO, LISA or BBO. However, low-scale models could still produce a detectable signal at frequencies accessible to BBO or DECIGO. For comparison, we have also computed the analogous background from some chaotic inflation models and obtained similar results to those of other groups. The discovery of such a background would open a new observational window into the very early universe, where the details of the process of reheating, i.e. the Big Bang, could be explored. Thus, it could also serve as a new experimental tool for testing the Inflationary Paradigm.

1 Introduction

Gravitational waves (GW) are ripples in space-time that travel at the speed of light, and whose emission by relativistic bodies represents a robust prediction of General Relativity. Theoretically, it is expected that the present universe should be permeated by a diffuse background of GW of either an astrophysical or cosmological origin [1]. Fortunately, these backgrounds have very different spectral signatures that might, in the future, allow gravitational wave observatories like LIGO [2], LISA [3], BBO [4] or DECIGO [5], to disentangle their origin [1]. Unfortunately, the weakness of gravity will make this task extremely difficult, requiring a very high accuracy in order to distinguish one background from another.

There are, indeed, a series of constraints on some of these backgrounds, coming from the anisotropies in the Cosmic Microwave Background (CMB) [6], from Big Bang nucleosynthesis [7] or from millisecond pulsar timing [8]. Most of these constraints come at very low frequencies, from 10^{-18} Hz to 10^{-8} Hz, while present and future GW detectors (will) work at frequencies of order $10^{-3} - 10^{3}$ Hz. If early universe first order phase transitions [9, 10] or cosmic turbulence [11] occurred around the electro-weak (EW) scale, GW detectors could have a chance to measure the corresponding associated backgrounds. However, if those processes occurred at the GUT scale, their corresponding backgrounds will go undetected by the actual detectors, since these cannot reach the required sensitivity in the high frequency range of $10^{7} - 10^{9}$ Hz. There are however recent proposals to cover this range [12, 13], which may become competitive in the not so far future.

Cosmological observations seem to suggest that something like Inflation must have occurred in the very early universe. Approximately scale-invariant density perturbations, sourced by quantum fluctuations during inflation, seem to be the most satisfying explanation for the CMB anisotropies. Together with such scalar perturbations one also expects tensor perturbations (GW) to be produced, with an almost

[1]E-mail: juan.garciabellido@uam.es
[2]E-mail: daniel.figueroa@uam.es

scale-free power spectrum [14]. The detection of such a background is crucial for early universe cosmology because it would help to determine the absolute energy scale of inflation, a quantity that for the moment is still uncertain, and would open the exploration of physics at very high energies.

However, in the early universe, after inflation, other GWB could have been produced at shorter wavelengths, in a more 'classical' manner rather than sourced by quantum fluctuations. In particular, whenever there are large and fast moving inhomogeneities in a matter distribution, one expects the emission of GW. At large distances from a source, the amplitude of the GW is given by $h_{ij} \simeq G\ddot{Q}_{ij}/c^4 r$, with Q_{ij} the quadrupole moment of the mass distribution. The larger the velocity of the matter distribution, the larger the amplitude of the radiation produced. However, because of the weakness of gravity, in order to produce a significant amount of gravitational radiation, it is required a very relativistic motion (and high density contrasts) in the matter distribution of a source. Fortunatelly, this is indeed believed to be the situation at the end of inflaton, during the conversion of the huge energy density driving inflation into radiation and matter, at the so-called *reheating* of the Universe [15], i.e. at the Big Bang.

Note that any background of GW coming from the early universe, if generated below Planck scale, immediately decoupled upon production and, whatever their spectral signatures, they will retain their shape throughout the expansion of the Universe. Thus, the characteristic frequency and shape of the GWB generated at a given time should contain information about the very early state of the Universe in which it was produced. Actually, it is conceivable that, in the not so far future, the detection of these GW backgrounds could be the only way we may have to infer the physical conditions of the Universe at such high energy scales. However, the same reason that makes GW ideal probes of the early universe $-$ the weakness of gravity $-$ is responsible for the extreme difficulties we have for their detection on Earth.

In Refs. [16, 17] we described the stochastic background predicted to arise from reheating after hybrid inflation. Here we will review the various processes involved in the production of such a background. In the future, this background could serve as a new tool to discriminate among different inflationary models, since reheating in each model would give rise to a different GWB with very characteristic spectral features. The details of the dynamics of preheating depend very much on the model and are often very complicated because of the non-linear, non-perturbative and out-of-equilibrium character of the process itself. However, all the cases have in common that only specific resonance bands of the fields suffer an exponential instability, which makes their occupation numbers grow by many orders of magnitude. The shape and size of the spectral bands depend very much on the inflationary model. If one translates this picture into position-space, the highly populated modes correspond to large time-dependent inhomogeneities in the matter distributions which acts, in fact, as a powerful source of GW. For example, in single field chaotic inflation models, the coherent oscillations of the inflaton during preheating generates, via parametric resonance, a population of highly occupied modes that behave like waves of matter. They collide among themselves and their scattering leads to homogenization and local thermal equilibrium. These collisions occur in a highly relativistic and very asymmetric way, being responsible for the generation of a stochastic GWB [18, 19, 20, 21, 22] with a typical frequency today of the order of $10^7 - 10^9$ Hz, corresponding to the present size of the causal horizon at the end of high-scale inflation.

However, there are models like hybrid inflation in which the end of inflation is sudden [23] and the conversion into radiation occurs almost instantaneously. Indeed, hybrid models preheat very violently, via the spinodal instability of the symmetry breaking field that triggers the end of inflation, irrespective of the couplings that this field may have to the rest of matter. Such a process is known as *tachyonic preheating* [24, 25] and could be responsible for copious production of dark matter particles [26], lepto and baryogenesis [27], topological defects [24], primordial magnetic fields [28], etc. In Ref. [25], it was shown that the process of symmetry breaking in hybrid preheating, proceeds via the nucleation of dense bubble-like structures moving at relativistic speeds, which collide and break up into smaller structures (see Figs. 7 and 8 of Ref. [25]). We conjectured at that time that such collisions would be a very strong source of GW, analogous to the GW production associated with strongly first order phase transitions [9]. As we will show here, this is indeed the case during the nucleation, collision and subsequent rescattering of the initial bubble-like structures produced after hybrid inflation. During the different stages of reheating in this model, gravity waves are generated and amplified until the Universe finally thermalizes and enters into the radiation era of the Standard Model of Cosmology. From that moment until now, this cosmic GWB will be redshifted as a radiation-like fluid, totally decoupled from any other energy-matter content of the universe, such that today's ratio of energy stored in these GW to that in radiation, could range from $\Omega_{\rm GW} h^2 \sim 10^{-8}$, peaked around $f \sim 10^7$ Hz for the high-scale models, to $\Omega_{\rm GW} h^2 \sim 10^{-11}$, peaked around $f \sim 1$ Hz for the low-scale models.

Finally, since the first paper by Khlebnikov and Tkachev [18], studing the GWB produced at reheating after chaotic inflation, there has been some developments. The idea was soon extended to hybrid inflation in Ref. [19]. It was also revisited very recently in Ref. [20, 21] for the $\lambda\phi^4$ and $m^2\phi^2$ chaotic scenarios, and reanalysed again for hybrid inflation in Refs. [16, 17], using the new formalism of tachyonic preheating [24, 25]. Because of the increase in computer power of the last few years, we are now able to perform precise simulations of the reheating process in a reasonable time scale. Moreover, understanding of reheating has improved, while gravitational waves detectors are beginning to attain the aimed sensitivity [2]. Furthermore, since these cosmic GWBs could serve as a deep probe into the very early universe, we should characterize in the most detailed way the information that we will be able to extract from them.

2 Gravitational Wave Production

Our main purpose here is to study the details of the stochastic GWB produced during the reheating stage after hybrid inflation (sections 2 and 3). Nevertheless, we also study more briefly the analogous background from reheating in some chaotic models (section 4). Thus, in this section we derive a general formalism for extracting the GW power spectrum in any scenario of reheating within the (flat) Friedman-Robertson-Walker (FRW) universe. The formalism will be simplified when applied to scenarios in which we can neglect the expansion of the universe, like in the case of Hybrid models.

A theory with an inflaton scalar field χ interacting with other Bose fields ϕ_a, can be described by

$$\mathcal{L} = \frac{1}{2}\partial_\mu\chi\partial^\mu\chi + \frac{1}{2}\partial_\mu\phi_a\partial^\mu\phi_a + \frac{R}{16\pi G} - V(\phi,\chi) \tag{1}$$

with R the Ricci scalar. For hybrid models, we consider a generic symmetry breaking 'Higgs' field Φ, with N_c real components. We can take $\Phi^\dagger\Phi = \frac{1}{2}\sum_a \phi_a^2 \equiv |\phi|^2/2$, with a running for the number of Higgs' components, *e.g.* $N_c = 1$ for a real scalar Higgs, $N_c = 2$ for a complex scalar Higgs or $N_c = 4$ for a $SU(2)$ Higgs, etc. The effective potential then becomes

$$V(\phi,\chi) = \frac{\lambda}{4}\left(|\phi|^2 - v^2\right)^2 + g^2\chi^2|\phi|^2 + \frac{1}{2}\mu^2\chi^2\,. \tag{2}$$

For chaotic scenarios, we consider a massless scalar field ϕ interacting with the inflaton χ via

$$V(\chi,\phi) = \frac{1}{2}g^2\chi^2\phi^2 + V(\chi)\,, \tag{3}$$

with $V(\chi)$ the inflaton's potential. Concerning the simulations we show in this paper, we concentrate in the $N_c = 4$ case for the hybrid model and consider a potential $V(\chi) = \frac{\lambda}{4}\chi^4$ for the chaotic scenario.

The classical equations of motion of the inflaton and the other Bose fields are

$$\ddot\chi + 3H\dot\chi - \frac{1}{a^2}\nabla^2\chi + \frac{\partial V}{\partial\chi} = 0\,, \qquad \ddot\phi_a + 3H\dot\phi_a - \frac{1}{a^2}\nabla^2\phi_a + \frac{\partial V}{\partial\phi_a} = 0 \tag{4}$$

with $H = \dot a/a$. On the other hand, GW are represented here by a transverse-traceless (TT) gauge-invariant metric perturbation, h_{ij}, on top of the flat FRW space $ds^2 = -dt^2 + a^2(t)\left(\delta_{ij} + h_{ij}\right)dx^i dx^j$, with $a(t)$ the scale factor and the tensor perturbations verifying $\partial_i h_{ij} = h_{ii} = 0$. Then, the Einstein field equations can be splitted into the background and the perturbed equations. The former describe the evolution of the flat FRW universe through

$$-\frac{\dot H}{4\pi G} = \dot\chi^2 + \frac{1}{3a^2}(\nabla\chi)^2 + \dot\phi_a^2 + \frac{1}{3a^2}(\nabla\phi_a)^2 \tag{5}$$

$$\frac{3H^2}{4\pi G} = \dot\chi^2 + \frac{1}{a^2}(\nabla\chi)^2 + \dot\phi_a^2 + \frac{1}{a^2}(\nabla\phi_a)^2 + 2V(\chi,\phi) \tag{6}$$

where any term in the r.h.s. of (5) and (6), should be understood as spatially averaged.

On the other hand, the perturbed Einstein equations describe the evolution of the tensor perturbations [35] as

$$\ddot{h}_{ij} + 3H\dot{h}_{ij} - \frac{1}{a^2}\nabla^2 h_{ij} = 16\pi G\,\Pi_{ij}\,, \tag{7}$$

with $\partial_i \Pi_{ij} = \Pi_{ii} = 0$. The source of the GW, Π_{ij}, contributed by both the inflaton and the other scalar fields, will be just the transverse-traceless part of the (spatial-spatial) components of the total anisotropic stress-tensor

$$\mathrm{T}_{\mu\nu} = \left[\partial_\mu\chi\partial_\nu\chi + \partial_\mu\phi_a\partial_\nu\phi_a + g_{\mu\nu}(\mathcal{L} - \langle p\rangle)\right]/a^2, \tag{8}$$

where $\mathcal{L}(\chi, \phi_a)$ is the lagrangian (1) and $\langle p\rangle$ is the background homogeneous pressure. As we will explain in the next subsection, when extracting the TT part of (8), the term proportional to $g_{\mu\nu}$ in the r.h.s of (8), will be dropped out from the GW equations of motion. Thus, the effective source of the GW will be just given by the TT part of the gradient terms $\partial_\mu\chi\partial_\nu\chi + \partial_\mu\phi_a\partial_\nu\phi_a$.

2.1 The Transverse-Traceless Gauge

A generic (spatial-spatial) metric perturbation δh_{ij} has six independent degrees of freedom, whose contributions can be split into [35] scalar, vector and tensor metric perturbations $\delta h_{ij} = \psi\,\delta_{ij} + E_{,ij} + F_{(i,j)} + h_{ij}$, with $\partial_i F_i = 0$ and $\partial_i h_{ij} = h_{ii} = 0$. By choosing a transverse-traceless stress-tensor source Π_{ij}, we can eliminate all the degrees of freedom (d.o.f.) but the pure TT part, h_{ij}, which represent the only physical d.o.f which propagate and carry energy out of the source (i.e. GW). Thus, taking the TT part of the anisotropic stress-tensor, we ensure that we only source the physical d.o.f. that represent GW.

Let us switch to Fourier space. The GW equations (7) then read

$$\ddot{h}_{ij}(t,\mathbf{k}) + 3H\dot{h}_{ij}(t,\mathbf{k}) + \frac{k^2}{a^2}h_{ij}(t,\mathbf{k}) = 16\pi G\,\Pi_{ij}(t,\mathbf{k})\,, \tag{9}$$

where $k = |\mathbf{k}|$. Assuming no GW at the beginnig of reheating (i.e. the end of inflation t_e), the initial conditions are $h_{ij}(t_e) = \dot{h}_{ij}(t_e) = 0$, so the solution to Eq. (9) for $t > t_e$ will be just given by a causal convolution with an appropriate Green's function $G(t, t')$,

$$h_{ij}(t,\mathbf{k}) = 16\pi G\int_{t_e}^{t} dt'\, G(t,t')\Pi_{ij}(t',\mathbf{k})\,. \tag{10}$$

Therefore, all we need to know for computing the GW is the TT part of the stress-tensor, Π_{ij}, and the Green's function $G(t', t)$. However, as we will demonstrate shortly, we have used a numerical method by which we don't even need to know the actual form of $G(t', t)$. To see this, let us extract the TT part of the total stress-tensor. Given the symmetric anisotropic stress-tensor $\mathrm{T}_{\mu\nu}$ (8), we can easily obtain the TT part of its spatial components in momentum space, $\Pi_{ij}(\mathbf{k})$. Using the spatial projection operators $P_{ij} = \delta_{ij} - \hat{k}_i\hat{k}_j$, with $\hat{k}_i = k_i/k$, then [36] $\Pi_{ij}(\mathbf{k}) = \Lambda_{ij,lm}(\hat{\mathbf{k}})\mathrm{T}_{lm}(\mathbf{k})$, where

$$\Lambda_{ij,lm}(\hat{\mathbf{k}}) \equiv \Big(P_{il}(\hat{\mathbf{k}})P_{jm}(\hat{\mathbf{k}}) - \frac{1}{2}P_{ij}(\hat{\mathbf{k}})P_{lm}(\hat{\mathbf{k}})\Big)\,. \tag{11}$$

Thus, one can easily see that, at any time t, $k_i\Pi_{ij}(\hat{\mathbf{k}}, t) = \Pi^i_i(\hat{\mathbf{k}}, t) = 0$, as required, thanks to the identities $P_{ij}\hat{k}_j = 0$ and $P_{ij}P_{jm} = P_{im}$.

Note that the solution (10) is just linear of the non-traceless nor-transverse tensor T_{ij} (8). Therefore, we can write the TT tensor perturbations (i.e. the GW) as

$$h_{ij}(t,\mathbf{k}) = \Lambda_{ij,lm}(\hat{\mathbf{k}})u_{lm}(t,\mathbf{k}), \tag{12}$$

with $u_{ij}(t,\mathbf{k})$ the Fourier transform of the solution of the following equation

$$\ddot{u}_{ij} + 3H\dot{u}_{ij} - \frac{1}{a^2}\nabla^2 u_{ij} = 16\pi G\,\mathrm{T}_{ij}\,. \tag{13}$$

This Eq. (13) is nothing but Eq. (7), sourced with the complete T_{ij} (8), instead of with its TT part, Π_{ij}. Of course, Eq. (13) contains unphysical (gauge) d.o.f.; however, in order to obtain the real physical

TT d.o.f. h_{ij}, we can evolve Eq.(13) in configuration space, Fourier transform its solution and apply the projector (11) as in (12). This way we can obtain in momentum space, at any moment of the evolution, the physical TT d.o.f. that represent GW, h_{ij}. Whenever needed, we can Fourier transform back to configuration space and obtain the spatial distribution of the gravitational waves.

Moreover, since the second term of the r.h.s of the total stress-tensor T_{ij} is proportional to $g_{ij} = \delta_{ij} + h_{ij}$, see (8), when aplying the TT projector (11), the part with the δ_{ij} just drops out, simply because it is a pure trace, while the other part contributes with a term $-(\mathcal{L} - \langle p \rangle)h_{ij}$ in the l.h.s of Eq.(9). However, $(\mathcal{L} - \langle p \rangle)$ is of the same order as the metric perturbation $\sim \mathcal{O}(h)$, so this extra term is second order in the gravitational coupling and it can be neglected in the GW Eqs. (9). This way, the effective source in Eq. (13) is just the gradient terms of both the inflaton and the other scalar fields,

$$\mathrm{T}_{ij} = (\nabla_i \chi \nabla_j \chi + \nabla_i \phi_a \nabla_j \phi_a)/a^2. \tag{14}$$

Therefore, the effective source of the physical GW, will be just the TT part of (14), as we had already mentioned before.

We have found the *commuting procedure* proposed (i.e. the fact that we first solve Eq. (13) and secondly we apply the TT projector to the solution (12), and not the other way around), very useful. We are able to extract the spectra or the spatial distribution of the GW at any desired time, saving a great amount of computing time since we don't have to be Fourier transforming the source at each time step. Most importantly, with this procedure we can take into account backreaction simultaneously with the fields evolution.

In summary, for solving the dynamics of reheating of a particular inflationary model, we evolve Eqs. (4) in the lattice, together with Eqs. (5)-(6), while for the GWs we solve Eq. (13). Then, only when required, we Fourier transform the solution of Eq. (13) and then apply (12) in order to recover the physical transverse-traceless d.o.f representing the GW. From there, one can easily build the GW spectra or take a snapshot of spatial distribution of the gravitational waves.

2.2 The energy density in GW

The energy-momentum tensor of the GW is given by [36]

$$t_{\mu\nu} = \frac{1}{32\pi G} \left\langle \partial_\mu h_{ij} \, \partial_\nu h^{ij} \right\rangle_{\mathrm{V}} , \tag{15}$$

where h_{ij} are the TT tensor perturbations solution of Eq. (7). The expectation value $\langle ... \rangle_{\mathrm{V}}$ is taken over a region of sufficiently large volume $V = L^3$ to encompass enough physical curvature to have a gauge-invariant measure of the GW energy-momentum tensor.

The GW energy density will be just $\rho_{\mathrm{GW}} = t_{00}$, so

$$\rho_{\mathrm{GW}} = \frac{1}{32\pi G} \frac{1}{L^3} \int d^3\mathbf{x} \, \dot{h}_{ij}(t,\mathbf{x}) \dot{h}_{ij}(t,\mathbf{x}) = \frac{1}{32\pi G} \frac{1}{L^3} \int d^3\mathbf{k} \, \dot{h}_{ij}(t,\mathbf{k}) \dot{h}^*_{ij}(t,\mathbf{k}) \, , \tag{16}$$

where in the last step we Fourier transformed each $\dot{h}_{ij}$ and used the definition of the Dirac delta. We can always write the scalar product in (16) in terms of the (Fourier transformed) solution u_{lm} of the Eq.(13), by just using the fact that $\Lambda_{ij,lm}\Lambda_{lm,rs} = \Lambda_{ij,rs}$. This way, we can express the GW energy density as

$$\rho_{\mathrm{GW}} = \frac{1}{32\pi G L^3} \int k^2 dk \int d\Omega \, \Lambda_{ij,lm}(\hat{\mathbf{k}}) \dot{u}_{ij}(t,\mathbf{k}) \dot{u}^*_{lm}(t,\mathbf{k}). \tag{17}$$

From here, we can also compute the power spectrum per logarithmic frequency interval in GW, normalized to the critical density ρ_c, as $\Omega_{\mathrm{GW}} = \int \frac{df}{f} \, \Omega_{\mathrm{GW}}(f)$, where

$$\Omega_{\mathrm{GW}}(k) \equiv \frac{1}{\rho_c} \frac{d\rho_{\mathrm{GW}}}{d\log k} = \frac{k^3}{32\pi G L^3 \rho_c} \int d\Omega \, \Lambda_{ij,lm}(\hat{\mathbf{k}}) \dot{u}_{ij}(t,\mathbf{k}) \dot{u}^*_{lm}(t,\mathbf{k}) \tag{18}$$

We have checked explicitely in the simulations that the argument of the angular integral of (18) is independent of the directions in **k**-space. Thus, whenever we plot the GW spectrum of any model, we will be showing the amplitude of the spectrum (per each mode k) as obtained after avaraging over all the directions in momentum space,

$$\Omega_{\rm GW}(k) = \frac{k^3}{8GL^3\rho_c}\left\langle \Lambda_{ij,lm}(\hat{\mathbf{k}})\dot{u}_{ij}(t,\mathbf{k})\dot{u}^*_{lm}(t,\mathbf{k})\right\rangle_{4\pi} \tag{19}$$

with $\langle f\rangle_{4\pi} \equiv \frac{1}{4\pi}\int f\mathrm{d}\Omega$.

Finally, we must address the fact that the frequency range, for a GWB produced in the early universe, will be redshifted today. We should calculate the characteristic physical wavenumber of the present GW spectrum, which is redshifted from any time t during GW production. So let us distinguish four characteristic times: the end of inflation, t_e; the time t_* when GW production stops; the time t_r when the universe finally reheats and enters into the radiation era; and today, t_0. Thus, today's frequency f_0 is related to the physical wavenumber k_t at any time t of GW production, via $f_0 = (a_t/a_0)(k_t/2\pi)$, with a_0 and a_t, the scale factor today and at the time t, respectively. Thermal equilibrium was established at some temperature T_r, at time $t_r \geq t$. The Hubble rate at that time was $M_P^2H_r^2 = (8\pi/3)\rho_r$, with $\rho_r = g_r\pi^2T_r^4/30$ the relativistic energy density and g_r the effective number of relativistic degrees of freedom at temperature T_r. Since then, the scale factor has increased as $a_r/a_0 = (g_{0,s}/g_{r,s})^{1/3}(T_0/T_r)$, with $g_{i,s}$ the effective entropic degrees of freedom at time t_i, and T_0 today's CMB temperature. Putting all together,

$$f_0 = \left(\frac{8\pi^3 g_r}{90}\right)^{\frac{1}{4}}\left(\frac{g_{0,s}}{g_{r,s}}\right)^{\frac{1}{3}}\frac{T_0}{\sqrt{H_rM_p}}\left(\frac{a_e}{a_r}\right)\frac{k}{2\pi}\,, \tag{20}$$

where we have used the fact that the physical wave number k_t at any time t during GW production, is related to the comoving wavenumber k through $k_t = (a_e/a_t)k$ with the normalization $a_e \equiv 1$.

From now on, we will be concerned with hybrid inflation, leaving chaotic inflation for section 4. Within the hybrid scenario, we will analyse the dependence of the shape and amplitude of the produced GWB on the scale of hybrid inflation, and more specifically on the *v.e.v.* of the Higgs field triggering the end of inflation. Given the natural frequency at hand in hybrid models, $m = \sqrt{\lambda}v$, whose inverse m^{-1} sets the characteristic time scale during the first stages of reheating, it happens that as long as $v \ll M_p$, the Hubble rate $H \sim \sqrt{\lambda}(v^2/M_p)$ is much smaller than such a frequency, $H \ll m$. Indeed, all the initial vacuum energy ρ_0 gets typically converted into radiation in less than a Hubble time, in just a few m^{-1} time steps. Therefore, we should be able to ignore the dilution due to the expansion of the universe during the production of GW, at least during the first stages of reheating. Our approach will be to ignore the expansion of the Universe, such that we fix the scale factor to one, $a = 1$. As we will see later, neglecting the expansion of the Universe for the time of GW production, will be completely justified *a posteriori*.

The system of equations that we have to solve numerically in a lattice for the hybrid model are

$$\ddot{u}_{ij} - \nabla^2 u_{ij} = 16\pi G\,\mathrm{T}_{ij} \tag{21}$$

$$\ddot{\chi} - \nabla^2\chi + \left(g^2|\phi|^2 + \mu^2\right)\chi = 0 \tag{22}$$

$$\ddot{\phi}_a - \nabla^2\phi_a + \left(g^2\chi^2 + \lambda|\phi|^2 - m^2\right)\phi_a = 0 \tag{23}$$

with T_{ij} given by Eq.(14) with the scale factor $a = 1$. We have explicitly checked in our computer simulations that the backreaction of the gravity waves into the dynamics of both the inflaton and the Higgs fields is negligible and can be safely ignored. We thus omit the backreaction terms in the above equations.

We evaluated during the evolution of the system the mean field values, as well as the different energy components. Initially, the Higgs field grows towards the true vacuum and the inflaton moves towards the minimum of its potential and oscillates around it. We have checked that the sum of the averaged gradient, kinetic and potential energies (contributed by both the inflaton and the Higgs), remains constant during reheating, as expected, since the expansion of the universe is irrelevant in this model. We have also checked that the time evolution of the different energy components is the same for different lattices, changing the number of points N, the minimum momentum $p_{\rm min} = 2\pi/L$ or the lattice spacing $a = L/N$, with L the lattice size. The evolution of the Higgs' *v.e.v.* follows three stages easily distinguished. First, an exponential growth of the *v.e.v.* towards the true vacuum. This is driven by the tachyonic instability of the long-wave modes of the Higgs field, that makes the spatial distribution of this field to form lumps and

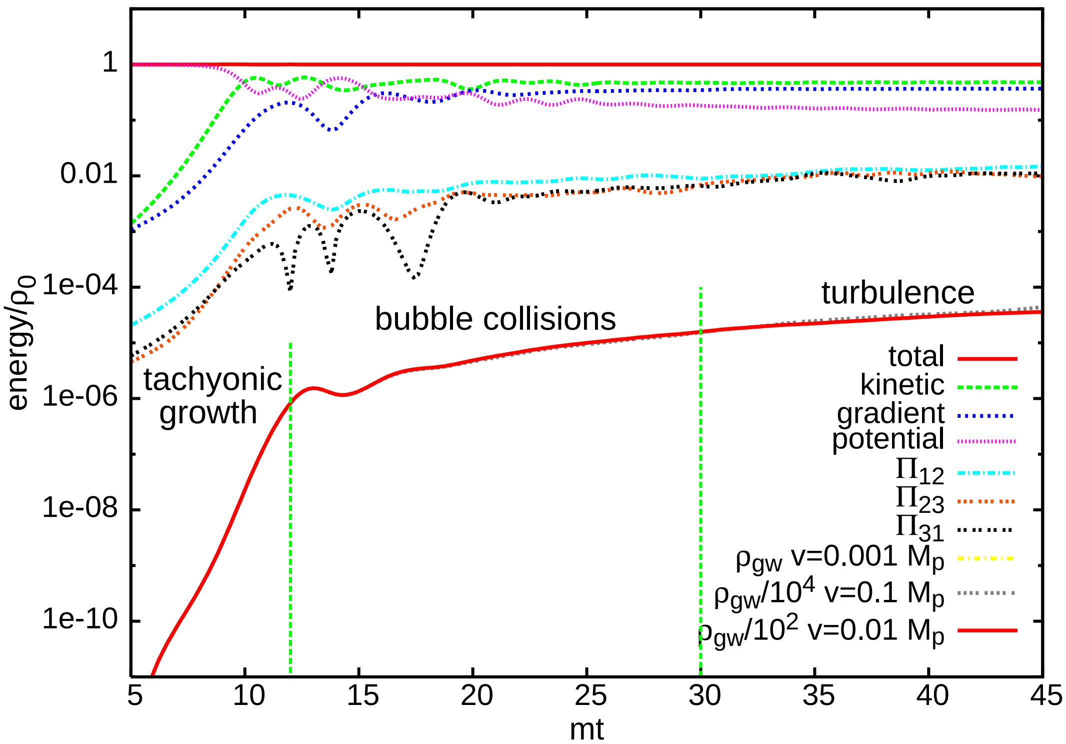

Figure 1: The time evolution of the different types of energy (kinetic, gradient, potential, anisotropic components and gravitational waves for different lattices), normalized to the initial vacuum energy, after hybrid inflation, for a model with $v = 10^{-3}\, M_P$. One can clearly distinguish here three stages: tachyonic growth, bubble collisions and turbulence.

bubble-like structures [24, 25]. Second, the Higgs field oscillates around the true vacuum, as the Higgs' bubbles collide and scatter off eachother. Third, a period of turbulence is reached, during which the inflaton oscillates around its minimum and the Higgs sits in the true vacuum. For a detailed description of the dynamics of these fields see Ref. [25]. Here we will be only concerned with the details of the gravitational wave production.

The initial energy density at the end of hybrid inflation is given by $\rho_0 = m^2 v^2/4$, with $m^2 = \lambda v^2$, so the fractional energy density in gravitational waves is

$$\frac{\rho_{\rm GW}}{\rho_0} = \frac{4 t_{00}}{v^2\, m^2} = \frac{1}{8\pi\, G v^2 m^2} \left\langle \dot h_{ij} \dot h^{ij} \right\rangle_{\rm V} , \tag{24}$$

where $\left\langle \dot h_{ij} \dot h^{ij} \right\rangle_{\rm V}$, defined as a volume average like $\frac{1}{\rm V} \int d^3{\bf x} \dot h_{ij} \dot h^{ij}$, is extracted from the simulations as

$$\left\langle \dot h_{ij} \dot h^{ij} \right\rangle_{\rm V} = \frac{4\pi}{V} \int d{\rm log}k\, k^3 \left\langle \Lambda_{ij,lm}(\hat{\bf k}) \dot u_{ij}(t,{\bf k}) \dot u^*_{lm}(t,{\bf k}) \right\rangle_{4\pi} \tag{25}$$

where $u_{ij}(t,{\bf k})$ is the Fourier transform of the solution of Eq. (21). Then, we can compute the corresponding density parameter today (with $\Omega_{\rm rad}\, h^2 \simeq 3.5 \times 10^{-5}$)

$$\Omega_{\rm GW}\, h^2 = \frac{\Omega_{\rm rad}\, h^2}{2G\, v^2\, m^2\, V} \int d{\rm log}k\, k^3 \left\langle \Lambda_{ij,lm}(\hat{\bf k}) \dot u_{ij}(t,{\bf k}) \dot u^*_{lm}(t,{\bf k}) \right\rangle_{4\pi} \tag{26}$$

which has assumed that all the vacuum energy ρ_0 gets converted into radiation, an approximation which is always valid in generic hybrid inflation models with $v \ll M_P$, and thus $H \ll m = \sqrt{\lambda}\, v$.

We have shown in Fig. 1 the evolution in time of the fraction of energy density in GW. The first (tachyonic) stage is clearly visible, with a (logarithmic) slope twice that of the anisotropic tensor Π_{ij}. Then there is a small plateau corresponding to the production of GW from bubble collisions; and finally

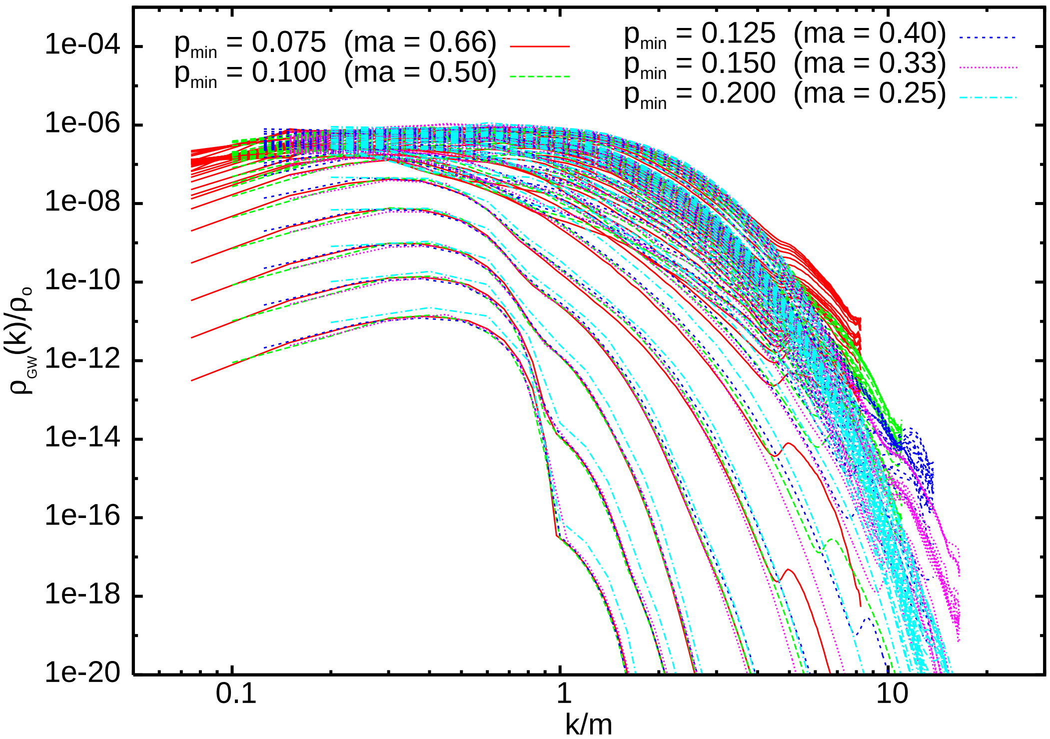

Figure 2: We show here the comparison between the power spectrum of gravitational waves obtained with increasing lattice resolution, to prove the robustness of our method. The different realizations are characterized by the the minimum lattice momentum ($\mathrm{p_{min}}$) and the lattice spacing (ma). The growth is shown in steps of $m\Delta t = 1$ up to $mt = 30$, and then in and $m\Delta t = 5$ steps up to $mt = 60$.

there is the slow growth due to turbulence. In the next section we will describe in detail the most significant features appearing at each stage.

Note that in the case that $H \ll m$, the maximal production of GW occurs in less than a Hubble time, soon after symmetry breaking, while turbulence lasts several decades in time units of m^{-1}. Therefore, we can safely ignore the dilution due to the Hubble expansion, up to times much greater than those of the tachyonic instability. Eventually the universe reheats and the energy in gravitational waves redshifts like radiation thereafter.

To compute the power spectrum per logarithmic frequency interval in GW, $\Omega_{\rm GW}(f)$, we just have to use (18). We can evaluate the power spectrum today from that obtained at reheating by converting the wavenumber k into frequency f. Simply using Eq. (20), with $g_{r,s}/g_{0,s} \sim 100$, $g_{r,s} \sim g_r$ and $a_e \sim a_*$, then

$$f = 6 \times 10^{10}\,\mathrm{Hz}\,\frac{k}{\sqrt{H\,M_p}} = 5 \times 10^{10}\,\mathrm{Hz}\,\frac{k}{m}\,\lambda^{1/4}\,. \tag{27}$$

We show in Fig. 2 the power spectrum of gravitational waves as a function of (comoving) wavenumber k/m. We have used different lattices in order to have lattice artifacts under control, specially at late times and high wavenumbers. We made sure by the choice of lattice size and spacing (i.e. $k_{\rm min}$ and $k_{\rm max}$) that all relevant scales fitted within the simulation. Note, however, that the lower bumps are lattice artifacts, due to the physical cutoff imposed at the initial condition, that rapidly disappear with time. We have also checked that the power spectrum of the scalar fields follows turbulent scaling after $mt \sim \mathcal{O}(100)$, and we can thus estimate the subsequent evolution of the energy density distributions beyond our simulations.

3 Lattice simulations

The problem of determining the time evolution of a quantum field theory is an outstandingly difficult problem. In some cases only a few degrees of freedom are relevant or else perturbative techniques are applicable. However, in our particular case, our interests are focused on processes which are necessarily non-linear and non-perturbative and involve many degrees of freedom. The presence of gravitational fields just contributes with more degrees of freedom, but does not complicate matters significantly.

In the present paper we will use the so called classical approximation to deal with the problem. It consists of replacing the quantum evolution of the system by its classical evolution, for which there are feasible numerical methods available. The quantum nature of the problem remains in the stochastic character of the initial conditions. This approximation has been used with great success by several groups in the past [34, 24]. The advantage of the method is that it is fully non-linear and non-perturbative.

Our approach is to discretize the classical equations of motion of all fields in both space and time. The time-like lattice spacing a_t must be smaller than the spatial one a_s for the stability of the discretized equations. In addition to the ultraviolet cut-off one must introduce an infrared cut-off by putting the system in a box with periodic boundary conditions. In this paper we have thouroughly studied a model with $g^2 = 2\lambda = 1/4$, but we have checked that other values of the parameters do not change our results significantly.

3.1 Initial conditions

The initial conditions of the fields follow the prescription from Ref. [25]. The Higgs modes ϕ_k are solutions of the coupled evolution equations, which can be rewritten as $\phi_k'' + (k^2 - \tau)\phi_k = 0$, with $\tau = M(t - t_c)$ and $M = (2V)^{1/3}m$. The time-dependent Higgs mass follows from the initial inflaton field homogeneous component, $\chi_0(t_i) = \chi_c(1 - Vm(t_i - t_c))$ and $\dot{\chi}_0(t_i) = -\chi_c Vm$. The Higgs modes with $k/M > \sqrt{\tau_i}$ are set to zero, while the rest are determined by a Gaussian random field of zero mean distributed according to the Rayleigh distribution

$$P(|\phi_k|)d|\phi_k|d\theta_k = \exp\left(-\frac{|\phi_k|^2}{\sigma_k^2}\right)\frac{d|\phi_k|^2}{\sigma_k^2}\frac{d\theta_k}{2\pi}\,, \tag{28}$$

with a uniform random phase $\theta_k \in [0, 2\pi]$ and dispersion given by $\sigma_k^2 \equiv |f_k|^2 = P(k, \tau_i)/k^3$, where $P(k, \tau_i)$ is the power spectrum of the initial Higgs quantum fluctuations, computed in the linear approximation in the background of the homogeneous inflaton. In the classical limit, the conjugate momentum $\dot{\phi}_k(\tau)$ is uniquely determined as $\dot{\phi}_k(\tau) = F(k, \tau)\phi_k(\tau)$, with $F(k, \tau) = \mathrm{Im}(if_k(\tau)\dot{f}_k^*(\tau))/|f_k(\tau)|^2$, see Ref. [25].

The rest of the fields (the inflaton non-zero modes and the gravitational waves), are supposed to start from the vacuum, and therefore they are semiclassically set to zero initially in the simulations. Their coupling to the Higgs modes will drive their evolution, giving rise to a rapid (exponential) growth of the GW and inflaton modes. Their subsequent non-linear evolution will be well described by the lattice simulations. In the next subsections we will describe the different evolution stages found in our simulations.

3.2 Tachyonic growth

In this subsection we will compare the analytical estimates with our numerical simulations for the initial tachyonic growth of the Higgs modes and the subsequent growth of gravitational waves. The first check is that the Higgs modes grow according to Ref. [25]. There we found that

$$k|\phi_k(t)|^2 \simeq v^2\, A(\tau)\, e^{-B(\tau)k^2}\,, \tag{29}$$

with $A(\tau)$ and $B(\tau)$ are given, for $\tau > 1$, as $A(\tau) = \frac{\pi^2(1/3)^{2/3}}{2\Gamma^2(1/3)}\,\mathrm{Bi}^2(\tau)$, and $B(\tau) = 2(\sqrt{\tau} - 1)$, where $\mathrm{Bi}(z)$ is the Airy function of the second kind. We have checked that the initial growth, from $mt = 6$ to $mt = 10$, follows precisely the analytical expression.

The comparison between the tensor modes $h_{ij}(k, t)$ and the numerical results is somewhat more complicated. We should first compute the effective anisotropic tensor $\mathrm{T}_{ij}(\mathbf{k}, t)$ (14) from the gradients of the Higgs field (those of the inflaton are not relevant during the tachyonic growth), as follows,

$$\tilde{\Pi}_{ij}(\mathbf{k}, t) = \int \frac{d^3\mathbf{x}\, e^{-i\mathbf{k}\mathbf{x}}}{(2\pi)^{3/2}}\left[\nabla_i\phi^a\,\nabla_j\phi^a(\mathbf{x}, t)\right]\,, \tag{30}$$

where $\nabla_i\phi^a(\mathbf{x},t) = \int \frac{d^3\mathbf{q}}{(2\pi)^{3/2}}\, iq_i\, \tilde{\phi}^a(\mathbf{q},t)\, e^{-i\mathbf{qx}}$. After performing the integral in $\mathbf{x}$ and using the delta function to eliminate $\mathbf{q}'$, we make a change of variables $\mathbf{q} \to \mathbf{q} + \mathbf{k}/2$, and integrate over $\mathbf{q}$. Finally, with the use of $\tilde{\Pi}_{ij}(\mathbf{k},t)$, we can compute the tensor fields,

$$h_{ij}(\mathbf{k},t) = (16\pi G)\int_0^t dt'\, \frac{\sin k(t-t')}{k}\, \tilde{\Pi}_{ij}, \qquad \partial_0 h_{ij}(\mathbf{k},t) = (16\pi G)\int_0^t dt'\, \cos k(t-t')\, \tilde{\Pi}_{ij}. \tag{31}$$

Using the analytic solutions one can perform the integrals and obtain expressions that agree surprisingly well with the numerical estimates. This allows one to compute the density in gravitational waves, $\rho_{\rm GW}$, at least during the initial tachyonic stage in terms of analytical functions, and we reproduce the numerical results. We will now compare these with the analytical estimates. The tachyonic growth is dominated by the faster-than-exponential growth of the Higgs modes towards the true vacuum. The (traceless) anisotropic strees tensor Π_{ij} grows rapidly to a value of order $k^2|\phi|^2 \sim 10^{-3}\, m^2 v^2$, which gives a tensor perturbation

$$\left|h_{ij}h^{ij}\right|^{1/2} \sim 16\pi G v^2 (m\Delta t)^2 10^{-3}\,, \tag{32}$$

and an energy density in GW,

$$\rho_{\rm GW}/\rho_0 \sim 64\pi G v^2\, (m\Delta t)^2 10^{-6} \sim G v^2\,, \tag{33}$$

for $m\Delta t \sim 16$. In the case at hand, with $v = 10^{-3}\, M_P$, we find $\rho_{\rm GW}/\rho_0 \sim 10^{-6}$ at symmetry breaking, which coincides with the numerical simulations at that time, see Fig. 1.

As shown in Ref. [25], the spinodal instabilities grow following the statistics of a Gaussian random field, and therefore one can use the formalism of [41] to estimate the number of peaks or lumps in the Higgs spatial distribution just before symmetry breaking. As we will discuss in the next section, these lumps will give rise via non-linear growth to lump invagination and the formation of bubble-like structures with large density gradients, expanding at the relativistic speeds and colliding among themselves giving rise to a large GWB. The size of the bubbles upon collision is essentially determined by the distance between peaks at the time of symmetry breaking, but this can be computed directly from the analysis of Gaussian random fields, as performed in Ref. [25]. This analysis works only for the initial (linear) stage before symmetry breaking. Nevertheless, we expect the results to extrapolate to later times since once a bubble is formed around a peak, it remains there at a fixed distance from other bubbles. This will give us an idea of the size of the bubbles at the time of collision.

3.3 Bubble collisions

The production of gravitational waves in the next stage proceeds through 'bubble' collisions. In Ref. [24] we showed that during the symetry breaking, the Higgs field develops lumps whose peaks grow up to a maximum value $|\phi|_{\rm max}/v = 4/3$, and then decrease creating approximately spherically symmetric bubbles, with ridges that remain above $|\phi| = v$. Finally, neighboring bubbles collide and high momentum modes are induced via field inhomogeneities. Since initially only the Higgs field sources the anisotropic stress-tensor Π_{ij}, then we expect the formation of structures in the spatial distribution of the GW energy density correlated with the Higgs lumps. In this sub-section we will give an estimate of the burst in GW produced by the first collisions of the Higgs bubble-like structures.

As for the collision of vaccum bubbles in first order phase transitions [9], we can give a simple estimate of the order of magnitude of the energy fraction radiated in the form of gravitational waves when two Higgs bubble-like structures collide. A similar stimation is indeed presented in [42, 22]. In general, the problem of two colliding bubbles has several time and length scales: the duration of the collision, Δt; the bubbles' radius R at the moment of the collision; and the relative speed of the bubble walls. The typical size of bubbles upon collisions, is of the order of $R \approx 10 m^{-1}$, while the growth of the bubble's wall is relativistic, see Ref. [25]. Then we can assume than the time scale associated with bubble collisions is also $\Delta t \sim R$. Assuming the bubble walls contain most of the energy density, it is expected that the asymmetric collisions will copiously produce GW.

Far from a source that produces gravitational radiation, the dominat contribution to the amplitude of GW is given by the acceleration of the quadrupole moment of the Higgs field distribution. Given the energy density of the Higgs field, $\rho_{\rm H}$, we can compute the (reduced) quadrupole moment of the Higgs field spatial distribution, $Q_{ij} = \int d^3x\,(x_ix_j - x^2\delta_{ij}/3)\,\rho_{\rm H}(x)$, such that the amplitude of the gravitational radiation, in the TT gauge, is given by $h_{ij} \sim (2G/r)\ddot{Q}_{ij}$. A significant amount of energy can be emitted in the form of gravitational radiation whenever the quadrupole moment changes significantly fast: through the bubble collisions in this case. The power carried by these waves can be obtained via (17) as

$$P_{\rm GW} = \frac{G}{8\pi}\int d\Omega\,\left\langle \dddot{Q}_{ij}\dddot{Q}^{ij}\right\rangle\,. \tag{34}$$

Omitting indices for simplicity, as the power emitted in gravitational waves in the quadrupole approximation is of order $P_{\rm GW} \sim G(\dddot{Q})^2$, while the quadrupole moment is of order $Q \sim R^5\rho_{\rm H}$, we can estimate the power emitted in GW upon the collision of two Higgs bubbles as

$$P_{\rm GW} \sim G\left(\frac{R^5\rho}{R^3}\right)^2 \sim G\rho_{\rm H}^2\,R^4 \tag{35}$$

The fraction of energy density carried by these waves, $\rho_{\rm GW} \sim P_{\rm GW}\Delta t/R^3 \sim P_{\rm GW}/R^2 \sim G\rho_{\rm H}^2\,R^2$, compared to that of the initial energy stored in the two bubble-like structures of the Higgs field, will be $\rho_{\rm GW}/\rho_{\rm H} = G\rho_{\rm H}R^2$. Since the expansion of the universe is negligible during the bubble collision stage, the energy that drives inflation, $\rho_0 \sim m^2v^2$, is transferred essentially to the Higgs modes during preheating, within an order of magnitude, see Fig. 1. Thus, recalling that $R \sim 10m^{-1}$, the total fraction of energy in GW produced during the bubble collisions to that stored in the Higgs lumps formed at symmetry breaking, is given by

$$\frac{\rho_{\rm GW}}{\rho_0} \sim 0.1\,G\rho_0\,R^2 \sim (v/M_p)^2\,, \tag{36}$$

giving an amplitude which is of the same order as is observed in the numerical simulations, see Fig. 1. Of course, an exhaustive analytical treatment of the production of GW during this stage of bubble collisions remains to be done, but we leave it for a future publication.

3.4 Turbulence

The development of a turbulent stage is expected from the point of view of classical fields, as turbulence usually appears whenever there exists an active (stationary) source of energy localized at some scale $k_{\rm in}$ in Fourier space. The oscillating inflaton zero-mode plays the role of the pumping-energy source, acting at a well defined scale $k_{\rm in}$ in Fourier space, given by the frequency of the inflaton oscillations. Apart from $k_{\rm in}$, there is no other scale in Fourier space where energy is accummulated, dissipated and/or infused. So, as turbulence is characterized by the transport of some conserved quantity, energy in our case, we should expect a flow of energy from $k_{\rm in}$ towards higher (direct cascade) or smaller (inverse cascade) momentum modes. In typical turbulent regimes of classical fluids, there exits a sink in Fourier space, corresponding to that scale at which the (direct) cascade stops and energy gets dissipated. However, in our problem there is no such sink so that the transported energy cannot be dissipated, but instead it is used to populate high-momentum modes. For the problem at hand, there exists a natural initial cut-off $k_{\rm out} \sim \lambda^{1/2}v$, such that only long wave modes within $k < k_{\rm out}$, develop the spinodal instability. Eventually, after the tachyonic growth has ended and the first Higgs' bubble-like structures have collided, the turbulent regime is established. Then the energy flows from small to greater scales in Fourier space, which translates into the increase of $k_{\rm out}$ in time.

When the turbulence has been fully established, if the wave (kinetic) turbulence regime of the fields' dynamics is valid, the time evolution of the variance of a turbulent field $f(\mathbf{x}, t)$, should follow a power-law-like scaling [43]

$${\rm Var}(f(t)) = \left\langle f(t)^2\right\rangle - \left\langle f(t)\right\rangle^2 \propto\, t^{-2p}\,, \tag{37}$$

with $p = 1/(2N-1)$ and N the number of scattering fields in a 'point-like collision'. In Fig. 3 we have plotted the time evolution of the variances of the Inflaton χ and of the Higgs modulus $\phi = \sqrt{\sum_a \phi_a^2}$, and fitted the data with a power-law like (37), obtaining

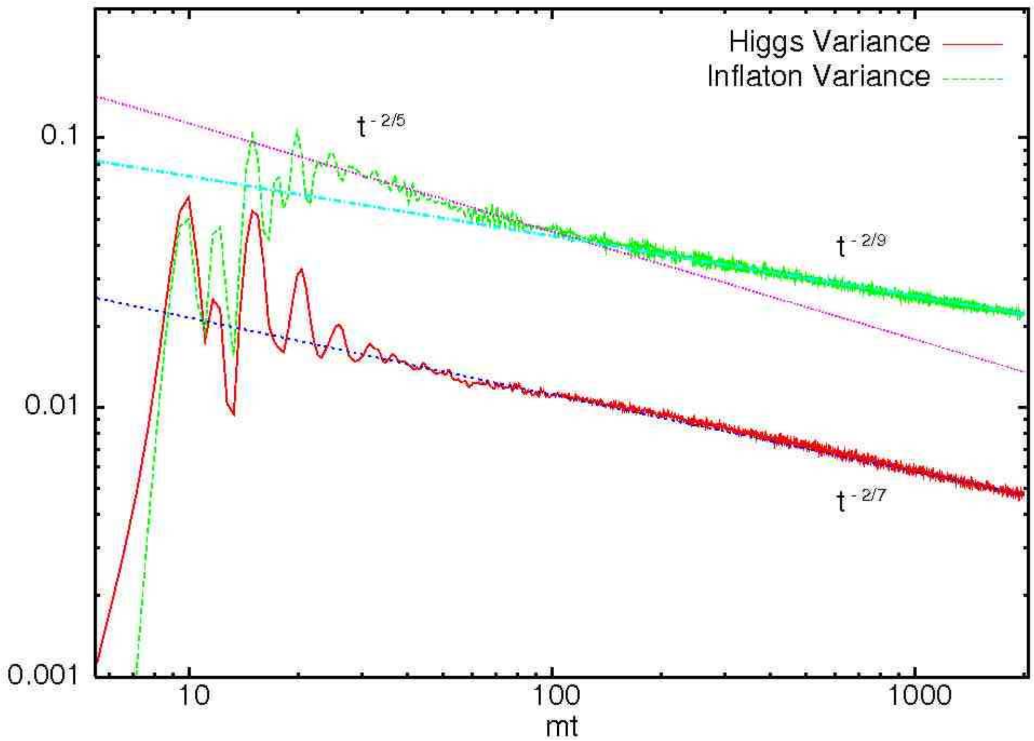

Figure 3: Variance of the Inflaton and the Higgs field as a function of time, the former normalized to its critical value, the latter normalized to its *v.e.v.*. As expected in a turbulent regime, these variances follow a power law $\sim t^{-2p}$ with p a certain critical exponent, although the slope of the Inflaton's variances evolves in time. The curves are produced from an average over 10 different statistical realizations.

$$\begin{aligned} \text{Inflaton:} \quad & p_{_I}^{-1} = 5.1 \pm 0.2, && [35{:}85] \\ \text{Inflaton:} \quad & p_{_I}^{-1} = 9.03 \pm 0.03, && [350{:}2000] \\ \text{Higgs:} \quad & p_{_H}^{-1} = 7.02 \pm 0.01, && [50{:}2000] \end{aligned}$$

where the last brackets on the right correspond to the range in time (in units of m^{-1}) for which we fitted the data. As can be seen in Fig. 3, the slope of the Higgs field (in logarithmic scale), $2p_{_H} \sim 2/7$, remains approximately constant in time, corresponding to a 4-field dominant interaction. However, the slope of the Inflaton's variance increases in time, i.e. the critical exponent $p_{_I}$ of the Inflaton decreases, until it reaches a stationary stage at $mt \sim 100$. We will not try to explain here the origin of such an effective critical exponents as extracted from the simulations. We will just stress that we have checked the robustness of those values under different lattice configurations $(N, p_{\rm min})$ and different statistical realizations. Actually, when turbulence has fully developed, it is expected that the distribution function of the classical turbulent fields, the inflaton and the Higgs here, follow a self-similar evolution [43]

$$n(k,t) = t^{-\gamma\, p} n_0(k\, t^{-p})\,, \tag{38}$$

with p the critical exponent of the fields' variances and γ a certain factor $\sim O(1)$, which depends on the type of turbulence developed. Looking at (38), we see that the exponent p determines the speed of the particles' distribution in momentum space: given a specific scale k_c that scale evolves in time as $k_c(t) = k_c(t_0)(t/t_0)^p$. In the simulations, we have seen that the evolution of the Higgs occupation number follows Eq. (38) with $p \approx 1/7$, as expected from the Higgs variance, and $\gamma \approx 2.7$. Whereas the evolution of the Inflaton occupation number follows (38) even more accurately than the Higgs, with an "effective" exponent (once the asymptotic regime is achieved) $p \approx 1/5$, and $\gamma \approx 3.9$. In Figs. 4 we have plotted the occupation numbers of the Higgs and the Inflaton, also inverting the relation of Eq. (38) in order to extract the *universal* time-independent $n_0(k)$ functions of each field. As shown in those figures,

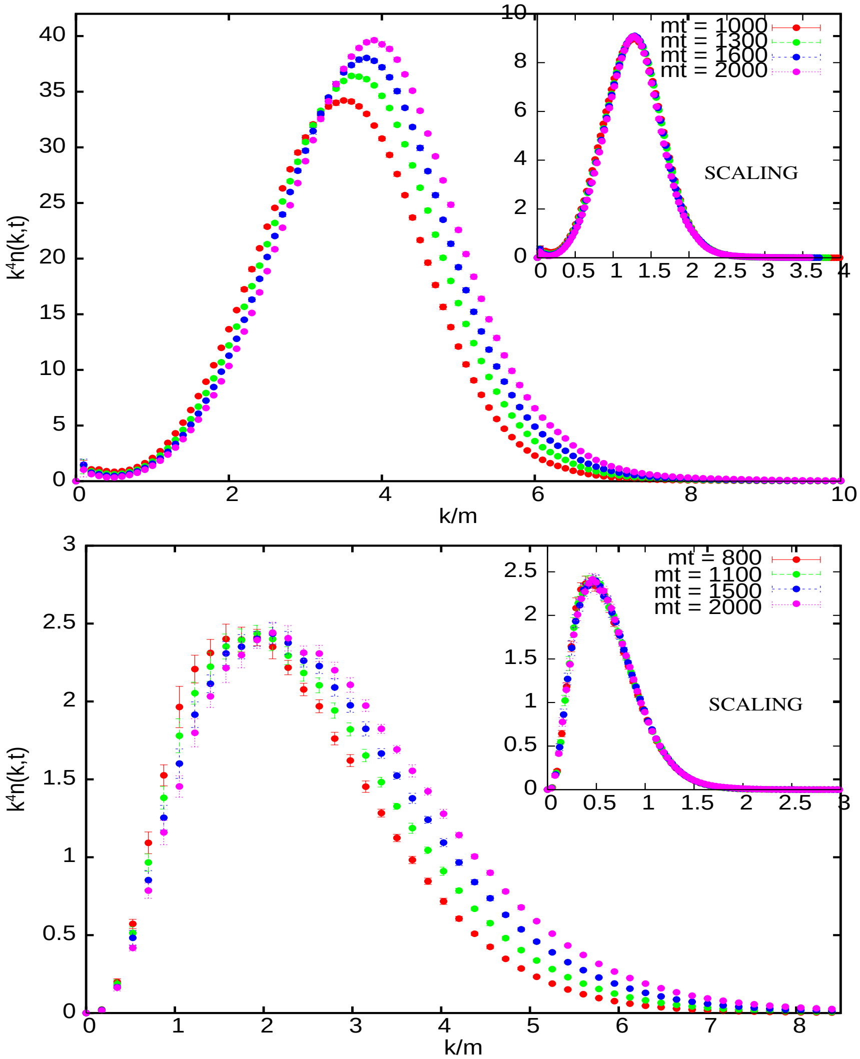

Figure 4: Some snapshots of the evolution of the spectral particle occupation numbers of the Higgs and the Inflaton fields at different times, each averaged over 10 statistical realizations. We multiply them by k^4 so we can see better the scaling behaviour. In the upper right corner, we plot the inverse relation of (38), $n_0(kt^{-p}) = t^{\gamma p} n(k,t)$, also averaged over 10 realizations for each time. The scaling behaviour predicted by wave kinetic turbulent theory [43], is clearly verified.

the distributions follow nicely the expected scaling behaviour. The universal functions $n_0(k)$ plotted in Figs. 4 have been obtained from averaging over ten statistical realizations for each time.

The advantage of the development of a turbulence behaviour is obvious: it allows us to extrapolate the time evolution of the fields' distributions till later times beyond the one we can reach with the simulations. Moreover, the fact that the turbulence develops so early after the tachyonic instability, also allow us to check for a long time of the simulation, the goodness of the description of the dynamics of the fields, given by the turbulent kinetic theory developed in Ref. [43]. We have fitted the averaged universal functions $n_0(k)$ with expressions of the form $k^4\, n_0(k) = P(k)e^{-Q(k)}$, with $P(k)$ and $Q(k)$ polynomials in k. There is no fundamental meaning associated with such a fit, but it is very useful to have an analytical control over $n_0(k)$, since this allows us to track the time-evolution of $n(k,t)$ through Eq. (38). Actually, the classical regime of the evolution of some bosonic fields ends when the system can be relaxed to the Bose-Einstein distribution. Since we cannot reach that moment, we can at least estimate the moment in which the initial energy density gets fully transferred to the Higgs classical modes. Using Eq.(38) and the fit to the universal $n_0(k)$ of the Higgs, we find that the initial energy density is totally transfered to

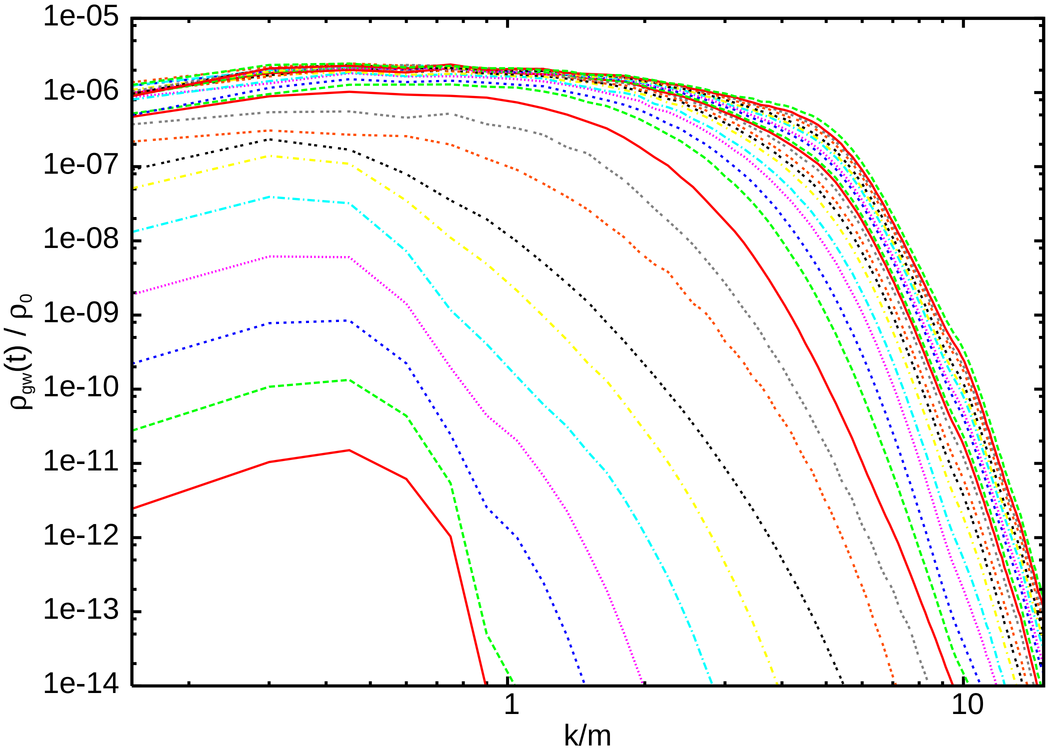

Figure 5: Time evolution of the GW spectra from mt = 6 to mt = 2000. The amplitude of the spectra seems to saturate after mt $\sim$ 100, although the high momentum tail still moves slowly to higher values of k during the turbulent stage.

the Higgs when (in units $m = 1$)

$$\rho_0 = \frac{1}{4\lambda} = \int \frac{dk}{k} \frac{k^3}{2\pi^2} \, k \, n(k,t) = \frac{7.565}{2\pi^2} \, t^{(4-\gamma)p} \,, \tag{39}$$

where we have assumed that the Higgs' modes have energy $E_k(k,t) = k\, n(k,t)$. In our case, with $\lambda = 1/8$, the conversion of the initial energy density into Higgs particles and therefore into radiation is complete by $t \sim 6 \times 10^4 m^{-1}$. Therefore, if we consider this value as a lower bound for the time that classical turbulence requires to end, we see that turbulence last for a very long time compared to the time-scale of the initial tachyonic and bubbly stages. Thus, if GW were significatively sourced during turbulence, one should take into account corrections from the expansion of the universe.

In Fig. 5, we show the evolution of the GW spectra up to times mt = 2000, for a lattice of $(\mathrm{N}, p_{\min})$ = $(128, 0.15)$. It is clear from that figure that the amplitude of the GW saturates to a value of order $\rho_{\mathrm{GW}}/\rho_0 \approx 2 \cdot 10^{-6}$. At mt $\approx$ 50, the maximum amplitude of the spectra has already reached $\rho_{\mathrm{GW}}/\rho_0 \approx 10^{-6}$, while at time mt $\approx$ 100, the maximum has only grown a factor of 2 with respect to mt $\approx$ 50. From times mt $\approx$ 150 till the maximum time we reached in the simulations, mt = 2000, the maximum of the amplitude of the spectrum does not seem to change significantly, slowly increasing from $\approx 2 \cdot 10^{-6}$ to $\approx 2.5 \cdot 10^{-6}$. Despite this saturation, we see in the simulations that the long momentum tail of the spectrum keeps moving towards greater values. This displacement is precisely what one would expect from turbulence, although it is clear that the amplitude of the new high momentum modes never exceed that of lower momentum. In order to disscard that this displacement towards the UV is not a numerical artefact, one should further investigate the role played by the turbulent scalar fields as a source of GW. Here, we just want to remark that the turbulent motions of the scalar fields, seem not to increase significatively anymore the total amplitude of the GW spectrum. Indeed, in a recent paper [22] where GW production at reheating is also considered, it is stated that GW production from turbulent motion of classical scalar fields, should be very supressed. That is apparently what we observe in our simulations although, as pointed above, this issue should be investigated in a more detailed way. Anyway, here we can conclude that the expansion of the Universe during reheating in these hybrid models, does not play an important role during the time of GW production, and therefore we can be safely ignore it.

4 Gravitational Waves from Chaotic Inflation

The production of a relic GWB at reheating was first addressed by Khlebnikov and Tkachev (KT) in Ref. [18], both for the quadratic and quartic chaotic inflation scenarios. Recently, chaotic scenarios were revisited in Ref. [20, 21]. Also very recently, Ref. [22] studied in a very detail way, the evolution of GW produced at preheating in the case of a massless inflaton with an extra scalar field.

In Refs. [18] and [20], the procedure to compute the GW from reheating relied on Weinberg's formula for flat space-time [45]. However, in chaotic models, the expansion of the universe cannot be neglected during reheating, so Weinberg's formula can only be used in an approximated way, if the evolution of the universe is considered as an adiabatic sequence of stationary universes. In Ref. [17], however, we adopted a different approach that takes into account the expansion of the universe in a self-consistent manner, and allows us to calculate at any time the energy density and power spectra of the GW produced at reheating (see section 2). Using our technique, we will show in this section that we reproduce, for specific chaotic models, similar results to those of other authors. In particular, we adapted the publicly available LATTICEEASY code [31], taking advantage of the structure of the code itself, incorparating the evolution of Eq. (7), together with the equations of the scalar fields, Eqs. (4), into the staggered leapfrog integrator routine.

Here we will concentrate only in an scenario with a massless inflaton χ, either accompanied or not by an extra scalar field ϕ. Such scenarios are described by the potential

$$V(\chi,\phi) = \frac{\lambda}{4}\chi^4 + \frac{1}{2}g^2\chi^2\phi^2 \tag{40}$$

Rescaling the time by and the physical fields by a conformal transformation as

$$\chi_c(\tau) = \frac{a(\tau)}{a(0)}\frac{\chi(\tau)}{\chi(0)}, \qquad \phi_c(\tau) = \frac{a(\tau)}{a(0)}\frac{\phi(\tau)}{\chi(0)}, \qquad d\tau = \frac{a(\tau)}{a(0)}\chi(0)\sqrt{\lambda}\,dt\,, \tag{41}$$

then the equations of motion of the inflaton and of the extra scalar field, Eq. (4), can be rewritten in terms of the conformal variables as

$$\chi_c'' - \nabla^2\chi_c - \frac{a''}{a}\chi_c + (\chi_c^2 + q\phi_c^2)\chi_c = 0 \tag{42}$$

$$\phi_c'' - \nabla^2\phi_c - \frac{a''}{a}\chi_c + q\chi_c^2\phi_c = 0\,, \tag{43}$$

where the prime denotes derivative with respect to conformal time. Since the universe expands as radiation-like in these scenarios, $a(\tau) \sim \tau$, so the terms proportional to a''/a in Eqs. (42) and (43) are soon negligible, as explicitly checked in the simulations. Thanks to this, the model is conformal to Minkowski.

The parameter $q \equiv g^2/\lambda$ controls the strength and width of the resonance. For the case of a massless inflaton without an extra scalar field, we just set $q = 0$ in Eq. (42) and ignore Eq. (43). However, in that case, fluctuations of the inflaton also grow via parametric resonance. Actually, they grow as if they were fluctuations of a scalar field coupled to the zero-mode of the inflaton with effective couplig $q = g^2/\lambda = 3$, see Ref. [46]. Following Refs. [18] and [20], we set $\lambda = 10^{-14}$ and $q = 120$. Since this case is also computed in [22], we can also compare our results with theirs. Moreover, we also present results for the pure $\lambda\chi^4$ model with no extra scalar field, a case only shown in Ref. [18].

We begin our simulations at the end of inflation, when the homogeneous inflaton verifies $\chi_0 \approx 0.342M_p$ and $\dot{\chi}_0 \approx 0$. We took initial quantum (conformal) fluctuations $1/\sqrt{2k}$ for all the modes up to a certain cut-off, and only added an initial zero-mode for the inflaton, $\chi_c(0) = 1$, $\chi_c(0)' = 0$. In Figs. 6 and 7, we show the evolution of $\Omega_{\rm GW}$ during reheating, normalized to the instant density at each time step, for the coupled and the pure case, respectively. In the case with an extra scalar field, the amplitude of the GWB saturates at the end of parametric resonance, when the fields variances have been stabilized. This is the beginnig of the turbulent stage in the scalar fields, which seems not to source anymore the production of

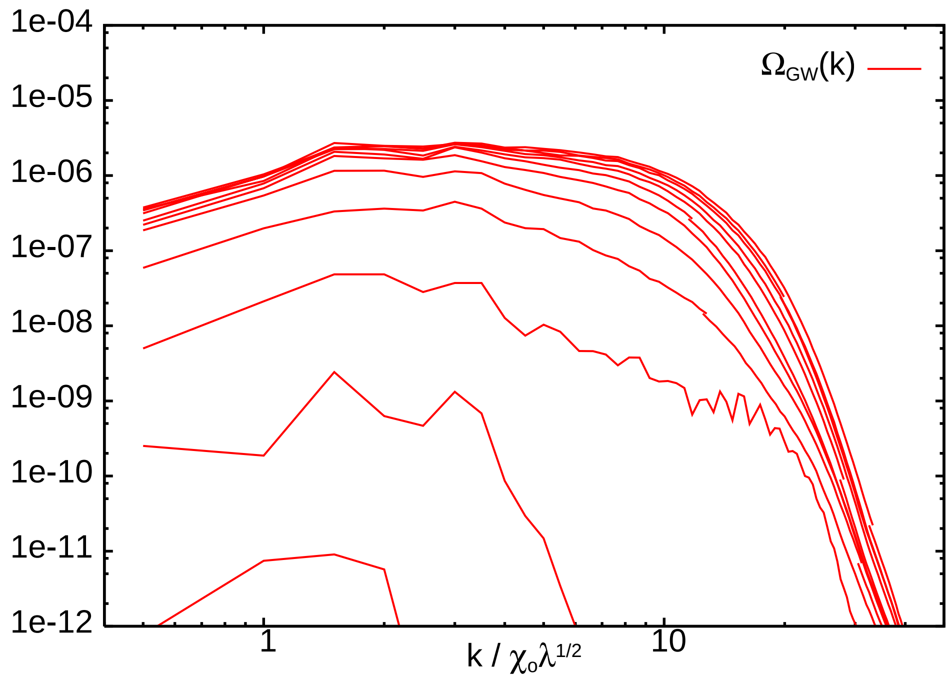

Figure 6: The spectrum of the gravitational waves' energy density, for coupled case with $\lambda = 10^{-14}$ and $g^2/\lambda = 120$. The spectrum is shown accumulated up to different times during GW production, so one can see its evolution. At each time, it is normalized to the total instant density. This plot corresponds to a N = 128 lattice simulation, from $\tau = 0$ to $\tau = 240$.

GWs, as already stated in Refs.[20, 22]. For the pure case, we also see the saturation of the amplitude of the spectra, see Fig. 7, although the high momentum tail seems to slightly move toward higher values.

Of course, in either case, with and without an extra field ϕ, in order to predict today's spectral window of the GW spectrum, we have first to normalize their energy density at the end of GW production to the total energy density at that moment; then to redshift the GW spectra from that moment of reheating, taking into account that the rate of expansion have changed significantly since the end of inflation, see Eq.(20). In particular, the shape and amplitude of GW spectra for the case with the extra scalar field coupled to the inflaton with $q = 120$, seems to coincide with the espectra shown in Ref. [22]. On the other hand, we also reproduce a similar spectra to the one shown in [18], for the case of the pure quartic model. Thanks to the tremendous gain in computer power, we were able to resolve the 'spiky' pattern of that spectrum with great resolution. For the first time, it is clearly observed the exponential tail for large frequencies, not shown in Ref. [18]. The most remarkable fact, is that we also confirm that the peak structure in the GW power spectrum, see Fig. 7, remains clearly visible at times much later than the one at which those peaks have dissapeared in the scalar fields' power spectrum. So, as pointed out in Ref. [18], this characteristic feature will allow us to distinguish this particular model from any other.

Let us emphasize that we have run the simulations till times much greater than that of the end of the resonance stage, both for the pure and the coupled case. The role of the turbulence period after preheating seems, therefore, not to be very important, despite its long duration. Apparently, the *no-go* theorem about the suppresion of GW at turbulence, discussed in [22], is fulfilled. In Refs. [27, 48] it was pointed out that gauge couplings or trilinear interactions could be responsible for a fast thermalization of the universe after inflation (see also Ref. [49]), but as long as this takes place after the end of the resonace stage, in principle this should not affect the results shown above.

5 Conclusions

To summarize, we have shown that hybrid models are very efficient generators of gravitational waves at preheating, in three well defined stages, first via the tachyonic growth of Higgs modes, whose gradients

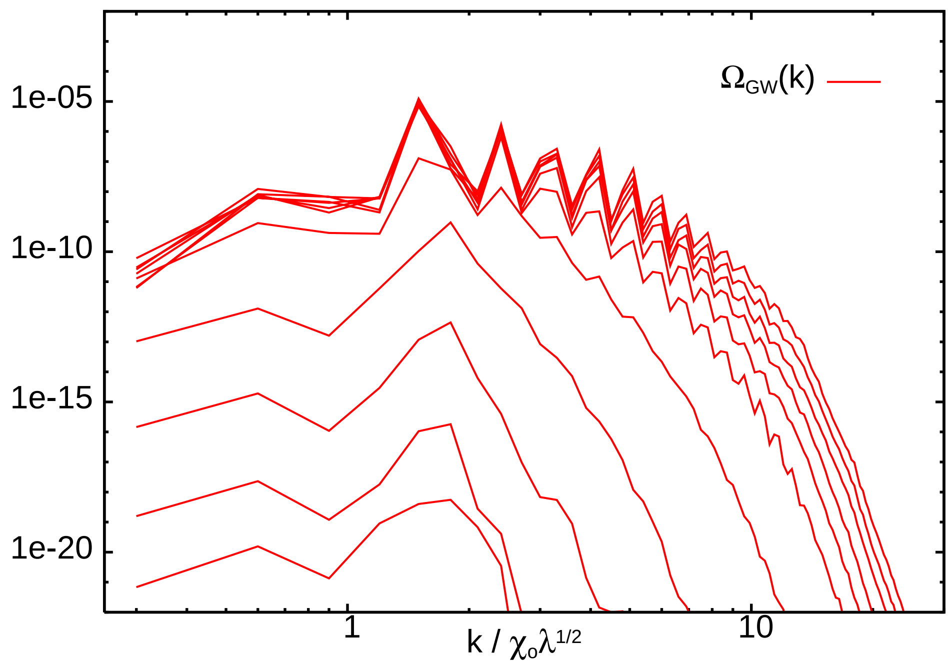

Figure 7: The spectrum of the gravitational waves' energy density, for the pure case, with $\lambda = 10^{-14}$. Again, we show the spectrum accumulated up to different times during GW production, normalized to the total instant density at each time. The plot corresponds to a N = 128 lattice simulation, from $\tau = 0$ to $\tau = 2000$.

act as sources of gravity waves; then via the collisions of highly relativistic bubble-like structures with large amounts of energy density, and finally via the turbulent regime (although this effect does not seem to be very significant in the presence of scalar sources), which drives the system towards thermalization. These waves remain decoupled since the moment of their production, and thus the predicted amplitude and shape of the gravitational wave spectrum today can be used as a probe of the reheating period in the very early universe. The characteristic spectrum can be used to distinguish between this stochastic background and others, like those arising from NS-NS and BH-BH coalescence, which are decreasing with frequency, or those arising from inflation, that are flat [50].

We have plotted in Fig. 8 the sensitivity of planned GW interferometers like LIGO, LISA and BBO, together with the present bounds from CMB anisotropies (GUT inflation), from Big Bang Nucleosynthesis (BBN) and from milisecond pulsars (ms pulsar). Also shown are the expected stochastic backgrounds of chaotic inflation models like $\lambda\phi^4$, both coupled and pure, as well as the predicted background from two different hybrid inflation models, a high-scale model, with $v = 10^{-3} M_P$ and $\lambda \sim g^2 \sim 0.1$, and a low-scale model, with $v = 10^{-5} M_P$ and $\lambda \sim g^2 \sim 10^{-14}$, corresponding to a rate of expansion $H \sim 100$ GeV. The high-scale hybrid model produces typically as much gravitational waves from preheating as the chaotic inflation models. The advantage of low-scale hybrid models of inflation is that the background produced is within reach of future GW detectors like BBO [4]. It is speculated that future high frequency laser interferometers could be sensitive to a GWB in the MHz region [12], although they are still far from the bound marked with an interrogation sign.

For a high-scale model of inflation, we may never see the predicted GW background coming from preheating, in spite of its large amplitude, because it appears at very high frequencies, where no detector has yet shown to be sufficiently sensitive, unless the spectrum can be extrapolated to lower frequencies, where there are interferometric detectors like BBO which could see a signal. On the other hand, if inflation occured at low scales, even though we will never have a chance to detect the GW produced during inflation in the polarization anisotropies of the CMB, we do expect gravitational waves from preheating to contribute with an important background in sensitive detectors like BBO. The detection and characterization of such a GW background, coming from the complicated and mostly unknown epoch of rehating of the universe,

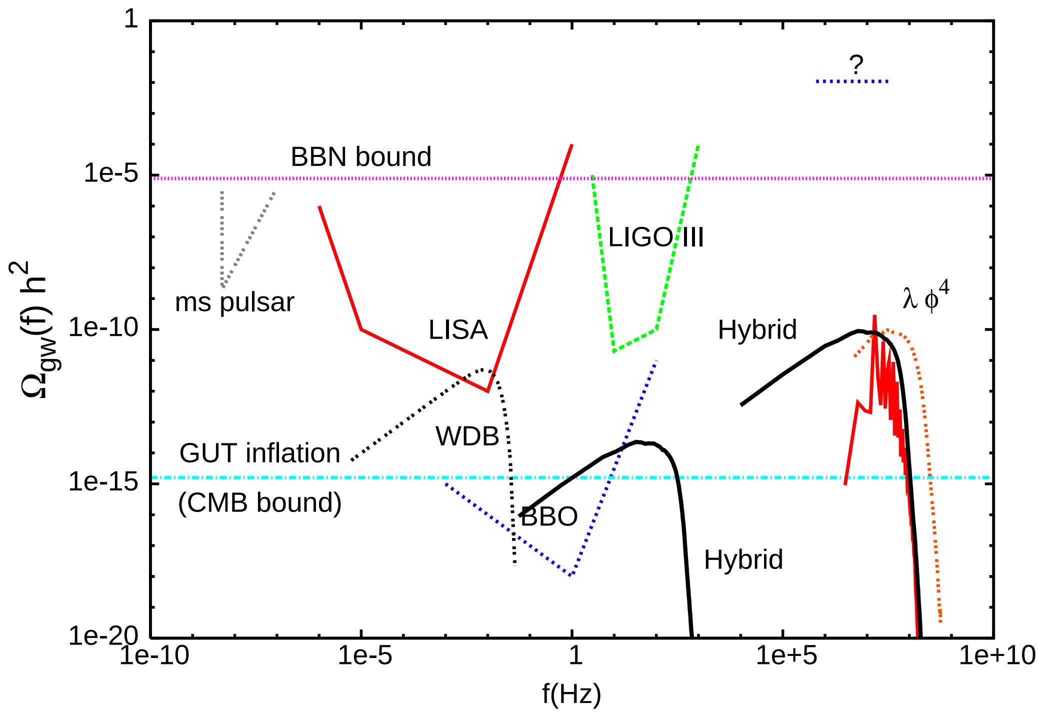

Figure 8: The sensitivity of the different gravitational wave experiments, present and future, compared with the possible stochastic backgrounds; we include the White Dwarf Binaries (WDB) [47] and chaotic preheating ($\lambda\phi^4$, coupled and pure) for comparison. Note the two well differentiated backgrounds from high-scale and low-scale hybrid inflation. The bound marked (?) is estimated from ultra high frequency laser interferometers' expectations [12].

may open a new window into the very early universe, while providing a new test on inflationary cosmology.

Acknowledgments

We wish to thank Alfonso Sastre for a very fruitful collaboration. JGB thanks the organisers of the Japan GRG 17th Meeting in Nagoya for a very enjoyable conference and legendary hospitality. This work is supported in part by CICYT projects FPA2003-03801 and FPA2006-05807, by EU network "UniverseNet" MRTN-CT-2006-035863 and by CAM project HEPHACOS S-0505/ESP-0346. D.G.F. and A.S. acknowledges support from a FPU-Fellowship from the Spanish M.E.C. We also acknowledge use of the MareNostrum Supercomputer under project AECT-2007-1-0005.

References

[1] M. Maggiore, Phys. Rept. **331**, 283 (2000); C. J. Hogan, arXiv:astro-ph/0608567; A. Buonanno, "Gravitational waves," arXiv:0709.4682 [gr-qc].

[2] B. Abbott *et al.* [LIGO Scientific Collaboration], Astrophys. J. **659**, 918 (2007) [arXiv:astro-ph/0608606]. LIGO Home Page: `http://www.ligo.caltech.edu/`

[3] S. A. Hughes, arXiv:0711.0188 [gr-qc]. LISA Home Page: `http://lisa.esa.int`

[4] V. Corbin and N. J. Cornish, Class. Quant. Grav. **23**, 2435 (2006); G. M. Harry, P. Fritschel, D. A. Shaddock, W. Folkner and E. S. Phinney, Class. Quant. Grav. **23**, 4887 (2006). BBO Home Page: `http://universe.nasa.gov/new/program/bbo.html`

[5] S. Kawamura *et al.*, Class. Quant. Grav. **23**, S125 (2006).

[6] T. L. Smith, E. Pierpaoli and M. Kamionkowski, Phys. Rev. Lett. **97**, 021301 (2006).

[7] B. Allen, gr-qc/9604033.

[8] I. H. Stairs, Living Rev. Rel. **6**, 5 (2003).

[9] A. Kosowsky, M. S. Turner and R. Watkins, Phys. Rev. Lett. **69**, 2026 (1992), Phys. Rev. D **45**, 4514 (1992); A. Kosowsky and M. S. Turner, Phys. Rev. D **47**, 4372 (1993); M. Kamionkowski, A. Kosowsky and M. S. Turner, Phys. Rev. D **49**, 2837 (1994).

[10] A. Nicolis, Class. Quant. Grav. **21**, L27 (2004); C. Grojean and G. Servant, "Gravitational waves from phase transitions at the electroweak scale and beyond," arXiv:hep-ph/0607107.

[11] A. Kosowsky, A. Mack and T. Kahniashvili, Phys. Rev. D **66**, 024030 (2002); A. D. Dolgov, D. Grasso and A. Nicolis, Phys. Rev. D **66**, 103505 (2002). G. Gogoberidze, T. Kahniashvili and A. Kosowsky, "The spectrum of gravitational radiation from primordial turbulence," arXiv:0705.1733 [astro-ph].

[12] A. Nishizawa *et al.*, "Laser-interferometric Detectors for Gravitational Wave Background at 100 MHz : Detector Design and Sensitivity," arXiv:0710.1944 [gr-qc]; A. M. Cruise and R. M. J. Ingley, Class. Quant. Grav. **23**, 6185 (2006).

[13] F. Pegoraro, L. A. Radicati, P. Bernard and E. Picasso, Phys. Lett. A **68**, 165 (1978); G. Gemme, A. Chincarini, R. Parodi, P. Bernard and E. Picasso, gr-qc/0112021; R. Ballantini *et al.*, gr-qc/0502054.

[14] A. A. Starobinsky, JETP Lett. **30**, 682 (1979) [Pisma Zh. Eksp. Teor. Fiz. **30**, 719 (1979)].

[15] L. Kofman, A. D. Linde and A. A. Starobinsky, Phys. Rev. Lett. **73**, 3195 (1994); L. Kofman, A. D. Linde and A. A. Starobinsky, Phys. Rev. D **56**, 3258 (1997).

[16] J. Garcia-Bellido and D. G. Figueroa, Phys. Rev. Lett. **98**, 061302 (2007) [arXiv:astro-ph/0701014].

[17] J. Garcia-Bellido, D. G. Figueroa and A. Sastre, "A Gravitational Wave Background from Reheating after Hybrid Inflation," arXiv:0707.0839 [hep-ph], to appear in PRD.

[18] S. Y. Khlebnikov and I. I. Tkachev, Phys. Rev. D **56**, 653 (1997).

[19] J. Garcia-Bellido, "Preheating the universe in hybrid inflation," Proceedings of the 33rd Rencontres de Moriond: Fundamental Parameters in Cosmology, Les Arcs, France, 17-24 Jan 1998, arXiv:hep-ph/9804205.

[20] R. Easther and E. A. Lim, JCAP **0604**, 010 (2006).

[21] R. Easther, J. T. . Giblin and E. A. Lim, "Gravitational Wave Production At The End Of Inflation," arXiv:astro-ph/0612294.

[22] J. F. Dufaux, A. Bergman, G. N. Felder, L. Kofman and J. P. Uzan, arXiv:0707.0875 [astro-ph].

[23] A. D. Linde, Phys. Rev. D **49**, 748 (1994); J. Garcia-Bellido and A. D. Linde, Phys. Rev. D **57**, 6075 (1998).

[24] G. N. Felder, J. Garcia-Bellido, P. B. Greene, L. Kofman, A. D. Linde and I. Tkachev, Phys. Rev. Lett. **87**, 011601 (2001); G. N. Felder, L. Kofman and A. D. Linde, Phys. Rev. D **64**, 123517 (2001).

[25] J. Garcia-Bellido, M. Garcia Perez and A. Gonzalez-Arroyo, Phys. Rev. D **67**, 103501 (2003);

[26] J. Garcia-Bellido and E. Ruiz Morales, Phys. Lett. B **536**, 193 (2002).

[27] J. Garcia-Bellido, D. Y. Grigoriev, A. Kusenko and M. E. Shaposhnikov, Phys. Rev. D **60**, 123504 (1999). J. Garcia-Bellido, M. Garcia Perez and A. Gonzalez-Arroyo, Phys. Rev. D **69**, 023504 (2004); A. Tranberg and J. Smit, JHEP **0311**, 016 (2003).

[28] A. Diaz-Gil, J. Garcia-Bellido, M. Garcia Perez and A. Gonzalez-Arroyo, PoS **LAT2005**, 242 (2006); PoS **LAT2007**, 052 (2007), arXiv:0710.0580 [hep-lat]; "Magnetic field production during preheating at the electroweak scale," arXiv:0712.4263 [hep-ph].

[29] MareNostrum Supercomputer Home Page:
`http://www.bsc.es/`

[30] IFT cluster Home Page:
`http://lattice.ft.uam.es/iftcluster/`

[31] G. N. Felder and I. Tkachev, arXiv: hep-ph/0011159;
`http://www.science.smith.edu/departments/`
`Physics/fstaff/gfelder/latticeeasy/`

[32] J. Garcia-Bellido, A. D. Linde and D. Wands, Phys. Rev. D **54**, 6040 (1996).

[33] R. Allahverdi, K. Enqvist, J. Garcia-Bellido and A. Mazumdar, Phys. Rev. Lett. **97**, 191304 (2006); R. Allahverdi, K. Enqvist, J. Garcia-Bellido, A. Jokinen and A. Mazumdar, JCAP **0706** (2007) 019 [arXiv:hep-ph/0610134].

[34] S. Y. Khlebnikov and I. I. Tkachev, Phys. Rev. Lett. **77**, 219 (1996); **79**, 1607 (1997); T. Prokopec and T. G. Roos, Phys. Rev. D **55**, 3768 (1997).

[35] V. F. Mukhanov, H. A. Feldman and R. H. Brandenberger, Phys. Rept. **215**, 203 (1992).

[36] S. Carroll, "*Spacetime and Geometry: An introduction to General Relativity*," Addison Wesley (2003).

[37] K. G. Wilson, Phys. Rev. D **10**, 2445 (1974).

[38] F. Cooper, S. Habib, Y. Kluger, E. Mottola, J. P. Paz and P. R. Anderson, Phys. Rev. D **50**, 2848 (1994) [arXiv:hep-ph/9405352]; F. Cooper, S. Habib, Y. Kluger and E. Mottola, Phys. Rev. D **55**, 6471 (1997) [arXiv:hep-ph/9610345].

[39] D. Boyanovsky, D. Cormier, H. J. de Vega, R. Holman, A. Singh and M. Srednicki, Phys. Rev. D **56**, 1939 (1997) [arXiv:hep-ph/9703327]; D. Boyanovsky, H. J. de Vega, R. Holman and J. Salgado, Phys. Rev. D **59**, 125009 (1999) [arXiv:hep-ph/9811273].

[40] J. Baacke, K. Heitmann and C. Patzold, Phys. Rev. D **55**, 2320 (1997) [arXiv:hep-th/9608006]; Phys. Rev. D **55**, 7815 (1997) [arXiv:hep-ph/9612264]; Phys. Rev. D **56**, 6556 (1997) [arXiv:hep-ph/9706274].

[41] J. M. Bardeen, J. R. Bond, N. Kaiser and A. S. Szalay, Astrophys. J. **304**, 15 (1986).

[42] G. N. Felder and L. Kofman, Phys. Rev. D **75** (2007) 043518 [arXiv:hep-ph/0606256].

[43] R. Micha and I. I. Tkachev, Phys. Rev. Lett. **90**, 121301 (2003); Phys. Rev. D **70**, 043538 (2004).

[44] http://lattice.ft.uam.es/gw

[45] S. Weinberg, "*Gravitation and Cosmology*", John Wiley & Sons, 1972.

[46] P. B. Greene, L. Kofman, A. D. Linde and A. A. Starobinsky, Phys. Rev. D **56**, 6175 (1997) [arXiv:hep-ph/9705347].

[47] A. J. Farmer and E. S. Phinney, Mon. Not. Roy. Astron. Soc. **346**, 1197 (2003).

[48] J. F. Dufaux, G. N. Felder, L. Kofman, M. Peloso and D. Podolsky, JCAP **0607**, 006 (2006).

[49] G. N. Felder and L. Kofman, Phys. Rev. D **63**, 103503 (2001).

[50] T. L. Smith, M. Kamionkowski and A. Cooray, Phys. Rev. D **73**, 023504 (2006).

Holography and Entanglement Entropy

Tadashi Takayanagi[1]

Department of Physics, Kyoto University, Kyoto 606-8502, Japan

Abstract

We review our recent formulation [1, 2] of computing entanglement entropy in a holographic way. The basic examples can be found by applying AdS/CFT correspondence and the holographic formula has successfully been checked in many examples of conformal field theories. We also explain the covariant formulation of holographic entanglement entropy which is closely related to the covariant entropy bound (Bousso bound) in an interesting way.

1 Introduction

In gravitational theories, the degree of freedom which is contained in a given region A is not proportional to the volume, but to the area of its boundary ∂A. This is because if we put a lot of materials inside A, then they eventually make a black hole and this gives the upper bound of the allowed entropy in A. In this way, the property of the gravitational theory is rather different from the familiar systems described by the law of quantum mechanics, where the entropy is extensive. This suggests that the true degree of freedom in a $d+2$ dimensional gravity is actually equally described by that of a $d+1$ dimensional quantum manybody system. This is known as the holographic principle [3]. This idea has been played crucial role in the recent development of the string theory, especially in the context of AdS/CFT correspondence [4]. The AdS/CFT relates the $d+2$ dimensional anti-de Sitter spacetime to a $d+1$ dimensional conformal field theory (CFT).

However, the holography in other spaces such as the de Sitter spacetime has not been studied well. This is because there is no simple way to realize such spaces in string theory, though in principle we can find (slightly complicated) examples for e.g. de-Sitter space [5]. Therefore it is intriguing and helpful to explore a general principle of holography which may allow us to find the holographic dual for any spacetime without relying on explicit examples in string theory. For this purpose, it is a nice idea to find a universal physical observables by which we can formulate the holographic principle generally. Clearly, the correlation functions, which are often quoted and studied in AdS/CFT, are not suitable for this aim, since we need to specify which operators we consider and thus we need to know the precise spectrum or field contents of the dual theory.

The purpose of this talk is to present a candidate of such a useful quantity. We claim that the quantity called entanglement entropy, which can be defined in any quantum mechanical systems, is a universal physical observable in holography. We will explain how the entanglement entropy in quantum field theories (QFTs) is related a certain geometrical quantity in the dual gravity background. In the first half, we assume that the spacetime is static for simplicity, where the entropy is time-independent. In the latter half, we extend the result in the static case to the time-dependent backgrounds by presenting a covariant formulation of holographic entanglement entropy. As will explain later, this construction has an interesting connection to the covariant entropy bound known as the Bousso bound.

This article is organized as follows. In section 2, we will offer an basic definition and properties of entanglement entropy. In section 3, we review the holographic calculation of entanglement entropy in a static spacetimes. In section 4, we consider its generalization to time-dependent spacetimes by looking at the covariant formulation. In section 5, we summarize the conclusions and discuss future problems.

[1] E-mail:takayana@gauge.scphys.kyoto-u.ac.jp

2 Definition and Properties of Entanglement Entropy

2.1 Definition

In order to define the entanglement entropy, we first divide a given quantum mechanical (manybody) system into two parts (or subsystems) A and B. Accordingly, the total Hilbert space is factorized as

$$H = H_A \otimes H_B. \tag{1}$$

A simple example is a spin chain, which is artificially divided into the left and right part of sites. Next we introduce the reduced density matrix

$$\rho_A = \mathrm{Tr}_B \rho, \tag{2}$$

for the subsystem A by tracing out H_B. ρ is the density matrix of the original system. Indeed, ρ_A is the density matrix when we consider an operator which only depends on the information of H_A. Finally, the entanglement entropy is defined as the von-Neumann entropy for ρ_A i.e.

$$S_A = -\mathrm{Tr}\rho_A \log \rho_A. \tag{3}$$

Notice that even if the total density matrix ρ is that of pure state (i.e. the entropy of ρ is vanishing), still we get a non-vanishing entropy $S_A > 0$ (except that A and B are totally decoupled) since we traced out B and this leads to some ambiguity of information, which is measured by the von-Neumann entropy S_A.

2.2 Basic Properties

Here we summarize the basic properties.

First of all, the entanglement entropy is not an extensive quantity and because of this it has a rather different property than the familiar thermal entropy. But, if we consider the high temperature limit, the entanglement entropy S_A includes a extensive part which is equal to the thermal entropy in A.

Let us assume that the total system is described by a pure state e.g. the system at zero temperature. Then we can show $S_A = S_B$ in a straightforwardly. However, this is violated when ρ is a mixed state.

It is also useful to consider the case where we divide the system in many parts. Especially assume that the Hilbert space is factorized as $H = H_A \otimes H_B \otimes H_C \otimes H_D$. Then we can show the inequality known as the strong subadditivity (see e.g. [6] for a review)

$$S_{A+B+C} + S_B \leq S_{A+B} + S_{B+C}. \tag{4}$$

This has been known to be the most strong constraint which the entanglement entropy should satisfy and it can be derived from the positivity of the norm of Hilbert space. By setting B to zero, (4) is reduced to the subadditivity $S_{A+C} \leq S_A + S_C$. The strong subadditivity represents the concave property of the von-Neumann entropy. For example, in [7], it has been shown that the strong subadditivity applied to 2D CFTs leads to the entropic version of the c-theorem.

2.3 Various Applications

The entanglement entropy has been played important roles in various areas in physics. First of all, it is a crucial quantity in the research of quantum information theory and quantum computation. In this context, the entanglement entropy measures the amount of quantum information [8].

Also recently it has been employed as a quantum order parameter in condense matter systems such as a spin systems, quantum Hall liquid and so on [9, 10]. Especially, it is expected that it can distinguish different quantum vacua such as the presence of anyons when the low energy limit is described by a topological field theory. Notice that in such a topological theory, the correlation functions behave trivial and are not useful. Also in the numerical simulation of quantum many body systems using the density matrix renormalization[2], the entanglement entropy measures the obstruction of the numerical simulation by approximating the degree of freedom by finite size matrices. Thus we expect that it diverges at the quantum phase transition point and this is the reason why the entanglement entropy plays the role of an order parameter.

[2] Roughly speaking this is a quantum version of the method of compressing information.

2.4 Entanglement Entropy in QFT and Area Law

Consider a QFT on a $d+1$ dimensional manifold $R_t \times N$, where R_t and N denote the time direction and the d dimensional space-like manifold, respectively. We define the subsystem by a d dimensional submanifold $A \subset N$ at fixed time $t = t_0$. We call its complement the submanifold B. The boundary of A, which is denoted by ∂A, divides the manifold N into two submanifolds A and B. Then we can define the entanglement entropy S_A by (3). Sometimes this kind of entropy is called geometric entropy as it depends on the geometry of the submanifold A. Since the entanglement entropy is always divergent in a continuum theory, we introduce an ultraviolet cut off a (or a lattice spacing). Then the coefficient in front of the divergence turns out to be proportional to the area of the boundary ∂A of the subsystem A as first pointed out in [11],

$$S_A = \gamma \cdot \frac{\mathrm{Area}(\partial A)}{a^{d-1}} + \text{subleading terms}, \tag{5}$$

where γ is a constant which depends on the system. This behavior can be intuitively understood since the entanglement between A and B occurs at the boundary ∂A most strongly. This result (5) was originally found from numerical computations [11] and checked in many later arguments.

The simple area law (5), however, does not always describe the scaling of the entanglement entropy in generic situations. As we will discuss in details in the next subsections, the entanglement entropy of 1D quantum systems at criticality scales logarithmically with respect to the linear size l of A, $S_A \sim \frac{c}{3} \log l/a$ where c is the central charge of the CFT that describes the critical point.

Before we proceed to further analysis of entanglement entropy, it might be interesting to notice that this area law (5) looks very similar to the Bekenstein-Hawking entropy (BH entropy) of black holes which is proportional to the area of the event horizon

$$S_{BH} = \frac{\text{Area of horizon}}{4G_N}, \tag{6}$$

where G_N is the Newton constant. Intuitively, we can regard S_A as the entropy for an observer who is only accessible to the subsystem A and cannot receive any signals from B. In this sense, the subsystem B is analogous to the inside of a black hole horizon for an observer sitting in A, i.e., outside of the horizon. Indeed, this similarity was an original motivation of considering the entanglement entropy in QFTs [12, 11]. An important motivation of our holographic calculations of the entanglement entropy is actually to explain this similarity from the holographic viewpoint.

2.5 Explicit Computations in 2D CFT

In order to find the entanglement entropy, we first evaluate $\mathrm{tr}_A\, \rho_A^n$, differentiate it with respect to n and finally take the limit $n \to 1$ (remember that ρ_A is normalized such that $\mathrm{tr}_A\, \rho_A = 1$)

$$\begin{aligned} S_A &= \lim_{n\to 1} \frac{\mathrm{tr}_A\, \rho_A^n - 1}{1-n} &(7)\\ &= -\frac{\partial}{\partial n} \mathrm{tr}_A\, \rho_A^n|_{n=1} = -\frac{\partial}{\partial n} \log \mathrm{tr}_A\ \rho_A^n|_{n=1}. &(8) \end{aligned}$$

This is called the replica trick. Therefore, what we have to do is to evaluate $\mathrm{tr}_A\ \rho_A^n$ in our 2D system. The first line of the above definition (7) without taking the $n \to 1$ limit defines the so-called Tsallis entropy, $S_{n,\mathrm{Tsallis}} = \frac{\mathrm{tr}_A\, \rho_A^n - 1}{1-n}$. [3]

This can be done in the path-integral formalism as follows. We first assume that A is the single interval $x \in [u, v]$ at $t_E = 0$ in the flat Euclidean coordinates $(t_E, x) \in R^2$. The ground state wave function Ψ can be found by path-integrating from $t_E = -\infty$ to $t_E = 0$ in the Euclidean formalism

$$\Psi\left(\phi_0(x)\right) = \int_{t_E=-\infty}^{\phi(t_E=0,x)=\phi_0(x)} D\phi\ e^{-S(\phi)}, \tag{9}$$

[3] The Tsallis entropy is related to the alpha entropy (Rényi entropy) $S_\alpha = \frac{\log \mathrm{tr}_A\, \rho_A^\alpha}{1-\alpha}$ through $S_{\alpha,\mathrm{Tsallis}} = \frac{1}{1-\alpha}[e^{(1-\alpha)S_\alpha} - 1]$. The $\alpha \to 1$ and $\alpha \to \infty$ limits of the alpha entropy give the von Neumann entropy and the single-copy entanglement entropy, respectively.

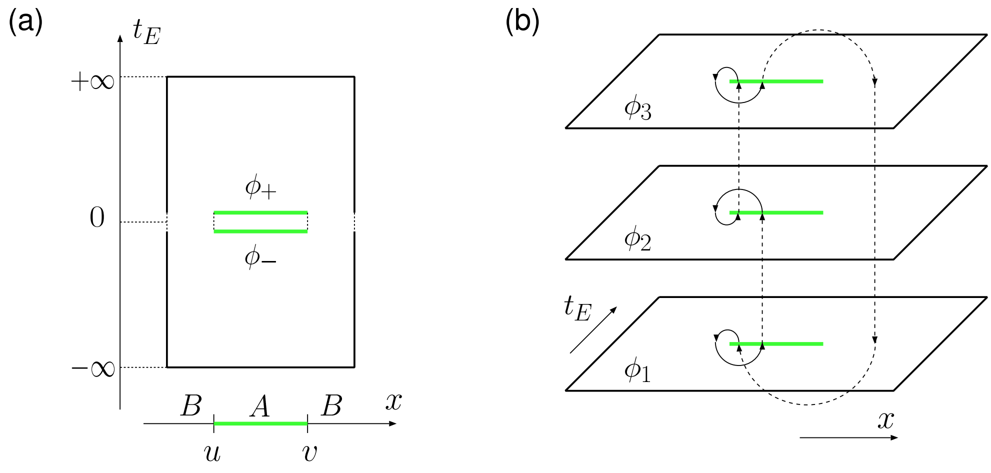

Figure 1: (a) The path integral representation of the reduced density matrix $[\rho_A]_{\phi_+\phi_-}$. (b) The n-sheeted Riemann surface $\mathcal{R}_n$. (Here we take $n = 3$ for simplicity.)

where $\phi(t_E, x)$ denotes the field which defines the 2D CFT. The values of the field at the boundary ϕ_0 depends on the spacial coordinate x. The total density matrix ρ is given by two copies of the wave function $[\rho]_{\phi_0\phi_0'} = \Psi(\phi_0)\bar{\Psi}(\phi_0')$. The complex conjugate one $\bar{\Psi}$ can be obtained by path-integrating from $t_E = \infty$ to $t_E = 0$. To obtain the reduced density matrix ρ_A, we need to integrate ϕ_0 on B assuming $\phi_0(x) = \phi_0'(x)$ when $x \in B$.

$$[\rho_A]_{\phi_+\phi_-} = (Z_1)^{-1} \int_{t_E=-\infty}^{t_E=\infty} D\phi \; e^{-S(\phi)} \prod_{x\in A} \delta\left(\phi(+0, x) - \phi_+(x)\right) \cdot \delta\left(\phi(-0, x) - \phi_-(x)\right), \tag{10}$$

where Z_1 is the vacuum partition function on R^2 and we multiply its inverse in order to normalize ρ_A such that $\mathrm{tr}_A \, \rho_A = 1$. This computation is sketched in Fig. 1 (a).

To find $\mathrm{tr}_A \, \rho_A^n$, we can prepare n copies of (10)

$$[\rho_A]_{\phi_{1+}\phi_{1-}} [\rho_A]_{\phi_{2+}\phi_{2-}} \cdots [\rho_A]_{\phi_{n+}\phi_{n-}}, \tag{11}$$

and take the trace successively. In the path-integral formalism this is realized by gluing $\{\phi_{i\pm}(x)\}$ as $\phi_{i-}(x) = \phi_{(i+1)+}(x)$ $(i = 1, 2, \cdots, n)$ and integrating $\phi_{i+}(x)$. In this way, $\mathrm{tr}_A \, \rho_A^n$ is given in terms of the path-integral on an n-sheeted Riemann surface $\mathcal{R}_n$ (see Fig. 1 (b))

$$\mathrm{tr}_A \, \rho_A^n = (Z_1)^{-n} \int_{(t_E, x)\in\mathcal{R}_n} D\phi \; e^{-S(\phi)} \equiv \frac{Z_n}{(Z_1)^n}. \tag{12}$$

To evaluate the path-integral on $\mathcal{R}_n$, it is useful to introduce replica fields. Let us first take n disconnected sheets. The field on each sheet is denoted by $\phi_k(t_E, x)$ $(k = 1, 2, \cdots, n)$. In order to obtain a CFT on the flat complex plane C which is equivalent to the present one on $\mathcal{R}_n$, we impose the twisted boundary conditions

$$\phi_k(e^{2\pi i}(w - u)) = \phi_{k+1}(w - u), \quad \phi_k(e^{2\pi i}(w - v)) = \phi_{k-1}(w - v), \tag{13}$$

where we employed the complex coordinate $w = x + it_E$. Equivalently we can regard the boundary condition (13) as the insertion of two twist operators $\Phi_n^{+(k)}$ and $\Phi_n^{-(k)}$ at $w = u$ and $w = v$ for each (k−th) sheet. Thus we find

$$\mathrm{tr}_A \, \rho_A^n = \prod_{k=0}^{n-1} \langle \Phi_n^{+(k)}(u) \Phi_n^{-(k)}(v) \rangle. \tag{14}$$

When ϕ is a real scalar field, this is a non-abelian orbifold. To make the situation simple, assume that ϕ is a complex scalar field. Then we can diagonalize the boundary condition by defining n new fields $\tilde{\phi}_k = \frac{1}{n}\sum_{l=1}^{n} e^{2\pi i lk/n}\phi_l$. They obey the boundary condition

$$\tilde{\phi}_k(e^{2\pi i}(w-u)) = e^{2\pi i k/n}\tilde{\phi}_k(w-u), \quad \tilde{\phi}_k(e^{2\pi i}(w-v)) = e^{-2\pi i k/n}\tilde{\phi}_k(w-v). \tag{15}$$

Thus in this case we can conclude that the system is equivalent to $n-$disconnected sheets with two twist operators $\sigma_{k/n}$ and $\sigma_{-k/n}$ inserted in the $k-$th sheet for each values of k. In the end we find

$$\mathrm{tr}_A\, \rho_A^n = \prod_{k=0}^{n-1} \langle \sigma_{k/n}(u)\sigma_{-k/n}(v)\rangle \sim (u-v)^{-4\sum_{k=0}^{n-1}\Delta_{k/n}} = (u-v)^{-\frac{1}{3}(n-1/n)}, \tag{16}$$

where $\Delta_{k/n} = -\frac{1}{2}\left(\frac{k}{n}\right)^2 + \frac{1}{2}\frac{k}{n}$ is the (chiral) conformal dimension of $\sigma_{k/n}$. When we have m such complex scalar fields we simply obtain

$$\mathrm{tr}_A\, \rho_A^n = \prod_{k=0}^{n-1} \langle \sigma_{k/n}(u)\sigma_{-k/n}(v)\rangle \sim (u-v)^{-\frac{c}{6}(n-1/n)}, \tag{17}$$

setting the central charge $c = 2m$.

To deal with a general CFT with central charge c, we need to go back to the basis (13). The paper [13] showed that the result (17) is generally correct. The argument is roughly as follows. Define the coordinate z as follows

$$z = \left(\frac{w-u}{w-v}\right)^{\frac{1}{n}}. \tag{18}$$

This maps $\mathcal{R}_n$ to the z-plane C. In this simple coordinate system we easily find $\langle T(z)\rangle_C = 0$. Via Schwartz derivative term in the conformal map we obtain a non-vanishing value of $\langle T(w)\rangle_{\mathcal{R}_n}$. From that result, we can learn that twist operators $\Phi_n^{\pm(k)}$ in (14) have conformal dimension $\Delta_n = \frac{c}{24}(1-n^{-2})$. Thus we find the same result (17) for general CFTs as follows from (14).

Applying the formula (8) to (17), we find[4] the famous result [14]

$$S_A = \frac{c}{3}\, \log \frac{l}{a}, \tag{19}$$

where a is the UV cut off (or lattice spacing) and we set $l \equiv v - u$.

By applying appropriate conformal maps, we can compactify a direction of the two dimensional flat space. If we do so in the space direction, after some computations we find the entanglement entropy on a circle with the length L [13] as follows

$$S_A = \frac{c}{3}\log\left(\frac{L}{\pi a}\sin\frac{\pi l}{L}\right), \tag{20}$$

where $l < L$ is the length of the subsystem A.

On the other hand, if we periodically identify the (Euclidean) time direction, we get the result at finite temperature $T = \beta^{-1}$ [13]

$$S_A = \frac{c}{3}\log\left(\frac{\beta}{\pi a}\sinh\frac{\pi l}{\beta}\right). \tag{21}$$

3 Holographic Entanglement Entropy for Static Spacetime

3.1 The Setup of Holography

As we have reviewed we can define the entanglement entropy S_A in any QFTs for each choice of the boundary ∂A. In this sense we always have infinite different quantities for a given QFT. Even though

[4] Here we neglect a constant term which does not depend on l, L and a.

in two dimensional CFT they can be analytically computed by using the conformal map method as in [13], the calculations in higher dimensional QFTs or CFTs are generally complicated and difficult. Nevertheless, we expect that the entanglement entropy play the role of order parameter of quantum phase transitions and it is quite useful if we can compute this quantity explicitly in a strongly coupled theories.

For this purpose, the holographic dual computation, if it exists, will be very useful because we expect that a quantum physical observable in the QFT side corresponds to a certain classical geometrical quantity in the dual gravity theory as is so in the AdS/CFT. Therefore we would like to consider the holographic calculation of the entanglement entropy in QFTs in this section.

The arguments below are not necessarily restricted to the setup of AdS/CFT correspondence, but we consider a rather general setup of the holography.

We will work in the general setup of holography where the (quantum) gravity in the bulk $d+2$ dimensional spacetime M is dual to a QFT on its $(d+1)$ dimensional boundary ∂M. If we stick to the AdS/CFT correspondence, M is the asymptotically AdS spacetime and the gravity on M is dual to a QFT with a UV fixed point defined on the boundary ∂M.

We assume that the spacetime M is static to make the argument simple. We will later discuss general time-dependent cases in the next section. Then we can express M as $M = R_t \times N$, where the d dimensional manifold N represents the time slice and R_t is the time direction. Also on the boundary we have $\partial M = R_t \times \partial N$.

3.2 Holographic Entanglement Entropy

To define the entanglement entropy, we divide the time slice N into A and B as we explained before. Since we are interested in the bulk gravity dual calculation, we would like to somehow extend this division to the bulk spacetime M. Our principle is as follows; as is clear in the area law of entanglement entropy, the boundary ∂A is the most physically important object. So we extend ∂A to a surface γ_A in the entire M such that $\partial\gamma_A = \partial A$. Notice that this is a surface in the time slice N, which is a Euclidean manifold. Of course, there are infinitely many different choices of γ_A. We claim that we have to choose the minimal area surface among them. This is uniquely determined and we call this γ_A below.

We are now in a position to present our holographic formula. We argue that the holographic entanglement entropy is simply given by

$$S_A = \frac{\mathrm{Area}(\gamma_A)}{4G_N^{(d+2)}}, \tag{22}$$

where $G_N^{(d+2)}$ is the Newton constant in the gravity theory on M. The above formula is reminiscent of the Bekenstein-Hawking formula of black hole entropy, though in our case γ_A is no longer than a horizon.

Indeed, we can motivate our formula (22) from the following intuitive argument. The holography relates the bulk gravity to a non-gravitational theory on its boundary. Thus we expect that a part of the bulk corresponds to the information of a certain region in the boundary. In our setup, we relate the information includes B in the boundary theory, whose amount is measure by S_A, to the bulk region defined by the one inside γ_A. The reason why we take the minimal area surface is that we are applying the idea of the entropy bound and we are trying to find the most strict bound. This part will be discussed in detail in the next section.

If we restrict to the AdS/CFT setup, we can formally derive the holographic formula (22) from the bulk to boundary relation (GKPW relation) [15] as shown in [16]. As we have explained in the previous section, the computation of $Tr\rho_A^n$, whose derivative about n in the limit $n \to 1$ leads to the entropy S_A, is equivalent to that of the partition function on the n-copied of the original manifold with the cut along ∂A. In other words, the manifold is defined by putting the negative deficit angle $2\pi(1-n)$ on the original spacetime. Following the AdS/CFT, what we have to do is to extend this geometry on the boundary toward the bulk region. We assume that the deficit angle surfaces extends to the entire the bulk AdS. This is denoted by γ_A. Then the Ricci scalar behaves like a delta function

$$R = 4\pi(1-n)\delta(\gamma_A). \tag{23}$$

Then we plug this in the gravity action

$$S_{AdS} = -\frac{1}{16\pi G_N^{(d+2)}}\int_M dx^{d+2}\sqrt{g}(R+\Lambda)+\cdots, \tag{24}$$

where we only make explicit the bulk Einstein-Hilbert action. Other parts which come from the boundary terms and the other fields contributions do not affect our computation here.

The basic principle of AdS/CFT i.e. the bulk to boundary relation [15] equates the partition function of CFT with the one of AdS gravity. Thus we can holographically calculate the entanglement entropy S_A as follows

$$S_A = -\frac{\partial}{\partial n}\log Tr\rho_A^n|_{n=1} = -\frac{\partial}{\partial n}\left[\frac{(1-n)\mathrm{Area}(\gamma_A)}{4G_N^{d+2}}\right]_{n=1} = \frac{\mathrm{Area}(\gamma_A)}{4G_N^{d+2}}. \tag{25}$$

This reproduces our holographic formula (22). The action principle in the gravity theory requires that γ_A is the minimal area surface.

Finally we would like to point that this holographic formulation assumes the existence of non-trivial minimal surfaces. In the spacetime with a warp factor as in AdS spaces, we expect this property. We think this is an interesting constraint on the spacetime which has a holographic interpretation.

3.3 Many Evidences for the Holographic Formula

Since the above arguments are pretty formal and assume the AdS/CFT correspondence, we need to check explicitly this claim by comparing both sides directly. Indeed, several different checks have been made until now and they have turn out to be all successful. In this subsection we would like to give a very brief overview of these agreements.

- The area law (5) known in QFT can be easily reproduced holographically. The warp factor in the AdS space leads to the UV divergence of the dual CFT [1]. Since the leading contribution to the area of γ_A comes from the region near the boundary, it should be proportional to the area of the boundary i.e. ∂A. This leading divergence of the area clearly scales as $\sim a^{-(d-1)}$ for AdS_{d+2}, which indeed agrees with the area law.

- We find perfect agreements in the lowest dimensional case of the AdS_3/CFT_2 setup [1]. In this case γ_A is a geodesic line which connects the two points which define the division into A and B. It is also possible to show that the entanglement entropy at finite temperature can be reproduced from the geodesics length in the BTZ black holes. These arguments will be reviewed in the next subsection.

- Though in the higher dimension, it is not easy to calculate the entanglement entropy in QFTs analytically, still we can show the semi-qualitative agreements between the CFT and AdS calculations. In particular, for the logarithmic terms of the entropy we can show the precise agreement as its coefficient is proportional to a linear combination of central charges. For details, refer to the second paper of [1].

- In the presence of a horizon, the minimal surface γ_A tends to wrap the (apparent) horizon. Then the wrapped part gives a extensive contribution to the holographic entanglement entropy. This agrees with the fact that the entanglement entropy includes the thermal part and we know that thermal entropy is dual to the black hole entropy which is given by the Bekenstein-Hawking area formula. In other words, our holographic formula generalizes the black hole entropy formula.

- We can holographically derive the strong subadditivity (4) in a very simple way [17] (see also [6]).

- If we apply the holographic formula to the AdS_2/CFT_1 setup, which comes from the near horizon limit of 4D or 5D extremal black holes, then it reproduces the Wald entropy formula in the presence of the higher derivative correction to the Einstein-Hilbert action [18].

- The holographic formula is nontrivially consistent with the covariant entropy bound (Bousso bound). This will be discussed in the next section.

3.4 Holographic Entanglement Entropy in AdS_3/CFT_2

Here we present a detailed analysis of the holographic entanglement entropy in AdS_3/CFT_2. According to AdS/CFT correspondence [4], the gravitational theories on this space are dual to $1+1$ dimensional conformal field theories with the central charge [19]

$$c = \frac{3R}{2G_N^{(3)}}, \tag{26}$$

where $G_N^{(3)}$ is the Newton constant in three dimensional gravity. In the global coordinate, the metric of AdS_3 becomes

$$ds^2 = R^2(-\cosh^2\rho dt^2 + d\rho^2 + \sinh^2\rho d\theta^2). \tag{27}$$

At the boundary $\rho = \infty$ of the AdS_3, the metric is divergent. To regulate relevant physical quantities we need to put a cutoff ρ_0 and restrict the space to the bounded region $\rho \le \rho_0$. This procedure corresponds to the ultra violet (UV) cutoff in the dual conformal field theory. If we define the dimensionless UV cutoff δ ($\propto$ *length*), then we find the relation $e^{\rho_0} \sim \delta^{-1}$. In the example of the previous section, δ should be identified with

$$e^{\rho_0} \sim \delta^{-1} = L/a. \tag{28}$$

Remember that L is the total length of the system and a is the lattice spacing (or UV cutoff). Notice that there is actually an ambiguity about the $\mathcal{O}(1)$ numerical coefficient in this relation[5].

In the global coordinate of AdS_3 (27), the $1+1$ dimensional spacetime, in which the CFT_2 is defined, is identified with the cylinder (t, θ) at the (regularized) boundary $\rho = \rho_0$. Then we consider the AdS dual of the setup of computing the entanglement entropy. The subsystem A corresponds to $0 \le \theta \le 2\pi l/L$ and we can discuss the entanglement entropy by applying our proposal (22). In this lowest dimensional example, the minimal surface γ_A, which plays the role of the holographic screen [3, 20], becomes one dimensional. In other words, it is the geodesic line which connects the two boundary points at $\theta = 0$ and $\theta = 2\pi l/L$ with t fixed (see Fig. 2) .

Then to find the entropy we calculate the length of the geodesic line γ_A. The geodesics in AdS_{d+2} spaces are given by the intersections of two dimensional hyperplanes and the AdS_{d+2} in the ambient $R^{2,d+1}$ space such that the normal vector at the points in the intersections is included in the planes. The explicit form of the geodesic in AdS_3, expressed in the ambient $\vec{X} \in R^{2,2}$ space, is

$$\vec{X} = \frac{R}{\sqrt{\alpha^2-1}}\sinh(\lambda/R)\cdot\vec{x} + R\left[\cosh(\lambda/R) - \frac{\alpha}{\sqrt{\alpha^2-1}}\sinh(\lambda/R)\right]\cdot\vec{y}, \tag{29}$$

where $\alpha = 1 + 2\sinh^2\rho_0\sin^2(\pi l/L)$; x and y are defined by

$$\begin{aligned}\vec{x} &= (\cosh\rho_0\cos t, \cosh\rho_0\sin t, \sinh\rho_0, 0),\\ \vec{y} &= (\cosh\rho_0\cos t, \cosh\rho_0\sin t, \sinh\rho_0\cos(2\pi l/L), \sinh\rho_0\sin(2\pi l/L)).\end{aligned} \tag{30}$$

The length of the geodesic can be found as

$$\text{Length} = \int ds = \int d\lambda = \lambda_*, \tag{31}$$

where λ_* is defined by

$$\cosh(\lambda_*/R) = 1 + 2\sinh^2\rho_0\ \sin^2\frac{\pi l}{L}. \tag{32}$$

Assuming that the UV cutoff energy is large $e^{\rho_0} \gg 1$, we can obtain the entropy (22) as follows (using (26))

$$S_A \simeq \frac{R}{4G_N^{(3)}}\log\left(e^{2\rho_0}\sin^2\frac{\pi l}{L}\right) = \frac{c}{3}\log\left(e^{\rho_0}\sin\frac{\pi l}{L}\right). \tag{33}$$

Indeed, this entropy exactly coincides with the known 2D CFT result (20), including the (universal) coefficients after we remember the relation (28).

[5]However, this ambiguity does not affect universal quantities which do not depend on the cut off a and we will consider such quantities in the later arguments.

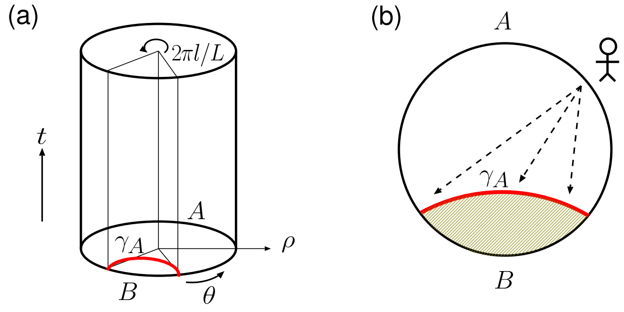

Figure 2: (a) AdS_3 space and CFT_2 living on its boundary and (b) a geodesics γ_A as a holographic screen.

It may be useful to repeat the similar analysis in the Poincare coordinates of AdS_3 $ds^2 = \frac{R^2}{z^2}(-dt^2 + dz^2 + dx^2)$. We pickup the spacial region (again call A) $-l/2 \le x \le l/2$ and consider its entanglement entropy. We can find the geodesic line γ_A between $x = -l/2$ and $x = l/2$ for a fixed time t_0

$$(x, z) = \frac{l}{2}(\cos s, \sin s), \qquad (\epsilon \le s \le \pi - \epsilon). \tag{34}$$

The infinitesimal ϵ is the UV cutoff and leads to the cutoff z_{UV} as $z_{UV} = \frac{l\epsilon}{2}$. Since $e^\rho \sim x^i/z$ near the boundary, we find $z \sim a$. The length of γ_A can be found as

$$\mathrm{Length}(\gamma_A) = 2R\int_\epsilon^{\pi/2} \frac{ds}{\sin s} = -2R\log(\epsilon/2) = 2R\log\frac{l}{a}. \tag{35}$$

Finally the entropy can be obtained as follows

$$S_A = \frac{\mathrm{Length}(\gamma_A)}{4G_N^{(3)}} = \frac{c}{3}\log\frac{l}{a}. \tag{36}$$

This again agrees with the well-known result (19) as expected.

Next we consider how to explain the entanglement entropy at finite temperature $T = \beta^{-1}$ from the viewpoint of AdS/CFT correspondence. Since we assumed that the spacial length of the total system L is infinite, we have $\beta/L \ll 1$. In such a high temperature circumstance, the gravity dual of the conformal field theory is described by the Euclidean BTZ black hole [22]. Its metric looks like

$$ds^2 = (r^2 - r_+^2)d\tau^2 + \frac{R^2}{r^2 - r_+^2}dr^2 + r^2 d\varphi^2. \tag{37}$$

The Euclidean time is compactified as $\tau \sim \tau + \frac{2\pi R}{r_+}$ to obtain a smooth geometry. We also impose the periodicity $\varphi \sim \varphi + 2\pi$. By taking the boundary limit $r \to \infty$, we find the relation between the boundary CFT and the geometry (37)

$$\frac{\beta}{L} = \frac{R}{r_+} \ll 1. \tag{38}$$

The subsystem for which we consider the entanglement entropy is given by $0 \le \varphi \le 2\pi l/L$ at the boundary. Then by applying our proposal (22), the entropy can be computed from the length of the space-like geodesic starting from $\varphi = 0$ and ending to $\varphi = 2\pi l/L$ at the boundary $r = \infty$ for a fixed time. To find the geodesic line, it is useful to remember that the Euclidean BTZ black hole at temperature T is equivalent to thermal AdS_3 at temperature $1/T$. If we define the new coordinates

$$r = r_+\cosh\rho, \quad \tau = \frac{R}{r_+}\theta, \quad \varphi = \frac{R}{r_+}t, \tag{39}$$

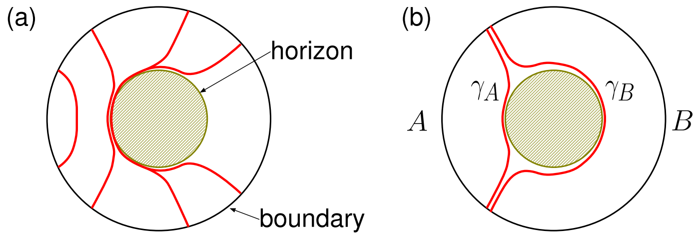

Figure 3: (a) Minimal surfaces γ_A in the BTZ black hole for various sizes of A. (b) γ_A and γ_B wrap the different parts of the horizon.

then the metric (37) indeed becomes the one in the Euclidean Poincare coordinates with t replaced by it. Now the computation of the geodesic line is parallel with what we did just before. We only need to replace $\sinh\rho$ and $\sin t$ with $\cosh\rho$ and $\sinh t$. In the end we find (31) with λ_* is now given by

$$\cosh\left(\frac{\lambda_*}{R}\right) = 1 + 2\cosh^2\rho_0 \sinh^2\left(\frac{\pi l}{\beta}\right), \tag{40}$$

where we took into account the UV cutoff $e^{\rho_0} \sim \beta/a$. Then our area law (22) precisely reproduces the known CFT result (21).

It is also intriguing to understand these calculations geometrically. The geodesic line in the BTZ black hole takes the form shown in Fig. 3(a). When the size of A is small, it is almost the same as the one in the ordinary AdS$_3$. As the size becomes large, the turning point approaches the horizon and eventually, the geodesic line covers a part of the horizon. This is the reason why we find a thermal behavior of the entropy when $l/\beta \gg 1$ i.e. $S_A \sim \frac{\pi c l}{3\beta}$. The thermal entropy in a conformal field theory is dual to the black hole entropy in its gravity description via the AdS/CFT correspondence. In the presence of a horizon, it is clear that S_A is not equal to S_B (remember B is the complement of A) since the corresponding geodesic lines wrap different parts of the horizon (see Fig. 3(b)). This is a typical property of entanglement entropy at finite temperature as we mentioned in section 2.2.

Also as shown recently in [18], when A is very closed to the total system, γ_A is divided into two pieces, the circle which wraps the horizon and the one localized at the boundary. This leads the precise relation between the entanglement entropy on the circle S_A and the BTZ black hole entropy S_{BH}

$$\lim_{l\to 0}\left(S_A(l) - S_A(L-l)\right) = S_{BH}, \tag{41}$$

where again L is the total length of the boundary.

4 Covariant Holographic Entanglement Entropy and Covariant Entropy Bound

4.1 Covariant Entropy Bound

So far we have only discussed static spacetimes. However, it is much more interesting to consider holography in a time-dependent spacetime as eventually we would like to understand cosmological backgrounds such as the de-Sitter space from a holographic viewpoint. Here we assume that there is a time-like boundary where the metric diverges as is so in the time-dependent asymptotically AdS spaces.

In the previous argument, we assumed a time slice on which we can define minimal surfaces since its signature is Euclidean. However, in our time-dependent case there is no longer a natural choice of the time-slices as we have infinitely many different ways of defining the time slices. Thus we need to consider the entire Lorentzian spacetime. Then we are in a trouble since in Lorentzian geometry there is no minimal area surface as the area vanishing if the surface extends in the light-like direction. In order to resolve this issue, let us remember an analogous problem; the covariant entropy bound so called the Bousso bound.

In general, if we get heavy objects together in a small region and continue to bring another one into the region, this system eventually experiences the gravitational collapse. Therefore we have a upper bound of the mass and entropy which can be included inside of the surface Σ. The bound for the entropy in flat space time is called the Bekenstein bound and it is given by

$$S_\Sigma \leq \frac{\text{Area}(\Sigma)}{4G_N}, \tag{42}$$

where Σ is a codimension two closed surface in the spacetime. It is also more interesting to generalize this bound to any time-dependent backgrounds like the cosmological ones. This requires to find a covariant description. It is obvious that the Bekenstein bound (42) is not covariant since the definition of the entropy included inside Σ is not covariant but depends on the choice of the time slice. The covariant entropy bound was eventually formulated by Bousso [20] and it is given by

$$S_{L(\Sigma)} \leq \frac{\text{Area}(\Sigma)}{4G_N}. \tag{43}$$

The light-like manifold $L(\Sigma)$ is called the light-sheet of Σ. This is defined by the manifold which is generated by the null geodesics starting from the surface Σ. We require that the expansion θ of the null geodesic is non-positive $\theta \leq 0$. In the flat spacetime, this is just a half of light-cone and the same is true for the AdS spacetime as it is conformally flat. Then the quantity $S_{L(\Sigma)}$ means the entropy which pass through the light sheet $L(\Sigma)$, which is covariantly well-defined. One more interesting thing of the Bousso bound is that we can apply the bound even if the surface Σ has boundaries, which is quite useful in the holographic setup as we employ below.

4.2 Covariant Holographic Entanglement Entropy

Now we would like to return to our original question of the covariant holographic entanglement entropy. Our final claim [2] is given by

$$S_A(t) = \frac{\text{Area}(\gamma_A(t))}{4G_N^{d+2}}, \tag{44}$$

where $\gamma_A(t)$ is the extremal surface in the entire Lorentzian spacetime M with the boundary condition $\partial\gamma_A(t) = \partial A(t)$. The time t is the time on the time slice in the boundary ∂M and there is no unique way to extend it to the bulk spacetime M.

This covariant formula (44) has been originally motivated from the Bousso bound (43) in [2]. To see let us remember the fact that the AdS/CFT correspondence with a UV cut off $z > a$ can be regarded as a brane-world setup (RS2 [21]). Since we assume that the cut off is close to the UV $a << R$, the gravity on the $d+1$ dimensional brane theory is very weak as

$$\frac{1}{G_N^{brane}} \sim \frac{R^d}{G_N^{bulk}} \int_a^\infty \frac{dz}{z^d} = \frac{R^d}{(d-1)a^{d-1}} \frac{1}{G_N^{bulk}} >> \frac{R}{G_N^{bulk}}, \tag{45}$$

where we assume the standard metric

$$ds^2 = R^2 \frac{dz^2 + g_{ij}(x)dx^i dx^j}{z^2}, \tag{46}$$

where g_{ij} is the metric on the brane.

Now we would like to ask what is the Bousso bound on the brane gravity theory (see fig.4 in the simplest case of AdS_3/CFT_2). We expect that the brane theory with quantum corrections taken into account is dual to the bulk gravity theory which is classical, based on the standard idea of AdS/CFT correspondence. Therefore we argue that the quantum corrected Bousso bound on the brane can be found as the classical Bousso bound on the brane. First we start with the setup of Bousso bound at the boundary ∂M. We pick up a (closed) surface $\partial\Sigma$ which separates a time slice into the subsystem A and B such that $\partial A = \partial\Sigma$. Now we define the light-sheet for Σ. We consider both the future and past directed ones and call them $\partial L^+(\Sigma)$ and $\partial L^-(\Sigma)$. The reason why we put the symbol ∂ is that we are

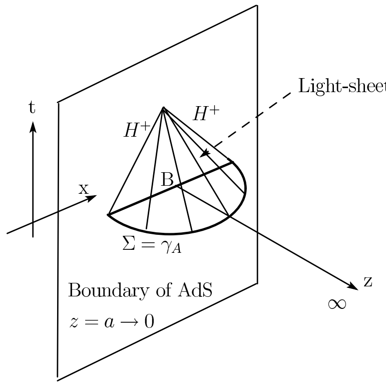

Figure 4: The setup of Bousso bound applied to the AdS_3/CFT_2 in the Poincare coordinate $ds^2 = \frac{R^2}{z^2}(-dt^2 + dz^2 + dx^2)$. In this simplified case, the future Cauchy horizon H^+ coincides with the future light-sheet $\partial L^+(\Sigma)$. In the above figure we only write the future light-sheet and not the past one just for simplicity.

interested in their bulk extensions $L^{\pm}(\Sigma)$. Again there are infinitely many different ways of extending the boundary light-sheets toward the bulk. We define the surface Σ by the intersection $L^+(\Sigma) \cap L^-(\Sigma)$. For each of such a Σ, we get the Bousso bound (43).

Here the condition of non-positive expansions of the null geodesics on the light-sheets i.e. $\theta^{\pm} \leq 0$ come into play. If there were not this condition we can choose arbitrary Σ and we can take them to be light-like. However, the condition is rather strong enough that the area of allowed Σ takes a non-trivial minimum and therefore we can define an analogue of the minimal surface in this Lorentzian spacetime. The minimum of the area corresponds to the most strict Bousso bound for a given boundary surface $\partial\Sigma$ or equally the choice of the subsystem A.

This minimum of the area occurs when the expansions on the two light-sheets are both vanishing $\theta^{\pm} = 0$. This condition is actually equal to the statement that the surface Σ is an extremal surface again called γ_A, which is defined by the saddle point of the area functional in the Lorentzian spacetime.

The final observation is that the quantum Bousso bound on the brane will be saturated by the entanglement entropy. This is motivated by the fact that the entanglement entropy represents a thermal entropy plus quantum corrections and that it is defined by assuming that the subsystem B is completely smeared, which will be expected to lead to the maximal entropy allowed in the region. If we assume this, then we immediately reach the holographic entanglement entropy formula (44).

Before we conclude, let us discuss an example where we can apply the above covariant formula. We consider the AdS Vaidya solution

$$ds^2 = -(r^2 - m(v))dv^2 + 2dvdr + r^2 d\phi^2. \tag{47}$$

This is the solution to the Einstein equation with the negative cosmological constant in the presence of null matter whose EM tensor looks like $T_{vv} = \frac{1}{2r}\frac{dm(v)}{dv}$. The null energy condition requires $T_{vv} \geq 0$ and thus we find that $m(v)$ is a monotonically increasing function of the (light-cone) time v.

This background is asymptotically AdS_3 and if we assume that $m(v)$ is a constant, then it is equivalent to the static BTZ black hole [22] with the mass m. Thus our background (47) describes an idealized collapse of a radiating star in the presence of negative cosmological constant. The dual theory is expected to be a CFT in a time-dependent background. The time-dependence comes from the time-dependent temperature. We can now apply the covariant entanglement entropy formula (44) and in the end we find

$$S_A(v) = \frac{c}{3}\left[\log\frac{l}{a} + \frac{m(v)l^2}{6} + \cdots\right], \tag{48}$$

as the expansion of small $m(v)$. The null energy condition guarantees that this is a monotonically increasing function of time. This shows that the entanglement entropy in this background is a monotonically increasing function of time as is so in the second law of the thermal entropy. We believe this behavior of entanglement entropy in black hole formation processes is rather general. However, we would like to stress that we are not claiming that the entanglement entropy is always increasing. For example if we start with the system with maximally entangled, the entanglement entropy will decrease after a small perturbation due to the de-coherence phenomenon.

We would also like to mention that if we stay with the brane-world setup we mentioned before and consider the brane-world black hole, then the holographic formula (44) tells us that the quantum corrected entropy of the black hole on the brane is equal to the entanglement entropy in the same theory as pointed out in [23]. This is because the horizon of this black hole is actually an extremal surface.

5 Conclusions and Discussions

In this talk we have presented the holographic formula which computes the entanglement entropy in the dual QFTs. It takes the form of the area law and can be regarded as a generalization of the Bekenstein-Hawking entropy formula. We also gives a covariant formulation which is useful to analyze the holographic dual of the time-dependent background.

There are many interesting future problems. We will mention a few of them here. One thing which would hopefully be clear in near future is the question how much information the entanglement entropy contains. Since we have infinitely many choices of the subsystem A, the entanglement entropy include infinite amount of information. The natural question is whether the information of entanglement entropy in a given QFT is enough to extract the metric of its holographic dual spacetime.

Another intriguing future problem is to understand any implications of holography in cosmological background such as a de-Sitter space from the viewpoint of entanglement entropy. This will be directly related to the understanding of the mysterious horizon entropy of de-Sitter space.

Acknowledgments

I would like to thank very much the organizers of JGRG17 for the wonderful conference. I am also grateful to my collaborators: T. Azeyanagi, M. Headrick, T. Hirata, V. Hubeny, T. Nishioka, M. Rangamani, and S. Ryu.

References

[1] S. Ryu and T. Takayanagi, Phys. Rev. Lett. **96** (2006) 181602 [arXiv:hep-th/0603001]; "Holographic derivation of entanglement entropy from AdS/CFT," Phys. Rev. Lett. **96** (2006) 181602 [arXiv:hep-th/0603001].

[2] V. E. Hubeny, M. Rangamani and T. Takayanagi, "A covariant holographic entanglement entropy proposal," JHEP **0707**, 062 (2007) [arXiv:0705.0016 [hep-th]].

[3] G. 't Hooft, "Dimensional reduction in quantum gravity," [arXiv:gr-qc/9310026]; L. Susskind, "The World as a hologram," J. Math. Phys. **36**, 6377 (1995) [arXiv:hep-th/9409089]; D. Bigatti and L. Susskind, "TASI lectures on the holographic principle," [arXiv:hep-th/0002044].

[4] J. M. Maldacena, "The large N limit of superconformal field theories and supergravity," Adv. Theor. Math. Phys. **2**, 231 (1998) [Int. J. Theor. Phys. **38**, 1113 (1999)] [arXiv:hep-th/9711200]; O. Aharony, S. S. Gubser, J. M. Maldacena, H. Ooguri and Y. Oz, "Large N field theories, string theory and gravity," Phys. Rept. **323**, 183 (2000) [arXiv:hep-th/9905111].

[5] S. Kachru, R. Kallosh, A. Linde and S. P. Trivedi, "De Sitter vacua in string theory," Phys. Rev. D **68**, 046005 (2003) [arXiv:hep-th/0301240].

[6] T. Hirata and T. Takayanagi, "AdS/CFT and strong subadditivity of entanglement entropy," JHEP **0702** (2007) 042 [arXiv:hep-th/0608213].

[7] H. Casini and M. Huerta, "A finite entanglement entropy and the c-theorem," Phys. Lett. B **600** (2004) 142 [arXiv:hep-th/0405111].

[8] See for example, M. Nielsen, and I. L. Chuang, “Quantum Computation and Quantum Information”, Cambridge university press, (2000).

[9] G. Vidal, J. I. Latorre, E. Rico and A. Kitaev, “Entanglement in quantum critical phenomena”, Phys. Rev. Lett. **90**, 227902 (2003) [arXiv:quant-ph/0211074].

[10] A. Kitaev and J. Preskill, “Topological entanglement entropy,” Phys. Rev. Lett. **96**, 110404 (2006) [arXiv:hep-th/0510092]; M. Levin and X. G. Wen, “Detecting topological order in a ground state wave function,” Phys. Rev. Lett. **96**, 110405 (2006) [arXiv:cond-mat/0510613].

[11] L. Bombelli, R. K. Koul, J. H. Lee and R. D. Sorkin, “A Quantum Source Of Entropy For Black Holes,” Phys. Rev. D **34**, 373 (1986); M. Srednicki, “Entropy and area,” Phys. Rev. Lett. **71**, 666 (1993) [arXiv:hep-th/9303048].

[12] G. ’t Hooft, “On The Quantum Structure Of A Black Hole,” Nucl. Phys. B **256**, 727 (1985).

[13] P. Calabrese and J. Cardy, “Entanglement entropy and quantum field theory,” J. Stat. Mech. **0406**, P002 (2004) [arXiv:hep-th/0405152]; “Entanglement entropy and quantum field theory: A non-technical introduction,” [arXiv:quant-ph/0505193].

[14] C. Holzhey, F. Larsen and F. Wilczek, “Geometric and renormalized entropy in conformal field theory,” Nucl. Phys. B **424**, 443 (1994) [arXiv:hep-th/9403108].

[15] S. S. Gubser, I. R. Klebanov and A. M. Polyakov, “Gauge theory correlators from non-critical string theory,” Phys. Lett. B **428**, 105 (1998) [arXiv:hep-th/9802109]; E. Witten, “Anti-de Sitter space and holography,” Adv. Theor. Math. Phys. **2**, 253 (1998) [arXiv:hep-th/9802150].

[16] D. V. Fursaev, “Proof of the holographic formula for entanglement entropy,” JHEP **0609**, 018 (2006) [arXiv:hep-th/0606184].

[17] M. Headrick and T. Takayanagi, “A holographic proof of the strong subadditivity of entanglement entropy,” Phys. Rev. D **76**, 106013 (2007) [arXiv:0704.3719 [hep-th]].

[18] T. Azeyanagi, T. Nishioka and T. Takayanagi, “Near Extremal Black Hole Entropy as Entanglement Entropy via AdS2/CFT1,” arXiv:0710.2956 [hep-th].

[19] J. D. Brown and M. Henneaux, “Central Charges in the Canonical Realization of Asymptotic Symmetries: An Example from Three-Dimensional Gravity,” Commun. Math. Phys. **104** (1986) 207.

[20] R. Bousso, “A Covariant Entropy Conjecture,” JHEP **9907** (1999) 004 [arXiv:hep-th/9905177].

[21] L. Randall and R. Sundrum, “An alternative to compactification,” Phys. Rev. Lett. **83**, 4690 (1999) [arXiv:hep-th/9906064].

[22] M. Banados, C. Teitelboim and J. Zanelli, “The Black hole in three-dimensional space-time,” Phys. Rev. Lett. **69**, 1849 (1992) [arXiv:hep-th/9204099].

[23] R. Emparan, “Black hole entropy as entanglement entropy: A holographic derivation,” [arXiv:hep-th/0603081].

MOA II Gravitational Microlensing Survey
— A new generation microlensing survey —

F. Abe[1], I. A. Bond[2], A. C. Gilmore[3], J. B. Hearnshaw[3] , Y. Itow[1], K. Kamiya[1]
P. M. Kilmartin,[3] , K. Masuda[1] , Y. Matsubara[1], Y. Muraki[4]
T. Sako[1], D. J. Sullivan[5]
P. Tristram[3], and P. C. M. Yock[6]

[1]*Solar-Terrestrial Environment Laboratory, Nagoya University, Nagoya Aichi 464-8601, Japan*
[2]*Institute of Information and Mathematical Sciences, Massey University at Albany Auckland, New Zealand*
[3]*Department of Physics and Astronomy, University of Canterbury Christchurch, New Zealand*
[4]*Department of Physics, Konan University Kobe, Japan*
[5]*School of Chemical and Physical Sciences, Victoria University Wellington, New Zealand*
[6]*Department of Physics, University of Auckland Auckland, New Zealand*

Abstract

Observing gravitational microlensing events has become a powerful technique for studying dark objects and the surface profiles of distant stars. The MOA II microlensing survey is a Japan-New Zealand collaboration that detects microlensing events towards the Galactic Bulge and the Magellanic Clouds. A recently installed 1.8-m wide-field telescope, equipped with a large CCD camera, enabled us to make high-cadence observations of most bulge microlensing events for the first time. This new type of microlensing survey opened new vistas in the search for planets by microlensing, and also in the search for MACHOs. In this paper we review past observations and science of microlensing, and then describe the MOA II project and its strategy.

1 Introduction

Gravitational microlensing is both a natural application of the general theory of relativity, and also a potentially powerful tool in astronomy. The concept of gravitational lensing [1] was introduced by Einstein in 1936. In his paper, Einstein predicted two phenomena. One was the "Einstein ring". If two stars are perfectly aligned on a line of sight, the rays of light from the more distant star are bent by the gravitational field of the nearer star. As the bending angle is independent of the azimuthal angle, the rays form a circular image, the so-called Einstein ring. If the stars are nearly aligned, a pair of arcs is produced. However, Einstein said in his paper, "Of course, there is no hope of observing this phenomenon directly." In spite of 70 year's progress in observational technology, Einstein rings (or arcs) are still difficult to observe. The resolution of the current largest optical interferometer VLTI (Very Large Telescope Interferometer) is 2.2 msec. This may be compared with the diameter of the Einstein ring which is typically less than 2 msec. To date, only one attempt has been made to directly resolve such an image [2, 3], and this was not successful [2]. The other phenomenon that Einstein predicted was magnification. This is the apparent increase in brightness of the distant star caused by the gravitational lensing of the nearer star, when the integrated light of the Einstein ring or arcs is detected. This phenomenon was also thought to be difficult to observe. Einstein said "Therefore, there is no great chance of observing this

[1]E-mail:abe@stelab.nagoya-u.ac.jp
[2]However, Einstein arcs and rings have been observed with aligned galaxies, for which the characteristic angle is of order secs [4]

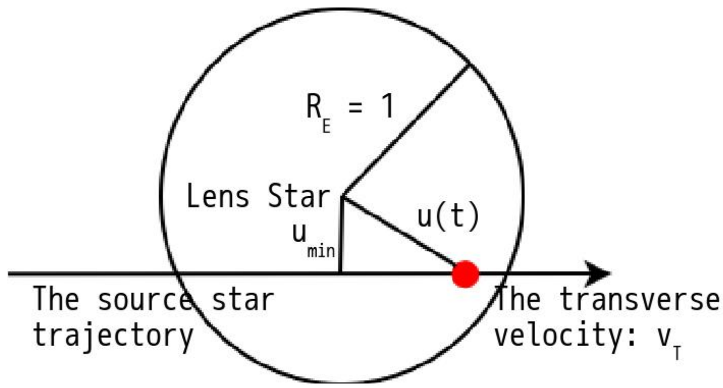

Figure 1: Configuration and definitions of parameters of a single lens event.

phenomenon, even if dazzling by the light of the much nearer star B is disregarded." However, modern technology now permits us to observe hundreds of microlensing events annually through the magnification effect.

The microlensing technique has been applied in a number of areas of astronomy. Because the effect is independent of the luminosity of the nearer star (i.e., the lens star), the technique can be applied to search for dark objects that are very difficult to detect by other means. Such dark objects might be, for example, MAssive Compact Halo Objects (MACHOs) [5], black holes [6], brown dwarfs, free-floating planets, and extrasolar planets. Microlensing can also be used to probe the more distant star (i.e., the source star). The magnification caused by microlensing depends sensitively on the angular separation between the lens and source stars, especially when the separation is small and the magnification is high. This enables the surface profile of a distant star to be resolved with remarkably high precision, allowing its atmosphere to be probed [7] or, in one case, its shape to be determined [8].

The search for MACHOs using microlensing [9] was originally proposed by Paczyński. If the stars in an external galaxy can be resolved, dark objects in the Halo in our galaxy may cause gravitational microlensing of them. This could be detectable through a change of the brightness of a resolved star. The magnification $A(t)$ by a single lensing object is

$$A(t) = \frac{u(t)^2 + 2}{u(t)(u(t)^2 + 4)^{1/2}}, \tag{1}$$

where, $u(t)$ is the projected distance between the source and the lens (see Fig.1),

$$u(t) = (u_{min}^2 + (v_T(t - t_0)/R_E)^2)^{1/2}, \tag{2}$$

u_{min} is the minimum $u(t)$, t_0 is the time of minimum, and R_E is the Einstein ring radius,

$$R_E^2 = \frac{4GMD}{c^2}, D = \frac{D_l D_{ls}}{D_s}, \tag{3}$$

where, G is the gravitational constant, M is the mass of the lens, c is the velocity of light, and D_l, D_{ls}, D_s are the distances between the observer and the lens, the lens and the source, the observer and the source, respectively. The variation of the brightness with time, i.e. the light curve, is symmetric before and after the peak (at t_0) and it is achromatic. The timescale of the event is characterized by the Einstein radius crossing time $t_E = R_E/v_T$. Typical values of t_E depend primarily on the masses of possible lenses, and are estimated to be $t_E > 200days$ for black holes, $6 < t_E < 150days$ for stars, $2 < t_E < 6days$ for brown dwarfs, and $t_E < 2days$ for planetary mass objects. As the time scales of most of events are expected to be several days or more, most past microlensing surveys included only one or a few observations/night.

The probability for a microlensing event to occur is expressed by the optical depth τ. Here τ is the probability for microlensing to occur on a star at a given instant. If the mass density of the lensing objects $\rho(D_l)$ is known, then τ can be deduced from the relationship

$$\tau = \int_0^{D_s} \frac{4\pi GD}{c^2} \rho(D_l) dD_l. \tag{4}$$

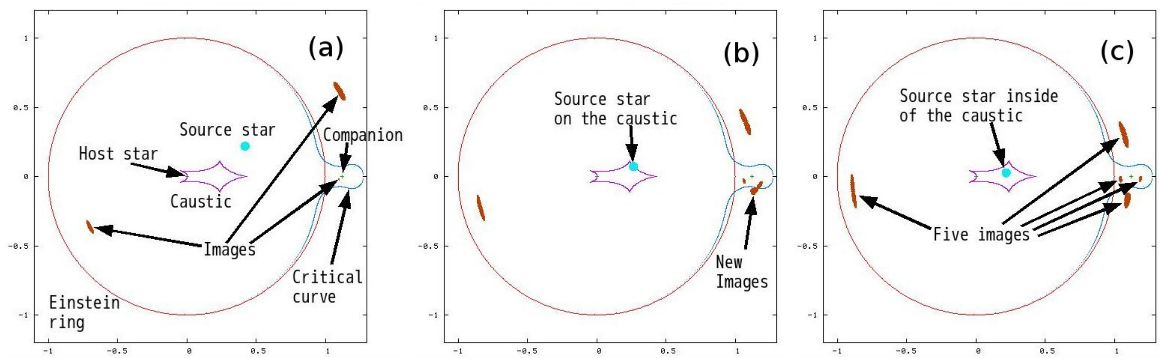

Figure 2: Configuration of binary lensing projected to the lens (host star and a companion) plane. When the source star is outside of the caustic (a), the number of images is 3. If the source star is on the caustic (b), new images appear. If the source star is inside of the caustic (c), the number of images is 5.

Typical estimated values of τ are $\sim 10^{-6}$. This implies that more than 10^6 stars must be monitored to find microlensing events. Thus, observations must be carried out toward crowded stellar fields (Magellanic Clouds, Galactic Bulge, or other galaxies), and wide-field surveys are necessary.

Using Paczyński's scheme, first generation surveys were performed to search for any dark matter in the form of MACHOs. These were conducted by MACHO (MAsive Compact Halo Object) [5], EROS (Expérience pour la Recherche d'Objects Sombres) [10], and OGLE (Optical Gravitational Lensing Experiment) [11]. Microlensing events towards the Large Magellanic Cloud (LMC) were reported by the MACHO and EROS groups, and toward the Galactic Bulge by the OGLE group. Since then, more than 3,000 microlensing events have been discovered, mostly in bulge fields. As the number density of stars in our Galaxy increases as the stellar mass decreases, the majority of microlensing events in the Galactic Bulge are expected to be caused by lenses that are low-mass red dwarfs.

A large fraction of the stars in our galaxy have companions. Such binary stars are expected to act as lenses for microlensing events too. But the magnification by a binary lens is complex compared with that of a single lens. The rays of light are bent by the host and the companion stars and are folded by each other. The magnification pattern on the source plane is divergent on closed lines named caustics. If the source star passes over a caustic, the light curve is singular. The magnification caused by binary lensing can be calculated by solving the lens equation,

$$\boldsymbol{\beta} = \boldsymbol{\theta} - \left(q_1 \frac{\boldsymbol{\theta}}{|\boldsymbol{\theta}|^2} - q_2 \frac{\boldsymbol{\theta} - \boldsymbol{l}}{|\boldsymbol{\theta} - \boldsymbol{l}|^2} \right) \tag{5}$$

where, β is the source position vector projected onto the lens plane in units of R_E, θ is the image position vector, l is the position vector of the companion (the host star is assumed at the origin), and q_1 and q_2 are the mass ratio of the host star and the companion, respectively. Solutions [12] to Eq. 5 were obtained by Scheneider and Weiβ. Recently, a simpler method [13] was devised by Asada. Figure 2(a-c) show images for a binary configuration determined by Asada's method. As seen in the figures, there are three images when the source star lies outside the caustic. When the source star moves inside the caustic, the number of images becomes five. Integrating over the images, the magnification of the lens may be calculated. Alternatively, the Inverse-Ray Shooting (IRS) method may be used for binary and more complex lenses. In the IRS method, rays of light generated by a hypothetical point source at the position of the observer are traced through the lens to the source plane. The density of rays on the source plane represents the magnification.

The light curve for binary lensing is generally quite complex and asymmetric. If the lens star has a planet, the lens may be treated as a binary with a small mass ratio. The detectability of extrasolar planets by gravitational microlensing was first treated in this manner[14]. The method is particularly effective for finding planets in the "lensing zone" which is an annular region from 0.6 to 1.6 R_E centred on the lens star. In this region, the anomaly caused by a planet is amplified. Simulations show that planets down to Earth-mass or less [15, 16] could be discovered in this region. A typical Einstein ring radius is

$2-4AU$ in bulge microlensing events. This region corresponds to that occupied by the asteroid belt in our solar system. As mentioned above, most Galactic Bulge microlensing events are caused by low-mass red dwarfs, so planets orbiting such low-mass stars are the most common target of the microlensing method. Planets may thus be detected by microlensing in very different regions from those explored by the radial velocity and transit techniques.

In summary, the MOA II project aims to seek and identify a fraction of Galactic Dark Matter that may exist in the form of MACHOs, and also to seek and identify extrasolar planets by gravitational microlensing. The present paper is organized as follows. Our previous project, MOA I, is described in Sec. 2, and extrasolar planets in Sec. 3. The MOA II project is introduced in Sec. 4. This includes discussion of the observing strategy that is being used in MOA II. Finally, a summary is given in Sec. 5.

2 MOA I project

Japan-New Zealand collaboration MOA (Microlensing Observations in Astrophysics) project was started in 1995. The observations were done toward Magellanic Clouds because the primary target was the MACHO search. Due to the raising interest of extrasolar planet, observations toward Galactic bulge were started later. The observations were performed with use of 61 cm B & C telescope in Mt. John university observatory ($170.°28'E, 43.°59'S$), New Zealand. The first CCD camera was MOA-cam1 which had 9 $1k \times 1k$ TI chips. Large mosaic CCD camera MOA-cam2 [17] which had 3 $2k \times 4k$ SITe CCD chips was installed in 1998. One of the advantages of Mt. John is its unique location. Mt. John is the southernmost astronomical observatory in the world except for Antarctica. In winter (June and July), the Galactic bulge passes close to the zenith at midnight. Due to the high latitude, the bulge observation can be continued more than 13 hours. Mt. John is a good observation site for Magellanic Clouds too. Due to the high latitude, Magellanic Cloud don't set. Observations can be done anytime in clear nights.

In spite of the small aperture, MOA I obtained a number of scientific results: measurement of optical depth toward Galactic bulge [18], measurements of the atmosphere [19] and the shape [8] of a distant star, period-luminosity relation of long-period variables in LMC [20], Candidate of extrasolar planet transits [21], etc. The highlight of MOA I is discovery of the first extrasolar planet with microlensing [22]. We will mention this discovery in Sec. 3. The MOA I microlensing alert was started in 2000 and continued until 2005. The numbers of alerts were 13-74 alerts/year. After 10 years MOA I survey, MOA II took over microlensing survey.

3 Extrasolar planets

Finding planets outside of the solar system is one of the most exciting issues in current astronomy. Since first discovery [23] of extrasolar planet orbiting around a sun-like star, more than 200 planets [24] have been discovered. Most of them were discovered with radial-velocity method which detects periodic change of radial velocity of the host star caused by the planet. As this method is more sensitive to massive close-in planets, most of the planets discovered are massive or close-in planets. Discovery of a number of close-in giant planets named "hot Jupiters" raized discussions [25] wheter our solar system is special or not. However this question is hard to answere because access to low-mass wide orbit planets have been very difficult.

Looking back to our solar system, eight planets are orbiting around the sun. They can be categorized into three types: rocky (terrestrial) planets, gas giants (Jovian planets), and icy (uraniun) planets. Inner four planets (Mercury, Venus, Earth, and Mars) are rocky planets which have solid rocky surfaces. Jupiter and Saturn are gas giants which don't have solid surface and covered with hydrogen and helium gases. Outer two planets (Uranus and Neptune) are icy planets which have solid ice surfaces.

The standard model of the planet formation is the core-accretion model [26]. In this model, dusts in the protoplanetary disk are coagulated then formed kilo-meter size planetesimals. The main component of the dusts is expected to be silicates at inside and ice at outside (less than melding point). Thus the core of the planets are formed with rocks at inside and ices at out side. The planetesimals are collide each other and form larger objects named protoplanets. Planets are formed by giant collisions of protoplanets. At the final stage of planet formation, the cores of planets at right outside of the "snow line" absorb the

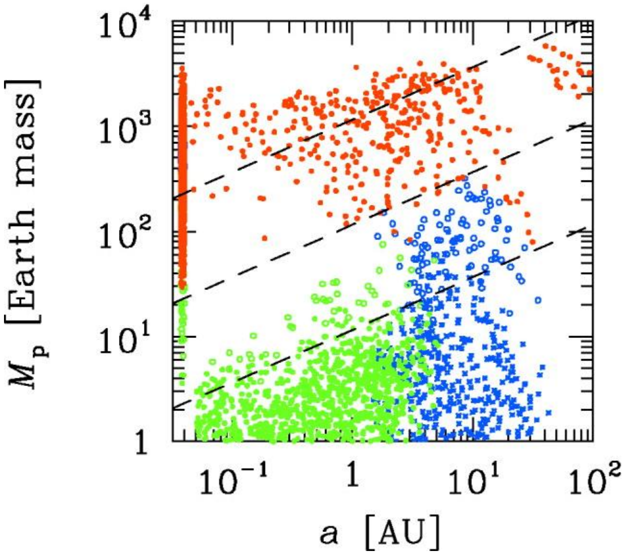

Figure 3: A result of a simulation [27] of the core-accretion model. Planet mass vs. semi-major axis. Red points represent gas giants, blue points are icy planets, and green points are rocky planets.

gas around them and gas giants are generated. This model succeeded to explain our solar system very well. A number of simulation studies have been made with this model. Figure 3 shows one of the results [27] of the simulation for a sun-like star. As shown in the figure, there are a number of rocky planets inside of the snow line ($\sim 2 - 3AU$) and icy planets in the outside. However, access to the low-mass rocky or icy planets was very difficult with conventional planet search. To confirm core-accretion model at extrasolar planetary system, new method has been necessary.

As we have mentioned, the microlensing planet search [14] was proposed by Mao and Paczyńscky in 1992. But the real discovery was difficult. After several pioneering attempt, the first extrasolar planet with microlensing [22] was discovered in 2003 by MOA I and OGLE. Anomaly in the light curve was discovered in OGLE 2003-BLG-235/MOA 2003-BLG-053 microlensing event. Figure 4 shows the light curve of OGLE 2003-BLG-235/MOA 2003-BLG-053. From the detailed analysis of the light curve, the mass ratio of the planet and the host star was determined to be $0.0039^{+0.0011}_{-0.0007}$ and separation to be 1.120 ± 0.007. To determine absolute values of the masses and the separation, determination of the distance to the lens system is necessary. As the determination of the distance from the observations is very difficult, the first estimate was done using stochastic method with a Galactic model. The obtained values were about $1.5M_J$ for the planet mass and about $3AU$ for the separation. In 2006, Hubble Space Telescope observed [28] the motion of the host star, then the proper motion and the distance were constrained. Using this constraint, the planet mass and the separation were better determined to be $2.6^{+0.8}_{-0.6}M_J$ and $4.3^{+2.5}_{-0.8}AU$, respectively. The microlensing planet search is thought to be potential method to discover down to earth-mass planet or less [15, 16]. But the first discovery was still a giant planet.

4 MOA II project

The MOA II project was started in 2002. New telescope which has 1.8-m aperture was installed in Mt. John Observatory in 2004. Figure 5 shows the 1.8-m telescope and the dome. To achieve very wide field of view, a prime focus optics with a parabolic primary mirror and four corrector lenses was adopted (see Fig. 6). This optics was effective to make wide-field telescope in a limited cost, because making primary mirror become much easier than short-focal length Ritchey-Crétien optics and no secondary mirror was needed. A new CCD camera named MOA-Cam3 [29] which has 10 $2k \times 4k$ E2V CCD chips was installed at the focal point. Figure 7 shows MOA-cam3 CCD camera. This system has strong advantages compared

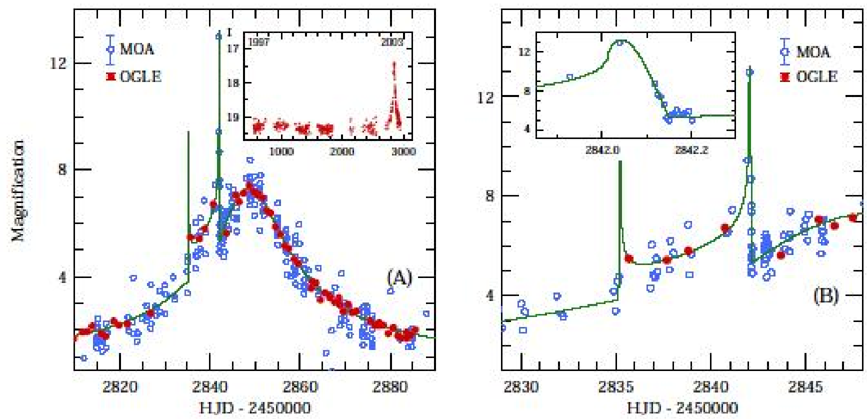

Figure 4: Discovery of first extrasolar planet with microlensing. The light curve of the microlensing event OGLE 2003-BLG-235/MOA 2003-BLG-053 [22] is shown. Two sharp peaks are caused by caustic crossing.

to past and on-going microlensing surveys. Table 1 shows comparison of the performances of microlensing surveys. The field of view was $2.2 degree^2$ which is about 6 times wider than that of OGLE. This wide field of view enabled us to take new observation strategy: high-cadence observation. There are two kinds of strategies in microlensing planet search: high magnification and high-cadence observations for all of the events. The difference of the strategies is due to the shape of the caustics of the planetary microlensing.

Figure 8 shows a magnification pattern of a planetary lensing. There are two kinds of caustics in the planetary lensing: central caustics and planetary caustics. The central caustics are always around the host star, thus the anomaly by the central caustics always appear [30] around the peak of high-magnification event. On the other hand, planetary caustics are hard to predict where they are. That means predicting anomaly is impossible for the planetary caustics. To detect anomaly caused by central caustics, watching peaks of high-magnification events is a clear very efficient strategy because observers can be concentrated into limited number of events and limited time. Once such event is discovered, no large CCD cameras are required. There are four major groups in microlensing observations: OGLE, MOA, PLANET/ROBOnet, and μFUN. In these groups, OGLE and MOA have large CCD cameras and working on microlensing event surveys. As the primary target is to find microlensing events, most of the telescope times are used for the microlensing survey. The other groups PLANET/ROBOnet and μFUN are working on follow-up observations of the events discovered by OGLE and MOA. These observations are done in target of opportunity base and no large CCD camera is used. Thus their observations are concentrated around the peaks of high-magnification events and specific target events they are interested in.

Table 1: Comparison of microlensing surveys

	MACHO	EROS	OGLE	MOA I	MOA II
Aperture (m)	1.27	1.0	1.3	0.61	1.8
FOV (deg^2)	0.5	0.938	0.325	1.27	2.18
Site	Australia	Chile	Chile	NZ	NZ
Status	Finished	Finished	Active	Finished	Active

In spite of the effectiveness of the high-magnification strategy, this method is thought to be inefficient to find low-mass planets. The size of the central caustic is proportional [31] to the mass ratio q and shrinks quickly with the mass ratio decrease. On the other hand, the size of the planetary caustics are

Figure 5: MOA II 1.8 m telescope at its opening ceremony.

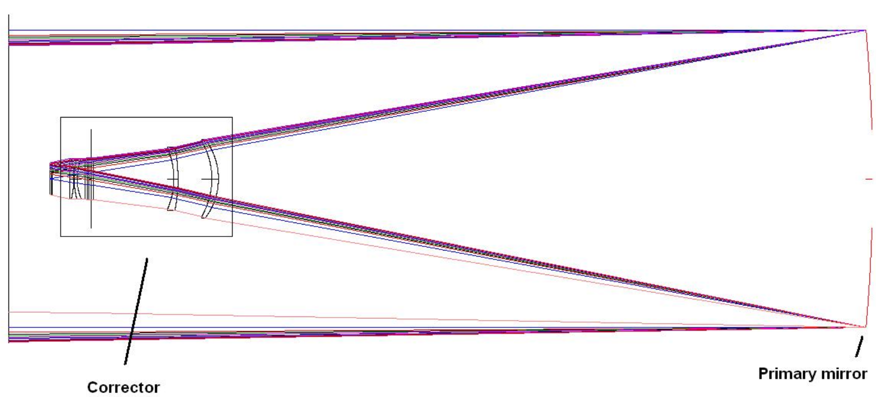

Figure 6: Optics of the MOA II telescope. A simple prime focus with a parabolic primary mirror and for corrector lenses was adopted.

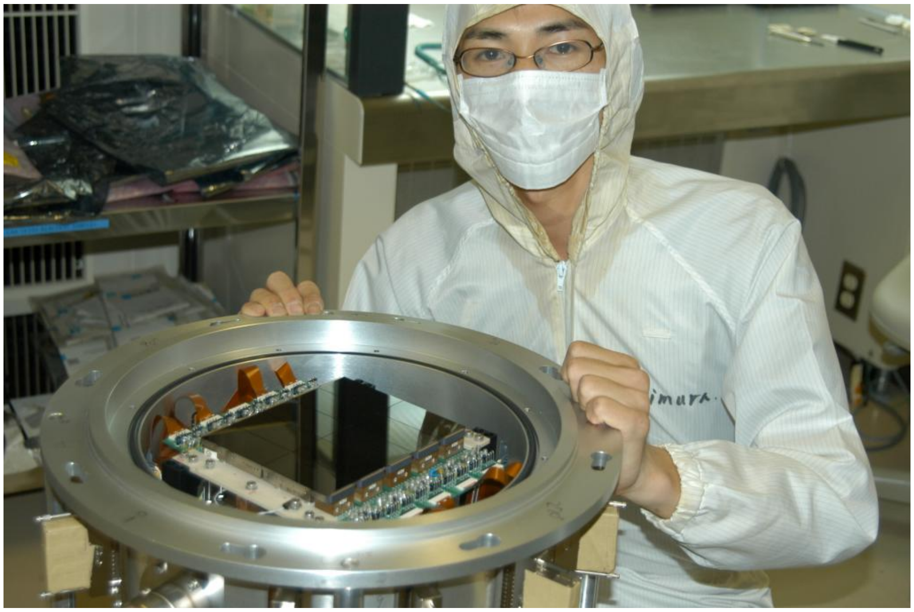

Figure 7: A large CCD camera MOA-cam3. The effective area is $12cm \times 15cm$.

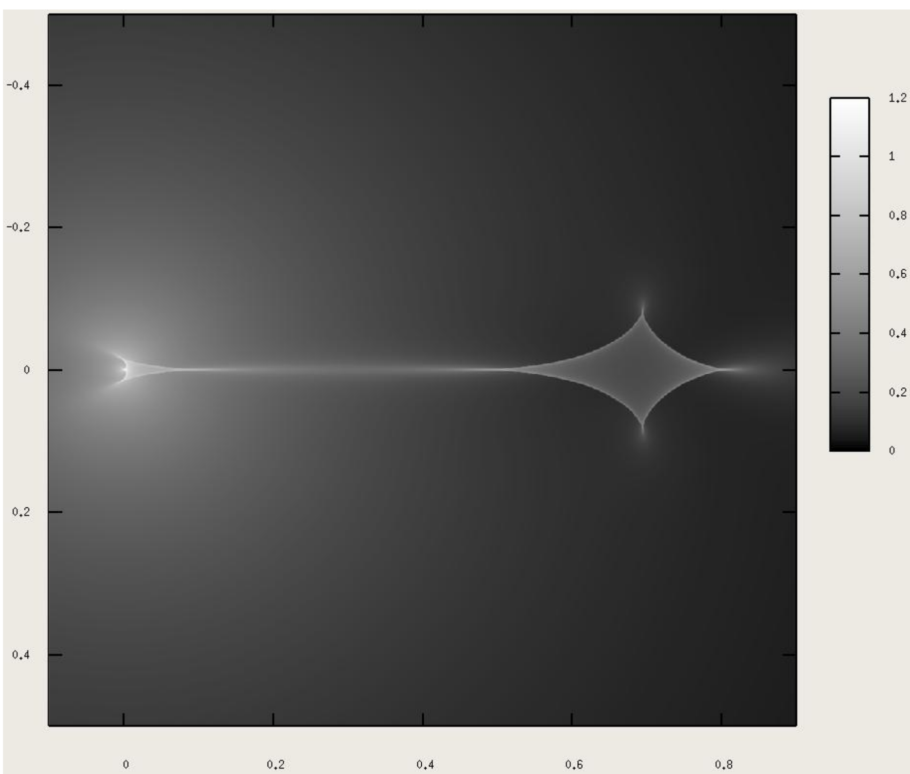

Figure 8: A magnification pattern of a planetary lensing. The host star is at origin, and the separation of the planet is 1.4 (outside of this figure). The mass ratio is 0.01. The small wedge shape caustic (left) is the central caustic and a large diamond shape caustic (right) is the planetary caustic.

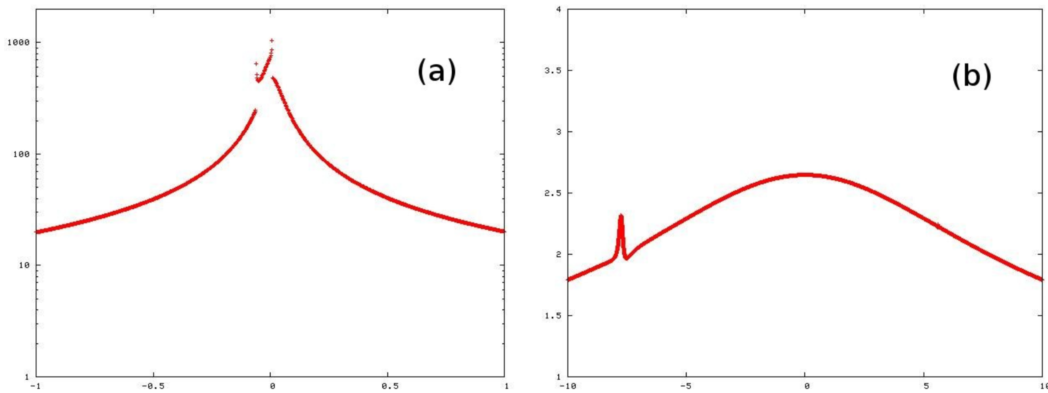

Figure 9: Light curves of a central caustic event (a) and a planetary caustic event (b). The anomaly by a central caustic always appear around the peak of a high-magnification event. The anomaly by a planetary caustic is hard to predict.

proportional [32] to the square root of the mass ratio. Anomaly shrinks both in time and change of brightness as the size of the caustic decrease. Thus finding planetary caustics are expected to be more efficient than finding central caustics. However, finding planetary caustic is more difficult because there is no prediction of anomaly to appear. Taking strong strategy such as high magnification is impossible to find planetary anomaly. Simply watching most of the events almost uniformly in time is only possible strategy. In this scheme, wider field of view is more efficient because higher-cadence observation can be done for most of the microlensing events.

The MOA II observation has started in 2005. The observations are being done for the 22 Galactic bulge fields. The exposure time is 60 seconds each. These 48 $degree^2$ are scanned every one hour. To find very short anomaly caused by low-mass planet, central 2 fields are observed every 10 minutes. A real time analysis is beeing done to find microlensing events on time. To find microlensing events efficiently, a Difference Image Analysis (DIA) [33] is used in the real time analysis. The MOA II microlensing alert system has started in 2006 for the Galactic bulge fields. The number of events were 168 in 2006 and 488 in 2007.

In 2005, an exciting microlensing event OGLE 2005-BLG-390 [34] was occurred. Figure 10 shows the light curve of this event. As seen in the figure, a small bump appeared on a single lens curve. From detailed analysis of the light curve, the bump is found to be caused by a low-mass planet. The mass of the planet was estimated to be $5.5^{+5.5}_{-2.7}M_{\oplus}$ and the separation to be $2.6^{+1.5}_{-0.6}AU$, where $M_{\oplus}$ is the mass of the Earth. At that time, it was the lowest mass planet discovered outside of the solar system. The host star was a low-mass ($M = 0.22^{+0.22}_{-0.11}M_{\odot}$) M dwarf. Combined with the separation, the surface temperature was estimated to be $\sim 50K$, a cool icy planet. It is the first discovery of extrasolar icy planet. MOA II succeeded to observe second peak caused by the planetary caustic. That means the MOA II wide-field survey itself can be a powerful follow-up observation for most of the microlensing events. The discovery of the low-mass planet shows possibilities of discovery of Earth-mass planet with microlensing in near future.

In spite of the microlensing surveys by MACHO and EROS groups, the fraction of MACHOs in the Galactic halo is still not well determined and a controversial issue in the dark matter problems. In 2000, the MACHO group reported [35] that the fraction of MACHOs is 20% for a typical halo model with a 95% confidence interval of 8%-50%. Although some of them were found to be variable stars, the reanalysis [36] of the data showed that the MACHO fraction is still 0.16 ± 0.06. On the other hand, EROS group reported a microlensing event in LMC previously. However they reported later that the events are not due to the microlensing but a variable star. They analyzed all of their LMC data and concluded that they have no candidate and set an upper limit [37] to the MACHO fraction. Figure 12 shows the final result of EROS group and that of MACHO group for comparison. As shown in the figure, there are discrepancies between EROS and MACHO results although a common small allowed region around $0.2 < M < 1.0$ and $0.05 < f < 0.1$. In addition, there are lots of discussions about the locations of the lensing objects:

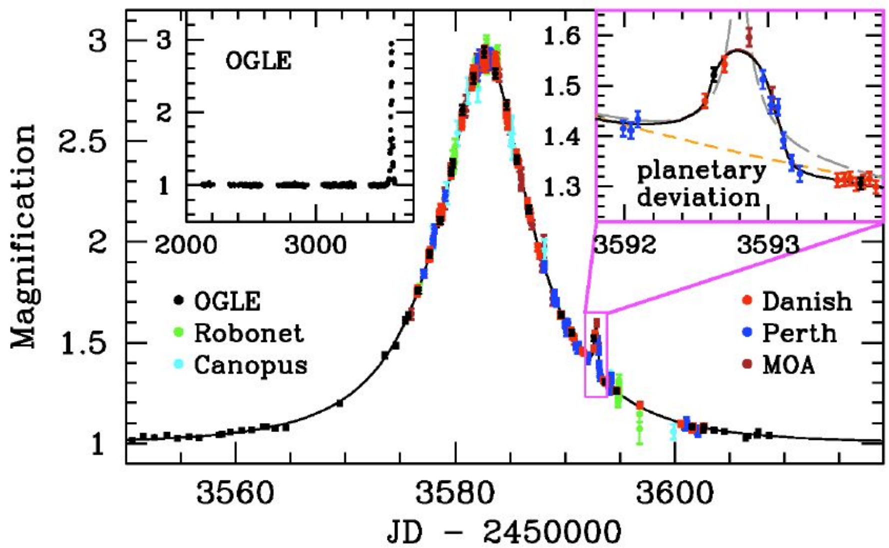

Figure 10: Discovery of first extrasolar icy planet. Light curve [34] of the microlensing event OGLE 2005-BLG-390 is shown.

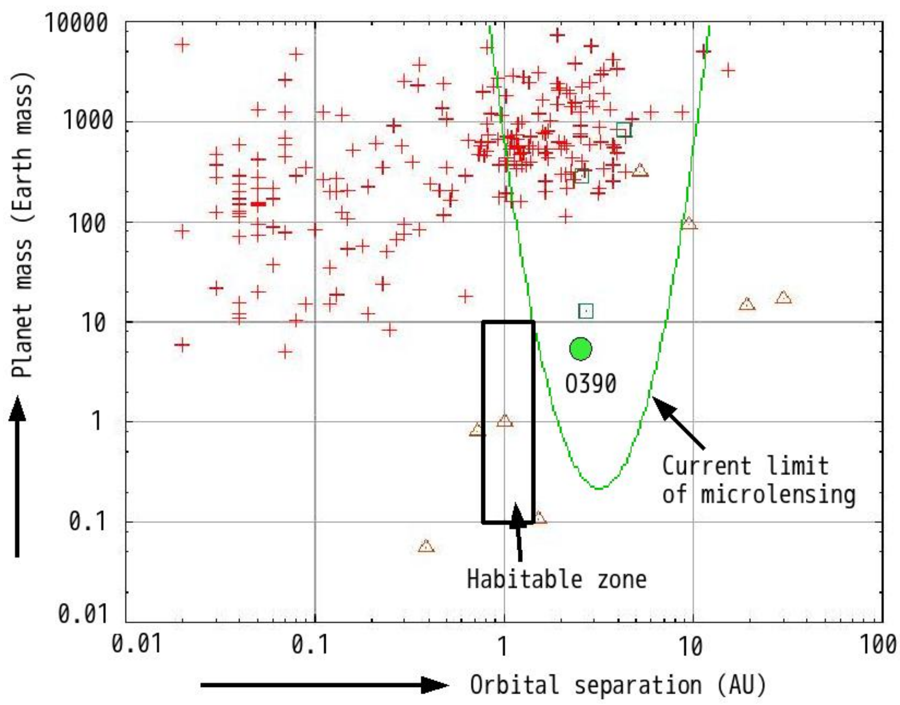

Figure 11: Extrasolar planets discovered with radial velocity and microlensing. The planet masses vs. the orbital separations are shown. The red crosses are discoveries with radial velocity method. Green squares are discoveries with microlensing. The brown triangles show solar system planets. The green circle is the planet discovered in OGLE 2005-BLG-390.

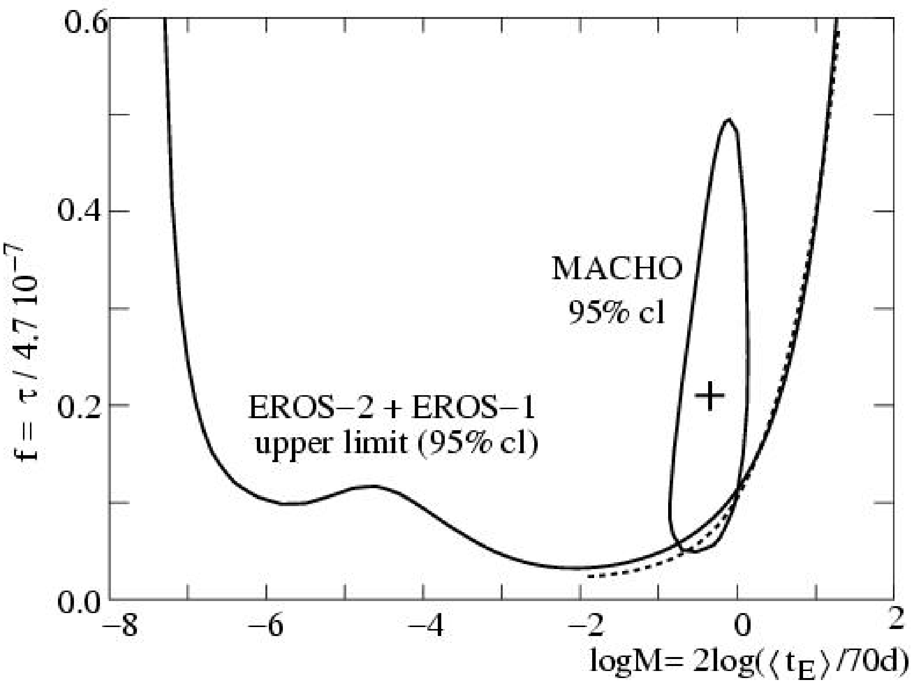

Figure 12: Results of past microlensing surveys toward Magellanic Clouds. The fraction [37] of MACHOs in the Galactic halo vs. the mass are shown. The 95% cl allowed area imposed by MACHO group and 95% cl upper limit imposed by EROS group are shown. The solid lines show LMC results. The dased line show EROS result including a SMC event.

lensings by MACHOs or lensing by LMC stars.

One of the aims of the MOA II project is to solve the MACHO problem and obtain well constrained value of the MACHO fraction. There are several advantages in MOA II to study MACHOs compared to other groups. The larger aperture enables us to observe more stars then to obtain more statistics of the microlensing events. The wide field of view enables us high-cadence observations to obtain well sampled light curves. Well sampled light curves are useful to discriminate background supernovae as well as variable stars. The locations of the lensing objects can be expected to be inferred from detailed analyses of the light curves if the parallax or finite source effect takes place. Well sampled light curves are useful for such analyses too. The high-sampled data around the peak of microlensing events are useful to find finite-source effects. From the analyses of finite-source effects, distances to the lens objects can be constrained. Durations of anomalies caused by finite-source effect are expected to be several hours to several days. In the past surveys, observations have been limited to a few times per night. Detecting short anomalies have been difficult. We are observing 14 LMC fields and 2 SMC fields in 300 second exposure time each. The central three fields are being observed every 30 minutes, while other fields are observed a few times every night. The MOA II survey is expected to obtain high sampled well constrained results in the MACHO problems.

5 Summary

Thanks to progress made in recent years in modern CCD technology, microlensing observations have become a powerful tool in astronomy. Observations of microlensing have been applied to seek dark objects and to probe distant stars. The first planet detection by microlensing was made jointly by MOA I and OGLE. Following this discovery, the method has matured and become a powerful method for planet hunting. Observations with the 1.8-m MOA II telescope commenced in 2005 using the MOA-cam3 CCD camera. Its wide field of view is being utilized to carry out high-cadence observations towards the Galactic Bulge and the Magellanic Clouds. This observational strategy has opened new channels for planet discovery, including the discovery of low-mass planets. The discovery of a 5.5 Earth-mass planet in OGLE 2005-BLG-390 event confirmed the efficacy of the high-cadence strategy. In the MACHO search, high-cadence observations toward the LMC and the SMC are expected to impose strict constraints on the fraction of MACHOs in halo of our galaxy.

The MOA II project is supported by the Ministry of Education, Culture, Sports, Science and Technology (MEXT), the Japan Society for Promotion of Science (JSPS), and the Marsden Fund of New Zealand.

References

[1] Einstein, A., Science 84, 506, 1936.

[2] Delplancke, F., Górski, K. M., Richichi, A., A & A 375, 2001.

[3] Rattenbury, N. J., Mao, S., MNRAS 365, 792, 2006.

[4] Cahntry, V. and Magain, P., A & A 470, 467, 2007.

[5] Alcock, C. et al., Nature 365, 621, 1993.

[6] Bennett, D. P., ApJ 579, 639, 2002.

[7] Alcock, C. et al., ApJ 491, 436, 1997.

[8] Rattenbury, N. J. et al., A & A 439, 645, 2005.

[9] PaczyńNatureski, B., ApJ 304, 1, 1986.

[10] Aubourg, E. et al., Nature 365, 623, 1993.

[11] Udalski, A. et al, Acta Astron. 43, 289, 1993.

[12] Scheneider, P. and Weiβ, A., A & A 164, 237, 1986.

[13] Asada, H., A & A 390, L11, 2002.

[14] Mao, S. and Paczyński, B., ApJ 374, 37, 1991.

[15] Bennett, D. P. and Rhie S. H., ApJ 472, 660, 1996.

[16] Dominik, M. et al., MNRAS 380, 792, 2007.

[17] Yanagisawa, T. et al., Exper. Astron. 10, 519, 2000.

[18] Sumi, T. et al., ApJ 541, 204, 2003.

[19] Abe, F., A & A 411, L493, 2003.

[20] Noda, S. et al., MNRAS 330, 137, 2002.

[21] Abe, F. et al., MNRAS 364, 325, 2005.

[22] Bond I. A. et al., ApJ 606, L155, 2004.

[23] Major, M. and Queloz, D., Nature 378, 355, 1995.

[24] Schneider, J., http://exoplanet.eu/

[25] Beer, M. E. et al., MNRAS 354, 763, 2004.

[26] Kokubo, E., and Ida, S., ApJ 581, 666, 2002.

[27] Ida, S. and Lin, D. N. C., ApJ 616, 567, 2004.

[28] Bennett, D. P., et al., ApJ 647, L171, 2006.

[29] Sako, T. et al., Exper. Astron., to be published.

[30] Griest, K., and Safizadeh, N., ApJ 500, 37, 1998.

[31] Chung, S.-J. et al., ApJ 630, 535, 2005.

[32] Han, C., ApJ 638, 1080, 2006.

[33] Bond, I. A. et al., MNRAS 327, 868, 2001.

[34] Beaulieu, J.-P. et al., Nature 439, 437, 2006.

[35] Alcock, C. et al., ApJ 542, 281, 2000.

[36] Bennett, D. P., ApJ 633, 906, 2005.

[37] Tisserand, P. et al., A & A 469, 387, 2007.

Dynamics of Plasma around Black Hole and the Relativistic Jet Formation
— Power of GRMHD simulations —

Shinji Koide[1]

[1] *Department of Physics, Kumamoto University, Kumamoto 860–8555, Japan*

Abstract

We review the topics of the relativistic jets in the universe and plasma around the black hole, which was presented in our talk at JGRG17. Expecially, we emphasize the power of general relativistic magnetohydrodynamics (GRMHD) numerical simulations in analyzing the physics of relativistic plasmas around the black holes.

1 Introduction

Superluminal motions have been observed from active galactic nuclei (AGNs), such as the elliptical galaxy M87 and the classical quasar (QSO) 3C273 [1, 2]. The apparent speed of the superluminal motion from M87 is $v_{\rm ap} = (5 \sim 6)c$, where c is the light speed. These motions are explained by the propagation of blobs which are directed almost toward us with the Lorentz factor larger than $v_{\rm ap}/c$. This is believed to be an evidence of the relativistic jet ejected from AGNs. The scale of this kind of jets reaches to several Mega light-years.

In out galaxy, superluminal motions were also observed from radio objects such as GRS1915+105 [3]. The apparent speed of this superluminal motion is several times light speed, and then the velocity of the jet is estimated to be $(0.8 - 0.9)c$. These objects are called micro-quasars (micro-QSOs). The scale of this jets is several light-years. Recently, observations suggest that gamma-ray bursts (GRBs) also include the relativistic jets. The Lorentz factor of this jet is several hundreds and its scale is several light-years [4].

In spite of the drastic differences of the Lorentz factors and the scales of the relativistic jets, their formation mechanism may be common. That is, at the footpoint of the relativistic jet, a rapidly rotating black hole exists, and the drastic phenomena in the disk around the black hole cause the relativistic jet [5]. However, the distinct mechanism of the jet, that is, the acceleration of the plasma near the black hole to the relativistic regime and the collimation of the relativistic plasma flow, has not been confirmed yet. A number of mechanisms have been proposed until now. These mechanisms are classified by the kinds of driven force of the jet: the forces are magnetic force, radiation pressure, and gas pressure. Recently, the magnetic mechanism has been considered most promising among them, because it can explain both the acceleration and collimation of the jet at once. Here we concentrate on the feature with respect to the magnetic mechanism of the jet formation. To investigate the magnetic mechanism of the relativistic jet formation around the black hole, we have to consider the interaction between the plasma and the magnetic field around (near) the black hole. The simplest approximation of the plasma in the magnetic field around the black hole is given by the ideal general relativistic magnetohydrodynamics (GRMHD) equations. The ideal GRMHD equations are constituted by the general relativistic conservation laws of particle number, momentum, and energy, and the general relativistic Maxwell equations with zero electric resistivity. Here, we usually use the adiabatic equation of state, which is not so good approximation of the relativistic plasmas [6].

At early stage, the GRMHD was studied analytically with the assumptions of the steady-state and the axisymmetry of the plasma and magnetic field around the black hole [7]. The equations consist of the poloidal wind equation (Bernoulli equation) and the MHD equilibrium equation of magnetic flux surfaces (Grad-Shafranov equation). Recently, the equations were solved within the approximation of special relativistic poloidal wind equation and the region far from the black hole [8]. The solution shows

[1] E-mail:koidesin@sci.kumamoto-u.ac.jp

clearly that the parabolic collimation relativistic jet whose Lorentz factor is several tens can be formed. However, it does not clearly show the solution around the footpoint of the relativistic jet near the black hole. Generally speaking, it is difficult to solve the GRMHD equations analytically in the neighborhood of the black hole to the infinity. Here, the numerical method becomes demanded because it provides the solution of the whole region from the closed vicinity of the black hole to the infinity consistently. Within the ideal GRMHD, the numerical technique similar to that of nonrelativistic MHD is applicable [9, 10, 11], and this has caused the rapid development of GRMHD simulations recently.

2 GRMHD numerical simulations

To present the power of the GRMHD numerical simulations for analysis of the relativistic plasma around the black hole, we show two topics with respect to the energy extraction from the black hole through the magnetic field and the formation of the relativistic jet from the black hole magnetosphere.

2.1 Energy extraction from rotating black hole through magnetic field

We performed numerical GRMHD simulations of rather simple system of the initially uniform rare plasma and the uniform strong magnetic field around the rapidly rotating black hole whose rotation parameter is $a = 0.99995$ [12, 13]. The numerical simulations showed that the magnetic field lines across the ergosphere are twisted by the frame-dragging effect quickly. The twist of the magnetic field lines propagates along the magnetic field lines as torsional Alfven waves. Through the torsional Alfven waves, the electromagnetic energy is emitted from the ergosphere powerfully. The energy-at-infinity of the plasma decreases and eventually it becomes negative. The negative energy-at-infinity corresponds to the negative mass. When the plasma with the negative energy-at-infinity falls into the black hole, the energy of the black hole swallowing the negative energy-at-infinity plasma reduces. This process clearly shows the energy extraction from the black hole through the magnetic field. This process is called "MHD Penrose process" [14] because it extracts the black hole energy through the negative energy-at-infinity of the matter, like the Penrose process [15]. To realize the negative energy-at-infinity, the plasma have to get the angular momentum opposite to the that of the black hole, like the Penrose process. The total angular momentum is conserved, and thus the redistribution of the angular momentum is needed to realize the negative energy-at-infinity. The Penrose process uses the particle fission to redistribute the angular momentum, while in the MHD Penrose process, the magnetic tension redistributes the angular momentum. It is noted that the Blandford-Znajek mechanism [16] uses the negative electromagnetic energy-at-infinity, while the MHD Penrose process uses the negative energy-at-infinity of plasma [13].

2.2 Relativistic jet formation

This is the one of the main subjects of the GRMHD numerical simulations. In the case of initially uniform magnetic field, the whole plasma falls into the black hole along the magnetic field, while the electromagnetic energy propagates outwardly along the magnetic field lines. This shows the uniform magnetic field severely forms the jet from the ergosphere, at least without the disk around the black hole. This is because the centrifugal force can't accelerate the plasma outwardly effectively. In the case of the split monopole type initial magnetic field, the relativistic outflow is formed due to the centrifugal force [17]. The frame-dragging effect of the rapidly rotating black hole whose rotation parameter is $a = 0.99995$ twists the magnetic field lines across the horizon. The magnetic field lines are shaped like a propeller screw. The rapidly rotating propeller screw accelerates the plasma around the black hole outwardly effectively. The Lorentz factor reached to 2.0 in the numerical simulation at $t = 6.5\tau_S$, where τ_S is a unit of time, which is defined as the Schwarzschild radius r_S divided by the light speed c. This type of outflow formation was also shown in the nonrelativistic MHD calculations of the system consisted of a central star, an accretion disk, and magnetic field across the disk with both the analytical and numerical methods [18, 19, 20]. The relativistic outflow shown by the GRMHD simulation is not collimated and does not become a relativistic jet. The split monopole magnetic field forms the relativistic outflow, but not the relativistic jet. The jet formation depends on the magnetic configuration around the black hole sensitively.

Next we performed the simulations with more realistic magnetic configurations. Generally speaking, the dynamo effect in the accretion disk creates the closed magnetic field lines. Such a closed line of force is unstable for magnetorotational instability [21]. The inner part of the magnetic field line falls into the black hole, while the outer part of the line of force shifts outwardly. Then the magnetic field line bridges between the ergosphere and the disk. Such a "magnetic bridge" between the ergosphere and the disk may be plausible around the black hole. We performed the GRMHD simulations with the magnetic bridge between the ergosphere and the disk around the rapidly rotating black hole as an initial condition (Fig. 1) [22]. The numerical results showed that the magnetic bridge is twisted by the frame dragging effect rapidly and the magnetic pressure in the magnetic bridge increases quickly. The large gradient of the magnetic pressure blows off the plasma near the black hole and the outflow is collimated by the magnetic tension to form the jet eventually. Similar type jet formation was found in the non-relativistic MHD simulations of the system with a star, disk, and the dipole magnetic field [23]. Unfortunately, the velocity of the jet shown by the GRMHD simulation is $(0.5 - 0.6)c$, i.e., sub-relativistic. Recently, longer-term, larger-scale GRMHD simulations were performed by McKinney [24]. They showed that in the large scale ($\sim 10^4 r_{\rm S}$), the relativistic low-density jet is formed, whose Lorentz factor is $5 \sim 7$.

3 Summary and future prospects

In this report, we review the numerical results of GRMHD briefly. Especially, we focused on two topics: the energy extraction from the rotating black hole and the magnetically driven formation of the relativistic jets. The former confirms the realization of the MHD Penrose process [12, 13] and the latter clarified the detailed structure of the magnetically-driven relativistic jet formation [24]. Here we briefly mention the future prospects of the GRMHD simulations for each astrophysical object.

1. **AGN jets, micro-QSO jets:** In these objects, the radiation can not be neglected. To include this effect, we have to develop the numerical technique of "radiation GRMHD". The electron-positron pair creation/annihilation is also important, and the other atomic processes should be considered.

2. **GRB jets:** With respect this type of jet, the radiation and the atomic processes are important, especially the neutrino creation/annihilation is important when we consider a collapsar as a model of the progenitor [25]. The self-gravity of the disk around the black hole should also be considered. To include this effect, we have to solve the Einstein equations [26].

In the point of the plasma physics, we have to consider the electric resistivity. In the "resistive" GRMHD, magnetic reconnection is properly calculated. The magnetic reconnection may cause crucial phenomena near the black hole, e.g., the magnetic reconnection in the ergosphere may extract the rotation energy of the black hole [27]. The other effect of the plasma such as the Hall effect may be important. To include these effects, we have to use the generalized Ohm's law or general relativistic two-fluid approximation instead of the GRMHD. The beak-down of the GRMHD approximation near the black hole will be examined with these new numerical methods.

Acknowledgments
We thank M. Koide for her important comments on this manuscript.

References

[1] Biretta, J. A., Sparks, W. B., & Macchetto, F. 1999 Astrophys. J., 520, 621.

[2] Pearson, T. J. & Zensus, J. A. 1987, in *Superluminal Radio Sources*, edited by J. A. Zensus and T. J. Pearson (Cambridge Univ., London), 1.

[3] Mirabel, I. F. & Rodriguez, L. F. 1994, Nature, 371, 46.

[4] Kulkarni, S. R. 1999, Nature, 398, 389.

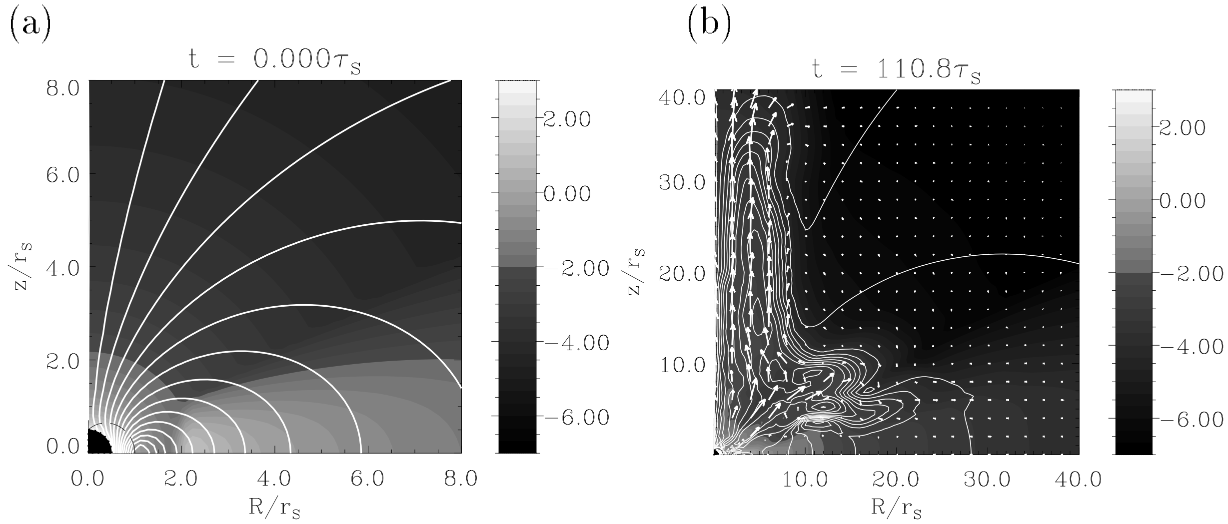

Figure 1: A result of GRMHD numerical simulation of the case with current loop around the rapidly rotating black hole whose rotation parameter is $a = 0.99995$ [22]. The black quarter circle region in the lower-left corner shows the inside of the black hole horizon, and the broken line shows the surface of the ergosphere. The white solid lines indicate the magnetic surfaces, the arrows are the plasma poloidal velocity, and the grey-scale shows the plasma density. The panel (a) shows the initial condition, and the panel (b) shows the result at $t = 110.8\tau_S$. The initial magnetic field is created by the current loop located at the circle $r = r_S$ on the equatorial plane, and the initial velocity of the accretion disk plasma is Kepler velocity. The magnetic bridge between the ergosphere and the disk is twisted rapidly due to the frame-dragging effect, and the magnetic pressure in the bridge increases quickly. The magnetic bridge expands vertically by the large gradient of the magnetic pressure, and the jet is formed. At the last stage, the anti-parallel magnetic field is formed, where the magnetic reconnection may be caused easily. However, as we use ideal GRMHD, the magnetic reconnection is forbidden. The magnetic islands in the panel (b) is caused artificially due to the numerical error. It is noted that the scales of the two panels are different.

[5] Meier, D. L., Koide, S., Uchida, Y. 2001, Science, 291, 84.

[6] Ryu, D., Chattopadhyay, I., & Choi, E. 2006, Astrophys. J. Suppl. Ser., 166, 410.

[7] Camenzind, M. 1986, Astrophys. Astron., 156, 137.

[8] Tomimatsu, A., & Takahashi, M. 2003, Astrophys. J., 592, 321.

[9] Koide, S, Shibata, K. & Kudoh, T. 1998 Astrophys. J., 495, L63.

[10] Koide, S, Shibata, K. & Kudoh, T. 1999 Astrophys. J., 522, 727.

[11] Koide, S, Meier, D. L., Shibata, K. & Kudoh, T. 2000, Astrophys. J., 536, 668.

[12] Koide, S, Shibata, K. Kudoh, T. & Meier, D. L. 2002, Science, 295, 1688.

[13] Koide, S 2003, Phys. Rev. D 67, 104010.

[14] Hirotani, K., Takahashi, M., Nitta, S.-Y., & Tomimatsu, A. 1992, Astrophys. J., 386, 455.

[15] Penrose, R. 1969, Nuovo Cimento, 1, 252.

[16] Blandford, R. D. & Znajek, R. 1977, Mon. Not. R. Astron. Soc. 179, 433.

[17] Koide, S 2004, Astrophys. J. Lett., 606, L45.

[18] Blandford, R. D. & Payne, D. 1982, Mon. Not. R. Astron. Soc. 199, 883.

[19] Uchida, Y. & Shibata, K. 1985, Publ. Astron. Soc. Jpn. 37, 515.

[20] Shibata, K. & Uchida, Y. 1986, Publ. Astron. Soc. Jpn. 38, 631.

[21] Balbus, S. A. & Hawley, J. F. 1991 Astrophys. J. 376, 214.

[22] Koide, S, Shibata, K. & Kudoh, T. 2006, Phys. Rev. D, 74, 044005.

[23] Hayashi, M. R., Shibata, K. & Matsumoto, R. 1996, Astrophys. J. Lett. 468, L37.

[24] McKinney, J. C. 2006, Mon. Not. R. Astron. Soc., 368, 1561.

[25] MacFadyen, A. I., & Woosley, S. E. 1999, Astrophys. J., 524, 262.

[26] Shibata, M., & Sekiguchi, Y. I. 2005, Phys. Rev. D, 72, 044014.

[27] Koide, S, & Arai, K. 2008, submitted.

From Gravity Probe B to STEP: Testing Einstein in Space

James Overduin[1]

[1] *Gravity Probe B, Hansen Experimental Physics Laboratory, Stanford University, Stanford, CA 94305, USA*

Abstract

I summarize the history, current status and preliminary findings of the Gravity Probe B (GPB) mission, which seeks to make the first direct measurements of the geodetic and frame-dragging effects predicted by Einstein's theory of general relativity. I then discuss the planned Satellite Test of the Equivalence Principle (STEP), which will test the underlying *assumption* of Einstein's theory, the equivalence of gravitational and inertial mass. STEP will place important constraints on theories that seek to go beyond general relativity, such as unified field theories based on higher dimensions (string theory) and theories of dynamical dark energy (quintessence), both of which predict the existence of new fields that may violate the equivalence principle.

1 Background to the Gravity Probe B Experiment

By coincidence, the successful launch of Gravity Probe B on 20 April 2004 (Fig. 1) came exactly 100 years after the earliest published accounts of frame-dragging experiments, by August Föppl in Munich in 1904 [1]. Föppl, working as he was before general (and for that matter special) relativity, was investigating the possibility of a coupling between the spin of the Earth and that of a pair of heavy flywheels whose rotation axis could be aligned along either lines of latitude or longitude (Fig. 2). He was probably inspired by earlier experiments of countrymen Immanuel and Benedict Friedlaender (1896) involving torsion balances in the vicinity of spinning millstones, and by the writings of Ernst Mach, who famously speculated in 1883 that water in a spinning bucket might not exhibit the effects of centrifugal force "if the sides of the vessel increased in thickness and mass until they were ultimately several leagues thick." A sufficiently

Figure 1: Launch of Gravity Probe B

[1] E-mail:overduin@relgyro.stanford.edu

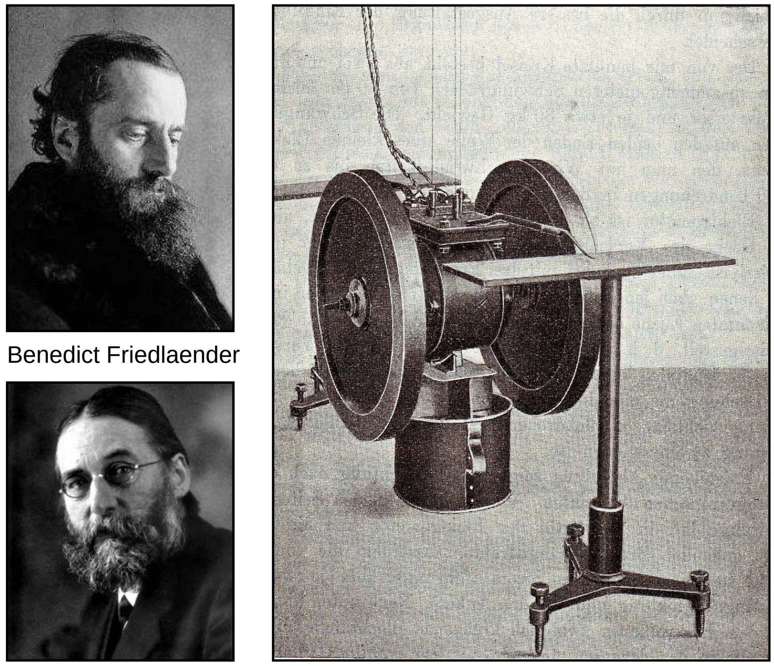

Benedict Friedlaender

August Föppl

Föppl's experimental setup

Figure 2: Experiments in frame-dragging before general relativity

massive bucket, in other words, might carry the local inertial frame of the water around with it. Mach's Principle, as this idea came to be known, has proved to be of limited scientific value (Ref. 1 lists 21 different formulations of it in the literature, some mutually contradictory). Nevertheless Gravity Probe B (GPB) can be seen as a modern-day realization of Mach's proposal with an earth-sized bucket and the role of water played by orbiting gyroscopes more than a million times more sensitive than the best inertial navigation gyros on earth.

Albert Einstein was strongly influenced by Mach's ideas, and his early attempts at gravitational field theories all exhibited frame-dragging effects. It is somewhat surprising, therefore, that he did not attempt to work out the Machian implications of general relativity himself. That was left to Hans Thirring and Josef Lense (1918), after whom the general relativistic frame-dragging effect is often named. (In a nice reversal of the usual course of events, Thirring had wanted to build an improved Föppl-type experiment and only reluctantly settled for doing the theoretical calculation after he was unable to obtain funding [1].) The terms "frame-dragging" and "Lense-Thirring" are sometimes used interchangeably with "gravitomagnetic", based on the close analogy between Maxwell's equations and a subset of Einstein's field equations in the low-velocity, weak-field limit [2]. Such analogies did not begin with general relativity; their existence was already suspected in 1849 by Michael Faraday, who designed experiments to search for "gravitational induction." The terminology must be used with care, however; for just as in ordinary electrodynamics, the distinction between gravitomagnetic and gravitoelectric is frame-dependent, and other phenomena besides frame-dragging are at least partly "gravito-electromagnetic." An example is the geodetic effect, which involves the transport of angular momentum through a gravitational field and was already studied two years before the Lense-Thirring effect by Willem de Sitter (1916). He showed that the earth-moon system would precess in the field of the sun, an effect now called the solar geodetic effect (although "heliodetic" might be more descriptive). De Sitter's calculation was extended to rotating test bodies such as the earth by Jan Schouten (1918) and Adriaan Fokker (1920), and the solar geodetic effect is now sometimes referred to as the de Sitter or Fokker-de Sitter effect.

These effects became widely known when they were mentioned by Arthur Eddington in his textbook of 1924. The idea of attempting to observe them with terrestrial gyroscopes was briefly considered in the 1930s by P.M.S. Blackett, who discarded it as impractical [3]. Technological progress during World


Leonard Schiff


George Pugh

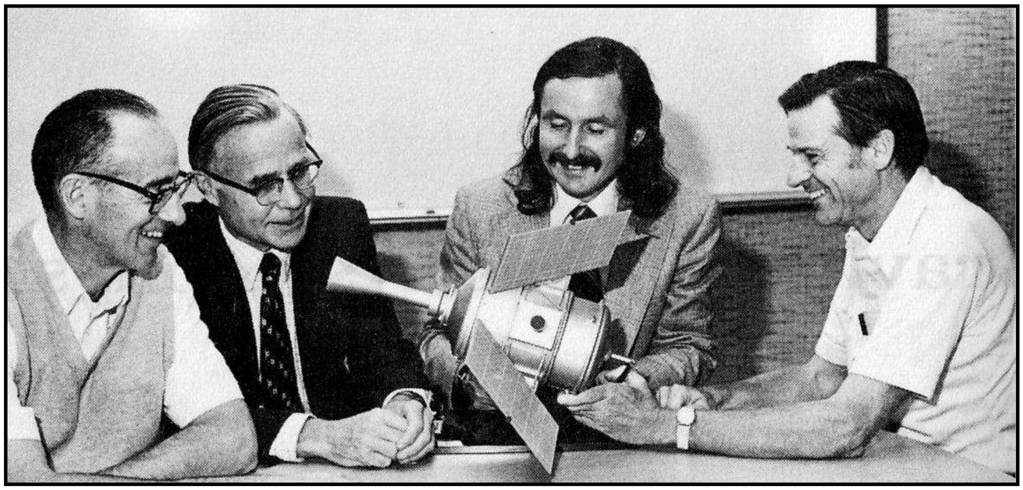
Dan Debra, Bill Fairbank, Francis Everitt and Bob Cannon with a model of GPB, 1980

Figure 3: Genesis of Gravity Probe B

War II, however, brought the problem back into the realm of possibility. An advertisement for a new "cryogenic gyroscope" in the December 1959 issue of *Physics Today* stimulated Leonard Schiff to revisit some earlier calculations involving tests of Mach's Principle and led to his elegant re-derivation of both the geodetic and frame-dragging effects in the form now known as the Schiff formula:

$$\vec{\Omega}_{\rm GR} = \vec{\Omega}_{\rm geo} + \vec{\Omega}_{\rm f-d} = \frac{3GM}{2c^2r^3}\left(\vec{r}\times\vec{v}\right) + \frac{GI}{c^2r^3}\left[\frac{3\vec{r}}{r^2}\left(\vec{S}\cdot\vec{r}\right) - \vec{S}\right], \tag{1}$$

where M, I and $\vec{S}$ refer to the mass, moment of inertia and angular momentum of the central body and r and $\vec{v}$ are the orbital radius and instantaneous velocity of the gyroscope. In a nice example of scientific synchronicity, essentially the same results were arrived at independently months earlier by George Pugh, a researcher at the Pentagon who also contributed the ingenious suggestion of shielding an orbiting gyroscope from non-gravitational disturbances inside a drag-free satellite.

Frame-dragging arises due to a spin-spin interaction between the gyroscope and rotating earth, analogous to the interaction of a magnetic dipole with a magnetic field. In a polar orbit 642 km above the earth, it causes a gyroscope's spin axis to precess in the east-west direction by 39 milliarcsec/yr, an angle so tiny that it is equivalent to the angular width of the object *Pluto* as seen from earth. The geodetic effect is somewhat larger; it arises partly as a spin-orbit interaction between the spin of the gyroscope and the "mass current" of the moving earth in the gyro rest frame. This is the analog of Thomas precession in electromagnetism. The spin-orbit interaction accounts for one-third of the total geodetic precession; the other two-thirds are not gravito-electromagnetic in origin, but arise due to space curvature around the massive earth (an effect sometimes referred to as the "missing inch" [2]). In a 642 km polar orbit, the geodetic effect causes a gyroscope's spin axis to precess in the north-south direction by 6606 milliarcsec/yr, an angle comparable to that subtended by the planet *Mercury* as seen from earth. The measurement of precessions this small would eventually pose immense technical and scientific challenges, an obstacle which fortunately did not deter Schiff (a theorist), Bill Fairbank (a low-temperature experimentalist) and Bob Cannon (a gyroscope specialist) when they met one sunny afternoon in 1960 in the Stanford university swimming pool to discuss the idea seriously for the first time (Fig. 3). GPB received its first NASA funding in March 1964.

2 The Gravity Probe B Mission and Preliminary Results

In concept the experiment is simplicity itself: a gyroscope, a readout mechanism to monitor its spin axis, and a telescope to compare this axis with the line of sight to a distant guide star (Fig. 4). In practice GPB

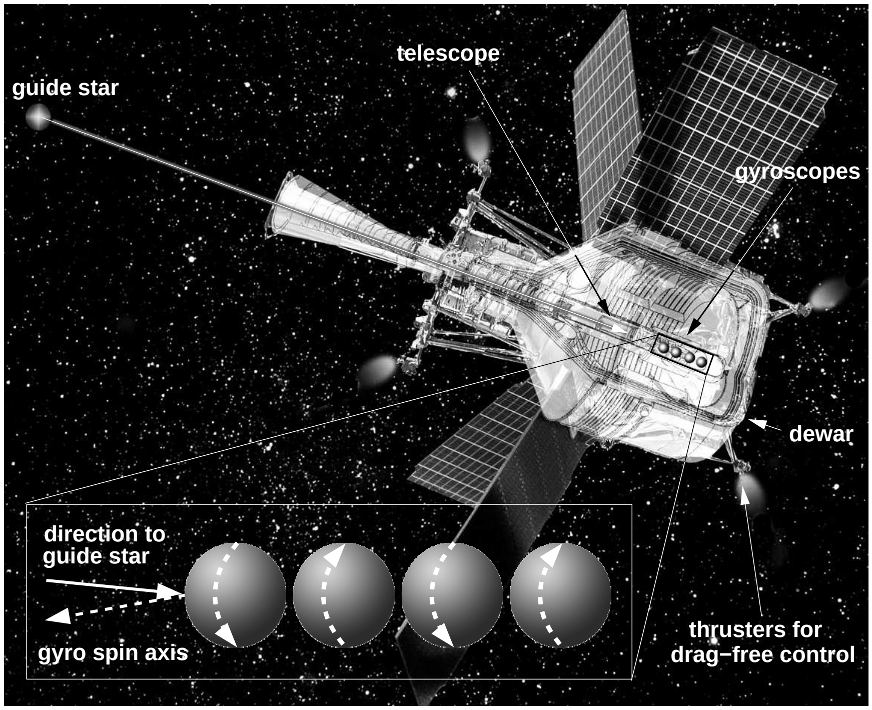

Figure 4: Gravity Probe B concept

grew into one of the most complex experiments ever flown, requiring at least a dozen new technologies that did not exist when it was conceived. Among these are the world's roundest and most homogeneous gyroscope rotors and a suspension system operating to levitate and maintain them within microns of their housings over a dynamic range of eleven orders of magnitude in force. A novel readout scheme based on the superconducting London moment was developed using ultra-sensitive superconducting quantum interference device (SQUID) magnetometers. Expandable nested lead shields were employed to reduce the ambient magnetic field. New techniques were invented to spin up the gyros, reduce vacuum pressure and remove charge buildup on the rotors. Perturbing forces were suppressed by a drag-free control system whereby any one of the gyroscopes could be isolated as an inertial "plumb line"; the rest of the spacecraft was made to follow its motion by means of helium boiloff vented through a revolutionary porous plug and specially designed thrusters. (This porous plug has since proved vital to other NASA missions including COBE, IRAS, WMAP and Spitzer.) The resolution of the onboard telescope, fastened to the gyro assembly by a novel quartz bonding technique, was enhanced by means of a beam splitter and image dividers. Non-inertial motions of the guide star, IM Pegasi, were compensated by the use of long-baseline radio interferometry to monitor its position relative to distant background quasars.

Once in orbit, GPB underwent an initial orbit checkout phase, which lasted until 27 August 2004 and has been described in detail elsewhere [4]. The science phase which followed lasted until 14 August 2005 (or 353 days, just under the original goal of one full year). The final post-flight calibration phase then continued for a further 46 days until there was no longer enough liquid helium to maintain the experiment at cryogenic temperatures. Fig. 5 shows one year's worth of preliminary north-south data. The predicted geodetic effect is already seen in the unprocessed gyro data to an accuracy level of 1%. Table 1 shows the general relativistic predictions in both the north-south (NS) and east-west (EW) directions compared to preliminary GPB results[5] (all figures in milliarcsec/yr). These numbers should be regarded as preliminary. As might be expected in an experiment that goes six or more orders of magnitude in gyro drift rate beyond anything that has gone before, two unexpected factors have cropped up to complicate the data analysis. First, it became apparent during the science phase of the mission that there were variations in the polhode rate of the gyros (polhode motion had been expected, but its period had not been expected to change appreciably over the mission lifetime, given characteristic

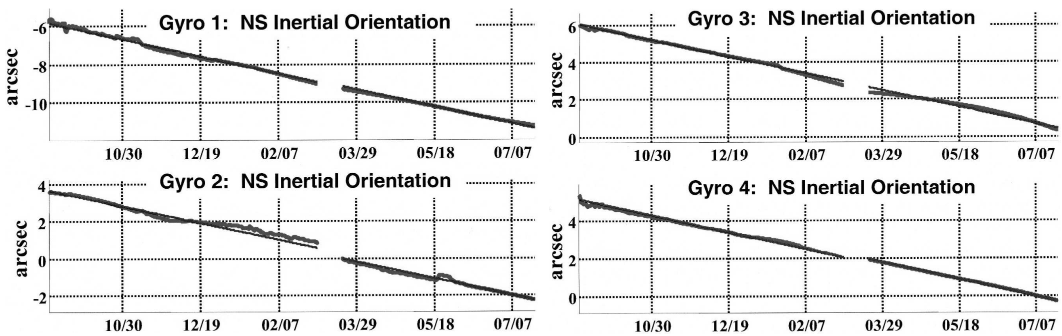

Figure 5: Seeing general relativity directly

gyro spin-down periods on the order of 10,000 years). It is critical to understand and model these polhode variations in order to combine the data from successive orbits and thereby reduce the noise as far as possible within the limits inherent in the SQUID readout system (roughly 1 milliarcsec in 5 hrs). Second, misalignment torques (torques proportional to the angle between the spacecraft roll axis and the line of sight to the guide star) appeared during the post-flight calibration phase that were larger than expected. These classical torques must also be understood and modeled, because they can mimic the desired relativity signal. Both factors have been traced to larger-than-anticipated electrostatic patches on the gyroscopes. The misalignment torques are due to interactions between these patches and similar ones on the gyro housings, and the time-varying polhode periods are caused by the fact that these interactions extract energy from the spinning rotors, albeit at a rate that would be imperceptible were the rotors not so perfect. (The energy loss amounts to $\sim 10^{-13}$ W, four orders of magnitude below the loss due to *heat radiation* of $\sim 10^{-9}$ W for rotors at 2.2 K.) A current worst-case upper bound on systematic error due to both factors together is 97 milliarcsec/yr in both directions (Table 1) [5]. However this will go down significantly. In expectation of the unexpected, GPB was designed to take various kinds of "redundant" data, and these are now proving their worth. In particular trapped-flux modeling is allowing the data analysis team to reconstruct the behavior of the gyro rotors in real time. This, in combination with more sophisticated method of data analysis, is expected to yield accuracies close to those originally envisioned for the experiment. Final results are to be announced in 2008.

Table 1: Preliminary GPB results (initial year-long 4-gyro average [5])

	(Terrestrial) geodetic	Solar geodetic	Guide star proper motion	Net predicted ($\Omega_{\rm GR}$)	Observed ($\Omega_{\rm obsd}$)
NS	-6606	+7	$+28 \pm 1$	-6571 ± 1	-6578 ± 9 (1σ)
EW	-39	-16	-20 ± 1	-75 ± 1	-87 ± 9 (1σ)

The final results from GPB will constitute a sixth and seventh test of general relativity, supplementing the three "classical tests" (gravitational redshift, perihelion precession and light deflection), the Shapiro time delay, and the spin-down of the binary pulsar in accordance with expectations based on the emission of gravitational radiation [6]. They will strengthen constraints on metric theories as possible extensions of general relativity, by placing new independent limits on the parameter γ of the Parametrized Post-Newtonian (PPN) formalism [7]. (In principle the GPB data can also constrain a second PPN parameter, the preferred-frame parameter α_1, but this effect is probably too small to be observed.) They may also impose new constraints on a wide variety of other "generalizations of general relativity." Examples are theories involving torsion (Hayashi and Shirafuji 1979 [8] and Halpern 1984 [9]; see Mao *et al.* 2006 [10] and Flanagan *et al.*[11]), extra dimensions (Overduin and Wesson 1997 [12]; see Liu and Overduin 2000 [13]) and violations of Lorentz invariance (Bailey and Kostelecký 2006 [14]; see Overduin 2008 [15]).

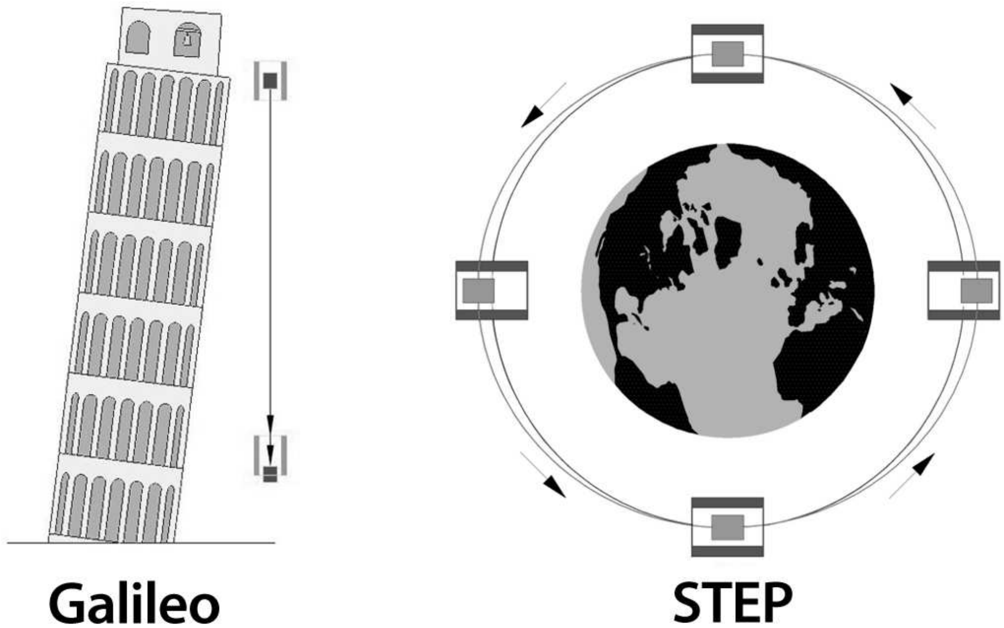

Figure 6: STEP concept: Galileo's free-fall experiment in orbit

3 Satellite Test of the Equivalence Principle

By contrast with GPB, which has carried out two new tests of predictions of general relativity, STEP will probe the underlying *foundation* of Einstein's theory, the (local) equivalence of gravitational and inertial mass. The equivalence principle (EP) originated in Newton's clear recognition (1687) of the strange experimental fact that mass fulfills two conceptually independent functions in physics, as both the source of gravitation and the seat of inertia. Einstein's "happiest thought" (1907) was the realization that the local equivalence of gravitational and inertial mass tells us something very deep about gravity: it tells us that the phenomenon of gravitation does not depend on the properties of matter (for it can be transformed away by moving to the same accelerated frame, regardless of the mass or composition of the falling object). Rather, the phenomenon of gravity must spring from the properties of spacetime itself. Einstein eventually identified the property of spacetime that is responsible for gravitation as its curvature. General relativity, our currently accepted "geometrical" theory of gravity, thus rests on the validity of the EP. But it is now widely expected that general relativity must break down at some level, in order to be united with the other fields making up the standard model (SM) of particle physics. It therefore becomes crucial to test the EP as carefully as possible.

Historically, there have been four distinct ways of testing equivalence: (1) Galileo's free-fall method, (2) Newton's pendulum experiments, (3) Newton's celestial method (his dazzling insight that moons and planets could be used as test masses in the field of the sun) and (4) Eötvös' torsion balance. Of these, (3) and (4) are by far the most exact: the celestial method now makes use of lunar laser ranging to place limits on the relative difference in acceleration toward the sun of the earth and moon of 3×10^{-13} [16], and similar constraints come from modern state-of-the-art torsion balance experiments [17]. But both these methods are subject to fundamental limitations (modeling uncertainties and seismic noise) and it is unlikely that they will advance significantly beyond the 10^{-13} level. STEP is conceptually a return to Galileo's free-fall method, but one that uses a 7000 km high "tower" that constantly reverses its direction to give a continuous periodic signal, rather than a quadratic 3 s drop (Fig. 6). A free-fall experiment in space has two principal advantages over terrestrial torsion-balance tests: a larger driving acceleration (sourced by the entire mass of the earth) and a quieter "seismic" environment, particularly if drag-free technology is used. These and other factors will enable STEP to improve existing constraints on EP violation by *five to six orders of magnitude*, from $\sim 10^{-13}$ to 10^{-18}.

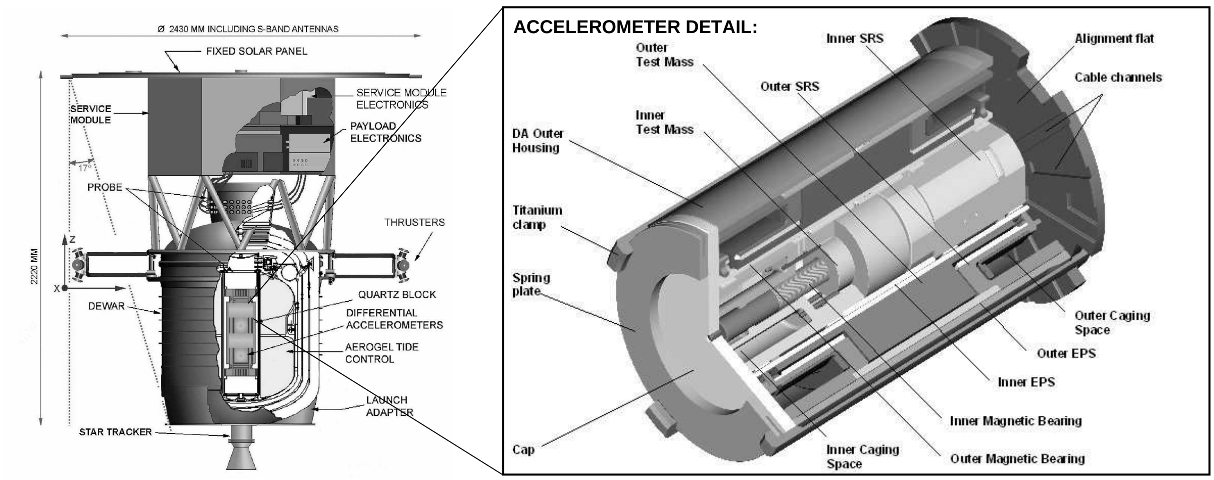

Figure 7: Schematic cutaway of the STEP spacecraft (left) with solar panel (top) and dewar (below) containing quartz block and four accelerometers (detail at right)

The STEP design calls for four pairs of concentric test masses, currently composed of Pt-Ir alloy, Nb and Be in a "cyclic condition" to eliminate possible sources of systematic error (the total acceleration difference between A-B, B-C and C-A must be sero for three mass pairs AB, BC and CA). This choice of test-mass materials is not yet fixed, but results from extensive theoretical discussions in the 1990s suggesting that EP violations are likely to be tied to three potential determinative factors that can be connected to a general class of string-inspired models: baryon number, neutron excess and nuclear electrostatic energy [18, 19]. The test masses are constrained by superconducting magnetic bearings to move in one direction only; they can be perfectly centered by means of gravity gradient signals, thus avoiding the pitfall of most other free-fall methods (unequal initial velocities and times of release). Their accelerations are monitored with very soft magnetic "springs" coupled to a cryogenic SQUID-based readout system. The SQUIDs are inherited from GPB, as are many of the other key STEP technologies, including test-mass caging mechanisms, charge measurement and UV discharge systems, drag-free control algorithms and proportional helium thrusters using boiloff from the dewar as propellant (Fig. 7). Prototypes of key components including the accelerometer are in advanced stages of development. STEP is to be submitted for NASA Phase A study as a Small Explorer (SMEX)-class mission in early 2008.

Theoretically, the range $10^{-18} \lesssim \Delta a/a \lesssim 10^{-13}$ is an extremely interesting one. This can be seen in at least three ways. The simplest argument is a dimensional one. New effects in any theory of quantum gravity must be describable at low energies by an effective field theory with new terms like $\beta(m/m_{\rm QG}) + \mathcal{O}(m/m_{\rm QG})^2$ where β is a dimensionless coupling parameter not too far from unity and $m_{\rm QG}$ is the quantum-gravity energy scale, which could be anywhere between the grand unified theory (GUT) scale $m_{\rm GUT} \sim 10^{16}$ GeV and the Planck scale $m_{\rm Pl} \sim 10^{19}$ GeV. In a theory combining gravity with the SM, m could plausibly lie anywhere between the mass of an ordinary nucleon ($m_{\rm nuc} \sim 1$ GeV) and that of the Higgs boson ($m_{\rm H} \sim 100$ GeV). With these numbers one finds that EP-violating effects should appear between $(m_{\rm nuc}/m_{\rm Pl}) \sim 10^{-19}$ and $(m_{\rm H}/m_{\rm GUT}) \sim 10^{-14}$ — exactly the range of interest. This makes STEP a potential probe of quantum gravity [20].

The dimensional argument, of course, is not decisive. A second approach is then to look at the broad range of specific theories that are sufficiently mature to make quantitative predictions for EP violation. There are two main categories. On the high-energy physics side, EP violations occur in many of the leading unified theories of fundamental interactions, notably *string theories* based on extra spatial dimensions. In the low-energy limit, these give back classical general relativity with a key difference: they generically predict the existence of a four-dimensional scalar dilaton partner to Einstein's tensor graviton, and several other gravitational-strength scalar fields known as moduli. In the early universe, these fields are naturally of the same order as the gravitational field, and some method has to be found to get rid of them in the universe we observe. If they survive, they will couple to SM fields with the

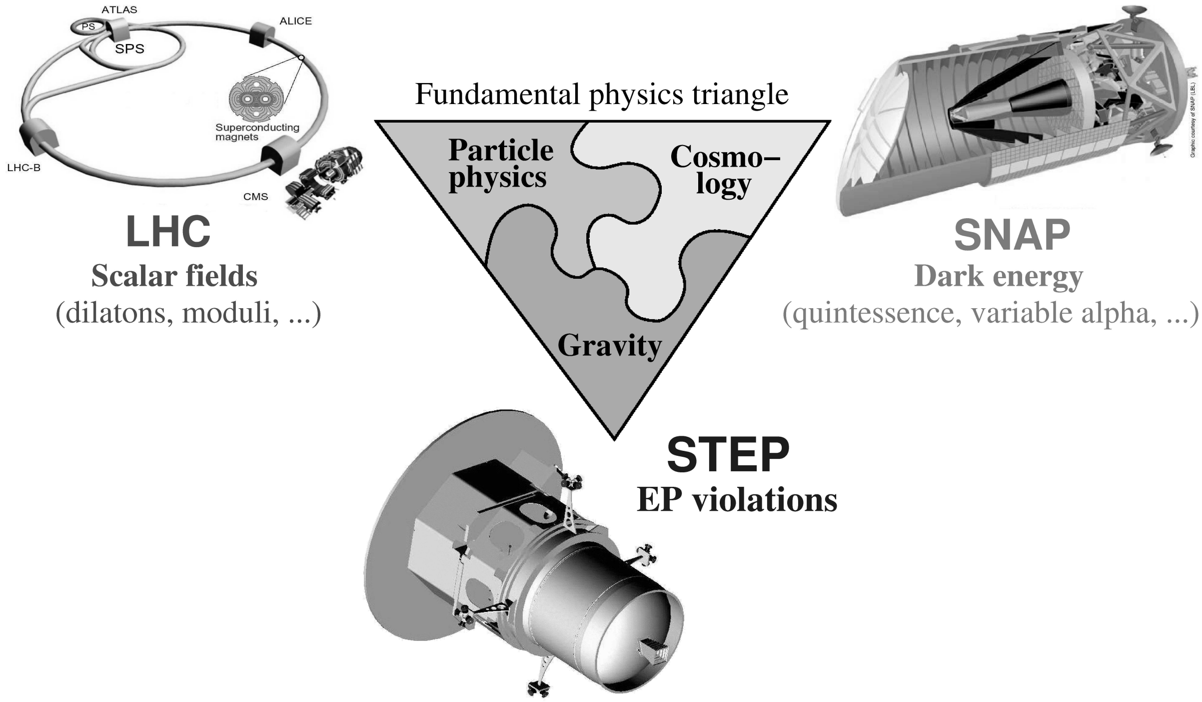

Figure 8: Investigating nature on all three scales — small, large *and intermediate*

same strength as gravity, producing drastic violations of the EP. One conjecture is that they acquire large masses and thus correspond to very short-range interactions, but this solution, though widely accepted, entails grave difficulties (the Polonyi or "moduli problem") because the scalars are so copiously produced in the early universe that their masses should long ago have overclosed the universe, causing it to collapse. Another possibility involves a mechanism whereby a massless "runaway dilaton" (or moduli) field is cosmologically attracted toward values where it almost, but not quite, decouples from matter; this results in EP violations that lie in the same range as that identified above and can reach $\sim 10^{-14}$ [21]. Similar comments apply to another influential model, the TeV "little string" theory [22]. The second category of specific EP-violating theories occurs at the opposite extremes of mass and length, in the field of cosmology. The reason is the same, however: a new field is introduced whose properties are such that it should naturally couple with gravitational strength to SM fields, thus influencing their motion in violation of the EP. The culprit in this case is usually *dark energy*, a catch-all name for the surprising but observationally unavoidable fact that the expansion of the universe appears to be undergoing late-time acceleration. Three main explanations have been advanced for this phenomenon: either general relativity is incorrect on the largest scales, or there is a cosmological constant (whose value is extremely difficult to understand) — or dark energy is *dynamical*. Most theories of dynamical dark energy (also known as quintessence) involve one or more species of new, light scalar fields that could violate the EP [23]. The same thing is true of new fields that may be responsible for producing cosmological variations in the electromagnetic fine-structure constant α [24].

In all or most of these specific theories, EP violations are predicted to appear in the STEP range, $10^{-18} \lesssim \Delta a/a \lesssim 10^{-13}$. To understand the reasons for this, it is helpful to look at the third of the arguments alluded to above for regarding this range as a particularly rich and interesting one from a theoretical point of view. This line of reasoning shares some of the robustness of the dimensional argument, in that it makes the fewest possible assumptions beyond the SM, while at the same time being based upon a convincing body of detailed calculations. Many authors have done work along these lines, with perhaps the best known being that of Carroll in 1998 [25], which we follow in outline here. Consider the simplest possible new field: a scalar ϕ (as motivated by observations of dark energy, or alternatively by the dilaton or supersymmetric moduli fields of high-energy unified theories such as string theory). Absent some protective symmetry (whose existence would itself require explanation), this new field ϕ couples to SM fields via dimensionless coupling constants β_k (one for each SM field) with values not too far from unity. Detailed but standard calculations within the SM (modified only to incorporate ϕ) show that these couplings are tightly constrained by existing limits on violations of the EP. The current bound of order $\Delta a/a < 10^{-12}$ translates directly into a requirement that the dominant coupling factor (the one associated with the gauge field of quantum chromodynamics or QCD) cannot be larger than $\beta_{\rm QCD} < 10^{-6}$. This is very small for a dimensionless coupling constant, though one can plausibly "manufacture" dimensionless quantities of this size (e.g. $\alpha^2/16\pi$), and many theorists would judge that anything smaller is almost certainly zero. Now STEP will be sensitive to violations as small as 10^{-18}. If none are detected at *this* level, then the corresponding upper bounds on $\beta_{\rm QCD}$ go down like the square root of $\Delta a/a$; i.e., to $\beta_{\rm QCD} < 10^{-9}$, which is no longer a natural coupling constant by any current stretch of the imagination. For perspective, recall the analogous "strong CP" problem in QCD, where a dimensionless quantity of order 10^{-8} is deemed so unnatural that a new particle, the axion, must be invoked to drive it toward zero. This argument does not say that EP violations inside the STEP range are inevitable; rather it suggests that violations *outside* that range would be so unnaturally fine-tuned as to not be worth looking for. As Ed Witten has stated, "It would be surprising if ϕ exists and would not be detected in an experiment that improves bounds on EP violations by 6 orders of magnitude" [26]. Only a space test of the EP has the power to force us to this conclusion.

The fundamental nature of the EP makes such a test a "win-win" proposition, regardless of whether violations are actually detected. A positive detection would be equivalent to the discovery of a new force of nature, and our first signpost toward unification. A null result would imply either that no such field exists, or that there is some deep new symmetry that prevents its being coupled to SM fields. A historical parallel to a null result might be the Michelson-Morley experiment, which reshaped physics because it found nothing. The "nothing" finally forced physicists to accept the fundamentally different nature of light, at the cost of a radical revision of their concepts of space and time. A non-detection of EP violations at the 10^{-18} level would strongly suggest that gravity is so fundamentally different from the other forces that a similarly radical rethinking will be necessary to accommodate it within the same theoretical framework as the SM based on quantum field theory.

STEP should be seen as the integral "intermediate-scale" element of a concerted strategy for fundamental physics experiments that also includes high-energy particle accelerators (at the smallest scales) and cosmological probes (at the largest scales), as suggested in Fig. 8. Accelerators such as the Large Hadron Collider (LHC) may provide indirect evidence for the existence of new fields via their missing-energy signatures. Astronomical observatories such as the SuperNova Acceleration Probe (SNAP) may produce *direct* evidence of a quintessence-type cosmological field through its bulk equation of state. But *only a gravitational experiment such as STEP can go further and reveal how or whether that field couples to the rest of the standard model.* It is at once complementary to the other two kinds of tests, and a uniquely powerful probe of fundamental physics in its own right.

Acknowledgments

Thanks go to Ron Adler, Quentin Bailey, Francis Everitt, Hans Fahr, Takao Fukui, Bob Kahn, Mac Keiser, Alan Kostelecký, Barry Muhlfelder, Holger Müller, Tom Murphy, Alex Silbergleit, Martin Tajmar and Bob Wagoner for valuable discussions.

References

[1] J.B. Barbour and H. Pfister eds., *Mach's Principle: From Newton's Bucket to Quantum Gravity*, Birkhäuser, Bston, 1995

[2] K.S. Thorne in J.D. Fairbank *et al.*, eds., *Near Zero*, W.H. Freeman, New York, 1988, p. 573

[3] C.W.F. Everitt in J.D. Fairbank *et al.*, eds., *Near Zero*, W.H. Freeman, New York, 1988, p. 587

[4] G.M. Keiser *et al.*, in V.A. Kostelecký, ed., *Third Meeting on CPT and Lorentz Symmetry*, World Scientific, Singapore, 2005, p. 115

[5] C.W.F. Everitt, presentation at the 18th Meeting on General Relativity and Gravitation (GRG18), Sydney, Australia, July 2007

[6] C.M. Will, Theory and Experiment in Gravitational Physics (Cambridge University Press, 1993), p. 210

[7] C.M. Will, Living Reviews in Relativity 3 (2006); `http://relativity.livingreviews.org/Articles/lrr-2006-3/`

[8] K. Hayashi and T. Shirafuji, Phys. Rev. D19 (1979) 3524

[9] L. Halpern, Int. J. Theor. Phys. 23 (1984) 843

[10] Y. Mao *et al.*, Phys. Rev. D76 (2007) 104029; arXiv:gr-qc/0608121 (2006)

[11] É.É. Flanagan and E. Rosenthal, Phys. Rev. D75 (2007) 124016; arXiv:0704.1447 (2007)

[12] J.M. Overduin and P.S. Wesson, Phys. Rep. 283 (1997) 303; arXiv:gr-qc/9805018

[13] H. Liu and J.M. Overduin, Astrophys. J. 538 (2000) 386; arXiv:gr-qc/0003034

[14] Q.G. Bailey and V.A. Kostelecký, Phys. Rev. D74 (2006) 045001; arXiv:gr-qc/0603030

[15] J.M. Overduin, in A. Kostelecký, ed., proc. Meeting on CPT Violation, Indiana University, 2007 (World Scientific, 2008), in press

[16] J.G. Williams *et al.*, Phys. Rev. Lett. 93 (2004) 261101

[17] E. Adelberger, Class. Quant. Grav. 18 (2001) 2397

[18] T. Damour, Class. Quant. Grav. 13 (1996) A33

[19] J.P. Blaser, Class. Quant. Grav. 18 (2001) 2515

[20] R. Adler, "Gravity," in *The New Physics for the Twenty-First Century* (Cambridge University Press, 2006), p. 41

[21] T. Damour, F. Piazza and G. Veneziano, Phys. Rev. Lett. 89 (2002) 08160

[22] I. Antoniadis and S. Dimopoulos, J. High Energy Phys. 5 (2001) 055

[23] R. Bean *et al.*, *Dark Energy Task Force* white paper, arXiv:astro-ph/0510059 (2005)

[24] G. Dvali and M. Zaldarriaga, Phys. Rev. Lett. 88 (2002) 091303

[25] S.M. Carroll, Phys. Rev. Lett. 81 (1998) 3067

[26] E. Witten, in D.B. Cline, ed., *Sources and Detection of Dark Matter and Dark Energy in the Universe* (World Scientific, 2000), p. 27

Properties of Rotating Black Holes

Roy Patrick Kerr

University of Canterbury

Christchurch, New Zealand

The Schwarzschild Solution

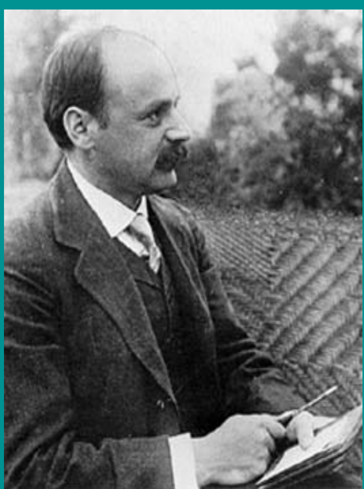

$$ds^2 = (1-\tfrac{2M}{R})^{-1}dr^2 + r^2 d\Omega^2 - (1-\tfrac{2M}{R})dt^2,$$
$$d\Omega^2 = d\theta^2 + \sin^2\theta d\phi^2.$$

Eddington - Finkelstein Coordinates

$$ds^2 = -dt^2 + dx^2 + dy^2 + dz^2 + \tfrac{2m}{r}(dr+dt)^2,$$
$$= \text{Minkowski metric} + \tfrac{2m}{r}(dr+dt)^2.$$

The search for a rotating generalisation of Schwarzschild

- It was known that the field outside any isolated spherically symmetric gravitational source must be Schwarzschild. This is time independent, although its interior can collapse to a “singularity” inside the event horizon.
- For 40 years Relativists searched for a rotating generalisation, a spinning black hole.
- The obvious approach was to assume the exterior field to be rotationally symmetric and time independent. This eliminates two out of the four coordinates in Einstein’s equations, leaving (r,z).
- The equations where put into many elegant and beautiful forms (particularly by Papapetrou) but no rotating solution was found.

Some additional assumption was needed.

Alexey Z. Petrov (1910-71)

•Petrov studied the algebraic form of the curvature tensor for an empty Einstein space (the conformal tensor) and showed that it is characterized by four null eigenvectors at each point. If these are written as spinors,

$$k^{\alpha} = \sigma^{\alpha}_{A\dot{B}} k^{A\dot{B}} \quad \text{then} \quad |\,\mathrm{k}\,|^2 = 0 \quad \Rightarrow \quad k^{A\dot{B}} = \varsigma^{A}\varsigma^{\dot{B}}.$$

•The conformal tensor corresponds to a completely symmetric four index spinor and its eigenvectors satisfy,

$$\Psi_{ABCD}\varsigma^{A}\varsigma^{B}\varsigma^{C}\varsigma^{D} = 0.$$

•This is a quartic equation for the ratio of the two components of the null spinor.

•It was observed that almost all known solutions of Einstein’s equations were “Algebraically Special”, i.e. two of the eigenvectors coincided.

Let’s look for “Algebraically Special” solutions of the empty Einstein equations!

Ivor Robinson Andrzej Trautman

They made the further assumption that the null vector was a gradient.
This lead to the Robinson-Trautman metrics in 1962.

$$ds^2 = r^2 P^{-2}(dx^2 + dy^2) - 2du dr - [\Delta \ln P - 2r(\ln P)_{,u}]du^2 - \frac{2m(u)}{r} du^2$$

$$\Delta\Delta(\ln P) + 12m(\ln P)_{,u} - 4m_{,u} = 0, \qquad \Delta = P^2(\partial_x^2 + \partial_y^2)$$

STILL NOT ROTATING!!

Previous attempts to find most general Algebraically Special metric

- Ivor Robinson continued his study of the most general algebraically special space-times. This would be completed later.
- In 1962-3 a group centred in Pittsburgh announced that they had solved the complete problem and that there was there was only a fairly non-interesting generalisation of Schwarzschild, NUT space.
- I had been studying the same problem and was very surprised at this result. Ivor Robinson told me later that he and and Andrzej Trautman also disbelieved it.
- A preprint containing the proof was sent to Alfred Schild and Alan Thompson at the University of Texas in Austin. I was also there at that time, and was in the same small apartment building as Alan.
- Neither Alan nor Alfred could see anything wrong with the paper. Alan then gave it to me to see why there were no interesting algebraically special Einstein spaces.

Examining the paper

- I thumb through the paper to see where this surprising result came from – which equation told them that the search was futile.
- I find a simple equation that seemed to be the key to their result,
- I do not know what A is but this equation seems to be the crux of their argument, so I look back to see where it came from and find that it cannot be true. The coefficients must sum to zero because of the "Bianchi Identities" .
- I rush next door and tell Alan that the conclusions are false. We calculate the first of the three terms and find that it is incorrect. The equation now reads
- I then calculate the correct field equations for Algebraically Special spaces. This is announced at a conference in New York. The author of the original paper says "Yes, but the second coefficient was a misprint. The equation is
- I say "OK, then the third must be wrong!" Alan and I calculate it that night and find that the correct equation is

$$1A + 2A - 3A = 0 \;\Rightarrow\; 0 = 0!$$

Examining the paper

- I thumb through the paper to see where this surprising result came from – what equation told them that the search was futile.
- I find a simple equation that seemed to be the key to their result,

$$2A + A - 2A = 0 \;\Rightarrow\; A = 0!$$

- I do not know what A is but this equation seems to be the crux of their argument, so I look back to see where it came from and find that it cannot be true. The coefficients must sum to zero because of the "Bianchi Identities" .
- I rush next door and tell Alan that the conclusions are false. We calculate the first of the three terms and find that it is incorrect. The equation now reads

$$A + A - 2A = 0 \;\Rightarrow\; 0 = 0!$$

- I then calculate the correct field equations for Algebraically Special spaces. This is announced at a conference in New York. The author of the original paper says "Yes, but the second coefficient was a misprint. The equation is

$$A + 2A - 2A = 0 \;\Rightarrow\; A = 0!$$

- I say "OK, then the third must be wrong!" Alan and I calculate it that night and find that the correct equation is

$$2A + A - 3A = 0 \;\Rightarrow\; 0 = 0!$$

Path to Kerr Solution

Assumed algebraically special. Five of the Einstein equations were solved and the metric was then written

$$ds^2 = (r^2+\Sigma^2)P^{-2}(d\varsigma d\bar\varsigma) - 2(dr + W d\varsigma + \overline{W} d\bar\varsigma)(du + L d\varsigma + \bar L d\bar\varsigma)$$
$$+2\left(-\tfrac{1}{2}K + r(\ln P)_{,u} + \frac{mr + M\Sigma}{r^2+\Sigma^2}\right)(du + L d\varsigma + \bar L d\bar\varsigma)^2,$$

$$\partial = \partial_\varsigma - L\partial_u, \qquad \Sigma = \frac{i}{2}P^2(\partial\bar L - \bar\partial L),$$
$$K = 2P^{-2}\mathrm{Re}[\partial(\bar\partial\,\mathrm{Ln}P - \bar L_{,u})], \qquad W = -(r+i\Sigma)L_{,u} + i\partial\Sigma.$$

The metric's dependence on the radial coordinate, "r", is given explicitly. When P is chosen to be 1 the remaining field equations are

$$M = \mathrm{Im}(\bar\partial\bar\partial\partial L),$$
$$\partial(m+iM) = 3(m+iM)L_{,u},$$
$$\partial_u[m - \mathrm{Re}(\bar\partial\bar\partial\partial L)] = |\partial_u \partial L|^2.$$

Arbitrary Killing vector

Any Killing vector (infinitesimal symmetry) can be written as

$$K = \alpha\partial_\varsigma + \bar\alpha\partial_{\bar\varsigma} + \mathrm{Re}(\alpha_\varsigma)(u\partial_u - r\partial r) + V\partial_u,$$
$$\text{where} \qquad \alpha = \alpha(\varsigma), \qquad V = V(\varsigma,\bar\varsigma).$$

Where a general coordinate system is being used, not necessarily one where *P=1*.

The coordinates can be chosen so that

$$K = \partial_u, \qquad \text{or} \qquad \mathrm{K} = \tfrac{i}{2}(\varsigma\partial_\varsigma - \bar\varsigma\partial_{\bar\varsigma}) = \partial_\theta.$$

Assumed independent of time. Now the equations are getting better, but no general solution has been found It is interesting to note that if ds_0^2 is any time-independent solution then so is

$$ds^2 = ds_0^2 + \frac{2m_0 r}{r^2 + \Sigma^2}(du + L d\varsigma + \bar{L} d\bar{\varsigma})^2.$$

where m_0 is a constant.

Assume axially symmetry. This reduces the field equations down to ordinary differential equations which can be solved.

The space-time now depends on four real numbers, or parameters. These characterise the metric completely. Getting near!!

Since I am looking for a physically interesting space-time I require the space to be Minkowski space (special relativity) at large distances. Two parameters are removed.

This leaves a solution with only two parameters, (M, a).

Kerr metric in Kerr-Schild form

The metric is rather nasty in the coordinates originally used to find it, but it can be put into the simple Kerr-Schild form,

$$ds^2 = dx^2 + dy^2 + dz^2 - c^2 dt^2 + \frac{2GMr^3}{r^4 + a^2 z^2}(cdt + ...)^2,$$
$$\frac{x^2 + y^2}{r^2 + a^2} + \frac{z^2}{r^2} = 1.$$

When a = 0 the metric reduces to Schwarzschild with mass M.

DOES IT ROTATE WHEN “a” IS NONZERO?

I tell Alfred Schild, the director of the “Gravitational Research Centre” in Austin, that I am going to my office to calculate the angular momentum of the last remaining hope. He says “Fine, I am coming too!”

Alfred sits in an armchair smoking his pipe while I chain smoke cigarettes and calculate.

The first thing to do was to expand the metric in inverse powers of R, the usual radial distance form the origin,

$$ds^2 = dx^2 + dy^2 + dz^2 - dt^2 + \frac{2M}{R}(dt + dR)$$
$$- \frac{4Ma}{R^3}(xdy - ydx)(dt + dR) + O(R^{-3}).$$

Now if $x^\mu \to x^\mu + a^\mu$ is an infinitesimal coordinate transformation, then the metric changes by $ds^2 \to ds^2 + 2da_\mu dx^\mu$. If we choose

$$a_\mu dx^\mu = -MaR^{-2}(xdy - ydx) \quad \Rightarrow$$
$$da_\mu dx^\mu = -2MaR^{-3}(xdy - ydx)dR,$$

Then the asymptotic metric becomes

$$ds^2 = dx^2 + dy^2 + dz^2 - dt^2 + \frac{2M}{R}(dt + dR)$$
$$- \frac{4Ma}{R^3}(xdy - ydx)dt + O(R^{-3}).$$

The leading terms in the linear approximation for the gravitational field around a rotating body were well known. The contribution from the angular momentum vector, **J**, is

$$4R^{-3}\varepsilon_{ijk}J^i x^j dx^k dt$$

At this point I turned to Alfred, puffing away in his armchair, and said

YES!!

"It rotates with angular momentum Ma about the z-axis. The parameter a is the angular momentum per unit mass." We then went out to celebrate.

Kerr metric in Kerr-Schild form

$$ds^2 = dx^2 + dy^2 + dz^2 - c^2dt^2 + \frac{2GMr^3}{c^2(r^4 + a^2z^2)}(k_\alpha dx^\alpha)^2,$$

$$k_\alpha dx^\alpha = cdt + \frac{z}{r}dz + \frac{r}{r^2 + a^2}(xdx + ydy) - \frac{a}{r^2 + a^2}(xdy - ydx),$$

Where the “radial” function r is given by

$$\frac{x^2 + y^2}{r^2 + a^2} + \frac{z^2}{r^2} = 1.$$

Event Horizons for Kerr Black Hole

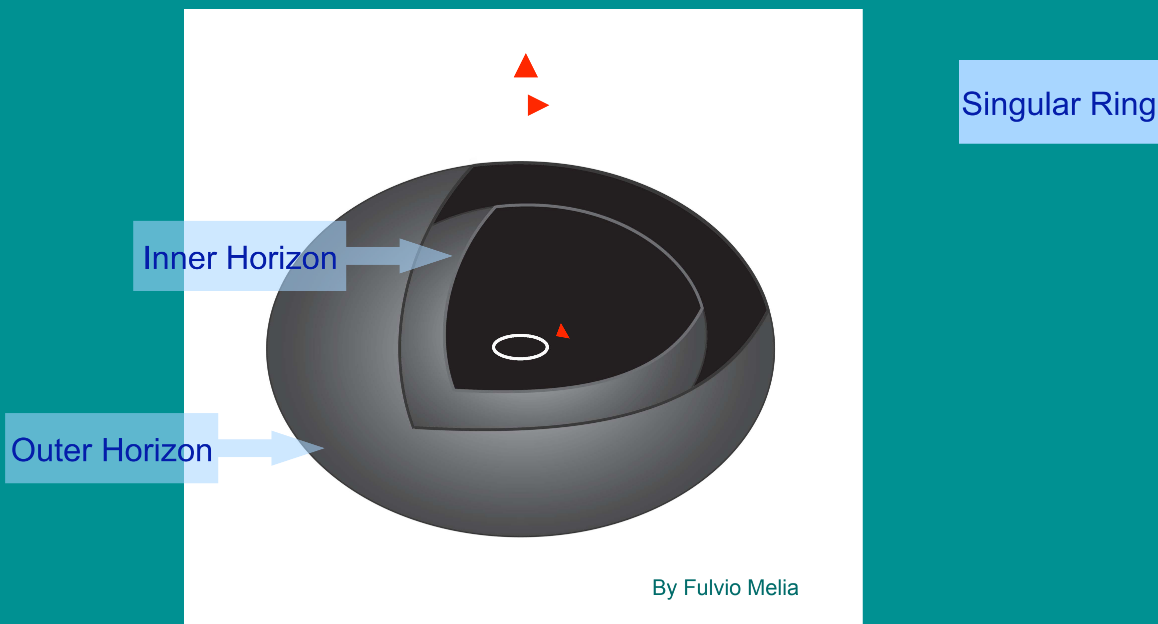

Quasars

- In the late 1950s many strange radio sources were discovered. Hundreds were discovered, and then in 1960 3C 48 was shown to have an optical counterpart, a faint blue “star” with an anomalous spectrum. John Bolton thought that it had a large redshift, but this was not believed by others.

- In 1962 the closest quasar, 3C 273, was occulted by the moon. Cyril Hazard and Bolton took observations allowing Marteen Schmidt to identify it.

- When he observed its spectrum he realised it was that for hydrogen, red-shifted, and so quasars were identified as galactic objects.

- If they were as far away as their redshifts implied, then they were far too energetic for all “reasonable” explanations.

- Possible explanations: antimatter, white holes, ….

First Texas Symposium on Gravitation and Astrophysics

- In December 1963 a meeting is arranged in Dallas Texas to discuss the newly discovered and highly energetic objects in the sky. These will later be called “Quasars”, short for “QUASi-stellAR radio sources”. At least 300 astronomers/astrophysicists and 50 Relativists attend.

- There are many theories presented but none that have broad appeal.

- Hoyle and Burbidge suggest a giant star with the mass of at least a million suns. Even this does not produce enough energy to power the observed quasars. Black holes are mentioned but the non-rotating Schwarzschild metric is far too unlikely.

- On hearing that Roger Penrose is going to give a talk on my solution, I tell the organisers that that is my pleasure, and then I give a 10-15 minute talk explaining its geometry, including its double event horizon, and that it rotates.

- The astronomers are totally uninterested and ignore my talk.

- Papapetrou screams at them that he and others have worked for 30 years to find this metric and that they should listen. They ignore this.

Kerr-Schild metrics

- Around Christmas 1963, after the First Texas Symposium in Dallas, I spend a morning investigating whether there are other Algebraically Special spaces that have the Kerr-Schild form. There seem to be a large class that depend on a "function of a complex variable" and include the Kerr rotating solution but none of the others are of physical interest so I just leave them on my desk.
- Jerzy Plebansky, a very well-known Polish relativist visits Austin for Christmas. Alfred Schild holds one of his excellent parties for Jerzy. During this I hear them mention their interest in spaces of the Kerr-Schild form (that name had not been invented at that time, of course).
- I say "I think I know of a large group of those, but the result was not checked and may be rubbish".
- Alfred and I retire to his office and do a small calculation that shows that any metric of this type has to be Algebraically Special.
- Next day we redo my original calculations, verifying that they were correct.
- We subsequently add an electromagnetic field to the problem, and find that there is a natural charged version of Kerr, the Kerr-Newman charged black holes. This is also discovered by Ted Newman by testing various ways that charged Schwarzschild (Reissner-Nordstrom) and Kerr might be amalgamated!

The Kerr-Schild metric can be parameterised so that

$$\begin{aligned} ds^2 &= -dt^2 + dx^2 + dy^2 + dz^2 + \lambda k^2, \\ k &= (du + \bar{Y} d\varsigma + Y d\bar{\varsigma} + Y\bar{Y} dv)/(1 + Y\bar{Y}) \\ u &= z + t, \quad v = t - z, \quad \varsigma = x + iy. \end{aligned}$$

If the metric satisfies Einstein's equations,

$$\lambda = 2m\mathrm{Re}(2Y_{,\varsigma}), \qquad Y^2\bar{\varsigma} + 2zY - \varsigma + F(Y) = 0.$$

The only asymptotically non-singular, let alone flat, example is the original Kerr metric where the arbitrary function, *F(Y) = - 2iaY.*

$$Y^2\bar{\varsigma} + 2(z - ia)Y - \varsigma = 0.$$

This equation has branch points on the ring where the discriminant is zero,

$$\varsigma\bar{\varsigma} + (z - ia)^2 = 0 \quad \Rightarrow \quad \mathrm{x}^2 + \mathrm{y}^2 = 0, \quad z = 0.$$

There are two roots for this equation,

$$Y_1 = \frac{r\varsigma}{(z+r)(r-ia)}, \qquad 2Y_{1,\varsigma} = +\frac{r^3+iarz}{r^4+a^2z^2},$$
$$Y_2 = \frac{r\varsigma}{(z-r)(r+ia)}, \qquad 2Y_{2,\varsigma} = -\frac{r^3+iarz}{r^4+a^2z^2}.$$

Where the surfaces of constant, r are ellipsoids with "foci" on the singular ring,

$$\frac{x^2+y^2}{r^2+a^2}+\frac{z^2}{r^2}=1.$$

This is a quadratic equation for r^2 with ONE positive root for r^2 and therefore ONE positive root for r.

The coefficient of k^2 in the metric is

$$\lambda = 2m\mathrm{Re}(2Y_{,\varsigma}) = \pm\frac{2mr^3}{r^4+a^2z^2}$$

Charged Kerr Schild

We could not prove that the congruences had to be geodesic, so we assumed that. The congruences are then same as in the uncharged case. Th electromagnetic field depends on two functions. We could not solve the remaining equations unless we put the first to zero, leaving an arbitrary analytic function,

$$\lambda = 2m\mathrm{Re}(2Y_{\varsigma}) - |\psi(Y)|^2|2Y_{\varsigma}|^2.$$

The electromagnetic potential is

$$f = d\left[P(\psi Z+\overline{\psi}\overline{Z})k + \tfrac{1}{2}(\chi d\overline{Y}+\overline{\chi}dY)\right]$$
$$\chi = \int P^{-2}\psi(Y)dY, \qquad (\overline{Y}\text{ constant}).$$

The simplest of these metrics is the Kerr-Newman metric.

The metric can be parametrised so that

$$ds^2 = -dt^2 + dx^2 + dy^2 + dz^2 + \lambda k^2,$$
$$k = (du + \bar{Y}d\varsigma + Yd\bar{\varsigma} + Y\bar{Y}dv)/(1 + Y\bar{Y})$$
$$u = z + t, \quad v = t - z, \quad \varsigma = x + iy.$$

If the metric satisfies Einstein's equations,

$$\lambda = 2m\mathrm{Re}(2Y_\varsigma), \qquad Y^2\bar{\varsigma} + 2zY - \varsigma + F(Y) = 0.$$

The only asymptotic example is the original Kerr metric where the arbitrary function, *F(Y),* is quadratic in *Y.*

Afterwards

- It is proved a few years later by David Robinson, another New Zealander, that there are no other spinning black hole solutions. All properties of the star are lost when it collapses, except for its mass, angular momentum and electric charge. John Archibald Wheeler coined the phrase “Black Holes have no hair” to express this.
- Do Black Holes really exist? Probably. We appear to be seeing millions or more black holes in the universe. It may be that every galaxy formed around a Black Hole that was created soon after the “Big Bang”. We do not know whether this is so, but Black Holes have something to do with the formation of galaxies.
- Are Black Holes truly represented by the Kerr solution? Yes, but only in the limit as they age. We can never see a Black Hole collapse inside its event horizon. For us, it is always just on the verge of doing so.
- The most famous example is at the centre of our own galaxy. It is Sagitarius A* and is around 4,000,000 times as heavy as the Sun. Astronomers expect to be able to photograph it within the next ten years.

Black Hole passing in front of a galaxy

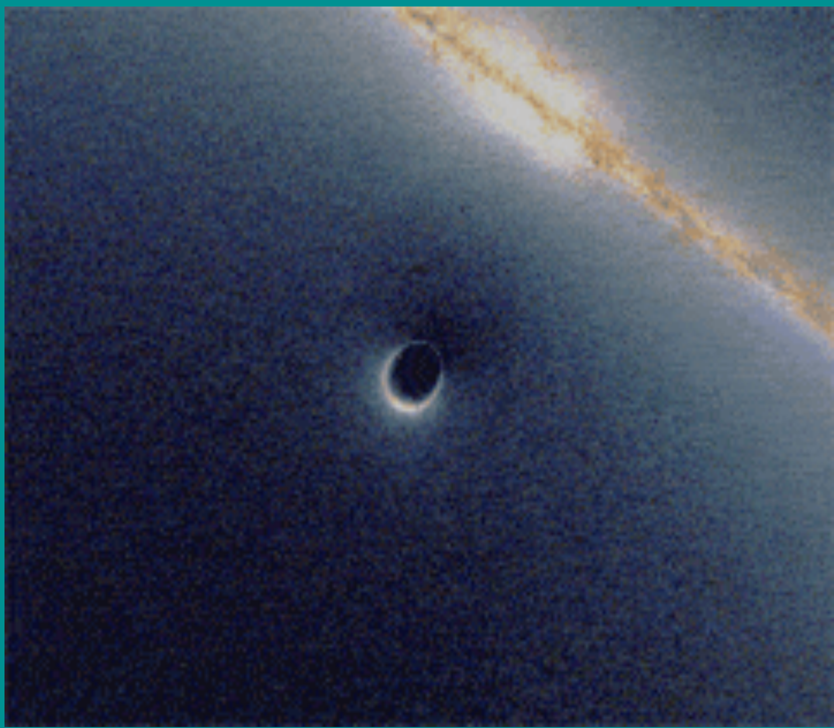

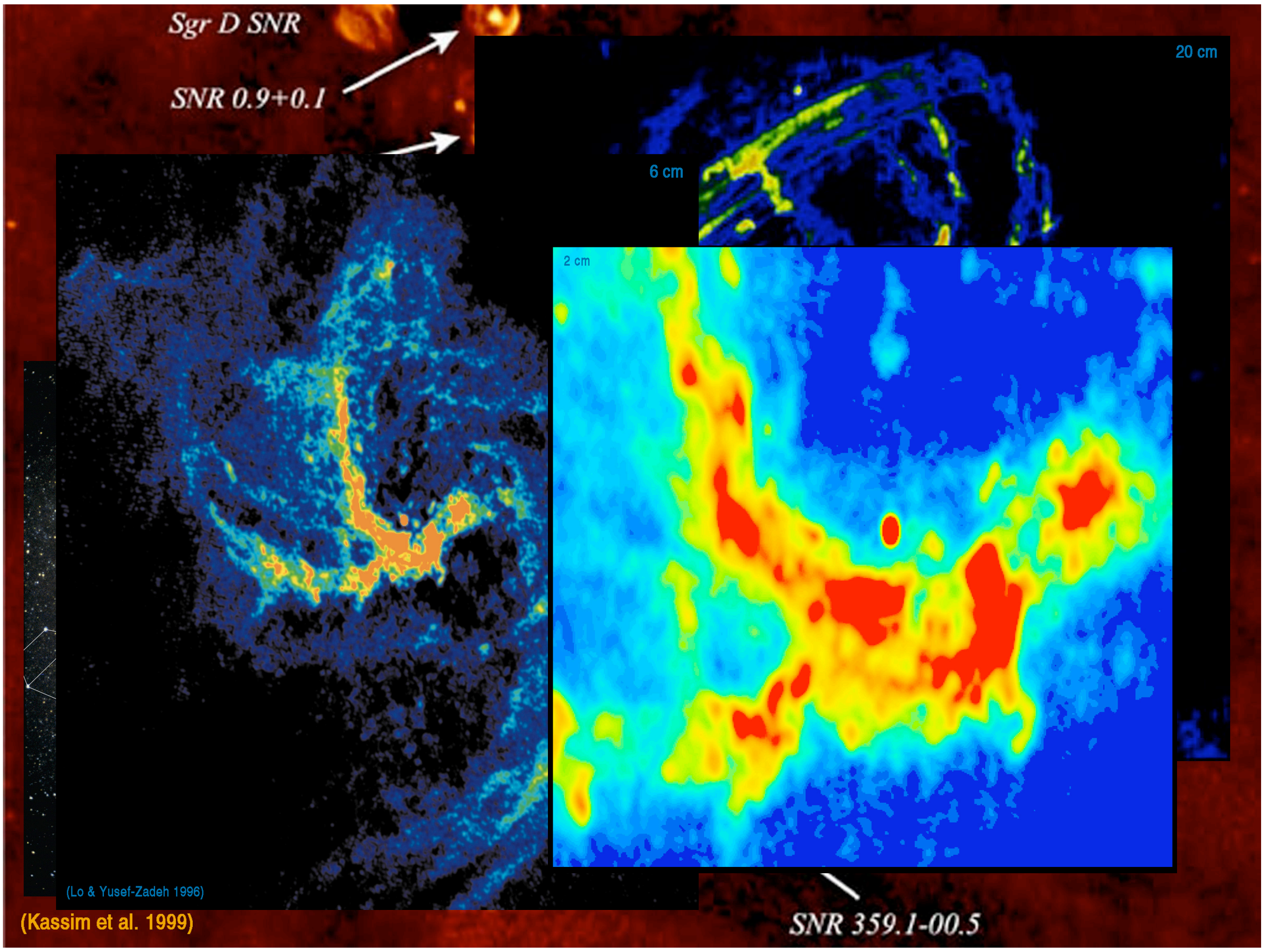

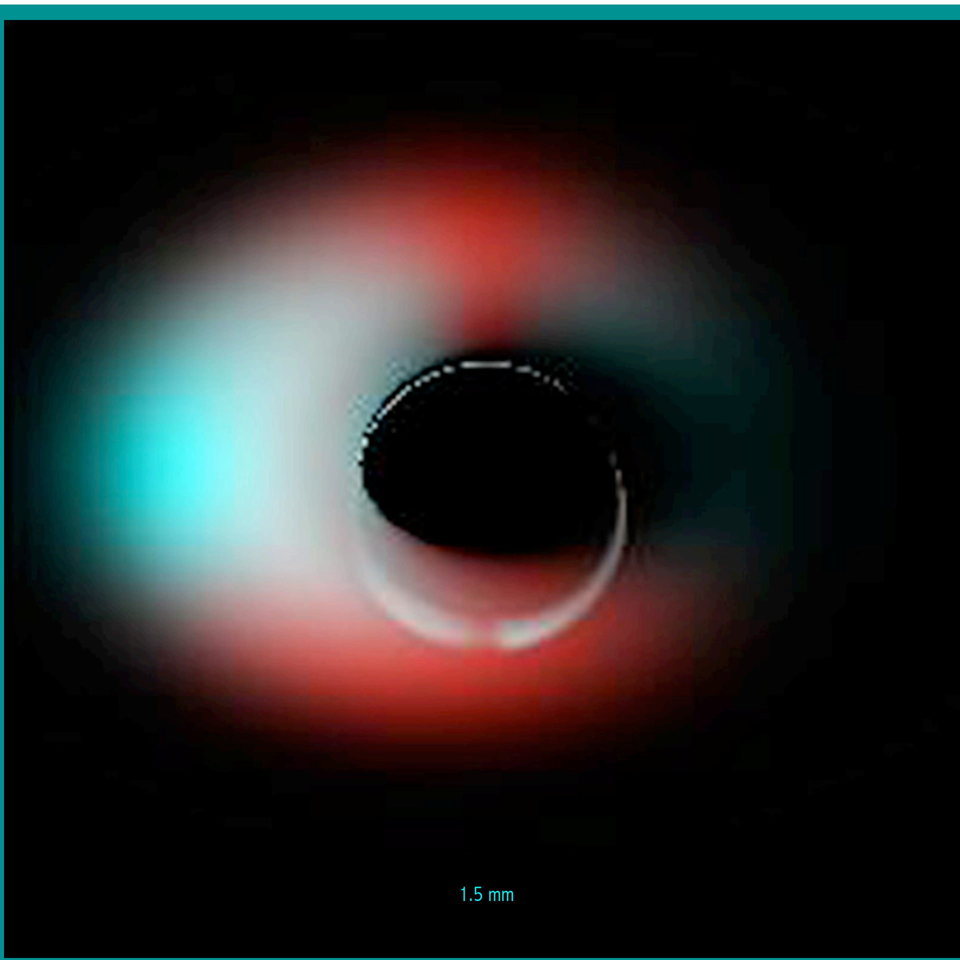

Stars circling Black Hole at Galactic Centre

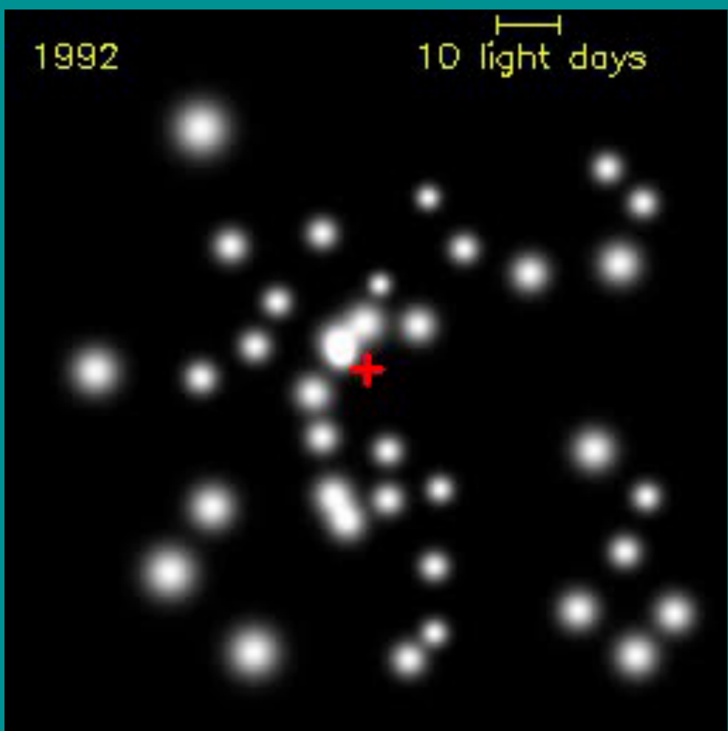

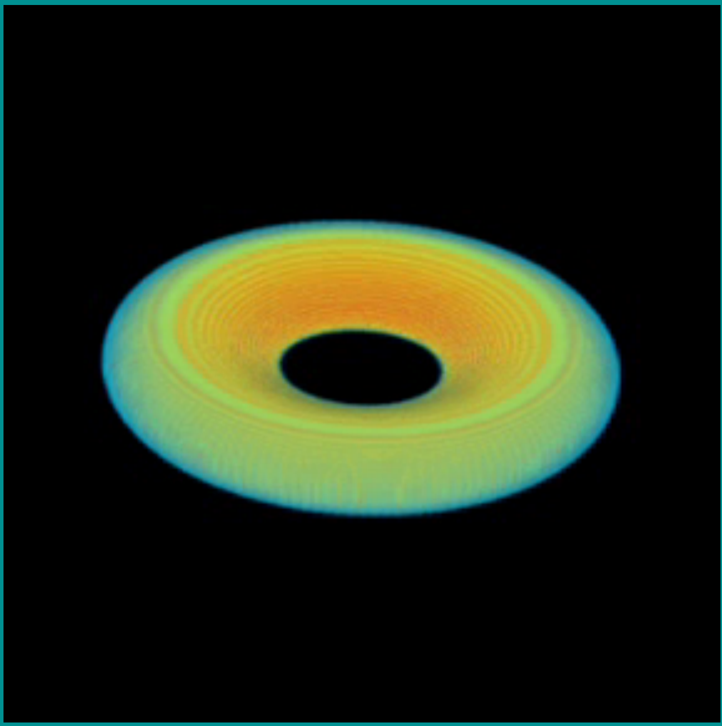

Overall 3D

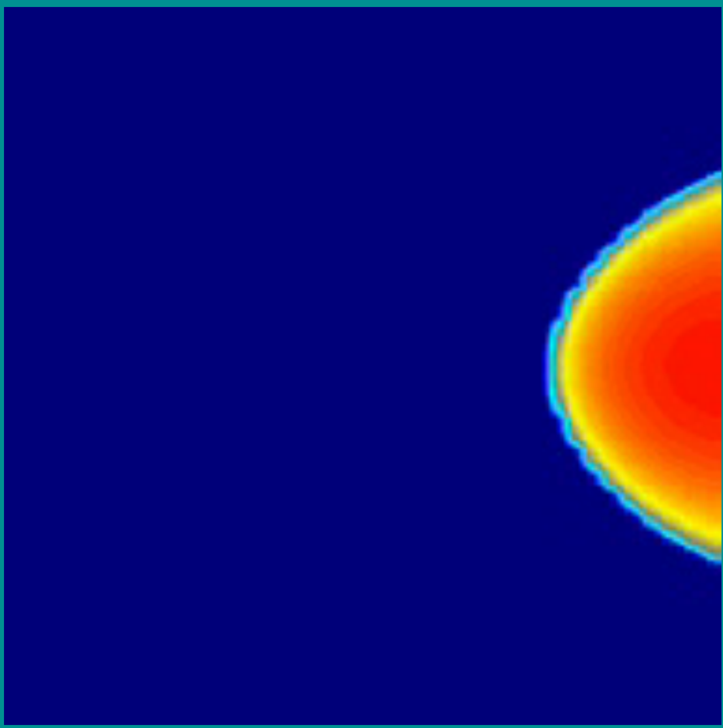

3DRZmovie

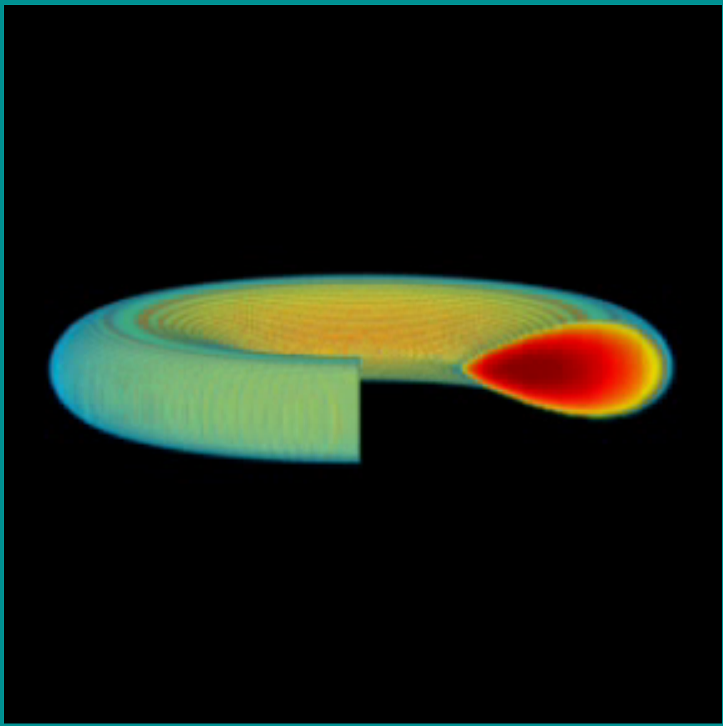

DensityMinChunk

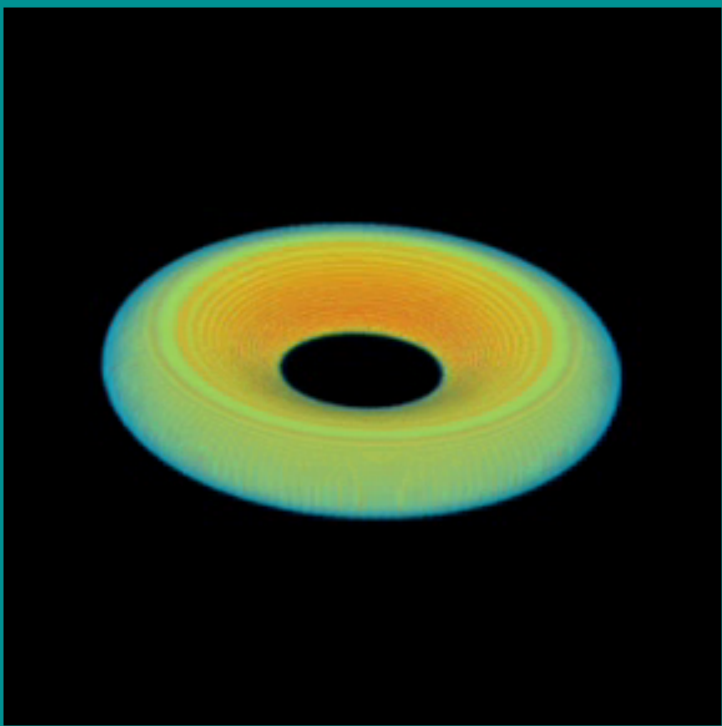

Equatorial Plane,   John F Hawley

Seyfert Galaxy

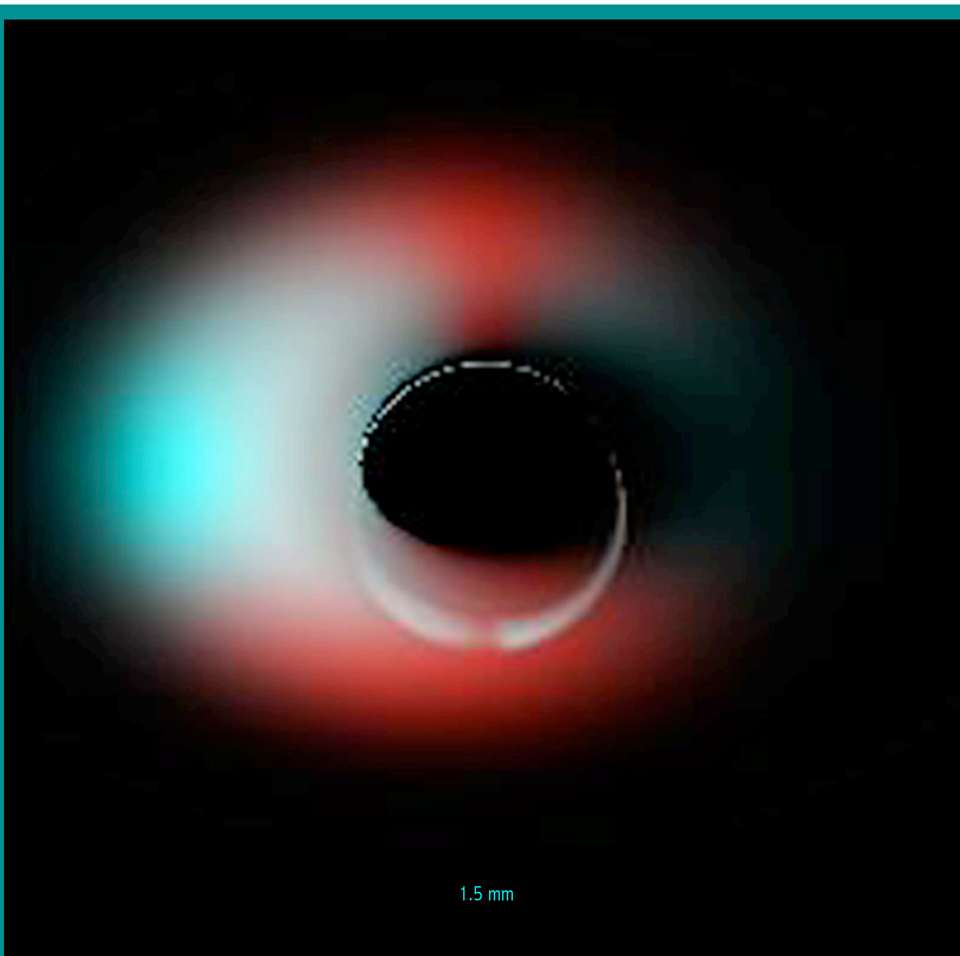

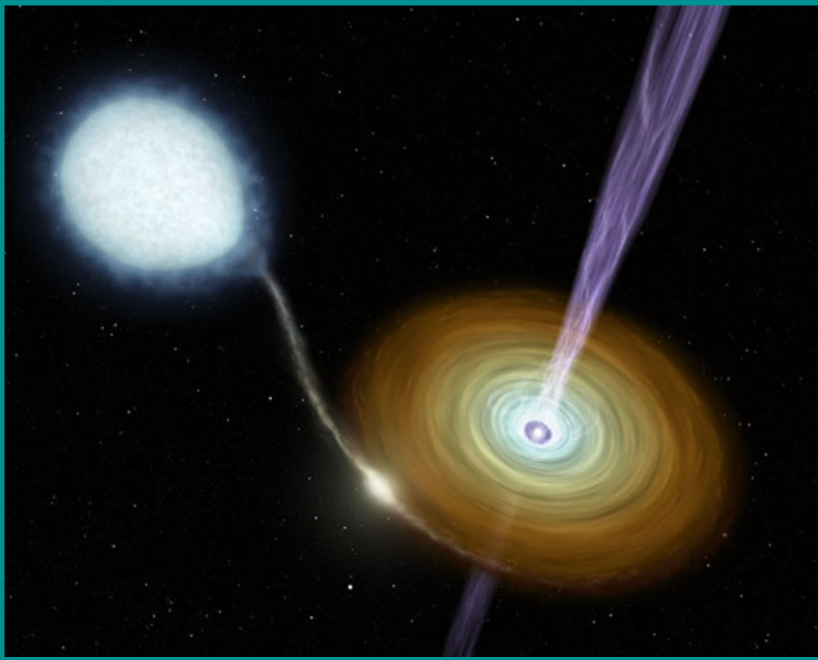


(NASA)

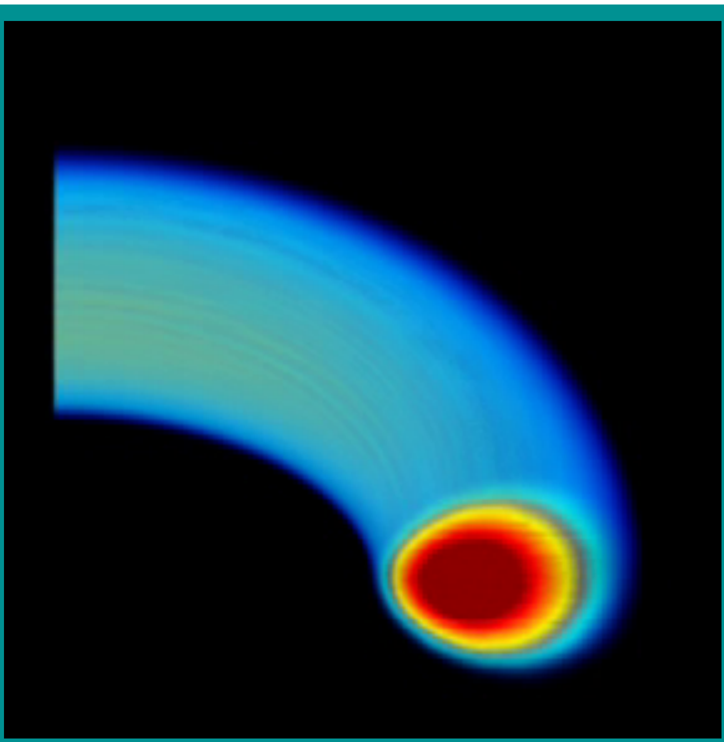

RunF01

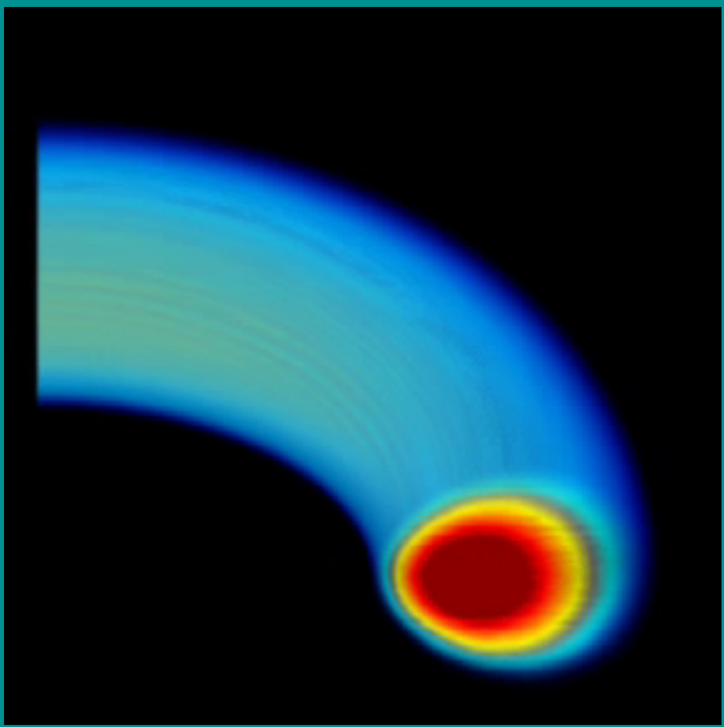

RunFZoom

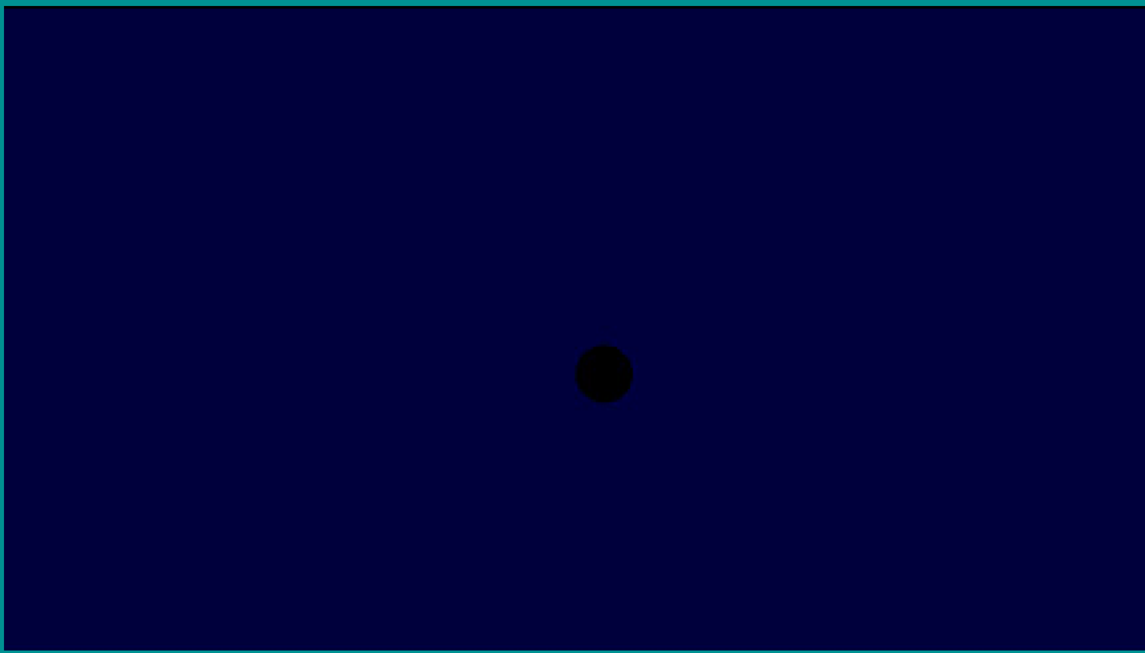

Jet Formation, John F Hawley

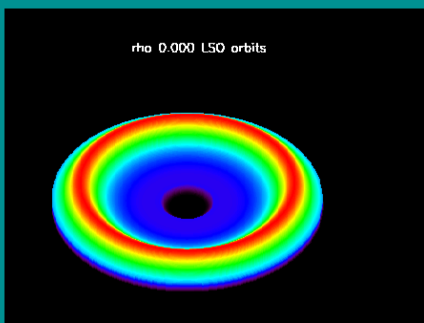

Tagger and Melia (2006)

Unravelling Einstein’s Secrets

Professor Roy Patrick Kerr

University of Canterbury, New Zealand

Newton’s Theory of Gravitation

The inverse square law: The force between two bodies is proportional to the product of their masses and inversely proportional to the square of the distance between them.

$$\boxed{F = \frac{GM_1M_2}{R^2}}$$

If one of the bodies moves then an immediate change is felt across the universe. This means the speed of gravitational signals is infinite. Newton thought that this was ridiculous, but he could not think of a good alternative

1905 - Special Relativity

Lorentz

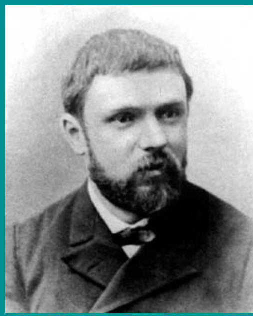

Grossman

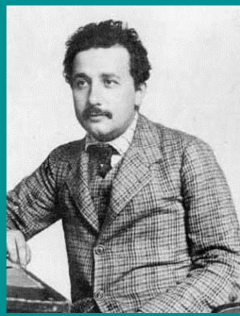

Einstein

- The velocity of light, *c,* is the same for all observers.
- The equations of physics are the same for all.
- No signal travels faster than light.
- Newton's theory says gravitation acts instantaneously.

$$\boxed{E = mc^2}$$

Newton's theory is inconsistent with Special Relativity

General Relativity

Albert Einstein

Marcel Grossmann

David Hilbert

"Matter and energy curve space and time"

$$\boxed{G^{\mu\nu} = 8\pi G T^{\mu\nu}}$$

The geometry of space-time determines the motion of all bodies in it. The quickest path between two space-time events is called a geodesic and this is the equivalent of a straight line in Euclidean space. As the Earth moves around the sun it thinks that it is moving on a straight line!

The first test of General Relativity

- The Perihelion of Mercury: It was already known that if Newton's theory was replaced with one that was consistent with special relativity so that there was no longer instantaneous action at a distance, then half of the precession could be explained.
- As soon as Einstein had formulated his theory he calculated the motion of small bodies (the planets) around a much larger central body (the sun). He did not need an exact solution for the gravitational field around the sun, although Schwarzschild's solution appeared soon afterwards
- When this was applied to Mercury's orbit the calculated precession was in agreement with the previous experimental results, 43" per century!
- This result was enough for Einstein to have complete faith that his theory was correct.

Solar System

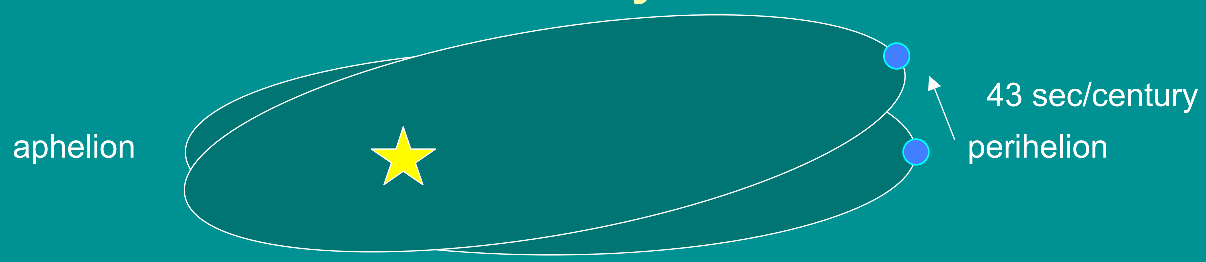

- The place where a planet is furthest from the sun is called the "perihelion".
- In Newton's theory this remains the same, orbit after orbit.
- It was observed that the perihelion of the planet Mercury advances by 43" (43 seconds of arc) per century, and so it rotates completely around the sun every 3,000,000 years.
- The same is true for the other planets but the effect is much smaller

Second Test: Bending of Light

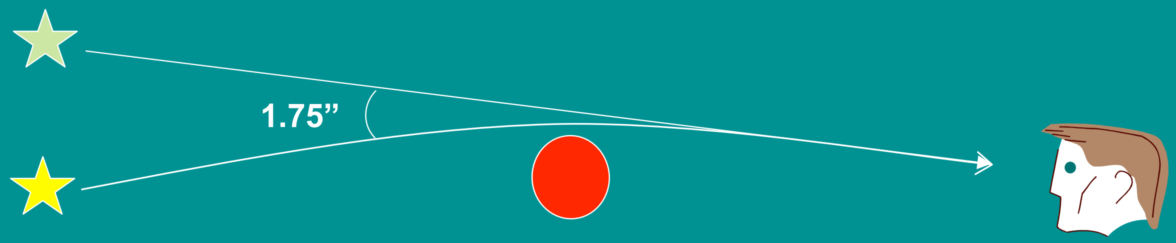

- Einstein’ theory predicted that light passing close to a massive body would curve towards it. This amounts to 1.75” close to the sun. The only time that photographs can be taken successfully near the sun is during a solar eclipse so the observations had to wait for a suitable moment. This did not occur until after World War I.

Bending of Light around the Sun

- Light bending by a strong gravitational field was not a new idea. In 1801 J. Soldner had pointed out that Newtonian gravity predicts that starlight will bend around a massive object, but the effect is only half that predicted by General Relativity and calculated by Einstein.

- Sir Arthur Eddington organised two of the most famous scientific expeditions in history to observe this bending during a solar eclipse in 1919. He led the first of these to Principe in Africa and sent a second to Sobral in Brazil, in case it was raining at the first site. In fact, the weather was bad in Principe but Eddington was still able to take some useful photographs.

Agreement with Relativity, disagreement with the Newtonian alternative

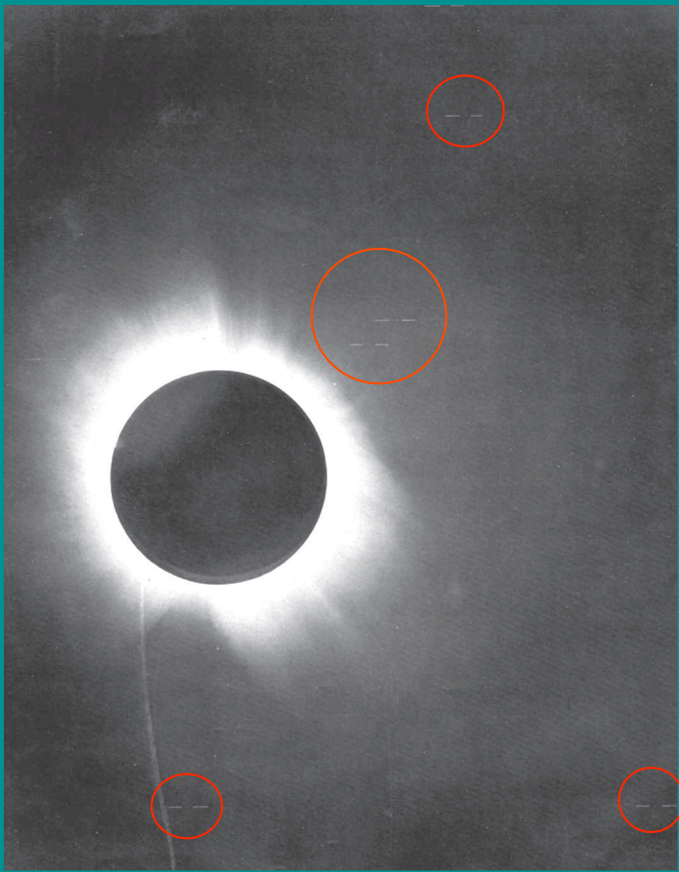

A reproduction of one of the negatives taken by Eddington's group using the 4-inch lens at Sobral, in Brazil. The positions of several stars are indicated with bars. When compared to other photographs taken of the same region of the sky, it became apparent that those closest to the rim of the Sun appeared to have shifted slightly.

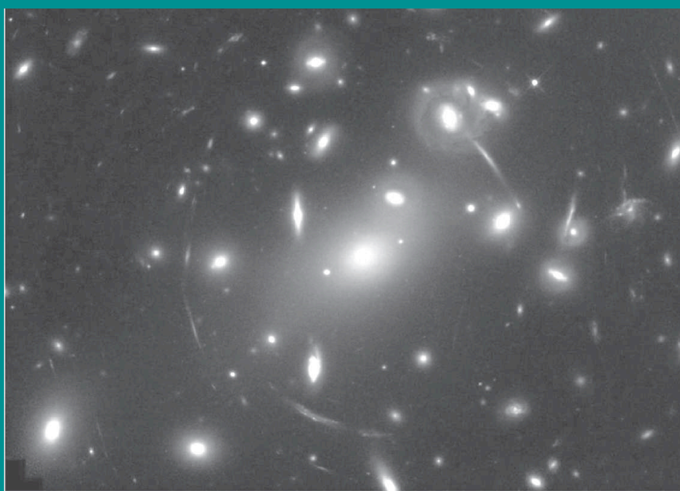

A modern example of light-bending . There is a Quasar behind the bright galaxy in the centre of the picture, but 5 times further away. Its light forms an “Einstein ring”.

This bending of light is being used to study the universe. The amount of distortion of images tells us about the total mass in any region. This is the best evidence for the existence of dark matter clustered around galaxies formed from standard matter.

Question: Does dark matter clustering cause ordinary matter to collect around it

1873-1916

The Schwarzschild Solution

Within a year of Einstein proposing his theory, Professor Karl Schwarzschild constructed a metric that was to be the most important solution of Einstein's equations for the next 40+ years. It gave the gravitational field outside a "spherically symmetric" body, i.e. one that looks the same from all directions.

$$\boxed{ds^2 = \left(1 - \frac{2GM}{rc^2}\right)^{-1} dr^2 + r^2(d\theta^2 + \sin^2\theta d\phi^2) - \left(1 - \frac{2GM}{rc^2}\right) c^2 dt^2}$$

There was something strange happening at what is called the Schwarzschild radius where the factor in brackets is zero. The sphere with this radius is called the event horizon.

$$\boxed{r = \frac{2GM}{c^2}}$$

At first it was thought that the metric was "singular" on this sphere, i.e. that the curvature became infinite as one approached it.

Eddington Coordinates

1882-1944

In 1924 Sir Arthur Eddington showed that the Schwarzschild solution is not singular at the Schwarzschild radius. He did this by changing to a new set of coordinates,

$$\boxed{ds^2 = dx^2 + dy^2 + dz^2 - c^2dt^2 + \frac{2GM}{rc^2}(dr + cdt)^2}$$

When the mass is zero the last part vanishes and the metric is that for flat space, the space-time of special relativity. This is usually called the Minkowski metric.

The only singular point for this metric is at the centre where the radius, r, is zero.

This simple form of Eddington will appear again in this talk. For historical reasons it is now called the Kerr-Schild form,

$$\boxed{ds^2 = \text{flat space} + \lambda(.....)^2}$$

The dreaded "Black Hole" appears!

- Eddington showed that the event horizon is well behaved but there is something strange happening there.
- A spaceship can approach as close as it likes to this surface and still escape from the gravitational field of the central body, but if it ventures inside the event horizon then there is no return. It is drawn rapidly to the central singularity.
- For a normal body such as the earth or the sun, the event horizon would be deep inside. However, it is then a meaningless concept as Schwarzschild gives the gravity outside, and not on the inside of the physical object.
- If the Earth and the Sun were to collapse to black holes then the radii of their event horizons would be 1cm and 3km respectively.
- The density of the Sun as it collapsed inside its event horizon is 20,000,000,000,000 kg per cubic centimetre, denser than a Neutron star.
- The Sun is 300,000 time heavier than the Earth. The density of the Earth as it collapsed inside its event horizon would therefore be

  1,800,000,000,000,000,000,000,000 kg per cubic centimetre.

It cannot happen!

The search for "rotating Schwarzschild"

- The gravitational field outside any non-rotating spherical star must be that found by Schwarzschild. This field is constant in time, even though the matter inside may evolve.
- If the star collapses inside its "event horizon" it becomes a black hole. No object or message can be sent from the inside to the outside of this sphere.
- All bodies in the universe rotate. Although it may be only small, nothing is ever absolutely still. Schwarzschild is a beautiful solution but nature likes rotation. Furthermore, as a body collapses it rotates faster.

The search for a rotating generalisation of Schwarzschild

- Physicists wondered whether a spinning object could form a Black Hole or whether the spin would make the event horizon disappear.
- For 40 years they searched for a spinning black hole solution of Einstein's equations.
- For simplicity, the star was assumed to be rotationally symmetric (like a normal bottle or glass) and unchanging with time.
- The equations were then put into many elegant and beautiful forms but no rotating solution was constructed.

Some additional assumption was needed.

Alexey Z. Petrov (1910-71)

- Alexey Petrov was a Russian who studied general properties of the curvature in an Einstein space (such as our universe!)
- For almost all known physical solutions of Einstein's equation, including that of Schwarzschild, the curvature had a special property. They were all "Algebraically Special".
- This property also seems to be true for the gravitational field far from any source.

1960: Let's look for "Algebraically Special" solutions of the empty Einstein equations!

Ivor Robinson

Andrzej Trautman

They made a further assumption, leading to the Robinson-Trautman metrics in 1962.

$$ds^2 = r^2 P^{-2}(dx^2 + dy^2) - 2dudr - [\Delta \ln P - 2r(\ln P)_{,u} - 2m(u)/r]du^2$$

$$\Delta\Delta(\ln P) + 12m(\ln P)_{,u} - 4m_{,u} = 0, \qquad \Delta = P^2(\partial_x^2 + \partial_y^2)$$

STILL NOT ROTATING!!

Previous attempts

- Ivor Robinson continued his study of the most general lgebraically special space-times. This would be completed later.
- In 1962-3 a group centred in Pittsburgh announced that they had solved the complete problem and that there was there was only a fairly non-interesting generalisation of Schwarzschild, NUT space.
- I had been studying the same problem and was very surprised at this result, as were Ivor Robinson and Andrzej Trautman.
- A preprint containing the proof was sent to Alfred Schild and Alan Thompson at the University of Texas in Austin. I was also there at that time, and was in the same small apartment building as Alan.
- Neither Alan nor Alfred could see anything wrong with the paper. Alan then gave it to me to see why there were no interesting algebraically special Einstein spaces.

Examining the paper

- I thumb through the paper to see where this surprising result came from – what equation told them that the search was futile.
- I find a simple equation that seemed to be the key to their result,

$$\boxed{2A + A - 2A = 0 \text{ gives } A = 0!}$$

- I do not know what A is but this equation seems to be the crux of their argument, so I look back to see where it came from and find that it cannot be true. The coefficients must sum to zero because of the "Bianchi Identities" .
- I rush next door and tell Alan that the conclusions are false. We calculate the first of the three terms and find that it is incorrect. The equation now reads

$$\boxed{A + A - 2A = 0 \text{ gives } 0 = 0!}$$

- I then calculate the correct field equations for Algebraically Special spaces. This is announced at a conference in New York. The author of the original paper says "Yes, but the second coefficient was a misprint. The equation is

$$\boxed{A + 2A - 2A = 0 \text{ gives } A = 0!}$$

- I say "OK, then the third must be wrong!" Alan and I calculate it that night and find that the correct equation is

$$\boxed{2A + A - 3A = 0 \text{ gives } 0 = 0!}$$

Path to Kerr Solution

- Assumed algebraically special. This reduces the ten Einstein equations to five, and the metrics dependence on the radial coordinate, "r", is known. However, the equations are much worse than those of Robinson and Trautman so something else is needed.
- Assumed independent of time. Now the equations are getting better, but they are still intractable.
- Assume axially symmetry. This reduces the field equations down to ordinary differential equations which can be solved.
- The space-time now depends on four real numbers, or parameters. These characterise the metric completely. Getting near!!
- Since I am looking for a physically interesting space-time I require the space to be Minkowski space (special relativity) at large distances. Two parameters are removed.

This leaves a solution with only two parameters, (M, a).

Kerr metric in Kerr-Schild form

The metric is rather nasty in the coordinates originally used to find it, but I realise that it can be put into the simple Kerr-Schild form,

$$\boxed{ds^2 = dx^2 + dy^2 + dz^2 - c^2dt^2 + \frac{2GMr^3}{r^4 + a^2z^2}(cdt + ...)^2}$$

When a = 0 the metric reduces to Schwarzschild mass with mass M

DOES IT ROTATE WHEN "a" IS NONZERO?

I tell Alfred Schild, the director of the "Gravitational Research Centre" in Austin, that I am going to my office to calculate the angular momentum of the last remaining hope. He says "Fine, I am coming too!"

Alfred sits in an armchair smoking his pipe while I chain smoke cigarettes and calculate. Finally, I announce

YES!!

Kerr metric in Kerr-Schild form

$$ds^2 = dx^2 + dy^2 + dz^2 - c^2dt^2 + \frac{2GMr^3}{c^2(r^4 + a^2z^2)}(k_\alpha dx^\alpha)^2,$$

$$k_\alpha dx^\alpha = cdt + \frac{z}{r}dz + \frac{r}{r^2+a^2}(xdx + ydy) - \frac{a}{r^2+a^2}(xdy - ydx),$$

Where the "radial" function r is given by

$$\boxed{\frac{x^2+y^2}{r^2+a^2} + \frac{z^2}{r^2} = 1.}$$

Event Horizons for Kerr Black Hole

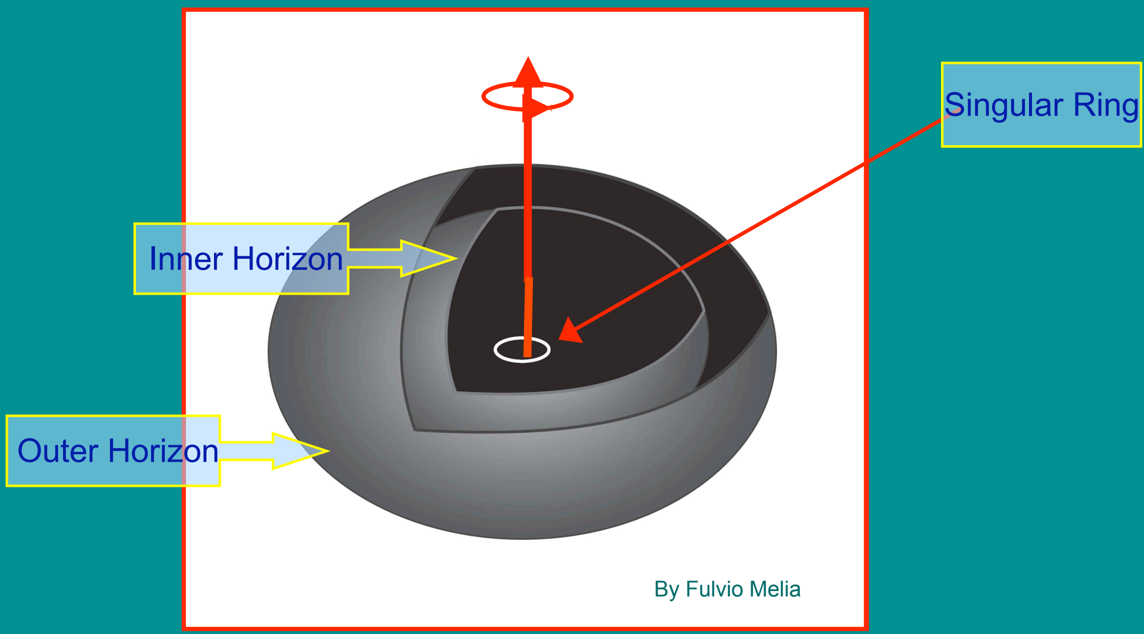

First Texas Symposium on Gravitation and Astrophysics

- In December 1963 a meeting is arranged in Dallas Texas to discuss the newly discovered and highly energetic objects in the sky. These will later be called “Quasars”, short f or “QUASi-stellAR radio sources”. At least 300 astronomers/astrophysicists and 50 Relativists attend.
- There are many theories presented but none that have broad appeal.
- Hoyle and Burbidge suggest a giant star with the mass of at least a million suns. Even this does not produce enough energy to power the observed quasars. Black holes are mentioned but the non-rotating Schwarzschild metric is far too unlikely.
- On hearing that Roger Penrose is going to give a talk on my solution, I tell the organisers that that is my pleasure, and then I give a 10-15 minute talk explaining its geometry and that it rotates.
- The astronomers are totally uninterested and ignore my talk.
- Papapetrou screams at them that he and others have worked for 30 years to find this metric and that they should listen. They ignore this.

Kerr-Schild metrics

- Around Christmas 1963, after the First Texas Symposium in Dallas, I spend a morning investigating whether there are other Algebraically Special spaces that have the Kerr-Schild form. There seem to be a large class that depend on a "function of a complex variable" and include the Kerr rotating solution but none of the others are of physical interest so I just let them lie.
- Jerzy Plebansky, a very well-known Polish relativist visits Austin for Christmas. Alfred Schild holds one of his excellent parties for Jerzy. During this I hear them mention their interest in spaces of the Kerr-Schild form (that name had not been invented at that time, of course).
- I say "I think I know of a large group of those, but the result was not checked and may be rubbish".
- Alfred and I retire to his office and do a small calculation that shows that any metric of this type has to be Algebraically Special.
- Next day we redo my original calculations, verifying that they were correct.
- We subsequently add an electromagnetic field to the problem, and find that there is a natural charged version of Kerr, the Kerr-Newman charged black holes. This is also discovered by Ted Newman by testing various ways that charged Schwarzschild (Reissner-Nordstrom) and Kerr might be amalgamated!

Powerpoint\Jena-TwistedPants_m4.avi

Afterwards

- It is proved a few years later by David Robinson, another New Zealander, that there are no other spinning black hole solutions. All properties of the star are lost when it collapses, except for its mass, angular momentum and electric charge. John Archibald Wheeler coined the phrase “Black Holes have no hair” to express this.
- Do Black Holes really exist? Probably. We appear to be seeing millions or more black holes in the universe. It may be that every galaxy formed around a Black Hole that was created soon after the “Big Bang”. We do not know, but Black Holes have something to do with the formation of galaxies.
- Are Black Holes truly represented by the Kerr solution? Yes, but only in the limit as they age. We can never see a Black Hole collapse inside its event horizon. For us, it is always just on the verge of doing so.
- The most famous example is at the centre of our own galaxy. It is called Sagitarius A* and is around 4,000,000 times as heavy as the Sun. Astronomers expect to be able to photograph it within the next ten years.

Black Hole in front of a spiral galaxy

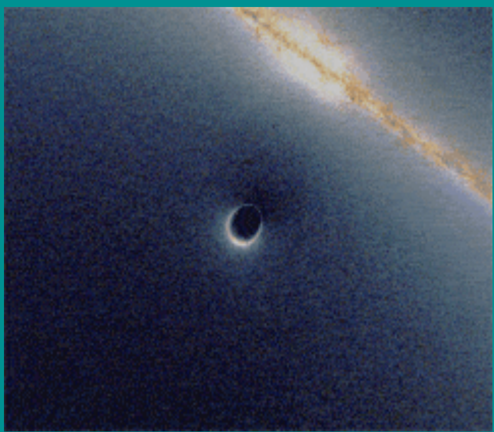

- This is the picture of a nearby Black Hole and a distant galaxy. It is a spiral galaxy with a central bulge, just like ours, seen side on. Of course, no such event has actually been photographed. It is just a computer simulation.
- Notice how the light from the galaxy bends around the back of the Black Hole. It gets very complicated as the Black Hole crosses in front of the galaxy.

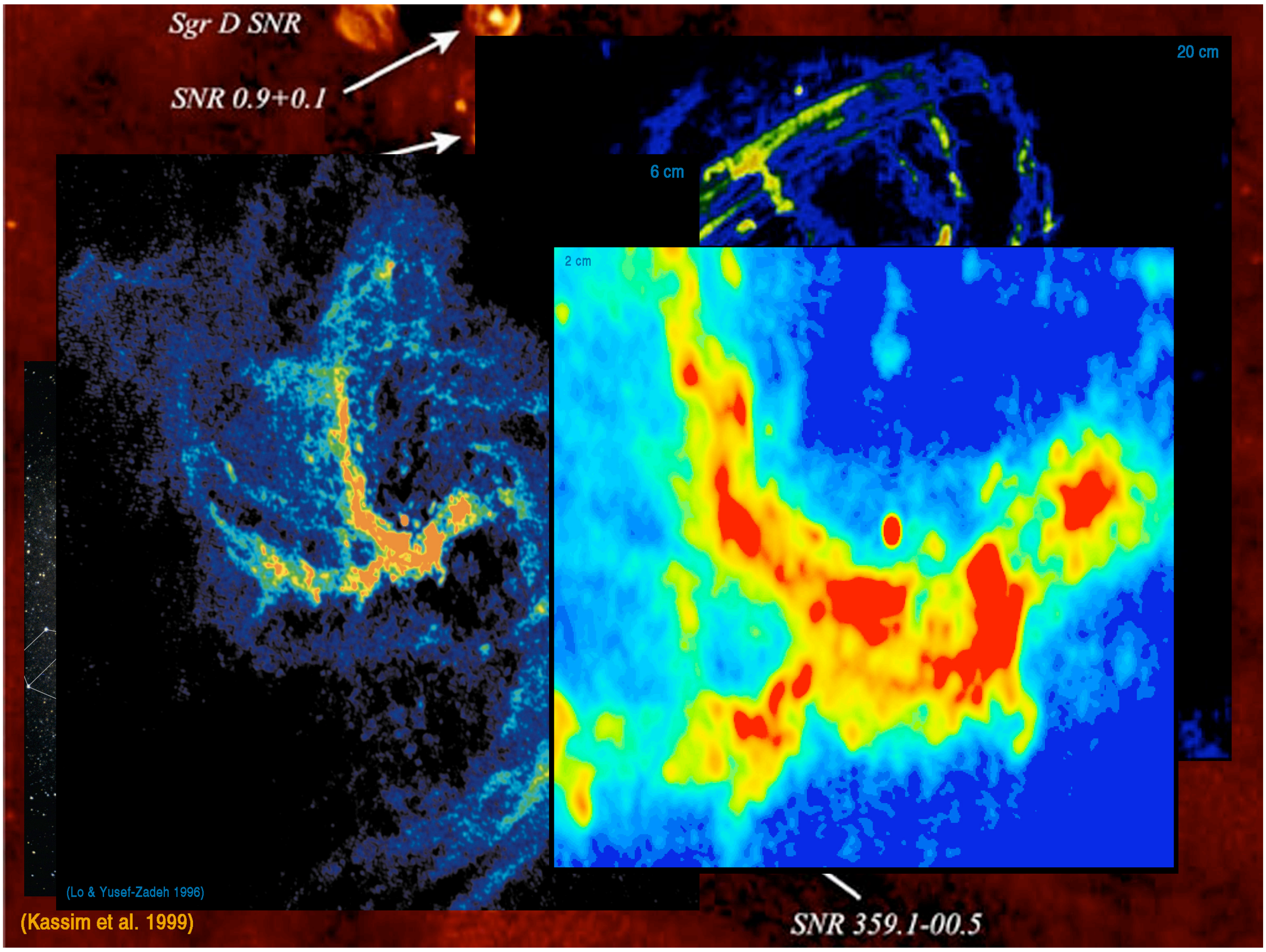

Stars circling Black Hole at Galactic Centre

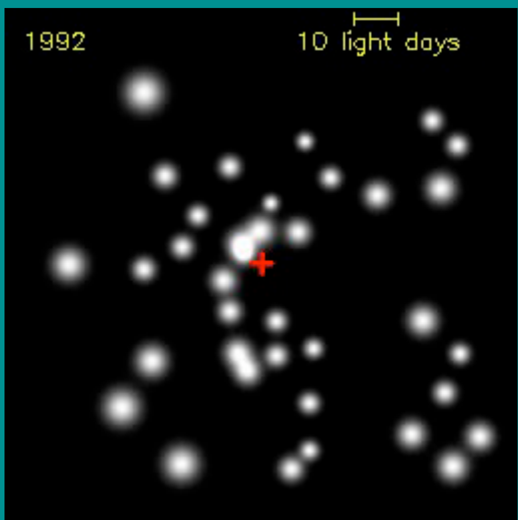

This is a series of real photographs of the stars circling the Black Hole at the centre of our very own galaxy. The star coming in from the top left on a cometary orbit takes 13 years to circle the Black Hole. It has now been observed for one complete orbit. From these orbits the mass of the central object has been calculated to be almost 4,000,000 times the mass of our Sun.

Black hole production at the LHC

Hirotaka Yoshino[1]

[1] *Department of Physics, University of Alberta, Edmonton, Alberta, Canada T6G 2G7*

Abstract

In the TeV gravity scenarios, black holes are expected to be produced at the Large Hadron Collider (LHC) in CERN. In this article, we review the current status of the theoretical studies on this issue. After a brief overview, we explain our studies on the apparent horizon (AH) formation in high-energy particle collisions.

1 Introduction

Almost a decade ago, scenarios in which the Planck energy M_p could be O(TeV) were proposed [1]. In these scenarios, our 3-dimensional space is a brane floating in large extra dimensions, and gauge particles and interactions are confined on the brane. Since the TeV scale energy will be reached by the Large Hadron Collider (LHC) in CERN, we have a possibility to observe quantum gravity phenomena by experiments. Specifically, in the collision with the energy much higher than the Planck scale, the black hole production is expected [2]. Since the LHC is planned to begin operation in 2008, the black hole production at the LHC is a very timely topic. In this article, we review the theoretical studies on this issue. We give a brief overview in the next section. In Sec. 3, we focus attention to our studies on the apparent horizon (AH) formation in high-energy particle collisions.

2 Brief overview

The LHC is designed so that protons collide with the center-of-mass energy 14 TeV. In the collisions, the partons interact with each other and black holes could be produced in these processes. If a black hole is produced, it emits mainly the gravitational wave and become a stationary higher-dimensional Kerr black hole (the balding phase). Then, the black hole will evaporate by the Hawking radiation (evaporation). The particles emitted in this process can be observed by the detectors such as the ATLAS. In the final phase of evaporation, the quantum gravity effects may become important (the Planck phase). Let us look at these issues one by one.

2.1 Production rate

The black holes with mass (few)M_p are expected to exist, since its gravitational radius is larger than the Planck length. Then the trans-Planckian collision is expected to cause the gravitational collapse if the impact parameter is smaller than the gravitational radius $r_h(\sqrt{\tau s})$ of the parton-pair system. Thus the parton-parton cross section for the black hole production is estimated as $\sigma_{ij\to bh}(\tau s) \sim \pi[r_h(\sqrt{\tau s})]^2$. In order to obtain the proton-proton cross section for the black hole production, one should multiply the parton distribution functions and take the sum over all possible parton pairs:

$$\sigma_{pp\to bh}(\tau_m, s) = \sum_{ij}\int_{\tau_m}^{1} d\tau \int_{\tau}^{1}\frac{dx}{x}f_i(x)f_j(\tau/x)\sigma_{ij\to bh}(\tau s). \qquad (1)$$

Based on this calculation, the black hole production rate is expected to be 1Hz in the most optimistic estimate [2]. We remark that the production rate depends on the effect of balding and the black hole threshold mass. Also, the value of $\sigma_{ij\to bh}$ should be estimated by a direct calculation. The topics in Sec. 3 are related to these issues.

[1] E-mail:hyoshino@phys.ualberta.ca

2.2 Balding phase

Once a black hole is produced, it decays through several phases. The first phase is the so-called balding phase. In this phase, the produced black hole emits gauge and gravitational radiations and eventually becomes a stationary higher-dimensional Kerr black hole. The gravitational radiation is expected to be larger than the gauge radiation. The characteristic time scale is estimated from the quasinormal frequency as $t_{\text{balding}} \sim M_p^{-1}(M/M_p)^{1/(D-3)}$, where D is the spacetime dimensionality.

Since the radiations carry part of the system energy and angular momentum, the final mass and angular momentum of the black hole is determined by the amount of the radiations. For this reason, the study of the balding phase is important in order to estimate the distribution of the mass and angular momentum of produced black holes. However, because of the highly nonlinear nature of high-energy particle systems, the study of this process is very difficult even numerically. So far there are no reliable estimates of the amount of radiations, although several attempts have been made including the interesting one by Pretorius [3].

2.3 Evaporation

The produced black hole evaporates by the Hawking radiation. The evaporation phase is further divided into two phases: the spin-down phase and the Schwarzschild phase. In the spin-down phase, the angular momentum of the black hole is extracted by emission of spin particles. After that, the black hole is Schwarzschild-like and the emission becomes almost isotropic. The characteristic time scale is estimated as $t_{\text{evaporation}} \sim M_p^{-1}(M/M_p)^{(D-1)/(D-3)}$, which is larger than t_{balding} for $M \gg M_p$. The energy spectrum of emitted particles are almost thermal and the temperature is $T_H = (D-3)/4\pi r_h(M)$. Since the number of brane fields is much larger than that of the bulk fields, the black hole radiates mainly on the brane [4] (though there are several subsequent discussions on this issue).

The emitted particles can be detected at the LHC. If the 10TeV mass black hole is produced, the signals have the following features: (i) $\sim$ 50 quanta with energy 150-200 GeV; (ii) Large transverse momentum; (iii) $\sim$ 10% hard leptons and $\sim$ 2% hard photons. The S/N ratio of lepton and photon events is very large, and it makes the detection easier. In fact, the ATLAS group demonstrated that the detection of black hole events is relatively easy by constructing the event generator [5].

We comment on the studies of the greybody factors. Because of the curvature scattering, part of the emitted particles is absorbed by the black hole and the spectrum differs from that of the black body. These effects were studied by many authors. The greybody factors of the Schwarzschild black hole were numerically calculated for both brane fields and bulk gravitons [6]. The greybody factors of the Kerr black hole were studied by full numerical calculations for brane fields [7]. Thanks to their studies, the temporal evolution of the evaporation can be calculated quite accurately. The recently constructed event generator takes account of the effects of these greybody factors [8]. Note that the greybody factor of the Kerr black hole for bulk gravitons is left as a remaining problem.

2.4 Planck phase

As the black hole evaporates, the mass decreases and becomes close to the Planck mass M_p. In this phase, the quantum gravity effects may become important. Currently there are no reliable predictions for this phase since we have no theory of quantum gravity. Rather, we can able to learn the dynamics of quantum gravity from the experiments. This opens up an interesting possibility to construct the quantum gravity theory based on the experiments. If this is the case, we might be able to resolve e.g. the information loss problem.

3 Studies on the apparent horizon formation

Now, we turn to the studies on the apparent horizon (AH) formation in high-energy particle collisions by ourselves. Motivation for our studies is as follows. In Sec. 2.1, the parton-parton cross section for the black hole production is assumed to be $\sigma_{ij\to bh} = \pi[r_h(2p)]^2$, where p denotes the energy of each incoming particle. Since this is just the order estimate, the realistic cross section will be $\sigma_{ij\to bh} = F_{ij}(D)\pi[r_h(2p)]^2$, where $F_{ij}(D)$ depends on the characters of the incoming particles such as charges and spins as well as the dimensionality D. It is necessary to obtain the reliable cross sections by direct calculations.

The AH is defined as a closed $(D-2)$-dimensional spacelike surface whose outgoing null geodesic congruence has zero expansion. Assuming the cosmic censorship, the AH existence is the sufficient condition for the black hole formation when the null energy condition is satisfied. Therefore, the AH is a good indicator for the black hole formation. We studied the AH formation in the grazing collision of Aichelburg-Sexl (AS) particles [9, 10]. The charge effect and the effects of spin and duration were discussed in [11] and [12], respectively. We briefly review these studies one by one.

3.1 Aichelburg-Sexl particle collision

In [9, 10], we studied the AH formation in the collision of AS particles with the impact parameter b, using the $(D \geq 4)$-dimensional general relativity. By using the AS particles, we ignored charges and spins of incoming particles, the brane tension and the structure of extra dimensions. By numerically calculating the cross section $\sigma_{\rm AH}$ for the AH formation, we found a lower bound on $\sigma_{ij\to bh}$.

The AS particle is a simple massless pointlike particle whose metric for $D \geq 5$ is

$$ds^2 = -dudv + \sum_i dx_i^2 + \Phi(r)\delta(u)du^2, \quad \Phi(r) = \frac{16\pi G p}{(D-4)\Omega_{D-3} r^{D-4}}, \tag{2}$$

where $r := \sqrt{\sum_i x_i^2}$ and the particle is located at $r = 0$. The gravitational field is distributed in the transverse plane to the motion, and it propagates at the speed of light along $u = 0$. We can set up the collision of two AS particles by just combining two metrics, since they do not interact before the collision. In this spacetime, the two incoming waves propagate along $u = 0$ and $v = 0$, and collide at $u = v = 0$. The locations of particles in the transvese plane are $x_i = (\pm b, 0, ..., 0)$, where b is the impact parameter.

The equation and the boundary conditions for determining the AH on the slice $u \leq 0 = v$ and $v \leq 0 = u$ were derived by Eardley and Giddings, and they solved the AH analytically in the case $D = 4$ [13]. Unfortunately, their method could not be applied to the higher-dimensional cases, and myself and Nambu [9] developed a numerical code to solve this problem. In Ref. [10], myself and Rychkov improved this result by solving the AH on a different slice, $u \geq 0 = v$ and $v \geq 0 = u$. The results of these two works are summarized as follows:

D	4	5	6	7	8	9	10	11
$\sigma_{\rm YN}/\pi r_h^2(2p)$ [9]	0.65	1.08	1.34	1.52	1.64	1.74	1.82	1.88
$\sigma_{\rm YR}/\pi r_h^2(2p)$ [10]	0.71	1.54	2.15	2.52	2.77	2.95	3.09	3.20

These values give the reliable lower bounds on $\sigma_{ij\to bh}$ for the case of AS particle collisions. In addition, using the area theorem, we could find the lower bound $M_{\rm AH}$ on the mass of final state of the produced black hole $M_{\rm BH}$ by calculating the AH area (i.e. $M_{\rm BH} > M_{\rm AH}$). $M_{\rm AH}$ has the tendency to decrease as the impact parameter b and the dimensionality D are increased. Our results were used in e.g. [14] in order to improve the estimate of the black hole production rate at the LHC. Specifically, they compared the two cases $M_{\rm BH} = 2p$ and $M_{\rm BH} = M_{\rm AH}$. The result is that the two estimates of the black hole production rate differ by a factor 10^3–10^6, indicating the importance of the studies on the balding phase.

3.2 Charge effect

In [11], myself and Mann discussed the effect of electric charge on the AH formation. In that paper, we ignored the confinement of electromagnetic fields on the brane. Namely, using the higher-dimensional classical Einstein-Maxwell theory, we introduced the charged version of the AS particle as the particle model as the first step. We studied only the head-on collision cases for simplicity.

The metric of the charged AS particle is similar to Eq. (2), but the function $\Phi(r)$ has the correction term due to the charge:

$$\Phi(r) = \frac{16\pi G p}{(D-4)\Omega_{D-3} r^{D-4}} - \frac{16\pi^2 (2D-5)!! G\gamma q^2}{(D-3)(2D-7)(2D-4)!! r^{2D-7}}, \tag{3}$$

where q is the D-dimensional charge and γ is the Lorentz factor. Since the correction term is negative, it is expected that the charge makes the AH formaton difficult. In fact, we solved the AH analytically and found that the condition for the AH formation is roughly given as $\gamma q^2 \lesssim Gp^2$. This is rewritten as $\alpha C_\mathrm{b}^{D-4}(M_p/m)(M_p/p) \lesssim 1$ with the fine structure constant α, the brane thickness C_b in the unit of the Planck length, and the rest mass m. This condition cannot be satisfied at the LHC, and our result might indicate that the black hole production rate is highly suppressed by the charge effect. However, in the regime where the AH formation is prohibited in this model, the QED effects are found to be important by evaluating the so-called classical radius. Therefore, further improvement is required to obtain the definite conclusion.

3.3 Effects of spin and duration

In [12], myself, Zelnikov and Frolov discussed the effects of spin and duration on the AH formation using the gyraton model [15], which represents the gravitational field of a spinning radiation beam pulse. Although the gyraton is a classical model, it can be regarded as a toy model of the quantum wavepackets with spin. For simplicity, we considered only the head-on collision in four dimensions.

The gyraton metric is given by

$$ds^2 = -dudv + dr^2 + r^2 d\phi^2 - 8Gp\chi_p(u)\log r du^2 + 4GJ\chi_j(u)dud\phi, \tag{4}$$

where J is the angular momentum (spin) and the last term causes the repulsive gravitational field around the center. $\chi_p(u)$ and $\chi_j(u)$ are the functions normalized as $\int \chi_p(u)du = \int \chi_j(u)du = 1$, which specify the energy and angular momentum distributions. The characteristic width of $\chi_p(u)$ and $\chi_j(u)$ is the duration L of the gyraton. Using this model, we studied the AH formation numerically, and found that the condition for the AH formation is roughly expressed as $L \simeq r_h(2p)$ and $J \lesssim 0.4pr_h(2p)$. By assuming L to be the Lorentz contracted proton size $\sim 1.5 \times 10^{-4}$fm and J to be $\hbar/2$, the above two conditions are satisfied at the LHC. Therefore the spin effects might not have such a significant effect for the black hole production rate, though it could be changed by a factor.

References

[1] N. Arkani-Hamed, S. Dimopoulos and G. R. Dvali, Phys. Lett. B **429**, 263 (1998).

[2] S. Dimopoulos and G. Landsberg, Phys. Rev. Lett. **87**, 161602 (2001);
S. B. Giddings and S. Thomas, Phys. Rev. D **65**, 056010 (2002).

[3] F. Pretorius, arXiv:0710.1338 [gr-qc].

[4] R. Emparan, G. T. Horowitz and R. C. Myers, Phys. Rev. Lett. **85**, 499 (2000).

[5] J. Tanaka, T. Yamamura, S. Asai and J. Kanzaki, Eur. Phys. J. C **41**, 19 (2005).

[6] V. Cardoso, M. Cavaglia and L. Gualtieri, Phys. Rev. Lett. **96**, 071301 (2006).

[7] D. Ida, K. y. Oda and S. C. Park, Phys. Rev. D **67**, **71**, 124039 (2005); **73**, 124022 (2006).

[8] D. C. Dai, G. Starkman, D. Stojkovic, C. Issever, E. Rizvi and J. Tseng, arXiv:0711.3012 [hep-ph].

[9] H. Yoshino and Y. Nambu, Phys. Rev. D **67**, 024009 (2003).

[10] H. Yoshino and V. S. Rychkov, Phys. Rev. D **71**, 104028 (2005).

[11] H. Yoshino and R. B. Mann, Phys. Rev. D **74**, 044003 (2006).

[12] H. Yoshino, A. Zelnikov and V. P. Frolov, Phys. Rev. D **75**, 124005 (2007).

[13] D. M. Eardley and S. B. Giddings, Phys. Rev. D **66**, 044011 (2002).

[14] L. A. Anchordoqui, J. L. Feng, H. Goldberg and A. D. Shapere, Phys. Lett. B **594**, 363 (2004).

[15] V. P. Frolov and D. V. Fursaev, Phys. Rev. D **71**, 104034 (2005).

Surface terms and matching conditions in $f(R)$ gravity

Yuuiti Sendouda[1], Nathalie Deruelle[2] and Misao Sasaki[1]

[1] *Yukawa Institute for Theoretical Physics, Kyoto University, Kita-shirakawa Oiwake-cho, Sakyo-ku, Kyoto 606-8502, Japan*

[2] *APC, UMR 7164 (CNRS, Université Paris 7, CEA, Observatoire de Paris), 10, rue Alice Domon et Lonie Duquet, 75205 Paris Cedex 13, France*

Abstract

Within the framework of $f(R)$ gravity where f is an arbitrary function of the Ricci scalar, we obtain a surface term for action which allows initial-value formulation with Dirichlet boundary conditions. Based on the action principle, we find matching conditions for two spacetimes across a codimension-one brane/shell, which are generalisation of the Israel junction conditions in the Einstein gravity.

1 Introduction

Recent trends in studies of gravitation have been strongly motivated by the progresses in string theories, where we are urged to face some of the essences of the fundamental theories; Here one is higher dimensionality of the universe, while another is non-linear curvature corrections to the Einstein gravity. It is an urgent task to construct viable models in which those two aspects are appropriately taken into account.

For that purpose, we shall here consider D-dimensional spacetimes on which the following higher-curvature action for gravity is defined:

$$S_{\mathrm{g}} = \frac{1}{2}\int_{\mathcal{M}} \sqrt{-g} f(R), \tag{1}$$

where f is an arbitrary function of the Ricci scalar R. The idea of braneworld [1] is a simple way to extend the theory to higher dimensions without giving rise to immediate inconsistencies, where matters are confined in a lower-dimensional object, called brane. We shall focus on a particular case of codimension one, where the matter energy–momentum tensor can be written as

$$T_{ab} = S_{ab}\delta(y), \tag{2}$$

where y is the Gaussian coordinate normal to the brane.

Prior to more general analyses, the concept of "Einstein limit" provides some clue to the problem, in which "$f(R) \to R$" is brought about. In such a limit, the theory is naively expected to recover the ordinary Einstein gravity, however, an obstacle arises since the Einstein limit is not a *smooth* limit; To illuminate this, first vary the action with respect to the metric to find the fourth-order field equation

$$f'(R)G_{ab} + \frac{1}{2}(Rf'(R) - f(R))g_{ab} + (g_{ab}\Box - \nabla_a\nabla_b)f'(R) = S_{ab}\delta(y), \tag{3}$$

where we took brane into account as the matter source. Assuming continuity of metric and R, integration of the field equation across the brane leads to the following jump conditions

$$-f'(R)[K_{ab} - K\gamma_{ab}]^+_- + f''(R)[\partial_y R]^+_-\gamma_{ab} = S_{ab}, \quad [K]^+_- = [R]^+_- = 0, \tag{4}$$

where γ_{ab} is the metric induced on the brane and K_{ab} is the extrinsic curvature. $[A]^+_- \equiv A|_{y=+0} - A|_{y=-0}$ means jump across the brane. We see that the continuity imposed on K remains no matter how the theory approaches Einstein, where $f' \to 1, f'' \to 0$, thereby claiming a discrepancy between this and the usual Israel junction conditions [2].

Puzzled by this phenomenon, at least we can imagine the importance of serious investigation into junction conditions in $f(R)$ gravity. The remainder of this article is dedicated to developing matching condition for $f(R)$ gravity theories in a rigorous manner.

2 First-order action for $f(R)$ gravity

We start with an initial-value formulation of the $f(R)$ gravity since the matching conditions for spacetimes will be given as boundary conditions at a given surface. As a rigorous way to find all the dynamical degrees of freedom and necessary boundary conditions, we employ canonical formulation of $f(R)$ gravity. For the time being we concentrate on vacuum gravity. We will discuss coupling to matter in the next section.

2.1 Equivalent scalar–tensor theory

We introduce two scalar fields ρ and Φ related by an algebraic constraint $\Phi = f'(\rho)$, and use them to rewrite the $f(R)$ action in the following way

$$S_{\mathrm{g}} = \frac{1}{2}\int_{\mathcal{M}} \sqrt{-g}(\Phi R - \rho\Phi + f(\rho)). \tag{5}$$

In vacuum, this action gives coupled equations of motion for g_{ab} and Φ

$$\begin{aligned} &\Phi G_{ab} + \frac{1}{2}(\rho\Phi - f(\rho))g_{ab} + (g_{ab}\Box - \nabla_a\nabla_b)\Phi = 0, \\ &R - \rho = 0. \end{aligned} \tag{6}$$

As this form is of Brans–Dicke-type scalar–tensor theory, it is clear that there is an additional scalar degree of freedom in gravity other than metric. It is easily seen that these field equations are combined to give the original fourth-order field equation (3).

2.2 Surface term via $(D-1)+1$ canonical decomposition

Suppose that the spacetime $\mathcal{M}$ is foliated by a one-parameter family of hypersurfaces $\{\Sigma_y\}$ labeled by a coordinate y and that the spacetime boundary $\partial\mathcal{M}$ is for convenience identified as one of those constant-y surfaces Σ_{y_0}. We discuss within the portion corresponding to $y \geq y_0$. We denote the unit vector normal to Σ_y as n^a, by which the metric induced on Σ_y is given as $\gamma_{ab} = g_{ab} - \epsilon n_a n_b$, where $\epsilon = n_a n^a = \pm 1$ for the cases the normal is spacelike and timelike, respectively. The signature of n_a is chosen so that it directs to the direction of increasing y. We define the extrinsic curvature of Σ_y by $K_{ab} = \gamma_a{}^c\nabla_c n_b$. Then we decompose the metric together with the lapse $N(>0)$ and the shift N^a as

$$g_{ab}\mathrm{d}x^a\mathrm{d}x^b = \gamma_{ab}(N^a\mathrm{d}y + \mathrm{d}x^a)(N^b\mathrm{d}y + \mathrm{d}x^b) + \epsilon N^2\mathrm{d}y^2. \tag{7}$$

By the Gauss relation, the action is represented by quantities that are totally parallel or perpendicular to the hypersurfaces:

$$\begin{aligned} S_{\mathrm{g}} = &\frac{1}{2}\int_{\mathcal{M}} \sqrt{|\gamma|}N(\Phi\bar{R} - \epsilon\Phi(K_{ab}K^{ab} - K^2) + 2\epsilon K\partial_n\Phi - 2\bar{\Box}\Phi - \rho\Phi + f(\rho)) \\ &- \epsilon\int_{\mathcal{M}} \sqrt{-g}\nabla_a(\Phi K n^a - \Phi a^a - \epsilon\bar{\nabla}^a\Phi), \end{aligned} \tag{8}$$

where and hereafter the bar represents $(D-1)$-dimensional quantities, and where $a^a = n^b\nabla_b n^a$, $\partial_n = n^a\nabla_a$, and $\bar{\Box} = \bar{\nabla}_a\bar{\nabla}^a$. To cancel the second derivative along the normal direction, we have to add a surface term

$$\bar{S}_{\mathrm{g}} = -\epsilon\int_{\partial\mathcal{M}} \sqrt{|\gamma|}\Phi K. \tag{9}$$

Then we get an action that contains normal derivatives only up to first order.

2.3 Boundary conditions in vacuum

Now canonical formulation for $f(R)$ gravity is ready. The result[1] tells that we have two dynamical variables $\{\gamma_{ab}, \Phi\}$ with canonical conjugate momenta

$$\pi_\gamma^{ab} = \epsilon\frac{\sqrt{|\gamma|}}{2}(-\Phi(K^{ab} - K\gamma^{ab}) + \gamma^{ab}\partial_n\Phi), \quad \pi_\Phi = \epsilon\sqrt{|\gamma|}K, \tag{10}$$

[1] We defer its full result until our accompanied paper [3].

respectively. In vacuum, we find variation of the action on-shell to be

$$\delta(S_{\mathrm{g}}+\bar{S}_{\mathrm{g}}) = -\int_{\partial\mathcal{M}} (\pi_\gamma^{ab}\delta\gamma_{ab} + \pi_\Phi\delta\Phi), \tag{11}$$

which vanishes if the fields satisfy Dirichlet conditions at the boundary.

3 Coupling to matter on a boundary and junction conditions

Next we take into account matters on the boundary $\partial\mathcal{M}$ which couples to gravitational fields γ_{ab} and Φ. In presence of matter on the boundary, variations of the matter action $\bar{S}_{\mathrm{m}}[\gamma_{ab},\Phi]$ give rise to source terms; The variational principle tells that we have boundary conditions

$$\pi_\gamma^{ab}|_{\partial\mathcal{M}} = \frac{\delta\bar{S}_{\mathrm{m}}}{\delta\gamma_{ab}}, \quad \pi_\Phi|_{\partial\mathcal{M}} = \frac{\delta\bar{S}_{\mathrm{m}}}{\delta\Phi}. \tag{12}$$

Now we move to the braneworld picture where two spacetimes $\mathcal{M}_+$ and $\mathcal{M}_-$ are matched at the boundary. In both of the portions we use the common unit normal vector n^a by choosing its signature so that it directs from $\mathcal{M}_-$ to $\mathcal{M}_+$. The notion $[\cdots]_-^+$ means jump across the boundary such as $[A]_-^+ \equiv A|_{\partial\mathcal{M}_+} - A|_{\partial\mathcal{M}_-}$. Then we find the junction conditions for the jumps of the canonical momenta, which are conveniently rearranged into the following expression

$$\Phi[K_{ab}]_-^+ = -\left(S_{ab} - \frac{S-\Phi F}{D-1}\gamma_{ab}\right), \quad [\partial_n\Phi]_-^+ = \frac{S+(D-2)\Phi F}{D-1}, \tag{13}$$

where

$$S_{ab} \equiv \epsilon\frac{-2}{\sqrt{|\gamma|}}\frac{\delta\bar{S}_{\mathrm{m}}}{\delta\gamma^{ab}}, \quad F \equiv \epsilon\frac{1}{\sqrt{|\gamma|}}\frac{\delta\bar{S}_{\mathrm{m}}}{\delta\Phi}. \tag{14}$$

It is seen that the Israel junction condition is recovered only when

$$\Phi F = -\frac{S}{D-2} \tag{15}$$

is satisfied by the matter on the boundary.

4 Conformal equivalence

A well-known fact for Brans–Dicke-type scalar–tensor theories is that a suitable conformal transformation takes to a particular frame in which the gravitational theory appears to be familiar Einstein–scalar theory. To see this, let us introduce another scalar field defined by

$$\phi = \sqrt{\frac{D-1}{D-2}}\ln\Phi, \tag{16}$$

where we assume $\Phi > 0$, and perform the following conformal transformation

$$g_{ab} = \mathrm{e}^{-2\phi/\sqrt{(D-1)(D-2)}}\tilde{g}_{ab}. \tag{17}$$

Then the action is given in terms of the Einstein-frame variables as

$$S = \frac{1}{2}\int_{\mathcal{M}}\sqrt{-\tilde{g}}(\tilde{R} - (\tilde{\partial}\phi)^2 - 2V(\phi)) - \epsilon\int_{\partial\mathcal{M}}\sqrt{|\tilde{\gamma}|}\tilde{K} + \bar{S}_{\mathrm{m}}[\tilde{\gamma}_{ab},\phi] \tag{18}$$

with the scalar potential given in terms of f

$$V(\phi) = \frac{\rho f'(\rho) - f(\rho)}{2f'(\rho)^{D/(D-2)}}, \tag{19}$$

where ρ is parametrically defined to satisfy $\phi = \sqrt{\frac{D-1}{D-2}} \ln f'(\rho)$. Thus the following junction conditions are obtained

$$[\tilde{K}_{ab}]^+_- = -\left(\tilde{S}_{ab} - \frac{\tilde{S}}{D-2}\tilde{\gamma}_{ab}\right), \quad [\tilde{\partial}_n \phi]^+_- = -\epsilon \frac{1}{\sqrt{|\gamma|}} \frac{\delta \bar{S}_{\rm m}[\tilde{\gamma}_{ab}, \phi]}{\delta \phi}, \tag{20}$$

where

$$\tilde{S}_{ab} = \epsilon \frac{-2}{\sqrt{-\tilde{\gamma}}} \frac{\delta \bar{S}_{\rm m}}{\delta \tilde{\gamma}^{ab}}. \tag{21}$$

Therefore the set of junction conditions in the original frame (13) has been shown to be equivalent to the familiar Israel conditions plus a jump condition for $\tilde{\partial}_n \phi$, which were utilised in, e.g., [5].

5 Summary

We showed that the Brans–Dicke-type action supplemented by a surface term

$$S_{\rm g} = \frac{1}{2} \int_{\mathcal{M}} \sqrt{-g}(\Phi R - \rho \Phi + f(\rho)) - \epsilon \int_{\partial \mathcal{M}} \sqrt{|\gamma|} \Phi K \tag{22}$$

allows well-defined initial-value formulation for the equivalent $f(R)$ gravity with Dirichlet conditions imposed on the boundary.

In presence of a brane, the junction conditions in this frame were given as

$$\Phi[K_{ab}]^+_- = -\left(S_{ab} - \frac{S - \Phi F}{D-1}\gamma_{ab}\right), \quad [\partial_n \Phi]^+_- = \frac{S + (D-2)\Phi F}{D-1}. \tag{23}$$

where S_{ab} and F were defined in (14).

Acknowledgement

YS was supported by Grant-in-Aid for JSPS Fellows No. 7852. MS was supported in part by JSPS Grant-in-Aid for Scientific Research (B) No. 17340075, (A) No. 18204024, and by JSPS Grant-in-Aid for Creative Scientific Research No. 19GS0219. The authors thank the Yukawa Institute for Theoretical Physics at Kyoto University, where this work was partially done during the scientific program on "Gravity and Cosmology 2007" and the workshop YITP-W-07-10 on "String Phenomenology and Cosmology." ND and MS also acknowledge financial support from the CNRS–JSPS Exchange Programme "Sakura."

References

[1] K. Akama, Lect. Notes Phys. **176** (1982) 267; V. A. Rubakov and M. E. Shaposhnikov, Phys. Lett. B **125** (1983) 136; N. Arkani-Hamed, S. Dimopoulos and G. R. Dvali, Phys. Lett. B **429** (1998) 263; I. Antoniadis, N. Arkani-Hamed, S. Dimopoulos and G. R. Dvali, Phys. Lett. B **436** (1998) 257; L. Randall and R. Sundrum, Phys. Rev. Lett. **83** (1999) 3370; *ibid.* 4690.

[2] W. Israel, Nuovo Cim. B **44** (1966) 1 [Erratum-ibid. B **48** (1967) 463].

[3] N. Deruelle, M. Sasaki and Y. Sendouda, in preparation.

[4] N. Deruelle, M. Sasaki and Y. Sendouda, Prog. Theor. Phys., in press [arXiv:0711.1150 [gr-qc]].

[5] K. i. Maeda and D. Wands, Phys. Rev. D **62** (2000) 124009; D. Langlois and M. Rodriguez-Martinez, Phys. Rev. D **64** (2001) 123507.

Dynamical black holes in Einstein-Gauss-Bonnet gravity

Masato Nozawa[1][1] and Hideki Maeda[2,3][2]

[1]*Department of Physics, Waseda University, Tokyo 169-8555, Japan*
[2]*Centro de Estudios Científicos (CECS), Arturo Prat 514, Valdivia, Chile*
[3]*Department of Physics, International Christian University, 3-10-2 Osawa, Mitaka-shi, Tokyo 181-8585, Japan*

Abstract

We explored several properties of dynamical black holes in Einstein-Gauss-Bonnet gravity. In the present paper, we assume that the spacetime is pseudo-spherically symmetric and the Gauss-Bonnet coupling constant is non-negative. Depending on the existence or absence of the general relativistic limit, solutions are classified into GR and non-GR branches, respectively. Assuming the null energy condition on matter fields, we show that a future outer trapping horizon in the GR branch possesses the same properties as that in general relativity. In contrast, that in the non-GR branch is shown to be non-spacelike with its area non-increasing into the future. We can recognize this peculiar behavior to arise from a fact that the null energy condition necessarily leads to the null convergence condition for radial null vectors in the GR branch, but not in the non-GR branch. The energy balance law yields the first law of a trapping horizon, from which we can read off the entropy of a trapping horizon reproducing Iyer-Wald's expression. The entropy of a future outer trapping horizon is shown to be non-decreasing in both branches along its generator.

1 Preliminaries

The action in $n(\geq 5)$-dimensional spacetime is given by

$$S = \frac{1}{2\kappa_n^2}\int\Big[R - 2\Lambda + \alpha(R^2 - 4R_{\mu\nu}R^{\mu\nu} + R_{\mu\nu\rho\sigma}R^{\mu\nu\rho\sigma})\Big] + S_{\rm matter}, \tag{1}$$

where the natural volume element is omitted. Here, R and Λ are the n-dimensional Ricci scalar and the cosmological constant, respectively. $S_{\rm matter}$ in Eq. (1) is the action for matter fields and $\kappa_n := \sqrt{8\pi G_n}$, where G_n is the n-dimensional gravitational constant. In four-dimensional spacetime, the Gauss-Bonnet term does not contribute to the field equations since it becomes a total derivative. α with the dimension of length-squared is the coupling constant of the Gauss-Bonnet term. We assume $\alpha \geq 0$ throughout this paper, as motivated by string theory. The gravitational equation derived from the action (1) is

$$G_{\mu\nu} + \alpha H_{\mu\nu} + \Lambda g_{\mu\nu} = \kappa_n^2 T_{\mu\nu}, \tag{2}$$

where $G_{\mu\nu} := R_{\mu\nu} - g_{\mu\nu}R/2$ is the Einstein tensor and

$$H_{\mu\nu} := 2\Big[RR_{\mu\nu} - 2R_{\mu\alpha}R^{\alpha}_{\ \nu} - 2R^{\alpha\beta}R_{\mu\alpha\nu\beta} + R_{\mu}^{\ \alpha\beta\gamma}R_{\nu\alpha\beta\gamma}\Big] - \frac{1}{2}g_{\mu\nu}(R^2 - 4R_{\mu\nu}R^{\mu\nu} + R_{\mu\nu\rho\sigma}R^{\mu\nu\rho\sigma}) \tag{3}$$

and $T_{\mu\nu}$ is the energy-momentum tensor of matter fields. The field equations (2) contain up to the second derivatives of the metric and linear in that term.

Suppose the n-dimensional spacetime $(\mathcal{M}^n, g_{\mu\nu})$ has symmetries corresponding to the isometries of an $(n-2)$-dimensional constant curvature space (K^{n-2}, γ_{ij}), which we call pseudo-spherical symmetry. Namely, the line element is written by the direct product as

$$g_{\mu\nu}{\rm d}x^\mu{\rm d}x^\nu = g_{ab}(y){\rm d}y^a{\rm d}y^b + r^2(y)\gamma_{ij}(z){\rm d}z^i{\rm d}z^j, \tag{4}$$

where $a, b = 0, 1;\ i, j = 2, ..., n-1$. Here r is a scalar on (M^2, g_{ab}) with $r = 0$ defining its boundary, and γ_{ij} is the unit metric on (K^{n-2}, γ_{ij}) with its sectional curvature $k = \pm 1, 0$. We assume that (K^{n-2}, γ_{ij}) is compact. Then the trapped region is expressed simply as the region where $(\nabla r)^2 < 0$.

[1]E-mail:nozawa@gravity.phys.waseda.ac.jp
[2]E-mail:hideki@cecs.cl

The generalized Misner-Sharp mass [1] is a scalar function on (M^2, g_{ab}) with the dimension of mass such that

$$m := \frac{(n-2)V_{n-2}^k}{2\kappa_n^2}\left\{-\tilde{\Lambda}r^{n-1} + r^{n-3}[k-(Dr)^2] + \tilde{\alpha}r^{n-5}[k-(Dr)^2]^2\right\}, \tag{5}$$

where $\tilde{\alpha} := (n-3)(n-4)\alpha$, $\tilde{\Lambda} := 2\Lambda/[(n-1)(n-2)]$, D_a is a metric compatible linear connection on (M^2, g_{ab}) and $(Dr)^2 := g^{ab}(D_a r)(D_b r)$. V_{n-2}^k is the area of the unit $(n-2)$-dimensional space of constant curvature. The quasi-local mass is defined by the quasi-local geometrical quantity on the boundary of a spatial surface and dependent only on the metric and first derivatives. The equations in the following analysis can be transcribed in a comprehensible form by using the quasi-local mass. The definition reduces to the Misner-Sharp mass when $\Lambda = 0$ [3], which characterizes the local nature of spherically symmetric spacetime [4].

Here we recapitulate basic properties that the quasi-local mass exhibits [2]. First, our geometrical definition is physically justified in that it is rederived as an integral of energy flux. Let us define the Kodama vector $K^\mu = -\epsilon^{\mu\nu}\nabla_\nu r$, from which K^μ is timelike in the trapped region. The existence of a timelike vector field irrespective of a highly dynamical setting is a direct consequence of the pseudo-spherical symmetry. Straightforward calculations show that $\nabla_\mu K^\mu = 0$, $G^{\mu\nu}\nabla_\mu K_\nu = 0$ and $H^{\mu\nu}\nabla_\mu K_\nu = 0$. Using these facts, we can show that the integral of the Kodama current, J^μ, yields our quasi-local mass:

$$m = -\int_\Sigma J^\mu n_\mu, \qquad J^\mu = -T^\mu{}_\nu K^\nu, \tag{6}$$

where Σ is some spatial region without an inner boundary and n^μ is its future-directed unit normal. It can be also derived by the locally conserved energy flux, from which the quasi-local mass is recognized as a total amount of energy enclosing the spatial surface [2].

The second criterion that we may recognize it as a well-defined mass is that whether it satisfies the first law. This is indeed the case. Define the pressure and the Bondi-flux localization as

$$P = -\frac{1}{2}T^a{}_a, \qquad \psi^a = T^a{}_b D^b r + P D^a r, \tag{7}$$

then the variation of m is written by manifestly satisfactory form

$$\mathrm{d}m = A\psi_a \mathrm{d}x^a + P\mathrm{d}V, \tag{8}$$

where $A = V_{n-2}^k r^{n-2}$ and $V = V_{n-2}^k r^{n-1}/(n-1)$. It follows from the unified first law (8) that $m = M =$ const.. In the case of $k + (Dr)^2/2\tilde{\alpha} \neq 0$ and $(\nabla r)^2 \neq 0$, the Kodama vector K^μ becomes hypersurface-orthogonal and then the spacetime is locally isometric to the Boulware-Deser-Wheeler solution (Birkhoff's theorem). In the asymptotic regions (asymptotically flat region at spatial infinity and asymptotic anti-de Sitter region), the values of quasi-local mass converges to the constancy representing the total energy of the system. If we assume the dominant energy condition and under some technical assumptions, the quasi-local mass shows monotonicity and positivity properties. All of the above properties supports the physical interpretation of our definition of quasi-local mass. We summarize the fundamental properties of the quasi-local mass in Table 1.

Table 1: Properties of the quasi-local mass.

	$k=1$	$k=0$	$k=-1$
Unified first law	Yes	Yes	Yes
Higher-dim. ADM mass	Yes	n/a	n/a
Monotonicity	Yes	Yes	Yes
Positivity	Yes	See [2]	See [2]

2 Dynamical black holes

By utilizing the quasi-local mass, we investigate the nature of trapping horizons (especially, future outer trapping horizons since we are mainly focusing our attention to the dynamical nature of black holes).

Black-hole formation typically entails the trapped region, from which even the outgoing null rays are converging. This is the local characterization of dynamical aspects of black holes. We investigated the nature of *trapping horizons*, which is the $(n-1)$-dimensional surface foliated by marginal surfaces. Let $\theta_\pm$ be two expansions associated with null vectors orthogonal to K^{n-2}. For the black-hole spacetimes, future ($\theta_- < 0$) outer ($\theta_{+,u} < 0$) trapping horizons are relevant, in which case the trapping horizon is located at $\theta_+ = 0$.

Now noting that $(Dr)^2$ is proportional to $\theta_+\theta_-$, the local nature of spacetime is encoded in quasi-local mass. But it is quadratic in $\theta_+\theta_-$ unlike general relativistic case so that two branches appear by solving (5) inversely

$$\theta_+\theta_- \propto -k - \frac{r^2}{2\tilde{\alpha}}\left(1 \mp \sqrt{1 + \frac{8\kappa_n^2\tilde{\alpha}m}{(n-2)V_{n-2}^k r^{n-1}} + 4\tilde{\alpha}\tilde{\Lambda}}\right). \tag{9}$$

We call *GR-branch* (the upper sign) and *non-GR branch* (lower sign) according to their general relativistic limit. Thus the nature of trapping horizons are very sensitive to branches. It follows from (9) that the trapping horizons are absent in the case of $k = 0, 1$ for non-GR branches and $r < \sqrt{2\tilde{\alpha}}$ ($r > \sqrt{2\tilde{\alpha}}$) regions with $k = -1$ for the GR (non-GR) branch. Whether the region is trapped or not is judged by the inequality of the quasi-local mass. The value of quasi-local mass

$$m_{\rm h} := \frac{(n-2)V_{n-2}^k}{2\kappa_n^2} r_{\rm h}^{n-3}\left(k + \frac{\tilde{\alpha}k^2}{r_{\rm h}^2} - \tilde{\Lambda}r_{\rm h}^2\right). \tag{10}$$

at trapping horizon $r = r_{\rm h}$ is naturally regarded as the mass of trapping horizon. Let us consider a spacetime containing a trapping horizon. The quasi-local mass satisfies the Penrose inequality $m \geq (\leq) m_{\rm h}$ for the GR (non-GR) branch under the dominant energy condition. For $k = 1$ and $\Lambda < 0$ case, this inequality gives more severe lower and upper bound than mere positivity.

Now it is well known fact that Killing horizons exhibit thermodynamical nature. To derive the formulae of black-hole thermodynamics, we have made full use of the stationarity conditions. Hence, it is not clear in dynamical situations that how these laws are altered. But for the case of trapping horizons (and especially for the pseudo-spherically symmetric case), similar laws seem to be valid. Taking the Kodama vector as a substitute of horizon-generator, we found that the trapping horizons exhibit thermodynamical properties as for Killing horizons, irrespective of its highly non-stationary situations. The symmetric derivative of the Kodama vector along itself reduces to

$$K^b D_{(b}K_{a)} = \frac{r\kappa_n^2}{n-2}\left(1 + \frac{2\tilde{\alpha}}{r^2}[k - (Dr)^2]\right)^{-1}\psi_a, \tag{11}$$

Eq. (11) reveals that ψ^a vanishes if K^a is a Killing vector on (M^2, g_{ab}), implying that $K^\mu = K^a(\partial/\partial x^a)^\mu$ is a hypersurface-orthogonal Killing vector on $(\mathcal{M}^n, g_{\mu\nu})$. This fact also lends support to the physical interpretation of ψ^a. Since $\psi_a K^a = T_{ab}K^aK^b$ on the trapping horizon where $D^a r = K^a$ holds, ψ^a is not in general proportional to K^a in a dynamical setting. Then the surface gravity of a trapping horizon should be defined by $K^b D_{[b}K_{a]} = \kappa_{\rm TH}K_a$. Thus we have

$$\kappa_{\rm TH} = \frac{1}{2}D^2 r = -\frac{1}{2}\epsilon^{ab}D_a K_b, \tag{12}$$

where the evaluation is performed on the trapping horizon. Transform the unified first law and project onto the generator of trapping horizon, we have the first law of the trapping horizon

$$A\psi_a {\rm d}'x^a = \frac{\kappa_{\rm TH}}{\kappa_n^2}{\rm d}'\left[A\left(1 + \frac{2(n-2)\tilde{\alpha}k}{(n-4)r^2}\right)\right], \tag{13}$$

where ${\rm d}'$ is the derivative along the trapping horizon. From the first law, we can read off the entropy of the trapping horizon as

$$S_{\rm TH} := \frac{V_{n-2}^k r_{\rm h}^{n-2}}{4G_n}\left[1 + \frac{2(n-2)(n-3)\alpha k}{r_{\rm h}^2}\right]. \tag{14}$$

This coincides with Iyer and Wald's definition of dynamical black-hole entropy, which has several plausible properties among other things. Their entropy is independent of the potential ambiguity of the Lagrangian and associated with a Noether charge. Moreover, it agrees with a non-stationary perturbation of the entropy of a stationary black hole and reduces to the entropy of a stationary black hole in the stationary case.

The first and second piece in the entropy expression corresponds to the one quarter of the area the deviation from the general relativistic case. We can show that under the null energy conditions, the area of future outer trapping horizon is non-decreasing (non-increasing) along the generator of the trapping horizon for the GR (non-GR) branch, whereas its entropy is non-decreasing in both branches. One may wonder why the non-GR branch shows the counter-intuitive behaviors. This peculiarity is best understood as follows. Let k^μ be radial null vector. The field equations and our definition of quasi-local mass combine to give

$$\pm R_{\mu\nu}k^\mu k^\nu \sqrt{1+\frac{8\kappa_n^2\tilde{\alpha}m}{(n-2)V_{n-2}^k r^{n-1}}+4\tilde{\alpha}\tilde{\Lambda}} = \kappa_n^2 T_{\mu\nu}k^\mu k^\nu. \qquad (15)$$

This equation shows that the null convergence condition violates if the null energy condition is strictly satisfied.

It also follows from (15) and Raychaudhuri's equation that under the null energy condition, an outer (inner) trapping horizon in the GR branch is non-timelike (non-spacelike), while it is non-spacelike (non-timelike) in the non-GR branch. The timelike nature for the non-GR branch is also counter-intuitive since light rays emanating from a point on the trapping horizon can propagate into both sides, which does not capture the idea that the black hole should be a region of no escape. This can be again recognized as the 'divergence condition' is satisfied for the non-GR branch.

For concreteness, let us consider the Hawking evaporation of a black hole, in which the null energy condition is violated. A black hole in the GR branch continues to lose its mass and reduce its area. In other words, the signature of a trapping horizon becomes non-spacelike and shrinks. Whereas in the non-GR branch, a black hole defined by a future outer trapping horizon increases its size as it "evaporates." A fundamental cause of this arises from the sign flip in Eq. (15) for a radial null vector k^μ, which makes the non-GR-branch solutions quite eccentric. But we have not explicitly shown whether this sign change is special to radial null vectors or an artifact of our spacetime ansatz (4).

To conclude we sum up the upshots obtained in [5] in Table 2.

Table 2: Properties of the future trapping horizon under the null energy condition. Each quoted term denotes that it has the meaning of time evolution only if the trapping horizon is null, since the area and entropy laws are formulated along the generator of the trapping horizon.

	GR branch		non-GR branch	
	future outer	future inner	future outer	future inner
signature	non-timelike	non-spacelike	non-spacelike	non-timelike
trapped side	future	exterior	interior	past
area law	"non-decreasing"	non-increasing	non-increasing	"non-decreasing"
entropy law	"non-decreasing"	non-increasing	non-decreasing	"non-increasing"

References

[1] H. Maeda, Phys. Rev. D **73**, 104004 (2006).

[2] H. Maeda and M. Nozawa, arXiv:0709.1199 [hep-th].

[3] C. W. Misner and D. H. Sharp, Phys. Rev. **136**, B571 (1964).

[4] S. A. Hayward, Phys. Rev. D. **53**, 1938 (1996).

[5] M. Nozawa and H. Maeda, arXiv:0710.2709 [gr-qc].

Hybrid compactifications and brane gravity in six dimensions

Tsutomu Kobayashi[1] and Yu-ichi Takamizu[2]

Department of Physics, Waseda University, Okubo 3-4-1, Shinjuku, Tokyo 169-8555, Japan

Abstract

We consider a six-dimensional axisymmetric Einstein-Maxwell model of warped braneworlds. The bulk is bounded by two branes, one of which is a conical 3-brane and the other is a 4-brane wrapped around the axis of symmetry. The latter brane is assumed to be our universe. The 3-brane folds the internal two-dimensional space in a narrow cone, making sufficiently small the Kaluza-Klein circle of the 4-brane. An arbitrary energy-momentum tensor can be accommodated on this ring-like 4-brane. We study linear perturbations sourced by matter on the brane, and show that weak gravity is apparently described by a four-dimensional scalar-tensor theory. The extra scalar degree of freedom can be interpreted as the fluctuation of the internal space volume, the effect of which turns out to be suppressed at long distances. Consequently, four-dimensional Einstein gravity is reproduced on the brane.

1 Introduction

Probably one of the most interesting recent developments in particle physics and cosmology has been the idea of braneworlds. Models with extra dimensions are motivated theoretically, as in superstring theory, which is a very promising approach to unification, requiring ten spacetime dimensions. Braneworld scenarios are further motivated by their phenomenologically interesting aspects. Among them are the possible effect of having the fundamental scale as low as the weak scale and some modification of the gravity law on submillimeter scales [1], both of which are accessible by experiments. So far five-dimensional (5D) Randall-Sundrum-type braneworlds [1] have been the most extensively studied examples, whereas more recently there has been growing interest in six- or higher dimensional models. In the present paper we will be focusing on 6D braneworlds with Maxwell fields. Since two extra dimensions are enough to admit flux-stabilized compactifications while keeping the setup as simple as possible, such brane models allow us to explore some of the interesting features which would be less easily addressed in more string theoretical settings. Perhaps the simplest exact solution of this type of warped braneworlds has been constructed in [2]. Codimension two branes are often considered in the above approaches, and they are unfortunately associated with the problem of the localization of matter. Namely, a strict codimension two defect does not allow for arbitrary energy-momentum tensor localized on it. Gravitational aspects of such higher dimensional braneworlds have not been explored thoroughly yet because of this fact. The hybrid Kaluza-Klein / Randall-Sundrum construction of [3] evades this problem by assuming that our universe is a 4-brane in six dimensions, with one of the spatial directions compactified on a circle. Refs. [4, 5, 6, 7] also exploit essentially the same idea to resolve codimension two singularities. The specific model we consider in this paper is most closely similar to that of [3], but not exactly the same. In [3] the bulk with axisymmetry closes regularly at the point where the axial Killing vector vanishes. In contrast, ours does not, permitting a conical singularity there, corresponding to a tensional 3-brane. The conical 3-brane can fold the internal 2D space in a narrow cone, yielding a small Kaluza-Klein circle of the 4-brane wrapped around the symmetry axis. (For this idea we are indebted to [8].) To study in more detail the behavior of weak gravity sourced by matter in the braneworld, we provide a rigorous treatment of metric and matter perturbations in this paper. We use the technique of [9], which was originally developed for studying linear perturbations in the Randall-Sundrum model and was developed by [4, 6] in the context of 6D brane models.

[1]E-mail:tsutomu@gravity.phys.waseda.ac.jp
[2]E-mail:takamizu@gravity.phys.waseda.ac.jp

2 The model

Our 6D bulk is described by the Einstein-Maxwell action. In our setup the bulk cosmological constant may be positive or negative or zero, and so we write $\Lambda_6 = \epsilon \frac{10}{\ell^2}$, $\epsilon = \pm 1,\ 0$. The 6D field equations derived from the above action and they admit the following bulk solution [3]:

$$g_{MN}dx^M dx^N = \xi^2 \eta_{\mu\nu}dx^\mu dx^\nu + \ell^2 \left[\frac{d\xi^2}{f(\xi)} + \beta^2 f(\xi) d\theta^2 \right], \tag{1}$$

where $f(\xi) := -\epsilon\xi^2 + \frac{\mu}{\xi^3} - \frac{q^2}{\xi^6}$. Only the $(\xi\theta)$ component of the field strength is nonvanishing, given by $F_{\xi\theta} = 2\sqrt{3}\frac{\beta\ell}{\kappa}\frac{q}{\xi^4}$. Let ξ_0 be the positive zero of $f(\xi)$. We consider the region in which $\xi \geq \xi_0$ and $f(\xi) \geq 0$. More specifically, ξ_0 is the largest positive zero of $f(\xi_0)$ for $\epsilon = -1$. For $\epsilon = 0$, we have $\xi_0 = (q^2/\mu)^{1/3}$. In the $\epsilon = 1$ case, ξ_0 is the second largest positive zero, and we consider the region $\xi_0 \leq \xi < \xi_1$, with ξ_1 being the largest zero. Accordingly, we have a deficit angle $\delta = 2\pi\left[1 - \beta f'(\xi_0)/2\right]$, corresponding to a conical 3-brane placed at $\xi = \xi_0$ with tension $\kappa^2\sigma = 2\pi\left[1 - \frac{\beta f'(\xi_0)}{2}\right]$. As in [3], one may impose $\beta = 2/f'(\xi_0)$, leading to the regular geometry without a 3-brane. In the present paper, however, we do not do so and allow for a conical deficit. We follow the construction of [3] and add a ring-like 4-brane at a point $\xi_* > \xi_0$, which is assumed to be our universe. The brane action is given by $S_{\rm brane} = \int d^5x\sqrt{-\gamma}\left(-\lambda + \mathcal{L}_m\right)$, where λ is the tension of the 4-brane and $\mathcal{L}_m$ is the matter Lagrangian. We denote by γ_{ab} the induced metric on the brane. Let $\mathcal{M}$ be the spacetime in which ξ ranges from ξ_0 to ξ_*. We impose Z_2 symmetry about ξ_*, and glue $\mathcal{M}$ and a copy of $\mathcal{M}$ together at $\xi = \xi_*$. In so doing we assume that the metric and F_{MN} are continuous across the brane.[3] The first derivative of the metric is subject to the Israel conditions. We now consider a vacuum brane. In this case the Israel conditions determines the brane position as $\xi_* = 2\left(\frac{q^2}{5\mu}\right)^{1/3}$. Since our brane model includes one Kaluza-Klein direction, we must impose that the circumference of the ring, $\mathcal{C} = 2\pi\beta\ell\sqrt{f_*}$, is not too large (say $\mathcal{C} \lesssim 10^{-16}\,$cm), whereas if the scale of the "braneworld compactification" is as large as $\ell \sim 10^{-2}\,$cm it will be particularly interesting. Clearly, this can be achieved by requiring $\beta\sqrt{f_*} \ll 1$. In other words, if the tension of the conical brane is fine-tuned to be very close to the critical value, $\kappa^2\sigma \simeq 2\pi$, the bulk will look like a narrow sliver with a small Kaluza-Klein circle. The required fine-tuning is $1 - \frac{\kappa^2\sigma}{2\pi} \sim \frac{\mathcal{C}}{\ell}$. We will keep using the conical brane to set the boundary of the system.

We can express the parameters μ and q^2 in terms of ξ_0 and ξ_*: $\mu = -\epsilon\frac{8\xi_0^5}{5\alpha^3 - 8}$, $q^2 = -\epsilon\frac{5\alpha^3\xi_0^8}{5\alpha^3 - 8}$, where $\alpha := \frac{\xi_*}{\xi_0}$. Note that the above expression is valid only for $\epsilon \neq 0$. Introducing the new coordinate $z := \xi/\xi_0$, we write $f = \xi_0^2\overline{f}(z)$, where $\overline{f}(z) := -\epsilon\left(z^2 + \frac{8}{5\alpha^3 - 8}\frac{1}{z^3} - \frac{5\alpha^3}{5\alpha^3 - 8}\frac{1}{z^6}\right)$. The background solution apparently depends on ξ_0, but it can be eliminated by performing an appropriate coordinate rescaling. Thus, it turns out that the background configuration in the $\epsilon \neq 0$ models is characterized by two parameters, α and the 3-brane tension σ. We see that $(1 <)\ \alpha^3 < 8/5$ for $\epsilon = +1$ and $\alpha^3 > 8/5$ for $\epsilon = -1$. If α is very close to $2/5^{1/3}$, we have a large circumference, $\mathcal{C} \propto |\alpha - 2/5^{1/3}|^{-1/2}$. Large α also tends to give a large Kaluza-Klein radius, $\mathcal{C} \propto \alpha$. Therefore, in what follows we will assume $\alpha \sim O(1)$ but not too close to $2/5^{1/3}$. The special case with $\epsilon = 0$ $(\alpha^3 = 8/5)$ should be considered separately. Since the 6D cosmological constant vanishes, the typical compactification scale is given solely by the Maxwell field: $\kappa^2F^2 = (24/\ell_0^2)z^{-8} \sim 1/\ell_0^2$, where $\ell_0 := \frac{\xi_0^4\ell}{q}$.

3 Linear perturbations

Let us now analyze linear perturbations on the brane model. We are interested in a length scale much larger than the circumference of the ring, and hence we focus on perturbations homogeneous in the θ-direction. Linear perturbations are split into scalar, vector, and tensor modes under the Lorentz group in the external spacetime. Here let us consider scalar and tensor perturbations. (Vector modes are of no particular interest.) For the transverse and traceless tensor perturbation, $h_{\mu\nu}$, the Einstein equations

[3] We impose the same boundary condition as in [3] for the Maxwell field. This is different from [4, 5, 6], in which F_{MN} is discontinuous at the 4-brane due to the Stückelberg term included in the brane action.

simply give $\left(\xi^4 f h'_{\mu\nu}\right)' + \xi^2\ell^2\Box h_{\mu\nu} = 0$, where $\Box := \eta^{\mu\nu}\partial_\mu\partial_\nu$. For the scalar perturbations, it is convenient to employ the 6D longitudinal gauge. The $(\mu\nu)$, $(\xi\xi)$, and $(\theta\theta)$ components of the Einstein equations are combined to give two basic equations as $\Omega'' + 2\left(\frac{f'}{f} + \frac{5}{\xi}\right)\Omega' + \ldots = 0$ and $\Psi'' + \frac{4}{\xi}\Psi' + \ldots = 0$. The remaining variables are obtained from $\Xi = \Psi + \Omega$ and $\delta A_\theta = \frac{\beta\ell\xi^3}{2\sqrt{3}\kappa q}\left[f\left(\xi\Omega' + 2\Omega\right) + \xi f'(\Omega + 2\Psi)\right]$. We now proceed to discuss boundary conditions. At the point where the geometry pinches off, $\xi = \xi_0$, we impose some regularity conditions on the perturbations. For the tensor mode, we require that both $h_{\mu\nu}$ and $h'_{\mu\nu}$ are regular at $\xi = \xi_0$. The regularity conditions for the scalar modes are $f\Omega|_{\xi_0} = 0$ and $(f\Omega)' + 2f'\Psi|_{\xi_0} = 0$. The perturbed field strength in the Gaussian-normal gauge must be continuous at $\xi = \xi_*$. Since we are assuming the $\mathbb{Z}_2$ symmetry across the ring, it leads to the condition $\delta A_{\theta *} + A'_{\theta *}\zeta = 0$, where the equation is written in terms of the 6D longitudinal gauge perturbations and hence includes the brane bending mode $\zeta = \zeta(x)$. In the 6D longitudinal gauge, the location of the brane is perturbed in general: $\xi_* \to \xi_* + \zeta(x)$. We now investigate the long-distance behavior of weak gravity on the 4-brane. Using the Israel condition we can put the bulk equation of motion and the boundary condition into a single equation with a source term:

$$\mathcal{O}h_{\mu\nu} := \left(\xi^4 f h'_{\mu\nu}\right)' + \xi^2\ell^2\Box h_{\mu\nu} = -\mathcal{S}_{\mu\nu}\delta(\xi - \xi_*), \tag{2}$$

where we define $\mathcal{S}_{\mu\nu} \equiv 2\ell\xi_*^2\sqrt{f_*}\kappa^2\left(T_{\mu\nu} - \frac{1}{3}T_\lambda^{\ \lambda}\gamma_{\mu\nu}\right) + 4\ell^2\xi_*^2\zeta_{,\mu\nu}$. We use the standard Green function method to solve Eq. (2). The Green function is explicitly given by $G_R = -\int\frac{d^4k}{(2\pi)^4}e^{ik\cdot(x-x')}\sum\frac{u_i(\xi)u_i(\xi')}{m_i^2 + \mathbf{k}^2 - (\omega + i\epsilon)^2}$, where $u_i(\xi)$ are a complete set of eigenfunctions of

$$\left(\xi^4 f u_i'\right)' = -\xi^2\ell^2 m_i^2 u_i. \tag{3}$$

The eigenfunctions must be normalized. We are mainly interested in the long-range gravity on the brane and hence the zero-mode solution of (3) is the most important. Setting $m_0^2 = 0$ and integrating once, we obtain $u_0' = \xi^{-4}f^{-1}U$, where U is an integration constant. However, from the regularity condition at $\xi = \xi_0$ we must impose $U = 0$. Therefore, the zero-mode solution is given by $u_0 = L^{-1} =$ constant. The normalization is determined as $L = \ell\sqrt{\frac{2}{3}(\xi_*^3 - \xi_0^3)}$. The zero-mode truncation of the Green function leads to $h_{\mu\nu} \approx -\frac{1}{L^2}\Box^{-1}\mathcal{S}_{\mu\nu}$. Now we would like to compute the Ricci tensor $R^{(4)}_{\mu\nu}$ of the 4D metric $\overline{g}_{\mu\nu} = \xi_*^2[(1 + 2\overline{\Psi}_*)\eta_{\mu\nu} + h_{\mu\nu}]$. Here $\overline{\Psi}_*$ is the metric perturbation in the Gaussian-normal gauge, which is related to the longitudinal gauge quantities. We write $R^{(4)}_{\mu\nu} = -\frac{1}{2}\Box h_{\mu\nu} - \frac{2\xi_*^2\ell^2}{L^2}\zeta_{,\mu\nu} - \frac{\ell^2}{L^2}\gamma_{\mu\nu}\Box\zeta - (2\partial_\mu\partial_\nu + \eta_{\mu\nu}\Box)\Upsilon$, where we defined $\Upsilon := \overline{\Psi}_* - \frac{\ell^2}{L^2}\xi_*^2\zeta$. Finally, we can evaluate

$$R^{(4)}_{\mu\nu} \approx \kappa_4^2\left(\overline{T}_{\mu\nu} - \frac{1}{2}\overline{T}_\lambda^{\ \lambda}\gamma_{\mu\nu}\right) - (2\partial_\mu\partial_\nu + \eta_{\mu\nu}\Box)\Upsilon, \tag{4}$$

where $\overline{T}_{ab} := \mathcal{C}T_{ab}$ is the energy-momentum tensor integrated along the θ-direction, and we defined the 4D Newton constant as $\kappa_4^2 := \frac{\xi_*^2\kappa^2}{2\pi L^2\beta}$. Thus, we see that the first three terms help to recover a 4D gravitational theory. However, brane gravity looks different from Einstein gravity at this stage because of the additional scalar degree of freedom encoded in Υ. It should be stressed here that the brane bending mode is crucial for reproducing the 4D tensor structure. The role of the brane bending here is the same as that of the Randall-Sundrum braneworld [9], and it has been shown that the same mechanism works in a slightly different setup of 6D braneworlds [4, 6].

Let us evaluate the effect of Υ. For $\ell^2\Box = 0$ we have the exact solutions, where four integration constants $c_1(x), \cdots$ etc. are to be determined by the boundary conditions. In general cases with $T_{ab} \neq 0$ we have nonzero integration constants. From the regularity conditions, one can express c_3 and c_4 in terms of c_1 and c_2. Then, we can write ζ in terms of c_1 and c_2. For $\epsilon \neq 0$ we find $\Upsilon = \frac{(\xi_*^3 - \xi_0^3)(\xi_*^3 + 8\xi_0^3)}{72\xi_*^3\xi_0^6}\hat{c}(x)$, where $\hat{c} := 8\xi_0^3 c_1 - c_2$. Using the Israel conditions, we finally arrive at

$$\Upsilon = \mathcal{F}(\alpha)\ell^2\ \kappa_4^2\left(\frac{1}{3}\overline{T}_\lambda^{\ \lambda} - \overline{T}_\theta^{\ \theta}\right), \tag{5}$$

where $\mathcal{F}(\alpha) := -\frac{\epsilon}{1440}\alpha^2(5\alpha^3 - 8)(\alpha^3 + 8)$. Eqs. (4) and (5) imply that the effect of Υ is suppressed on scales much greater than $\sqrt{\mathcal{F}}\ell$. For $\alpha \sim O(1)$, the coefficient $\sqrt{\mathcal{F}}$ is not large, so that the critical scale may be given by ℓ. The critical scale becomes large for $\alpha \gg 1$, but this is not the case we are considering. In the $\epsilon = 0$ case, a straightforward computation can be similarly done and the effect of Υ is negligible on scales much greater than ℓ_0. To illustrate the geometrical interpretation of the scalar mode Υ, we compute the perturbations of the internal space volume and the circumference of the brane. It then turns out that $\delta\mathcal{V} \propto \delta\mathcal{C} \propto \hat{c}$. Namely, Υ ($\propto \hat{c}$) can be interpreted as the perturbations of the internal space volume and the circumference of the ring. It is reasonable that standard 4D gravity is recovered when the matter fields on the brane do not perturb the internal space much.

So far we have seen that the zero-mode sector of perturbations can reproduce standard 4D gravity on the brane. Basically, the effect of discrete Kaluza-Klein modes are Yukawa-suppressed, and hence we can safely neglect these massive modes at long distances. In this subsection, we compute the mass spectrum of the Kaluza-Klein modes for completeness. To do so we rewrite Eq. (3) in terms of z and $\overline{f}(z)$, so that we would like to solve $\frac{d}{dz}\left[z^4\overline{f}(z)\frac{du_i}{dz}\right] + \nu_i^2 z^2 u_i = 0$, $\nu_i^2 := \frac{m_i^2\ell^2}{\xi_0^2}$, supplemented with the boundary conditions. For $\epsilon = 0$ we replace ℓ^2 in ν_i^2 by ℓ_0^2. In the case of $\epsilon = 0$ we have analytic solutions for the Kaluza-Klein mode functions. The Kaluza-Klein mass spectrum can be calculated from the boundary condition and we can find $\nu_1 \simeq 7.42$, $\nu_2 \simeq 13.6$, $\nu_3 \simeq 19.7, \cdots$. The Kaluza-Klein masses measured by an observer on the ring are $\nu_i\ell_0^{-1}(\xi_0/\xi_*) \simeq 0.855 \times \nu_i\ell_0^{-1}$. In the case of $\epsilon \neq 0$ we compute the mass spectra fully numerically. As before, the Kaluza-Klein masses measured by an observer on the ring are $\nu_i\ell^{-1}\alpha^{-1}$. We are considering the case with $\alpha \sim O(1)$, and so we have $m_i/\xi_* \gtrsim \ell^{-1}$.

4 Summary

We have considered a warped braneworld in six dimensions. The background is given by the model of [3] with a slight modification, in which our universe is assumed to be a 4-brane wrapped around the axisymmetric internal space. Since the codimension of the brane is one, this construction allows for localized matter on the brane. We have performed a linearized perturbation analysis in order to study the long-distance behavior of weak gravity sourced by arbitrary matter on the brane. We have found that there are two scalar modes, ζ and Υ, relevant to brane gravity. The first one, ζ, describes the shift of the brane position and plays an important role in recovering the tensor structure of 4D gravity. The mode Υ encodes the fluctuation of the volume of the internal space (or that of the circumference of the 4-brane) and signals a scalar-tensor theory of gravity. However, the effect of Υ was shown to be suppressed on scales greater than ℓ (or ℓ_0). Discrete Kaluza-Klein modes are Yukawa-suppressed at long distances. Thus, we have successfully obtained standard 4D gravity on the brane. The hybrid braneworld does not eliminate the hierarchy problem with relatively "large" extra dimensions, because one of the extra dimensions will be quite small compared to the other. Indeed, we find $M_{\rm Pl}^2 = (M_6^4)\ell\mathcal{C}\,\frac{2(\xi_*^3-\xi_0^3)}{3\xi_*^2\sqrt{f_*}} \sim (M_6^4)\ell\mathcal{C}$. (For $\epsilon = 0$, we find $M_{\rm Pl}^2 = 2(M_6^4)\ell_0\mathcal{C}/\sqrt{15}$.) The circumference of the ring must be $\mathcal{C} \lesssim 10^{-16}$ cm. Thus, for $\ell \lesssim 10^{-2}$ cm we get the fundamental scale $M_6 \gtrsim 10^7$ GeV.

References

[1] L. Randall and R. Sundrum, Phys. Rev. Lett. **83**, 3370 (1999); Phys. Rev. Lett. **83**, 4690 (1999).

[2] S. Mukohyama, Y. Sendouda, H. Yoshiguchi and S. Kinoshita, JCAP **0507**, 013 (2005).

[3] J. Louko and D. L. Wiltshire, JHEP **0202**, 007 (2002).

[4] M. Peloso, L. Sorbo and G. Tasinato, Phys. Rev. D **73**, 104025 (2006).

[5] E. Papantonopoulos, A. Papazoglou and V. Zamarias, JHEP **0703**, 002 (2007).

[6] T. Kobayashi and M. Minamitsuji, Phys. Rev. D **75**, 104013 (2007).

[7] C. P. Burgess, D. Hoover and G. Tasinato, arXiv:0705.3212 [hep-th].

[8] N. Kaloper, arXiv:hep-th/0702206.

[9] J. Garriga and T. Tanaka, Phys. Rev. Lett. **84**, 2778 (2000).

General Relativity and Gravitation

Bulk dominated fermion emission on a Schwarzschild background

H. T. Cho[1], A. S. Cornell[2], Jason Doukas[3], Wade Naylor[4]

[1] *Department of Physics, Tamkang University, Tamsui, Taipei, Taiwan, Republic of China*
[2] *Université Lyon 1, Institut de Physique Nucléaire de Lyon, France*
[3] *School of Physics, University of Melbourne, Parkville, Victoria 3010, Australia*
[4] *Department of Physics, Ritsumeikan University, Kusatsu, Shiga 525-8577, Japan*

Abstract

Using the WKBJ approximation we obtain semi-analytic expressions of the absorption probability for Dirac fermions on a higher dimensional Schwarzschild background. We then relate the absorption probability to the absorption cross-section, and then use these results to plot the emission rates. Our results lead to the interesting conclusion that for $d > 5$ bulk fermion emission dominates brane localised emission.

Introduction

Large extra-dimensional scenarios [1] have led to the somewhat striking prediction that black holes (BHs) may be observed at particle accelerators such as the LHC [2]. However, in order to suppress a rapid proton decay quarks and leptons need to be physically separated in the higher dimension(s). Such models are generically called split fermion models [3, 4]. Note that in supersymmetric versions of this idea the localizing scalars and bulk gauge fields will also have fermionic bulk superpartners.

In a previous work we applied conformal methods, which allowed us to separate the Dirac equation on a higher dimensional spherically symmetric background, to discuss the quasinormal modes (QNMs) for Schwarzschild BHs [5]. In this work we used this same method to calculate the greybody factors [6] and emission rates for Dirac perturbations on a d-dimensional Schwarzschild background by writing the background as:

$$ds^2 = -f(r)dt^2 + f^{-1}(r)dr^2 + r^2 d\Omega_{d-2}^2 \ , \tag{1}$$

with $f(r) = 1 - \left(\frac{r_H}{r}\right)^{d-3}$ and where the horizon is at $r = r_H$.

After the conformal transformation [5], the Dirac equation separates into a time-radial part and a $(d-2)$-sphere. Moreover, the radial part reduces to a Schrödinger-like equation in the tortoise coordinate r_*:

$$\left(-\frac{d^2}{dr_*^2} + V_1\right) G = E^2 G \ , \tag{2}$$

where $dr = f(r)dr_*$, and the potential is given by $V_1(r) = \kappa^2 \frac{f}{r^2} + \kappa f \frac{d}{dr}\left[\frac{\sqrt{f}}{r}\right]$, with $\kappa = \ell + \frac{d-2}{2}$. Note that the above potential reduces to the brane-localized results when we set $\kappa = \ell + 1$, and therefore provides an alternate derivation of the brane localized potential.

Absorption probabilities via the WKBJ approximation

In a recent work by two of the authors [7] we applied the intermediate WKBJ approximation (up to first order) to evaluate the absorption probability of a graviton to a static BH. The WKBJ approximation can, however, be applied at all energies (including low energy) as has been discussed in reference [8].

[1] htcho"at"mail.tku.edu.tw
[2] cornell@ipnl.in2p3.fr
[3] j.doukas"at"physics.unimelb.edu.au
[4] naylor"at"se.ritsumei.ac.jp

Low Energy WKBJ

In terms of the WKBJ approximation, in general, it will be convenient to make a change of variables to $x = Er$ [7]. Writing $E^2 Q(x_*) = E^2 - V_1$ the Schrödinger equation, equation (2), takes the form:

$$\left(\frac{d^2}{dx_*^2} + Q\right) G = 0 \ . \tag{3}$$

The low energy absorption probability corresponds to the probability for a particle to tunnel through the potential barrier. The result to first order in the low energy WKBJ approximation is given by:

$$|\mathcal{A}_\kappa(E)|^2 = \exp\left[-2\int_{x_1}^{x_2} \frac{dx'}{f(x')}\sqrt{-Q(x')}\right] \ , \tag{4}$$

where x_1 and x_2 are the turning points, $Q(x_{1,2}) = 0$. This approximation is valid for $V_1 \gtrsim E^2$ and as long as we can solve for the turning points in $V_1(x) = E^2$. Note that we can numerically integrate equation (4) for each energy E to obtain the absorption probability as a function of E.

Intermediate Energy: 3rd Order WKBJ

An adapted form of the WKBJ method can be employed to find the QNMs, or the absorption probability (which we are primarily interested in here), when the scattering takes place near the top of the potential barrier. In the following we shall use the same notation as reference [9], where we have confirmed their results to fourth order. However, for the purposes of this work, we shall consider only up to and including third order, in which case we express the absorption probability as:

$$|\mathcal{A}_\kappa(E)|^2 = \frac{1}{1 + e^{2S(E)}} \ , \tag{5}$$

where $S(E)$ has been defined in reference [5].

It should be noted that as we go to higher orders the approximation becomes valid for lower energies. However, as can be seen from figure 1, even orders in the intermediate WKBJ method drop back down to zero for large energy. For this reason we shall work to third order in our calculations, as odd orders have the nice property that $|A|^2 \to 1$ for large energy. Note also that the WKBJ approximation, in general, is accurate for larger angular momentum channels, whereas the Unruh approach [10] is valid for only the lowest angular momentum channels and $\varepsilon \ll 1$ (namely small BHs). However, it is interesting to note that although the low energy WKBJ result does not agree exactly with the Unruh result, they both tend to zero for $\varepsilon \to 0$. On the other hand, unlike the Unruh result, the low energy WKBJ is valid for energies up to $\varepsilon \sim \mathcal{O}(1)$, where it matches onto the intermediate WKBJ. For a more in depth discussion of this method see references [5].

High Energy

For high energies the absorption probability tends to unity, and the cross-section reduces to that of the classical cross-section, see reference [7]. However, as discussed in reference [8], there will always be small corrections to the large energy limit. A high energy WKBJ approach can be applied in this limit, but for the purposes of this current study it will be sufficient to use $|\mathcal{A}_\kappa(E)|^2 = 1$.

Emission Rates

The emission rate for a massless fermion from a BH is related to the cross-section by a $d^{d-1}k$ dimensional momentum integral times a fermionic thermal temperature distribution:

$$\frac{d\mathcal{E}}{dt} = \sum_{\lambda,E} \sigma_{\lambda,E} \frac{E}{e^{\frac{E}{T_H}} + 1} \frac{d^{d-1}k}{(2\pi)^{d-1}} \ , \tag{6}$$

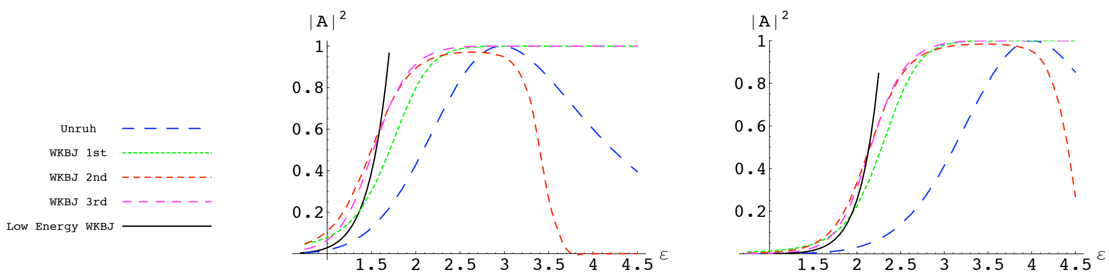

Figure 1: *Plots of the absorption probability, via various schemes, for $d = 7$ and the first two angular momentum channels: $\ell = 0$ (left) and $\ell = 1$ (right). Note the Unruh result is only valid for $\varepsilon \ll 1$.*

where T_H is the Hawking temperature, $\sigma_{\lambda,E}$ are the greybody factors and the sum is a generic sum over all angular momentum and momentum variables. We were able to relate the greybody factor to the absorbtion probability by considering the results of reference [11]:

$$\sigma_{\lambda,E} = \frac{1}{2\Omega_{d-2}} \left(\frac{2\pi}{E}\right)^{d-2} \sum_{\kappa} D_\kappa |\mathcal{A}_\kappa(E)|^2 \ . \tag{7}$$

In the above we have used D_κ as the degeneracy. Given that the angular integration over the momentum for a massless field ($|k| = E$) leads to the Jacobian $\int d^{d-1}k = \int \Omega_{d-2} E^{d-2} dE$, the fermion emission rate can be expressed solely in terms of the absorption probability. However, as the sum over κ is for $\kappa = \pm\left(\frac{d}{2} - 1\right), \pm\frac{d}{2}, \pm\left(\frac{d}{2} + 1\right)$ and since the integrand depends only on the absolute value of κ, we shall sum for $\kappa \geq 0$ and multiply by a factor of two. Therefore, after changing variables to $\varepsilon = E r_H$, and using the fact that the Hawking temperature is $T_H = (d-1)/(4\pi r_H)$, we obtain:

$$\frac{d^2\mathcal{E}}{dEdt} = \frac{1}{\pi r_H} \sum_{\kappa>0} \frac{\varepsilon}{e^{\frac{4\pi\varepsilon}{d-1}} + 1} D_\kappa |\mathcal{A}_\kappa(\varepsilon)|^2 \ . \tag{8}$$

Results and Conclusions

We have calculated the total power by integrating over ε, see equation (8). The results are shown in Table 1. From these results we find that for $d > 5$ the emission is predominantly into the bulk. Note that in order to obtain convergence in equation (8) we must choose some value of $\kappa_{max} > \varepsilon$, and to ensure this we have taken $\kappa_{max} = 34 + \frac{d}{2}$.

Dimension d	5	6	7	8	9	10
$d\mathcal{E}_{\text{Bulk}}/dt$	0.0579	0.1771	0.3380	1.4731	3.56403	18.2606
$d\mathcal{E}_{\text{brane}}/dt$	0.0708	0.1172	0.204	0.3435	0.554892	0.860165
$\frac{d\mathcal{E}_{\text{Bulk}}/dt}{d\mathcal{E}_{\text{brane}}/dt}$	0.8181	1.5109	1.6587	4.2880	6.42292	21.9019

Table 1: *A comparison of the bulk and brane-localised power spectrum up to $d = 10$, where we have changed units from r_H to M and set $M = 1$.*

Our results for the Hawking emission rate of a massless Dirac field on a bulk d-dimensional Schwarzschild background, using the method we developed in reference [5], conclude that fermions are mainly emitted into the bulk for $d > 5$, as we have shown, see Table 1, which is in contrast to the scalar field case and for bulk to brane photons [12]. This is an example contrary to the conjecture that BHs radiate mainly on the brane [13]. Furthermore, bulk dominated fermion emission is also consistent with the original motivation for split-fermions, namely that of a suppression of a rapid proton decay [3]. Note that these results also agree qualitatively with our work for the QNMs on such a background [5], where the BH damping rate was found to increase with dimension.

We have also highlighted how semi-analytic results can be obtained by considering different versions of the semi-classical WKBJ approximation, where we also compared this to the low energy analytic results derived from the method first developed in reference [10], see figure 1. Note also that in a recent work these methods have been used to investigate the effect of brane tension on bulk fermion emission, with the result that QNMs were damped by the tension of the brane [14].

References

[1] N. Arkani-Hamed, S. Dimopoulos and G. R. Dvali, Phys. Lett. B **429**, 263 (1998); I. Antoniadis, N. Arkani-Hamed, S. Dimopoulos and G. R. Dvali, Phys. Lett. B **436**, 257 (1998) [arXiv:hep-ph/9804398].

[2] P. C. Argyres, S. Dimopoulos and J. March-Russell, Phys. Lett. B **441**, 96 (1998); S. Dimopoulos and G. Landsberg, Phys. Rev. Lett. **87**, 161602 (2001); S. B. Giddings and S. D. Thomas, Phys. Rev. D **65**, 056010 (2002); R. Casadio and B. Harms, Int. J. Mod. Phys. A **17**, 4635 (2002) [arXiv:hep-th/0110255].

[3] N. Arkani-Hamed and M. Schmaltz, Phys. Rev. D **61**, 033005 (2000); N. Arkani-Hamed, Y. Grossman and M. Schmaltz, Phys. Rev. D **61**, 115004 (2000); T. Han, G. D. Kribs and B. McElrath, Phys. Rev. Lett. **90**, 031601 (2003);

[4] D. C. Dai, G. D. Starkman and D. Stojkovic, Phys. Rev. D **73**, 104037 (2006) [arXiv:hep-ph/0605085].

[5] H. T. Cho, A. S. Cornell, J. Doukas and W. Naylor, Phys. Rev. D **75** (2007) 104005 [arXiv:hep-th/0701193]; H. T. Cho, A. S. Cornell, J. Doukas and W. Naylor, arXiv:0709.1661 [hep-th].

[6] S. R. Das, G. W. Gibbons and S. D. Mathur, Phys. Rev. Lett. **78** (1997) 417 [arXiv:hep-th/9609052].

[7] A. S. Cornell, W. Naylor and M. Sasaki, JHEP **0602** (2006) 012 [arXiv:hep-th/0510009].

[8] H. T. Cho and Y. C. Lin, Class. Quant. Grav. **22** (2005) 775 [arXiv:gr-qc/0411090].

[9] C. M. Will and J. W. Guinn, Phys. Rev. A **37** (1988) 3674; S. Iyer and C. M. Will, Phys. Rev. D **35** (1987) 3621.

[10] W.G. Unruh, Phys. Rev. **D 14**, 3251 (1976).

[11] V. Cardoso, M. Cavaglia and L. Gualtieri, JHEP **0602**, 021 (2006) [arXiv:hep-th/0512116].

[12] E. Jung and D. K. Park, Nucl. Phys. B **766**, 269 (2007) [arXiv:hep-th/0610089]; C. M. Harris and P. Kanti, JHEP **0310**, 014 (2003) [hep-ph/0309054]; P. Kanti, Int. J. Mod. Phys. A **19** (2004) 4899 [arXiv:hep-ph/0402168].

[13] R. Emparan, G. T. Horowitz and R. C. Myers, Phys. Rev. Lett. **85**, 499 (2000) [arXiv:hep-th/0003118].

[14] H. T. Cho, A. S. Cornell, J. Doukas and W. Naylor, arXiv:0710.5267 [hep-th].

Braneworlds without Z_2 symmetry in n dimensions

Daisuke YAMAUCHI[1] and Misao SASAKI[2]

Yukawa Institute for Theoretical Physics, Kyoto University,
Kyoto 606-8502, Japan

Abstract

We consider a brane world in an arbitrary number of dimensions without Z_2 symmetry and derive the effective Einstein equation on the brane, where its right-hand side is given by the matter on the brane and the curvature in the bulk. This is achieved by first deriving the junction conditions for a non-Z_2 symmetric brane and second solving the Gauss equation, which relates the mean extrinsic curvature of the brane to the curvature in the bulk, with respect to the mean extrinsic curvature. The latter corresponds to formulating an explicit junction condition on the mean of the extrinsic curvature, analogue to the Israel junction condition for the jump of the extrinsic curvature. The derived equation is a basic equation for the study of Kaluza-Klein brane worlds in which some dimensions on the brane are compactified or for a regularization scheme for a higher codimension brane world, where the Kaluza-Klein compactification on the brane is regarded as a means to regularize the uncontrollable spacetime singularity created by the higher codimension brane.

1 Introduction

String theory suggests that our universe is not four dimensional but, rather, a submanifold (brane) embeded in a higher-dimensional spacetime (bulk). In particular, Randall and Sumdrum (RS) [2, 3] proposed an interesting brane world model. The RS model assumes a codimension-1 brane with Z_2 symmetry embeded in the bulk with a negative cosmological constant. However, to reconcile a higher-dimensional theory with the observed four-dimensional spacetime, the RS model is not sufficient. Since string theory suggests that the number of bulk dimensions is 10 or 11, the corresponding number of codimensions is 6 or 7. Therefore, we must consider a higher-codimension brane world. But a higher-codimension brane world has the serious problem that the brane becomes an uncontrollable spacetime singularity due to its self-gravity, except possibly for a codimension-2 brane world, which may give a reasonable cosmology. Thus it is necessary to develop a regularization method to realize a reasonable higher-codimension brane world.

For the above-stated purpose, we focus on a specific regularization scheme, which we now describe. Let us consider a codimenion-$(q+1)$ brane in an n-dimensional spacetime. We regularize this brane by expanding it into q-dimensions, so that it becomes a codimension-1 brane with q compact dimensions on the brane. Note that the resulting codimension-1 brane will not have the Z_2 symmetry. This regularization scheme is essentially the same as the Kaluza-Klein (KK) compactification of q spatial dimensions on the brane, which is called the KK brane world.

In this paper, partly to give a framework for the KK brane worlds and partly as a first step to formulate the above-mentioned regularization scheme for brane worlds of arbitrary codimension, we consider a codimension-1 brane world in an arbitrary number of spacetime dimensions without Z_2 symmetry and derive an effective Einstein equation on the brane, which is a generalization of the effective Einstein equation on the brane with Z_2 symmetry derived by Shiromizu, Maeda and Sasaki [4].

The work most relevant to the present one is that of Battye et al., [5] in which the non-Z_2 symmetric brane world is investigated. They study the junction condition in detail and point out that the effective Einstein equation has terms involving the mean of the extrinsic curvature across the brane which are not explicitly expressed in terms of either the matter on the brane or the curvature in the bulk. Then, they focused their investigation on a spatially homogeneous, isotropic brane. Our purpose here is to solve

[1]E-mail: yamauchi@yukawa.kyoto-u.ac.jp
[2]E-mail: misao@yukawa.kyoto-u.ac.jp

this problem and express the effective Einstein equation solely in terms of the matter on the brane and the curvature in the bulk, and also to present a straightforward generalization in which the number of spacetime dimensions of the bulk is extended from 5 to n.

Thoughout the paper, we use square brackets to denote the jump of a quantity across the brane and angled brackets to denote its mean. For an arbitrary tensor $\mathcal{A}$ (with tensor indices suppressed), we define $[\mathcal{A}] \equiv \mathcal{A}^+ - \mathcal{A}^-$, $\langle \mathcal{A} \rangle \equiv \frac{1}{2}(\mathcal{A}^+ + \mathcal{A}^-)$, where the superscript + denotes the side of the brane from which the normal vector n^A points toward the bulk.

2 Pre-effective Einstein equation on the brane

We consider a family of $(n-1)$-dimensional timelike hypersurfaces (slicing) in an n-dimensional spacetime and identify one of them as a brane (i.e., a singular hypersurface). We denote the bulk metric by g_{MN} where $M = 0, 1, \cdots, n-1$. We denote the vector field unit normal to the hypersurfaces by n^M. Then the induced metric γ_{MN} on the hypersurfaces is given by $\gamma_{MN} = g_{MN} - n_M n_N$. The metric $\gamma^A{}_B = \gamma^{AC} g_{CB}$ acts as a projection operator, projecting bulk tensors onto the brane. Here, the Gauss equation gives

$$\bar{R}_{ab} \quad = \quad \mathcal{F}_{ab} + K K_{ab} - K_a{}^c K_{bc} \,, \tag{1}$$

where $\bar{R}_{abcd}$ is the $(n-1)$-dimensional Riemann curvauture, K_{ab} is the extrinsic curvature on the brane. For convenience, we introduce the tensor $\mathcal{F}_{ab}$ defined by

$$\mathcal{F}_{ab} \equiv \frac{n-3}{n-2} \mathcal{R}_{AB} \gamma^A_a \gamma^B_b + \frac{1}{n-2} \mathcal{R}_{CD} \gamma^{CD} \gamma_{ab} - \frac{1}{n-1} \mathcal{R} \gamma_{ab} + \mathcal{E}_{ab} \,, \tag{2}$$

where $\mathcal{R}_{ABCD}$ is the n-dimensional Riemann curvature and $\mathcal{E}_{ab}$ is the projected Weyl curvature on the brane, defined by $\mathcal{E}_{ab} \equiv \mathcal{C}_{ACBD} n^C n^D \gamma^A_a \gamma^B_b$. Using the fact that the brane induced metric satisfies the junction condition $[\gamma_{ab}] = 0$, the Gauss equation can be decomposed into two equations,

$$\langle \bar{R}_{ab} \rangle = \bar{R}_{ab} = \langle \mathcal{F}_{ab} \rangle + \frac{1}{4}([K][K_{ab}] - [K^c_a][K_{bc}]) + \langle K \rangle \langle K_{ab} \rangle - \langle K^c_a \rangle \langle K_{bc} \rangle \,, \tag{3}$$

$$[\bar{R}_{ab}] = 0 = [\mathcal{F}_{ab}] + \langle K \rangle [K_{ab}] + [K] \langle K_{ab} \rangle - 2 \langle K_{(a}{}^c \rangle [K_{b)c}] \,, \tag{4}$$

where we use the relations between the jump and mean symbol$\langle \rangle, []$. We can construct the effective Einstein equation on the brane without any symmetry. For convenience, we decompose the $\mathcal{F}_{ab}$ and K_{ab} into trace and traceless parts, $\mathcal{F}_{ab} = \frac{\mathcal{F}}{n-1}\gamma_{ab} + \omega_{ab}$, $K_{ab} = \frac{K}{n-1}\gamma_{ab} + \sigma_{ab}$, respectively. The effective Einstein equation is derived from the mean of the Gauss equation (3). Inserting the Israel junction condition [6] ($[K\gamma_{ab} - K_{ab}] = \kappa^2_{(n)} \bar{T}_{ab} = \kappa^2_{(n)}(-\lambda \gamma_{ab} + \tau_{ab})$) into it, we obtain

$$\bar{G}_{ab} = -\bar{\Lambda} \gamma_{ab} + \kappa^2_{(n-1)} \tau_{ab} + \frac{\kappa^2_{(n-1)}}{\lambda} S_{ab} + \langle \Omega_{ab} \rangle - \langle \sigma_a{}^c \rangle \langle \sigma_{bc} \rangle \,, \tag{5}$$

where the each terms is defined by

$$\kappa^2_{(n-1)} = \frac{n-3}{4(n-2)} \kappa^4_{(n)} \lambda \,, \tag{6}$$

$$\bar{\Lambda} = \frac{n-3}{2(n-1)} \langle \mathcal{F} \rangle + \frac{1}{2} \kappa^2_{(n-1)} \lambda + \frac{(n-2)(n-3)}{2(n-1)^2} \langle K \rangle^2 - \frac{1}{2} \langle \sigma^{cd} \rangle \langle \sigma_{cd} \rangle \,, \tag{7}$$

$$S_{ab} = \frac{\tau}{n-3} \tau_{ab} - \frac{\tau^2}{2(n-3)} \gamma_{ab} - \frac{n-2}{n-3} \tau^c_a \tau_{bc} + \frac{n-2}{2(n-3)} \tau^{cd} \tau_{cd} \gamma_{ab} \,, \tag{8}$$

$$\langle \Omega_{ab} \rangle = \langle \omega_{ab} \rangle + \frac{n-3}{n-1} \langle K \rangle \langle \sigma_{ab} \rangle \,. \tag{9}$$

The first term $\bar{\Lambda}$ on the right-hand side of Eq. (5) represents the effective cosmological constant. We note, however, that this quantity may not be constant in general, as is clear from its expression in Eq. (7). The second and third terms are contributions from the energy-momentum tensor on the brane and its quadratic term, which are the same as in the Z_2 symmetric case [4]. The fourth traceless term, $\langle \Omega_{ab} \rangle$, which is traceless by definition, is an extension of the $\mathcal{E}_{ab}$ term in the Z_2 symmetric case. Finally, the last term is a new term, which has no analog in the Z_2 symmetric case. As is clear from its definition, this term arises from the square of the mean extrinsic curvature $\langle K_{ab}\rangle$, and it vanishes only if the traceless part of $\langle K_{ab}\rangle$ is zero. The above effective Einstein equation, (5), is completely general in the sense that no symmetry has been imposed. However, it is useless, except in the Z_2 symmetric case, because it depends strongly on the unknown mean extrinsic curvature $\langle K_{ab}\rangle$. In order to make it meaningful, it is necessary to express $\langle K_{ab}\rangle$ in terms of geometrical quantities in the bulk (i.e., the bulk metric and curvature) and the brane energy-momentum tensor.

3 The mean extrinsic curvature $\langle K_{ab}\rangle$

The equation we solve is (4),

$$-[\mathcal{F}_{ab}] = 2\kappa_{(n)}^2 \hat{\tau}_{(a}{}^c \langle K_{b)c}\rangle + \langle K\rangle [K_{ab}]\,. \tag{10}$$

where we use the Israel junction condition and for convenience we introduce the "hatted" energy-momentum tensor:

$$\hat{\tau}_{ab} \equiv \tau_{ab} - \frac{(n-3)\lambda - \tau}{2(n-2)}\gamma_{ab} = \bar{T}_{ab} - \frac{1}{2(n-2)}\bar{T}\gamma_{ab}\,. \tag{11}$$

Here we seek a general solution without particular assumptions concerning the brane energy-momentum tensor. Our method consists of two parts. First, we obtain the trace of the mean extrinsic curvature $\langle K\rangle$ by introducing the inverse of the hatted tensor $\hat{\tau}_{ab}$. Second, with $\langle K\rangle$ known, we rewrite the second Gauss equation as a matrix equation for $\langle K_{ab}\rangle$. This matrix equation can be solved by using the tetrad (more precisely, the vielbein) decomposition of $\hat{\tau}_{ab}$. Using this strategy, we obtain the general solution for the mean extrinsic curvature.

$$\begin{aligned}\kappa_{(n)}^2\langle K_{ab}\rangle &= -\frac{1}{2}(\hat{\tau}^{-1})_a{}^c[\mathcal{F}_{bc}] + \frac{(n-3)(\hat{\tau}^{-1})^{de}[\mathcal{F}_{de}]}{2((n-3)^2 - \hat{\tau}^m{}_m(\hat{\tau}^{-1})^n{}_n)}\left(\gamma_{ab} - \frac{\hat{\tau}^c{}_c}{n-3}(\hat{\tau}^{-1})_{ab}\right) \\ &\quad - \sum_{i\neq j}\frac{1}{\hat{\tau}_{(i)} + \hat{\tau}_{(j)}}\bar{e}_a^{(i)}\bar{e}_b^{(j)}[\omega_{(i)(j)}]\,. \end{aligned} \tag{12}$$

where $(\hat{\tau}^{-1})_{ab}$ is a inverse matrix of the "hatted" energy-momentum tensor $\hat{\tau}_{ab}$ and $\bar{e}_a^{(i)}$ is a local Lorentz frame in which the hatted tensor $\hat{\tau}_{ab}$ is diagonalized. We refer to this as the junction condition for the mean of the extrinsic curvature, which is a counterpart to the conventional junction condition for the jump of the extrinsic curvature, Israel junction condition [6]. We also note that this result is valid only if we have $\hat{\tau}_{(i)} + \hat{\tau}_{(j)} \neq 0$ for all possible pairs of (i) and (j). We need a special treatment in the case that any of the demonimators are zero.

4 Effect of $\langle K_{ab}\rangle$ on the brane

Low energy limit

We conjecture that the low energy regime, where $|\tau_{ab}| \ll \lambda$, Einstein gravity is recovered on the brane. For this reason, we believe that the contributions of the ω_{ab} and S_{ab} terms become negligibly small. To examine this, let us consider the solution for the mean extrinsic curvature up to $O(\tau_{ab}^2, \omega_{ab})$. In this case, the inverse of the hatted energy-momentum tensor is given by

$$(\hat{\tau}^{-1})^{ab} = \frac{2(n-2)}{n-3}\lambda^{-1}\left(\gamma^{ab} + \frac{2(n-2)}{n-3}\lambda^{-1}\left(\tau^{ab} - \frac{\tau}{2(n-2)}\gamma^{ab}\right) + \cdots\right)\,. \tag{13}$$

Then $\langle K_{ab}\rangle$ can be readily obtained as

$$\kappa_{(n)}^2\langle K_{ab}\rangle = \frac{[\mathcal{F}]}{2(n-1)\lambda}\left\{\gamma_{ab} + \frac{1}{\lambda}\left(\tau\gamma_{ab} - (n-2)\tau_{ab}\right)\right\} + \mathcal{O}(\tau_{ab}^2, \omega_{ab})\,. \tag{14}$$

Using this, the effective Einstein equation becomes

$$\bar{G}_{ab} = -\bar{\Lambda}^{LE}\gamma_{ab} + \kappa^2_{(n-1)}{}^{LE}\tau_{ab} + O(\tau^2_{ab}, \omega_{ab}), \tag{15}$$

where

$$\kappa^2_{(n-1)}{}^{LE} = \frac{n-3}{4(n-2)}\kappa^4_{(n)}\lambda - \frac{(n-2)(n-3)[\mathcal{F}]^2}{4(n-1)^2\kappa^4_{(n)}\lambda^3}\,, \tag{16}$$

$$\bar{\Lambda}^{LE} = \frac{n-3}{2(n-1)}\langle\mathcal{F}\rangle + \frac{n-3}{8(n-2)}(\kappa^2_{(n)}\lambda)^2 + \frac{(n-2)(n-3)[\mathcal{F}]^2}{8\kappa^4_{(n)}(n-1)^2\lambda^2}\,. \tag{17}$$

Thus, Einstein gravity is recovered. However, in contrast to our naive expectation, the contribution of the mean extrinsic curvature gives rise to new correction terms from the bulk, both to the gravitational constant and to the cosmological constant, which are not necessarily constant.

5 Conclusion

We considered a general codimension-1 brane in an arbitrary number of dimensions without Z_2 symmetry and we obtained expressions for both the jump and the mean of the extrinsic curvature in terms of the bulk curvature tensor and the brane energy-momentum tensor. With this result, we derived the effective Einstein equation on the brane in its most general form, which is a generalization of the Shiromizu-Maeda-Sasaki equation [4] to the case in which Z_2 symmetry does not exist. The derived effective Einstein equation has a new term arising from the mean extrinsic curvature, and this new term leads to the appearance effectively anisotropic matter on the brane.

Thus, our result is a basic equation for the hybrid brane world scenario, in which some spatial dimensions on the brane are Kaluza-Klein compactified. Also, it provides a basis for higher codimension brane worlds in which a higher codimension brane is regularized by a codimension-1 brane with extra dimensions on the brane compactified to an infinitesimally small size.

Acknowledgements

We would like to thank M. Minamitsuji for valuable and interesting discussions. We would also like to thank Y. Sendouda, and K. Izumi for useful comments. This work was supported in part by the Monbu-Kagakusho 21st century COE Program "Center for Diversity and Universality in Physics", and by JSPS Grants-in-Aid for Scientific Research [(B) No. 17340075, and (A) No. 18204024.]

References

[1] D. Yamauchi and M. Sasaki, Prog. Theor. Phys., **118**, 2,245 (2006) ; arXiv:0705.2443 [gr-qc].

[2] L. Randall and R. Sundrum, Phys. Rev. Lett. **83** (1999), 4690 ; hep-th/9906064.

[3] L. Randall and R. Sundrum, Phys. Rev. Lett. **83** (1999), 3370 ; hep-ph/9905221.

[4] T. Shiromizu, K. i. Maeda and M. Sasaki, Phys. Rev. D **62** (2000), 024012 ; gr-qc/9910076.

[5] R. A. Battye, B. Carter, A. Mennim and J. P. Uzan, Phys. Rev. D **64** (2001), 124007 ; hep-th/0105091.

[6] W. Israel, Nuovo Cim. B **44S10** (1966), 1 [Errata, **48** (1967 NUCIA,B44,1.1966) 463].

Modulus stabilization and low energy effective theory in six-dimensional supergravity braneworlds

Tsutomu Kobayashi[1], Frederico Arroja[2], Kazuya Koyama[3], and Tetsuya Shiromizu[4]

[1]*Department of Physics, Waseda University, Okubo 3-4-1, Shinjuku, Tokyo 169-8555, Japan*
[2,3]*Institute of Cosmology and Gravitation, University of Portsmouth, Portsmouth PO1 2EG, UK*
[3]*Department of Physics, Tokyo Institute of Technology, Tokyo 152-8551, Japan*

Abstract

We derive the low energy effective theory on a brane in six-dimensional chiral supergravity. The conical 3-brane singularities are resolved by introducing cylindrical codimension one 4-branes whose interiors are capped by a regular spacetime. The effective theory is described by the Brans-Dicke (BD) theory with the BD parameter given by $\omega_{\rm BD} = 1/2$. The BD field is originated from a modulus which is associated with the scaling symmetry of the system. If the dilaton potentials on the branes preserve the scaling symmetry, the scalar field has an exponential potential in the Einstein frame. Based on the effective theory, we discuss a possible way to stabilize the modulus to recover standard cosmology.

1 Introduction

Recently, much attention has been paid to six-dimensional supergravity. The most intriguing property of six-dimensional supergravity is that the four-dimensional spacetime is always Minkowski even in the presence of branes with tension. A 3-brane with tension induces only a deficit angle in the six-dimensional spacetime and the tension does not curve the four-dimensional spacetime within the brane. This feature is called self-tuning and it may solve the cosmological constant problem. This is the basis of the supersymmetric large extra-dimension (SLED) proposal.

In this paper, we derive a four-dimensional effective theory for the modulus in six-dimensional supergravity with resolved 4-branes by extending the analysis of Ref. [1] which studied the low energy effective theory in the Einstein-Maxwell theory. Arbitrary matter and potentials for the dilaton on 4-branes are allowed to exist. We use the gradient expansion technique to solve the six-dimensional geometry assuming that the deviation from the static solution is small. Using this method, it is possible to solve the non-trivial dependence of the bulk geometry on the four-dimensional coordinates. It is also possible to study whether we can reproduce sensible cosmology at low energies or not. We also study the possibility to stabilize the modulus using the potentials for the dilaton on the branes along the line of Ref. [2]. A detailed discussion is done in a much longer paper [3].

2 Basic equations

The relevant part of the supergravity action we consider is

$$S = \int d^6x\sqrt{-g}\left[\frac{M^4}{2}R - \frac{M^4}{2}\left(\partial\phi\right)^2 - \frac{1}{4}F^2e^{-\phi} - \frac{M^4}{2L_I^2}e^{\phi}\right], \tag{1}$$

where ϕ is the dilaton, M is the fundamental scale of gravity, $(\partial\phi)^2 := g^{MN}\partial_M\phi\partial_N\phi$, $F^2 := F_{MN}F^{MN}$, and $F_{MN} = \partial_M A_N - \partial_N A_M$ is the field strength of the gauge field A_M. For the moment we are interested in solving the 6D bulk equations of motion. In Sec. 4 we will add two 4-branes (at positions $y = y_\pm$)

[1]E-mail:tsutomu@gravity.phys.waseda.ac.jp
[2]E-mail:Frederico.Arroja@port.ac.uk
[3]E-mail:Kazuya.Koyama@port.ac.uk
[4]E-mail:shiromizu@phys.titech.ac.jp

and L_I denotes the different bulk curvature scales on either sides of the branes. We start with the axisymmetric metric ansatz

$$g_{MN}dx^M dx^N = L_I^2 e^{2\lambda(x)}\frac{dy^2}{f(y)} + \ell^2 e^{2[\psi(y,x)-\lambda(x)]}f(y)d\theta^2 + 2\ell b_\mu(y,x)d\theta dx^\mu + a^2(y)\bar{h}_{\mu\nu}(y,x)dx^\mu dx^\nu, \quad (2)$$

where capital Latin indices numerate the 6D coordinates while the Greek indices are restricted to the 4D coordinates. The evolution equations along the y-direction are given by

$$n^y\partial_y K_{\hat\mu}^{\hat\nu} + \hat{K}K_{\hat\mu}^{\hat\nu} = {}^5R_{\hat\mu}^{\hat\nu} - e^{-\lambda(x)}{}^5D_{\hat\mu}{}^5D^{\hat\nu}e^{\lambda(x)} - \partial_{\hat\mu}\phi\partial^{\hat\nu}\phi - \frac{1}{4L_I^2}e^\phi\delta_{\hat\mu}^{\hat\nu} - \frac{1}{M^4}\left(F_{\hat\mu M}F^{\hat\nu M} - \frac{1}{8}\delta_{\hat\mu}^{\hat\nu}F^2\right)e^{-\phi}, \quad (3)$$

where $n^y = e^{-\lambda}\sqrt{f}/L_I$, $K_{\hat\mu}^{\hat\nu}$ is the extrinsic curvature of $y=$ constant hypersurfaces, $\hat{K}$ is its 5D trace, ${}^5R_{\hat\mu}^{\hat\nu}$ is the 5D Ricci tensor and ${}^5D_{\hat\mu}$ is the covariant derivative with respect to the 5D metric. Here, $\hat\mu = \mu$ and θ. The Hamiltonian constraint is

$${}^5R + K_{\hat\mu}^{\hat\nu}K_{\hat\nu}^{\hat\mu} - \hat{K}^2 = -\frac{2}{M^4}\left(F_{yM}F^{yM} - \frac{1}{4}F^2\right)e^{-\phi} - 2(n^y\partial_y\phi)^2 + (\partial\phi)^2 + \frac{1}{L_I^2}e^\phi, \quad (4)$$

and the momentum constraints are ${}^5D_{\hat\nu}\left(K_{\hat\mu}^{\hat\nu} - \delta_{\hat\mu}^{\hat\nu}\hat{K}\right) = \frac{1}{M^4}F_{\hat\mu M}F^{yM}n_y e^{-\phi} + D_{\hat\mu}\phi\, n^y\partial_y\phi$, where $n_y = e^\lambda L_I/\sqrt{f}$. The Maxwell equations are given by $\nabla_M\left(e^{-\phi}F^{MN}\right) = 0$, where ∇_M is the covariant derivative with respect to the 6D metric. The dilaton equation of motion is $\nabla_M\nabla^M\phi + \frac{1}{4M^4}F^2e^{-\phi} - \frac{1}{2L_I^2}e^\phi = 0$.

3 Gradient expansion approach

In this section we will use the gradient expansion method to solve the 6D bulk equations. We assume that the length scale ℓ is of the same order of L_I. The small expansion parameter is the ratio of the bulk curvature scale to the 4D intrinsic curvature scale, $\varepsilon = \ell^2|R|$. We expand the various quantities as $\bar{h}_{\mu\nu} = h_{\mu\nu}(x) + \varepsilon \overset{(1)}{h}_{\mu\nu}(y,x) + \cdots$, $\psi = \psi^{(0)} + \varepsilon\psi^{(1)} + \cdots$, $\phi = \phi^{(0)} + \varepsilon\phi^{(1)} + \cdots$, $K_\mu^{\ \nu} = \overset{(0)}{K}{}_\mu^{\ \nu} + \varepsilon \overset{(1)}{K}{}_\mu^{\ \nu} + \cdots$, $K_\theta^{\ \theta} = \overset{(0)}{K}{}_\theta^{\ \theta} + \varepsilon \overset{(1)}{K}{}_\theta^{\ \theta} + \cdots$, $F_{y\theta} = \overset{(0)}{F}_{y\theta} + \varepsilon \overset{(1)}{F}_{y\theta} + \cdots$.

3.1 Zeroth order solutions

The zeroth order solutions are obtained as $a(y) = \sqrt{y}$, $f(y) = \frac{1}{4}\left(-y + \frac{\mu}{y} - \frac{q^2}{y^3}\right)$, $\lambda(x) = \frac{1}{2}\Phi(x)$, $\psi^{(0)}(y,x) = \Phi(x)$, $\phi^{(0)}(y,x) = -\ln y - \Phi(x)$, $\overset{(0)}{F}_{y\theta} = M^2\ell\frac{q}{a^4}e^{\phi^{(0)}+\psi^{(0)}} = M^2\ell\frac{q}{y^3}$, where μ and q are integration constants.

3.2 First order equations

The 4D traceless part of the evolution equations is found to be

$$\partial_y\left(y^2\sqrt{f}\,\mathbb{K}_\mu^{\ \nu}\right) = e^{\Phi/2}yL_I\mathbb{R}_\mu^{\ \nu}, \quad (5)$$

where we defined $\mathbb{K}_\mu^{\ \nu} := \overset{(1)}{K}{}_\mu^{\ \nu} - (1/4)\delta_\mu^{\ \nu}\overset{(1)}{K}{}_\lambda^{\ \lambda}$ and

$$\mathbb{R}_\mu^{\ \nu} := R_\mu^{\ \nu} - \frac{1}{4}\delta_\mu^{\ \nu}R - \left(\mathcal{D}_\mu\mathcal{D}^\nu\Phi - \frac{1}{4}\delta_\mu^{\ \nu}\mathcal{D}^2\Phi\right) - \frac{3}{2}\left[\mathcal{D}_\mu\Phi\mathcal{D}^\nu\Phi - \frac{1}{4}\delta_\mu^{\ \nu}(\mathcal{D}\Phi)^2\right], \quad (6)$$

where $\mathcal{D}^2\Phi := h^{\mu\nu}\mathcal{D}_\mu\mathcal{D}_\nu\Phi$ and $(\mathcal{D}\Phi)^2 := h^{\mu\nu}\mathcal{D}_\mu\Phi\mathcal{D}_\nu\Phi$. The general solution to the above equation is given by

$$\mathbb{K}_\mu^{\ \nu} = \frac{e^{\Phi/2}}{2\sqrt{f}}L_I\mathbb{R}_\mu^{\ \nu} + \frac{1}{y^2\sqrt{f}}\mathbb{C}_\mu^{\ \nu}(x), \quad (7)$$

where the traceless tensor $\mathbb{C}_\mu^{\ \nu}(x)$ is the integration "constant" to be fixed by the boundary conditions.

Now we define convenient quantities $\mathcal{J} := n^y \partial_y \phi^{(1)} + \frac{1}{2} \overset{(1)}{K}{}_\lambda^{\ \lambda}$ and

$$\mathcal{K} := \frac{3}{4} \overset{(1)}{K}{}_\lambda^{\ \lambda} + \overset{(1)}{K}{}_\theta^{\ \theta} + \frac{\sqrt{f}}{L_I} e^{-\Phi/2} \left(\frac{\partial_y f}{2f} - \frac{1}{2y} \right) \psi^{(1)} + \frac{y}{M^4 \ell^2 L_I \sqrt{f}} \overset{(0)}{F}_{y\theta}\, e^{-\Phi/2} A_\theta^{(1)} - \frac{\sqrt{f}}{L_I} \frac{e^{-\Phi/2}}{y} \phi^{(1)}. \tag{8}$$

The evolution equations for these variables can be derived using the above basic equations. With some manipulation one arrives at

$$\partial_y \left(y^2 \sqrt{f} \mathcal{J} \right) = \frac{1}{2} e^{\Phi/2} y L_I \left[R + \mathcal{D}^2 \Phi + \frac{1}{2} (\mathcal{D}\Phi)^2 \right], \tag{9}$$

$$\partial_y \left(y^2 \sqrt{f} \mathcal{K} \right) = \frac{1}{4} e^{\Phi/2} y L_I \left[R - 3\mathcal{D}^2 \Phi - \frac{7}{2} (\mathcal{D}\Phi)^2 \right]. \tag{10}$$

The two equations have the same structure as that of Eq. (5). The general solution for each evolution equation contains one integration "constant" which will be determined by the boundary conditions.

4 Junction conditions and effective theory on a regularized brane

The action of each brane is taken to be

$$S_{\rm brane} = - \int d^5 x \sqrt{-q} \left[V(\phi) + \frac{1}{2} U(\phi) (\partial_{\hat\mu} \Sigma - \mathrm{e} A_{\hat\mu})(\partial^{\hat\mu} \Sigma - \mathrm{e} A^{\hat\mu}) \right] + \int d^5 x \sqrt{-q}\, \mathcal{L}_{\rm m}, \tag{11}$$

where $q_{\hat\mu\hat\nu}$ is the induced metric on the 4-brane, $V(\phi)$ and $U(\phi)$ are the couplings to the dilaton, and $\mathcal{L}_{\rm m}$ is the Lagrangian of usual matter localized on the brane.

The jump conditions for the Maxwell field are $[[n^M F_{MN} e^{-\phi}]] = -\mathrm{e} U (\partial_N \Sigma - \mathrm{e} A_N)$, while for the dilaton field we have $[[n^M \partial_M \phi]] = \frac{1}{M^4} \left[\frac{dV}{d\phi} + \frac{1}{2} \frac{dU}{d\phi} (\partial_{\hat\lambda} \Sigma - \mathrm{e} A_{\hat\lambda})(\partial^{\hat\lambda} \Sigma - \mathrm{e} A^{\hat\lambda}) \right]$, where $[[F]]_{y_{\rm b}} := \lim_{\epsilon \to 0} (F|_{y_{\rm b}+\epsilon} - F|_{y_{\rm b}-\epsilon})$. Here and hereafter in this section all the quantities are evaluated at the position of the brane under consideration. The Israel conditions are given by $\left[\left[K_{\hat\mu}^{\ \hat\nu} - \delta_{\hat\mu}^{\ \hat\nu} \hat K \right]\right] = -\frac{1}{M^4} T_{\hat\mu ({\rm tot})}^{\ \hat\nu}$ where

$$T_{\hat\mu ({\rm tot})}^{\ \hat\nu} = -V \delta_{\hat\mu}^{\ \hat\nu} + U \left[(\partial_{\hat\mu} \Sigma - \mathrm{e} A_{\hat\mu})(\partial^{\hat\nu} \Sigma - \mathrm{e} A^{\hat\nu}) - \frac{1}{2} \delta_{\hat\mu}^{\ \hat\nu} (\partial_{\hat\lambda} \Sigma - \mathrm{e} A_{\hat\lambda})(\partial^{\hat\lambda} \Sigma - \mathrm{e} A^{\hat\lambda}) \right] + T_{\hat\mu}^{\ \hat\nu}, \tag{12}$$

and $T_{\hat\mu}^{\ \hat\nu}$ represents the matter energy-momentum tensor.

4.1 Zeroth order

The zeroth order junction conditions relate several parameters with each other, and the detail of the parameter counting of the configuration is found in Ref. [2].

The classical scaling symmetry is preserved by the special choice of the potentials $V(\phi) = v e^{\phi/2}, \quad U(\phi) = u e^{-\phi/2}$. In the following, we assume that at the zeroth order, the potentials are given by these scale-invariant ones. Then we expand the potentials as follows: $V(\phi) = V^{(0)}(\phi^{(0)}) + \varepsilon \left(V^{(1)}(\phi^{(0)}) + \frac{dV^{(0)}}{d\phi^{(0)}} \phi^{(1)} \right), U(\phi) = U^{(0)}(\phi^{(0)}) + \varepsilon \left(U^{(1)}(\phi^{(0)}) + \frac{dU^{(0)}}{d\phi^{(0)}} \phi^{(1)} \right)$, where $V^{(1)}(\phi^{(0)})$ and $U^{(1)}(\phi^{(0)})$ stand for the deviations from the zeroth order potentials.

4.2 First order

The 4D traceless part of the Israel conditions at first order is given by

$$[[\mathbb{K}_\mu^{\ \nu}]] = -\frac{1}{M^4} \mathbb{T}_\mu^{\ \nu}, \tag{13}$$

where $\mathbb{T}_\mu{}^\nu := T_\mu{}^\nu - (1/4)\delta_\mu{}^\nu T_\lambda{}^\lambda$. The 4D trace part of the Israel conditions reduces to

$$[[\mathcal{K}]] = \frac{1}{4M^4}T_\lambda{}^\lambda - \frac{1}{M^4}\Delta V. \tag{14}$$

where we defined $\Delta V = V^{(1)}(\phi^{(0)}) + \frac{1}{2}U^{(1)}(\phi^{(0)})\frac{e^{-\Phi}}{\ell^2 f}\left(n - \mathrm{e}A_\theta^{(0)}\right)^2$.

The $(\theta\theta)$ component of the Israel conditions and the dilaton jump condition are combined to give

$$[[\mathcal{J}]] = \frac{1}{2M^4}T_\theta{}^\theta - \frac{1}{M^4}\frac{d}{d\Phi}(\Delta V) - \frac{1}{2M^4}\Delta V. \tag{15}$$

Using Eqs. (13) and (14) together with the solution for $\mathbb{K}_\mu{}^\nu$ and $\mathcal{K}$ in terms of R and Φ, we end up with the effective equations

$$\begin{aligned} e^\Phi &\left(R_\mu{}^\nu[q^+] - \frac{1}{2}\delta_\mu{}^\nu R[q^+] - \Phi_{;\mu}^{;\nu} + \delta_\mu{}^\nu\Phi_{;\lambda}^{;\lambda} - \frac{3}{2}\Phi_{;\mu}\Phi^{;\nu} + \frac{5}{4}\delta_\mu{}^\nu\Phi_{;\lambda}\Phi^{;\lambda}\right) \\ &= \kappa_+^2\left(\overline{T}_\mu^{+\nu} - \overline{\Delta V}^+\delta_\mu^\nu\right) + \frac{a_-^2}{a_+^2}\kappa_-^2\left(\overline{T}_\mu^{-\nu} - \overline{\Delta V}^-\delta_\mu^\nu\right), \end{aligned} \tag{16}$$

where the 4D gravitational couplings are defined as $\kappa_\pm^2 := \frac{a_\pm^2}{2\pi\ell_*^2 M^4}$, with $\ell_*^2 = \ell\int_{y_S}^{y_N} L_I y dy$, ; denotes a covariant derivative with respect to the induced metric $q_{\mu\nu}^+ = a_+^2 h_{\mu\nu}$, $R_{\mu\nu}[q^+]$ is Ricci tensor computed from $q_{\mu\nu}^+$ and the potential integrated along the θ-direction is defined as $\overline{\Delta V} = 2\pi\ell\sqrt{f}e^{\Phi/2}\Delta V$.

The first order equations for $\mathcal{J}$ give the equation of motion for Φ:

$$(e^\Phi)_{;\mu}^{;\mu} = \frac{\kappa_+^2}{4}\left(\overline{T}_\lambda^{+\lambda} - \overline{T}_\theta^{+\theta} + 2\frac{d}{d\Phi}(\overline{\Delta V}^+) - 4\overline{\Delta V}^+\right) + \frac{a_-^2}{a_+^2}\frac{\kappa_-^2}{4}\left(\overline{T}_\lambda^{-\lambda} - \overline{T}_\theta^{-\theta} + 2\frac{d}{d\Phi}(\overline{\Delta V}^-) - 4\overline{\Delta V}^-\right). \tag{17}$$

5 Conclusions

In this paper, we derived the low energy effective theory in six-dimensional supergravity with resolved 4-branes. The gradient expansion method is used to solve the bulk geometry. The resultant effective theory is a Brans-Dicke theory with the Brans-Dicke parameter given by $\omega_{\mathrm{BD}} = 1/2$. If we choose the dilaton potentials on the branes so that they keep the scaling symmetry in the bulk and if we tune their amplitudes then there is no potential in the effective theory and the modulus is massless.

Our effective theory allows us to discuss cosmology with arbitrary matter on the brane. As the BD parameter is given by 1/2, it is impossible to reproduce realistic cosmology without stabilizing the modulus field. As it was suggested by Ref. [2], it is easy to generate a potential for the modulus Φ with a minimum by breaking the scaling symmetry from the dilaton potentials on the branes. Then it is possible to reproduce GR at low energies.

References

[1] S. Fujii, T. Kobayashi and T. Shiromizu, Phys. Rev. D **76**, 104052 (2007) [arXiv:0708.2534 [hep-th]].

[2] C. P. Burgess, D. Hoover and G. Tasinato, JHEP **0709**, 124 (2007) [arXiv:0705.3212 [hep-th]].

[3] F. Arroja, T. Kobayashi, K. Koyama and T. Shiromizu, JCAP **0712**, 006 (2007) [arXiv:0710.2539 [hep-th]].

Renormalized Newtonian Cosmic Evolution with Primordial Non-Gaussianity

Keisuke Izumi [1] and Jiro Soda [2]

Department of Physics, Kyoto University, Kyoto 606-8501, Japan

Abstract

We study Newtonian cosmological perturbation theory from a field theoretical point of view. We derive a path integral representation for the cosmological evolution of stochastic fluctuations. Our main result is the closed form of the generating functional valid for any initial statistics. Moreover, we extend the renormalization group method proposed by Matarresse and Pietroni to the case of primordial non-Gaussian density and velocity fluctuations. As an application, we calculate the nonlinear propagator and examine how the non-Gaussianity affects the memory of cosmic fields to their initial conditions. It turns out that the non-Gaussianity affect the nonlinear propagator. In the case of positive skewness, the onset of the nonlinearity is advanced with a given comoving wavenumber. On the other hand, the negative skewness gives the opposite result.

1 Introduction

The large scale structure in the universe has evolved from primordial fluctuations according to the gravitational instability. In the standard scenario of the structure formation, the primordial fluctuations are created quantum mechanically during the inflationary stage in the early universe. After exiting the horizon, the fluctuations are evolved linearly; which is well described by relativistic linear perturbation theory. Eventually the fluctuations re-enter into the horizon. After that, it is sufficient to treat the evolution of fluctuations by means of Newtonian gravity. Due to the Jeans instability, at some point, the density fluctuations become nonlinear. In this stage, usually we resort to the N-body simulations. However, since the numerical simulations are time consuming, the analytical calculation of the nonlinear evolution is still desired. The standard perturbative expansion method is developed for this purpose. In the quasi-nonlinear regime, the perturbative approach was successful. To obtain more accurate results, however, the non-perturbative analytic method would be necessary.

Recently, Crocce and Scoccimarro have developed a new formalism to study the large scale structure [1]. They described the perturbative solution by Feynman diagrams and identified three fundamental objects: the initial conditions, the vertex, and the propagator. They have found that the renormalization of the propagator is the most important one. Based on this finding, they have observed that, due to the rapid fall off of the nonlinear propagator, the memory of the cosmic fields to their initial conditions will be lost soon in the nonlinear regime.

Following their work, Matarrese and Pietroni reformulated the cosmological perturbation theory from the path integral point of view and developed the renormalization group (RG) techniques in cosmology [2, 3]. Matarrese and Pietroni have applied their formalism to the baryon acoustic oscillations (BAO) which takes place around the scale $k \sim 0.1\mathrm{Mpc}^{-1}$ [4]. On these scales, the nonlinear effects are relevant [5, 6]. They have found that the renormalization group method is useful to predict the BAO feature. Crocce and Scoccimarro have used their graphical approach to discuss BAO and found the renormalized perturbation approach gives a good agreements with results of numerical simulations [7]. This result is further confirmed by Nishimichi et al. [8].

These authors have discussed only the Gaussian initial conditions. Recently, however, it has been realized that the primordial non-Gaussianity can be produced in the inflationary scenario. If so, it is important to give a renormalization group formalism for the non-Gaussian initial conditions. Conventionary,

[1] E-mail:ksuke@tap.scphys.kyoto-u.ac.jp
[2] E-mail:jiro@tap.scphys.kyoto-u.ac.jp

the non-Gaussian curvature perturbation Φ is characterized by the following form

$$\Phi(\mathbf{x}) = \Phi_g(\mathbf{x}) + f_{NL}(\Phi_g^2(\mathbf{x}) - \langle\Phi_g^2\rangle), \tag{1}$$

where Φ_g is the Gaussian field and f_{NL} is the parameter to represent a deviation from the Gaussianity. There are several possible observational tests to constrain the non-Gaussianity. The most stringent limit comes from WMAP and the result is $-58 < f_{NL} < 134$ [9]. Planck and other tests will give a more stringent limit or detect the non-Gaussianity [10].

The purpose of our paper [11] is therefore to extend the analysis by Matarrese and Pietroni to the non-Gaussian initial conditions. Starting from the generating functional of the multi-point functions, we derive the path integral representation of the cosmic evolution of the cosmic fields. In contrast to the previous work, the non-Gaussianity is incorporated into the field theoretical scheme. In particular, we obtain the formula for the generating functional which allows us to use the Feynman diagram method to calculate various statistical quantities characterizing the large scale structure in the universe. We also derive the RG equation for the effective action. As an application, we calculate the nonlinear propagator and examine if the memory of the cosmic fields to their initial conditions has the tendency to be kept by the non-Gaussianity or not.

2 Basic equations for cosmic fields

In this section, we review the standard Newtonian cosmological perturbation theory. Here, we consider the Einstein-de Sitter universe for simplicity. Of course, it is possible to extend our analysis to other cosmological models.

First of all, let us consider the homogeneous cosmological background spacetime. Taking the conformal time and assuming the flat space, we can write down the metric

$$ds^2 = a^2(\tau)\left[-d\tau^2 + \delta_{ij}dx^i dx^j\right] \ . \tag{2}$$

The cosmological scale factor a is determined by solving FRW equations

$$\mathcal{H}^2 = \frac{8\pi G}{3}a^2\rho_0 \ , \quad \mathcal{H}' = -\frac{4\pi G}{3}a^2\rho_0 \ , \tag{3}$$

where ρ_0 is the averaged density field and we have defined $\mathcal{H} = da/d\tau/a = a'/a$.

Now, let us consider the inhomogeneous distribution of the matter. The evolution of the total matter density is determined by the gravity including the effect of cosmic expansion. The actual density $\rho(\mathbf{x},\tau)$ is deviated from the averaged density $\rho_0(\tau)$ Let us define the density fluctuation as

$$\delta(\mathbf{x},\tau) = \frac{\rho(\mathbf{x},\tau) - \rho_0(\tau)}{\rho_0(\tau)} = \int d^3k\delta(\mathbf{k},\tau)e^{-i\mathbf{k}\cdot\mathbf{x}} \ . \tag{4}$$

It obeys the equation of continuity and the peculiar velocity $\mathbf{v}$ is determined by the Euler equation in the presence of gravitational potential ϕ. The gravitational potential itself is governed by the Poisson equation. Thus, equations of motion for the cosmic fields, δ, $\mathbf{v}$, and ϕ, are given by

$$\frac{\partial\delta}{\partial\tau} + \nabla\cdot[(1+\delta)\,\mathbf{v}] = 0, \qquad \frac{\partial\mathbf{v}}{\partial\tau} + \mathcal{H}\mathbf{v} + (\mathbf{v}\cdot\nabla)\,\mathbf{v} = -\nabla\phi, \qquad \nabla^2\phi = \frac{3}{2}\mathcal{H}^2\delta \ . \tag{5}$$

On large scales, the assumption that the peculiar velocity is irrotational would be valid. Then, defining $\theta = \nabla\cdot\mathbf{v}$, we obtain the relation $\mathbf{v}(\mathbf{k},\tau) = i\mathbf{k}\theta(\mathbf{k},\tau)/k^2$. After eliminating the gravitational potential, we obtain equations of motion in the Fourier space where the index $a = 1, 2$ and $\eta = \log a(\tau)/a_{\rm in}$ denotes the e-folding number. The initial scale factor $a_{\rm in}$ can be taken arbitrarily.

$$(\delta_{ab}\partial_\eta + \Omega_{ab})\,\varphi_b(\mathbf{k},\eta) = e^\eta\gamma_{abc}(\mathbf{k},-\mathbf{p},-\mathbf{q})\varphi_b(\mathbf{p},\eta)\varphi_c(\mathbf{q},\eta), \tag{6}$$

$$\gamma_{121}(\mathbf{k},\mathbf{p},\mathbf{q}) = \frac{1}{2}\delta_D(\mathbf{k}+\mathbf{p}+\mathbf{q})\alpha(\mathbf{p},\mathbf{q}) = \gamma_{112}(\mathbf{k},\mathbf{q},\mathbf{p}), \quad \gamma_{222}(\mathbf{k},\mathbf{p},\mathbf{q}) = \delta_D(\mathbf{k}+\mathbf{p}+\mathbf{q})\beta(\mathbf{p},\mathbf{q}), \tag{7}$$

$$\varphi_a(\mathbf{k},\tau) \equiv \begin{pmatrix} \varphi_1(\mathbf{k},\tau) \\ \varphi_2(\mathbf{k},\tau) \end{pmatrix} \equiv e^{-\eta}\begin{pmatrix} \delta(\mathbf{k},\tau) \\ -\theta(\mathbf{k},\tau)/\mathcal{H} \end{pmatrix}, \quad \Omega = \begin{pmatrix} 1 & -1 \\ -3/2 & 3/2 \end{pmatrix}, \tag{8}$$

where other components are zero, the index $a=1,2$ and $\eta=\log a(\tau)/a_{\rm in}$ denotes the e-folding number. The initial scale factor $a_{\rm in}$ can be taken arbitrarily. Here, we have used the Einstein's sum rule

$$\varphi_a(-\mathbf{k},0)\varphi_b(\mathbf{k},0)\equiv\int d^3k\varphi_a(-\mathbf{k},0)\varphi_b(\mathbf{k},0)\ . \tag{9}$$

From now on, we should understand this convention is used when the same wavenumber vector appear twice in the same term.

3 Path Integral Representation and Renormalization Group

What we are interested in are the statistical quantities characterizing the large scale structure in the universe. The statistics of primordial cosmic fields $\varphi_a(\mathbf{k},0)$ are determined by the initial probability functional $P[\varphi_a(\mathbf{k},0)]$. To calculate desired quantities, we need to solve the nonlinear evolution equations and obtain the solution as a function of the initial fields. Namely, we have the statistics and the dynamics to be considered. More precisely, we want to calculate

$$\begin{aligned}&\left\langle \exp i\int d\eta J_a(-\mathbf{k},\eta)\varphi_a(\mathbf{k},\eta;\varphi(\mathbf{k},0))\right\rangle\\&\quad=\int d\varphi_a(\mathbf{k},0)P[\varphi_a(\mathbf{k},0)]\exp i\int d\eta J_a(-\mathbf{k},\eta)\varphi_a(\mathbf{k},\eta;\varphi_a(\mathbf{k},0)),\end{aligned} \tag{10}$$

where $P[\varphi_a(\mathbf{k},0)]$ is the general probability functional for the initial field $\varphi_a(\mathbf{k},0)$ and $\varphi_a(\mathbf{k},\eta;\varphi_a(\mathbf{k},0))$ is the solution of Eq.(6) with the initial condition $\varphi_a(\mathbf{k},0)$. This is a generating functional for multi-point correlation functions. Here, we shall combine the statistics and the dynamics in a unified framework. This can be achieved by the field theoretical path integral method. It is the path integral representation of the problem which can be used to perform the non-perturbative approximation.

Intrducing an auxiliary field $\chi(\mathbf{k},\eta)$, a generating function can be written as the path integral representation;

$$\begin{aligned}Z[J_a,K_b]\ &=\ \int D\varphi_a(\mathbf{k},\eta)D\chi_a(\mathbf{k},\eta)e^{C[\chi_a(\mathbf{k},0)]}\exp\left[i\int d\eta\chi_a(-\mathbf{k},\eta)\mathbf{L}\varphi_a(\mathbf{k},\eta)\right.\\&\qquad\left.+i\int d\eta J_a(-\mathbf{k},\eta)\varphi_a(\mathbf{k},\eta)+i\int d\eta K_a(-\mathbf{k},\eta)\chi_a(\mathbf{k},\eta)\right].\end{aligned} \tag{11}$$

where

$$\begin{aligned}C[\chi_a(\mathbf{k},0)]=(2\pi)^3\Big(&-\frac{1}{2}\chi_a(-\mathbf{k},0)P_{ab}\chi_b(\mathbf{k},0)\\&+\frac{i}{6}B_{abc}\left(\mathbf{k}_1,\mathbf{k}_2,\mathbf{k}_3\right)\chi_a(-\mathbf{k}_1,0)\chi_b(-\mathbf{k}_2,0)\chi_c(-\mathbf{k}_3,0)+\cdots\Big)\ .\end{aligned} \tag{12}$$

From the field theoretical point of view, $C[\chi_a(\mathbf{k},0)]$ can be regarded as the boundary action on the initial hypersurface $\eta=0$. In this sense, the field $\chi_a(\mathbf{k},0)$ is associated with the initial conditions.

Then, using the generator of the connected Green functions,

$$W[J_a,K_b]=-i\log Z[J_a,K_b]\ , \tag{13}$$

we can get

$$(2\pi)^3P_{ab}=-i\frac{\delta^2W}{\delta J_a\delta J_b}\ ,G_{ab}=-\frac{\delta^2W}{\delta J_a\delta K_b}\ ,(2\pi)^3B_{abc}=\frac{\delta^3W}{\delta J_a\delta J_b\delta J_c}\ . \tag{14}$$

The idea of the renormalization group introduced by Matarrese and Pietroni is as follows. First, we introduce a filter function with the UV cutoff λ in the P^0_{ab} and B^0_{abc}. This defines a fictious theory where the linear perturbation theory works well. We denote various quantities in the cutoff theory with the suffix

λ, for example like as $P_{ab,\lambda}$. When this cutoff scale λ goes to infinity, the original theory is recovered. As λ becomes large, nonlinear effects are incorporated gradually. This process can be expressed by the renormalization group equation. Then, we obtain

$$\begin{aligned}
\partial_\lambda W_\lambda \quad = \quad & \frac{(2\pi)^3}{2} \int d\eta_a d\eta_b \partial_\lambda P_{ab,\lambda} \delta(\eta_a)\delta(\eta_b) \left(\frac{\delta^2 W_\lambda}{\delta K_a(-\mathbf{p},\eta)\delta K_b(\mathbf{p},\eta)} + i \frac{\delta W}{\delta K_a(-\mathbf{p},\eta)} \frac{\delta W}{\delta K_b(\mathbf{p},\eta)} \right) \\
& + \frac{(2\pi)^3}{6} \int d\eta_a d\eta_b d\eta_c \partial_\lambda B_{abc,\lambda}(\mathbf{p}_1,\mathbf{p}_2,\mathbf{p}_3)\delta(\eta_a)\delta(\eta_b)\delta(\eta_c) \\
& \times \left(\frac{\delta^3 W}{\delta K_a(\mathbf{p}_1,\eta)\delta K_b(\mathbf{p}_2,\eta)\delta K_c(\mathbf{p}_3,\eta)} + i \left(\frac{\delta W}{\delta K_a(\mathbf{p}_1,\eta)} \frac{\delta^2 W}{\delta K_b(\mathbf{p}_2,\eta)\delta K_c(\mathbf{p}_3,\eta)} + (\mathrm{cyc.}[a,b,c]) \right) \right. \\
& \left. \quad - \frac{\delta W}{\delta K_a(\mathbf{p}_1,\eta)} \frac{\delta W}{\delta K_b(\mathbf{p}_2,\eta)} \frac{\delta W}{\delta K_c(\mathbf{p}_3,\eta)} \right) + \cdots .
\end{aligned} \tag{15}$$

Using this equation, we can obtain the renormalized propagator equation as

$$\begin{aligned}
& \partial_\lambda \frac{\delta^2 W_\lambda}{\delta J_a(-\mathbf{k},\eta_a)\delta K_b(\mathbf{k}',\eta_a)} = -\delta(\mathbf{k}-\mathbf{k}')\partial_\lambda G_{ab,\lambda}(k;\eta_a\eta_b) \\
& \quad = \left\{ \frac{(2\pi)^3}{2} \int d\eta_c d\eta_d \partial_\lambda P_{cd,\lambda} \delta(\eta_c)\delta(\eta_d) \frac{\delta^4 W_\lambda}{\delta J_a(-\mathbf{k},\eta_a)\delta K_b(\mathbf{k}',\eta_a)\delta K_c(-\mathbf{p},\eta_a)\delta K_d(\mathbf{p},\eta_a)} \right. \\
& \qquad + \frac{(2\pi)^3}{6} \int d\eta_c d\eta_d d\eta_e \partial_\lambda B_{cde,\lambda}(\mathbf{p}_1,\mathbf{p}_2,\mathbf{p}_3)\delta(\eta_c)\delta(\eta_d)\delta(\eta_e) \\
& \qquad \left. \left. \times \frac{\delta^5 W_\lambda}{\delta J_a(-\mathbf{k},\eta_a)\delta K_b(\mathbf{k}',\eta_a)\delta K_c(-\mathbf{p}_1,\eta_a)\delta K_d(-\mathbf{p}_2,\eta_a)\delta K_e(-\mathbf{p}_3,\eta_a)} + \cdots \right\} \right|_{J_a=0,K_a=0}
\end{aligned} \tag{16}$$

Solving this equation under some approximations [11], we find that the modes in the range $k > 0.1(1+z)\mathrm{Mpc}^{-1}$ or $k > 0.03\xi_{NL}^{-\frac{1}{2}}(1+z)^{3/2}\mathrm{Mpc}^{-1}$ seems to have already lost the memory to the initial conditions.

References

[1] M. Crocce and R. Scoccimarro, Phys. Rev. D **73**, 063519 (2006) [arXiv:astro-ph/0509418].

[2] S. Matarrese and M. Pietroni, arXiv:astro-ph/0702653.

[3] S. Matarrese and M. Pietroni, arXiv:astro-ph/0703563.

[4] D. J. Eisenstein *et al.* [SDSS Collaboration], Astrophys. J. **633**, 560 (2005) [arXiv:astro-ph/0501171].

[5] E. Huff, A. E. Schulz, M. White, D. J. Schlegel and M. S. Warren, Astropart. Phys. **26**, 351 (2007) [arXiv:astro-ph/0607061].

[6] D. Jeong and E. Komatsu, Astrophys. J. **651**, 619 (2006) [arXiv:astro-ph/0604075].

[7] M. Crocce and R. Scoccimarro, arXiv:0704.2783 [astro-ph].

[8] T. Nishimichi *et al.*, arXiv:0705.1589 [astro-ph].

[9] E. Komatsu *et al.* [WMAP Collaboration], Astrophys. J. Suppl. **148**, 119 (2003) [arXiv:astro-ph/0302223].

[10] N. Bartolo, E. Komatsu, S. Matarrese and A. Riotto, Phys. Rept. **402**, 103 (2004) [arXiv:astro-ph/0406398].

[11] Keisuke Izumi and Jiro Soda . Phys. Rev. **D76** 083517 (2007) [arXiv:0706.1604].

Leptogenesis from two flat directions

Kohei Kamada [1] and Jun'ichi Yokoyama

Research Center for the Early Universe (RESCEU),
Graduate School of Science, The University of Tokyo, Tokyo 113-0033, Japan

Abstract

We investigate Affleck-Dine mechanism when multiple flat directions have large values simultaneously. We consider in detail the case when both LH_u flat direction and H_uH_d flat direction with non-renormalizable superpotential work. We find that initial value is determined completely by the potential and there are no ambiguities how two flat directions are mixed. Moreover there is CP-violation even for large H which is due to A-term and cross coupling in F-term and lepton asymmetry is generated just after the end of inflation. There is no suppression factor $m_{3/2}/H_{osc}$ in the net lepton-to-entropy ratio.

1 Introduction

The Affleck-Dine (AD) mechanism [1] is one of the most promising scenarios among many models of baryogenesis that account for the origin of the observed baryon asymmetry of the universe. Especially a model of AD mechanism that Dine et al. developed [2] is very effective in the inflationary regime and many authors [3, 4, 5] have analyzed this model energetically.

Their analyses restricted only in the case where the configuration of flat direction can be parameterized in terms of one complex scalar field. There are, however, many flat directions even in the minimal supersymmetric standard model (MSSM), some of which carry $B-L$ charge but others do not. (Lepton asymmetry can be converted to baryon asymmetry through the sphaleron effect [6], which violates $B+L$ at the electroweak scale, where B and L are baryon and lepton charges respectively.) Therefore it is very important which flat direction, if any, is selected as the AD field. Moreover, there are multiple flat directions which do not give rise to any F-term in the renormalizable limit. Such directions can get large values at the same time and we can no longer parameterize them by one scalar field. If some of them carry $B-L$ charge and others do not, the degree of the mixing of multiple flat directions directly affects the net baryon asymmetry. It is not trivial whether the simple one-field analysis is applicable in such a case.

Previously, Senami and Yamamoto [7], and Enqvist et al. [8] have considered the case where multiple flat directions have large values in the MSSM and its extensions. However, their evaluation of the potential was insufficient and in particular they did not care how multiple flat directions mix. The purpose of this talk is to investigate how multiple flat directions mix and to evaluate the resultant baryon/lepton asymmetry.

2 Model

We adopt a non-renormalizable superpotential of the form [7],

$$\delta W = \frac{\lambda_{Lij}}{2M}(L_iH_u)(L_jH_u) + \frac{\lambda_H}{2M}(H_uH_d)(H_uH_d), \tag{1}$$

in addition to the lepton sector of the renormalizable superpotential of MSSM. Here M is some cut-off scale, λ_{Lij} and λ_H are coupling constants. We choose a basis which λ_{Lij} is diagonal and assume that $\lambda_{L22}, \lambda_{L33} \gg \lambda_H \sim \lambda_{L11} \equiv \lambda_L$. Note that this superpotential gives neutrino mass when Higgs field that couples up-type quark gets a nonvanishing expectation value,

$$m_{\nu_i} = \frac{\lambda_{Lii}}{M}\langle H_u\rangle^2. \tag{2}$$

[1] E-mail:kamada@resceu.s.u-tokyo.ac.jp

To realize inflation, we introduce an inflaton sector besides the MSSM sector. Coupling between the inflaton sector and the MSSM sector arises only with the gravitational strength in the supergravity scalar potential,

$$V = e^{K/M_G^2}\left(D_i W K^{i\bar{j}} D_{\bar{j}} W^* - \frac{3}{M_G^2}|W|^2\right), \tag{3}$$

where M_G is the reduced Planck mass. We also introduce non-minimal Kahler potential,

$$\delta K = \frac{a_a}{M_G^2}|I|^2|\phi_a|^2 \qquad \text{and} \qquad \delta K = \frac{b_a}{M_G} I|\phi_a|^2 + \text{h.c.}, \tag{4}$$

in addition to the canonical terms, where ϕ_a is scalar fields of MSSM and I is the inflaton, and a_a is real, b_a is complex parameter. We assume the F-term of inflaton dominates the universe during inflation.

By neglecting heavier leptons [7] (Hereafter L represents lightest lepton L_1) and restricting dynamics of scalar fields along flat directions, we can parameterize scalar fields as

$$L = \begin{pmatrix} 0 \\ \nu \end{pmatrix}, H_u = \begin{pmatrix} h_u \\ 0 \end{pmatrix}, H_d = \begin{pmatrix} 0 \\ h_d \end{pmatrix}, \tag{5}$$

without loss of generality. The resultant potential for ν, h_u and h_d during inflationary era becomes

$$\begin{aligned} V(\nu, h_u, h_d) =& \sum_{a=\nu,h_u,h_d} (m_a^2 - c_a H^2)|\phi_a|^2 \\ &+ \left|\frac{\lambda_L}{M}\nu^2 h_u + \frac{\lambda_H}{M} h_u h_d^2\right|^2 + \left|\frac{\lambda_H}{M} h_u^2 h_d\right|^2 + \left|\frac{\lambda_L}{M}\nu h_u^2\right|^2 \\ &+ \left[\frac{\lambda_L}{2M}(a_L H + A_L m_{3/2})\nu^2 h_u^2 + \text{h.c.}\right] + \left[\frac{\lambda_H}{2M}(a_H H + A_H m_{3/2}) h_d^2 h_u^2 + \text{h.c.}\right] + V_D, \end{aligned} \tag{6}$$

$$V_D = (g^2 + g'^2)(|\nu|^2 - |h_u|^2 + |h_d|^2)^2 \tag{7}$$

where c_a's are real and a_L, A_L, a_H and A_H are complex parameters with their magnitude presumably of order of unity. Here we also introduce the effect of SUSY breaking from hidden sector in terms of m_a, the soft mass of scalar field ϕ_a, and $m_{3/2}$, the gravitino mass. Terms including the Hubble parameter H arise due to the coupling of flat direction to the F-term of the inflaton $F_I \sim H_{inf} M_G$.

Inflaton oscillation era follows the inflationary era. In this era, a part of the potential of scalar fields change as

$$\frac{\lambda_L}{2M} a_L H \nu^2 h_u^2 + \text{h.c.} \rightarrow \frac{\lambda_L}{2\kappa M H_{inf}} a_L H^2 \nu^2 h_u^2 + \text{h.c.} \tag{8}$$

$$\frac{\lambda_H}{2M} a_H H h_d^2 h_u^2 + \text{h.c.} \rightarrow \frac{\lambda_H}{2\kappa M H_{inf}} a_H H^2 h_d^2 h_u^2 + \text{h.c.}, \tag{9}$$

where H_{inf} is the Hubble parameter in the inflationary era and κ is a numerical parameter of order of unity that depends on the inflation model. This change of potential is due to the change of time average of F_I. Moreover, thermal plasma from inflaton decay emerges and the potential for scalar fields acquires thermal correction [4].

3 Instability of one flat direction

Next we examine the necessity of considering multiple flat directions in the inflationary era. The mass terms of scalar fields are

$$-(c_\nu + c_u)H^2|\nu|^2 - (c_u + c_d)H^2|h_d|^2. \tag{10}$$

Here we neglect soft terms from hidden sector and set the D-flat condition $V_D = 0$. When the initial values are set near the origin, and if $c_\nu + c_u > 0$ and $c_u + c_d < 0$, h_d stays at the origin and we can take the one flat direction description. However, if $c_\nu + c_u > 0$ and $c_u + c_d > 0$, not only ν but also h_d stay away from the origin and we can no longer take the description. Moreover, even if only LH_u direction is selected in the beginning, H_d is unstable at the origin for large parameter region. We can see this by evaluating the eigenvalues of mass matrix for H_d around the local minimum of LH_u flat direction parameterized as $\nu = h_u = \phi \sim \sqrt{((c_\nu + c_u)/2)^{1/2} HM/\lambda_L}$, The eigenvalues of this matrix are

$$\left(\frac{\lambda_H}{M}\right)^2 |\phi|^4 - c_d H^2 \pm \left[\left(\frac{\lambda_L \lambda_H}{M^2}|\phi|^4 + \mathrm{Re}(a_H)\frac{\lambda_H H}{2M}|\phi|^2\right)^2 + \left(\mathrm{Im}(a_H)\frac{\lambda_H H}{2M}|\phi|^2\right)\right]^{1/2}. \tag{11}$$

As a consequence, if c_d or $|a_H|$ is a little larger than unity, for example, h_d is unstable around LH_u flat direction with a wide range of parameters. Therefore, considering multiple flat directions is more natural than one flat direction.

4 Dynamics of scalar fields and leptogenesis

In this section, we describe the motion of scalar fields and estimate number asymmetry of scalar fields-to-entropy ratio. Here we consider only homogeneous mode and neglect fluctuations around it because the curvature of the potential is much larger than the Hubble parameter and quantum fluctuation is sufficiently suppressed in this case.

In the Friedman universe scalar fields ϕ_a obey the equation of motion,

$$\ddot{\phi}_a + 3H\dot{\phi}_a + \frac{\partial V}{\partial \phi_a^*} = 0. \tag{12}$$

We analyzed the dynamics of three scalar fields in the inflationary era ($H = H_{inf} = const.$) and in the inflaton oscillation era ($H = (2/3)t^{-1}$) numerically.

In the inflationary era, scalar fields fall into one of potential minima like one field case [2] if the number of e-fold is large enough. Moreover we find the potential minima is unique except for the gauge freedom (Fig.1) although the potential is very complicated. As a consequence, in this model there remains no pre inflationary information.

Next we turn to the inflaton oscillation dominant era. We take the final value of scalar fields in the inflationary era as their initial value in the inflaton oscillation dominant era. In this era, the equation for angular motions of scalar fields becomes

$$\frac{\partial^2 \theta_a}{\partial z^2} + \frac{4}{9}\frac{e^{2z}}{(H_{inf}|\phi_a|)^2}\frac{\partial V}{\partial \theta_a} = 0, \tag{13}$$

where θ_a is the phase of ϕ_a and we define

$$z = \ln(t/t_f), \quad t_f = \frac{2}{3}H_{inf}^{-1} \tag{14}$$

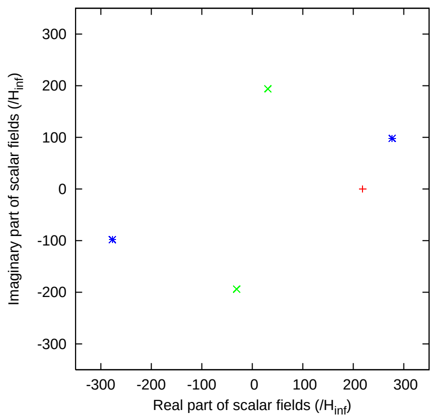

Figure 1: The value of scalar fields at the end of inflation, the real part (horizontal axis) and the imaginary part (vertical axis) after gauge transformation. Red crosses represent ν, blue x's represent h_u, and green stars represent h_d. The parameters: $c_\nu = 0.8, c_u = 1.0, c_d = 1.2, M/\lambda_L = 1.2 \times 10^5 H_{inf}, M/\lambda_H = 1.5 \times 10^5 H_{inf}, a_L = e^{i\pi/3}, a_H = i$. Initial values are chosen randomly in the range $0.01H_{inf} \sim 100.0H_{inf}$.

Potential minima in the angular direction change just after the end of inflation because of the change of potential (8), (9). Therefore, scalar fields acquire angular momenta, in other words, number asymmetry at once and some of their values oscillate without damping. The value of number asymmetry per comoving volume is fixed when the rotation around the origin, which is due to mass term or thermal potential[5], starts. Moreover, because the potential for the phase of h_u vanishes rapidly, the value of number asymmetry per comoving volume of h_u is fixed much earlier than other fields. The net value of number asymmetry to entropy ratio is evaluated as

$$\frac{n_{\nu(h_d)}}{s}(t) \simeq \frac{|a_{L(H)}|}{18}\left(\frac{g_*}{g_{*s}}\right)\frac{T_R M}{\lambda M_G^2}\sin(\delta_{eff}^{\nu(h_d)}) \tag{15}$$

for $\nu(h_d)$ (The number asymmetry of ν is the lepton asymmetry), and

$$\frac{n_{h_u}}{s}(t) \simeq \frac{|a_L| + |a_H|}{36\kappa} \left(\frac{g_*}{g_{*s}}\right) \frac{T_R M}{\lambda M_G^2} \sin(\delta_{eff}^{h_u}), \qquad (16)$$

for h_u, where $\delta_{eff}^{\phi_a}$ is the effective phase of oscillation of ϕ_a at the time of number asymmetry fixing. There is no suppression factor $m_{3/2}/H_{osc}$ which is emerged in Ref.5. We see this feature by numerical calculation (Fig. 2).

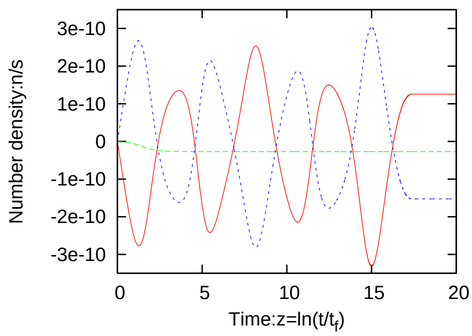

Figure 2: Time evolution of lepton asymmetry and number density of Higgs fields par comoving volume. Horizontal axis is time and vertical axis is lepton number density par comoving volume divided by entropy par comoving volume at the time when reheating is finished. Red solid line is lepton asymmetry, green dashed line is number density of h_u and blue dotted line is that of h_d. The parameters : $c_\nu = c_u = c_d = 1.0$, $H_{inf} = 1.0 \times 10^{13}$[GeV], $M/\lambda_L = 1.0 \times 10^{22}$[GeV] , $M/\lambda_H = 1.5 \times 10^{22}$[GeV] , $a_L = e^{i2\pi/3}$, $a_H = i$, $\kappa = 8$, and reheating temperature T_R is 5.0×10^6[GeV].

5 Conclusion

We have demonstrated two important results about Affleck-Dine leptogenesis via multiple flat directions with non-renormalizable superpotential and vanishing renormalizable F-term. First, when multiple flat directions have negative Hubble induced masses, we can no longer parameterize flat directions in terms of one complex scalar field and multi-dimensional motion of scalar fields must be considered. Moreover, scalar potential has unique minimum except for gauge freedom and phase inversion. Therefore the degree of the mixing of flat directions is determined only by the shape of the potential without ambiguities and initial values of dynamics of post inflationary are deterministic. Thus AD mechanism via multiple flat directions, there remains no pre inflationary information if inflation lasts long enough.

Second, there are CP-violation term even for large H which is due to cross coupling of scalar fields in non-renormalizable F-terms and the Hubble induced A-terms. Although the Hubble induced A-terms decreases rapidly after the end of inflation, they can give the angular momentum scalar fields. Therefore lepton asymmetry is generated just after the end of inflation. In particular, there is no suppression due to thermal effect [3]. Net lepton entropy ratio does not have suppression factor $m_{3/2}/H_{osc}$.

References

[1] I. Affleck and M. Dine, Nucl. Phys. B **249**, 361 (1985).

[2] M. Dine, L. Randall and S. D. Thomas, Nucl. Phys. B **458**, 291 (1996) .

[3] A. Anisimov and M. Dine, Nucl. Phys. B **619**, 729 (2001) .

[4] R. Allahverdi, B. A. Campbell and J. R. Ellis, Nucl. Phys. B **579**, 355 (2000) .

[5] M. Fujii, K. Hamaguchi and T. Yanagida, Phys. Rev. D **63**, 123513 (2001)

[6] V. A. Kuzmin, V. A. Rubakov and M. E. Shaposhnikov, Phys. Lett. B **191**, 171 (1987).

[7] M. Senami and K. Yamamoto, Phys. Rev. D **66**, 035006 (2002) .

[8] K. Enqvist, A. Jokinen and A. Mazumdar, JCAP **0401**, 008 (2004) .

Cosmology of Supersymmetric Axion Models

Kazunori Nakayama [1]

Institute for Cosmic ray Research, University of Tokyo, Kashiwa 277-8582, Japan

Abstract

We derive general cosmological constraints on supersymmetric extension of axion models, in particular paying careful attention to the cosmological effects of saxion. It is found that for every mass range of the saxion from $O(1)$ keV to $O(10)$ TeV, severe constraints on the energy density of the saxion are imposed. Together with constraints from axino, we obtain stringent upper bounds on the reheating temperature.

1 Introduction

Although the standard model in particle physics has achieved great successes, there still remain some theoretical problems. One is the strong CP problem, and another is the gauge hierarchy problem. In other words, these problems indicate the existence of the physics beyond the standard model.

A promising solution to the strong CP problem was proposed in the 1970's by Peccei and Quinn [1]. They introduced an anomalous U(1) symmetry, called PQ symmetry, which is spontaneously broken at some energy scale F_a. From astrophysical and cosmological arguments, F_a is constrained as 10^{10} GeV $\lesssim F_a \lesssim 10^{12}$ GeV. A coherent oscillation of the axion, which is a pseudo-Nambu-Goldstone boson associated with spontaneous breaking of PQ symmetry, can be the cold dark matter of the universe for $F_a \sim 10^{12}$ GeV.

On the other hand, supersymmetry (SUSY) is also well-motivated from particle physics point of view. First, SUSY provides a solution to the gauge hierarchy problem. Due to the symmetry between a scalar and fermion, radiative corrections to the Higgs scalar mass squared are canceled and quadratic divergent quantity disappears. Thus the weak scale becomes stabilized against the radiative correction, which explains why the Higgs mass should be around 100 GeV, as indicated by electroweak precision measurements at LEP. Next, the running of the gauge coupling constants are modified in SUSY, which realizes the gauge coupling unification at the energy scale $\sim 2 \times 10^{16}$ GeV. Thus Grand Unified Theory (GUT) is naturally realized in the framework of SUSY.

Therefore the combination these two paradigms, the SUSY axion model, has many attractive features. However, cosmology of SUSY axion model is highly non-trivial. In SUSY axion model, the axion forms a supermultiplet, which contains a scalar partner called *saxion* and fermionic superpartner, called *axino* [2]. Their interaction is suppressed by the PQ scale, and hence they are long-lived particles (or become stable for the axino). Such a long-lived particle has a potential to affect the cosmological evolution scenario like the gravitino [3]. In the present work, we have studied the cosmology of SUSY axion models, in particular paying careful attention to the effects of the saxion (see Ref. [4] for a detail).

2 Properties of Saxion

The saxion corresponds to a flat direction which does not feel the scalar potential, which is preserved by $U(1)_{\rm PQ}$ symmetry and the holomorphic property of the superpotential in SUSY limit. Thus the saxion obtains a mass only from SUSY breaking effects, and hence the saxion mass (m_s) is naturally expected to be of order of the gravitino mass ($m_{3/2}$). The gravitino mass ranges from $O(1)$ keV to $O(10)$ TeV depending on SUSY breaking models, such as gauge-, gravity- or anomaly-mediated SUSY breaking models. Here we regard the saxion (gravitino) mass as a free parameter within the above range.

Now we turn to the cosmological effects of the saxion. For cosmological arguments, it is important to know the production mechanism and decay modes.

[1] E-mail:nakayama@icrr.u-tokyo.ac.jp

Saxions are produced in the early universe in two ways. One is thermal production, where scattering processes of particles in thermal bath produce saxion. The other is the coherent oscillation. Because the saxion is a scalar field, it has large energy density with an initial amplitude s_i in the form of Bose-Einstein condensate. The former contribution, in terms of the saxion-to-entropy ratio, is given by

$$\left(\frac{\rho_s}{s}\right)^{(\mathrm{TP})} \sim 1.0 \times 10^{-9}\ \mathrm{GeV}\left(\frac{m_s}{1\ \mathrm{GeV}}\right)\left(\frac{T_R}{10^5\ \mathrm{GeV}}\right)\left(\frac{10^{12}\ \mathrm{GeV}}{F_a}\right)^2 \tag{1}$$

for $T_R \lesssim T_D \sim 10^9\mathrm{GeV}\ (F_a/10^{11}\mathrm{GeV})^2$, where T_R denotes the reheating temperature of the universe after inflation. For $T_R \gtrsim T_D$, saxions are thermalized and its abundance is given by $(\rho_s/s)^{(\mathrm{TP})} \sim 1.0 \times 10^{-3}\ \mathrm{GeV}(m_s/1\ \mathrm{GeV})$. The coherent oscillation contribution is estimated as

$$\left(\frac{\rho_s}{s}\right)^{(\mathrm{C})} = \frac{1}{8}T_R\left(\frac{s_i}{M_P}\right)^2 \simeq 2.1 \times 10^{-9}\ \mathrm{GeV}\left(\frac{T_R}{10^5\ \mathrm{GeV}}\right)\left(\frac{F_a}{10^{12}\ \mathrm{GeV}}\right)^2\left(\frac{s_i}{F_a}\right)^2 \tag{2}$$

for $\Gamma_I < m_s$ where Γ_I denotes the decay rate of the inflaton. For $\Gamma_I > m_s$, T_R in the above formula should be replaced with T_{osc}, which is the temperature at which the saxion oscillation begins. Importantly, both contributions are proportional to T_R for wide parameter regions, and hence cosmological constraints on the saxion abundance are rephrased by the upper bound on T_R.

Next let us investigate the saxion decay modes. First, the saxion can decay into two axions ($s \to 2a$). We can estimate the decay rate of the saxion into axions as

$$\Gamma(s \to 2a) \simeq \frac{f^2}{64\pi}\frac{m_s^3}{F_a^2}, \tag{3}$$

where $f = \sum_i q_i^3 v_i^2/F_a^2$ with the VEV of the i-th PQ scalar field v_i and its PQ charge q_i. If $f \sim 1$ as in many cases including the case with only one PQ scalar, this is the dominant decay mode of the saxion [5]. Then the lifetime is given by

$$\tau_s \simeq 1.3 \times 10^2 f^{-2}\ \sec\left(\frac{1\ \mathrm{GeV}}{m_s}\right)^3\left(\frac{F_a}{10^{12}\ \mathrm{GeV}}\right)^2. \tag{4}$$

As for the cosmological arguments, it is important to know whether the main saxion decay mode is into axions ($f \sim 1$) or not ($f \sim 0$), because such a decay mode does not affect BBN or CMB.

On the other hand, the saxion also decays into ordinary particles. For the KSVZ axion model, the saxion decays into two gluons through one-loop process with a decay rate given by

$$\Gamma(s \to 2g) \simeq \frac{\alpha_s^2}{64\pi^3}\frac{m_s^3}{F_a^2}, \tag{5}$$

for $m_s \gtrsim 1$ GeV. The decay rate into two photons is given by

$$\Gamma(s \to 2\gamma) \simeq \frac{\kappa^2\alpha_{\mathrm{EM}}^2}{512\pi^3}\frac{m_s^3}{F_a^2}, \tag{6}$$

where κ is a model dependent constant of $O(1)$.

For the DFSZ axion model, the saxion decays into fermion-anti-fermion pair. The decay rate into down-type quarks d_i $(i = 1, 2, 3)$ is represented as

$$\Gamma(s \to d_i\bar{d}_i) = \frac{3}{8\pi}\left(\frac{2x}{x + x^{-1}}\right)^2 m_s\left(\frac{m_{di}}{F_a}\right)^2\left(1 - \frac{4m_{di}^2}{m_s^2}\right)^{3/2}, \tag{7}$$

where $x = \tan\beta = \langle H_u\rangle/\langle H_d\rangle$. Decay rate into up-type quarks u_i $(i = 1, 2, 3)$ is similar,

$$\Gamma(s \to u_i\bar{u}_i) = \frac{3}{8\pi}\left(\frac{2x^{-1}}{x + x^{-1}}\right)^2 m_s\left(\frac{m_{ui}}{F_a}\right)^2\left(1 - \frac{4m_{ui}^2}{m_s^2}\right)^{3/2}. \tag{8}$$

Although those decay modes into ordinary particles may be sub-dominant if $f \sim 1$, only such a small fraction of the saxion decay may significantly affect cosmology, as we will see in the next section.

3 Cosmological Constraints

Now we briefly summarize various cosmological constraints on the saxion abundance.

Effective number of neutrinos : Decay products of the saxion increase the radiation energy density of the universe. Such extra radiation contributions accelerate the Hubble expansion and changes the predictions of BBN, CMB anisotropy and structure formation etc. In terms of the effective number of neutrino species, $\Delta N_\nu \lesssim 1$ must hold. Note that this constraint is relevant for the decay mode $s \to 2a$ [6], even if $\tau_s \ll 1$ sec.

Big-Bang nucleosynthesis : Decay produced photons or hadrons may significantly affect BBN for $\tau_s \gtrsim 10^{-2}$ sec [7]. For 10^{-2} sec $\lesssim \tau_s \lesssim 10^2$ sec, the main effect is $p \leftrightarrow n$ conversion due to injected pions, which results in ^{4}He overproduction. For later injection, the main effect is photo (hadro)-dissociation of light elements, for radiative (hadronic) decay modes.

Cosmic microwave background : For $\tau_s \gtrsim 10^6$ sec, injected radiations can not reach chemical equilibrium because double-Compton scattering processes are ineffective. Then the extra radiations distort the blackbody spectrum of CMB. The distortion is characterized by a chemical potential μ or Compton-y parameter, which is constrained by the COBE FIRAS measurement [8].

Diffuse X(γ)-ray background : For $\tau_s \gtrsim 10^{13}$ sec, the decay produced photons contribute to diffuse X(γ)-ray background [9]. But such a contributions are constrained from the observations of ASCA, HEAO1, COMPTEL, EGRET. This gives a stringent bound on the saxion abundance.

Reionization : For $\tau_s \gtrsim 10^{13}$ sec, depending on the photon energy and decay epoch, the decay-produced photon may escape the "transparency window", where photons can freely propagate the universe without interacting with intergalactic medium (IGM) [10]. If this is the case, decay-produced photons ionize the IGM and change the reionization history of the universe which results in too large optical depth to the last scattering surface to be consistent with the WMAP three year observaton.

Present matter density limit : If the saxion lifetime exceeds the present age of the universe, the energy density of the saxion itself contributes to the total matter density of the universe, $\Omega_m h^2$.

LSP overproduction : If the saxion is heavy enough to decay into SUSY particles, the non-thermally produced LSPs emitted by the saxion decay must not be overproduced [11]. Otherwise the LSPs give too large contribution to the matter density of the universe. Here we assume for $m_s \gtrsim 1$ TeV, such decay modes are open, and also the annihilation cross section of the LSP is small so that they do not annihilate with each other after the non-thermal production.

Gravitino and Axino overproduction : As is well known, gravitinos are produced through scattering of particles in thermal bath. The resulting abundance is proportional to the reheating temperature T_R [12]. For $m_{3/2} \lesssim 100$ GeV, the gravitino is stable and it contributes to the matter density of the universe. Similarly, axinos are also produced efficiently. Its abundance is also proportional to T_R [13]. (Here we assume the axino mass $m_{\tilde{a}}$ is equal to the gravitino mass.) Thus both set the upper bound on T_R.

In Fig. 1 we summarize the upper bound on the reheating temperature including all the above mentioned constraints. Four panels correspond to different models. Upper left : KSVZ with $f = 1$, upper right : KSVZ with $f = 0$, lower left : DFSZ with $f = 1$, lower right : DFSZ with $f = 0$. We can see that for almost all the saxion mass, the reheating temperature is severely constrained.

4 Summary

In this work, we have derived general cosmological constraints on SUSY axion models. It is found that the reheating temperature is severely constrained, compared with the bound from usual gravitino problem.

This has some implications on SUSY axion models. Because the reheating temperature is severely constrained, it is rather difficult to produce the correct amount of baryon asymmetry. In particular, thermal leptogenesis using right-handed neutrinos suffers from the low-reheating temperature. One possibility to generate baryon asymmetry is using Affleck-Dine mechanism. In fact, it can create a correct amount of baryon asymmetry even for such a low-reheating temperature [14]. Also, the present dark matter can be accounted for by the axion condensate or the axino. For an unstable axino, the neutralino LSP produced either thermally or non-thermally may also be the dark matter candidate.

As a final remark, the axion induces an isocurvature fluctuation with an amplitude proportional to the inflation scale. Hence a low-scale inflation model such as new inflation should be assumed [15].

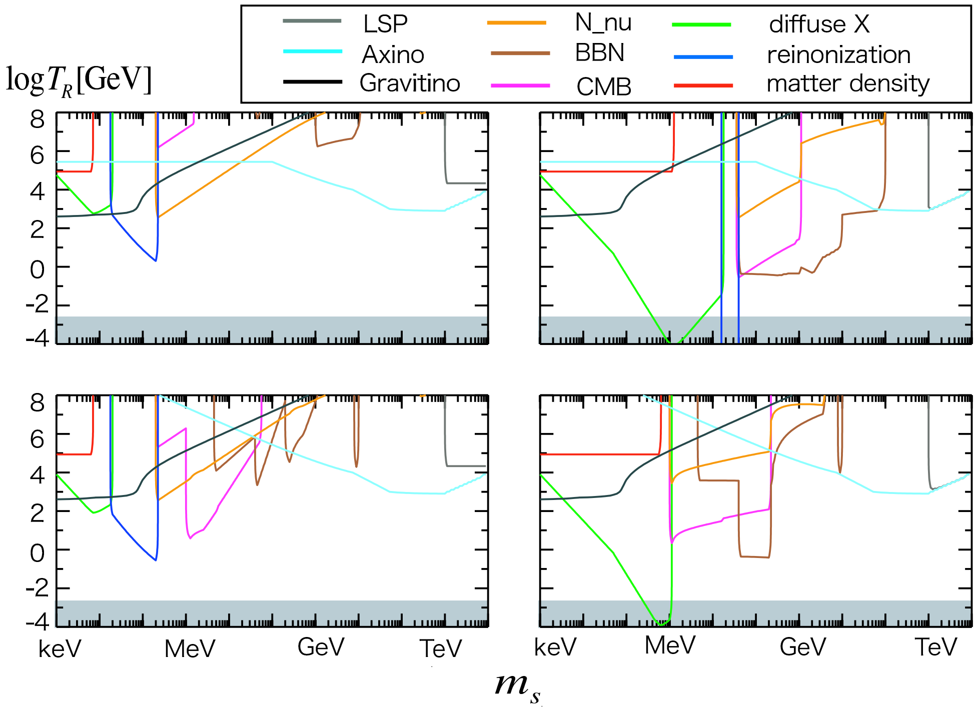

Figure 1: Upper bounds on the reheating temperature T_R for each model with $F_a = 10^{12}$ GeV [4]. The initial amplitude of the saxion is assumed to be $s_i \sim F_a$.

References

[1] R. D. Peccei and H. R. Quinn, Phys. Rev. Lett. **38**, 1440 (1977).

[2] K. Rajagopal, M. S. Turner and F. Wilczek, Nucl. Phys. B **358**, 447 (1991).

[3] M. Hashimoto, K. I. Izawa, M. Yamaguchi and T. Yanagida, Phys. Lett. B **437**, 44 (1998); T. Asaka and M. Yamaguchi, Phys. Rev. D **59**, 125003 (1999).

[4] M. Kawasaki, K. Nakayama and M. Senami, arXiv:0711.3083 [hep-ph].

[5] E. J. Chun and A. Lukas, Phys. Lett. B **357**, 43 (1995).

[6] K. Ichikawa, M. Kawasaki, K. Nakayama, M. Senami and F. Takahashi, JCAP **0705**, 008 (2007).

[7] M. Kawasaki, K. Kohri and T. Moroi, Phys. Lett. B **625**, 7 (2005); Phys. Rev. D **71**, 083502 (2005).

[8] D. J. Fixsen *et al.*, Astrophys. J. **473**, 576 (1996).

[9] M. Kawasaki and T. Yanagida, Phys. Lett. B **399**, 45 (1997).

[10] X. L. Chen and M. Kamionkowski, Phys. Rev. D **70**, 043502 (2004).

[11] M. Endo and F. Takahashi, Phys. Rev. D **74**, 063502 (2006).

[12] M. Bolz, A. Brandenburg and W. Buchmuller, Nucl. Phys. B **606**, 518 (2001).

[13] L. Covi, H. B. Kim, J. E. Kim and L. Roszkowski, JHEP **0105**, 033 (2001); A. Brandenburg and F. D. Steffen, JCAP **0408**, 008 (2004).

[14] M. Kawasaki and K. Nakayama, Phys. Rev. D **76**, 043502 (2007).

[15] For a recent analysis, see M. Kawasaki and T. Sekiguchi, arXiv:0705.2853 [astro-ph].

Non-Gaussianities from ekpyrotic collapse with multiple fields

Shuntaro Mizuno[1], Kazuya Koyama[2], Filippo Vernizzi[3] and David Wands[4]

[1]*Research Center for the Early Universe (RESCEU), School of Science, University of Tokyo, 7-3-1 Hongo, Bunkyo, Tokyo 113-0033, Japan*

[2,4] *Institute of Cosmology and Gravitation, Mercantile House, University of Portsmouth, Portsmouth PO1 2EG, United Kingdom*

[3] *Abdus Salam ICTP, Strada Costiera 11, 34100 Trieste, Italy*

Abstract

We compute the non-Gaussianity of the curvature perturbation generated by ekpyrotic collapse with multiple fields. The transition from the multi-field scaling solution to a single-field dominated regime converts initial isocurvature field perturbations to an almost scale-invariant comoving curvature perturbation. In the specific model of two fields, ϕ_1 and ϕ_2, with exponential potentials, $-V_i \exp(-c_i\phi_i)$, we calculate the bispectrum of the resulting curvature perturbation. We find that the non-Gaussianity is dominated by non-linear evolution on super-Hubble scales and hence is of the local form. The non-linear parameter of the curvature perturbation is given by $f_{NL} = 5c_j^2/12$, where c_j is the exponent of the potential for the field which becomes sub-dominant at late times.

1 Introduction

Recently, there has been progress in generating a scale-invariant spectrum for curvature perturbations in the ekpyrotic scenario with more than one field, which we will refer to as the new ekpyrotic scenario [1, 2, 3]. If these fields have steep negative exponential potentials, there exists a scaling solution where the energy densities of the fields grow at the same rate during the collapse. In this multi-field scaling solution background, the isocurvature field perturbations have an almost scale-invariant spectrum, owing to a tachyonic instability in the isocurvature field.

The multi-field scaling solution in the new ekpyrotic scenario can be shown to be an unstable saddle point in the phase space and the late-time attractor is the old ekpyrotic collapse dominated by a single field [4]. But the transition from the multi-field scaling solution to the single-field-dominated solution also provides a mechanism to automatically convert the initial isocurvature field perturbations about the multi-field scaling solution into comoving curvature perturbations about the late-time attractor [5].

On the other hand, the non-Gaussianity of the distribution of primordial curvature perturbations in the inflationary scenario has been extensively studied by many authors (see e.g. [6] for a review). Thus, as a natural extension of the study performed in [4, 5], in this paper [7] we compute the non-Gaussianity of the primordial curvature perturbations generated from the contracting phase of the multi-field new ekpyrotic cosmology.

2 Model and Homogeneous dynamics

We first review the model and the background dynamics of the new ekpyrotic cosmology with multiple scalar fields. During the ekpyrotic collapse the contraction of the universe is assumed to be described by a 4D Friedmann equation in the Einstein frame with n scalar fields with negative exponential potentials

$$3H^2 = V + \sum_j^n \frac{1}{2}\dot{\phi}_j^2 \,, \quad \text{where} \quad V = -\sum_j^n V_j e^{-c_j\phi_j} \,, \tag{1}$$

[1]E-mail:mizuno@resceu.s.u-tokyo.ac.jp
[2]E-mail:Kazuya.Koyama@port.ac.uk
[3]E-mail: vernizzi@ictp.it
[4]E-mail:David.Wands@port.ac.uk

and we take $V_i > 0$ and set $8\pi G$ equal to unity. From now on, for simplicity, we concentrate our attention on the case of two fields. In this case, it will be easier to work in terms of new variables,

$$\varphi = \frac{c_2\phi_1 + c_1\phi_2}{\sqrt{c_1^2 + c_2^2}}\,, \quad \chi = \frac{c_1\phi_1 - c_2\phi_2}{\sqrt{c_1^2 + c_2^2}}\,. \tag{2}$$

The potential can then be simply re-written as

$$V = -U(\chi)\, e^{-c\varphi}\,, \quad \text{with} \quad U(\chi) = V_1\, e^{-(c_1/c_2)c\chi} + V_2\, e^{(c_2/c_1)c\chi}\,, \quad \frac{1}{c^2} \equiv \sum_j \frac{1}{c_j^2}\,. \tag{3}$$

It can be shown that $U(\chi)$ has a minimum at $\chi = \chi_0$ and the multi-field scaling solution corresponds to the classical solution along this minimum $\chi = \chi_0$, while φ is rolling down the exponential potential. It is worth noting that the potential for χ has a negative mass-squared $m_\chi^2 \equiv \partial^2 V/\partial\chi^2 = c^2 V < 0$ around $\chi = \chi_0$ which makes the multi-field scaling solution unstable. Furthermore, the χ field evolution is nonlinear, with the cubic interaction being given by

$$V^{(3)} \equiv \frac{\partial^3 V}{\partial \chi^3} = \tilde{c} m_\chi^2\,, \quad \text{where} \quad \tilde{c} \equiv \frac{c_2^2 - c_1^2}{\sqrt{c_1^2 + c_2^2}}\,, \tag{4}$$

which becomes important when we consider the non-Gaussianity later in this paper. Another important solution is the single-field dominated scaling solution which is also appeared in the old ekpyrotic scenario. In this paper, we consider the case in which the background evolves from the multi-field scaling solution to the ϕ_2-dominated scaling solution without loss of generality.

3 Statistical correlators and δN-formalism

In the two-field new ekpyrotic cosmology, the isocurvature fluctuations acquired by the field χ during the multi-field scaling regime, play a crucial role to generate a scale-invariant spectrum of perturbations. On the other hand, the fluctuations of the field φ are negligible on large scales, because of its very blue spectral tilt. Thus, in the following we neglect $\delta\varphi$ fluctuations. To relate the non-Gaussianity of the scalar field fluctuations to observations, we need to calculate the three-point functions of the comoving curvature perturbation ζ. In order to do that, we can use the δN-formalism [8, 9]. In the δN-formalism, the comoving curvature perturbation ζ evaluated at some time $t = t_f$ coincides with the perturbed expansion integrated from an initial *flat* hypersurface at $t = t_i$, to a final *uniform density* hypersurface at $t = t_f$, with respect to the background expansion, i.e.,

$$\zeta(t_f, \mathbf{x}) \simeq \delta N(t_f, t_i, \mathbf{x}) \equiv N(t_f, t_i, \mathbf{x}) - N(t_f, t_i)\,, \tag{5}$$

with

$$N(t_f, t_i, \mathbf{x}) \equiv \int_{t_i}^{t_f} \mathcal{H}(\mathbf{x}, t)dt\,, \quad N(t_f, t_i) \equiv \int_{t_i}^{t_f} H(t)dt\,, \tag{6}$$

where $\mathcal{H}(\mathbf{x}, t)$ is the inhomogeneous Hubble expansion. We will choose the initial time t_i to be *during* the multi-field scaling regime. Furthermore, since φ is unperturbed, δN can be expanded in series of the initial field fluctuations $\delta\chi_i$. Retaining only terms up to second order, we obtain

$$\delta N = N_{,\chi_i}\delta\chi_i + \frac{1}{2} N_{,\chi_i\chi_i}(\delta\chi_i)^2\,, \tag{7}$$

where $N_{,\chi}$ denotes the derivative of N with respect to χ.

The bispectrum of the curvature perturbation ζ, which includes the first signal of non-Gaussianity, is defined as

$$\langle \zeta_{\mathbf{k}_1}\zeta_{\mathbf{k}_2}\zeta_{\mathbf{k}_3}\rangle \equiv (2\pi)^3 \delta^{(3)}(\sum_j \mathbf{k}_j) B_\zeta(k_1, k_2, k_3)\,, \tag{8}$$

where the left hand side of Eq. (8) can be evaluated by the δN-formalism using Wick's theorem,

$$\langle \zeta_{\mathbf{k}_1}\zeta_{\mathbf{k}_2}\zeta_{\mathbf{k}_3}\rangle = N_{,\chi_i}^3 \langle \delta\chi_{i\mathbf{k}_1}\delta\chi_{i\mathbf{k}_2}\delta\chi_{i\mathbf{k}_3}\rangle + \frac{1}{2} N_{,\chi_i}^2 N_{,\chi_i\chi_i} \langle \delta\chi_{i\mathbf{k}_1}\delta\chi_{i\mathbf{k}_2}(\delta\chi_i \star \delta\chi_i)_{\mathbf{k}_3}\rangle + \text{perms}\,. \tag{9}$$

In the above equation, a star $\star$ denotes the convolution and we have neglected correlators higher than the four-point.

Observational limits on the non-Gaussianity of the primordial curvature perturbations are usually given on the nonlinear parameter f_{NL} defined by

$$\frac{6}{5}f_{NL} \equiv \frac{\prod_j k_j^3}{\sum_j k_j^3}\frac{B_\zeta}{4\pi^4\mathcal{P}_\zeta^2}\,, \tag{10}$$

where $\mathcal{P}_\zeta$ is the power spectrum of the curvature perturbation ζ. If the non-Gaussianity is local, one can write ζ as

$$\delta N = \zeta_L + \frac{3}{5}f_{NL}\zeta_L^2\,, \tag{11}$$

where ζ_L is a Gaussian variable.

4 Non-Gaussianities

We consider the situation in which χ_i is perturbed on the $t = t_i$ hypersurface, while H_i assumes on this hypersurface a constant value. This is justified by the fact that the $t = t_i$ hypersurface is flat and since χ is an isocurvature field its fluctuations do not affect the local Hubble expansion. Furthermore, we assume that the transition into the single-field-dominated scaling solution at the time $t = t_T$, happens *instantaneously* on the hypersurface $\chi = \chi_T =$ const., where H_T is perturbed.

Under these assumptions, the expansion N defined by Eq. (6) can be split into

$$N = \int_{t_i}^{t_T} H dt + \int_{t_T}^{t_f} H dt\,, \tag{12}$$

where t_f is set sufficiently later than the transition time t_T. In Eq. (12), the first integral is over the multi-field scaling evolution and the last integral is over the ϕ_2-dominated phase.

The first term on the right hand side of Eq. (12) can be expressed as $-(1/\epsilon)\ln(H_i/H_T)$, where $\epsilon = c^2/2$, while the second term becomes $-(1/\epsilon_2)\ln(H_T/H_f)$, where $\epsilon_2 = c_2^2/2$. Then, for a fixed t_i and t_f, the expansion N can be expressed as

$$N = \frac{2}{c_1^2}\ln|H_T| + \text{const.}, \tag{13}$$

which depends only on the parameter c_1, besides the transition time t_T.

During the multi-field scaling regime, the linear evolution equation of χ on large scales is given by

$$\ddot{\chi} + 3H\dot{\chi} + m_\chi^2\chi = 0\,. \tag{14}$$

Including the cubic self-interaction $V^{(3)}$ given in Eq. (4), the large scale evolution equation for χ in the multi-field scaling regime becomes

$$\ddot{\chi} + 3H\dot{\chi} + m_\chi^2\chi = -\frac{1}{2}\tilde{c}m_\chi^2\chi^2. \tag{15}$$

The above evolution equation can be solved perturbatively. Given the solution to the linear equation (14), i.e., $\chi_L \propto H$, the growing-mode solution for χ is

$$\chi = \chi_L + \frac{1}{4}\tilde{c}\chi_L^2 = \alpha H + \frac{1}{4}\tilde{c}\alpha^2H^2\,, \tag{16}$$

where α is a constant parameter whose value distinguishes the different trajectories and shown to be close to Gaussian. Then, the simplest way to compute f_{NL} is to calculate the δN corresponding to the fluctuation $\delta\alpha$, i.e.,

$$\delta N = N_{,\alpha}\delta\alpha + \frac{1}{2}N_{,\alpha\alpha}(\delta\alpha)^2\,. \tag{17}$$

In order to compute $N_{,\alpha}$ and $N_{,\alpha\alpha}$ we want to use Eq. (13), and for this we need to know how H_T varies as a function of α at the transition from multi-field scaling to single-field ϕ_2-dominated scaling solution. Inverting Eq. (16) (to leading order in $\tilde{c}\chi$) gives

$$\alpha = \frac{\chi}{H}\left(1 - \frac{1}{4}\tilde{c}\chi\right) . \tag{18}$$

Assuming as in the linear case that the transition corresponds to a critical value of the tachyon field $\chi = \chi_T$, on the transition surface (constant χ_T) we have from (18) that $\alpha \propto H_T^{-1}$ and hence we find

$$\delta N = -\frac{2}{c_1^2}\frac{\delta\alpha}{\alpha} + \frac{1}{c_1^2}\left(\frac{\delta\alpha}{\alpha}\right)^2 , \tag{19}$$

which means

$$N_{,\alpha} = -\frac{2}{c_1^2}\frac{1}{\alpha}, \qquad N_{,\alpha\alpha} = \frac{2}{c_1^2}\frac{1}{\alpha^2} . \tag{20}$$

Taking $\delta\alpha$ to be a Gaussian random variable and comparing with Eq. (11) with $\zeta_L = -2\delta\alpha/(c_1^2\alpha)$ we obtain the nonlinear parameter for the curvature perturbation after the transition:

$$f_{NL} = \frac{5}{6}\frac{N_{,\alpha\alpha}}{N_{,\alpha}^2} = \frac{5}{12}c_1^2 . \tag{21}$$

5 Conclusion

In this paper we have studied the nonlinear evolution of perturbations in the multi-field new ekpyrotic cosmology. We have studied the simplest model based on two fields with exponential potentials and considered the specific scenario in which the nearly scale-invariant comoving curvature perturbation is generated by the transition from the multi-field scaling solution to the single-field dominated attractor solution. We have applied the δN-formalism, which is widely adopted to study the non-linearity of the primordial curvature perturbation. We find that after the transition to the single-field attractor solution the non-Gaussian parameter $f_{NL} = 5c_1^2/12$, where $-V_1 \exp(-c_1\phi_1)$ is the potential of the field ϕ_1 which becomes subdominant at late time. Since the non-Gaussianity is mainly generated by the nonlinear super-Hubble evolution, it is of the local form, and the nonlinear parameter is k independent. Since c_1^2 must be large, in order to generate an almost scale invariant spectrum, the non-Gaussianity is inevitably large. Thus, the model is strongly constrained by observational bounds on the spectral index and non-Gaussianity.

References

[1] J. L. Lehners, P. McFadden, N. Turok and P. J. Steinhardt, Phys. Rev. D **76**, 103501 (2007).

[2] E. I. Buchbinder, J. Khoury and B. A. Ovrut, arXiv:hep-th/0702154.

[3] P. Creminelli and L. Senatore, arXiv:hep-th/0702165.

[4] K. Koyama and D. Wands, JCAP **0704**, 008 (2007).

[5] K. Koyama, S. Mizuno and D. Wands, Class. Quant. Grav. **24**, 3919 (2007).

[6] N. Bartolo, E. Komatsu, S. Matarrese and A. Riotto, Phys. Rept. **402**, 103 (2004).

[7] K. Koyama, S. Mizuno, F. Vernizzi and D. Wands, JCAP **0711**, 024 (2007).

[8] A. A. Starobinsky, JETP Lett. **42**, 152 (1985) [Pisma Zh. Eksp. Teor. Fiz. **42**, 124 (1985)].

[9] M. Sasaki and E. D. Stewart, Prog. Theor. Phys. **95**, 71 (1996).

Constraints on brane inflation from WMAP3

Larissa Lorenz[1]

[1] *Institut d'Astrophysique de Paris, UMR 7095-CNRS, Université Pierre et Marie Curie, 98bis boulevard Arago, 75014 Paris, France*

Abstract

Considerable and ongoing effort is made to identify promising scalar field candidates in string theory to drive a cosmological period of inflation. At stake is the possibility that fundamental string parameters could be encoded in observables such as the CMB perturbation spectrum. In this contribution, we hold a concrete model of string inflation (KKLMMT) up against WMAP3 and discuss the constraints obtained.

1 Introduction

In recent years, the hope of embedding cosmological inflation into superstring theory has been put on more solid grounds. While they remain challenging, issues such as moduli stabilization are better understood, and scenarios for both open and closed string mode inflatons have been constructed. With its tight relation to observables of current and future CMB experiments, inflation could provide the decisive missing link between string theory and observation. We investigate if the WMAP3 data provides constraints on the parameters of one particular (open string) scenario, known as the KKLMMT model of brane inflation [1]. To this end, we identify its cosmological parameters and how they relate to the underlying string geometry, followed by a comparison to the WMAP3 data using numerical integration of the perturbations and MCMC methods [2] (see also [3]).

2 Setting the stage in string theory

The KKLMMT inflaton field $\phi = \sqrt{T_3}r$ corresponds to the distance r between a D3 and an anti-D3 brane in a 10d supergravity background. T_3 denotes the brane tension, $T_3 = 1/[(2\pi)^3 g_s \alpha'^2]$, with string coupling g_s and $\alpha' = l_s^2$ the string length squared. To understand the dynamics of ϕ and calculate its potential, one has to start from the 10d action of type IIB superstring theory and find solutions for the metric and all n-forms. A supergravity metric ansatz reads $\mathrm{d}s^2 = h^{-1/2}(r) g_{\mu\nu} \mathrm{d}x^\mu \mathrm{d}x^\nu + h^{1/2}(r)\mathrm{d}s_6^2$, i.e. a 4d extended space-time (along the worldvolume of the branes) and six compactified dimensions. The function $h(r)$ is called the warp factor. For the 6d section, the choice of interest (in view of the desired cosmological outcome) is $\mathrm{d}s_6^2 = \mathrm{d}r^2 + r^2 \mathrm{d}s_{T_{1,1}}^2$, with $\mathrm{d}s_{T_{1,1}}^2$ the conifold metric [4]. To enforce "warping" on $T_{1,1}$, non-vanishing background fluxes (which are characterized by an integer number $\mathcal{N}$ [5]) are given to certain n-forms. This geometry is called the Klebanov-Strassler (KS) throat, defined by the throat's bottom r_0, edge r_{UV} (where it is glued into the rest of the 6d manifold), and a dimensionless parameter v, measuring the relative size of the 5d conifold base. The KS throat is a an explicit example[2], but one may consider generic "warped throats" which appear in many flux compactifactions.

The (heavy) anti-D3 brane is embedded at r_0 within this deformed background; its presence adds a small warp factor perturbation $\delta h(r, r_0)$. The (light) D3 brane probes the resulting geometry: Inserted at $r_1 \gg r_0$ (far from the bottom, but below the edge r_{UV}), it experiences gravity and Ramond-Ramond interactions with the anti-D3 through closed string modes. The radial inter-brane distance $r = r_1 - r_0$ is interpreted as the inflation field ϕ (up to normalisation), and its potential $V(\phi)$ is calculated from the Coulomb-like force in the limit $r \gg l_s$ [1]. Inflation proceeds while the D3 approaches the anti-D3, hence ϕ decreases. At a critical ϕ_{strg}, when the branes' proper distance equals l_s, a tachyon (the lightest open string mode) appears, and $V(\phi)$ calculated from closed mode exchange is no longer valid. The two branes then annihilate in a complex process followed by the reheating era.

[1] lorenz@iap.fr

[2] where notably v is fixed at $v = 16/27$

The resulting effective four-dimensional action for the inflaton field ϕ in this model reads

$$S=-\frac{1}{2\kappa}\int R\sqrt{-g}\,\mathrm{d}^4x-\int\left[T(\phi)\sqrt{1+\frac{1}{T(\phi)}g^{\mu\nu}\partial_\mu\phi\partial_\nu\phi}+T(\phi)\right]\sqrt{-g}\,\mathrm{d}^4x, \qquad (1)$$

where $\kappa\equiv 8\pi/m_{\mathrm{Pl}}^2$, and $T(\phi)=T_3/\tilde{h}(\phi)$ is the position-dependent brane tension. $\tilde{h}(\phi)$ includes the anti-D3's perturbation and follows from the 10d Einstein equations. $T(\phi)$ represents an upper bound on the field's velocity; while $\dot{\phi}^2\ll T(\phi)$, one may expand the squareroot to obtain an action with standard kinetic term. The true field dynamics, however, are given by the stringy DBI expression in (1). A tool to quantify the DBI impact is the "Lorentz factor" $\gamma(\phi,\dot{\phi})=[1-\dot{\phi}^2/T(\phi)]^{-1/2}$, with $\gamma\approx 1$ in the standard phase, and $\gamma\gg 1$ when the stringy kinetic term is crucial [6]. In the expansion of (1), it is easy to identify the potential (using the explicit form of $\tilde{h}(\phi)$, see [1]):

$$V(\phi)=2T(\phi)=\frac{M^4}{1+(\mu/\phi)^4}\simeq M^4\left[1-\left(\frac{\mu}{\phi}\right)^4\right] \qquad (2)$$

The last expression is obtained for $\phi\gg\mu$. This potential is characterized by the overall scale of inflation M, and the relative scale μ for ϕ. Hence, together with ϕ_{UV} (below which the evolution must start) and ϕ_{strg} (where brane annihilation sets in), they give a set of four parameters. On the microscopic level, however, $(M,\mu,\phi_{\mathrm{UV}},\phi_{\mathrm{strg}})$ derive from the stringy quantities $(g_{\mathrm{s}},\alpha',M,v,\mathcal{N})$[3].

3 The standard inflation viewpoint and stringy aspects

Starting at some initial value $\mu\ll\phi_{\mathrm{in}}<\phi_{\mathrm{UV}}$, the inflaton moves across a period of standard inflation on the very flat potential (2). The slow-roll approximation can be used until the field reaches ϕ_ϵ; in usual inflation, this means the end of accelerated expansion[4]. There are, however, new stringy ingredients in the picture of (1): The kinetic term of ϕ is DBI, and hence Friedmann and Klein-Gordon equations are different from standard (though they reduce to the usual ones for $\gamma\approx 1$). In particular, inflation may continue after ϕ_ϵ, the inflaton eventually reaching (from a certain ϕ_{DBI} onwards) an ultrarelativistic regime where $\gamma\gg 1$. An analytical solution in the DBI dominated regime exists [2], which, however, is not inflating. This leaves the question if a significant amount of inflation is produced in the transitory regime $\phi_{\mathrm{DBI}}<\phi<\phi_\epsilon$, which would affect the matching of today's scales to those during inflation. Access to this regime is through numerics only, and ϕ_ϵ and ϕ_{DBI} are in fact of the same order, the number of e-folds produced inbetween typically being $\mathcal{O}(1)$. Hence, in the pure KKLMMT scenario, DBI dynamics do not significantly prolong inflation.

The second important point concerns the end of inflation: We do not forcibly have $\phi_{\mathrm{end}}=\phi_\epsilon$, since inflation really ends at ϕ_{strg}, the onset of mutual brane annihilation. ϕ_{strg} is calculated from the background parameters[5] $(g_{\mathrm{s}},M,v,\mathcal{N})$. Since ϕ_ϵ is known analytically, too, it is possible to express their ratio $\phi_\epsilon/\phi_{\mathrm{strg}}=f(g_{\mathrm{s}},M,v,\mathcal{N})$, i.e. as a function of background parameters. ϕ_{strg} could therefore lie "on either side" of ϕ_ϵ, meaning that in some cases $\phi_{\mathrm{end}}=\phi_{\mathrm{strg}}$ while slow-roll still holds. Since $f(g_{\mathrm{s}},M,v,\mathcal{N})$ depends on the scale M, fixed from normalization to COBE (which, in turn, needs a ϕ_{end} as an input), only the contour $\phi_\epsilon/\phi_{\mathrm{strg}}=1$ (at fixed g_{s}) can be traced unambiguously[6] in the parameter plane $(\ln v,\ln\mathcal{N})$, see figure 1. Depending on the choice of g_{s}, some $(\ln v,\ln\mathcal{N})$ belong to the region where $\phi_{\mathrm{end}}=\phi_{\mathrm{strg}}$, or where $\phi_{\mathrm{end}}=\phi_\epsilon$. There exists, however, a rescaling of $(\mathcal{N},v,g_{\mathrm{s}})$, illustrated by the lower panel in figure 1, that allows to remove the g_{s} dependence. In the rescaled parameter space $(\ln x,\ln\bar{v})$, the contour $\phi_\epsilon/\phi_{\mathrm{strg}}=1$ is unique.

We now turn to intrinsic parameter restrictions. First, consistency requires that the volume of the KS throat must not exceed the *total* volume V_6^{total} of the 6d compactification [7]. Since V_6^{total} enters into the calculation of the 4d Planck mass, this constraint can be re-written as a condition relating m_{Pl} to $(\mathcal{N},v,g_{\mathrm{s}},\alpha')$. This condition is a straight line with universal slope and α'-dependent offset, cutting

[3]where $\mu^4=\phi_0^4/\mathcal{N}$, $M^4=4\pi^2v\phi_0^4/\mathcal{N}$

[4]More precisely, we can distinguish $\phi_{\epsilon_1},\phi_{\epsilon_2}$ (the end of inflation vs. the end of slow-roll), where we find $\phi_{\epsilon_2}>\phi_{\epsilon_1}$.

[5]Note that the dependence on α' cancels out.

[6]COBE normalization is possible analytically when $\phi_{\mathrm{end}}=\phi_\epsilon$, see [2].

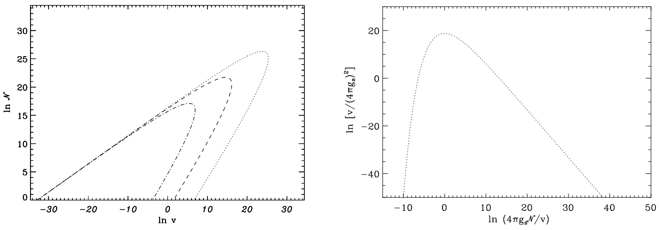

Figure 1: Upper panel: $\phi_\epsilon = \phi_{\rm strg}$ in the plane $(\ln \mathcal{N},\ \ln v)$, using COBE normalization with $N_* = 50$. The dotted line corresponds to $g_{\rm s} = 0.1$, dashed to 10^{-3} and dotted-dashed to 10^{-5}. The area enclosed is the region where $\phi_\epsilon > \phi_{\rm strg}$. The $g_{\rm s}$-dependence can be absorbed by rescaling the parameters. Lower panel: $\phi_\epsilon = \phi_{\rm strg}$ (universal for all values of $g_{\rm s}$) in the plane $(\ln x,\ \ln \bar{v})$, where $x = 4\pi g_{\rm s}\mathcal{N}/v$ and $\bar{v} = v/(4\pi g_{\rm s})^2$.

through the $(\ln x, \ln \bar{v})$ plane[7]. Second, we focus on the case where inflation takes place in one throat: We require $\phi_{\rm in} < \phi_{\rm UV}$, and the throat has to be "long enough" to accommodate ~ 60 e-folds of inflation. In the region where $\phi_{\rm end} = \phi_\epsilon$, this condition is another straight line, again with universal slope but an α'-dependent offset. Where $\phi_{\rm end} = \phi_{\rm strg}$, the shape of this condition has to be found numerically.

4 MCMC results

The KKLMMT model has four "cosmological" parameters $(M, \mu, \phi_{\rm strg}, \phi_{\rm UV})$, to which we add the dimensionless parameter R for the reheating era[8]. The most suitable set for MCMC sampling, however, is $[\log\left(10^{10}\mathcal{P}_*\right), \log(\sqrt{\kappa}\mu), \log(\sqrt{\kappa}\phi_{\rm UV}), \log(\phi_{\rm strg}/\mu), \ln R]$, where $\mathcal{P}_*$ is the amplitude of the scalar primordial spectrum at a given observable wavenumber k_*. Therefore, one has to implement the above restrictions as priors for these quantities. The numerics impose a lower limit of $\sqrt{\kappa}\mu > 10^{-3}$. For a detailed discussion of all priors, see [2].

We now briefly present the results of our MCMC comparison. First, one can show that the KKLMMT model reproduces ΛCDM parameters such as e.g. $\Omega_{\rm b}, \Omega_{\rm dm}, H_0$, as well as the correct perturbation amplitude and spectral indices. Second, figure 2 shows the mean likelihoods (ML) and marginalized probability distributions (MPD) for the sampled primordial parameters $[\log(\sqrt{\kappa}\mu), \log(\sqrt{\kappa}\phi_{\rm UV}), \log(\phi_{\rm strg}/\mu), \ln R]$. An interesting feature of the panels for $\log(\sqrt{\kappa}\mu), \log(\sqrt{\kappa}\phi_{\rm UV})$ is the *difference* between ML and MPD: The ML's are uniform because in the explored prior range, these parameters do not improve the fit to the data, while the drop in the MPD's shows that $\log(\sqrt{\kappa}\mu) < 1.1$ at 95% confidence level (CL). These shapes are explained by volume effects in the multi-dimensional parameter space due to strong correlations. $\log(\phi_{\rm strg}/\mu)$ and $\ln R$, on the other hand, are directly constrained by the data: $\log(\phi_{\rm strg}/\mu) < 1.4$ and $\ln R > -38$ at 95% CL. Third, we can derive the corresponding distributions of the remaining parameters: $\log(\sqrt{\kappa}M)$ and $\mathcal{P}_*$ are directly related, as is $\log(4\pi^2 v)$ to μ and M (see figure 2). In addition, the 2d probability distribution obtained without marginalising over $\log(\sqrt{\kappa}\mu)$ is shown, illustrating the strong correlations. In particular, the numerically motivated lower prior $\sqrt{\kappa}\mu > 10^{-3}$ directly translates into an upper (lower) limit for $\log(4\pi^2 v)$ $[\log(\sqrt{\kappa}M)]$. The respective other end of these distributions, however, is "physical" and gives the 95% CL constraints $\log(\sqrt{\kappa}M) < -2.9$ and $\log(4\pi^2 v) > -8.5$.

Do these probability distributions hold restrictions for fundamental string parameters, e.g. $g_{\rm s}$? We know that $(M, \mu, \phi_{\rm strg}, \phi_{\rm UV})$ really derive from the five quantities $(g_{\rm s}, \alpha', M, v, \mathcal{N})$, hence additional assumptions are necessary. In [2] this approach was explored, yielding a non-trivial degeneracy between $\mathcal{N}, g_{\rm s}$ and v at a certain α'. However, the corresponding MPD would not allow any quantitative restriction on these parameters.

5 Conclusions

A general result of this work is that, *in principle*, it seems possible to constrain stringy parameters from cosmology. However, the accuracy of present data does not suffice to break the degeneracies. Moreover,

[7] See figure 6 of [2].

[8] The definition of (and prior on) R is discussed in [2].

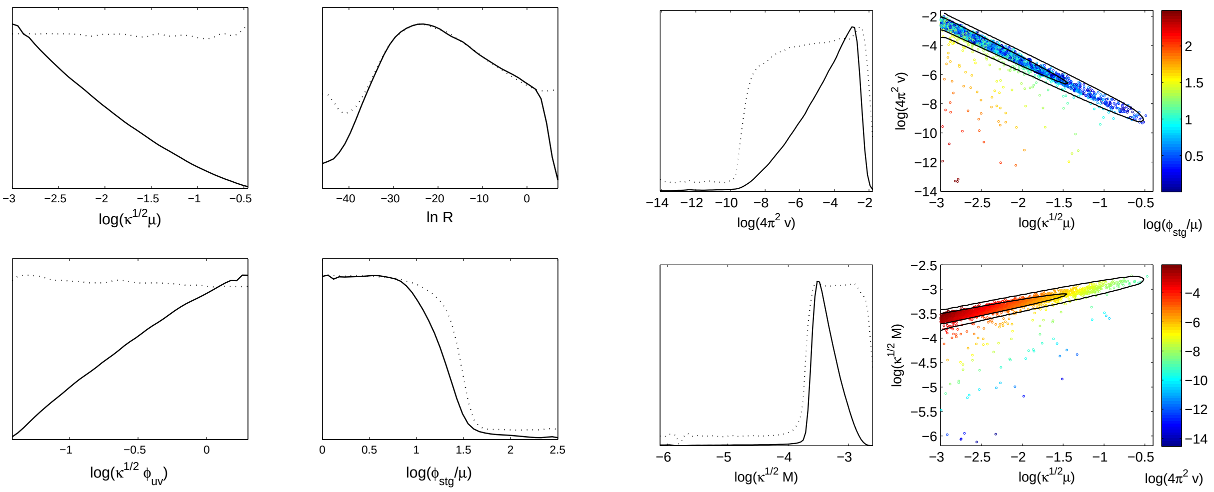

Figure 2: Left: MPD (solid lines) and ML (dotted lines) for the sampled primordial ΛCDM–KKLMMT parameters. Right: MPD and ML for M/m_{Pl} and v. On the very right are the 1σ- and 2σ-contours of the 2d posteriors obtained without marginalising over $\log(\sqrt{\kappa}\mu)$. The 2d probability is proportional to the point density while the colormap traces correlations with the third parameter.

one must not underestimate the strong *theoretical* prior that comes with any attempt at cosmological model building in string theory, since the testable inflationary quantities derive from fundamental (e.g. geometric) choices for the background.

In [2], we presented the first complete MCMC analysis of the pure KKLMMT model, considering g_{s} and α' as free parameters. We also suggest how to systematically scan the parameter space for arbitrary g_{s}, α'. The data favour those cases where inflation occurs in the usual slow-roll way, i.e. inflation ends at ϕ_ϵ and not earlier at brane annihilation. This is because $\phi_{\mathrm{end}} = \phi_{\mathrm{strg}} > \phi_\epsilon$ would push $n_{\mathrm{s}} \to 1$, while preserving a low level of gravitational waves (see [2]). A weak limit on v, i.e. on a parameter of the 6d compactification, is also obtained: $\log v > -10$ at 95% CL.

The choice of the pure KKLMMT scenario [1] comes with a considerable caveat: All moduli are considered stabilized, and various additional contributions to $V(\phi)$ are assumed to conspire in such a way as to only leave the Coulomb term (2). Recently, these contributions became calculable [8], and their general cancellation is unlikely. In practice, the full potential should be of the form $V(\phi) = V_{D\bar{D}}(\phi) + m^2\phi^2 + \ldots$, leading to a completely different inflaton evolution and notably rendering the DBI phase important. The next step would be to include these terms in our analysis, at the expense of introducing additional parameters.

References

[1] S. Kachru *et al.*, JCAP **0310** (2003) 013 [arXiv:hep-th/0308055].

[2] L. Lorenz, J. Martin and C. Ringeval, arXiv:0709.3758 [hep-th].

[3] R. Bean *et al.*, JCAP **0705** (2007) 004 [arXiv:hep-th/0702107].

[4] P. Candelas and X.C. de la Ossa, Nucl. Phys. **B342** (1990) 246-268.

[5] I. R. Klebanov and M. J. Strassler, JHEP **08** (2000) 052 [arXiv:hep-th/0007191].

[6] E. Silverstein and D. Tong, Phys. Rev. **D70** (2004) 103505 [hep-th/0310221].

[7] D. Baumann and L. McAllister, Phys. Rev. **D75** (2007) 123508 [arXiv:hep-th/0610285].

[8] D. Baumann *et al.*, Phys. Rev. Lett. **99** (2007) 141601 {arXiv:0705.3837 [hep-th]}; D. Baumann *et al.*, arXiv:0706.0360 [hep-th]; A. Krause and E. Pajer, arXiv:0705.4682 [hep-th].

Reconstruction of primordial fluctuation spectrum from WMAP-3yr data

Ryo Nagata and Jun'ichi Yokoyama

Research Center for the Early Universe (RESCEU), Graduate School of Science, The University of Tokyo, Tokyo, 113-0033, Japan

Abstract

We reconstruct the primordial curvature fluctuation spectrum from the cosmic microwave background temperature anisotropy spectrum of the Wilkinson Microwave Anisotropy Probe 3-year data by the maximum likelihood matrix inversion method which can potentially reproduce possible fine structure in the primordial spectrum. In the reconstructed primordial spectrum, the prominent oscillatory features found previously on the scales of the top and foot of the first Doppler peak are mildly smoothed except for the peaky structure on ≈ 750Mpc which might be a true signal of deviation from a featureless spectrum.

1 Introduction

The cosmic history during the inflationary stage of the early Universe is recorded in the primordial fluctuation spectrum which can be revealed by modern cosmological observations. In particular, the anisotropy spectrum of the cosmic microwave background (CMB) contains a great deal of such information. With the high quality data provided by the Wilkinson Microwave Anisotropy Probe (WMAP) mission and the clear linear perturbation theory, which relates the primordial spectrum to the observational CMB anisotropy spectrum, we can probe the shape of the primordial spectrum with good accuracy.

Since the first release of the WMAP data [1, 2, 3, 4, 5], it has been argued that the CMB temperature anisotropy spectrum have non-trivial features such as oscillatory behaviors on intermediate scales and lack of power on the largest scales already claimed before WMAP [6, 7]. Although some of the glitches and bites seen in the WMAP 1-year anisotropy spectrum have disappeared in the 3-year anisotropy spectrum [8, 9], still anomalous structure is observed and not well-understood. Those anomaly cannot be explained by a simple powerlaw primordial spectrum that is a generic prediction of conventional inflation models, hence they may have some implication for our understanding of early Universe. WMAP team managed to parametrize the primordial spectrum by decomposing it into ad hoc band-powers, but existence or non-existence of fine structure is still uncertain because it is beyond the scope of parameter fitting method. To evaluate the significance of such fine structure, we apply more flexible non-parametric method.

2 Maximum likelihood matrix inversion method

We introduce the maximum-likelihood matrix method to reconstruct the primordial power spectrum $P(k)$. Temperature anisotropy is decomposed into the coefficients of spherical harmonics as,

$$\frac{\delta T}{T}(\hat{n}) = \sum_{\ell,m} a_{\ell m} Y_{\ell m}(\hat{n}). \tag{1}$$

A theoretical angular power spectrum C_ℓ is the ensemble average of their norm which is related to $P(k)$ via a radiation transfer function $X_\ell(k)$,

$$C_\ell = \langle |a_{\ell m}|^2 \rangle = \frac{2}{\pi} \int d\ln k \;\; k^3 P(k) \left(\frac{X_\ell(k)}{2\ell+1} \right)^2 . \tag{2}$$

We define the primordial spectrum as the initial spectrum of curvature fluctuation, $P(k) = \langle|\Phi(0,k)|^2\rangle$. The probability distribution of a harmonic coefficient for a given $P(k)$ obeys to Gaussian statistics of a complex variable,

$$\mathcal{P}[a_{\ell m}|P(k)] = \frac{1}{\pi C_\ell}\exp\left(-\frac{|a_{\ell m}|^2}{C_\ell}\right) \qquad (m \neq 0), \tag{3}$$

$$\mathcal{P}[a_{\ell 0}\,|P(k)] = \frac{1}{\sqrt{2\pi C_\ell}}\exp\left(-\frac{|a_{\ell 0}|^2}{2C_\ell}\right). \tag{4}$$

Hence the probability of realizing a sky (i.e. a set of harmonic coefficients) is the product of them.

$$\mathcal{P}[\{a_{\ell m}\}|P(k)] = \prod_{\ell,\ m\geq 0} \mathcal{P}[a_{\ell m}|P(k)] \equiv e^{-\mathcal{L}[P(k)]}. \tag{5}$$

Here, following Tocchini-Valentini et al.[10, 11], we assume that $P(k)$ should be a sufficiently smooth function. As the prior for $P(k)$ we adopt

$$\mathcal{P}\left[P(k)\right] \propto \exp\left[-\epsilon\int dk\ \frac{1}{2}\left(\frac{dk^3P(k)}{dk}\right)^2\right] \equiv e^{-\epsilon\mathcal{R}[P(k)]}, \tag{6}$$

where ϵ is a parameter[10, 11]. According to the Bayes theorem, the conditional probability of $P(k)$ under the condition that each $a_{\ell m}$ takes some observed value reads,

$$\mathcal{P}\left[P(k)|\{a_{\ell m}\}\right] = \frac{\mathcal{P}\left[\{a_{\ell m}\}|P(k)\right]\mathcal{P}\left[P(k)\right]}{\mathcal{P}\left[\{a_{\ell m}\}\right]}. \tag{7}$$

The most probable primordial spectrum is obtained by solving the following equation as

$$\frac{\delta}{\delta P(k)}\Big(\mathcal{L}[P(k)] + \epsilon\mathcal{R}[P(k)]\Big) = 0. \tag{8}$$

We can interpret $\mathcal{L}[P(k)]+\epsilon\mathcal{R}[P(k)]$ as the action of a forced oscillator rolling around C_ℓ^{obs}, which assures that the reconstructed $P(k)$ restores the observation.

In our numerical treatment, we adopt the adiabatic initial condition and fiducial cosmological parameters found by the WMAP team [9] to calculate the transfer function. We incorporate the angular spectrum data from $\ell_{min} = 10$ to $\ell_{max} = 800$ and perform the reconstruction in the wave-number range as $k = 1.13\times10^{-5}$ Mpc^{-1} $\sim 2.06\times10^{-1}$ Mpc^{-1} which is divided into about 6000 bins, though the reliable range is limited only to the scales between 2.10×10^{-3} Mpc^{-1} and 2.73×10^{-2} Mpc^{-1} or equivalently between $\ell = 30$ and $\ell = 390$. The actual inversion formula is modified to include noise contribution and uncertainty from incomplete sky coverage. We employ the appropriately chosen $\epsilon(= 4\times10^{-4}\text{Mpc}^{-1})$ so that the resolution is as fine as possible while the power is positive on any scale. Test calculations using mock samples show that this method returns a smoother power spectrum than the original one, if latter has non trivial features. For implementing the inversion scheme, we employ the routines of CMBFAST code [12] to calculate the transfer functions.

3 Reconstructed primordial spectrum

The reconstruction maps also the cosmic variance on the anisotropy spectrum into k-space. Therefore we have to be careful about error estimation for extracting the reliable information of inflation dynamics. In order to incorporate observational errors, we employ Monte-Carlo method to calculate the covariance matrix of the reconstructed power spectrum K_{ij}. Producing 10000 anisotropy spectra from χ^2 distributed random numbers whose mean is the central value of the observational anisotropy spectrum and variance agrees with the diagonal element of the covariance matrix of C_ℓ, we obtain 10000 realizations of $P(k)$.

In the angular power spectrum, the dimension of persisting information of the primordial spectrum is fewer than ℓ_{max} due to smoothing by the convolution with the transfer function. To extract the mutually

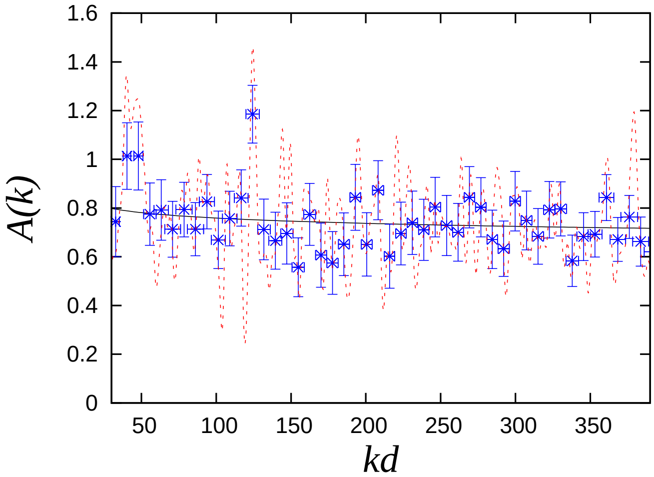

Figure 1: Primordial spectrum $P(k)$ reconstructed from the three-year WMAP data and its band-power decomposition where the vertical axis is normalized in the same way as that of CMBFAST code. The dashed curve represents the solution of the reconstruction formula. Each data point indicates the amplitude of diagonalized mode S defined in the text. The associated vertical bar is its expected dispersion and horizontal bar is 1σ width of the window matrix estimated by Gaussian fitting. The solid line drawn around the middle height is the best-fit powerlaw spectrum.

independent degree of freedom and estimate the reliable error bars, we disentangle this correlation by diagonalizing the covariance matrix [13]. We define a window matrix W by

$$W_{ij} = \frac{(K^{-1/2})_{ij}}{\sum_{m=1}^{N}(K^{-1/2})_{im}}. \tag{9}$$

$K^{-1/2}$ represents the inverse square root of K defined as the unitary transform of diag$(\lambda_1^{-1/2}, \lambda_2^{-1/2}, ...)$ where λ_i's are the eigenvalues of K. Convolving $P_\alpha(k_i)$ with this window function, we define a new statistical variable $S_\alpha(k_i)$ as

$$S_\alpha(k_i) \equiv \sum_{j=1}^{N} W_{ij} P_\alpha(k_j), \tag{10}$$

whose correlation matrix is diagonal and reads

$$\begin{aligned} &\langle\langle S_\alpha(k_i) S_\alpha(k_j)\rangle\rangle_\alpha - \langle\langle S_\alpha(k_i)\rangle\rangle_\alpha \langle\langle S_\beta(k_j)\rangle\rangle_\beta \\ &= (WK^tW)_{ij} = \left[\sum_{m=1}^{N}(K^{-1/2})_{im}\right]^{-2} \delta_{ij}, \end{aligned} \tag{11}$$

where $P_\alpha(k_i)$ represents the value of the reconstructed power spectrum at $k = k_i$ in the α-th realization and $\langle\langle\rangle\rangle$ represents the average of 10000 realizations.

Fig.1 is the result of band power analysis of WMAP 3-year data. In this graph i-th data point indicates the value of

$$\langle\langle S_\alpha(k_i)\rangle\rangle_\alpha = \sum_{j=1}^{N} W_{ij} \langle\langle P_\alpha(k_j)\rangle\rangle_\alpha ,$$

and the vertical error bar represents the variance

$$\left[\langle\langle S_\alpha^2(k_i)\rangle\rangle_\alpha - \langle\langle S_\alpha(k_i)\rangle\rangle_\alpha^2\right]^{1/2} = \left[\sum_{m=1}^{N}(K^{-1/2})_{im}\right]^{-1}.$$

Here k_i is the location of the peak of the i-th line of the window matrix W_{ij}. The horizontal bar, on the other hand, indicates the width of the window matrix. On most scales, the reconstructed band-powers agree with the best-fit power-law quite well. However, we find a prominent peak around $kd \approx 125$, or equivalently the length scale of ≈ 750Mpc, which would be a true signal of deviation from a simple power-law spectrum. It deviates from the best-fit power-law at about 4σ significance level. To evaluate the statistical significance of this deviation, we performed Monte Carlo simulation. Producing 10000 mock realizations of C_ℓ whose ensemble is supposed to be the best-fit power-law model, we apply our reconstruction procedure to each C_ℓ to collect the statistics of reconstructed band powers. We find that the statistical distribution of reconstructed band powers agrees with Gaussian distribution. We repeated the same analysis with the different value of ϵ many times, and in most cases observed the similar peak with similar statistical significance. We have also reconstructed power spectrum using the cosmic inversion method [14, 15, 16, 17, 18] and found a similar peak in the band power analysis at a slightly smaller wave-number with a larger statistical significance $\sim 5\sigma$.

4 Summary

In conclusion, we have reconstructed the power spectrum of primordial curvature perturbation and found a severe deviation from the best-fit power-law in a narrow band around $k* \simeq 0.009\text{Mpc}^{-1}$. The probability that such a deviation is realized in a simple power-law fluctuation is expected to be less than 10^{-4}, and this provides an interesting challenge to theories of generation of fluctuations.

References

[1] C. L. Bennett *et al.*, Astrophys. J. Suppl. **148**, 1 (2003).

[2] G. Hinshaw *et al.*, Astrophys. J. Suppl. **148**, 135 (2003).

[3] D. N. Spergel *et al.*, Astrophys. J. Suppl. **148**, 175 (2003).

[4] H. Peiris *et al.*, Astrophys. J. Suppl. **148**, 213 (2003).

[5] L. Page *et al.*, Astrophys. J. Suppl. **148**, 233 (2003).

[6] Y.-P. Jing and L.-Z. Fang, Phys. Rev. Lett. **73**, 1882 (1994).

[7] C. L. Bennett *et al.*, Astrophys. J. Lett. **464**, L1 (1996).

[8] G. Hinshaw *et al.*, Astrophys. J. Suppl. **170**, 288 (2007).

[9] D.N. Spergel *et al.*, Astrophys. J. Suppl. **170**, 377 (2007).

[10] D. Tocchini-Valentini, M. Douspis and J. Silk, *Mon. Not. Roy. Astron. Soc.* **359**, 31 (2005).

[11] D. Tocchini-Valentini, Y. Hoffman and J. Silk, *Mon. Not. Roy. Astron. Soc.* **367**, 1095 (2006).

[12] U. Seljak and M. Zaldarriaga, Astrophys. J. **469**, 437 (1996).

[13] R. Nagata and J. Yokoyama, in preparation.

[14] Matsumiya, M., Sasaki, M., and Yokoyama, J. Phys. Rev. D **65**, 083007 (2002).

[15] Matsumiya, M., Sasaki, M., and Yokoyama, J. *JCAP* **0302**, 003 (2003).

[16] Kogo, N., Sasaki, M., and Yokoyama, J. Phys. Rev. D **70**, 103001 (2004).

[17] Kogo, N., Sasaki, M., and Yokoyama, J. Prog. Theor. Phys. **114**, 555 (2005).

[18] Kogo, N., Matsumiya, M., Sasaki, M., and Yokoyama, J., Astrophys. J. **607**, 32 (2004).

Primordial non-Gaussianity generated during inflation

Shuichiro Yokoyama[1], Teruaki Suyama[2] and Takahiro Tanaka 3

[1,3]*Department of Physics, Kyoto University, Kyoto 606–8502, Japan*
[2]*Institute for Cosmic Ray Research, The University of Tokyo, Kashiwa 277-8582, Japan*

Abstract

We give a concise formula for the non-Gaussianity of the primordial curvature perturbation generated on super-horizon scales in multi-scalar inflation model without assuming slow-roll conditions.

1 Introduction

Non-Gaussianity of the primordial curvature perturbation is a potentially useful discriminator of the existing many inflation models [1]. PLANCK [2] is expected to detect the primordial non-Gaussianity if the so-called non-linear parameter, f_{NL}, which parameterizes the magnitude of the bispectrum, is larger than $3 \sim 5$ [1]. Hence it is important to theoretically understand the generation of non-Gaussianity. Standard single slow-roll inflation model predicts rather small level of the non-linear parameter, f_{NL}, suppressed by the slow-roll parameters. In this article, we give a useful formula for calculating the non-linear parameter in the multi-scalar inflation models including the models in which the slow-roll approximation is (temporarily) violated after the cosmological scales exit the horizon scale during inflation. Current observations do not exclude such models.

2 formulation

In this section, we derive a formula for calculating the non-linear parameter in the multi-scalar inflation models including the models in which the slow-roll approximation is (temporarily) violated after the cosmological scales exit the horizon scale during inflation [4, 5], based on δN formalism [3]. We use the unit $M_{\rm pl}^2 = (8\pi G)^{-1} = 1$. We consider a $\mathcal{N}$-component scalar field whose action is given by

$$S = -\int d^4x\sqrt{-g}\left[\frac{1}{2}h_{IJ}g^{\mu\nu}\partial_\mu\phi^I\partial_\nu\phi^J + V(\phi)\right] \ , \ \ (I, J = 1, 2, \cdots, \mathcal{N}) \ ,$$

where $g_{\mu\nu}$ is the spacetime metric and h_{IJ} is the metric on the scalar field space. In the main text, we restrict our discussion to the flat field space metric $h_{IJ} = \delta_{IJ}$ to avoid inessential complexities due to non-flat field space metric. Extension to the general field space metric was given in our paper [5]. We define $\varphi_i^I (i = 1, 2)$ as

$$\varphi_1^I \equiv \phi^I \ , \ \ \varphi_2^I \equiv \frac{d}{dN}\phi^I \ , \tag{1}$$

where $dN = Hdt$ with H and t being the Hubble parameter and cosmological time, respectively. Namely, we take e-folding number, N, as a time coordinate. For brevity, hereinafter, we use Latin indices at the beginning of Latin alphabet, a, b or c, instead of the double indices, I, i, i.e., $X^a = X_i^I$. Then, the background equation of motion for φ^a and Friedmann equation are respectively

$$\frac{d}{dN}\varphi^a = F^a(\varphi) \ , \text{ with } F_1^I = \varphi_2^I \ , \ F_2^I = -\frac{V}{H^2}\left(\varphi_2^I + \frac{V^I}{V}\right) \ , \tag{2}$$

$$H^2 = \frac{2V}{6 - \varphi_2^I\varphi_{2I}} \ , \tag{3}$$

[1]E-mail:shu@tap.scphys.kyoto-u.ac.jp

with $V^I = \delta^{IJ}(\partial V/\partial\phi^I)$ and $\varphi_{2I} = \delta_{IJ}\varphi_2^J$.

In the δN formalism [3], the evolution of the difference between two adjacent background solutions determines that of the primordial curvature perturbation on super-horizon scales. Here, we use the word "perturbation" to denote the difference between two adjacent background solutions. In this subsection, we analyze the time evolution of the perturbation and relate the result to the curvature perturbation. The solution of the background equation (2) is labelled by $2\mathcal{N}$ integral constants λ^a. Let us define $\delta\varphi^a$ as the perturbation, $\delta\varphi^a(N) = \varphi^a(\lambda + \delta\lambda; N) - \varphi^a(\lambda; N)$, where λ is abbreviation of λ^a and $\delta\lambda^a$ is a small quantity of $\mathcal{O}(\delta)$. For the purpose of calculating the leading bispectrum of the curvature perturbation, it is enough to know the evolution of $\delta\varphi^a(N)$ up to second order in δ. For later convenience, we decompose $\delta\varphi^a$ as $\delta\varphi^a = \delta\overset{(1)}{\varphi}{}^a + \frac{1}{2}\delta\overset{(2)}{\varphi}{}^a$, where $\delta\overset{(1)}{\varphi}{}^a$ and $\delta\overset{(2)}{\varphi}{}^a$ are first and second order quantities in δ, respectively. Evolution equation for $\delta\overset{(1)}{\varphi}{}^a$ is given by

$$\frac{d}{dN}\delta\overset{(1)}{\varphi}{}^a(N) = P^a_{\ b}(N)\delta\overset{(1)}{\varphi}{}^b(N)\ ,\ \text{with}\ \ P^a_{\ b} \equiv \left.\frac{\partial F^a}{\partial\varphi^b}\right|_{\varphi=\overset{(0)}{\varphi}(N)}\ . \tag{4}$$

Here $\overset{(0)}{\varphi}(N)$ represents the unperturbed trajectory. Formally, solution of this equation can be written as

$$\delta\overset{(1)}{\varphi}{}^a(N) = \Lambda^a_{\ b}(N, N_*)\delta\overset{(1)}{\varphi}{}^b(N_*)\ , \tag{5}$$

$$\frac{d}{dN}\Lambda^a_{\ b}(N, N') = P^a_{\ c}(N)\Lambda^c_{\ b}(N, N')\ , \tag{6}$$

with the condition $\Lambda^a_{\ b}(N, N) = \Lambda^{Ij}_{iJ}(N, N) = \delta^I_{\ J}\delta_i^{\ j}$. Evolution equation for $\delta\overset{(2)}{\varphi}{}^a$ is given by

$$\frac{d}{dN}\delta\overset{(2)}{\varphi}{}^a(N) = P^a_{\ b}(N)\delta\overset{(2)}{\varphi}{}^b(N) + Q^a_{\ bc}(N)\delta\overset{(1)}{\varphi}{}^b(N)\delta\overset{(1)}{\varphi}{}^c(N)\ ,\ \text{with}\ Q^a_{\ bc} \equiv \left.\frac{\partial^2 F^a}{\partial\varphi^b\partial\varphi^c}\right|_{\varphi=\overset{(0)}{\varphi}(N)}\ . \tag{7}$$

Let us choose the integral constants λ^a as the initial values of φ^a at $N = N_*$, namely, $\lambda^a = \varphi^a(N_*)$. Then we have $\delta\varphi^a(N_*) = \delta\lambda^a$. Hence $\delta\overset{(2)}{\varphi}{}^a(N)$ vanishes at N_*. Under this initial condition, the formal solution of Eq. (7) is given by

$$\delta\overset{(2)}{\varphi}{}^a(N) = \int_{N_*}^{N} dN'\Lambda^a_{\ b}(N, N')Q^b_{\ cd}(N')\delta\overset{(1)}{\varphi}{}^c(N')\delta\overset{(1)}{\varphi}{}^d(N')\ . \tag{8}$$

According to the δN formalism, the curvature perturbation on large scales evaluated at a final time, $N = N_c$, is given by the perturbation of the e-folding number between an initial flat hypersurface at $N = N_*$ and a final uniform energy density hypersurface at $N = N_c$. Let us take N_* to be a certain time soon after the relevant length scale crossed the horizon scale, H^{-1}, during the scalar dominant phase and N_c to be a certain time after the complete convergence of the background trajectories has occurred. At $N > N_c$ the dynamics of the universe is characterized by a single parameter and only the adiabatic perturbations remain. Then, the e-folding number between N_* and N_c can be regarded as the function of the final time N_c and $\varphi^a(N_*)$, which we denote $N(N_c, \varphi(N_*))$. Based on δN formalism, the curvature perturbation on the uniform energy density hypersurface evaluated at $N = N_c$ is given by

$$\zeta(N_c) \simeq \delta N(N_c, \varphi(N_*)) = N_{a*}\delta\varphi^a_* + \frac{1}{2}N_{ab*}\delta\varphi^a_*\delta\varphi^b_* + \cdots\ , \tag{9}$$

where $\delta\varphi^a_* = \delta\varphi^a(N_*)$ represents the field perturbations and their time derivative on the initial flat hypersurface at $N = N_*$. Here we also defined $N_{a*} = N_a(N_*)$ and $N_{ab*} = N_{ab}(N_*)$ by

$$N_a(N) \equiv \left.\frac{\partial N(N_c, \varphi)}{\partial\varphi^a}\right|_{\varphi=\overset{(0)}{\varphi}(N)}\ ,\ N_{ab}(N) \equiv \left.\frac{\partial^2 N(N_c, \varphi)}{\partial\varphi^a\partial\varphi^b}\right|_{\varphi=\overset{(0)}{\varphi}(N)}\ , \tag{10}$$

evaluated at $N = N_*$. It is well known that the curvature perturbations on an uniform density hypersurface, ζ, remain constant in time for $N > N_c$. Hence, $\zeta(N_c)$ gives the final spectrum of the primordial perturbation. Let us take N_F to be a certain late time during the scalar dominant phase. Then we have

$$\zeta(N_c) \simeq \delta N(N_c, \varphi(N_F)) = N_{aF}\delta\varphi^a_F + \frac{1}{2}N_{abF}\delta\varphi^a_F\delta\varphi^b_F + \cdots\ . \tag{11}$$

where $\delta\varphi^a_F = \delta\varphi^a(N_F)$, $N_{aF} = N_a(N_F)$ and $N_{abF} = N_{ab}(N_F)$. During the period with $N_* < N < N_F$, we can use the solutions for $\delta\varphi^a$ given by Eqs. (5) and (8). Using these solutions, we obtain the relations;

$$N_{a*} = N_{bF}\Lambda^b{}_a(N_F, N_*) \ , \tag{12}$$

$$N_{ab*} = N_{cdF}\Lambda^c{}_a(N_F, N_*)\Lambda^d{}_b(N_F, N_*) + 2\int_{N_*}^{N_F} dN' N_c(N')Q^c{}_{de}(N')\Lambda^d{}_a(N', N_*)\Lambda^e{}_b(N', N_*) \tag{13}$$

with

$$N_a(N) \equiv N_{bF}\Lambda^b{}_a(N_F, N). \tag{14}$$

Using above basic equations, we derive a formula for the non-linear parameter f_{NL} by making use of the δN formalism. We first give the definition of f_{NL}. It is defined as the magnitude of the bispectrum of the curvature perturbation ζ,

$$B_\zeta(k_1, k_2, k_3) = \frac{6}{5}\frac{f_{NL}}{(2\pi)^{3/2}}\Big[P_\zeta(k_1)P_\zeta(k_2) + P_\zeta(k_2)P_\zeta(k_3) + P_\zeta(k_3)P_\zeta(k_1)\Big] \ , \tag{15}$$

where P_ζ is the power spectrum of ζ. The definitions of P_ζ and B_ζ are, respectively,

$$\langle\zeta_{\mathbf{k}_1}\zeta_{\mathbf{k}_2}\rangle \equiv \delta(\mathbf{k}_1 + \mathbf{k}_2)P_\zeta(k_1) \ , \tag{16}$$

$$\langle\zeta_{\mathbf{k}_1}\zeta_{\mathbf{k}_2}\zeta_{\mathbf{k}_3}\rangle \equiv \delta(\mathbf{k}_1 + \mathbf{k}_2 + \mathbf{k}_3)B_\zeta(k_1, k_2, k_3) \ . \tag{17}$$

Equation (15) restricts the form of the bispectrum. The bispectrum in general does not take that simple form. In fact, sub-horizon perturbations of fields give different k-dependent form of the bispectrum. However, the sub-horizon contribution to the bispectrum is suppressed by the slow-roll parameters evaluated at the time of horizon exit. In contrast, the super-horizon evolution always gives the bispectrum in the form of Eq. (15) independent of the number of fields (see below). If $f_{NL} \gtrsim 1$, which is an interesting case from the observational point of view, then the contribution due to super-horizon evolution dominates the total bispectrum. We assume that the slow-roll conditions are satisfied at $N = N_*$. Then, to a good approximation, $\delta\varphi^I_{1*}$ becomes a Gaussian variable with its variance given by $\langle\delta\varphi^I_{1*}\delta\varphi^J_{1*} \propto \delta^{IJ}$, and φ^I_2 becomes function of φ^I_1. Differentiating $\varphi^I_2 \simeq -\frac{V^I}{V}$, we have

$$\delta\varphi^I_{2*} = \left(\frac{V^I V_J}{V^2} - \frac{V^I{}_J}{V}\right)\delta\varphi^J_{1*} + \cdots. \tag{18}$$

The higher order terms are also suppressed by the slow-roll parameters. Hence, $\delta\varphi^I_{2*}$ is Gaussian as well as $\delta\varphi^I_{1*}$ to a good approximation. Then, we can write down the variance of $\delta\varphi^a_*$ as

$$\langle\delta\varphi^a_*\delta\varphi^b_*\rangle \simeq A^{ab}\left(\frac{H_*}{2\pi}\right)^2 \ . \tag{19}$$

At the first order both in the field perturbation and slow-roll limit, the matrix $A^{ab} = A^{IJ}_{ij}$ can be written as

$$A^{IJ}_{11} = \delta^{IJ} \ , \ A^{IJ}_{12} = A^{IJ}_{21} = \epsilon^{IJ} \ , \ A^{IJ}_{22} = \epsilon^I{}_K\epsilon^{KJ} \ , \tag{20}$$

where

$$\epsilon^{IJ} \equiv \left[\frac{V^I(\phi)V^J(\phi)}{V(\phi)^2} - \frac{V^{IJ}(\phi)}{V(\phi)}\right]_{\phi = \overset{(0)}{\phi}(N_*)} \ . \tag{21}$$

Since $\epsilon^{IJ} = O(\epsilon, \eta)$, we find that $\langle\delta\varphi^I_{1*}\delta\varphi^J_{2*}\rangle$ and $\langle\delta\varphi^I_{2*}\delta\varphi^J_{2*}\rangle$ are suppressed by the slow-roll parameters. Using these equations, to the leading order, the non-linear parameter is written as

$$\begin{aligned}\frac{6}{5}f_{NL} &\simeq \frac{N_{a*}N_{b*}N_{cd*}A^{ac}A^{bd}}{(N_{e*}N_{f*}A^{ef})^2} \\ &= \frac{1}{(N_{a*}\Theta^a_*)^2}\left[N_{abF}\Theta^a(N_F)\Theta^b(N_F) + \int_{N_*}^{N_F} dN' N_c(N')Q^c{}_{ab}(N')\Theta^a(N')\Theta^b(N')\right] \ , \end{aligned} \tag{22}$$

where

$$\Theta^a(N) \equiv \Lambda^a{}_c(N, N_*)A^{cb}N_{b*} \ , \tag{23}$$

and $\Theta^a_* = \Theta^a(N_*)$. As we mentioned before, we have neglected the non-Gaussianity from the sub-horizon contributions in deriving Eq. (22). Eq. (22) shows that, aside from N_{aF} and N_{abF} [2], f_{NL} is completely determined by the quantities $N_a(N)$ and $\Theta^a(N)$. These quantities obey the following closed differential equations,

$$\frac{d}{dN}N_a(N) = -N_b(N)P^b{}_a(N) \ , \ \frac{d}{dN}\Theta^a(N) = P^a_b(N)\Theta^b(N) \ . \tag{24}$$

First, we solve $N_a(N)$ backward till $N = N_*$ under the initial conditions $N_a(N_F) = N_{aF}$. Then we solve $\Theta^a(N)$ forward till $N = N_F$ under the initial conditions $\Theta^a(N_*) = A^{ab}N_{b*}$. Substituting these solutions into Eq. (22), we obtain f_{NL}.

3 Summary

In this article, Based on the δN formalism, we have derived a useful formula for calculating the primordial non-Gaussianity due to the super-horizon evolution of the curvature perturbation in multi-scalar inflation without imposing slow-roll conditions. This formula can apply for the inflation models with general field space metric, h_{IJ}, as long as super-horizon contributions are concerned. Generally, when one calculates the non-Gaussianity of the curvature perturbations, one has to solve the second order perturbation equations. In doing so for a multi-scalar inflation, there appear tensorial quantities with respect to the indices of the field components. Our formalism reduces the problem to calculate the non-linear parameter f_{NL} to solving only first order perturbation equations for two vector quantities. This reduces $\mathcal{O}(\mathcal{N}^2)$ calculations to $\mathcal{O}(\mathcal{N})$ ones where $\mathcal{N}$ is the number of the scalar field components. Hence our formalism has a great advantage for the numerical evaluation of f_{NL} in the inflation model composed of a large number of fields. We have not discussed the possibility of large non-Gaussianity, here. However, in our paper [5], we have studied the primordial non-Gaussianity in double inflation model as an example that violates slow-roll conditions by using our formalism. We found that, although f_{NL} defined for the curvature perturbation on a constant Hubble hypersurface exceeds 1 for a moment around the time when the slow-roll conditions are violated, the final value of f_{NL} is suppressed by the slow-roll parameters evaluated at the time of horizon exit. We have shown that this can be understood even analytically in the δN formalism. This result is straightforwardly extended to more general double inflation model and $\mathcal{N}$-flation model.

References

[1] E. Komatsu and D. N. Spergel, Phys. Rev. D **63**, 063002 (2001) [arXiv:astro-ph/0005036].

[2] [Planck Collaboration], arXiv:astro-ph/0604069.

[3] M. Sasaki and T. Tanaka, Prog. Theor. Phys. **99**, 763 (1998) [arXiv:gr-qc/9801017].

[4] S. Yokoyama, T. Suyama and T. Tanaka, JCAP **0707**, 013 (2007) arXiv:0705.3178 [astro-ph].

[5] S. Yokoyama, T. Suyama and T. Tanaka, arXiv:0711.2920 [astro-ph].

[2] Neglecting the later evolution of the curvature perturbations during the period with $N_c > N > N_F$, we can obtain explicit forms of N_{aF} and N_{abF} [5].

The interrelation between the generation of large-scale electric fields and that of large-scale magnetic fields in inflationary cosmology

Kazuharu Bamba[1]

Department of Physics, Kinki University, Higashi-Osaka, Osaka 577-8502, Japan

Abstract

We study the interrelation between the generation of large-scale electric fields and that of large-scale magnetic fields due to the breaking of the conformal invariance of the electromagnetic field in inflationary cosmology. It is shown that if large-scale magnetic fields with a sufficiently large amplitude are generated during inflation, the generation of large-scale electric fields is suppressed, and vice versa.

1 Introduction

Magnetic fields with the field strength $\sim 10^{-6}$G on a 1–10kpc scale have been observed in galaxies of all types, galaxies at cosmological distances, and clusters of galaxies (for a detailed review, see [1]). Moreover, the field strength of magnetic fields in clusters of galaxies is estimated at 10^{-7}–10^{-6}G and the scale is estimated at 10kpc–1Mpc scale. The origin of these magnetic fields, in particular magnetic fields in clusters of galaxies on a coherence scale as large as ∼Mpc, is not well understood yet. Although galactic dynamo mechanisms have been proposed to amplify very weak seed magnetic fields up to $\sim 10^{-6}$G, they require initial seed magnetic fields to feed on. Furthermore, the effectiveness of the dynamo amplification mechanism in galaxies at high redshifts or clusters of galaxies is not well established.

Although various generation mechanisms of seed magnetic fields have been proposed, it is difficult that these mechanisms generate the magnetic fields on megaparsec scales with sufficient field strength to account for the observed magnetic fields in galaxies and clusters of galaxies without requiring any dynamo amplification.

The most natural origin of such a large-scale magnetic field is electromagnetic quantum fluctuations generated in the inflationary stage [2]. This is because inflation naturally produces effects on very large scales, larger than Hubble horizon, starting from microphysical processes operating on a causally connected volume. Since the Friedmann-Robertson-Walker (FRW) metric usually considered is conformally flat and the classical electrodynamics is conformally invariant, the conformal invariance of the Maxwell theory must have been broken in the inflationary stage in order that electromagnetic quantum fluctuations could be generated at that time. Hence various conformal symmetry breaking mechanisms have been studied [2, 3, 4].

It follows from indications in higher-dimensional theories including string theory that there can exist the dilaton field coupled to the electromagnetic field. Moreover, there can exist non-minimal gravitational couplings between the scalar curvature and the electromagnetic field due to one-loop vacuum-polarization effects in curved spacetime. These couplings break the conformal invariance of the electromagnetic field. Such a coupling of non-trivial background fields that vary in time to the electromagnetic field is very interesting as the generation mechanism of large-scale magnetic fields with a sufficiently large amplitude. In Ref. [5], therefore, the present author and Sasaki studied the evolution of the electromagnetic field in a very general situation in which the conformal invariance is broken through the coupling of the form $IF_{\mu\nu}F^{\mu\nu}$ where I can be a function of any non-trivial background fields that vary in time, and $F_{\mu\nu} = \partial_\mu A_\nu - \partial_\nu A_\mu$ is the electromagnetic field-strength tensor. Here, A_μ is the $U(1)$ gauge field. In this case, not only large-scale magnetic fields but also large-scale electric fields can be generated during inflation. The conductivity of the universe in the inflationary stage is negligibly small because there are few charged particles at that time. Hence electric fields can exist during inflation.

[1]E-mail:bamba@phys.kindai.ac.jp

In the present paper [6] we consider the interrelation between the generation of large-scale electric fields and that of large-scale magnetic fields during inflation due to the breaking of the conformal invariance of the electromagnetic field through a coupling with non-trivial background fields that vary in time.

2 Conformal symmetry breaking of the electromagnetic field

We consider the following model action:

$$S = \int d^4x\sqrt{-g}\left(-\frac{1}{4}I\, F_{\mu\nu}F^{\mu\nu}\right), \tag{1}$$

where g is the determinant of the metric tensor $g_{\mu\nu}$, and I is an arbitrary function of non-trivial background fields at the moment.

From the action (1), the equation of motion for the electromagnetic field can be derived as follows:

$$-\frac{1}{\sqrt{-g}}\partial_\mu\left[\sqrt{-g}IF^{\mu\nu}\right] = 0\,. \tag{2}$$

We assume the spatially flat FRW space-time with the metric

$$ds^2 = -dt^2 + a^2(t)d\boldsymbol{x}^2 = a^2(\eta)(-d\eta^2 + d\boldsymbol{x}^2)\,, \tag{3}$$

where a is the scale factor, and η is the conformal time. We consider the evolution of the $U(1)$ gauge field in this background. Its equation of motion in the Coulomb gauge, $\partial^j A_j(t,\boldsymbol{x}) = 0$, and the case $A_0(t,\boldsymbol{x}) = 0$, reads

$$\ddot{A}_i(t,\boldsymbol{x}) + \left(H + \frac{\dot{I}}{I}\right)\dot{A}_i(t,\boldsymbol{x}) - \frac{1}{a^2}\overset{(3)}{\Delta} A_i(t,\boldsymbol{x}) = 0\,, \tag{4}$$

where $H = \dot{a}/a$ is the Hubble parameter, and a dot denotes a time derivative, $\dot{} = \partial/\partial t$. Moreover, $\overset{(3)}{\Delta} = \partial^i\partial_i$ is the flat 3-dimensional Laplacian.

Next, we consider the evolution of the $U(1)$ gauge field in generic slow-roll inflation. Here we shall quantize the $U(1)$ gauge field $A_\mu(t,\boldsymbol{x})$. It follows from the model Lagrangian in Eq. (1) that the canonical momenta conjugate to $A_\mu(t,\boldsymbol{x})$ are given by

$$\pi_0 = 0\,, \quad \pi_i = Ia(t)\dot{A}_i(t,\boldsymbol{x})\,. \tag{5}$$

We impose the canonical commutation relation between $A_i(t,\boldsymbol{x})$ and $\pi_j(t,\boldsymbol{x})$,

$$[A_i(t,\boldsymbol{x}), \pi_j(t,\boldsymbol{y})] = i\int \frac{d^3k}{(2\pi)^3} e^{i\boldsymbol{k}\cdot(\boldsymbol{x}-\boldsymbol{y})}\left(\delta_{ij} - \frac{k_i k_j}{k^2}\right), \tag{6}$$

where $\boldsymbol{k}$ is comoving wave number and $k = |\boldsymbol{k}|$. From this relation, we obtain the expression for $A_i(t,\boldsymbol{x})$ as

$$A_i(t,\boldsymbol{x}) = \int \frac{d^3k}{(2\pi)^{3/2}} \sum_{\sigma=1,2}\left[\hat{b}(\boldsymbol{k},\sigma)\epsilon_i(\boldsymbol{k},\sigma)A(k,t)e^{i\boldsymbol{k}\cdot\boldsymbol{x}} + \hat{b}^\dagger(\boldsymbol{k},\sigma)\epsilon_i^*(\boldsymbol{k},\sigma)A^*(k,t)e^{-i\boldsymbol{k}\cdot\boldsymbol{x}}\right], \tag{7}$$

where $\epsilon_i(\boldsymbol{k},\sigma)$ ($\sigma = 1,2$) are the two orthonormal transverse polarization vectors, and $\hat{b}(\boldsymbol{k},\sigma)$ and $\hat{b}^\dagger(\boldsymbol{k},\sigma)$ are the annihilation and creation operators which satisfy

$$\left[\hat{b}(\boldsymbol{k},\sigma), \hat{b}^\dagger(\boldsymbol{k}',\sigma')\right] = \delta_{\sigma,\sigma'}\delta^3(\boldsymbol{k}-\boldsymbol{k}')\,, \quad \left[\hat{b}(\boldsymbol{k},\sigma), \hat{b}(\boldsymbol{k}',\sigma')\right] = \left[\hat{b}^\dagger(\boldsymbol{k},\sigma), \hat{b}^\dagger(\boldsymbol{k}',\sigma')\right] = 0\,. \tag{8}$$

It follows from Eq. (4) that the mode function $A(k,t)$ satisfies the equation

$$\ddot{A}(k,t) + \left(H + \frac{\dot{I}}{I}\right)\dot{A}(k,t) + \frac{k^2}{a^2}A(k,t) = 0\,, \tag{9}$$

and that the normalization condition for $A(k,t)$ reads

$$A(k,t)\dot{A}^*(k,t) - \dot{A}(k,t)A^*(k,t) = \frac{i}{Ia}\,. \tag{10}$$

Replacing the independent variable t by η, we find that Eq. (9) becomes

$$A''(k,\eta) + \frac{I'}{I}A'(k,\eta) + k^2 A(k,\eta) = 0\,, \tag{11}$$

where the prime denotes differentiation with respect to the conformal time η.

We are not able to obtain the exact solution of Eq. (11) for the case in which I is given by a general function of η. In fact, however, we can obtain an approximate solution with sufficient accuracy by using the Wentzel-Kramers-Brillouin (WKB) approximation on subhorizon scales and the long-wavelength approximation on superhorizon scales, and matching these solutions at the horizon crossing $\eta = \eta_k \approx -/k$ [5]. As a result, we find that an approximate solution for $|A(k,\eta)|^2$ at late times is given by

$$A(k,\eta) = C(k) + D(k)\int_{\eta}^{\eta_{\mathrm{R}}} \frac{1}{I\left(\tilde{\eta}\right)}d\tilde{\eta}\,, \tag{12}$$

$$C(k) = \left.\frac{1}{\sqrt{2k}}I^{-1/2}\left[1 - \left(\frac{1}{2}I' + ikI\right)\int_{\eta}^{\eta_{\mathrm{R}}} \frac{1}{I\left(\tilde{\tilde{\eta}}\right)}d\tilde{\tilde{\eta}}\right]e^{-ik\eta}\right|_{\eta=\eta_k}\,, \tag{13}$$

$$D(k) = \left.\frac{1}{\sqrt{2k}}I^{-1/2}\left(\frac{1}{2}I' + ikI\right)e^{-ik\eta}\right|_{\eta=\eta_k}\,. \tag{14}$$

3 Evolution of large-scale electric and magnetic fields

The proper electric and magnetic fields are given by

$$E_i^{\mathrm{proper}}(t,\boldsymbol{x}) = a^{-1}E_i(t,\boldsymbol{x}) = -a^{-1}\dot{A}_i(t,\boldsymbol{x})\,, \tag{15}$$

$$B_i^{\mathrm{proper}}(t,\boldsymbol{x}) = a^{-1}B_i(t,\boldsymbol{x}) = a^{-2}\epsilon_{ijk}\partial_j A_k(t,\boldsymbol{x})\,, \tag{16}$$

where $E_i(t,\boldsymbol{x})$ and $B_i(t,\boldsymbol{x})$ are the comoving electric and magnetic fields, and ϵ_{ijk} is the totally antisymmetric tensor ($\epsilon_{123} = 1$).

Using Eqs. (12), (15) and (16), and multiplying quantities in Fourier space by the phase-space density, $4\pi k^3/(2\pi)^3$, we obtain the energy density of the large-scale electric and magnetic fields in the position space

$$\rho_E(L,\eta) = \frac{|D(k)|^2}{2\pi^2 k}\frac{k^4}{a^4}\frac{1}{I(\eta)}\,, \tag{17}$$

$$\rho_B(L,\eta) = \frac{k|C(k)|^2}{2\pi^2}\frac{k^4}{a^4}I(\eta)\,, \tag{18}$$

on a comoving scale $L = 2\pi/k$, respectively.

In order to study the property of generation of large-scale electric and magnetic fields more clearly, we consider the case in which the coupling function of non-trivial background fields to the electromagnetic field, I, is given by a specific form as follows:

$$I(\eta) = I_{\mathrm{s}}\left(\frac{\eta}{\eta_{\mathrm{s}}}\right)^{-\alpha}\,, \tag{19}$$

where η_{s} is some fiducial time during inflation, I_{s} is the value of $I(\eta)$ at $\eta = \eta_{\mathrm{s}}$, and α is a constant. In this case, the ratio of the energy density of the large-scale electric fields to that of the large-scale magnetic fields is given by

$$\frac{\rho_E(L,\eta)}{\rho_B(L,\eta)} = \frac{\alpha^2+4}{4\mathcal{C}}\left(\frac{k}{aH}\right)^{2\alpha}\,, \tag{20}$$

where $\mathcal{C}$ is a constant of order unity. Since we here consider the superhorizon scale, $k/(aH) \ll 1$, from Eq. (20) we see that if $\alpha > 0$, $\rho_B(L,\eta) > \rho_E(L,\eta)$, and that if $\alpha < 0$, $\rho_B(L,\eta) < \rho_E(L,\eta)$. Hence, if large-scale magnetic fields with a sufficiently large root-mean-square (rms) amplitude are generated during inflation, the generation of large-scale electric fields is suppressed, and vice versa. This result holds true for the case in which I is given by an arbitrary function of non-trivial background fields. From Eqs. (17) and (18), we see that $\rho_E(L,\eta) \propto 1/I(\eta)$ and $\rho_B(L,\eta) \propto I(\eta)$. If large-scale magnetic fields with a sufficiently large amplitude are generated during inflation, the value of the coupling function I must be extremely small in the beginning and increase rapidly over time during inflation [5]. In such a case, from the above relations we see that the generation of large-scale electric fields is suppressed.

It follows from Eqs. (15) and (16) that if the amplitude of the $U(1)$ gauge field $A_i(t,\boldsymbol{x})$ varies in time, electric fields are generated; on the other hand, if the amplitude of $A_i(t,\boldsymbol{x})$ varies in terms of space coordinates, magnetic fields are generated. When the amplitude of $A_i(t,\boldsymbol{x})$ greatly varies in time, the relative difference of the amplitude of $A_i(t,\boldsymbol{x})$ at each of the space-coordinate points becomes very small because the amplitude of $A_i(t,\boldsymbol{x})$ greatly grows (or decays) at all the space-coordinate points equally. It follows from the relation $A'(k,\eta) = -D(k)/I(\eta)$, which is derived from Eq. (12), that this situation is realized if the value of I decreases rapidly in time during inflation. On the other hand, when there can exist the large relative difference of the amplitude of $A_i(t,\boldsymbol{x})$ at each of the space-coordinate points, the variation of the amplitude of $A_i(t,\boldsymbol{x})$ in time must be small. This is because the relative difference of the amplitude of $A_i(t,\boldsymbol{x})$ at each of the space-coordinate points is dissipated by the large variation of the amplitude of $A_i(t,\boldsymbol{x})$ in time. This situation is realized if the value of I increases rapidly in time during inflation. Thus, increasing I which favors the small variation of the amplitude of $A_i(t,\boldsymbol{x})$ in time leads to stronger magnetic fields and vice versa.

Consequently, in this scenario there does not exist the possibility that both large-scale electric and magnetic fields with a sufficiently large amplitude are generated simultaneously. Hence large-scale magnetic fields with a sufficiently large amplitude can be generated during inflation without being inconsistent with the fact that the sum of the energy density of the generated electric and magnetic fields during inflation should be smaller than that of the inflaton. Furthermore, when large-scale magnetic fields with a sufficiently large amplitude are generated during inflation, the amplitude of the large-scale electric fields generated is very small. Hence the large-scale charge separation and additional fluctuations in the cosmic plasma, which could be generated during reheating due to the large-scale electric fields and which might make the evolution of the universe anisotropic, can be hardly generated. Consequently, this generation scenario of large-scale magnetic fields from inflation is consistent with the standard evolution of the universe suggested from the observation of the cosmic microwave background (CMB) radiation.

4 Conclusion

In the present paper [6] we have considered the interrelation between the generation of large-scale electric fields and that of large-scale magnetic fields due to the breaking of the conformal invariance of the electromagnetic field through the coupling IF^2 in inflationary cosmology. As a result, we have shown that if large-scale magnetic fields with a sufficiently large amplitude are generated during inflation, the generation of large-scale electric fields is suppressed, and vice versa.

References

[1] D. Grasso and H. R. Rubinstein, Phys. Rept. **348**, 163 (2001).

[2] M. S. Turner and L. M. Widrow, Phys. Rev. D **37**, 2743 (1988).

[3] B. Ratra, Astrophys. J. **391**, L1 (1992).

[4] K. Bamba and J. Yokoyama, Phys. Rev. D **69**, 043507 (2004); *ibid.* **70**, 083508 (2004).

[5] K. Bamba and M. Sasaki, JCAP **0702**, 030 (2007).

[6] K. Bamba, JCAP **0710**, 015 (2007).

Non-Gaussianity from a single field inflation during non slow-roll regime

Yoshiharu Tanaka[1] and Misao Sasaki[2]

Yukawa Institute for Theoretical Physics, Kyoto University, Kyoto 606–8502, Japan

Abstract

We estimated the bispectrum of curvature perturbations in the Starobinsky model in which a single inflaton field has a potential where there is a sudden change in its slope, and temporarily undergoes non slow-roll regime just after passing the change spot, by using the non-linear solution for curvature perturbations, constructed in gradient expansion. Then, we found that large non-Gaussianity may be produced in the model.

1 Introduction

It has been understood from the observations of CMB anisotropies that early universe must have undergone inflationary era. As CMB observations become more accurate, we will come to know abundance of informations about the inflationary era. As one among the observations, it has been studied if there exists the deviation of Gaussian statistics in the CMB fluctuations, i.e. non-Gaussianity. Measuring the non-Gaussianity is important because it plays a role to give much informations probably to distinguish inflation models. Due to the expectation, non-Gaussianity in many models has been studied. Though many authors have investigated non-Gaussianity in single field or multi fields models, there are not so many works, considering models in which slow-roll conditions are violated. It was claimed in Ref. [3] that enhancement or damping of curvature perturbations on superhorizon scales can be occurred in such a non slow-roll model. However, since such features are still studied only in linear theory, it might be worth studying them in non-linear theory, and then non-Gaussianity.

At this work, we consider the Starobinsky model, a single scalar field inflation in which slow-roll condition is violated temporarily in Einstein gravity, and use the nonlinear solutions of metric for single scalar system, which are constructed in gradient expansion [2], to evaluate the nonlinear consequences from non slow-roll regime. And finally we calculate the bispectrum in the model. In this approach based on gradient expansion, we consider only fluctuations on superhorizon scales, and don't deal with nonlinear evolutions on subhorizon scales.

2 Non-linear solutions in gradient expansion

Here, we present the non-linear solutions which are constructed in the existence of a minimal coupling single scalar field, in gradient expansion.

The metric is expressed as

$$ds^2 = (-\alpha^2 + \beta_k\beta^k)dt^2 + 2\beta_i dx^i dt + a^2(t)\, e^{2\mathcal{R}(t,x^k)}\, \tilde{\gamma}_{ij}(t,x^k)dx^i dx^j, \tag{1}$$

where α and β^i ($\beta^i = \gamma^{ij}\beta_j$) are the lapse function, shift vector respectively, $\det(\tilde{\gamma}_{ij}) = 1$, and the function $a(t)$ is the scale factor of a fiducial homogeneous and isotropic background universe.

The stress-energy tensor for a minimal coupling single scalar field is expressed as

$$T_{\mu\nu} = \nabla_\mu\phi\nabla_\nu\phi - \frac{1}{2}g_{\mu\nu}(\nabla^\alpha\phi\nabla_\alpha\phi + 2V(\phi)). \tag{2}$$

We have general and non-linear solutions for α and $\mathcal{R}$ which satisfy the Einstein equations in a minimal coupling single scalar field model as follows [2],

[1] E-mail:yotanaka@yukawa.kyoto-u.ac.jp
[2] E-mail:misao@yukawa.kyoto-u.ac.jp

$$
\begin{aligned}
\alpha &= 1+2\frac{\dot\phi_k}{a^3\dot\phi^3}\left[{}_{(2)}C(x^k)\left(2a\,\dot\phi+\frac{dV}{d\phi}\int_{-\infty}^{t}a(t')dt'\right)+{}_{(2)}D(x^k)\frac{dV}{d\phi}\right], &(3)\\
\mathcal{R} &= {}_{(0)}\mathcal{R}+\int_{t_k}^{t}(\alpha-1)H dt', &(4)
\end{aligned}
$$

where ${}_{(0)}\mathcal{R}$ and ${}_{(2)}D$ (the number indexes (0) and (2) indicate the leading-order and the next-order in gradient expansion, for the quantities attached by them) are arbitrary functions of the spatial coordinates (i.e. integration constants), t_k is actually arbitrary, but we take it to be the time at a few e-foldings after horizon crossing by choosing ${}_{(0)}\mathcal{R}$, $\dot\phi$ is indeed ${}_{(0)}\dot\phi(t)$ which satisfies the (local) Friedmann equations, and $C(x^k)$ is defined as

$$
{}_{(2)}C = \frac{8{}_{(0)}f^{ij}(\bar D_i\bar D_j e^{{}_{(0)}\mathcal{R}/2})-{}_{(0)}f^{kl}{}_{(2)}\bar R_{kl}e^{{}_{(0)}\mathcal{R}/2}}{48\pi G e^{5{}_{(0)}\mathcal{R}/2}a_k^2\dot\phi_{(0)}(t_k)}. \quad (5)
$$

For simplifying the problem, we ignore tensor modes, set ${}_{(0)}f_{ij}=\delta_{ij}$, and have

$$
{}_{(2)}C = \frac{2\partial^2{}_{(0)}\mathcal{R}+\delta^{ij}\partial_{i(0)}\mathcal{R}\partial_{j(0)}\mathcal{R}}{24\pi G\dot\phi_k}e^{-2{}_{(0)}\mathcal{R}} \quad (6)
$$

From Eqs. (3), (4) and (6) , we obtain

$$
\mathcal{R}={}_{(0)}\mathcal{R}+\int_{t_k}^{t}dt' H\frac{2\partial^2{}_{(0)}\mathcal{R}+\delta^{ij}\partial_{i(0)}\mathcal{R}\partial_{j(0)}\mathcal{R}}{12\pi G a^3\dot\phi^3}e^{-2{}_{(0)}\mathcal{R}}\left(2a\,\dot\phi+\frac{dV}{d\phi}\int_{-\infty}^{t'}a(t'')dt''\right)+\int_{t_k}^{t}\frac{2\dot\phi_k H}{a^3\dot\phi^3}{}_{(2)}D\frac{dV}{d\phi}dt'. \quad (7)
$$

3 Application of the nonlinear formalism

We shall estimate the bispectrum in a specific model, the Starobinsky model, using the nonlinear solution which we showed in the previous section. We briefly introduce the model below.

3.1 The Starobinsky model

In the Starobinsky model, a single scalar field has a potential in which there is a sudden change in its slope. The potential is described as

$$
V(\phi)=\begin{cases} V_0+A_+(\phi-\phi_0) & \text{for} \quad \phi>\phi_0\,,\\ V_0+A_-(\phi-\phi_0) & \text{for} \quad \phi<\phi_0\,,\end{cases} \quad (8)
$$

where A_+, A_- and ϕ_0 are assumed to be positive so that the scalar field evolves from a large positive value of ϕ toward $\phi=0$. Then, assuming the de Sitter approximation $3H^2=\kappa^2 V_0$, the scalar field ϕ in the (local) Friedmann spacetime satisfies

$$
3H\dot\phi=\begin{cases} -A_+ & \text{for} \quad \phi>\phi_0\,,\\ -\left(A_-+(A_+-A_-)e^{-3H(t-t_0)}\right) & \text{for} \quad \phi<\phi_0\,,\end{cases} \quad (9)
$$

where t_0 is the time at which $\phi=\phi_0$. Thus the scalar field slow-rolls at $\phi>\phi_0$, and violates the slow-roll condition temporarily at $\phi<\phi_0$. The evolution is decelerated if $A_+/A_->1$, or accelerated if $A_+/A_-<1$, compared to the slow-roll evolution.

3.2 Matching after horizon crossing

To determine the integration constants in Eq. (7), we consider a matching at a few e-foldings after horizon crossing, of quantum fluctuation in linear theory and the nonlinear solution. We refer the detail of the matching to Ref. [4] and avoid the argument here. After the matching, the integration constants are determined as follows,

$$
{}_{(0)}\mathcal{R} \;=\; \left[1+\frac{\partial^2}{12\pi G a_k^2\dot{\phi}_k^2}-\frac{\partial^2}{(a_k H)^2}\right]{}_{(0)}\mathcal{R}_H^{(\pm)}\,, \tag{10}
$$

where here ${}_{(0)}\mathcal{R}_H^{(\pm)}$ is defined in real space, and represents linear quantum curvature perturbations ${}_{(0)}\mathcal{R}_H^{(+)}$ for $t_k < t_0$ and ${}_{(0)}\mathcal{R}_H^{(-)}$ for $t_k > t_0$. And ${}_{(2)}D$ is determined as follows,

$$
{}_{(2)}D = \left(\frac{3H^2K^{(+)}}{8\pi G a_k^2 A_+^2}-\frac{K^{(+)}}{2a_k^2H^2}\right)\left[\frac{3H^2}{a_0^3A_+}\left(1+\frac{A_+}{A_-}\right)-\frac{6H^2}{A_+}\left(\frac{1}{a_0^3}-\frac{1}{a_k^3}\right)\right]^{-1}\,, \tag{11}
$$

where $K^{(+)}$ is defined as

$$
K^{(+)} \equiv 2(\partial^2{}_{(0)}\mathcal{R}_H^{(+)})(e^{-2{}_{(0)}\mathcal{R}_H^{(+)}}-1)+\delta^{ij}\partial_i{}_{(0)}\mathcal{R}_H^{(+)}\partial_j{}_{(0)}\mathcal{R}_H^{(+)}e^{-2{}_{(0)}\mathcal{R}_H^{(+)}}\,. \tag{12}
$$

By substituting Eq. (9) into Eq. (7) and evaluating the integrals in Eq. (7), it can be seen that in the case that $t_0 < t_k$ non-linear evolution doesn't occur. So, non-Gaussianity isn't generated on superhorizon scales in the case, and we focus only on the case that $t_0 > t_k$. Substituting Eqs. (10) and (11) into Eq. (7), and expanding the resulting formula w.r.t. ${}_{(0)}\mathcal{R}$ to second order of it, we obtain the final amplitude (at $t=\infty$) of curvature perturbations in Fourier space,

$$
\begin{aligned}
\mathcal{R}_k(t=\infty) \;=\;& {}_{(0)}\mathcal{R}_{H\mathbf{k}}^{(+)}+T\Big\{-2k^2{}_{(0)}\mathcal{R}_{H\mathbf{k}}^{(+)}\Big\}+T\Big\{4\int\frac{d^3k'd^3k''}{(2\pi)^3}k'^2{}_{(0)}\mathcal{R}_{H\mathbf{k}'}^{(+)}{}_{(0)}\mathcal{R}_{H\mathbf{k}''}^{(+)}\delta(-\mathbf{k}+\mathbf{k}'+\mathbf{k}'')\\
&-\int\frac{d^3k'd^3k''}{(2\pi)^3}\delta_{ij}k'^ik''^j{}_{(0)}\mathcal{R}_{H\mathbf{k}'}^{(+)}{}_{(0)}\mathcal{R}_{H\mathbf{k}''}^{(+)}\delta(-\mathbf{k}+\mathbf{k}'+\mathbf{k}'')\Big\}\,,
\end{aligned} \tag{13}
$$

where we supposed that $t_0 > t_k$, $\mathcal{R}=\int\frac{d^3k}{(2\pi)^3}\mathcal{R}_k e^{i\mathbf{k}\cdot\mathbf{x}}$, ${}_{(0)}\mathcal{R}_H^{(+)}=\int\frac{d^3k}{(2\pi)^3}{}_{(0)}\mathcal{R}_{H\mathbf{k}}^{(+)}e^{i\mathbf{k}\cdot\mathbf{x}}$, ${}_{(0)}\mathcal{R}_{H\mathbf{k}}^{(+)}=\frac{3iH^3}{\sqrt{2}k^{3/2}A_+}$, and T is defined as $T\equiv\frac{1}{5k_0^2}\left(\frac{A_+}{A_-}-1\right)$ where $k_0=a_0H$.

3.3 Bispectrum

We define the bispectrum $B_\mathcal{R}$ by the three point functions as follows,

$$
<\mathcal{R}_{k_1}\mathcal{R}_{k_2}\mathcal{R}_{k_3}> \;=\; (2\pi)^3B_\mathcal{R}(\mathbf{k_1},\mathbf{k_2},\mathbf{k_3})\delta^{(3)}(\mathbf{k_1}+\mathbf{k_2}+\mathbf{k_3})\,, \tag{14}
$$

where $<\cdots>$ represents an ensemble average of $\cdots$. We assume $<\mathcal{R}_\mathbf{k}>=0$. Thus, there is no disconnected part for $<\mathcal{R}_{k_1}\mathcal{R}_{k_2}\mathcal{R}_{k_3}>$, and $<\mathcal{R}_{k_1}\mathcal{R}_{k_2}\mathcal{R}_{k_3}>$ equals to a connected part, $<\mathcal{R}_{k_1}\mathcal{R}_{k_2}\mathcal{R}_{k_3}>_c$. We also assume that ${}_{(0)}\mathcal{R}_H^{(+)}$ is a Gaussian variable. Thus, the three point correlation function of $\mathcal{R}_k$ is to leading order,

$$
\begin{aligned}
<\mathcal{R}_{\mathbf{k_1}}\mathcal{R}_{\mathbf{k_2}}\mathcal{R}_{\mathbf{k_3}}>_c \;=\;& T\Big[\frac{4}{(2\pi)^3}(k_1^2+k_2^2)\delta^{(3)}(\mathbf{k_3}+\mathbf{k_1}+\mathbf{k_2})|{}_{(0)}\mathcal{R}_{H\mathbf{k_1}}^{(+)}|^2|{}_{(0)}\mathcal{R}_{H\mathbf{k_2}}^{(+)}|^2+\text{perms}\\
&-\frac{2}{(2\pi)^3}\delta_{ij}k_1^ik_2^j\delta^{(3)}(\mathbf{k_3}+\mathbf{k_1}+\mathbf{k_2})|{}_{(0)}\mathcal{R}_{H\mathbf{k_1}}^{(+)}|^2|{}_{(0)}\mathcal{R}_{H\mathbf{k_2}}^{(+)}|^2+\text{perms}\Big]\,.
\end{aligned} \tag{15}
$$

The two point correlation function of ${}_{(0)}\mathcal{R}_{H\mathbf{k}}^{(+)}$ is written as $<{}_{(0)}\mathcal{R}_{H\mathbf{k}}^{(+)}{}_{(0)}\mathcal{R}_{H\mathbf{k}'}^{(+)}>=(2\pi)^3|{}_{(0)}\mathcal{R}_{H\mathbf{k}}^{(+)}|^2\delta^{(3)}(\mathbf{k}+\mathbf{k}')=(2\pi)^3P_\mathcal{R}(k)\delta^{(3)}(\mathbf{k}+\mathbf{k}')$. From Eqs. (14) and (15), we have

$$B_{\mathcal{R}} = T\Big[4(k_1^2+k_2^2)|_{(0)}\mathcal{R}^{(+)}_{H\mathbf{k_1}}|^2|_{(0)}\mathcal{R}^{(+)}_{H\mathbf{k_2}}|^2 + \text{perms} \tag{16}$$
$$-2\delta_{ij}k_1^i k_2^j|_{(0)}\mathcal{R}^{(+)}_{H\mathbf{k_1}}|^2|_{(0)}\mathcal{R}^{(+)}_{H\mathbf{k_2}}|^2 + \text{perms}\Big]\,.$$

Next, we define the k-dependent f_{NL} as

$$B_{\mathcal{R}} = -\frac{6}{5}f_{NL}(\mathbf{k_1},\mathbf{k_2},\mathbf{k_3})\frac{\sum_i k_i^3}{\prod_{i=1}^{3}k_i^3}(P_{\mathcal{R}}(k)k^3)^2\,. \tag{17}$$

From Eqs. (16) and (17), we obtain

$$f_{NL}(\mathbf{k_1},\mathbf{k_2},\mathbf{k_3}) = -\frac{\left(\frac{A_+}{A_-}-1\right)}{6\sum_i k_i^3}\left[\sum_{i\neq j, j\neq k, k\neq i}\frac{2(k_i^2+k_j^2)k_k^3}{k_0^2} - \sum_{i\neq j, j\neq k, k\neq i}\frac{\mathbf{k_i}\cdot\mathbf{k_j}k_k^3}{k_0^2}\right]. \tag{18}$$

Evaluating this equation roughly, we have

$$f_{NL}(\mathbf{k_1},\mathbf{k_2},\mathbf{k_3}) \sim -\left(\frac{A_+}{A_-}-1\right)\sum_{i\neq j}\frac{(k_i^2+k_j^2)}{k_0^2}\,. \tag{19}$$

As you can see from this equation, considering the fact that $\frac{k_i}{k_0}<1$, we may have $|f_{NL}|\geq O(1)$ in case that $\frac{A_+}{A_-}>>1$. As k_i approaches to k_0, f_{NL} becomes larger, and maximum just at $k_i=k_0$. The maximum value is characterized by $\frac{A_+}{A_-}$. Thus, non-Gaussianity for the fluctuations which exit horizon just before t_0, may be large if $\frac{A_+}{A_-}$ is larger than unity. It should be noted that the sign of f_{NL} is always minus. One the other hand, non-Gaussianity for the fluctuations which exit horizon after t_0 is not produced at all.

4 Conclusion

We calculated the bispectrum in the Starobinsky model, in which a single scalar inflaton field has a potential where there is a sudden change in its slope, and undergoes non slow-roll regime temporarily just after passing the field value where the change occurs, by using non-linear solutions which were obtained in Ref. [2]. We found that as curvature fluctuations exit horizon scales at time ($t<t_0$) earlier than $t=t_0$, their non-Gaussianity becomes larger and maximally $\sim -\left(\frac{A_+}{A_-}-1\right)$. Then, we emphasize that the sign of f_{NL} is minus. On the other hand, for curvature fluctuations which exit horizon scales after t_0, non-Gaussianity is not produced at all. The Starobinsky model is indeed a toy model of non slow-roll ones. Thus, we guess that what we found here may also be seen similarly in other non slow-roll models.

References

[1] A. A. Starobinsky, JETP Lett. **55**, 489 (1992) [Pisma Zh. Eksp. Teor. Fiz. **55**, 477 (1992)].

[2] Y. Tanaka and M. Sasaki, Prog. Theor. Phys. **118**, 455 (2007) arXiv:0706.0678 [gr-qc].

[3] S. M. Leach, M. Sasaki, D. Wands and A. R. Liddle, Phys. Rev. D **64**, 023512 (2001).

[4] Y. Tanaka and M. Sasaki, in prepareation.

Simulating relativistic binaries with `Whisky`

Luca Baiotti

Department of Earth Science & Astronomy, College of Arts and Science, University of Tokyo, 3-8-1 Komaba, Meguro-ku, Tokyo, 153-8902, Japan

Abstract

We report about our first tests and results in simulating the last phase of the coalescence and the merger of binary relativistic stars. The simulations were performed using our code `Whisky` and mesh refinement through the `Carpet` driver.

1 Introduction

Despite the presence of numerous works in the literature [1, 2, 3, 4, 5], the relativistic *binary neutron star problem* still poses a fundamental challenge in general relativity and in theoretical and observational astrophysics, as well as in numerical relativity. Furthermore, binary systems of compact objects are considered one of the most important sources for gravitational-wave emission and are thought to be at the origin of some of the most violent events in the Universe: (short) γ-ray bursts.

Among the additional motivations that make this problem so interesting, there is surely the investigation of gravitational waves, of their consistency with Einstein's theory and of their detectabilty in the now-operating gravitational-wave detectors. Detection of gravitational waves from relativistic-star binaries will provide a wide variety of physical information on the component stars, including their mass, spin, radius and equation of state.

As said, the study of relativistic-star binary systems is also finalized to the understanding of the origin of some type of γ-ray bursts, because the short rise times of the bursts imply that their central sources have to be highly relativistic objects [6]. After the observational confirmation that γ-ray bursts a have cosmological origin, it has been estimated that the central sources powering these bursts must provide a large amount of energy ($\sim 10^{51}$ ergs) in a very short timescale, going from one millisecond to one second (at least for a subclass of them, called *short γ-ray bursts*). It has been suggested that the merger of relativistic-star binaries could be a likely candidate for the powerful central source. The typical scenario is based on the assumption that a system composed of a rotating black hole and a surrounding massive disc is formed after the merger. If the disc had a mass is $\gtrsim 0.1 M_\odot$, it could supply the large amount of energy by neutrino processes or by extracting the rotational energy of the black hole.

In our previous work [7, 8, 9, 10], we have described how we can perform - with our code `Whisky`, mesh refinement (through the `Carpet` driver [11]) and without excision - accurate three-dimensional relativistic simulation of rotating relativistic-star collapse and how we can extract the (weak) gravitational signal emitted until and past the newly formed black-hole ring-down phase. We have now started to apply the `Whisky` code to investigate the binary problem (where the gravitational-wave signal is expected to be much stronger) and we report here our initial setup.

Hereafter, unless explicitly shown otherwise for convenience, we use a system of units in which $c = G = M_\odot = 1$.

2 Basic equations and their implementation

The `Whisky` code solves the general-relativistic hydrodynamics equations on a three-dimensional numerical grid with Cartesian coordinates [12]. The code has been constructed within the framework of the `Cactus` Computational Toolkit (see [13] for details). While the `Cactus` code provides at each time step and on a spatial hypersurface the solution of the Einstein equations $G_{\mu\nu} = 8\pi T_{\mu\nu}$, where $G_{\mu\nu}$ is the Einstein tensor and $T_{\mu\nu}$ is the stress-energy tensor, the `Whisky` code provides the time evolution of the hydrodynamics equations, expressed through the conservation-equations for the stress-energy tensor $T^{\mu\nu}$ and for the matter current density J^μ

$$\nabla_\mu T^{\mu\nu} = 0 \, , \qquad \nabla_\mu J^\mu = 0 \, . \tag{1}$$

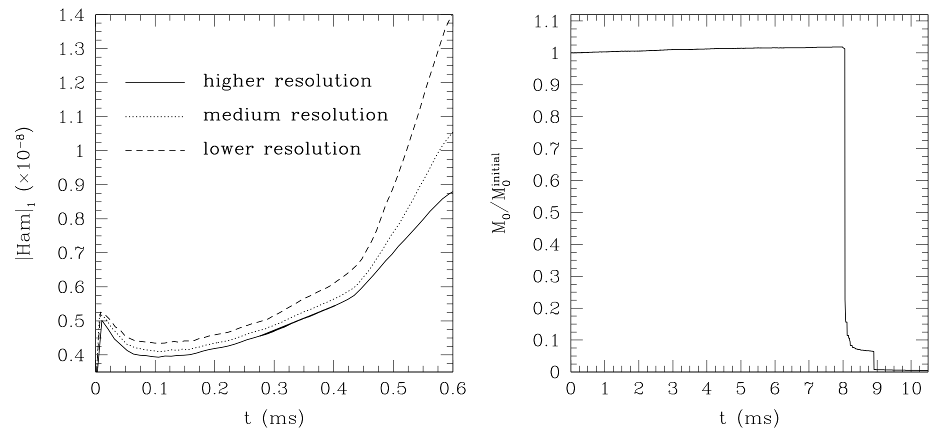

Figure 1: LEFT: Comparison of the Hamiltonian constraint violation for three resolutions. The spacing for the finest grid of the three resolutions are $0.016M$, $0.02M$ and 0.025. RIGHT: conservation of baryon mass.

Details on the system of field equations we use are given in [14] and in the previous `Whisky` articles [7, 8, 9, 10]. The code is designed to handle arbitrary shift and lapse conditions, which can be chosen as appropriate for a given spacetime simulation. More information about the possible families of spacetime slicings which have been tested and used with the present code can be found in [14, 15].

The singularity-avoiding properties of the above gauge choices have proved equally good both when using excision, as we did in [7] and [8], and when not using excision. In the latter case, these gauge choices are essential to "freeze" the evolution in those regions of the computational domain inside the apparent horizon, where the metric functions experience the growth of very large gradients. Furthermore, in this case a small additional dissipation in the metric and gauge terms is also necessary to obtain long-term stable evolutions [9].

An important feature of the `Whisky` code is the implementation of a *conservative formulation* of the hydrodynamics equations [16, 17, 18], in which the set of equations (1) is written in a hyperbolic, first-order and flux-conservative form of the type

$$\partial_t \mathbf{q} + \partial_i \mathbf{f}^{(i)}(\mathbf{q}) = \mathbf{s}(\mathbf{q}) \,, \tag{2}$$

where $\mathbf{f}^{(i)}(\mathbf{q})$ and $\mathbf{s}(\mathbf{q})$ are the flux-vectors and source terms, respectively [2]. Note that the right-hand side (the source terms) must not depend on derivatives of the stress-energy tensor.

Additional details on the formulation we use for the hydrodynamics equations can be found in [2]. We stress that an important feature of this formulation is that it has allowed to extend to a general-relativistic context the powerful numerical methods developed in classical hydrodynamics, in particular High-Resolution Shock-Capturing schemes based on exact [19, 20, 21] or approximate Riemann solvers (see [2] for a detailed bibliography). Such schemes are essential for a correct representation of shocks, whose presence is expected in several astrophysical scenarios.

3 Initial data and evolution

As initial data for relativistic-star binary simulations we use the ones produced by the group working at the Observatoire de Paris-Meudon [22, 23]. These data, which we refer to also as the *Meudon data*, are obtained under the simplifying assumptions of quasi-equilibrium and of conformally-flat spatial metric. These initial configurations are computed using a multi-domain spectral-method code named `LORENE`, which is a free software under the GNU General Public License; a specific routine then converts from spherical coordinates to a Cartesian grid of the desired dimensions and shape.

Except where explicitly indicated, the simulations we discuss here refer to evolutions of equal-mass irrotational initial data having the following properties: initial orbital period T=3.395 ms; rest mass of a star $M_0 = 1.625M_\odot$; gravitational mass of a star $M = 1.456M_\odot$; radius of a star R=13.68 km; coordinate distance between stellar

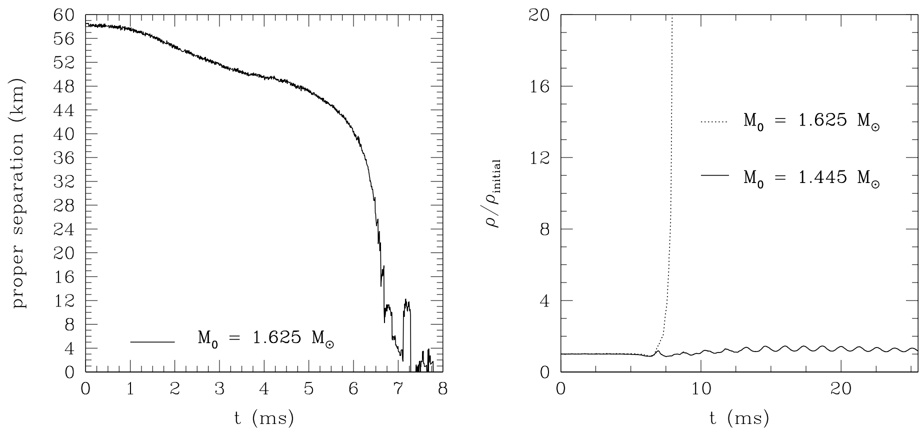

Figure 2: LEFT: Time evolution of the proper distance between the maximum–rest-mass-density points of the stars. RIGHT: Time evolution of the maximum of the rest-mass density, in the case of a prompt formation of black hole (dotted line) and in the case of the formation of an oscillating relativistic star.

centres 45km = 41 M_0 = 0.19 $\lambda_{\rm GW}$ = 3.4 R; compactness of a star M/R = 0.14; ratio of the polar to the equatorial radius of a star 0.93; polytropic exponent $\Gamma = 2$.

We performed evolutions with 8 refinement levels. In the case of the highest-resolution simulation, the finest grid covered only the interior of the stars, with a resolution of $\Delta x \simeq 0.016M$ and the coarsest one had the outer boundary at $\simeq 175M$. This is still work in progress, but the presently available data for the initial part of the time evolution seems to suggest that these resolutions are sufficient for reliable evolutions, as the time evolution of the rest mass also shows (right panel of Fig. 1). The rest mass should in principle be constant and the data represented in the figure indicate that the violation of the conservation, due to numerical errors, is less than 0.1%, until horizon formation, when this measure ceases to be meaningful. The convergence rate of the code for this kind of simulations, as measured through the norm of the Hamiltonian constraint violation, is 1.5. This is also shown in the left panel of Fig. 1.

One positive remark we can make at this point is that in our evolutions for the above-mentioned initial data we can follow the orbit of the stars for several periods, before the beginning of the plunge, as is shown in Fig. 2, which reports the time evolution of the proper distance between the maximum–rest-mass-density points (*i.e.* the centres) of the stars. Such a proper measure shows an approximately constant decrease of the distance, only slightly modulated by residual eccentricity. At the time of the beginning of the plunge, at around $t = 6$ ms, the proper distance between the stars is about 5 times the total initial ADM mass of the system. During the merger, the stars bounce shortly before collapsing as a single object to a black hole. This phase is illustrated in the figure by the spikes present between 6.5 and 8 ms. Even if for space reasons it is not reported in the present article, we can also simulate the ring-down phase of the newly formed black hole and extract the complete gravitational-wave signal.

The right panel of Fig. 2 shows the time evolution of the maximum of the rest-mass density. This illustrates two very different possible outcomes of the merger, namely the prompt collapse to a black hole, about 1 ms after the merger, and the formation of a compact object without (apparent) horizons. Such a compact object oscillates violently, emitting a persistent gravitational radiation of amplitude similar to the one emitted during the last phases of the coalescence. After dissipative effects (depending strongly on the equation of state) like shock heating and gravitational-radiation emission reduce the pressure and the angular momentum of the compact star, a delayed collapse to black hole is possible. Indeed, we observe this behaviour in some simulations now under investigation (not reported here).

In the near future, we plan to carry out a detailed study of relativistic-star mergers, investigating in particular the different dynamics and gravitational waveforms obtained with different initial data (masses) and different equations of state.

I want to thank Luciano Rezzolla for discussions and suggestions on the manuscript. The computations were performed on the clusters at the Albert Einstein Institute.

References

[1] Oohara K I and Nakamura T 1997 *Prog. Theor. Phys. Suppl.* **128** 183

[2] Font J A 2003 *Living Rev. Relativity* **6** 4 *http://www.livingreviews.org/Articles/lrr-2003-4*

[3] Shibata M and Uryū K 2000 *Phys. Rev. D* **61** 064001 gr-qc/9911058

[4] Shibata M and Nakamura T 1995 *Phys. Rev. D* **52** 5428

[5] Shibata M and Uryū K 2002 *Prog. Theor. Phys.* **107** 265

[6] Piran T 1999 *Phys. Rept.* **314** 575–667

[7] Baiotti L, Hawke I, Montero P J, Löffler F, Rezzolla L, Stergioulas N, Font J A and Seidel E 2005 *Phys. Rev. D* **71** 024035

[8] Baiotti L, Hawke I, Rezzolla L and Schnetter E 2005 *Phys. Rev. Lett.* **94** 131101

[9] Baiotti L and Rezzolla L 2006 *Phys. Rev. Lett.* **97** 141101

[10] Baiotti L, Hawke I, Rezzolla L and Schnetter E to be published in July 2007 in A S Olives and J Carot, eds, *XXIX Spanish Relativity Meeting (ERE 2006)* (Palma de Mallorca: Journal of Physics: Conference Series)

[11] Schnetter E, Hawley S H and Hawke I 2004 *Class. Quantum Grav.* **21**(6) 1465–1488

[12] Baiotti L, Hawke I, Montero P and Rezzolla L 2003 in R Capuzzo-Dolcetta, ed, *Computational Astrophysics in Italy: Methods and Tools* (Trieste: Mem. Soc. Astron. It. Suppl.) vol 1 p 210

[13] Cactus Computational Toolkit home page *http://www.cactuscode.org/*

[14] Alcubierre M, Brügmann B, Dramlitsch T, Font J A, Papadopoulos P, Seidel E, Stergioulas N and Takahashi R 2000 *Phys. Rev. D* **62** 044034

[15] Alcubierre M, Brügmann B, Pollney D, Seidel E and Takahashi R 2001 *Phys. Rev. D* **64** 061501(R)

[16] Martí J M, Ibáñez J M and Miralles J M 1991 *Phys. Rev. D* **43** 3794

[17] Banyuls F, Font J A, Ibáñez J M, Martí J M and Miralles J A 1997 *Astrophys. J.* **476** 221

[18] Ibáñez J, Aloy M, Font J, Martí J, Miralles J and Pons J 2001 in E Toro, ed, *Godunov methods: theory and applications* (New York: Kluwer Academic/Plenum Publishers)

[19] Martí J M and Müller E 1999 *Living Rev. Relativity* **2** 3 *http://www.livingreviews.org/lrr-1999-3*

[20] Rezzolla L and Zanotti O 2001 *Journ. of Fluid Mech.* **449** 395

[21] Rezzolla L, Zanotti O and Pons J A 2003 *Journ. of Fluid Mech.* **479** 199

[22] Gourgoulhon E, Grandclément P, Taniguchi K, Marck J and Bonazzola S 2001 *Phys. Rev. D* **63** 064029

[23] Taniguchi K and Gourgoulhon E 2002 *Phys. Rev. D* **66** 104019

Numerical Calculation of Force-free Black Hole Magnetospheres

Yosuke Takamori[1] , Hideki Ishihara[2] , Masashi Kimura[3] , Ken-ichi Nakao[4] ,
Masaaki Takahashi[5] and Chul-Moon Yoo[6]

[1,2,3,4] *Department of Mathematics and Physics, Graduate School of Science, Osaka City University, Osaka 558-8585, Japan*
[5] *Department of Physics, and Astronomy, Aichi University of Education, Kariya, Aichi, 448-8542, Japan*
[6] *Yukawa Institute for Theoretical Physics, Kyoto University, Kyoto 606–8502, Japan*

Abstract

We propose the numerical scheme to solve the Grad-Shafranov equation which represents stationary, axisymmetric and force-free electromagnetic field. In this article, firstly, we briefly surmmaraize the scheme to solve the Grad-Shafranov equation given by [1][2]. Then, we describe our numerical scheme. In our scheme, treatment of the light surface and the symmetry axis are improved from the method given by [1][2].

1 Introduction

It is widely believed that there is a supermassive black hole in the center of active galactic nuclei(AGN's) and it works as an engine of AGN. The mechanism of energy generation is roughly divided into two categories. One is due to a release of the gravitational energy of accreting matter, and the other is due to an extraction of the rotational energy from accretion disks or central rotating black holes. As the way to extract the rotational energy of the black hole, Penrose process, super-radiance, and Blandford-Znajek(B-Z) mechanism[3] are known. In paticular, B-Z mechanism is believed to play an important role in the jets formation in AGN's. Because the efficiency of energy extarction by B-Z mechanism would depend on the configuration of magnetic field around the black hole, it is important to study the electromagnetics around the black hole.

In this study we consider stationary, axisymmetric, and force-free magnetospheres, in which B-Z mechanism is shown. The configuration of magnetosphere is determined by only one equation called the Grad-Shafranov(G-S) equation. This equation is a quasi-linear second-order eliptic partial differential equation, and has the singularity called the light surface. Due to this singularity, it is difficult to solve the G-S equation in the domain including the light surfce. Recently Contopoulos et al.[4] proposed a method to solve the G-S equation for pulsar magnetospheres. After that, Uzdensky extended this method to black hole cases.

In this article we will briefly summarize the method to solve the G-S equation given by [1][2], and describe our numerical scheme. Through this article we use the geometrical units $c = G = 1$.

2 The Grad-Shafranov equation

Here, we consider stationary, axisymmetric, and force-free magnetospheres around a Kerr black hole. In Boyer-Lindquist coordinates (t, r, θ, ϕ), the metric of the Kerr black hole geometory is given by

$$ds^2 = -\left(1 - \frac{2Mr}{\rho^2}\right) dt^2 - \frac{4Mar\sin^2\theta}{\rho^2} dtd\phi + \frac{\rho^2}{\Delta} dr^2 + \rho^2 d\theta^2 + \frac{A\sin^2\theta}{\rho^2} d\phi^2, \tag{1}$$

[1]E-mail:takamori@sci.osaka-cu.ac.jp
[2]E-mail:ishihara@sci.osaka-cu.ac.jp
[3]E-mail:mkimura@sci.osaka-cu.ac.jp
[4]E-mail:knakao@sci.osaka-cu.ac.jp
[5]E-mail:takahashi@phyas.aichi-edu.ac.jp
[6]E-mail:yoo@yukawa.kyoto-u.ac.jp

where $\rho^2 = r^2 + a^2\cos^2\theta$, $\Delta = r^2 - 2Mr + a^2$, and $A = (r^2+a^2)^2 - a^2\Delta\sin^2\theta$. M and a are mass and spin parameter of the black hole, respectively. In order to describe the electromagnetic process around a Kerr black hole, we use ZAMO formalism introduced by Macdonaldand and Thorne[5]. In this formalism, the electric and magnetic fields are measured by zero-angular-momentum observers(ZAMOs). Because four-velocities of ZAMOs constitute the normal vector fields to the spacelike hypersurfaces labeled by t, this formalism is equivalent to the 3+1 dcomposition of the Maxwell equations. The intrinsic geometry of a spacelike hypersurface labeled by t is given by

$$ds^2_{3dim} = h_{ij}dx^i dx^j = \frac{\rho^2}{\Delta}dr^2 + \rho^2 d\theta^2 + \frac{A\sin^2\theta}{\rho^2}d\phi^2, \tag{2}$$

where $i, j, \dots$ runs over the three spatial coordinates (r, θ, ϕ).

Under the assumptions that the magnetosphere is stationary, axisymmetric and force-free, electric and magnetic fields can be expressed in terms of three scalar functions, $\Psi(r,\theta)$, $I(\Psi)$, and $\Omega_F(\Psi)$, which have the physical meanings of the total magnetic flux, the total current, and the angular velocity of the magnetic field lines, respectively. The G-S eqution is a partial differential equation for $\Psi(r,\theta)$,

$$D_i\left(\frac{D}{\alpha\varpi^2}D^i\Psi\right) + \frac{(\Omega_F - \omega)}{\alpha}\frac{d\Omega_F}{d\Psi}D_i\Psi D^i\Psi + \frac{16\pi^2 I}{\alpha\varpi^2}\frac{dI}{d\Psi} = 0, \tag{3}$$

where $\alpha^2 = \Delta\rho^2/A$, $\varpi^2 = A\sin^2\theta/\rho^2$, $\omega = 2Mar/A$, and $D = \alpha^2 - (\Omega_F - \omega)^2\varpi^2$.[5] D_i is the derivative oparator associated with h_{ij}. This equation is a quasi-linear second-order elliptic partial differential equation. From (3), it is easy to see that, in general, this equation has two kinds of singular surface. One is the event horizon defined by $\Delta = 0$, and the other is the so-called light surface defined by $D = 0$.

3 Numerical scheme to solve the Grad-Shafranov equation

3.1 Iterative method

Due to the light surface singularity, it is difficult to obtain a smooth solution of the G-S equation in the domain including the light surface. Recently, Contopoulos et al.[4] proposed an iterative method to obtain a smooth solution. They constructed the numerical scheme to solve the pulsar equation which corresponds to the G-S equation in the Mikowsiki back ground. Uzdensky extended this method to a black hole case [1][2]. We will briefly summarize his method(for details, see [1][2]) in this section.

To solve the G-S equation, Uzdensky defined the diffusion equation

$$\frac{\partial\Psi}{\partial t} = f(r,\theta)(\mathrm{LHS} - \mathrm{RHS}), \tag{4}$$

where

$$\begin{aligned}
\mathrm{LHS} &= \partial_r\left(\frac{D\Delta}{\rho^2}\partial_r\Psi\right) + \partial_\theta\left(\frac{D}{\rho^2}\partial_\theta\Psi\right) + \frac{D\Delta\sin\theta}{\rho^4}\left(\Delta\partial_r\Psi\partial_r\left(\frac{\rho^2}{\Delta\sin\theta}\right) + \partial_\theta\Psi\partial_\theta\left(\frac{\rho^2}{\Delta\sin\theta}\right)\right),\\
\mathrm{RHS} &= -16\pi^2 I\frac{dI}{d\Psi} - (\Omega_F - \omega)\varpi^2\frac{d\Omega_F}{d\Psi}D_i\Psi D^i\Psi.
\end{aligned} \tag{5}$$

The function $f(r,\theta)$ is an artificial multiplier introduced to accelerate convergence Eq.(4). We set boundary conditions and an initial condition, and specify I and Ω_F. We solve Eq.(4) numerically as a Cauchy problem. Since Ψ would be expected to satisfiy $\partial_t\Psi = 0$ after the sufficient time evolution, we obtain a solution of the G-S equation by solving Eq.(4). However, we have to treat the light surface singularity appropriatly to obtain a smooth solution in the domain including the light surface. At the light surface, we obatin the reguraliry conditon as

$$-16\pi^2 I\frac{dI}{d\Psi}\bigg|_{\mathrm{LS}} = D_i D D^i\Psi|_{\mathrm{LS}} + (\Omega_F - \omega)\varpi^2\frac{d\Omega_F}{d\Psi}D_i\Psi D^i\Psi|_{\mathrm{LS}}. \tag{6}$$

In Uzdensky's method, Eq.(6) is treated as an equation which determine $I\frac{dI}{d\Psi}$. Then, the numerical procedure to solve the G-S equation given by Uzdensky is as follows:

1. We choose an initial traial magnetic flux function $\Psi_{\rm ini}(r,\theta)$, and set boundary conditions on the boundary of computational domain.
2. By solving Eq.(6), we obtain the initial current distribution $I\frac{dI}{d\Psi}$.
3. By solving Eq.(4), we obtain next time step magntic flux function $\Psi(\delta t, r, \theta)$.
4. We use $\Psi(\delta t, r, \theta)$ to determine new $I\frac{dI}{d\Psi}$.

We repeat steps 2-4 until $\partial_t\Psi = 0$.

3.2 New Method

The method given in [1][2] does not guarantee that the values of $\partial_r^2\Psi$ and $\partial_\theta^2\Psi$ are continuous across the light surface. To obtain a smooth solution of the G-S equation, we construct the numerical scheme which guarantee the finiteness of $\partial_r^2\Psi$ and $\partial_\theta^2\Psi$ acrross the light surface in section 3.2.1. In section 3.2.2, we introduce the boundary condition at the polar axis, $\theta = 0$, which is the symmetry axis. We choose the boundary condition at the polar axis such that total magntic flux Ψ and its derivative $\partial_\theta\Psi$ vanish there.

3.2.1 Condition at the light surface

As a first step for our study, we assume the constant angular velocity of magnetic field lines, i.e.,$\Omega_F =$ constant. There are two light surfaces in the black-hole spacetime. On one light surface, we determine $I\frac{dI}{d\Psi}$. Another light surfce is treated as the boundary of numerical domain.

In order to guarantee that $\partial_r^2\Psi$ and $\partial_\theta^2\Psi$ are continuous across the light surface, we rewrite Eq.(3) as

$$\frac{\Delta}{\rho^2}\partial_r^2\Psi + \frac{\sin\theta}{\rho^2}\partial_\theta\left(\frac{\partial_\theta\Psi}{\sin\theta}\right) + \frac{N}{D} = 0, \tag{7}$$

$$N = (D_i D)(D^i\Psi) + 16\pi^2 I\frac{dI}{d\Psi}. \tag{8}$$

At the light surfce, N and D are vanishing, we see that

$$\lim_{r\to r_{\rm LS}}\frac{N}{D} = \left.\frac{\partial_r N}{\partial_r D}\right|_{\rm LS}. \tag{9}$$

Then, Eq.(7) at the light surfce is given by

$$\frac{\Delta}{\rho^2}\partial_r^2\Psi|_{\rm LS} + \frac{\sin\theta}{\rho^2}\partial_\theta\left.\left(\frac{\partial_\theta\Psi}{\sin\theta}\right)\right|_{\rm LS} + \left.\frac{\partial_r N}{\partial_r D}\right|_{\rm LS} = 0. \tag{10}$$

3.2.2 Boundary condition at the polar axis

The coditions $\Psi(r,0) = 0$ and $\partial_\theta\Psi(r,0) = 0$ imply that Ψ behaves as $\Psi \propto \theta^2$ near the symmetry axis. Thus we rewrite $\Psi(r,\theta)$ as $\Psi(r,\theta) = \sin^2\theta\hat{\Psi}(r,\theta)$. Substituting this into Eq.(7), we obtain the factorized G-S equation

$$\frac{\Delta}{\rho^2}\partial_r^2\hat{\Psi} + \frac{1}{\rho^2}\partial_\theta^2\hat{\Psi} + \frac{3}{\rho^2\tan\theta}\partial_\theta\hat{\Psi} - \frac{2}{\rho^2}\hat{\Psi} + \frac{N}{D\sin^2\theta} = 0. \tag{11}$$

To avoid the singurarity at the symmetry axis, $\partial_\theta\hat{\Psi} = 0$ at $\theta = 0$ should hold. This is a boundary condition on $\hat{\Psi}$ at the symmetry axis.

The diffusion equation to solve the factorized G-S equation (11) is

$$\partial_t\hat{\Psi} = \frac{\Delta}{\rho^2}\partial_r^2\hat{\Psi} + \frac{1}{\rho^2}\partial_\theta^2\hat{\Psi} + \frac{3}{\rho^2\tan\theta}\partial_\theta\hat{\Psi} - \frac{2}{\rho^2}\hat{\Psi} + \frac{\hat{N}}{D}, \tag{12}$$

$$\hat{N} = \frac{\Delta}{\rho^2}\partial_r D\partial_r\hat{\Psi} + \frac{1}{\rho^2}\partial_\theta D\left(\partial_\theta\hat{\Psi} + \frac{2\hat{\Psi}}{\tan\theta}\right) + \frac{16\pi^2 I}{\sin^2\theta}\frac{dI}{d\Psi}. \tag{13}$$

At the light surface and the symmetry axis $\theta = 0$, we solve the following equations

$$\partial_t \hat{\Psi} = \frac{\Delta}{\rho^2}\partial_r^2 \hat{\Psi} + \frac{1}{\rho^2}\partial_\theta^2 \hat{\Psi} + \frac{3}{\rho^2 \tan\theta}\partial_\theta \hat{\Psi} - \frac{2}{\rho^2}\hat{\Psi} + \frac{\partial_r \hat{N}}{\partial_r D} \qquad \text{at the light surface} \tag{14}$$

and

$$\partial_t \hat{\Psi} = \frac{\Delta}{\rho^2}\partial_r^2 \hat{\Psi} + \frac{4}{\rho^2}\partial_\theta^2 \hat{\Psi} - \frac{2}{\rho^2}\hat{\Psi} + \frac{\hat{N}}{D} \qquad \text{at } \theta = 0, \tag{15}$$

respectively.

4 Summary

We proposed the numerical scheme to obtain a smooth solution of the G-S equation for the case of $\Omega_F =$ constant. In our scheme, treatment of the light surface and the symmetry axis are improved from the method given in [1][2]. We have already constructed the numerical code, and we will report numerical solutions by this code in near future.

References

[1] D.A.Uzdensky, Astro.Phys.J,603,652(2004)

[2] D.A.Uzdensky, Astro.Phys.J,620,889(2005)

[3] R.D.Blandford and R.L.Znajek, Mon.Not.R.Astro.Soc,179,433(1977)

[4] I.Contopoulos, D.Kazanas and C.Fendt, Astro.Phys.J,511,351(1999)

[5] D.Macdonald and K.S.Thorne, Mon.Not.R.Astro.Soc,198,345(1982)

Superradiant illumination of a disk in a black hole magnetosphere

Taichi Kobayashi[1], Kohei Onda[2], and Akira Tomimatsu[3]

Department of Physics, Nagoya University, Nagoya 464–8602, Japan

Abstract

Using the Kerr-Schild formalism to solve the Einstein-Maxwell equations, we consider the superradiance in the black hole-disk system, which may work as a mechanism to illustrate a disk licated on the equatorial plane. In this paper, we illustrate the energy extraction from the black hole and the energy transport to the disk, using a specific example. As a result, we obtain the disk illumination by the black hole superradiance.

1 Introduction

It is widely believed that there exists a rotating black hole surrounded by a disk in the central region of high energetic astrophysical objects, such as active galactic nuclei (AGNs), X-ray binary systems, and gamma-ray bursts (GRBs). However, in this view, recent observation of extremely broad and red-shifted Fe Kα line emission from a nearby Seyfert 1 galaxy [1] cannot be explained. To explain the observed spectrum a very steep emissivity profile is required. This result motivate us to consider the energy transport from the black hole to the disk in the disk-black hole systems.

It is important to consider magnetic fields in the processes of disk radiation, jet production, and so on. As was emphasized in [2, 3], if a black hole is magnetically connected with a disk, the energy and angular momentum fluxes can be transported between them along the magnetic field lines through a mechanism analogous to the Blandford-Znajek effect [4]. The energy supply to an accretion disk due to spin-down of a rapidly rotating black hole will enhance the disk radiation [5, 6]. Then this may be relevant to the observational result.

Though it is possible to construct stationary magnetospheric models representing the magnetic connection (e.g., see [7, 8, 9] for vacuum and force-free models with disk currents), the stability of such a configuration is not confirmed. In fact, recent numerical simulation of general relativistic magnetohydrodynamics (GRMHD) rather claim that the magnetic connection should be disrupted to produce open field lines threading the event horizon and extending to infinity [10, 11, 12]. Such a change of configuration of magnetic field lines can develop turbulent disturbances in the inner magnetospheric region, and the Poynting flux of strongly disturbed electromagnetic fields may propagate toward the equatorial plane to illuminate the disk surface. The subsequent dissipation of the supplied electromagnetic energy inside the disk should contribute to a disk heating. Hence, as a possible mechanism of energy transport to the disk we would like to pay our attention to the process of disk illumination caused by persistent excitation of electromagnetic disturbances in the black hole-disk system. However, using the superradiance, the process of energy transport to the disk have been never studied.

2 Superradiance in the black hole-disk system

In general, the injected electromagnetic disturbances should be scattered away to infinity, or absorbed by a black hole. Here we are not interested in the scattered outgoing part. We rather consider absorption by a thin disk, which corresponds to the boundary condition that the energy flux is transported to the equatorial plane both from the upper side and from the lower one. Of course, the exact analysis based on GRMHD is required to study the time evolution of electromagnetic fields in black hole magnetospheres.

[1]E-mail:kobayashi@gravity.phys.nagoya-u.ac.jp
[2]E-mail:onda@gravity.phys.nagoya-u.ac.jp
[3]E-mail:atomi@gravity.phys.nagoya-u.ac.jp

Nevertheless, we focus on the analysis of the vacuum Maxwell equations under the disk boundary condition as a first step to approach the problem of disk illumination. This is because our main purpose is to reveal the superradiance effect in Kerr background geometry which transports the energy from a central black hole to "a surrounding disk". If there exists no disk, the efficiency of superradiance of vacuum electromagnetic waves to amplify the energy radiated away to infinity well-known [13]. We expect that such an amplification can also occur in the process of disk illumination, by which a hot spot may appear on the disk surface near the inner edge.

3 Kerr-Schild formalism

To treat vacuum electromagnetic fields in the disk-black hole system, it is convenient to use the Kerr-Schild formalism [14] for solving the Einstein-Maxwell equation. If this formalism is applied to obtain electromagnetic perturbations on Kerr background, it is known that all the field components are simply derived by two arbitrary complex functions ψ and ϕ [15], where arbitrary complex functions ψ and ϕ are function of $Y = e^{i\tilde{\varphi}}\tan(\theta/2)$ and $\tau = \tilde{t} + r + ia\cos\theta$. Here, $\tilde{t}$ and $\tilde{\varphi}$ denote the time and the azimuthal angle in Kerr-Schild coordinates.

We consider some constraints to ψ and ϕ, which will be useful to see clearly the superradiant energy transport in the disk-black hole system. Recall that superradiant modes with frequency ω have the form $f(r,\theta)e^{i(m\varphi-\omega t)}$, if no disk boundary exists. This motivate us to assume that the ψ is written by the form

$$\psi(Y,\tau) \equiv \psi(X), \;\; X \equiv e^{-i\omega\tau}Y = e^{-i\omega\tau+i\tilde{\varphi}\tan(\theta/2)}, \tag{1}$$

Next, to impose the similar constraint on ϕ, let us consider an energy flux vector $\mathcal{E}^\mu$ defined in the Boyer-Lindquist frame as

$$\mathcal{E}^\mu \equiv -T^\mu_{\ t}, \tag{2}$$

where $T_{\mu\nu}$ is the stress-energy tensor of electromagnetic field. Considering energy extraction on the horizon, we impose the constraint on ϕ written by

$$\phi(Y,\tau) = e^{-i\omega\tau}\left[(r_{\rm H}+ia)i\omega + 1\right]\frac{\psi_{,X}}{r_{\rm H}}, \tag{3}$$

where $r_{\rm H}$ is the horizon radius. This means that the energy extraction may be more efficient at an intermediate region between the pole and the equator, producing a hot spot on the disk surface slightly apart from the horizon through the propagation of the Poynting flux. For example, we obtain the electromagnetic component written by Boyer-Lindquist coordinate system as follows

$$F_{tr} = \mathrm{Re}\left[\frac{\psi}{(r+ia\cos\theta)^2} + \frac{a}{\Delta}\frac{iX\psi_{,X}}{2r_{\rm H}(r+ia\cos\theta)}K(r,\theta)\right], \tag{4}$$

$$F_{t\theta} = \mathrm{Re}\left[-\frac{ia\sin\theta\psi}{(r+ia\cos\theta)^2} + \frac{X\psi_{,X}}{r_{\rm H}(r+ia\cos\theta)\sin\theta}K(r,\theta)\right], \tag{5}$$

$$F_{t\varphi} = \mathrm{Re}\left[\frac{iX\psi_{,X}}{2r_{\rm H}(r+ia\cos\theta)}K(r,\theta)\right], \tag{6}$$

$$F_{\theta\varphi} = \mathrm{Re}\left[-\frac{i(r^2+a^2)\sin\theta\psi}{(r+ia\cos\theta)^2} + \frac{a\sin\theta X\psi_{,X}}{r_{\rm H}(r+ia\cos\theta)}K(r,\theta)\right], \tag{7}$$

$$F_{r\varphi} = \mathrm{Re}\left[\frac{a\sin^2\theta\psi}{(r+ia\cos\theta)^2} + \frac{r^2+a^2}{\Delta}\frac{iX\psi_{,X}}{2r_{\rm H}(r+ia\cos\theta)}K(r,\theta)\right], \tag{8}$$

$$F_{r\theta} = \frac{\Sigma}{\Delta\sin\theta}\mathrm{Re}\left[\frac{X\psi_{,X}}{r_{\rm H}(r+ia\cos\theta)}K(r,\theta)\right], \tag{9}$$

where $\Delta = (r^2+a^2)^2 - 2Mr$, $K(r,\theta) \equiv (r-r_{\rm H}) + is\cos\theta(1-\omega/\Omega(r))$, $\Omega(r) \equiv a/(rr_{\rm H}) + a^2$, and then $\Omega_{\rm H} \equiv \Omega(r_{\rm H})$ is the angular velocity of the black hole.

4 Disk boundary conditions

In the Kerr-Schild formalism, the electromagnetic fields are described by the only two arbitrary complex functions. It is well-known that any complex function which is not a constant cannot be regular every where on the complex plane. We will assume the existence of a branch cut in ψ placed on the complex X-plane, which corresponds to the existence of a disk current on the equatorial plane $\theta = \pi/2$. This means that the components $F_{t\theta}$, $F_{\theta\phi}$, and $F_{r\theta}$ (namely, the imaginary part of ψ and the real part of $X\psi_{,X}$) become discontinuous at $\theta = \pi/2$

5 Distribution of electromagnetic energy flux

Now let us discuss the energy flux distribution given by the electromagnetic fields. The energy flux vectors are defined by Eq. (2). Note that the complex variable X in ψ is oscillatory with respect to the Kerr-Schild time $\tilde{t}$ (as well as the azimuthal angle $\tilde{\varphi}$). Then, the energy flux vector $\mathcal{E}^\mu$ contains oscillatory terms. To estimate a real efficiency of the energy transport, we must consider the time averaged quantities such that

$$\langle A\rangle \equiv \frac{\omega}{2\pi}\int_0^{2\pi/\omega} A d\tilde{t}. \tag{10}$$

Furthermore, to illustrate the distribution of electromagnetic energy flux, the complex functions $\psi(X)$ is assumed to be

$$\psi(X) = \psi_0\left[(X^{-2}+X^2)^{3/2} - X^{-3} - X^3\right]^2 \tag{11}$$

where ψ_0 is a real constant.

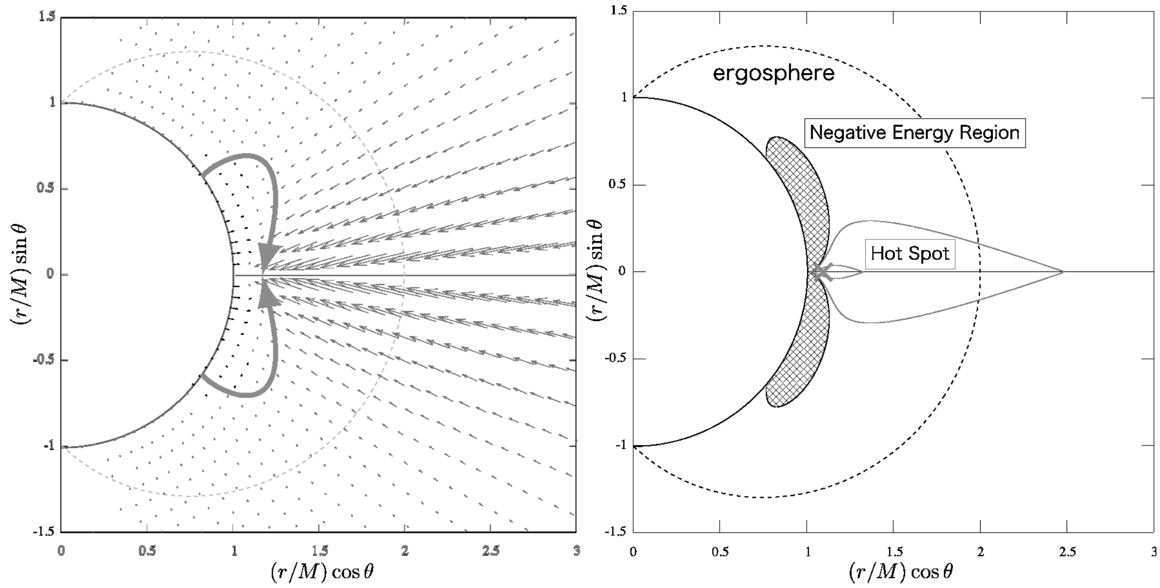

Figure 1: Left-hand side:Time-averaged energy transport in the disk-black hole system. The electromagnetic disturbance is given by Eq. (11) with the wave frequency $\omega \simeq 0.76238\Omega_{\rm H}$, an the spin parameter a is chosen as $a = 0.99999M$. The arrows show the poloidal energy flux with the component $\langle\mathcal{E}^r\rangle$ and $\sqrt{\Delta}\langle\mathcal{E}^\theta\rangle$, which are normalized by ${\psi_0}^2/M^4$. The dark gray and light gray arrows correspond to the flux with $\langle\mathcal{E}^r\rangle > 0$ and $\langle\mathcal{E}^r\rangle < 0$, respectively. Right-hand side:Contour of time-averaged energy density for the electromagnetic disturbance given by Eq. (11). The wave frequency and the spin parameter are assumed to be $\omega \simeq 0.76238\Omega_{\rm H}$ and $a = 0.99999M$. The negative energy region is shown as the shaded region. The position of the maximum energy density $\langle\mathcal{E}^t\rangle_m$ is at $r \simeq 1.0535M$ shown as cross point. The surface giving $\langle\mathcal{E}^t\rangle = \langle\mathcal{E}^t\rangle_m/2$ (which may be explained as the boundary of the hot spot) is shown by the short gray line.

In Fig. 1, it is easy to see that energy extracted from the black hole, extracted energy transported to the disk, and then energy deposited to the disk region. If the deposited electromagnetic energy density dissipates to heat up the disk, a hot spot is expected to appear on the inner part of the disk.

6 Summary

The superradiance process is confirmed in disk-black hole system. Then, the rotational energy is extracted from the black hole, and transported to the disk. Finally, the High energy density region is formed in the inner part of disk near the horizon.

References

[1] J. Wilms, C. S. Reynolds, M. C. Begelnar, J. Reeves, S. Molendi, R. Staubert, and E. Kendziorra, Mon. Not. R. Astron. Soc. **328**, L27 (2001).

[2] L.-X. Li, ApJ **567**, 463 (2002a).

[3] M. H. P. M. van Putten and A. Levinson, ApJ **584**, 937 (2003).

[4] R. D. Blandford and R. L. Znajek, Mon. Not. R. Astron. Soc. **179**, 433 (1977).

[5] L.-X. Li, A& A **392**, 469 (2002b).

[6] Z.-M. Gan, D.-X. Wang, and Y. Li, Mon. Not. R. Astron. Soc. **376**, 1695 (2007).

[7] A. Tomimatsu and M. Takahashi, ApJ **552**, 710 (2001).

[8] D. A. Uzdensky, ApJ **603**, 652 (2004).

[9] D. A. Uzdensky, ApJ **620**, 889 (2005).

[10] J. C. McKinney and C. F. Gammie, ApJ **611**, 977 (2004).

[11] J. C. McKinney, Mon. Not. R. Astron. Soc. **368**, 1561 (2006).

[12] S. Koide, T. Kudoh, and K. Shibata, Phys. Rev. D **74**, 044005 (2006).

[13] S. A. Teukolsky and W. H. Press, ApJ **193**, 443 (1974).

[14] G. C. Debney, R. P. Kerr, and A. Schild, J. Math. Phys. **10**, 1842 (1969).

[15] A. Burinskii, E. Elizalde, S. R. Hildebrandt, and G. Magli, Grav. Cosmol. **12**, 115 (2006), `astro-ph/0610036`.

Analysis of Non-Axisymmetric Shock Stability in Black Hole Geometry by Numerical Simulation and Linear Analysis

Hiroki Nagakura[1] and Shoichi Yamada[2]

[1]*Science and Engineering, Waseda University, 3-4-1 Okubo, Shinjuku, Tokyo 169-8555, Japan*
[2]*Advanced Research Institute for Science and Engineering, Waseda University, 3-4-1 Okubo, Shinjuku, Tokyo 169-8555, Japan*

Abstract

We study about the multidimensional stability of standing shock waves in advection-dominated accretion flows into a Schwarzschild black hole by 2D general relativistic hydrodynamical simulations and linear analysis in the equatorial plane. We demonstrate that the accretion shock is stable against axisymmetric perturbations but becomes unstable to non-axisymmetric perturbations. The results of dynamical simulations are good consistent with linear analysis such as stability, oscillation and growing timescale. However, our analysis does not support previous work suggestion which is the instability mechanism is based on Papaloizou-Pringle type. It seems due to the wavelength of perturbation is too large for discussion about reflection point. In non-linear phases, it is found not only short-term random fluctuations by turbulent motions but also quasi periodic oscillations taking place on longer time scales in the latter phase. We discuss possible implications of Black Hole SASI for Quasi Periodic Oscillation (QPO) and central engine for Gamma Ray Bursts (GRB).

1 Introduction

Many theoretical astrophysicists have long studied about the accretion flow with a shock. Hydrodynamical instabilities of shocked accretion flows may explain the time variability of the emission from many black hole candidates, since the shock wave is a good candidate mechanism for transforming potential gravitational energy into radiation.

The multiple critical points are essential conditions for existence standing shocks. In order to produce them, the flow need to have adequate injection parameters such as specific angular momentum and Bernoulli constant. Under setting adequate conditions, we can generally obtain two possible shock locations. However, as is well known for a long time, inner shock is already unstable against radial perturbations. Recently, [1, 2] pointed out by linear analysis that the outer shock wave is also unstable to non-radial perturbations. He argued that the advection-acoustic cycle could be responsible for the instability. In this mechanism the velocity and entropy fluctuations initially generated at the shock are advected inward, producing pressure perturbations, which then propagate outward and reach the shock and generate new entropy and velocity fluctuations there, thus repeating the cycle with an increased amplitude. The so-called standing accretion shock instability or SASI is currently attracting much attention as Black Hole Accretion Disk and also Supernova context.

The non-axisymmetric shock stability also has a focus of much attention. The author of [3] performed 2D simulations of a shocked adiabatic flow by using pseudo-Newtonian potential and found a non-axisymmetric instability. To investigate the mechanism of this instability, [4, 5] performed linear analysis under isothermal flow or adiabatic flow, respectively. They concluded that the mechanism seems to be Papaloizou-Pringle type instability which is based on the cycle of acoustic waves between the corotation radius and the shock point.

As mentioned above, many efforts have been made for clarifying non-radial (including non-axisymmetric) instability, but the complete understanding of these mechanisms are still uncertain. It is because the background accretion structure, which strongly affect to clarify the instability mechanism, is completely different and complex in each case. For example, in supernova context, since the shock behavior is

[1]E-mail:hiroki@heap.phys.waseda.ac.jp
[2]E-mail:shoichi@heap.phys.waseda.ac.jp

strongly affected by neutrino luminosity, we should take into account them adequately. On the other hand, in black hole accretion disks, gravitational fields should be treated appropriately, because it is one of the main factor to determine flow structure such as sonic points and shock points. However complete general relativistic hydrodyanamical flow is much complex than Newton gravity, thus, the shock stability has been investigated only under Newtonian or approximate general relativistic (GR) treatment Thus far, there is no self-consistent work for studying non-radial shock stability under fully GR treatment.

In the present research, we performed the first time analyzing non-axisymmetric shock stability in the advection-dominated accretion flows into a Schwarzschild black hole under fully general relativistic hydrodynamical treatment. In so doing, we consider only the equatorial plane, assuming that θ component of four-velocity (u^θ) and vertical differentiation are negligible. We investigate the stability of shock by using both linear approach and non-linear dynamical simulations. We show that the shock is indeed unstable against non-axisymmetric perturbations and forms a spiral arm structure as the instability grows. We analyze each phases and discuss the instability mechanisms by comparing with previous works. Besides, we also discuss possible implications of our findings for GRBs: the fluctuations in the jet that will produce the internal shocks and black hole QPO which can be also explained by the shock quasi-periodic oscillation and rotation.

2 Basic Equations and Initial Conditions

The basic equations are relativistic continuity, energy momentum tensor conservations.

$$(\rho_0 u^\mu)_{;\mu} = 0 \quad (1)$$
$$(T^{\mu\nu})_{;\nu} = 0 \quad (2)$$

in Schwarzschild geometry. As all of our calculations, we employed a Γ-law EOS. The procedure for constructing initial data which is steady axisymmetric accretion flow with standing shock is as follows.

First we set adequate injection parameters for multiple critical points, then we solve an ordinally diferential equation numerically from each critical points. After making two transonic solutions, we search locations for satisfying relativistic Rankine-Hugonit relations. As mentioned already, the two possible locations are generally obtained but we only consider the outer one because it is stable against axisymmetric perturbations, in contrast inner one is unstable. For convincing this fact, we performed axisymmetric shock stability analysis by linear perturbed method and dynamical simulations. We observed that outer shock is truly axisymmetrically stable which are obtained by both methods. Moreover, it is interested that perturbation is added against inner shock, then this shock goes down to black hole or approach to outer shock location and eventually stop there. According to this fact, we conclude that the outer shock is strong axisymmetric stable, indeed.

3 Dynamical Simulations and Basic Behavior

The dynamical simulations for the growth of the initial perturbations were computed with a multi-dimensional general relativistic hydrodynamics code, which is based on a recent modern technique, the so-called high-resolution central scheme. We use kerr-schild coordinates to evolve the system. The computational domain is a part of the equatorial plane with $1.5M_* \le r \le 200M_*$ and computing time is about $t = 6 \times 10^4 M_*$ where M_* indicates black hole mass. We employed $600(r) \times 60(\phi)$ grid points in every cases which radial grids are chosen as non-uniform grids. The most inner resolution is $\Delta r = 0.1M_*$ and grid spacing increases geometrically toward outer boundary by 0.34% per zone.

The procedure of adding initial perturbations are determined by linear analysis results in order to extract purely single mode and node in linear evolution phase. Tnanks to perturbed methods, we can figure out that not only distinguish each mode is stable or unstable but also radial and azimuthal distribution of perturbed quantities. In this paper, we only explain about one Model whose Bernoulli constant and specific angular momentum are set as 1.004 and $3.43M_*$, respectively. According to linear analysis, this shock is unstable against $m = 1$ mode perturbations. We choose the most unstable eigenfrequency case in $m = 1$ mode and determine the initial perturbed quantities and the initial shock displacement is set as 1%.

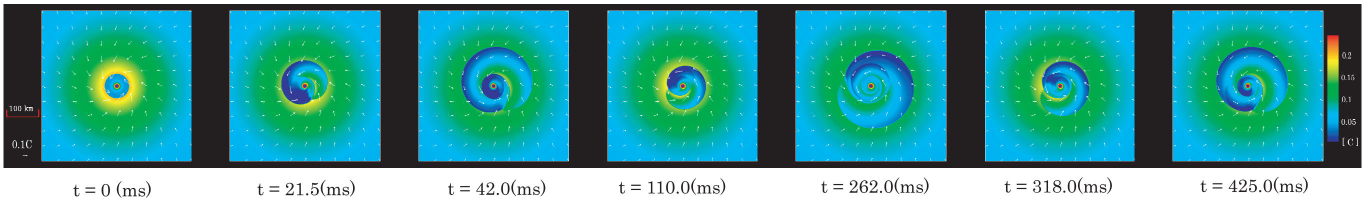

Figure 1: Velocity evolution for Standard Model. Color counter means the magnitude of radial velocity. Side of red is supersonic and side of blue indicates subsonic. The arrow represents the velocity magnitud and directions. The region of center(blue) indicates the black hole. As shown this figure, due to the shock existence, the velocity is decelerate from supersonic to subsonic. However, because the azimuthal velocity doesn't change so much between pre and post shock region, the arrow direction become along the azimuthal direction at post shock location.

Figure 1 shows that the example of system evolutions about this Model. The time and radius which are shown in cgs units correspond to $M_* = 3M_{sun}$ case. At first, the shock starts to fluctuate and rotation pattern can be found. This pattern rotates to same directions of back ground matter rotations. Besides, the shock not only rotates but also starts to increase axisymmetrically. After several revolutions, the spiral arm structure develops and the more complex shocked features are constructed. In these non-linear regime, some shocks generate and are interacted each other by collision. The flow becomes new axially asymmetric configure with dominat $m = 1$ mode in non-linear phase. In other cases, the basic evolutional path is similar but the growth rate and oscillation period and growth timescale are quantatively large difference. The discussion of these results are done in following paper [6].

4 Comparison with linear analysis

For clarifying instability mechanisms and confirmation of dynamical simulations, we implement the linear perturbed analysis. When we solve the linearlized equations about 1 and 2, we have to set boundary conditions which locate at shock surface and inner sonic point. At shock surface, the boundary conditions are set as pre-shock region doesn't fluctuate. On the other hand, the inner sonic point, we impose the regularity condition at this point.

Thanks to solving linearlized equations under these boundary conditions, we find out that the unstable eigenfrequencies in each mode. We obtain that about Standard Model, the oscillation period is about 3.7 ms, the growth period is about 20 ms in the most unstable eigenfrequency of $m = 1$ mode. As shown in Figure 2, the dynamical simulation shows good agreement with oscillation and growth time scale of $m = 1$ mode until 10 ms. After this time, the non-linear coupling can not be ignored (please see Figure 3 which shows that $m = 0$ evolution), thus it starts to line off gradually. According to this result, we confine that our numerical simulation is correct and the shock is really unstable against non-axisymmetric perturbations.

Besides, linear analysis gives us information that counter-rotating modes $m < 0$ are stable. Actually our dynamical simulations demonstrate that the shock pattern rotates same directions of background matter rotation. It means that the rotation stabilize the counter rotating mode.

5 Summary and Conclusions

The main results of the present work are as follows

1. As mentioned already, the standing shock is generally unstable against non-axisymmetric perturbations, and a spiral arm structure can be constructed. This is typically one-armed, which indicates that the dominant mode in the non-linear phase is m=1.

2. In the linear phase, the dynamical simulations are consistent with the linear analysis in such features as stability, oscillation timescale and growth timescale. The direction of deformed shock pattern is

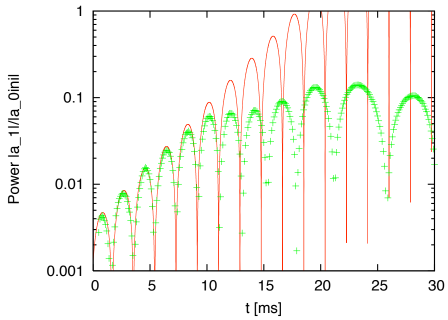

Figure 2: Comparison of linear analysis and dynamical simulation results in linear growing phase. The red line indicates the expected evolution of growing $m = 1$ mode by linear analysis, and green dots indicate that calculation from GRHD simulation results.

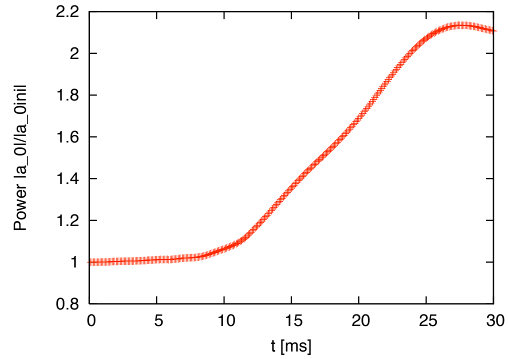

Figure 3: The evolution of $m = 0$ mode until 30 ms in M1 case.

also consistent woth the linear analysis.

3. The growth of axisymmetric mode is also induced by the non-axisymmetric instability. It seems to be quasi-periodic in longer timescale. Other higher modes also have each specific frequency period. In the non-linear phases, due to the axisymmetric growth, these oscillation periods become slightly longer than expected in the linear analysis.

4. Even though strong perturbations are added initially, the shock system isn't disrupted. Thus, if the outer boundary continues to satisfy the shock producing conditions, the shock would remain in a quasi-steady state.

5. The effects of higher modes to a axisymmetric mode become weaker even though the higher mode growth rate is larger than the lower modes.

6. The reflection point can not be identified unambiguously in the present work. It is because the wavelength of perturbations is much longer than the scale height. Thus, the Papaloizou-Pringle type Mechanism which is cycle between corotation point and shock doesn't always happen. Actually the timescale of acoustic cycle are different from their growth timescale.

7. The Black Hole SASI can contribute to QPO. Moreover, it may have an implication for GRB since it is a nature source of fluctuations for internal shocks.

We conducted more systematic investigations, such as initial mode or backgournd dependency.etc. For more details, please see [6]

References

[1] Foglizzo, T., 2001 [arXiv:astro-ph/0101056]

[2] Foglizzo, T., 2002 [arXiv:astro-ph/0206274]

[3] Molteni, D., Toth, G. and Kuznetsov, O. A., 1999 Astrophys. J. **516**, 411

[4] Gu, Wei-Min and Foglizzo, T. 2003, A & A 409, 1-7

[5] Gu, Wei-Min and Lu, Ju-Fu 2005 MNRAS, 365, 2, 647-652 [arXiv:astro-ph/0710.219v1]

[6] Nagakura, H., Yamada, S. in preparation

On cylindrically symmetric gravitational waves in expanding spacetimes

Makoto Narita[1]

Department of Mathematics, National Taiwan University, No.1, Roosevelt Rd. Sec. 4, Taiwan[2]

Abstract

We show a global existence theorem for the vacuum Einstein equations with cylindrical symmetry. Also Kasner-like solutions near initial singularity are constructed. These results support the validity of the strong cosmic censorship.

One of the most important problems in general relativity is the understanding of the global behavior of solutions to the Einstein equations. It is known that the Einstein equations lead to the formation of singularities. Typical examples are given by the Friedman-Robertson-Walker (spatially homogeneous and isotropic) spacetime, which evolves from the "big bang" singularity, and the Schwarzschild (stationary and spherically symmetric) spacetime, which has the central singularity. Then, the question of whether singularities generally occur in physical spacetimes or not, has been an important question for year. Penrose and Hawking have given some answers by their *singularity theorems* [4]. Rephrased in the words of the initial value problem, the question is that of the timelike and null geodesic completeness of the maximal future Cauchy development. The singularity theorems give us negative answers, i.e. generic spacetimes are timelike or null geodesically incomplete.

If the singularities can be seen, this means violation of predictability, because we cannot put appropriate boundary conditions on the singularities. Since predictability is a fundamental requirement of classical physics, it seems reasonable to require it to be valid whole spacetime. This implies that physical spacetimes should be globally hyperbolic in Leray's sense. Motivated by these considerations, Penrose proposed the strong cosmic censorship conjecture:

Conjecture 1 (Klainerman [6]) *Generic Cauchy data sets have maximal Cauchy developments which are locally inextendible as Lorentzian manifolds.*

This is one of the most important and unsolved questions in classical general relativity. We need two steps to prove the validity of the conjecture: (1) show global existence theorems for solutions to the Einstein(-matter) equations in an appropriate time coordinate, (2) analyze asymptotic behavior of the solutions and show inextendiblity of spacetime manifold. Thus, an important aspect of this strong cosmic censorship conjecture is relation to the global Cauchy problem for the Einstein(-matter) equations.

Unfortunately, the problem of proving global existence theorems for the full Einstein-matter equations is beyond the reach of the mathematics presently available. To make some progress, it is necessary to concentrate on simplified models. The most common simplifications are to look at solutions with various types of symmetry and solutions for small data.

Recently, new spacetimes which describe cylindrical gravitational waves in expanding universe are proposed [3]. The metric of the (generalized) spacetimes is given by

$$g = -e^{2(\eta-U)}dt^2 + e^{2(\eta-U)}dr^2 + e^{2U}(dx + Ady)^2 + e^{-2U}R^2dy^2, \tag{1}$$

where $\partial/\partial x$ and $\partial/\partial y$ are Killing vector fields generating the $U(1)\times R$ group action, and η, U, A and R are functions of $t \in (0,\infty)$ and $r \in (0,\infty)$. These new spacetimes would model localized inhomogeneities in Big Bang cosmology. Now we put a gauge condition, $R = rt$ [3]. The system of the evolution part of the Einstein equations is equivalent with the following wave maps $u : (M^{2+1}, G) \mapsto (N^2, h)$:

$$S_{\rm WM} = \int dtdr\sqrt{-G}G^{\alpha\beta}h_{AB}\partial_\alpha u^A\partial_\beta u^B, \tag{2}$$

[1] E-mail:narita@math.ntu.edu.tw

[2] Present address: Department of Integrated Arts and Science, Okinawa National College of Technology, 905, Aza-Henoko, Nago, 905-2192, Japan, E-mail: narita@okinawa-ct.ac.jp

where

$$G = -dt^2 + dr^2 + t^2 r^2 d\psi^2, \qquad h = dU^2 + \frac{e^{4U}}{4r^2 t^2} dA^2.$$

One of our main results is to show existence of global solutions for the above system and by using this we can prove the following theorem:

Theorem 1 *Let $(\mathcal{M}, g)$ be the maximal Cauchy development of C_0^∞ initial data for the cylindrically symmetric system. Then, $\mathcal{M}$ can be covered by Cauchy surfaces of constant time t with each value in the range $(0, \infty)$. Moreover, this maximal Cauchy development is timelike future geodesically complete, hence inextendible into the future direction.*

The method of the proof is the standard energy estimate (so-called *light cone estimate*). Theorems of Christodoulou-Tahvildar-Zadeh are also used [1, 2].

Another result is to construct Kasner-like (asymptotically velocity-terms dominated (AVTD)) solutions as $t \to 0$. To do this we will apply the Fuchsian algorithm developed by Kichenassamy and Rendall [5] to our system. This algorithm consists of the following steps:

- Decompose the unknown into a prescribed singular part and a regular part $\mathcal{U}$.
- If the system can be written as a Fuchsian system of the form

$$t\partial_t \mathcal{U} + N(x)\mathcal{U} = t^\alpha f(t, x, \mathcal{U}, \partial_x \mathcal{U}), \qquad \alpha > 0, \tag{3}$$

one can use the following theorem:

Theorem 2 *(Kichenassamy-Rendall [5]) Assume that N is an analytic matrix near $x = 0$ such that there is a constant C with $\| \sigma^N \| \leq C$ for $0 < \sigma < 1$, where σ^N is the matrix exponential of $N \ln \sigma$. Also, suppose that f is a locally Lipschitz function of $\mathcal{U}$ and $\partial_x \mathcal{U}$ which preserves analyticity in x and continuity in t. Then, the Fuchsian system (3) has a unique solution in a neighborhood of $x = 0$ and $t = 0$ which is analytic in x and continuous in t, and tends to zero as $t \to 0$.*

Remark 1 *The sufficient condition for N is non-negativity of eigenvalues of N.*

Now, the Geroch-Ernst potential, given by

$$\dot{A} = -Re^{-4U} w', \qquad A' = -Re^{-4U} \dot{w},$$

will be used for the convenience of computation. From this and replacing U by $z/2$, the evolution part of the Einstein equations become

$$\begin{aligned} D^2 z - t^2 \Delta z &= -e^{-2z} \left((Dw)^2 - t^2 (\nabla w)^2 \right), & (4) \\ D^2 w - t^2 \Delta w &= 2 \left(Dz Dw - t^2 \nabla z \nabla w \right), & (5) \end{aligned}$$

where

$$D := t\partial_t, \qquad \Delta := \partial_r^2 + \frac{1}{r}\partial_r + \frac{1}{r^2}\partial_\phi^2, \qquad \nabla f \nabla g := \partial_r f \partial_r g + \frac{1}{r^2} \partial_\phi f \partial_\phi g.$$

To avoid a coordinate singularity at $r = 0$, the Cartesian coordinate will be used:

$$x = r\cos\phi, \qquad y = r\sin\phi, \qquad \Delta := \partial_x^2 + \partial_y^2, \qquad \nabla f \nabla g := \partial_x f \partial_x g + \partial_y f \partial_y g.$$

Note that the form of the evolution equations does not change. Dropping the spatial derivative parts from equations (4) and (5) and solving the equations, we have the following formal solutions:

$$\begin{aligned} z(t,x,y) &= k(x,y)\ln t + \phi(x,y) + t^\epsilon u(t,x,y), & (6) \\ w(t,x,y) &= w_0(x,y) + t^{2k(x,y)} \left(\psi(x,y) + v(t,x,y) \right), & (7) \end{aligned}$$

where $\epsilon > 0$ is a small constant. Next, the Fuchsian system (3) for u and v will be reduced with the following conditions: $\alpha = 1$, $f = f(t, x, y, \mathcal{U}_i)$ is a regular function and

$$\begin{aligned} \mathcal{U} &= (\mathcal{U}_1, \mathcal{U}_2, \mathcal{U}_3, \mathcal{U}_4, \mathcal{U}_5, \mathcal{U}_6, \mathcal{U}_7, \mathcal{U}_8) \\ &:= (u, Du, t\partial_x u, t\partial_y u, v, Dv, t\partial_x v, t\partial_y v) \end{aligned} \tag{8}$$

$$N = \begin{bmatrix} 0 & -1 & 0 & 0 & 0 & 0 & 0 & 0 \\ \epsilon^2 & 2\epsilon & 0 & 0 & 0 & 0 & 0 & 0 \\ 0 & 0 & 0 & 0 & 0 & 0 & 0 & 0 \\ 0 & 0 & 0 & 0 & 0 & 0 & 0 & 0 \\ 0 & 0 & 0 & 0 & 0 & -1 & 0 & 0 \\ 0 & 0 & 0 & 0 & 0 & 2k & 0 & 0 \\ 0 & 0 & 0 & 0 & 0 & 0 & 0 & 0 \\ 0 & 0 & 0 & 0 & 0 & 0 & 0 & 0 \end{bmatrix}, \quad 0 < \epsilon < \min\{2k, 2-2k\}. \tag{9}$$

By using the theorem 2, we have

Theorem 3 *Suppose that k, ϕ, w_0 and ψ are real analytic functions of r and $0 < \epsilon < \min\{2k, 2-2k\}$. Then, there is a unique solution of the Einstein equations (4) and (5) of the form (6) and (7) in a neighborhood of $t = 0$ such that u and v tend to zero as $t \to 0$.*

Thus, solutions become AVTD (Kasner-like) ones near singularities at $t = 0$. In this case, the Kretschmann invariant $R_{\mu\nu\lambda\delta}R^{\mu\nu\lambda\delta}$ blows up as $t \to 0$, thus our spacetime is inextendible into the past direction if the solution (6) and (7) is generic. Combining our two theorems, it has been verified the validity of the strong cosmic censorship conjecture for our spacetimes.

References

[1] D. Christodoulou and A. S. Tahvildar-Zadeh, *On the regularity of spherically symmetric wave maps*, Comm. Pure Appl. Math. **46** (1993), 1041-1091.

[2] D. Christodoulou and A. S. Tahvildar-Zadeh, *On the asymptotic behavior of spherically symmetric wave maps*, Duke Math. J. **71** (1993), 31-69.

[3] R. H. Gowdy and B. D. Edmonds, *Cylindrical gravitational waves in expanding universe: Models for waves from compact sources*, Phys. Rev. **D75** (2007), 084011.

[4] S. W. Hawking and G. F. R. Ellis, *The large scale structure of space-time*, Cambridge Monographs on Mathematical Physics, (Cambridge University Press, London, 1973).

[5] Rendall, A. D. and Kichenassamy, S., *Analytic description of singularities in Gowdy spacetimes*, Class. Quantum Grav. **15**, (1998) 1339-1355.

[6] S. Klainerman, *Mathematical challenges of general relativity*, in Proceedings of the Ninth Marcel Grossmann Meeting, edited by V. G. Gurzadyan, R. T. Jantzen and R. Ruffini, (World Scientific), 28-43, (2002).

Circular Polarization of Primordial Gravitational Waves due to Stringy Effects

Masaki Satoh[1], Sugumi Kanno[2] and Jiro Soda[3]

[1,3]*Department of Physics, Kyoto University, Kyoto 606-8501, Japan*
[2]*Department of Physics, McGill University, Montréal, QC H3A 2T8, Canada*

Abstract

We study a mechanism to produce the circular polarization of primordial gravitational waves. The circular polarization is generated during the super-inflation driven by the Gauss-Bonnet term in the string-inspired cosmology. The instability in the tensor mode caused by the Gauss-Bonnet term and the parity violation due to the gravitational Chern-Simons term are the essential ingredients of the mechanism. This circularly polarized signal may be an interesting target for observations to verify the superstring theory.

1 Introduction

It is widely believed that the most promising candidate for an unified theory including quantum gravity is superstring theory. It is therefore interesting to prove or disprove superstring theory from an observational point of view. To this end, primordial gravitational waves have been considered as the most efficient probe, since the gravitational waves can carry the information of the universe at the Planck time.

In this paper, we focus on a robust prediction of superstring theory, namely, the parity violation due to the gravitational Chern-Simons term. In fact, the Chern-Simons term appears in the Green-Schwarz mechanism which is necessary to cancel the anomaly in the theory [1]. It also arises as a string correction [2]. Intriguingly, the existence of the Chern-Simons term can be probed by the primordial gravitational waves. This is because the Chern-Simons term can generate the circular polarization of gravitational waves through the parity violation. While it is difficult to find other effects to produce the circular polarization of primordial gravitational waves. Hence, if we detect the circular polarization in the primordial gravitational waves, it would be a strong indication of existence of the Chern-Simons term in the early universe. Thus, it can be interpreted as an evidence of superstring theory.

According to several works [3], it turned out that, however, there exists no observable amount of circular polarization of gravitational waves, in the standard slow-roll inflation. The point is that the Chern-Simons term is not the only term that could be induced by the stringy corrections. There is another term, the so-called Gauss-Bonnet term. Taking into both term, we can expect a different result. This is because there exists an instability in gravitational wave modes during the super-inflationary stage [5]. It is this instability that generates the circular polarization of primordial gravitational waves. In fact, we show the primordial gravitational waves are fully polarized due to the Gauss-Bonnet term [6].

2 Basic equations in Gauss-Bonnet-Chern-Simons Gravity

We start with the action motivated from string theory given by [4]

$$S = \frac{1}{2}\int \mathrm{d}^4x\sqrt{-g}R - \int \mathrm{d}^4x\sqrt{-g}\left[\frac{1}{2}\nabla^\mu\phi\nabla_\mu\phi + V(\phi)\right] - \frac{1}{16}\int \mathrm{d}^4x\sqrt{-g}\xi(\phi)R^2_{\mathrm{GB}} + \frac{1}{16}\int \mathrm{d}^4x\sqrt{-g}\omega(\phi)R\tilde{R}\ , \tag{1}$$

[1]E-mail:satoh@tap.scphys.kyoto-u.ac.jp
[2]E-mail:sugumi@hep.physics.mcgill.ca
[3]E-mail:jiro@tap.scphys.kyoto-u.ac.jp

where the first term of action is the Einstein-Hilbert term and g is the determinant of the metric $g_{\mu\nu}$. We have set the unit $8\pi G = 1$. In the above action (1), we have taken into account the Gauss-Bonnet term $R^2_{\rm GB}$ and Chern-Simons term $R\tilde{R}$

$$R^2_{\rm GB} = R^{\alpha\beta\gamma\delta}R_{\alpha\beta\gamma\delta} - 4R^{\alpha\beta}R_{\alpha\beta} + R^2 \ , \quad R\tilde{R} = \frac{1}{2}\epsilon^{\alpha\beta\gamma\delta}R_{\alpha\beta\rho\sigma}R_{\gamma\delta}{}^{\rho\sigma} \ , \tag{2}$$

where $\epsilon^{\alpha\beta\gamma\delta}$ is the Levi-Civita tensor density. We have also allowed the coupling of the inflaton field both to the Gauss-Bonnet $\xi(\phi)$ and Chern-Simons terms $\omega(\phi)$. Otherwise, these topological terms vanish identically. It should be noted that, as is well known, the Chern-Simons term does not contribute to the dynamics of the isotropic and homogeneous universe. From now on, for simplicity, we consider a typical potential, $V = 1/2m^2\phi^2$.

2.1 Background spacetime

Let us consider the background spacetime with spatial isotropy and homogeneity. Then, the metric is given by

$$ds^2 = g_{\mu\nu}{\rm d}x^\mu {\rm d}x^\nu = a^2(\eta)\left[-d\eta^2 + \delta_{ij}{\rm d}x^i{\rm d}x^j\right] \ . \tag{3}$$

Here, we have also assumed the flat space and used the conformal time η. Taking the variations of the action (1), we have equations

$$3\mathcal{H}^2 = \frac{1}{2}\phi'^2 + \frac{1}{2}m^2a^2\phi^2 + \frac{3}{2a^2}\mathcal{H}^3\xi' \tag{4}$$

$$(2\mathcal{H}' + 3\mathcal{H}^2)\left(1 - \frac{1}{2a^2}\mathcal{H}\xi'\right) + \mathcal{H}^2\left(1 + \frac{\mathcal{H}}{2a^2}\xi' - \frac{1}{2a^2}\xi''\right) - m^2a^2\phi^2 = 0 \tag{5}$$

$$\phi'' + 2\mathcal{H}\phi' + \frac{3}{2a^2}\mathcal{H}^2\mathcal{H}'\xi_{,\phi} + m^2a^2\phi = 0, \tag{6}$$

where we have defined $\mathcal{H} = a'/a$. Here, the prime denotes the derivative with respect to the conformal time η.

In the presence of the Gauss-Bonnet term, the force due to the Gauss-Bonnet term becomes dominant for a large value of ϕ. If the scalar field start with a negative value, the force term accelerate the scalar field and makes the kinetic term dominant. Hence, the situation, $\mathcal{H}^2 \ll \phi'^2, m^2a^2\phi^2 \ll \phi'^2$, is realized. Thus, Eqs.(4) and (5) become

$$a^2\phi'^2 + 3\mathcal{H}^3\xi' = 0 \tag{7}$$

$$(2\mathcal{H}' + 3\mathcal{H}^2)\xi' + \mathcal{H}\left(\xi'' - \mathcal{H}\xi'\right) = 0 \ . \tag{8}$$

The scalar field ϕ rolls down from the negative side towards zero according to the above equations (7) and (8). Now, it is easy to solve Eqs.(7) and (8) as

$$\phi = -\sqrt{15/16}(-\eta)^{5/6} \ , \quad a(\eta) = (-\eta)^{-1/6} \ , \quad \mathcal{H} = \frac{1}{(-6\eta)} \ , \quad \eta < 0 \ . \tag{9}$$

We note that the super-inflation $H' > 0$ is realized in this phase. Here, $H = \mathcal{H}/a$ is the Hubble parameter. As the scalar field rolls down, the Gauss-Bonnet term decreases. Eventually, the conventional Hubble friction overcome the Gauss-Bonnet effect and the slow-roll inflation commences. A typical evolution of the spacetime is shown in Fig.1. In the super-inflationary phase $H' > 0$, the weak energy condition is violated. Hence, the system may show the instability. Of course, as you can see in Fig. 1, this instability is a transient one. This diagram shows that the super-inflationary phase will be followed by the standard phase where the Hubble parameter is decreasing.

2.2 Action for gravitational waves

Let us consider the tensor perturbation

$$ds^2 = g_{\mu\mu}{\rm d}x^\mu{\rm d}x^\nu = a^2(\eta)\left[-{\rm d}\eta^2 + (\delta_{ij} + h_{ij}){\rm d}x^i{\rm d}x^j\right] \ , \tag{10}$$

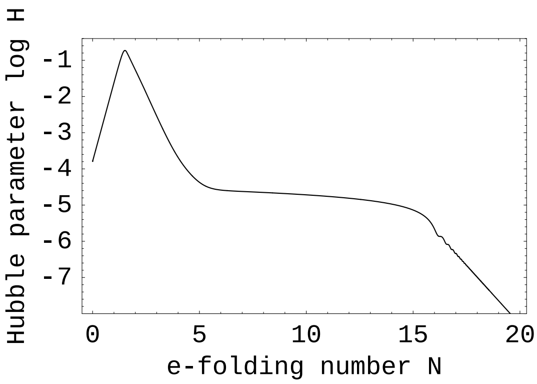

Figure 1: A typical evolution of the background spacetime is numerically calculated and displayed. A short period of the super-inflationary phase is followed by a long period of the slow-roll inflationary phase.

where h_{ij} satisfies the transverse-traceless conditions $h_{ij,j} = h_{ii} = 0$. We expand h_{ij} by plane waves

$$\frac{h_{ij}(\eta, \mathbf{x})}{\sqrt{2}} = \sum_{A=\mathrm{R,L}} \int \frac{\mathrm{d}^3 k}{(2\pi)^3} \psi^A_{\mathbf{k}}(\eta) \mathrm{e}^{i\mathbf{k}\cdot\mathbf{x}} p^A_{ij} \ , \tag{11}$$

here p^A_{ij} denotes polarization tensor for circular polarizations. Some calculations leads to the action for gravitational waves

$$S^{\mathrm{GW}} = \sum_{A=\mathrm{R,L}} \frac{1}{2} \int \mathrm{d}\eta \frac{\mathrm{d}^3 k}{(2\pi)^3} \left[|\mu'^A_{\mathbf{k}}|^2 - \left(1 + \frac{\mathcal{H}\xi'}{z_A^2} - \frac{\xi''}{2z_A^2} \right) k^2 |\mu^A_{\mathbf{k}}|^2 + \frac{z''_A}{z_A} |\mu^A_{\mathbf{k}}|^2 \right] , \tag{12}$$

where we have defined

$$z_A = a(\eta) \sqrt{1 - \frac{\mathcal{H}\xi'}{2a^2} - \lambda^A k \frac{\omega'}{2a^2}} \ , \qquad \lambda^{\mathrm{R}} = 1 \ , \quad \lambda^{\mathrm{L}} = -1, \tag{13}$$

and $\mu^A_{\mathbf{k}} \equiv z^A_{\mathbf{k}} \psi^A_{\mathbf{k}}$. Thus, the equation of motion becomes

$$(\mu^A_{\mathbf{k}})'' + \left[\left(1 + \frac{\mathcal{H}\xi'}{z_A^2} - \frac{\xi''}{2z_A^2} \right) k^2 - \frac{z''_A}{z_A} \right] \mu^A_{\mathbf{k}} = 0 \ . \tag{14}$$

The term z''_A/z_A can be interpreted as the effective potential. The coefficient of the wavenumber k may be interpreted as the square of the speed of sound waves.

3 A mechanism to produce Circular Polarization

Eq.(14) show that the speeds of sound for gravitational waves are different for right- and left-handed waves. And if the square of the speed of sound becomes negative, exponentially growing mode appears. Hence, we can expect that this growing mode appears only in one-handed waves. Actually, in sub-horizon scale, $\mathcal{H} \ll k$ or $-k\eta \gg 1/6$, this equation can be approximated as

$$(\mu^A_{\mathbf{k}})'' + k^2 \left(1 - \lambda^A \frac{8}{3} \frac{1}{-k\eta} \right) \mu^A_{\mathbf{k}} = 0 \ . \tag{15}$$

This equation shows that only right-handed waves would be amplified exponentially.

What we want to calculate is the degree of the circular polarization defined as the difference between the power of right and left-handed circularly polarized gravitational waves at the end of the super inflation phase:

$$\Pi(k) \equiv \frac{\langle \mu^{\mathrm{R}}_{\mathbf{k}}(\eta_{\mathrm{end}}) \rangle^2 - \langle \mu^{\mathrm{L}}_{\mathbf{k}}(\eta_{\mathrm{end}}) \rangle^2}{\langle \mu^{\mathrm{R}}_{\mathbf{k}}(\eta_{\mathrm{end}}) \rangle^2 + \langle \mu^{\mathrm{L}}_{\mathbf{k}}(\eta_{\mathrm{end}}) \rangle^2} \ , \tag{16}$$

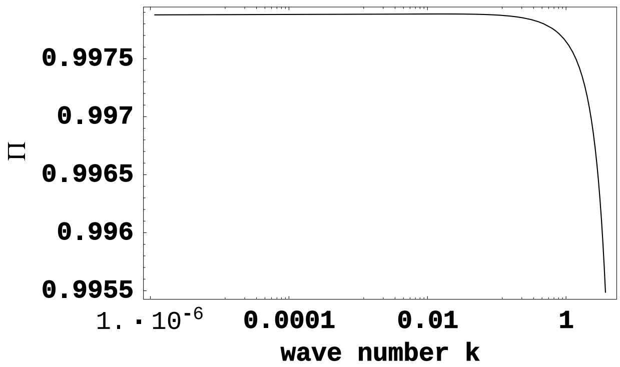

Figure 2: The degree of the polarization $\Pi(k)$ as a function of wave numbers k is shown. As expected, the gravitational waves are almost 100% circularly polarized.

where $\eta_{\rm end}$ represents the time when the super-inflation ends, and numerical result is shown inf Fig.2. The resultant polarization is sufficiently large and hence detectable by BBO or DECIGO.

4 Conclusion

We have studied a mechanism to produce the circular polarization of gravitational waves in the string-inspired cosmology. It turned out that the circularly polarized gravitational waves are ubiquitous in string cosmology. There are two key terms in string theory, namely, the Chern-Simons term and the Gauss-Bonnet term. The Chern-Simons term violates the parity invariance, therefore it makes a room for the circularly polarized gravitational waves to be produced. However, in the previous works [3], it had been shown that there is no significant circular polarization of gravitational waves within the conventional inflationary scenario. In this paper, we have shown that the Gauss-Bonnet term reversed the previous conclusion. The Gauss-Bonnet term has changed the background evolution in such a way that the super-inflationary epoch appears during the conventional inflationary stage. During the super-inflation, there exists an instability in the tensor modes. It is the instability that produces a significant circular polarization $\Pi \sim 1$. This result shows the possibility for verification of superstring theory by observing circular polarization.

References

[1] M. B. Green and J. H. Schwarz, Phys. Lett. B **149**, 117 (1984).

[2] I. Antoniadis, E. Gava and K. S. Narain, Phys. Lett. B **283**, 209 (1992) [arXiv:hep-th/9203071].

[3] A. Lue, L. M. Wang and M. Kamionkowski, Phys. Rev. Lett. **83**, 1506 (1999) [arXiv:astro-ph/9812088]; S. Alexander and J. Martin, Phys. Rev. D **71**, 063526 (2005) [arXiv:hep-th/0410230]; D. H. Lyth, C. Quimbay and Y. Rodriguez, JHEP **0503**, 016 (2005) [arXiv:hep-th/0501153].

[4] I. Antoniadis, J. Rizos and K. Tamvakis, Nucl. Phys. B **415**, 497 (1994) [arXiv:hep-th/9305025].

[5] S. Kawai, M. a. Sakagami and J. Soda, Phys. Lett. B **437**, 284 (1998) [arXiv:gr-qc/9802033]; J. Soda, M. a. Sakagami and S. Kawai, arXiv:gr-qc/9807056; S. Kawai, M. a. Sakagami and J. Soda, arXiv:gr-qc/9901065.

[6] M. Satoh, S. Kanno and J. Soda, to appear in Phys. Rev. D, arXiv:0706.3585[astro-ph].

Laser-interferometric detectors for gravitational wave background at 100 MHz

Atsushi Nishizawa[1], Seiji Kawamura[2], Tomotada Akutsu[3], Koji Arai[2], Kazuhiro Yamamoto[2], Daisuke Tatsumi[2], Erina Nishida[4], Masa-aki Sakagami[1], Takeshi Chiba[5], Ryuichi Takahashi[6], Naoshi Sugiyama[6]

[1] *Graduate School of Human and Environmental Studies, Kyoto University, Kyoto 606-8501, Japan*
[2] *TAMA Project, National Astronomical Observatory of Japan, Mitaka, Tokyo 181-8588, Japan*
[3] *Department of Astronomy, School of Science, University of Tokyo, Bunkyo-ku, Tokyo 113-0033, Japan*
[4] *Ochanomizu University, Bunkyo-ku, Tokyo 112-8610, Japan*
[5] *Department of Physics, College of Humanities and Sciences, Nihon University, Tokyo 156-8550, Japan*
[6] *Graduate School of Science, Nagoya University, Nagoya 467-8602, Japan*

Abstract

Recently, observational searches for gravitational wave background (GWB) have been developed and given constraints on the energy density of GWB in a broad range of frequencies. However, at 100 MHz, there is no strict upper limit from *direct* observation. In this article, we will propose a direct observation with interferometers. We investigated the detector designs, which can effectively respond to GW at high frequencies, and an optimal location of two detectors for correlation analysis of GWB.

1 Introduction

There are many theoretical predictions of gravitational wave background (GWB) in a broad range of frequencies, $10^{-18} - 10^{10}$ Hz. Some models in cosmology and particle physics predict relatively large stochastic GWB at ultra high frequency ~ 100 MHz; the quintessential inflation model [1], preheating [2], pre-big-bang scenarios in string cosmology [3], black strings in the Randall-Sundrum model [5], the binary evolution and coalescence of primordial black holes produced in the early universe [4]. For the inquiry of high energy physics, testing these models with gravitational wave (GW) detectors for high frequencies is very important.

Upper limits on GWB in wide-frequency ranges have been obtained from various observations [6, 7]. Nevertheless, as far as we know, no direct experiment has been done above 10^5 Hz except for the experiment by A. M. Cruise and R. M. J. Ingley [8]. They have used electromagnetic waveguides and obtained an upper limit on the amplitude of GW backgrounds, $h \leq 10^{-14}$ corresponding to $h_{100}^2 \Omega_{\rm gw} \leq 10^{34}$ at 100 MHz, where h_{100} is the Hubble constant normalized with $100\,{\rm km\,sec^{-1}\,Mpc^{-1}}$ and $\Omega_{\rm gw}$ is the energy density of GWB per logarithmic frequency bin normalized by the critical energy density of the universe [7]. This constraint is much weaker than the constraints at other frequencies. Therefore, a much tighter bound above 10^5 Hz is needed to test various theoretical models.

In this paper, we propose a method of direct detection of GWB at 100 MHz with laser interferometers. At high frequencies, the GW wavelength is comparable to the size of a detector, for example, which is the order of a few meters around 100 MHz. Thus, a so-called long-wave approximation that the GW wavelength is much larger than the detector size is not valid in the freqency band. In this case, the phase of GW changes during the one-way trip of light between mirrors. Therefore, we have to use a detector design that is able to integrate GW signals efficiently. In addition, to detect GWB with smaller amplitude than detector noise, one has to take correlation of signals from two detectors in order to distinguish GW signals from noises. The analytical method has been well developed [7, 11]. In these references, they assume the long-wave approximaiton, however, which is not valid in our situation around 100 MHz. This means the relative location of the two SRIs significantly affects the correlation sensitivity to GWB and the response function of a detector should be taken into account properly. Thus, in this paper, we will extend the previous analytical method of correlation, including the response functions of the detectors, and evaluate the dependence of the sensitivity on the relative location of two detectors.

[1] E-mail:atsushi.nishizawa@nao.ac.jp

2 Synchronous-recycling interferometer

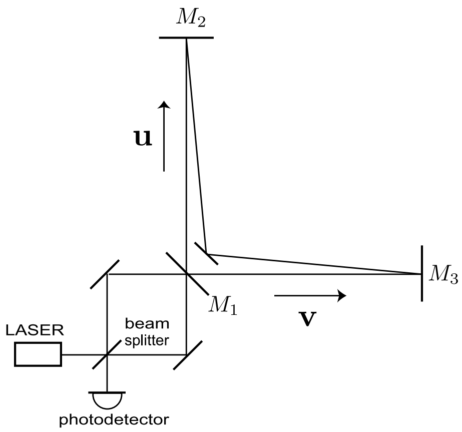

Figure 1: Design of synchronous recycling interferometer (SRI).

In our previous paper [9], we considered three designs of a interferometer: synchronous recycling interferometer (SRI) [10], ordinary Fabry-Perot Michelson interferometer (FPMI), and L-Shaped Michelson interferometer (LMI). According to the detailed investigation of the detector response functions, we found that SRI can effectively respond to GW at high frequencies, where the wavelength of GW is comparable to the detector size. The design is shown in Fig. 1. The advantage of SRI is that GW signals at certain frequencies are effectively accumulated and amplified because the light beams experience GWs with the same sign of phases during round trips in the folded cavity. The GW signal of SRI resonates at 100 MHz if one select the arm length as $L = 0.75\,\mathrm{m}$ [14].

The GW response of a SRI can be written in the form $\tilde{\delta\Phi}(f, \hat{\mathbf{\Omega}}) = \alpha(f)\,\tilde{\delta\phi}(f, \hat{\mathbf{\Omega}})$, where $\tilde{\delta\phi}(f, \hat{\mathbf{\Omega}})$ denotes the Fourier component of phase shift due to GW during the round trip of light in a recycling cavity and $\alpha(f)$ denotes an optical amplification factor of light in the cavity [9]. The specific expressions are written as

$$\tilde{\delta\phi}(f, \hat{\mathbf{\Omega}}) = 2\,\omega\tau\, e^{-2\pi i f \hat{\mathbf{\Omega}}\cdot\vec{\mathbf{X}}/c}\,(1 - e^{-4\pi i f\tau}) \sum_p \mathbf{e}^p \tilde{h}_p : \frac{1}{2}\left[(\hat{\mathbf{u}}\otimes\hat{\mathbf{u}})\mathcal{T}(f, \hat{\mathbf{\Omega}}\cdot\hat{\mathbf{u}}) - (\hat{\mathbf{v}}\otimes\hat{\mathbf{v}})\mathcal{T}(f, \hat{\mathbf{\Omega}}\cdot\hat{\mathbf{v}})\right], \quad (1)$$

$$\alpha(f) = -\frac{R_E T_F^2}{(R_F - R_E)(1 - R_F R_E\, e^{-8\pi i f\tau})}\,, \quad (2)$$

$$\mathcal{T}(f, \hat{\mathbf{\Omega}}\cdot\hat{\mathbf{u}}) \equiv \frac{-\,e^{-2\pi i f\tau}}{2\pi f\tau\,\{1 - (\hat{\mathbf{\Omega}}\cdot\hat{\mathbf{u}})^2\}}\left[\sin(2\pi f\tau) - i\,(\hat{\mathbf{\Omega}}\cdot\hat{\mathbf{u}})\left\{e^{-2\pi i f\tau\,\hat{\mathbf{\Omega}}\cdot\hat{\mathbf{u}}} - \cos(2\pi f\tau)\right\}\right], \quad (3)$$

where $\tau \equiv L/c$, ω is the angular frequency of laser, $\vec{\mathbf{X}}$ is a position vector of the mirror M_1, R_F is the amplitude reflectivity of a front mirror, and R_E is the composite amplitude reflectivity of other three mirrors of the cavity. $\hat{\mathbf{u}}$, $\hat{\mathbf{v}}$ are the unit vectors directed in the arms and $\hat{\mathbf{\Omega}}$ is that directed in GW propagation. We call $\mathcal{T}$ arm's response function that describes the effect of finite arm length on propagating light. In the detector whose arm length is much smaller than the wavelength of GW, this function is approximated to unity, while in our detector whose detector size is comparable to GW wavelength, the function significantly affects the response of the detector.

3 Correlation analysis

We use the formalism of correlation analysis for GWB in [7, 11] and extend it including the response function of SRI. Details of this section is described in [13]. We assume that GWB is (i) isotropic, (ii) unpolarized, (iii) stationary, and (iv) Gaussian, and (v) has small amplitude compared with that of noise. The SNR for GWB is given by

$$\mathrm{SNR} = \frac{3H_0^2}{10\pi^2}\sqrt{T}\left[\int_{-\infty}^{\infty} df\,\frac{\gamma^2(f)\Omega_{\mathrm{gw}}^2(f)}{f^6 P_1(f)P_2(f)}\right]^{1/2}, \quad (4)$$

where $H_0 = 100\, h_{100}\, \mathrm{km\, s^{-1}\, Mpc^{-1}}$, T is observation time. $P_i(f),\, i = 1, 2$ are the one-sided power spectrum density of noise defined by $\langle \tilde{n}_i^*(f)\tilde{n}_i(f')\rangle \equiv \frac{1}{2}\delta(f-f')P_i(f),\, i = 1, 2$. $\gamma(f)$ is called the overlap reduction function and is given by

$$\gamma(f) \equiv \frac{5}{8\pi}\sum_p \int_{S^2} d\hat{\mathbf{\Omega}}\, e^{2\pi i f \hat{\mathbf{\Omega}}\cdot\Delta\vec{\mathbf{X}}/c} F_1^{p\,*}(f, \hat{\mathbf{\Omega}}) F_2^p(f, \hat{\mathbf{\Omega}})\,, \tag{5}$$

where the separation of two detectors is $\Delta\vec{\mathbf{X}} \equiv \vec{\mathbf{X}}_1 - \vec{\mathbf{X}}_2$. This function describes how GW signals in two detectors are correlated, and equals unity for colocated and coaligned detectors in low frequency limit. The angular response function $F_p(f, \hat{\mathbf{\Omega}})$ and the detector tensor $\mathbf{D}(f, \hat{\mathbf{\Omega}})$ are defined by

$$\begin{aligned} F_p(f, \hat{\mathbf{\Omega}}) &\equiv \mathbf{D}(f, \hat{\mathbf{\Omega}}) : \mathbf{e}_p(\hat{\mathbf{\Omega}})\,. \\ \mathbf{D}(f, \hat{\mathbf{\Omega}}) &\equiv \frac{1}{2}\left[(\hat{\mathbf{u}}\otimes\hat{\mathbf{u}})\mathcal{T}(f, \hat{\mathbf{\Omega}}\cdot\hat{\mathbf{u}}) - (\hat{\mathbf{v}}\otimes\hat{\mathbf{v}})\mathcal{T}(f, \hat{\mathbf{\Omega}}\cdot\hat{\mathbf{v}})\right]\,. \end{aligned} \tag{6}$$

where $\mathbf{e}_p(\hat{\mathbf{\Omega}})$, $p = +, \times$ are polarizarion tensors of GW, and $\mathcal{T}$ is the arm's response function introduced in Eq. (3). The meaning of $\gamma(f)$ in this paper is slightly different from those in other papers [7, 11] because it includes $\mathcal{T}$ and does not give unity even for colocated and coaligned detector at high frequencies. Namely, the function means not only the overlap of GW signals in two detectors, but also the loss of GW signals in each detector at high frequencies.

The SNR is significantly influenced by the relative location of two detectors through $\gamma(f)$ when the wavelength of GW is comparable to the size of a detector. $\gamma(f)$ can be calculated numerically from Eq. (5) using the arm's response function $\mathcal{T}$ given in Eq. (3). We will fix the frequency at 100 MHz and consider $\gamma(f)$, because SRI has a narrow frequency band and what we are most interested in is γ at 100 MHz. Each configuration of detectors is characterized by the relative position $\Delta\vec{\mathbf{X}} = \vec{\mathbf{X}}_1 - \vec{\mathbf{X}}_2$ and the relative angle β. In Fig. 2 and Fig. 3, the angle of detectors is fixed and the locations are translated. In an initially coaligned case ($\beta = 0$) in Fig. 2, $\gamma(f)$ has its maximum at $\Delta X = 0$ and keep the moderate value in a range $\Delta X = \pm 0.2\,\mathrm{m}$. However, the maximal value is ≈ 0.377, not unity. This is because we defined $\gamma(f)$ including $\mathcal{T}$, which drops at high frequencies due to the effect of the phase change of GW during the round trip of light in the detector. In an initially reversed case ($\beta = \pi$) in Fig. 3, when the detector is translated to the direction $(\hat{\mathbf{u}}+\hat{\mathbf{v}})/\sqrt{2}$, the peak of $\gamma(f)$ is shifted. This is because the overlap of two detectors is better when their arms are overlapped geometrically.

We will calculate the sensitivity achievable with correlation analysis. From the results obtained above, the best location is obviously colocated and coaligned case, and gives $\gamma(f)|_{100\,\mathrm{MHz}} \approx 0.377$ (this value is not considerably affected if two detectors are in a range $\pm 0.2\,\mathrm{cm}$). Assuming the detectors are shot-noise limited, with experimental parameters $L = 0.75\,\mathrm{m}$, $\omega = 1.77\times 10^{15}\,\mathrm{rad\, s^{-1}}$, and $\alpha \approx 10^5$ at 100 MHz, we have the power spectral density of noise $P_i(f) \approx 4.65\times 10^{-42}\,\mathrm{Hz^{-1}}$, i = 1, 2 around 100 MHz. Therefore, from Eq. (4),one can calculate the cross-correlation sensitivity to GWB with flat spectrum [12] and obtain $h_{100}^2\Omega_{\mathrm{gw}} \approx 1.4\times 10^{14}$.

4 Conclusions

In this paper, we investigated the optimal location of two SRI and derived its cross-correlation sensitivity to GWB. At 100 MHz, the wavelength of GW is comparable to the size of a detector, where the GW response of the detector is less effective than one in long wavelength limit. In addition, the sensitivity is significantly affected by the location of detectors. We included the effect due to the finite size of a detector into the overlap reduction function and evaluated it. As a result, SNR is worsened by a factor of $(0.377)^{-1} \approx 2.65$ at 100 MHz in contrast to the case where long wave approximation is valid. However, SNR is almost optimal value if two detectors are in the range of $\pm 0.2\,\mathrm{m}$ and in coaligned. Using this configuration and experimentally realized parameters of two SRIs, one can achieve the sensitivity to GWB with flat spectrum, $h_{100}^2\Omega_{\mathrm{gw}} \approx 1.4\times 10^{14}$. This constraint on GWB would be much tighter than that obtained by current direct observation [8].

This research was supported by the Ministry of Education, Science, Sports and Culture, Grant-in-Aid for Scientific Research (A), 17204018.

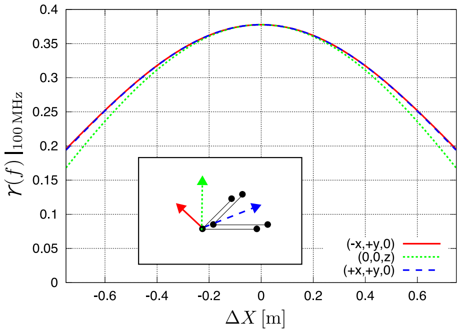

Figure 2: Overlap reduction function when the detector is initially colocated and coaligned ($\beta = 0$) and is translated in certain directions. Each curve means the direction of translation. $(+x, +y, 0)$, $(-x, +y, 0)$, and $(0, 0, z)$ are the direction of $(\hat{\mathbf{u}} + \hat{\mathbf{v}})/\sqrt{2}$, $(\hat{\mathbf{u}} - \hat{\mathbf{v}})/\sqrt{2}$, and the direction perpendicular to $\hat{\mathbf{u}}\,\hat{\mathbf{v}}$ plane, respectively.

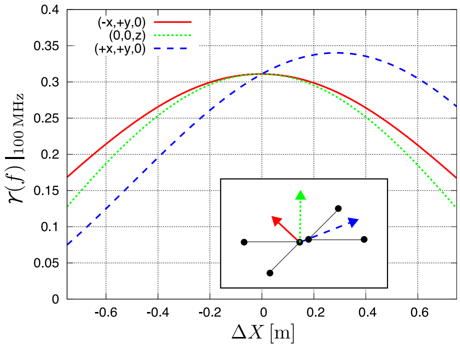

Figure 3: Overlap reduction function when the detector is initially colocated and reversed ($\beta = \pi$) and is translated in certain directions. Each curve means the translation to the same direction as shown in Fig. 2.

References

[1] M. Giovannini, Phys. Rev. D 60, 123511 (1999); M. Giovannini, Phys. Rev. D 58, 083504 (1998); A. Riazuelo and J. Uzan, Phys. Rev. D 62, 083506 (2000)

[2] R. Easther and E. A. Lim, astro-ph/0601617; J. Garcia-Bellido and D. G. Figueroa, Phys. Rev. Lett. 98, 061302 (2007); J. Dufaux, A. Bergman, G. Felder, L. Kofman, and J. Uzan, arXiv:0707.0875

[3] M. Gasperini and M. Giovannini, Phys. Rev. D 47, 1519 (1993); R. Brustein, M. Gasperini, M. Giovannini, and G. Veneziano, Phys. Lett. B 361, 45 (1995)

[4] T. Nakamura, M. Sasaki, T. Tanaka, and K. S. Thorne, Astrophys. J. 487, L139 (1997); K. Ioka, T. Chiba, T. Tanaka, and T. Nakamura, Phys. Rev. D 58, 063003 (1998); K. T. Inoue and T. Tanaka, Phys. Rev. Lett., 91, 021101 (2003)

[5] S. S. Seahra, C. Clarkson, and R. Maartens, Phys. Rev. Lett. 94, 121302 (2005); C. Clarkson and S. S. Seahra, Class. Quantum. Grav. 24, F33 (2007)

[6] T. L. Smith, M. Kamionkowski, and A. Cooray, Phys. Rev., D 73, 023504 (2006); F. A. Jenet *et al.*, Astrophys. J. 653, 1571 (2006); J. W. Armstrong, L. Iess, P. Tortora, and B. Bertotti, Astrophys. J., 599, 806 (2003); B. Abbott *et al.*, Astrophys. J. 659, 918 (2007)

[7] M. Maggiore, Phys. Rep. 331, 283 (2000)

[8] A. M. Cruise and R. M. J. Ingley, Class. Quantum. Grav. 23, 6185 (2006)

[9] A. Nishizawa *et al.*, arXiv:0710.1944

[10] R. W. P. Drever, Gravitational Radiation, edited by N. Deruelle and T. Piran (North-Holland, Amsterdam, 1983), pp.321-338

[11] B. Allen and J. D. Romano, Phys. Rev. D 59, 102001 (1999)

[12] T. Chiba, Y. Himemoto, M. Yamaguchi, and J. Yokoyama, Phys. Rev. D 76, 043516 (2007)

[13] A. Nishizawa *eq al.*, in preparation

[14] The arm length is defined as the length between M_1 and M_2, or M_3. Note that we assume Sagnac part in front of the cavity is much smaller than the cavity.

Equivalence Principle and Holography: a possible clash in the extra dimensions?

Fabio Scardigli[1] and Roberto Casadio[2]

[1] *Yukawa Institute for Theoretical Physics, Kyoto University, Kyoto 606-8502, Japan*
[2] *Dipartimento di Fisica, Università di Bologna and I.N.F.N., Sezione di Bologna, via Irnerio 46, 40126 Bologna, Italy*

Abstract

It has been recently debated whether a class of generalized uncertainty principles that include gravitational sources of error are compatible with the holographic principle in models with extra spatial dimensions. We had in fact shown elsewhere that the holographic scaling is lost when more than four space-time dimensions are present. However, we shall show here that the validity of the holographic counting can be maintained also in models with extra spatial dimensions, but at the intriguing price that the equivalence principle for a point-like source be violated and the inertial mass differ from the gravitational mass in a specific non-trivial way.

1 Introduction

The topic of generalized uncertainty principles (GUP) is a rather old one. Recently, it has been revived with the addition of gravitational contributions which provide a minimum length of the order of the Planck scale (for a review and examples, see Ref. [1]). An attempt in this direction was taken by Ng and van Dam [2] who suggested to include an error due to the space-time curvature induced by the measuring device, the latter being described, along the lines of Wigner's 1958 paper [3], as a system made of a clock, a photon detector and a photon gun, with total mass m and diameter $d = 2\,a$ (spherical symmetry is assumed for simplicity). A given length l is then measured by timing the photon travel from the gun to a suitably placed (ideally weightless) mirror and back. Photons are also supposed to be emitted in spherical waves, in order to avoid recoil and back-reaction effects on the clock's position. This leads to a GUP which yields the remarkable consequence of suggesting that four-dimensional space-time actually contains (gravitational) degrees of freedom which scale in agreement with the holographic principle [4].

However, if one tries to extend this result to models with extra spatial dimensions [5, 6], the latter property becomes questionable. It was in fact shown in Ref. [7] that a straightforward extension does not work. Before we proceed, let us recall why it is sensible to place on the same footing a "fundamental" uncertainty principle such as Heisenberg's and an (apparently) phenomenological gravitational source of error. On general grounds, one understands that in Einstein's general relativity space-time is a dynamical concept and its quantum description must involve uncertainty. Constructions such as that of Ref. [2] make it clear that the two sources of uncertainty are closely related: the photon shot by the gun moves in a Schwarzschild metric with ADM mass equal to m minus the photon energy E. Since we are timing the photon's travel, the time-energy uncertainty relation implies that E has an uncertainty $\Delta E \sim \hbar/\Delta t_{\rm em}$ if $\Delta t_{\rm em}$ is the uncertainty in the time of emission. Correspondingly, we cannot determine with infinite accuracy the length of the photon optical path, say from $r_0 > r_{\rm g}$ to $r > r_0$ (in the detector's frame), with $r_{\rm g}(m) = 2\,G_{\rm N}\,m/c^2$, but can just find the lower and upper bounds

$$\int_{r_0}^{r} \frac{{\rm d}\rho}{1-\frac{r_{\rm g}^{+}}{\rho}} \equiv c\,\Delta t_{\rm max} \gtrsim c\,\Delta t \gtrsim c\,\Delta t_{\rm min} \equiv \int_{r_0}^{r} \frac{{\rm d}\rho}{1-\frac{r_{\rm g}^{-}}{\rho}}\ , \qquad (1)$$

where $r_{\rm g}^{\pm} = r_{\rm g}(m - E \pm \Delta E)$. Ref. [2] then suggests to add to other sources of errors the uncertainty in the length of the optical path as the difference

$$\delta l_{\rm C} \simeq c\,(\Delta t_{\rm max} - \Delta t_{\rm min})\ . \qquad (2)$$

[1]E-mail: fabio@yukawa.kyoto-u.ac.jp
[2]E-mail: casadio@bo.infn.it

The aim of this paper is to take the opposite perspective with respect to some previous works and *to show* that the GUP of Refs. [2, 7] and the holographic principle *can* be both kept valid consistently. However, we shall then show that this leads to another principle being violated, namely the detector's inertial mass and gravitational mass must differ in models with extra spatial dimensions. We shall write explicitly the fundamental constants c, $\hbar$ and Newton's constant $G_{\rm N}$ or, alternatively, the Planck length $\ell_{\rm p} = (G_{\rm N}\,\hbar/c^3)^{1/2}$ or mass $M_{\rm p} = \hbar/2\,c\,\ell_{\rm p}$ [respectively replaced by $G_{(n+4)}$, $\ell_{(4+n)} = (G_{(4+n)}\,\hbar/c^3)^{\frac{1}{2+n}}$ and $M_{(4+n)} = \hbar/2\,c\,\ell_{(4+n)}$ in $4+n$ dimensions].

2 Gravitational GUP

Suppose we wish to measure a distance l with the detector described in the *Introduction.* If Δx is the initial uncertainty in the position of the clock, after the time $T = 2\,l/c$ taken by the photon to return to the detector, the uncertainty in the actual length of the segment l becomes $\Delta x_{\rm tot} = \Delta x + T\,\Delta v = \Delta x + \frac{\hbar\,T}{2\,m\,\Delta x}$, where Δv is the uncertainty in the detector's velocity from Heisenberg's principle. Upon minimizing $\Delta x_{\rm tot}$ with respect to Δx we obtain Wigner's quantum mechanical error [3]

$$\delta l_{\rm QM} \simeq 2\left(\frac{\hbar\,l}{m\,c}\right)^{1/2} , \tag{3}$$

which we seem to be able to reduce as much as we want by choosing m very large. But gravity now gets in the way as mentioned before. In fact, we need now to include in the computation the gravitational error of Eq. (2) with $r = a + l > r_0 = a \gg r_{\rm g}$. We consider for $r_{\rm g}^{\pm}$ the lower and upper bounds allowed by total energy conservation, corresponding to the two limiting cases $E - \Delta E = 0$ and $E + \Delta E = m$, respectively. This yields, for distances $l \gtrsim a$,

$$\delta l_{\rm C} \simeq r_{\rm g}\,\log\left(\frac{a+l}{a}\right) \gtrsim r_{\rm g}\log 2 \simeq \frac{r_{\rm g}}{2}\,. \tag{4}$$

Note that $\delta l_{\rm C}$ increases with increasing detector's mass and the total error becomes

$$\delta l_{\rm tot} = \delta l_{\rm QM} + \delta l_{\rm C} \simeq 2\left(\frac{\hbar\,l}{m\,c}\right)^{1/2} + \frac{G_{\rm N}\,m}{c^2}\,. \tag{5}$$

For a given l, this error can only be minimized with respect to the mass of the clock, which yields

$$(\delta l_{\rm tot})_{\rm min} \simeq 3\left(\ell_{\rm p}^2\,l\right)^{1/3} , \tag{6}$$

for $m = 2\,M_{\rm p}(l/l_{\rm p})^{1/3}$. The global uncertainty on l therefore contains precisely the term proportional to $l^{1/3}$ required by the holography. Unfortunately, in $4+n$ dimensions this does not seem to work. When $a+l$ is shorter than the size L of the extra dimensions, one can use the $4+n$-dimensional Schwarzschild metric [8] ${\rm d}s^2 = g_{\mu\nu}\,{\rm d}x^\mu\,{\rm d}x^\nu = -F(r)\,c^2\,{\rm d}t^2 + F(r)^{-1}\,{\rm d}r^2 + r^2\,{\rm d}\Omega_{n+2}^2$, where Greek indices run from 0 to $3+n$ (Latin indices will denote spatial coordinates) with

$$F(r) = 1 - C/r^{1+n}\,, \qquad \text{and} \qquad C = \frac{16\,\pi\,G_{4+n}\,m}{(2+n)\,A_{2+n}\,c^2}\,, \tag{7}$$

A_{2+n} being the surface area of the unit $(2+n)$-sphere. Upon repeating analogous steps, one then finds [7]

$$(\delta l_{\rm tot})_{\rm min} \sim \left(a^{-n}\,\ell_{(4+n)}^{2+n}\,l\right)^{1/3} . \tag{8}$$

The above expression, even in the rather ideal case $a \sim \ell_{(4+n)}$, yields the following scaling for the number of degrees of freedom in a volume V of size l,

$$\mathcal{N}(V) = \left(\frac{l}{(\delta l_{\rm tot})_{\rm min}}\right)^{3+n} \sim \left(\frac{l}{\ell_{(4+n)}}\right)^{2\left(1+\frac{n}{3}\right)} , \tag{9}$$

and the holographic counting holds in four-dimensions ($n = 0$) but is lost when $n > 0$.

3 GUP, Holography and the Equivalence Principle

Let us now point out that, beside the GUP proposed by Ng and van Dam, the result in Eq. (8) deeply relies on the use of the black hole metric (7) and its dependence on the mass m. In particular, the expression for the parameter C is obtained by taking the weak field limit [8] in which the metric can be written as $g_{\mu\nu} = \eta_{\mu\nu} + h_{\mu\nu}$, with $|h_{\mu\nu}| \ll 1$ in the asymptotic region far from any source. The linearized metric $h_{\mu\nu}$, in the harmonic gauge, obeys the Poisson equation

$$\nabla^2 h_{\mu\nu} = -\frac{16\,\pi\,G_{4+n}}{c^4}\,\bar{T}_{\mu\nu}\ , \tag{10}$$

with a source $\bar{T}_{\mu\nu}$ related to the stress-energy tensor by $\bar{T}_{\mu\nu} = \left(T_{\mu\nu} - \frac{1}{2+n}\,\eta_{\mu\nu}\,T\right)$. The condition that the system be non-relativistic means that time derivatives can be considered much smaller than spatial derivatives, so that the components of the stress energy tensor can be ordered as $|T_{00}| \gg |T_{0i}| \gg |T_{ij}|$. A solution to Eq. (10) is then given by

$$h_{\mu\nu}(x) \simeq \frac{16\,\pi\,G_{4+n}}{(1+n)\,A_{2+n}\,c^4}\,\frac{1}{r^{1+n}}\int \bar{T}_{\mu\nu}\,\mathrm{d}^{3+n}y + \frac{16\,\pi\,G_{4+n}}{A_{2+n}\,c^4}\,\frac{x^k}{r^{3+n}}\int y^k\,\bar{T}_{\mu\nu}\,\mathrm{d}^{3+n}y + \dots\ , \tag{11}$$

where the approximate equality is obtained by expanding for $r = |x|$ very large (far from the central source). Myers and Perry define the $4+n$-dimensional ADM mass m as

$$\int \bar{T}_{00}\,\mathrm{d}^{3+n}x = m\,c^2\ , \tag{12}$$

so that one obtains the natural generalization of the Newtonian potential to $4+n$ dimensions, $h_{00} \simeq C/r^{1+n}$. One can now wonder if the metric defined by Eq. (7) can be modified in such a way that the holographic principle be fulfilled also in $4+n$ dimensions, thus suitably changing the counting of degrees of freedom given in Eq. (9). In other words, we shall assume the holographic principle as a constraint to fix the form of the $4+n$-dimensional black hole metric. Of course, this new metric must still satisfy the $4+n$-dimensional Einstein equations (10), which is a very strong constraint and it seems therefore sensible to change the original metric (7) as little as possible. On the other hand, we note that the Myers-Perry solution exhibits a complete $3+n$-dimensional spherical symmetry, which means that it ignores the weight of the brane. All things considered, the deformation of the metric (7) which we shall use consists in allowing for a departure from a linear relation between the inertial mass and the gravitational ADM mass of the form

$$\int \bar{T}_{00}\,\mathrm{d}^{3+n}x = M_{(4+n)}\,c^2\,\left(\frac{m}{M_{(4+n)}}\right)^{\gamma(n)}\ , \tag{13}$$

where γ is a (yet) unspecified function of n. Although this *ansatz* is not the only one that can in principle be conceived, it really is one of the simplest possible, as Eq. (13) means that the gravitational mass M and inertial mass m of the source (the detector) are related by

$$M = M_{(4+n)}\,\left(\frac{m}{M_{(4+n)}}\right)^{\gamma(n)}\ . \tag{14}$$

The equivalence principle would thus be violated for any function $\gamma \neq 1$. Eq. (14) yields a total error in length measurements given by

$$\delta l_{\mathrm{tot}} = \delta l_{\mathrm{QM}} + \delta l_{\mathrm{C}} \simeq \frac{J}{\sqrt{m}} + K m^{\gamma}\ , \tag{15}$$

where $J = 2(\hbar\,l/c)^{1/2}$; $K = \frac{2^n-1}{n\,2^n\,a^n}\,\frac{16\,\pi\,G_{4+n}\,M_{4+n}^{(1-\gamma)}}{(2+n)\,A_{2+n}\,c^2}$. Upon minimizing δl_{tot} with respect to m, one obtains

$$(\delta l_{\mathrm{tot}})_{\mathrm{min}} \sim l^{\frac{\gamma}{2\,\gamma+1}}\ . \tag{16}$$

Hence, if we require that holography holds, namely $(\delta l_{\rm tot})_{\rm min} \sim (l)^{\frac{1}{3+n}}$, we must also have $\gamma/(2\,\gamma+1) = 1/(3+n)$. In this way we see that the holographic scaling can be preserved also in $4+n$ dimensions, with a Schwarzschild-like metric for point-like sources, provided we define the gravitational mass M as in Eq. (14) with

$$\gamma = \frac{1}{1+n} \ . \tag{17}$$

Therefore, the equivalence principle must be violated at distances shorter than the size L of the extra dimensions, as well as Newton's law is modified in $4+n$ dimensions (*i.e.*, $F \sim 1/r^{2+n}$).

4 Conclusions

We have shown how a gravitational error originated by the quantum mechanical uncertainty in the ADM mass of a detector inevitably affects any measurements of length. This leads to Ng and van Dam's GUP, which has the remarkable property of respecting the holographic counting in four dimensions. When extra spatial dimensions are present, the holographic scaling is violated. However, holography can be restored if one instead allows for a violation of the equivalence principle at short distances (below the size of extra dimensions). This violation could in principle be tested (see, *e.g.*, Ref. [9]), and its extent is related to the number of extra dimensions. The connections of the present scenario with other models where the equivalence principle is also violated are worth of further investigation. To this aim, the results reported for example in Refs. [10] seem to be particularly promising. Such results, although sometimes worked out in a stringy oriented scenario (for example D-brane induced gravity) or in the framework of loop quantum gravity, seem anyway to match, at least for the key aspects, the more phenomenological arguments given here.

References

[1] C.N. Yang, Phys. Rev. **72**, 874 (1947); F. Karolyhazy, Nuovo Cim. A **42**, 390 (1966); L.J. Garay, Int. J. Mod. Phys. A **10**, 145 (1995); F. Scardigli, Phys. Lett. B **452**, 39 (1999); R.J. Adler, P. Chen and D.I. Santiago, Gen. Rel. Grav. **33**, 2101 (2001).

[2] Y.J. Ng and H. van Dam, Mod. Phys. Lett. **A 9**, 335 (1994); Mod. Phys. Lett. **A 10**, 2801 (1995); Phys. Lett. **B 477**, 429 (2000); Y.J. Ng, Phys. Rev. Lett. **86**, 2946 (2001).

[3] E.P. Wigner, Rev. Mod. Phys. **29**, 255 (1957); H. Salecker, E.P. Wigner, Phys. Rev. **109**, 571 (1958).

[4] L. Susskind, L. Thorlacius and J. Uglum, Phys. Rev. D **48**, 3743 (1993); G. 't Hooft, "Dimensional Reduction in Quantum Gravity", gr-qc/9310026; L. Susskind, J. Math. Phys. **36**, 6377 (1995).

[5] N. Arkani-Hamed, S. Dimopoulos and G. Dvali, Phys. Lett. **B 429**, 263 (1998); Phys. Rev. D **59**, 086004 (1999); I. Antoniadis, N. Arkani-Hamed, S. Dimopoulos and G. Dvali, Phys. Lett. **B 436**, 257 (1998); C. Kokorelis, Nucl. Phys. **B 677** 115 (2004).

[6] L. Randall and R. Sundrum, Phys. Rev. Lett. **83**, 3370 (1999); Phys. Rev. Lett. **83**, 4690 (1999).

[7] F. Scardigli and R. Casadio, Class. Quantum Grav. **20**, 3915 (2003).

[8] R.C. Myers and M.J. Perry, Ann. Phys. NY **172**, 304 (1986); P.C. Argyres, S. Dimopoulos, J. March-Russell, Phys. Lett. B **441**, 96 (1998); R. Casadio, B. Harms, Phys. Lett. B **487**, 209 (2000).

[9] C. Lammerzahl, Lect. Notes Phys. **631**, 367 (2003).

[10] S.L. Dubovsky, V.A. Rubakov, Phys. Rev. D **67**, 104014 (2003); P.S. Wesson, Int. J. Mod. Phys. **D14**, 2315 (2005); J. Ellis, N.E. Mavromatos, D.V. Nanopoulos, A.S. Sakharov, Int. J. Mod. Phys. **A19**, 4413 (2004); E. Anderson and R. Tavakol, JCAP **0510**, 017 (2005); J.M. Overduin, Phys. Rev. D **62**, 102001 (2000).

Numerical experiments of adjusted BSSN systems for controlling constraint violations

Kenta Kiuchi[1] and Hisa-aki Shinkai[2]

[1]*Department of Physics, Waseda University, 3-4-1 Okubo, Shinjuku-ku, Tokyo 169-8555, Japan*
[2]*Faculty of Information Science and Technology, Osaka Institute of Technology, 1-79-1 Kitayama, Hirakata, Osaka 573-0196, Japan*

Abstract

We present our numerical comparisons between the BSSN formulation widely used in numerical relativity today and its adjusted versions using constraints. We performed three testbeds: gauge-wave, linear wave, and Gowdy-wave tests, proposed by the Mexico workshop on the formulation problem of the Einstein equations. We tried three kinds of adjustments, which were previously proposed from the analysis of the constraint propagation equations, and investigated how they improve the accuracy and stability of evolutions. As a result, we observe that in some cases (e.g., gauge-wave or Gowdy-wave tests) the simulations using the adjusted systems last 10 times as long as those using the original BSSN.

1 Introduction

Numerical integration of the Einstein equations is the only way to investigate highly dynamical and nonlinear gravitational space-time. The detection of gravitational wave requires templates of waveform, among them mergers of compact objects are the most plausible astrophysical sources. Numerical relativity has been developed with this purpose over decades.

A number of scientific numerical simulations for compact binary sytems such as Neutron star (NS) - NS binary, NS-Black hole (BH) binary, and BH-BH binary, have been done so far, and we are now at the level of discussing the actual physics of the phenomena, including the effects of the equations of state, hydrodynamics, and general relativity by evolving various initial data [1, 2, 3, 4].

Almost all the groups which apply the above conventional approach use the so-called BSSN variables, which stands for Baumgarte-Shapiro [5] and Shibata-Nakamura [6], the modified Arnowitt-Deser-Misner formulation initially proposed by Nakamura [6]. There have already been several efforts to explain why the combination of this recipe works from the point of view of the well-posedness of the partial differential equations (e.g. [7, 8]). However, the question remains whether there exists an alternative evolution system that enables more long-term stable and accurate simulations. The search for a better set of equations for numerical integrations is called the formulation problem for numerical relativity, of which earlier stages are reviewed by one of the authors [9].

In this article, we report our numerical tests of modified versions of the BSSN system, the *adjusted BSSN systems*, proposed by Yoneda and Shinkai [10]. The idea of their modifications is to add constraints to the evolution equations like Lagrange multipliers and to construct a robust evolution system which evolves to the constraint surface as the attractor. Their proposals are based on the eigenvalue analysis of the constraint propagation equations (the evolution equations of the constraints) on the perturbed metric. Our numerical examples are taken from the proposed problems for testing the formulations of the Mexico Numerical Relativity Workshop 2001 participants [11], which are sometimes called the Apples-with-Apples test.

2 Original and adjusted BSSN equations

We start by presenting the standard BSSN formulation, where we follow the notations of [5], which are widely used among numerical relativists.

[1]E-mail:kiuchi@gravity.phys.waseda.ac.jp
[2]E-mail:shinkai@is.oit.ac.jp

The idea of the BSSN formulation is to introduce auxiliary variables to those of the Arnowitt-Deser-Misner (ADM) formulation for obtaining longer stable numerical simulations. The basic variables of the BSSN formulation are $(\phi, \tilde{\gamma}_{ij}, K, \tilde{A}_{ij}, \tilde{\Gamma}^i)$, which are defined by

$$\phi = \frac{1}{12}\log(det\gamma_{ij}), \tag{1}$$

$$\tilde{\gamma}_{ij} = e^{-4\phi}\gamma_{ij}, \tag{2}$$

$$K = \gamma^{ij}K_{ij}, \tag{3}$$

$$\tilde{A}_{ij} = e^{-4\phi}\left[K_{ij} - \frac{1}{3}\gamma_{ij}K\right], \tag{4}$$

$$\tilde{\Gamma}^i = \tilde{\gamma}^{jk}\tilde{\Gamma}^i_{jk}, \tag{5}$$

where (γ_{ij}, K_{ij}) are the intrinsic and extrinsic ADM 3-metric. The conformal factor ϕ is introduced so as to set $\tilde{\gamma} \equiv det[\tilde{\gamma}_{ij}]$ as unity, $\tilde{A}_{ij}$ is supposed to be traceless, and $\tilde{\Gamma}^i$ is treated independently in evolution equations. Therefore these three requirements turn into the new constraints [below (8)-(10)].

For saving the space, we don't explicitly show the set of the BSSN evolution equations, but the constraints equations in the BSSN system (see [13]). The two "kinematic" constraints, the Hamiltonian and momentum constraint equations, are expressed in terms of the BSSN basic variables and are written as

$$\mathcal{H} = e^{-4\phi}\tilde{R} - 8e^{-4\phi}(\tilde{D}^i\tilde{D}_i\phi + \tilde{D}^i\phi\tilde{D}_i\phi) + \frac{2}{3}K^2 - \tilde{A}_{ij}\tilde{A}^{ij} - \frac{2}{3}\mathcal{A}K \approx 0, \tag{6}$$

$$\mathcal{M}_i = 6\tilde{A}^j{}_i\tilde{D}_j\phi - 2\mathcal{A}\tilde{D}_i\phi - \frac{2}{3}\tilde{D}_iK + \tilde{D}_j\tilde{A}^j{}_i \approx 0. \tag{7}$$

Additionally, the BSSN formulation requires three "algebraic" constraint relations;

$$\mathcal{G}^i = \tilde{\Gamma}^i - \tilde{\gamma}^{jk}\tilde{\Gamma}^i_{jk} \approx 0, \tag{8}$$

$$\mathcal{A} = \tilde{A}_{ij}\tilde{\gamma}^{ij} \approx 0, \tag{9}$$

$$\mathcal{S} = \tilde{\gamma} - 1 \approx 0, \tag{10}$$

where (8) and (9) are from the definitions of (5) and (4), respectively. Equation (10) is from the requirement on $\tilde{\gamma}$.

To understand the stability property of the BSSN system, Yoneda and Shinkai [10] studied the structure of the evolution equations in detail, especially how the modifications using the constraints, (6)-(10), affect to the stability. They investigated the signature of the eigenvalues of the constraint propagation equations (dynamical equations of constraints), and explained that the standard BSSN dynamical equations are balanced from the viewpoints of constrained propagations, including a clarification of the effect of the replacement using the momentum constraint equation.

Moreover, they predicted that several combinations of modifications have a constraint-damping nature, and named them *adjusted* BSSN systems. (Their predictions are based on the signature of eigenvalues of the constraint propagations, and the negative signature implies a dynamical system which evolves toward the constraint surface as the attractor.)

Among them, in this work, we test the following three adjustments:

1. An adjustment of the $\tilde{A}$-equation with the momentum constraint:

$$\partial_t\tilde{A}_{ij} = \partial_t^B\tilde{A}_{ij} + \kappa_A\alpha\tilde{D}_{(i}\mathcal{M}_{j)}, \tag{11}$$

   where $\kappa_{\mathcal{A}}$ is predicted (from the eigenvalue analysis) to be positive in order to damp the constraint violations.

2. An adjustment of the $\tilde{\gamma}$-equation with $\mathcal{G}$ constraint:

$$\partial_t\tilde{\gamma}_{ij} = \partial_t^B\tilde{\gamma}_{ij} + \kappa_{\tilde{\gamma}}\alpha\tilde{\gamma}_{k(i}\tilde{D}_{j)}\mathcal{G}^k, \tag{12}$$

   with $\kappa_{\tilde{\gamma}} < 0$.

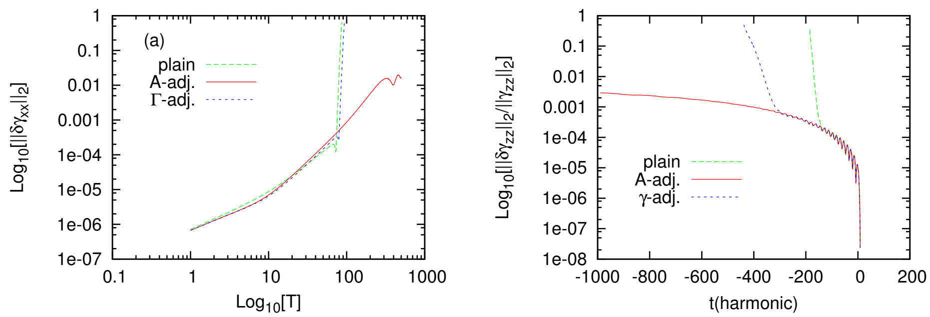

Figure 1: Evaluation of the accuracy of (a) the one-dimensional gauge-wave and (b) Gowdy wave testbeds. The lines in Fig. (a) are the L2 norm of the error in γ_{xx} with the plain BSSN, the adjusted BSSN with $\mathcal{A}$-equation, and with $\tilde{\Gamma}$-equation. The lines in Fig. (b) are the L2 norm of the error in γ_{zz}, rescaled by the L2 norm of γ_{zz}, for the plain BSSN, adjusted BSSN with $\tilde{\mathcal{A}}$-equation, and with $\tilde{\gamma}$-equation.

3. An adjustment of the $\tilde{\Gamma}$-equation with $\mathcal{G}$ constraint:

$$\partial_t \tilde{\Gamma}^i = \partial_t^B \tilde{\Gamma}^i + \kappa_{\tilde{\Gamma}} \alpha \mathcal{G}^i. \tag{13}$$

with $\kappa_{\tilde{\Gamma}} < 0$.

These three adjustments are chosen as samples of "best candidates", Eq. (4.9)-(4.11) in [10].

3 Numerical Testbed Models

Following the proposals of the Mexico Numerical Relativity Workshop [11], we perform three kinds of tests;

- One dimensional Gauge wave test with amplitude 10^{-2}
- One dimensional Linear wave test with amplitude 10^{-8}
- One dimensional Gowdy wave test in collapsing direction

The details of the testbeds are represented in [11].

4 Numerical Results

For saving sapce, we only show the result of the Gauge wave and Gowdy wave test because the linear wave testbed does not produce a significant constraint violation even for the plain BSSN system and the adjusted system can reproduce the same result as the plain system.

In Fig. 1(a), we plot the L2 norm of the error in γ_{xx} with the function of time. Three lines correspond to the result of the plain BSSN system, $\tilde{A}$-eq. adjusted, and $\tilde{\Gamma}$-eq. adjusted BSSN system, respectively. The $\tilde{\Gamma}$-adjustment makes the life-time slightly longer than that of the plain BSSN, while $\tilde{A}$-adjustment increases the life-time of the simulation by a factor of 10. However, it is also true that the error grows in time in all the three cases.

Figure 1(b) shows the normalized error in γ_{zz} versus time for the plain BSSN, adjusted BSSN with $\tilde{\mathcal{A}}$-equation, and adjusted BSSN with $\tilde{\gamma}$-equation systems. We find that these three systems produce accurate results up to $t = 200$, $t = 1000$, and $t = 400$, respectively. This proves that the adjustments work effectively, i.e, they make possible a stable and accurate simulation, especially the $\mathcal{A}$-adjusted BSSN system.

5 Summary and Discussion

In this article, we presented our numerical comparisons of the BSSN formulation and its adjusted versions using constraints. We can summarize our tests as follows:

- Among the adjustments we tried, we observed that the adjusted BSSN system with the $\tilde{A}$-eq. (11) is the most robust for all the testbeds examined in this study. It gives us an accurate and stable evolution compared to the plain BSSN system. Quantitatively, the life-time of the simulation becomes 10 times longer for the gauge-wave testbed and 5 times longer for the Gowdy-wave testbed than the life-time of the plain BSSN system. However, it should be noted that for the gauge-wave testbed, the convergence feature is lost at a comparatively early time, the 200 crossing-time in the Hamiltonian constraint and the 50 crossing-time in the momentum constraint.

In [12], it is argued that the gauge condition in the Gauge wave testbed has a residual freedom in the form $H \to e^{\lambda t}H$, where λ is an arbitrary and H is a function in the Gauge wave testbed. Of course, our set up corresponds to the $\lambda = 0$ case, but numerical error easily excites modes that result in either exponentially increasing or decaying metric amplitude. Actually, we find the amplitude of the error decays with time in this testbed. So, we conclude that due to the adjustment, the growing rate of the gauge mode is suppressed and the life-time of the simulation is extended as a result.

- The other type of adjustments (12 and 13) show their apparent effects while depending on a problem. The $\tilde{\Gamma}$-adjustment for the gauge-wave testbed makes the life-time longer slightly. The $\tilde{\gamma}$-adjustment for the Gowdy-wave testbed makes possible a simulation twice as long as the plain BSSN system.

Although the testbeds used in this work are simple, it might be rather surprising to observe the expected effects of adjustments with such a slight change in the evolution equations. We therefore think that our demonstrations imply a potential to construct a robust system against constraint violations even in highly dynamical situations, such as black hole formation via gravitational collapse, or binary merger problems. We are now preparing our strong-field tests of the adjusted BSSN systems using large amplitude gravitational waves, black hole space-time, or non-vacuum space-time, which will be reported on in the near future.

References

[1] M. Shibata, K. Taniguchi and K. Uryu, Phys. Rev. D **68**, 084020 (2003), Phys. Rev. D **71**, 084021 (2005)

[2] F. Pretorius, Phys. Rev. Lett. **95**, 121101 (2005)

[3] M. Campanelli, C. O. Lousto, P. Marronetti and Y. Zlochower, Phys. Rev. Lett. **96**, 111101 (2006)

[4] M. Shibata and K. Uryu, Phys. Rev. D **74**, 121503 (2006), Class. Quant. Grav. **24**, S125 (2007)

[5] T.W. Baumgarte and S.L. Shapiro, Phys. Rev. D **59**, 024007 (1999).

[6] T. Nakamura, K. Oohara and Y. Kojima, Prog. Theor. Phys. Suppl. **90**, 1 (1987). M. Shibata and T. Nakamura, Phys. Rev. D **52**, 5428 (1995).

[7] H. Beyer, and O. Sarbach, Phys. Rev. D **70**, 104004 (2004).

[8] C. Gundlach, J. M. Martin-Garcia, Phys. Rev. D **74**, 024016 (2006).

[9] H. Shinkai and G. Yoneda, gr-qc/0209111.

[10] G. Yoneda and H. Shinkai, Phys. Rev. D **66**, 124003 (2002).

[11] M. Alcubierre *et al.*, Class. Quant. Grav. **21**, 589 (2004)

[12] M. C. Babiuc *et al.* [Apples With Apples Collaboration], arXiv:0709.3559 [gr-qc].

[13] K. Kiuchi and H. a. Shinkai, arXiv:0711.3575 [gr-qc] appeared in PRD.

Gravitational self force on a particle in orbit around a Schwarzschild black hole

Leor Barack and Norichika Sago[1]

School of Mathematics, University of Southampton, Southampton, SO17 1BJ, United Kingdom

Abstract

We calculate the gravitational self force acting on a pointlike particle orbiting a Schwarzschild black hole. For this purpose, first, we solve the (1+1)-dim field equations for the Lorenz-gauge perturbations by using a time-domain code. Then we derive each multipole mode of the full force from the given perturbation. Finally, we apply the "mode sum" scheme to obtain the physical self force. We evaluate the correction to the orbital frequency due to the conservative self-force effect. We also show that the temporal component of the self force balances with the total energy flux of the gravitational-wave radiated to infinity and through the event horizon.

1 Introduction

The problem of calculating the back-reaction force, or *self force* (SF), experienced by a point particle as it moves in curved spacetime is now understood well enough to allow actual computations of this effect in systems comprising of a small object orbiting a large black hole. The fundamental formulation of the problem and its solution was set in works by Mino, Sasaki and Tanaka [1] and Quinn and Wald [2] for gravitational case. An alternative formulation was introduced by Detweiler and Whiting [3], also clarifying the relation between the SF picture ("forced motion on a background geometry") and the standard description based on the principle of equivalence ("geodesic motion in a perturbed geometry"). A number of authors later devised a practical method of calculating the SF in black hole spacetimes, so-called the "mode sum scheme", which is based on multipole decomposition of the retarded field, and relies on standard methods of black hole perturbation theory [4]. This method has since been implemented by various authors on a case-by case basis, so far mostly for calculations of the *scalar field* SF. The *gravitational* SF has been calculated so far only for radial trajectories in Schwarzschild [5] and for static particles in Schwarzschild [6]. The case of an orbiting particle has been tackled only under the post-Newtonian (PN) approximation [7].

The main challenge in extending the analysis from the scalar-field toy model to the gravitational case has to do with the gauge freedom in the latter case. The problem can be summarized as follows. The gravitational perturbation in the vicinity of the point particle is best described using the *Lorenz* gauge, which preserves the local isotropic nature of the point singularity. On the other hand, the field equations that govern the global evolution of the metric perturbation are more tractable in gauges which comply well with the global symmetry of the black hole background—best known examples of which are the "radiation" gauges [8] or the Regge-Wheeler gauge [9]. Now, in calculating the local SF we need, essentially, to subtract a suitable local, divergent piece of the perturbation from the full (retarded) perturbation field. In doing so, both fields (local and global) must be given in the same gauge; the "gauge problem" arises since the two fields are normally calculated in different gauges. Indeed, the only fully-worked-out example of the gravitational SF so far is the case of radial orbits in Schwarzschild [5], where the gauge problem is avoided simply because, in this particular setup, the singular piece of the Regge-Wheeler perturbation happens to coincide with that of the Lorenz-gauge perturbation.

Our strategy to settle the problem is that we solve the perturbation equations directly in the Lorenz gauge. The calculation is therefore done entirely within the Lorenz gauge, the "subtraction" procedure necessary for constructing the SF is implemented in a straightforward way, and the gauge problem is avoided altogether. Other advantages of working in the Lorenz gauge include the fact that the field equations then take a fully hyperbolic form (making them especially suitable for time-domain integration);

[1] E-mail:sago@soton.ac.uk

r_0/M	$(M/\mu)^2 F^t$	$(M/\mu)^2 F_t/u_0^t$	$(M/\mu)^2 \dot{E}_{\rm total}$	rel. diff.
6.0	-1.99476×10^{-3}	9.40338×10^{-4}	9.40190×10^{-4}	1.6×10^{-4}
10.0	-9.19067×10^{-5}	6.15158×10^{-5}	6.15047×10^{-5}	1.8×10^{-4}
20.0	-2.25549×10^{-6}	1.87151×10^{-6}	1.87111×10^{-6}	2.2×10^{-4}
50.0	-2.10849×10^{-8}	1.96249×10^{-8}	1.96203×10^{-8}	2.3×10^{-4}
100.0	-6.46305×10^{-10}	6.23806×10^{-10}	6.23628×10^{-10}	2.9×10^{-4}
150.0	-8.47172×10^{-11}	8.27475×10^{-11}	8.27279×10^{-11}	2.4×10^{-4}

Table 1: The t component of the SF, as a function of the orbital radius. The estimated fractional error in F^t is less than 10^{-4} for all radii considered. The third and fourth columns compare between the work done by the temporal SF and the total flux of energy radiated in gravitational waves. The error in the total flux is roughly estimated at $O(10^{-4})$. The last column displays the relative difference $\left|\dot{E}_{\rm total}/(F_t/u_0^t) - 1\right|$, showing that the balance equation (1) is satisfied within the numerical accuracy, and providing a strong quantitative check of our results.

and the fact that the Lorenz-gauge metric perturbation is better behaved near the particle compared with the perturbation in other gauges [10] (which, again, makes it more suitable for numerical implementation).

Our "all-Lorenz-gauge" approach is made possible (at least is the Schwarzschild case) following a recent work by Barack and Lousto [11], which provided a practical formulation of the Lorenz-gauge perturbation equations in the Schwarzschild geometry and developed a time-domain code to solve them. Recently, by using this approach, we calculated the gravitational SF for circular geodesic orbits in Schwarzschild geometry. In this paper, we give a brief summary of the results we obtained in our recent work. The details of our numerical code and full results are shown in [12].

Throughout this work, we denote the masses of a orbiting point particle and a central Schwarzschild black hole as μ and M, respectively. Also we use standard geometrized units with $c = G = 1$ and metric signature $(-+++)$.

2 Results

Temporal component : We calculated the temporal component of the SF, F^t, for 29 values of the orbital radius r_0, in the range from $r_0 = 6M$ to $r_0 = 150M$. Some of the results are displayed in Table 1 (The full table is shown in [12]). The computation error in F^t is estimated at $\lesssim 10^{-4}$ for all radii considered.

The t component of the SF is related to the momentary rate of change of the specific orbital energy parameter $\mathcal{E}$ as $\dot{\mathcal{E}} = -(\mu u_0^t)^{-1} F_t$, where an overdot denotes d/dt, and $u_0^t = (1 - 3M/r_0)^{-1/2}$. If we assume that the radiation reaction is negligible over an orbital period $T_{\rm orb}$, then, for a circular orbit, $\dot{\mathcal{E}}$ also represents the average rate of change of $\mathcal{E}$ over $T_{\rm orb}$. This must be balanced by the flux of gravitational-wave energy radiated to infinity and through the horizon, averaged over $T_{\rm orb}$. If we denote the former by $\dot{E}_\infty$ and the latter by $\dot{E}_{\rm EH}$, we have the energy balance formula

$$\dot{E}_{\rm total} \equiv \dot{E}_\infty + \dot{E}_{\rm EH} = -\mu\dot{\mathcal{E}} = F_t/u_0^t. \tag{1}$$

In Table 1, we also list $-(\mu u_0^t)^{-1} F_t$ and $\dot{E}_{\rm total}$. This shows, for each of the radii considered, how the work done by the temporal component of the local SF is balanced by the total flux of radiated energy.

Radial component : We calculated the radial component of the SF, F^r, for 29 values of the orbital radius, in the range from $r_0 = 6M$ to $t_0 = 150M$. We plot them as a function of r_0 in Fig. 1. The radial SF is "repulsive" (i.e, acting outward, away from the central black hole) for all r_0. At large orbital radii the numerical data can be fitted analytically as

$$F^r(r_0 \gg M) \simeq \frac{\mu^2}{r_0^2}\left[a_0 + a_1\frac{M}{r_0} + a_2\left(\frac{M}{r_0}\right)^2 + a_3\left(\frac{M}{r_0}\right)^3\right], \tag{2}$$

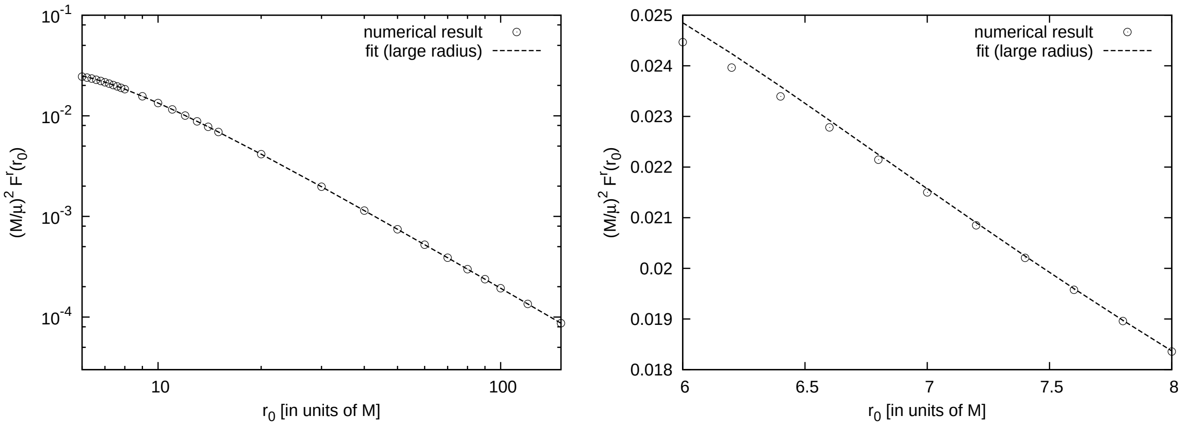

Figure 1: The radial component of the SF. The left figure shows $F^r(r_0)$ for $6M \le r_0 \le 150M$. The right shows a expansion of the ISCO area. The dashed line is a plot of the large-r_0 fit given in Eq. (2).

with

$$a_0 = 1.999991, \quad a_1 = -6.9969, \quad a_2 = 6.29, \quad a_3 = -24.6. \tag{3}$$

This formula reproduces the numerical data within the numerical accuracy [$\lesssim 10^{-3}$] for all $r_0 \ge 8M$. The leading-order term, $F^r \simeq a_0\mu^2/r_0^2 \simeq 2\mu^2/r_0^2$ is consistent with the "Keplerian" SF describing the back-reaction effect from the motion of the black hole about the system's center of mass (cf. below).

Conservative effect on the orbital frequency : Given F^r, we can calculate the shift in the orbital frequency induced by the conservative SF effect as

$$\Omega^2 = \Omega_0^2\left[1 - \left(\frac{r_0(r_0-3M)}{M\mu}\right)F_r\right] + O((\mu/M)^2), \tag{4}$$

where $\Omega_0^2 = M/r_0^3$. At large r_0 we obtain, using Eq. (2),

$$\Omega^2(r_0 \gg M) \simeq \Omega_0^2\left\{1 + \frac{\mu}{M}\left[-a_0 + c_1\frac{M}{r_0} + c_2\left(\frac{M}{r_0}\right)^2 + c_3\left(\frac{M}{r_0}\right)^3\right]\right\}, \tag{5}$$

where $c_1 = 3a_0 - a_1$, $c_2 = 3a_1 - a_2$, and $c_3 = 3a_2 - a_3$, with the coefficients a_n given in Eq. (3). The term proportional to $a_0(\simeq 2)$ is precisely the "Newtonian" SF, [see, e.g., Eq. (2) of [13]], which dominates the SF effect at $r_0 \gg M$. This piece of the force is simply the $O(\mu)$ difference between the standard Keplerian frequency $\Omega^2 = (M+\mu)/R^3$ (expressed in terms of the separation R) and $\Omega_0^2 = M/r_0^3$, with the separation R related to the "center-of-mass" distance r_0 through $M(R - r_0) = \mu r_0$.

3 Summary

In this work, we compute the gravitational SF in an example of a particle orbiting a black hole, demonstrating the applicability of our approach, whose main elements are (i) direct solution for the metric perturbation, in the Lorenz gauge; (ii) numerical evolution in the time domain; and (iii) use of the mode-sum scheme to derive the local SF. In the case of a strictly circular orbit, the analysis of the local SF provides us with little new physics: The radiative effect is well known from energy-balance analysis, and the conservative force does not have a strict gauge-invariant significance. Calculation of gauge invariant conservative effects (like the shift in the ISCO frequency, or the correction to the rate of perihelion precession) requires analysis of non-circular orbits. In follow-up work we intend to extend our analysis to eccentric orbits, which would gain us access to this more interesting physics.

Self-force calculations bring about major issues of computational cost and computational efficiency. We need to sophisticate our time-domain code to studying more general orbits. There are a few obvious ways by which one may improve the efficiency of the numerical algorithm: (1) We may try to improve the finite difference scheme used in our evolution code. In our current code, we adopt a 2nd-order-convergent finite difference scheme. By replacing it to a higher order scheme, we can obtain more accurate results. (We already have developed a code to solve the Lorenz-gauge perturbation equations by using 4th-order-convergent scheme in our coming work [14].) (2) Our evolution code currently utilizes a uniform grid. This is very inefficient, since the resolution requirement near the worldline is much higher than anywhere else on the 2-dimensional grid. A mesh-refinement technique may settle this inefficiency [15].

Since our code is based on time-domain evolution (with no frequency decomposition), it is readily extensible to deal with any orbit in Schwarzschild spacetime. The finite-difference algorithm would change slightly, but the stability features and resolution requirements of the code would not change. Work to extend our analysis to eccentric orbits is now in progress [14].

It is more challenging to apply our approach for orbits in Kerr spacetime. In this case we may no longer rely on a spherical-harmonic decomposition of the field equations, and—insisting on a time-domain analysis in the Lorenz gauge—we would have to apply time evolution in 2+1-D. The challenge here is two-fold: Firstly, the solutions to the 2+1-D field equations are no longer continuous along the worldline (as in the 1+1-D case), but rather diverge there logarithmically. Secondly, a stable numerical scheme for evolution of Lorenz-gauge perturbations in $2+1$D is yet to be developed. A numerical scheme for dealing with the first of the above difficulties had been outlined in Sec. V of BL, and was recently implemented for a scalar-field toy model [16].

Acknowledgements

This work was supported by PPARC through grant number PP/D001110/1.

References

[1] Y. Mino, M. Sasaki and T. Tanaka, Phys. Rev. D **55**, 3457 (1997) [arXiv:gr-qc/9606018].

[2] T. C. Quinn and R. M. Wald, Phys. Rev. D **56**, 3381 (1997) [arXiv:gr-qc/9610053].

[3] S. Detweiler and B. F. Whiting, Phys. Rev. D **67**, 024025 (2003) [arXiv:gr-qc/0202086].

[4] L. Barack, Y. Mino, H. Nakano, A. Ori and M. Sasaki, Phys. Rev. Lett. **88**, 091101 (2002) [arXiv:gr-qc/0111001].

[5] L. Barack and C. O. Lousto, Phys. Rev. D **66**, 061502 (2002) [arXiv:gr-qc/0205043].

[6] T. S. Keidl, J. L. Friedman and A. G. Wiseman, arXiv:gr-qc/0611072.

[7] W. Hikida, H. Nakano and M. Sasaki, Class. Quant. Grav. **22**, S753 (2005) [arXiv:gr-qc/0411150].

[8] P. L. Chrzanowski, Phys. Rev. D **11**, 2042 (1975).

[9] T. Regge and J. A. Wheeler, Phys. Rev. **108**, 1063 (1957).

[10] L. Barack and A. Ori, Phys. Rev. D **64**, 124003 (2001) [arXiv:gr-qc/0107056].

[11] L. Barack and C. O. Lousto, Phys. Rev. D **72**, 104026 (2005) [arXiv:gr-qc/0510019].

[12] L. Barack and N. Sago, Phys. Rev. D **75**, 064021 (2007) [arXiv:gr-qc/0701069].

[13] S. Detweiler, Class. Quant. Grav. **22**, S681 (2005) [arXiv:gr-qc/0501004].

[14] L. Barack and N. Sago, in preparation.

[15] L. Barack and J. Thornburg, in preparation.

[16] L. Barack and D. A. Golbourn, Phys. Rev. D **76**, 044020 (2007) [arXiv:0705.3620 [gr-qc]].

Collapse of differentially rotating relativistic stars: Post black hole formation stage

Motoyuki Saijo[1] and Ian Hawke[2]

School of Mathematics, University of Southampton, Southampton SO17 1BJ, United Kingdom

Abstract

We investigate the collapse of differentially rotating supermassive stars (SMSs) by means of 3+1 hydrodynamic simulations in general relativity. We particularly focus on the onset of collapse to understand the final outcome of collapsing SMSs. We find that the estimated ratio between the black hole (BH) and the surrounding disk from the equilibrium star is roughly the same as the results from numerical simulation. This statement suggests that the picture of axisymmetric collapse is adequate in the absence of nonaxisymmetric instabilities for illustrating the final state of the collapse. We also find that when the newly formed BH is almost an extreme Kerr, a corotation resonance can be triggered by the oscillation of a BH. In this case, nonaxisymmetric instabilities are triggered by corotation resonance and make a significant difference in the gravitational waveforms. This alternative scenario for the collapse of differentially rotating SMSs might be observable by LISA.

There exists plenty of evidence that supermassive black holes (SMBHs) exists in the centre of galaxies, but their actual formation process has been a mystery for many decades [1]. Several different scenarios have been proposed, some based on stellar dynamics, others on gas hydrodynamics, and still others that combine the processes. Here we consider a possibility of forming an SMBH from the collapse of a supermassive star (SMS).

There are two categories of collapsing rotating SMSs based on their angular momentum distribution. One is the collapse of a uniformly rotating SMS. This happens when momentum transport is large, either through viscous turbulence or magnetic process, which drives the star to rotate uniformly. The other is the collapse of differentially rotating SMSs. This happens when the viscous and the magnetic effects are small, which allows the star to rotate differentially. One of the representative scenarios for forming a differentially rotating star is as follows. First, a gas cloud gathers in an almost spherical configuration with some amount of angular momentum in the system. Next the almost spherical star contracts, conserving the specific angular momentum due to the lack of viscosity, to form a differentially rotating star, and possibly a disk at the end of the contraction.

During the contraction of the differentially rotating SMS, prior to forming a supermassive disk, two possible instabilities may arise that terminate the contraction. One is the post-Newtonian gravitational instability, which leads the star to collapse dynamically. The other is the dynamical bar mode instability, which changes the angular momentum distribution of the star to form a bar, and possibly leads to the central core of the star collapsing to a black hole (BH) due to the angular momentum loss.

Here we focus on the post-Newtonian gravitational instability in differentially rotating SMSs. We particularly focus on the case where the final estimated BH is very close to the extreme Kerr BH, which potentially leads to rotational instabilities if they occur. In particular, we plan to answer the following questions. Does the BH form coherently? What are the features of the dynamics? Does the newly formed disk lead to contain various instabilities? Can this system act as an efficient source of gravitational waves (GWs)? In order to answer these questions, three dimensional general relativistic hydrodynamics are desirable. A more detailed discussion will be presented in the forthcoming paper [2]. Throughout this paper, we use the geometrized units with $G = c = 1$ and adopt Cartesian coordinates (x, y, z) with the coordinate time t.

[1] Email address: ms1@maths.soton.ac.uk
[2] Email address: I.Hawke@soton.ac.uk

Table 1: Four different rotating equilibrium SMSs for evolution.

Model	$\rho_0^{\max(a)}$	$M^{(b)}$	$J/M^{2(c)}$	$M/R_{\rm e}{}^{(d)}$	$m_{\rm disk}{}^{(e)}$	$(a/M)^{({\rm BH})(f)}$
I	1.56×10^{-5}	4.88	0.99	2.56×10^{-2}	0.044	0.98
II	1.56×10^{-5}	5.07	1.03	2.63×10^{-2}	—	$\gtrsim 1$
III	1.56×10^{-5}	5.31	1.07	2.78×10^{-2}	—	$\gtrsim 1$
IV	1.56×10^{-5}	5.75	1.10	3.47×10^{-2}	—	$\gtrsim 1$

(a): Maximum rest mass density
(b): Gravitational mass
(c): J: Total angular momentum
(d): R_e: Equatorial proper radius
(e): Ratio of the estimated rest mass of the disk from the equilibrium star to the rest mass of the equilibrium star
(f): Estimated Kerr parameter of the final hole from the equilibrium star

We perform 3+1 hydrodynamic simulations in general relativity using CACTUS[3] (gravitational physics), CARPET[4] (mesh refinement of space and time), WHISKY[5] (general relativistic hydrodynamics). Spacetime is evolved using the BSSN formulation with generalised hyperbolic K-driver for the lapse and generalised hyperbolic $\tilde{\Gamma}$-driver for the shift (e.g. [2]). We set the outermost boundary of the computational grid for all direction as $x_{\rm max} = 111 - 131M$, imposing plane symmetry across the $z = 0$ plane, and use $4 - 10$ refinement levels.

We first investigate the onset of collapse by evolving four differentially rotating equilibrium stars. We use the perfect fluid approximation with a Γ-law equation of state, choosing $\Gamma = 4/3$ to represent a SMS (the pressure is dominated by radiation pressure). We also impose a high degree of differential rotation, $\Omega_{\rm c}/\Omega_{\rm e} \approx 10$, to construct the equilibrium star, where Ω_c and Ω_e represents the angular velocity at the center and the equatorial surface, respectively. We choose the z-axis as the rotational one of the equilibrium star. The character of the equilibrium stars is summarized in Table 1. Since we use the polytropic equation of state $P = \kappa \rho_0^{\Gamma}$ (P: pressure, κ: constant, ρ_0: rest mass density, Γ: adiabatic exponent) when constructing initial data sets, all physical quantities are rescalable in terms of κ. Therefore, we represent all physical quantities in a nondimensional one in this paper, which is equivalent to setting $\kappa = 1$. To trigger collapse we deplete pressure by 1%. Checking the maximum rest mass density of the rotating stars throughout the evolution, we conclude that models I and II are radially unstable, while models III and IV are stable [2].

Next we trace the mass and angular momentum of the newly formed BH throughout the evolution using the technique of dynamical horizon. A dynamical horizon is defined as the spacelike marginally trapped tube which is composed of future-marginally trapped surface, i.e. apparent horizon. In order to compute the gravitational mass and the total angular momentum of the BH locally, we need to construct the timelike and the rotational Killing vectors intrinsic to the horizon, should they exist on the horizon numerically (e.g. [3]). Using these Killing vectors, we monitor the gravitational mass, total angular momentum and the Kerr parameter of the newly formed BH throughout the evolution (Fig. 1). The BH mass, the spin and the Kerr parameter increase monotonically after the BH has formed, by swallowing much of the surrounding material. This stage lasts roughly until the matter is swallowed, located inside the radius of the innermost stable circular orbit of the final BH.

We have also confirmed that the estimated mass and spin of the BH from the equilibrium configuration of the collapsing SMS are in good agreement with the results from the dynamics. For instance, the estimated Kerr parameter from the equilibrium star of model I is 0.98 (Table 1), while the result of numerical simulation is ≈ 0.97 (Fig. 1). Also the ratio between the estimated rest mass of the disk and the rest mass of the equilibrium star of model II is 0.044 (Table 1), while the result of numerical simulation is ≈ 0.05 (Fig. 2).

[3]http://www.cactuscode.org
[4]http://www.carpetcode.org
[5]http://www.whiskycode.org

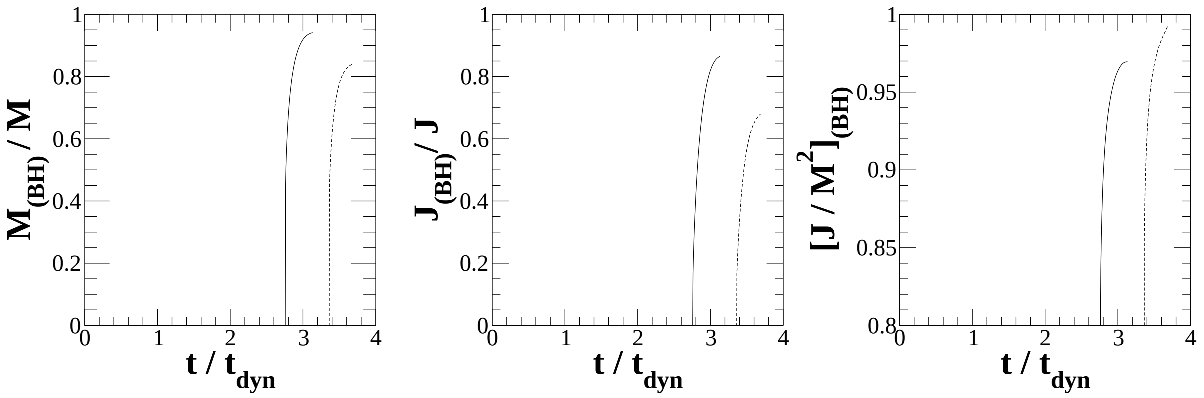

Figure 1: Gravitational mass ($M_{(\mathrm{BH})}$), total angular momentum ($J_{(\mathrm{BH})}$) and Kerr parameter ($(J/M^2)_{(\mathrm{BH})}$) of a newly formed BH as a function of time. Solid and dashed line represent models I and II, respectively. Hereafter t_{dyn} represents the dynamical time defined as $t_{\mathrm{dyn}} = \sqrt{R_e^3/M}$.

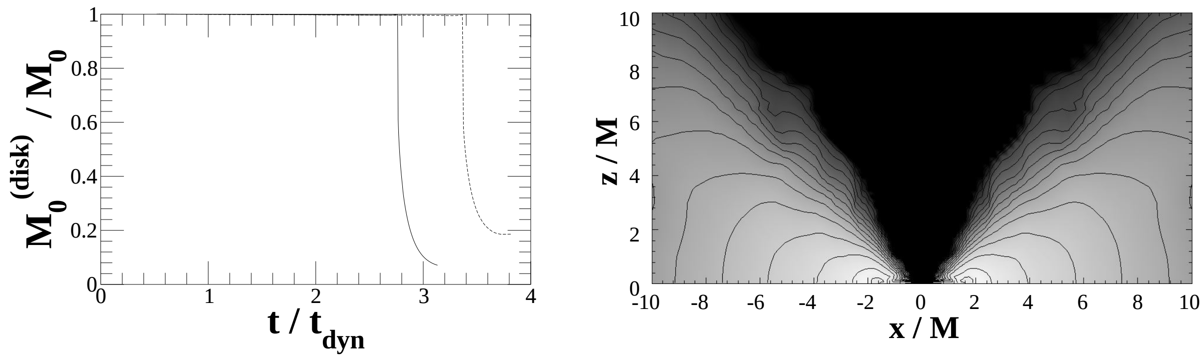

Figure 2: (Left panel) Disk mass as a function of time. We defined the disk mass as the rest mass outside the apparent horizon of the newly formed BH. Solid and dashed line represent models I and II, respectively.
(Right panel) Snapshot of the rest mass density in the meridional plane for model III at $t = 3.82 t_{\mathrm{dyn}}$. The contour lines denote $\rho_0/\rho_0^{\max} = 10^{-0.4(20-i)}$ $(i = 1, \cdots, 20)$, where $\rho_0^{\max} = 8.56 \times 10^{-5}$. Note that the radius of the apparent horizon in the equatorial plane is $r \approx 0.16M$ in coordinate units.

We furthermore study the formation of a massive disk from the collapse of differentially rotating SMSs. We trace the rest mass of the disk by defining the rest mass outside the apparent horizon of the newly formed BH for models I and II (Fig. 2). The rest mass of the disk monotonically decreases once the BH has formed, since the newly formed BH grows monotonically by swallowing the surrounding materials. One noticeable feature in Fig. 2 is that there is a plateau at the final stage of model II. This indicates that the self gravity, the centrifugal force, and the pressure gradient are roughly balanced so that the disk can maintain Keplarian orbital motion around the BH. We also illustrate the snapshot of the rest mass density in the meridional plane of model II (Fig. 2). The maximum of the rest mass density is located around $r \approx 2M$ in coordinate units.

Finally we investigate the gravitational waveform from the collapsing object. We introduce the Weyl scalar Ψ_4 to study the outgoing gravitational waves. If we put the observer sufficiently far from the source, the Weyl scalar Ψ_4 roughly represents the outgoing gravitational waves, ignoring the radiation back scattered by the curvature. We observe the waveform (the real component of Ψ_4) along the x-axis in the equatorial plane at coordinate location $r \approx 60M$ for models I and II. Note that the equatorial radius of the equilibrium star is $r \approx 38.0M - 39.1M$ for models I and II. We find that the waveform contains three different stages. The first stage is the burst. This happens around horizon formation of

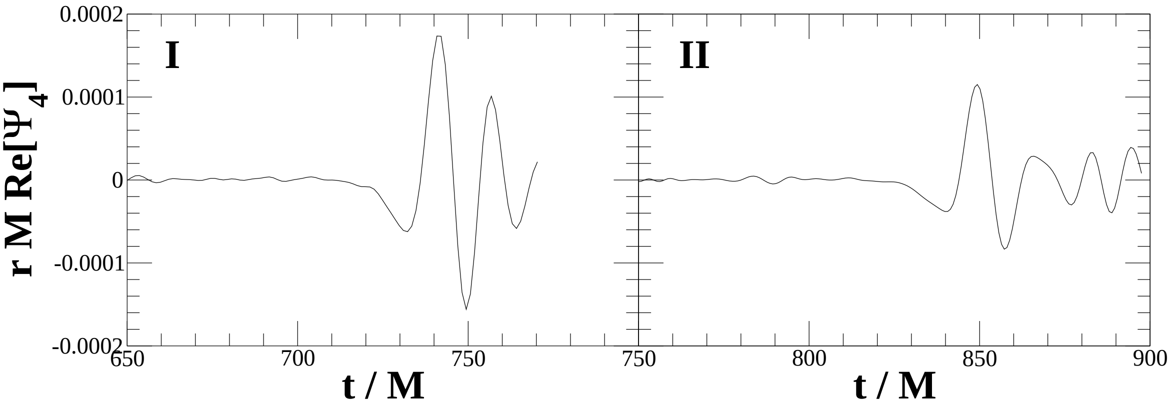

Figure 3: Gravitational waveform measured with the Weyl scalar Ψ_4 observed along the x-axis in the equatorial plane at $r = 61.43M$ for model I and $r = 59.20M$ for model II. Note that the time at which the apparent horizon is first detected is $t = 676M$ for model I and $t = 788M$ for model II, respectively. Taking the wave propagation time from the source to the observer into account, the apparent horizon formation in the waveform is roughly just before the peak due to the burst.

collapsing SMS. The dominant contribution of the burst comes from the axisymmetric mode due to the radial instability. The second stage is the quasinormal ringing of a newly formed BH. The dominant contribution is again the axisymmetric mode. The final stage might be related to an instability in the disk, and only appears in the model II. In fact when the spin of the newly formed BH is very close to the extreme Kerr, the amplitude of the gravitational wave signal gradually grows after the quasinormal ringing. We also check the azimuthal m modes of the rest mass density traced at the certain radius in the equatorial plane, and found that the $m = 2$ mode starts growing exponentially after the ringdown. One possible explanation for the exponential growth of the $m = 2$ mode at late times is the existence of corotation resonance of the newly formed disk triggered by the vibration of the hole. The dominant quasinormal mode of the BH has the frequency is $M\omega_{\rm qnm} = 0.43$ for $a/M = 0.9998$ [4], where $\omega_{\rm qnm}$ is a frequency of the quasinormal mode and a is the Kerr parameter. If the corotation resonance is triggered by quasinormal ringing, the necessary condition for triggering a corotation resonance is $\omega_{\rm qnm} = m\Omega$ (e.g. [5]) at a certain radius of the star, where Ω is the angular velocity. Since the inner part of the disk has $M\Omega \approx 0.38$ and $r \approx 0.79M$ in coordinate unit (Fig. 2), there exists a radius inside the disk which satisfies the above condition. In order to confirm the growth in the amplitude and the possible interpretation as corotation resonance, further time integration from our termination time of the three dimensional hydrodynamics in general relativity is necessary. Since we terminate the time integration by hand, there is no obstacle of continuing our simulation except for the computational time.

We investigate the collapse of differentially rotating SMSs, especially focusing on the post BH formation stage, by means of three dimensional hydrodynamic simulations in general relativity. We particularly focus on the onset of collapse to form a rapidly rotating hole as the final outcome.

We have found that the evolutional results about the feature of the final hole and the disk behaves quite similar to the estimation from the equilibrium configuration when the estimated, final BH has $J_{\rm (BH)}/M_{\rm (BH)}^2 < 1$. This result suggests that in the absence of a nonaxisymmetric instability, the estimation of the BH mass and the disk mass agree with a simple axisymmetric picture that the specific angular momentum is conserved throughout the evolution and the newly formed BH swallows the matter up to the radius of the innermost stable circular orbit.

We have also found that when the newly formed BH is "very" close to the extreme Kerr with sufficient matter around it, a corotational resonance of the matter may be triggered by the quasi-normal mode of the BH. As the Kerr parameter goes to 1, the radius of the innermost stable circular orbit coincides with that of the event horizon. Hence the necessary condition for the corotation resonance triggered by the vibration of the BH is satisfied. Therefore the system potentially emits gravitational waves effectively due to the resonance. However, further time integration of the post BH formation stage is necessary to confirm the above statement.

References

[1] M. Rees, in *The Future of Theoretical Physics and Cosmology*, edited by G. W. Gibbons, E. P. S. Shellard and S. J. Rankin (Cambridge Univ. Press, Cambridge, 2003), 17.

[2] M. Saijo and I. Hawke, in preparation (2008).

[3] E. Schnetter, B. Krishnan and F. Beyer, Phys. Rev. D **74**, 024028 (2006).

[4] E. W. Leaver, Proc. R. Soc. London A **402**, 285 (1985).

[5] M. Saijo and S.'i. Yoshida, Mon. Not. R. Astron. Soc. **368**, 1429 (2006).

Time-Symmetric Initial Data of Brane-Localized Black hole in RS-II Model

Norihiro Tanahashi[1] and Takahiro Tanaka[2]

Department of Physics, Kyoto University, Kyoto 606–8502, Japan

Abstract

In the aim of shedding a new light on the classical black hole evaporation conjecture, we investigate time-symmetric initial data with a brane-localized apparent horizon (AH) and analyzed its properties. As a result, we unambiguously confirm that initial data with an arbitrarily large AH area do exist. We compare the ADM mass and the horizon area of our initial data with that of the black string (BS) solution, and further investigate what kind of configuration realizes the minimum mass for the same AH area. All the results of the analysis are consistent with the classical BH evaporation conjecture.

1 Introduction

The Randall-Sundrum II (RS-II) model [1] is a brane world model, which provides a way to realize our four-dimensional world in a higher-dimensional spacetime. RS-II model is composed of five-dimensional bulk spacetime with negative cosmological constant and a four-dimensional brane with positive tension. It is known that the weak gravitational field on the brane obeys the usual four-dimensional Newton law with a correction suppressed at a large distance from the gravitational source [1, 2], though the extra-dimension extends infinitely in this model. This fact means that it is difficult to distinguish this model from an ordinary four-dimensional model as long as we investigate the weak gravity regime. Thus we turn focus on strong gravity phenomena, such as gravitational collapse on the brane.

Naively, a static black hole (BH) whose horizon is localized near the brane will be formed as a final state of gravitational collapse on the brane. There is an exact static solution with an event horizon, which is black string (BS) [3], but it seems unlikely that a BS is formed as a result of gravitational collapse since it is singular and also unstable due to so-called Gregory-Laflamme instability [4]. A static solution of a large BH localized on the brane, however, has not been discovered yet, despite lots of effort on this issue (e.g. Ref. [5]. Numerical solution of a static brane-localized BH has been constructed when the horizon size is not much larger than the bulk curvature scale, but the construction becomes harder as the horizon size becomes larger [6, 7]. This fact does not exclude the possibility that a static solution of brane-localized BH larger than the bulk curvature scale does exist, but we do not have any strong evidence of its existence. As an explanation of the lack of static solution, there is a conjecture that brane-localized static BHs larger than bulk curvature scale do not exist in RS-II model based on the AdS/CFT correspondence [8, 9].

There are several works related to this conjecture (e.g. [10, 11]), but no definite conclusion is obtained yet. It is desirable to investigate the properties of static black hole solution directly in order to test the validity of this conjecture, but it is technically difficult to construct a static large BH solution numerically. Thus, we consider time-symmetric initial data which have a brane-localized apparent horizon (AH) [12], expecting that their properties may give some insight into the brane-localized BH.

2 Initial data construction method

In this section we introduce a construction method of time-symmetric initial data with a brane-localized AH in RS-II model. The model is composed of two copies of five-dimensional empty bulk with negative cosmological constant Λ separated by a $\mathbb{Z}_2$-symmetric positive tension brane. The tension of the brane

[1] E-mail:tanahashi@tap.scphys.kyoto-u.ac.jp
[2] E-mail:tama@scphys.kyoto-j.ac.jp

satisfies the RS condition $\lambda = 3k/4\pi G_5$ with $k = \sqrt{-\Lambda/6}$, where G_5 is the five-dimensional gravitational constant. The setup is compatible with a Minkowski brane with AdS bulk with the bulk curvature length being k^{-1}. The initial data we consider have $O(3)$-symmetry in the spacelike dimension as well as the symmetry with respect to time reversal. These symmetries are property shared with static brane-localized BH solutions. Hence, we think it appropriate to restrict our attention to this class of initial data.

The starting point of our construction procedure is to choose an asymptotically AdS vacuum solution of the Einstein equations with negative cosmological constant Λ. In this study, we use the well-known AdS Schwarzschild (the case with $\beta = +1$ below) solution and its extensions (the cases with $\beta = 0$ and -1 below), which are called "topological BH in AdS" [13]. The metric is given by

$$ds^2 = -U(r)dt^2 + \frac{dr^2}{U(r)} + r^2\sigma_{IJ}(x)dx^I dx^J, \tag{1}$$

where

$$U(r) = \beta + k^2r^2 - \frac{\mu}{r^2} \quad (\beta = +1, 0, -1), \quad \sigma_{IJ}(x)dx^I dx^J = \begin{cases} d\chi^2 + \sin^2\chi d\Omega_{\rm II}^2 & (\beta = +1) \\ d\chi^2 + \chi^2 d\Omega_{\rm II}^2 & (\beta = 0) \\ d\chi^2 + \sinh^2\chi d\Omega_{\rm II}^2 & (\beta = -1) \end{cases}.$$

Here μ is the mass parameter and $d\Omega_{\rm II}^2 = d\theta^2 + \sin^2\theta\, d\phi^2$. The spacetime described by this metric is asymptotically AdS, and has an spherical event horizon at $r = r_g$ where $U(r)$ vanishes when $\beta = +1$. In the other two cases ($\beta = 0$ and -1), $r = r_g$ defined by $U(r_g) = 0$ becomes a surface on which the expansion Θ of the outgoing null geodesic congruence vanishes. We refer to these solutions as spherical ($\beta = +1$), flat ($\beta = 0$) and hyperbolic ($\beta = -1$) AdS BHs, respectively, in this literature. In the following discussion we set k to unity by rescaling the unit of length. In this sense, this background spacetime has only one free parameter μ, which becomes one of free parameters of the initial data.

Let us consider a three surface on a t =constant hypersurface Σ_t. If the expansion Θ of the outgoing null geodesic congruence on this three-surface vanishes, it becomes a candidate of an AH. Even if the surface is not closed in the original spacetime, it might be made compact after we introduce a $\mathbb{Z}_2$-symmetric brane. Hence, we refer to such a surface with $\Theta = 0$ as an apparent horizon candidate (AHC). We denote the unit vector normal to an AHC in Σ_t as s^i. Here Latin indices starting from the middle of the alphabet $(i, j, \cdots)$ run over all spatial coordinates. Then the condition of vanishing expansion of the outgoing null geodesic congruence emanating from this AHC is given by $K - K_{ij}s^is^j - D_is^i = 0$, where K_{ij} is the extrinsic curvature of the surface Σ_t and K is its trace. D_i is the covariant differentiation with respect to the induced metric on Σ_t. Since we have $K_{ij} = 0$ by the assumption of time-symmetric initial data, this equation is reduced to

$$D_is^i = 0, \tag{2}$$

which determines the position of the AHC. Assuming $O(3)$-symmetry of AHC, we specify its trajectory by $(r, \chi) = (r_{\rm AH}(\zeta), \chi_{\rm AH}(\zeta))$, where ζ is the proper radial length along the AHC measured from the axis of the $O(3)$-symmetry. These $r_{\rm AH}(\zeta)$ and $\chi_{\rm AH}(\zeta)$ satisfy

$$U^{-1}r'^2_{\rm AH} + r^2_{\rm AH}\,\chi'^2_{\rm AH} = 1, \tag{3}$$

where a prime means a differentiation with respect to the argument, which is ζ here. Then, the spacelike unit vector normal to the AHC is

$$s_\mu = \left(\sqrt{U}r_{\rm AH}\chi'_{\rm AH}, -\frac{r'_{\rm AH}}{\sqrt{U}r_{\rm AH}}\right). \tag{4}$$

Then Eq. (2) and Eq. (3) can be recasted into a set of two ordinary differential equations, whose explicit form for the spherical AdS BH bulk is given by

$$\frac{\sqrt{U}r_{\rm AH}}{r'_{\rm AH}}\chi''_{\rm AH} + 4\sqrt{U}\chi'_{\rm AH} - \frac{2\cot\chi_{\rm AH}}{\sqrt{U}r_{\rm AH}}r'_{\rm AH} = 0, \quad -\frac{1}{\sqrt{U}r_{\rm AH}\chi'_{\rm AH}}r''_{\rm AH} + 3\sqrt{U}\chi'_{\rm AH} + \frac{r'_{\rm AH}}{2U^{3/2}r_{\rm AH}\chi'_{\rm AH}}\left(\frac{dU}{dr}r'_{\rm AH} - 4U\chi'_{\rm AH}\cot\chi_{\rm AH}\right) = 0. \tag{5}$$

The expression for the hyperbolic AdS BH bulk is obtained by simply replacing $\cot\chi_{\rm AH}$ with $\coth\chi_{\rm AH}$. We solve this equation setting $\chi_{\rm AH}(0) = 0$. We can freely choose the value of $r_{\rm AH}(0)$, which specifies the position of the AHC in the background spacetime. This $r_0^{\rm AH} \equiv r_{\rm AH}(0)$ becomes one of free parameters of the initial data we construct. The boundary condition at $\zeta = 0$ is given by $r'_{\rm AH}(0) = 0$, which comes from the regularity of the AHC on the axis. We solve Eq. (5) with this boundary condition numerically to obtain the trajectories of AHCs.

Next we put a vacuum brane with $\mathbb{Z}_2$-symmetry in the AdS BH bulk. We denote the unit normal of the brane by $\tilde{s}_\mu$. We take this $\tilde{s}_\mu$ in the direction toward the bulk from the brane. We introduce the induced metric $\tilde{\gamma}_{\mu\nu} \equiv g_{\mu\nu} - \tilde{s}_\mu \tilde{s}_\nu$ on the brane. The extrinsic curvature $\tilde{K}_{ab}$ on the brane is defined by $\tilde{K}_{ab} = -\tilde{\gamma}_a{}^\mu \tilde{\gamma}_b{}^\nu \nabla_\mu \tilde{s}_\nu$. Here Latin indices starting from the beginning of the alphabet $(a, b, \cdots)$ run the four-dimensional coordinates on the brane. A vacuum brane has the four-dimensional energy-momentum tensor localized on the brane given by $T_{ab} = -\lambda \tilde{\gamma}_{ab}$. Israel's junction condition [14] on the brane is given by $\tilde{K}_{ab} - \tilde{K}\tilde{\gamma}_{ab} = \frac{1}{2} \cdot 8\pi G_5 T_{ab}$, where we used $\mathbb{Z}_2$-symmetry across the brane. At the moment of the time-reversal symmetry, we only have to solve the Hamiltonian constraint, which is the (t,t)-component of the junction condition. Using the normal vector $\tilde{s}^\mu$, this equation is written as

$$D_i \tilde{s}^i = -3k. \tag{6}$$

As before, we assume $O(3)$-symmetry, and we specify the brane trajectory by $(r, \chi) = (r_b(\xi), \chi_b(\xi))$, where ξ is the proper radial length along the brane. The spacelike unit normal $\tilde{s}_\mu$ is given by Eq. (4), replacing $r_{\rm AH}$ and $\chi_{\rm AH}$ with r_b and χ_b respectively. Then the Hamiltonian constraint (6) becomes a second order ODE of $r_b(\xi)$ and $\chi_b(\xi)$. The explicit expression for the spherical AdS BH becomes Eq. (5), replacing $r_{\rm AH}$ and $\chi_{\rm AH}$ with r_b and χ_b on the left hand sides, and 0 with $-3k$ on the right hand sides.

As we are not interested in the spacetime interior of the AHC, we solve the brane trajectory from a point on the AHC. The choice of the starting point on the AHC is arbitrary. This degree of freedom becomes one of free parameters of the initial data we construct. The boundary condition for Eq. (6) at this point is determined by the regularity of the AH across the brane. Namely, the AH should intersect the brane perpendicularly, i.e. $\tilde{s}_\mu s^\mu = 0$. This leads to the condition, $(r'_b, \chi'_b) = \left(\sqrt{U} r_{\rm AH}\, \chi'_{\rm AH}, -\frac{r'_{\rm AH}}{\sqrt{U} r_{\rm AH}}\right)$, at the crossing point. We solve Eq. (6) numerically to obtain the brane trajectory. Once the AHC is truncated by the brane, it becomes a closed surface with vanishing expansion, $\Theta = 0$. However, the AH is not simply a compact surface with $\Theta = 0$ but it must be the outermost one among such surfaces. Thus we have to check if there is no other $\Theta = 0$ hypersurface in the region outside of the AHC. If there is no such a hypersurface with $\Theta = 0$, the original AHC is the genuine AH. In the case that true AH exists outside AHC, such initial data will be also given by other values of free parameters in the parameter space. Hence, we just discard such initial data, and analyze only the data which have no outer AH.

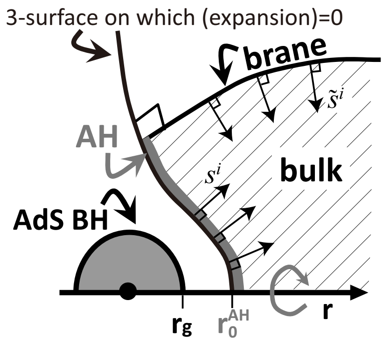

Figure 1: Schematic figure of the initial data.

3 Analysis of the Initial Data Property and Discussion

We find that a three-parameter family of such initial data can be constructed by simply placing a brane on a constant time surface of Schwarzschild anti-de Sitter space. Since there is no static brane-localized BH solution with a large horizon area, one may suspect that time-symmetric initial data with a large AH do not exist. However, we found no difficulty in constructing initial data with a large AH. Our method of constructing the initial data requires just solving ordinary differential equations. Hence, the conclusion that initial data with an arbitrarily large AH area exist is quite robust.

We can calculate the four-dimensional ADM mass of the initial data from the induced metric on the brane. We compared this ADM mass and the horizon area of our initial data with that of the black string (BS) solution. If there is a sequence of static brane-localized BH solutions, such solutions should be contained in the time-symmetric initial data. Moreover, if they are stable, it will have a smaller mass compared with the BS solution with the same horizon area. However, we found that any initial data constructed by this method do not have a smaller mass than the BS solution when the horizon area is larger than the size determined by the bulk curvature scale. In the following sense, this result is consistent with the scenario that these initial data evolve into configurations similar to BS, which is unstable through Gregory-Laflamme instability. The event horizon, which must exist outside the AH area, should have a larger area than AH. The area theorem tells that the area of the event horizon does not decrease as a course of time evolution, while the mass will not increase when there is no incoming energy flux from infinity. Hence, if there is an initial data whose horizon area is significantly larger than that of BS with the same mass, such an initial data cannot evolve into the configuration close to BS.

We further investigated what kind of configuration realizes the minimum mass for the same AH area. The configuration that realizes the smallest mass turned out to be the one close to the BS truncated by a cap. One may think that this indicates the existence of a static brane-localized BH solution. However, since our three-parameter family of initial data does not include the configuration resembling the BS solution, this minimum of mass may just reflect the expected minimum of mass corresponding to the BS solution.

We conducted the same analysis also in the case of four-dimensional bulk spacetime since the situation looks quite different in this case. The BS solution does not exist, but we have an exact brane-localized BH solution found by Emparan, Horowitz and Myers (EHM), instead. Nevertheless, the results of the analyses as to the time-symmetric initial data were quite similar to the five-dimensional case. We found that the area of the initial data is always larger than the EHM solution with the same mass, which is in harmony with the naive expectation that the EHM solution is the most stable black object in four-dimensional RS-II model.

These results were all consistent with the classical BH evaporation conjecture, but unfortunately they did not provide a strong indication about the classical evaporation conjecture because the initial data that we examined were very limited. However, it is a remarkable progress that we have shown that time-symmetric initial data with a large AH area can be constructed. As a next step, we can consider the time evolution of these initial data. The family of initial data we constructed in this study will be a good starting point for researches in this direction.

References

[1] L. Randall and R. Sundrum, Phys. Rev. Lett. **83**, 4690 (1999)

[2] J. Garriga and T. Tanaka, Phys. Rev. Lett. **84**, 2778 (2000)

[3] A. Chamblin, S. W. Hawking and H. S. Reall, Phys. Rev. D **61**, 065007 (2000)

[4] R. Gregory, Class. Quant. Grav. **17**, L125 (2000)

[5] D. Karasik, C. Sahabandu, P. Suranyi and L. C. R. Wijewardhana, Phys. Rev. D **69**, 064022 (2004)

[6] H. Kudoh, T. Tanaka and T. Nakamura, Phys. Rev. D **68**, 024035 (2003)

[7] H. Kudoh, Phys. Rev. D **69**, 104019 (2004) [Erratum-ibid. D **70**, 029901 (2004)]

[8] T. Tanaka, Prog. Theor. Phys. Suppl. **148**, 307 (2003)

[9] R. Emparan, A. Fabbri and N. Kaloper, JHEP **0208**, 043 (2002)

[10] P. R. Anderson, R. Balbinot and A. Fabbri, Phys. Rev. Lett. **94**, 061301 (2005)

[11] T. Tanaka, arXiv:0709.3674 [gr-qc].

[12] N. Tanahashi and T. Tanaka, arXiv:0712.3799 [gr-qc].

[13] D. Birmingham, Class. Quant. Grav. **16**, 1197 (1999) [arXiv:hep-th/9808032].

[14] W. Israel, Nuovo Cim. B **44S10**, 1 (1966) [Erratum-ibid. B **48**, 463 (1967 NUCIA,B44,1.1966)].

A counterexample of the self-similarity hypothesis for perfect fluid gravitational collapse

Eiji Mitsuda[1] and Akira Tomimatsu[2]

Department of Physics, Nagoya University, Nagoya 464–8602, Japan

Abstract

It has been postulated as the so-called self-similarity hypothesis that a self-similar behavior may be an attractor behavior which becomes dominant near a central dense region as gravitational collapse starting from generic initial conditions proceeds to final stages. Whether this hypothesis holds is an important problem for understanding the geometrical structure and the fluid motion at final stages in gravitational collapse. In this paper, through the analytical treatment of the Einstein's equation for the perfect fluid, we show that the self-similarity hypothesis does not necessarily hold for spherically symmetric gravitational collapse of a low pressure perfect fluid.

1 Introduction

Spherically symmetric gravitational collapse of a perfect fluid with pressure P given by the equation of state $P = \alpha\rho$ has been extensively studied in general relativity to understand fundamental features of relativistic motion of non-dust fluids and geometrical structure in gravitational contraction. In particular, some attention after the discovery of the critical phenomena has been given to generality of the self-similar behaviors governed by the Einstein's equations reduced to a set of ordinary differential equations with respect to a dimensionless variable such as $z \equiv r/t$, where r and t may be comoving radial and time coordinates. For this problem the self-similarity hypothesis proposed by Carr (see [1] for a recent review) may assert that a self-similar behavior is a general behavior which becomes dominant near the central dense region in the final or intermediate stage of the initially non-self-similar gravitational collapse starting from general initial conditions. Though this hypothesis strongly motivates us to study extensively self-similar hydrodynamics, the prerequisites for it should be also understood through detailed comparisons between evidence and counterevidence.

The remarkable evidence for the self-similarity hypothesis was given by the numerical simulations for the parameter range $0 < \alpha \lesssim 0.03$ [2] which showed the appearance of a self-similar behavior in the final stage for some initial data sets. In addition it was also shown that such a self-similar behavior can be well described by the general relativistic Larson-Penston solution or the flat Friedmann solution. However we recently showed that the flat Friedmann solution for sufficiently small values of α ($0 < \alpha \ll 1$) is unstable for spherically symmetric non-self-similar and inhomogeneous perturbations. This suggests that for a variety of initial data sets, the spacetime metrics and the fluid motion in the final stage are always well approximated by the general relativistic Larson-Penston solution. It is interesting to note that the general relativistic Larson-Penston solution for the parameter range $0 < \alpha \lesssim 0.0105$ describes the shell-focusing naked singularity formation [4]. Whether the transition to the general relativistic Larson-Penston stage occurs for all possible initial conditions is an important problem to be examined in the light of the analytical treatment of the dynamical field equations in relation to not only the universality of the final stage dynamics but also the cosmic censorship conjecture.

In this paper we analytically study spherically symmetric perfect fluid gravitational collapse through the non-perturbative analysis of the Einstein's field equations. Using the rescaling formula such as $z \rightarrow x \equiv z/\alpha^{3/2}$ and the low pressure limit $\alpha \rightarrow 0$, we reduce the several partial differential field equations to the single master equation without vanishing the effects of pressure. By analyzing this master equation, we succeed in the derivation of the sufficient condition with respect to the initial density profile for non-appearance of a self-similar behavior in the final stage.

[1]E-mail: emitsuda@gravity.phys.nagoya-u.ac.jp
[2]E-mail: atomi@gravity.phys.nagoya-u.ac.jp

2 Field equations for the low pressure perfect fluid

Throughout this paper, we consider spherically symmetric line element given by

$$ds^2 = -e^{2\nu(t,r)}dt^2 + e^{2\lambda(t,r)}dr^2 + R^2(t,r)\left(d\theta^2 + \sin^2\theta d\varphi^2\right) \tag{1}$$

with the comoving coordinates t and r. As was mentioned in Sec. 1, the collapsing matter is assumed to be a prefect fluid with the equation of state $P = \alpha\rho$ for a constant α lying in the range $0 < \alpha \leq 1$, where P and ρ are the pressure and the energy density, respectively. To discuss the self-similar behavior later, we use a new variable z defined by $z \equiv r/t$, instead of r. In addition we also introduce the following dimensionless functions:

$$S(t,z) \equiv \frac{R}{r}\ , \qquad \eta(t,z) \equiv 8\pi r^2\rho\ , \qquad M(t,z) \equiv \frac{2m}{r}\ , \tag{2}$$

where the function $m(t,r)$ is the Misner-Sharp mass.

From the Einstein's field equations, we can obtain the four equations governing the functions ν, λ, S and η. By virtue of the choice of the comoving coordinates, the two equations lead to the relations

$$e^{\nu} = C_\nu(t)(z^2)^{\alpha/(1+\alpha)}\eta^{-\alpha/(1+\alpha)}\ , \tag{3}$$
$$e^{\lambda} = C_\lambda(r)\eta^{-1/(1+\alpha)}S^{-2}\ , \tag{4}$$

where C_ν and C_λ are arbitrary functions. Thus the remaining two equations become the equations for only the two unknown functions S and η and are written by

$$M + M' = \eta S^2(S + S')\ , \tag{5}$$
$$\dot{M} - M' = -\alpha\eta S^2(\dot{S} - S')\ , \tag{6}$$
$$M(t,z) = S\left\{1 + e^{-2\nu}z^2\left(\dot{S} - S'\right)^2 - e^{-2\lambda}\left(S + S'\right)^2\right\}\ , \tag{7}$$

where the dot and the prime represent the partial derivative with respect to $\log|t|$ and $\log|z|$, respectively.

It was pointed out in [4] that the general relativistic Larson-Penston solution does not correspond to the Lemaítre-Tolman-Bondi solution even in the limit $\alpha \to 0$. In order to examine the generality of the transition to the general relativistic Larson-Penston stage in the low pressure limit $\alpha \to 0$, we introduce the following rescaled variables:

$$S_0(t,x) \equiv \alpha S, \qquad \eta_0(t,x) \equiv \eta/\alpha^3, \qquad x \equiv -z/\alpha^{3/2}\ . \tag{8}$$

By taking the low pressure limit $\alpha \to 0$ with keeping the functions S_0 and η_0 and the variable x finite, we can derive the following single partial differential equation for only S_0 from the field equations (5), (6) and (7):

$$\frac{V_0^2 - 1}{(S_0 + S_0')^2}\left(S_0'' + S_0'\right) + y^2\left(\ddot{S}_0 - 2\dot{S}_0' - \dot{S}_0\right) + \frac{1}{2S_0^2} - \frac{2}{S_0} = 0\ , \tag{9}$$

where the function V_0 is defined as

$$V_0(t,x) \equiv x\left(S_0 + S_0'\right)\ . \tag{10}$$

This master equation is expected to be useful for the analytical study of various classes of motions of the low pressure perfect fluid. The remaining two variables η_0 and M are given by

$$M = 1\ , \qquad \eta_0 = S_0^{-2}\left(S_0 + S_0'\right)^{-1}\ . \tag{11}$$

It should be noted that the function V_0 can be written as

$$V_0 = V/\sqrt{\alpha}\ , \qquad V(t,z) \equiv ze^{\lambda-\nu}\ . \tag{12}$$

The function V means the velocity of $z =$ const. surface relative to the fluid element. Thus the point $x = x_s(t)$ at which $V_0^2 = 1$ is called as the sonic point. It is easily found from Eq. (9) that the second derivative of the function S_0 with respect to x cannot be determined at the sonic point. This makes us confirm that our method do not miss the pressure effect by virtue of the rescaling formula (8). It should be also noted that the last term in the left hand side of Eq. (9) also appears by virtue of the rescaling formula.

3 Asymptotic solution and initial density profiles

It is easily found that there is a class of solutions of Eq. (9) for which the functions V_0 and S_0^{-1} become much larger than unity in the region $x \gg 1$. In the region $x \gg 1$ the function S_0 for such a class of solutions is approximated by

$$S_0(t,x) \simeq \left\{ \frac{3(1+K(\tilde{r})x)}{2x} \right\}^{2/3} , \tag{13}$$

where K is an arbitrary function dependent on only $\tilde{r}$ defined as $\tilde{r} \equiv r/\alpha^{3/2}$. It should be noted that the function S_0 for the flat Friedmann solution and the general relativistic Larson-Penston solution is expressed by this asymptotic form in the region $x \gg 1$. Although this may not necessarily hold for all physically allowable self-similar or non-self-similar solutions, we focus on the solutions approximated by Eq. (13) in the region $x \gg 1$ in this section.

In order to see the relation between the arbitrary function K and the initial density profile, we consider the coordinate transformation as $r \to r_*$ defined as

$$r_* = r \left\{ \frac{3}{2} \left(\frac{K}{\alpha^{3/2}} - \frac{L}{r} \right) \right\}^{2/3} , \tag{14}$$

where L is an arbitrary constant. Then we can rewrite the asymptotic form of the area radial function R to the same form as R for the marginally bound Lemaítre-Tolman-Bondi solution as follows,

$$R(t,r_*) \simeq r_* \left\{ 1 + \frac{3}{2}\sqrt{\frac{r(r_*)}{r_*^3}}\,(t-L) \right\}^{2/3} . \tag{15}$$

Because the area radial function R corresponds to the radial coordinate r_* at $t = L$, we regard the constant L as the initial time. The initial density profile $\rho(L, r_*) \equiv \rho_{\rm init}(r_*)$ is given from the field equations as

$$\rho_{\rm init}(r_*) = \frac{1}{4\pi r_*^2}\frac{dm}{dr_*}. \tag{16}$$

From Eq. (11), the Misner-Sharp mass m is found to be written as

$$m(r_*) = r(r_*)/2 . \tag{17}$$

This equation and Eq. (16) mean that if the initial density profile is determined, then the function K is also determined through Eq. (14).

In general, the initial density profile $\rho_{\rm init}$ is expanded around the regular center $r_* = 0$ as

$$\rho_{\rm init}(r_*) = \frac{3}{4\pi L^2} \left\{ 1 - \left(\frac{r_*}{r_0} \right)^2 \right\} + O(r_*^3) , \tag{18}$$

where r_0 is positive constants. Note that the value of $\rho_{\rm init}$ at the center $r_* = 0$ is uniquely determined as $3/(4\pi L^2)$ because we define the time coordinate t so that the central singularity appears at $t = 0$. Eq. (18) corresponds to the following expansion of the function K:

$$K(\tilde{r}) = K_0 \tilde{r}^{-1/3} + O(\tilde{r}^{1/3}) , \tag{19}$$

where K_0 is a constant explicitly given by A and B. The validity of the expansion (18) is restricted to the region $r_* \ll r_0$. At $t = L$ this region corresponds to

$$x \ll \left(\frac{r_0}{\sqrt{\alpha}L} \right)^3 . \tag{20}$$

Hence, if the constants L and r_0 satisfy the condition

$$\frac{r_0}{L} \gg \sqrt{\alpha} , \tag{21}$$

then the asymptotic form of the solution S_0 in the region $1 \ll x \ll \{r_0/(\sqrt{\alpha}L)\}^3$ is given by

$$S_0(t,x) \simeq \left[\frac{3\left\{1 + K_0 x^{2/3}(-t)^{-1/3}\right\}}{2x} \right]^{2/3} . \tag{22}$$

4 Conclusion

Now let us consider the behavior of the solution S_0 for the initial density profile satisfying the condition (21). It is easily found from the asymptotic form (22) that the solution S_0 monotonically increases to the infinity with non-self-similar manner in the region $1 \ll x \ll \{r_0/(\sqrt{\alpha}L)\}^3$ as $t \to 0$ along a $x = \mathrm{const}$ line. In order to see whether a self-similar behavior appears in the central region $0 \leq x \lesssim 1$, we would like to note that the value of the function S_0 for the self-similar solutions must be $1/4$ at the sonic point because of the regularity, which is easily understood from the master equation (9). That is, the value of the function S_0 at the sonic point $x = x_s(t)$ must approach $1/4$ with lapse of time if the system near the central region in the final stage is approximately described by the general relativistic Larson-Penston solution. Next, we note that the function S_0 for the solutions describing the monotonical gravitational contraction must monotonically decrease with respect to x at any fixed time t. This means that the value of the function S_0 at the sonic point cannot settle on $1/4$ because S_0 in the region $1 \ll x \ll \{r_0/(\sqrt{\alpha}L)\}^3$ monotonically increases to the infinity with lapse of time. This leads us to the conclusion that a self-similar behavior does not appear even in the central region.

In this paper we have derived the sufficient condition (21) as to the initial density profile for non-appearance of a self-similar behavior in the final stage of spherically symmetric low pressure perfect fluid collapse. The constant r_0 in this condition can be regarded as the scale of the inhomogeneity near the center. Therefore we can give a physical interpretation of the condition (21) such that the speed of the collapse of the inhomogeneity scale to the singularity is much larger than the speed of sound.

References

[1] B. J. Carr and A. A. Coley, Gen. Relativ. Gravit. **37**, 2165 (2005).

[2] T. Harada and H. Maeda, Phys. Rev. D **63**, 084022 (2001).

[3] E. Mitsuda and A. Tomimatsu, Phys. Rev. D **74**, 104019 (2006).

[4] A. Ori and T. Piran, Phys. Rev. D **42**, 1068 (1990).

Apparent shapes of charged rotating black holes and naked singularities

Kenta Hioki[1] and Umpei Miyamoto[2]

[1] *Department of Physics, Waseda University, Okubo 3-4-1, Tokyo 169-8555, Japan*
[2] *Racah Institute of Physics, Hebrew University, Givat Ram, Jerusalem 91904, Israel*

Abstract

Sen black hole is a solution in a low energy limit of the heterotic string theory, which has a rotation and charges associated with the electro-magnetic, dilaton, and axion fields. In this paper, we investiagate null geodesics on the Sen black hole in detail and determine the position and the optical shape, i.e., the "shadow", of this black hole observed at infinity. Then, the shape and position is compared with those of the Kerr-Newman (KN) class spacetimes, including both black-hole and naked-singular spacetimes, in a wide range of parameters. It is found that the Sen black hole forms the shadow irrespective of the charge and forbid the "anti-world" of negative r to be observable, while the corresponding KN spacetime of the identical extremality does not. As a by-product of the analysis, an irreducible rank-2 Killing tensor of the Sen spacetime is obtained.

1 Introduction

There are some evidence for the existence of a black hole in the Galactic center associated with the ultra compact radio source Sagittarius A*. The possibility of direct observation of the black hole by the future interferometers became high. However, the research of an observation of black hole and collapsed object in theoretical approach is still lacking.

The theory of gravitational lensing has been developed in the weak field approximation and has been succeed to explain many physical and astronomical observations. The influence of the strong gravity of the black hole and other collapsed object appears when the photon passes the vicinity of the origin of the gravity. In order to obtain physical information of black hole and other collapsed object with strong gravity, the direct imaging and the apparent shapes are important to be investigated [1–5].

As the final state of realistic gravitational collapse, the solutions of Einstein equations with strong gravity generally possess a spacetime singularity. If the spacetime singularity has appeared from physically reasonable initial conditions the spacetime singularity is hidden to within the event horizon, so-called cosmic censorship hypothesis proposed by Penrose is well-known. It implies that a naked singularity which is a spacetime singularity uncovered by event horizon does not existed. Since no proof is known for the cosmic censorship hypothesis, it is one of the most important problem in general relativity. There is a possibility that the candidate of the black hole could be naked singularity. The research for observing naked singularity is important [6].

In the Einstein-Maxwell theory, the uniqueness theorem implies that when the solution has no monopole magnetic charge the Kerr-Newman solution is the most general solution which describing an isolated stationary axially symmetric solution. Determinating the parameters of black hole from observations is important in astrophysics. It is also interesting to consider of other fields like dilaton and axion field to investigate the influences to observations [7–9].

2 Sen black hole

The action of a low effective action of the heterotic string theory is given by

$$S = \frac{1}{16\pi}\int d^4x\sqrt{-g}\left[R - 2\left(\nabla\phi\right)^2 - e^{-2\phi}F^2 - \frac{1}{12}e^{-4\phi}H^2\right] \ . \tag{1}$$

[1] E-mail:hioki@gravity.phys.waseda.ac.jp
[2] E-mail:umpei@phys.huji.ac.il

Here, ϕ is a dilaton, and F and H are field strength of an electromagnetic and axion fields, respectively. The line element of the Sen solution [10] in Boyer-Lindquist coordinates is given by

$$ds^2 = -\left(\frac{\Delta - a^2\sin^2\theta}{\Sigma}\right)dt^2 - \frac{4\mu ra\cosh^2\beta\sin^2\theta}{\Delta}dtd\varphi + \frac{\Sigma}{\Delta}dr^2 + \Sigma d\theta^2 + \frac{\Lambda\sin^2\theta}{\Sigma}d\varphi^2 \ ,$$
$$A_\mu dx^\mu = \frac{\mu r\sinh 2\beta}{\sqrt{2}\Sigma}(dt - ad\varphi) \ , \quad B_{t\varphi} = 2a^2\sin^2\theta\frac{\mu r\sinh^2\beta}{\Sigma} \ , \quad \phi = -\frac{1}{2}\ln\frac{\Sigma}{r^2 + a^2\cos^2\theta} \ , \tag{2}$$

where

$$\Delta := r^2 - 2\mu r + a^2 \ , \quad \Sigma := r^2 + a^2\cos^2\theta + 2\mu r\sinh^2\beta \ ,$$
$$\Lambda := \left[r(r + 2\mu\sinh\beta^2) + a^2\right]^2 - \Delta a^2\sin^2\theta \ . \tag{3}$$

Fields A_μ and $B_{\mu\nu}$ are the potentials of field F and H, respectively. Parameters μ, β and a are related to the physical quanties such as the mass M, $U(1)$ charge Q, and angular momentum J by

$$M = \frac{\mu}{2}(1 + \cosh 2\beta) \ , \quad Q = \frac{\mu}{\sqrt{2}}\sinh^2 2\beta \ , \quad J = \frac{a\mu}{2}(1 + \cosh 2\beta) \ . \tag{4}$$

Inequality $|J| \leq M^2 - Q^2/2$ has been satisfied for the above solution to be a regular black hole. The Sen solution (2) without the rotation ($J = 0$) coincides with the Gibbons-Maeda solution [11, 12] with coupling constant $\alpha = 1$. In the rest of this paper, we denote the physical charges of KN, RN and GM spacetimes by corresponding subscripts as M_{KN}, M_{RN} and M_{GM}.

3 Shadows of Sen black holes

We construct the irreducible rank-2 Killing tensor $K^{\mu\nu}$ from the integrability of the Hamilton-Jacobi equation, which satisfies $\nabla_{(\lambda}K_{\mu\nu)} = 0$.

$$K^{\mu\nu} = \delta^\mu_\theta\delta^\nu_\theta + \csc^2\theta\delta^\mu_\varphi\delta^\nu_\varphi - 2a\delta^{(\mu}_\varphi\delta^{\nu)}_t + a^2\sin^2\theta\left(\delta^\mu_t\delta^\nu_t - \cot^2\theta g^{\mu\nu}\right) \ . \tag{5}$$

Sen spacetime is not algebraically special and is of type-I in the Petrov classification. Thus, it is not so trivial that Killing tensor (5) exists, which is related to a hidden symmetry [13].

Now, we can write the first-order form of null geodesic motion, due to the existence of the symmetry, as

$$\Sigma\dot{r} = \sigma_r\sqrt{R} \ ,$$
$$\Sigma\dot{\theta} = \sigma_\theta\sqrt{\Theta} \ ,$$
$$\Sigma\dot{t} = \frac{1}{\Delta}(\Lambda E - 2MraL_z) \ ,$$
$$\Sigma\dot{\varphi} = \frac{1}{\Delta}[2MarE + L_z\csc^2\theta(\Sigma - 2Mr)] \ , \tag{6}$$

where $\dot{X} := dX/d\lambda$. We have defined

$$R := \left[r(r + r_0) + a^2 - a\xi\right]^2 - \Delta\left[\eta + (a - \xi)^2\right] \ ,$$
$$\Theta := \eta + (a - \xi)^2 - (a\sin\theta - \xi\csc\theta)^2 \ . \tag{7}$$

which ξ and η are impact parameters of the null geodesics [7]. The sign functions $\sigma_r = \pm$ and $\sigma_\theta = \pm$ are indpendent each other and the sign changes at a turning points of the geodesic motion. The new parameter r_0 is defined by $r_0 := Q^2/M$.

We consider circular photon orbits of radius r_{circ}, which satisfy $R(r_{\mathrm{circ}}) = \partial_r R\ |_{r_{\mathrm{circ}}} = 0$ and is important class of orbits to construct apparent shapes (shadows) of spacetime. For nonrotating case $J = 0$, existence of circular photon orbits of radius $r^{\mathrm{GM}}_{\mathrm{circ}}$ is clarified

$$r^{\mathrm{GM}}_{\mathrm{circ}} = \frac{1}{4}\left\{3(2M - r_0) + [(2M - r_0)(18M - r_0)]^{1/2}\right\} \ . \tag{8}$$

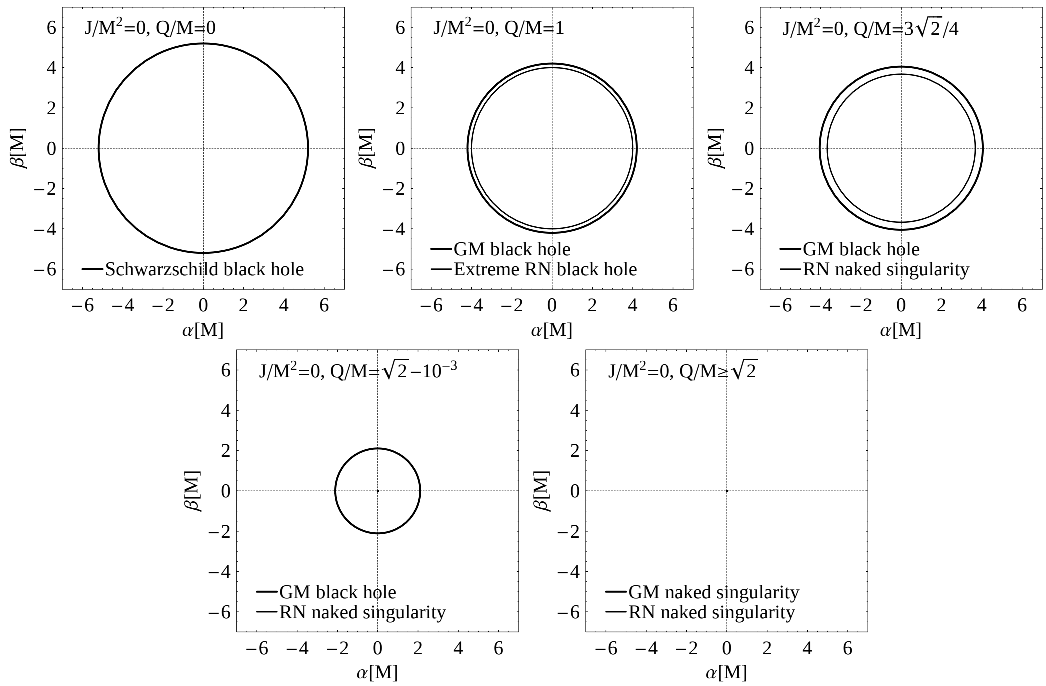

Figure 1: Contours of apparent shapes of black holes and naked singularities in Gibbons-Maeda (thick solid line) and Reissner-Nordström (thin solid line) spacetimes. For black holes, the inner region of the contours of apparent shapes are the dark region to be observed, while for naked singularities the inner region is not dark. For $Q_{\rm GM} \geq \sqrt{2} M_{\rm GM}$ ($Q_{\rm RN} > 3\sqrt{2} M_{\rm RN}/4$), we determine that the spacetimes can not be distinguished from observation.

We can easily see that unstable circular photon orbit exsists if and only if $r_0 < 2M$. Such properties are a very different points from RN spacetime. For rotating case $J \neq 0$, the impact parameters of a circular photon orbit of constant radius r are determined by

$$\xi^{\rm S}_{\rm circ} = \frac{1}{a(2r + r_0 - 2M)} \left[2M\left(r^2 - a^2\right) - (2r + r_0)\,\Delta\right] ,$$

$$\eta^{\rm S}_{\rm circ} = \frac{r^2}{a^2(2r + r_0 - 2M)} \left\{8a^2 M(2r + r_0) - \left[(r + r_0 - 2M)(2r + r_0) - 2Mr\right]^2\right\} . \tag{9}$$

If the cosmic censorship hypothesis is valid, unstable circular photon orbit only exist for the region,

$$r < -r_0/2 \ , \ M - M_0 - r_0/2 < r < r_- \ , \ r_+ < r \ , \tag{10}$$

while $-r_0/2 \leq M - M_0 - r_0/2 \leq r_- \leq r_+$ with $M_0 := \left\{M\left[(2M - r_0)^2 - 4a^2\right]/4\right\}^{1/3}$. We excluded $r = r_\pm$, $r = M - r_0/2 - M_0$ and $r = -r_0/2$, because their are principal null congruences.

We show apparent shapes of black holes and naked singularities in GM spacetime in Fig 1 and apparent shapes of Sen black holes in Fig 2. For every cases, we also plot KN and RN spacetime in cooresponding parameters. The apparent shape (shadow) is defined as the area which does not illuminated by light source. We consider that observer is at spatial infinity and some inclination angle. We must consider the tetrad components of the four momentum $\left(p^{(t)}, p^{(r)}, p^{(\theta)}, p^{(\varphi)}\right)$ with respect to locally nonrotating reference frames. Thus we find that, for an observer at infinity and inclination angle i, the celestial coordinate of the observer (α, β) is

$$\alpha = \lim_{r\to\infty} \frac{r p^{(\varphi)}}{p^{(r)}} = -\xi \csc i \ , \tag{11}$$

$$\beta = \lim_{r\to\infty} \frac{r p^{(\theta)}}{p^{(r)}} = \sqrt{\eta + a^2 \cos^2 i - \xi^2 \cot^2 i} \ . \tag{12}$$

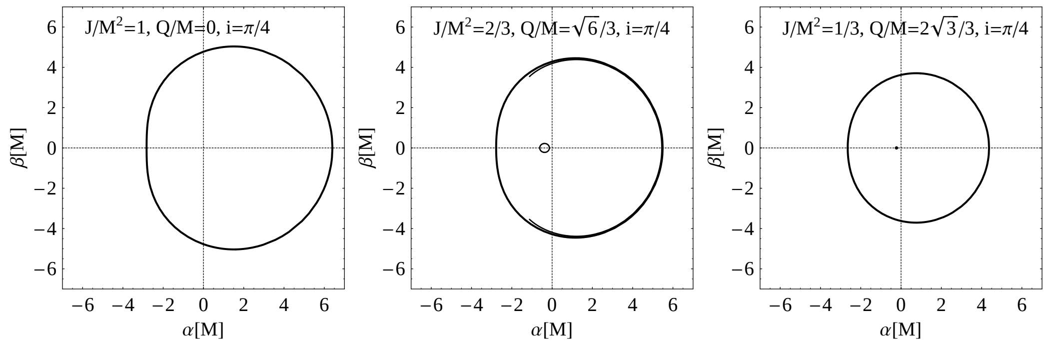

Figure 2: Contours of apparent shapes of Sen black holes (thick solid line) and naked singularites of corresponding parameters in Kerr-Newman spacetimes (thin solid line).

These relations coincide with its of KN spacetime. The apparent shape of the spacetime for an observer at infinity will be determined by the critical impact parameters $\xi^{\mathrm{S}}_{\mathrm{circ}}$ and $\eta^{\mathrm{S}}_{\mathrm{circ}}$.

4 Summary

We obtained the apparent shape of Sen and GM spacetimes. The influence of a dilaton and an axion on the apparent shape is clarified. In particular, the degeneracy of shape with similar kind of black holes, e.g., KN black hole, is carefully investigated. As a by-product of the analysis, the irreducible rank-2 Killing tensor in Sen spacetime is obtained. This is ramarkable fact since Sen spacetime is of type-I in Petrov classification. To obtain the apparent shapes of the naked singularity in Sen spacetime, the global structure has to be investigated since it plays a critical role for the apparent shape.

References

[1] A. F. Zakharov, A. A. Nucita, F. De Paolis, and G. Ingrosso, New Astron. **10** (2005) 479–489.

[2] R. Takahashi, Astrophys.J. **611** (2004) 996–1004, [astro-ph/0405099].

[3] H. Falcke, F. Melia, and E. Agol, Astrophys.J. **528** (2000) L13–L16, [astro-ph/9912263].

[4] A. de Vries, Class. Quant. Grav. **17** (2000) 123–144.

[5] J.-P. Luminet, Astron. Astrophys. **75** (may, 1979) 228–235.

[6] K.-i. Nakao, N. Kobayashi, and H. Ishihara, Phys. Rev. **D67** (2003) 084002, [gr-qc/0211061].

[7] G. N. Gyulchev and S. S. Yazadjiev, Phys. Rev. **D75** (2007) 023006, [gr-qc/0611110].

[8] N. Mukherjee and A. S. Majumdar, Gen. Rel. Grav. **39** (2007) 583–600, [astro-ph/0605224].

[9] A. Bhadra, Phys. Rev. **D67** (2003) 103009, [gr-qc/0306016].

[10] A. Sen, Phys. Rev. Lett. **69** (1992) 1006–1009, [hep-th/9204046].

[11] J.-i. Koga and K.-i. Maeda, Phys. Rev. **D52** (1995) 7066–7079, [hep-th/9508029].

[12] G. W. Gibbons and K.-i. Maeda, Nucl. Phys. **B298** (1988) 741.

[13] M. Walker and R. Penrose, Commun. Math. Phys. **18** (1970) 265–274.

Generic features of Einstein-Aether black holes

Takashi Tamaki[1] and Umpei Miyamoto[2]

[1]*Department of Physics, Waseda University, Okubo 3-4-1, Tokyo 169-8555, Japan*
[2]*Racah Institute of Physics, Kaplun Building, The Hebrew University of Jerusalem, Givat Ram, Jerusalem 91904, Israel*

Abstract

We reconsider spherically symmetric black hole solutions in Einstein-Aether theory with the condition that this theory has identical PPN parameters as those for general relativity, which is the main difference from the previous research.

1 Introduction

Identifying the contents of dark energy and dark matter (DE/DM) is one of the most important subjects in cosmology. It is frequently argued that gravitational theories are an alternative to DE/DM. Recently, tensor-vector-scalar (TeVeS) theories have attracted much attention since they do not only explain galaxy rotation curves but also satisfy many constraints from solar experiments [1].

However, it is nontrivial whether or not these theories satisfy the constraints by strong gravity tests. To study vector fields in a general form is difficult. Thus, as a first step, it is important to investigate a simplified model which is tractable and instructive for general cases. One such useful model would be Einstein-Aether (EA) theory [2], where all parameterized post-Newtonian (PPN) parameters can be the same as those in GR [3]. In EA theory, strong gravitational cases including black holes have been analyzed to some extent [4, 5, 6, 7]. Nevertheless, the analysis of black holes has been limited to the case in which the event horizon coincides with the spin-0 horizon [5], and this case does not necessarily satisfy weak fields tests. Thus, it is interesting to ask whether or not significant differences from the Schwarzschild black hole appear when weak fields tests are satisfied. For this reason, we argue black holes with the case in which the EA theory has identical PPN parameters as in GR [8]. We use units in which $c = 1$ and the sign convention $(-, +, +, +)$ for metrics.

2 Einstein-Aether theory

We consider the following action:

$$I = \frac{1}{16\pi G}\int d^4x\sqrt{-g}\, R - K^{ab}{}_{cd}\nabla_a u^c \nabla_b u^d + \lambda(u^2+1)\ , \tag{1}$$

$$K^{ab}{}_{cd} := c_1 g^{ab} g_{cd} + c_2 \delta^a_c \delta^b_d + c_3 \delta^a_d \delta^b_c - c_4 u^a u^b g_{cd}\ , \tag{2}$$

where u^a is a vector field and $u^2 := u^a u_a$. c_i $(i = 1, 2, 3, 4)$ are theoretical parameters in EA theory. λ is a Lagrange multiplier ensuring the vector field u^a to be unit timelike vector everywhere.

Varying this action with respect to λ and u^a, we have

$$u^2 + 1 = 0\ ,\quad c_4 \dot{u}^m \nabla_a u_m + \nabla_m J^m_{\ a} + \lambda u_a = 0\ , \tag{3}$$

where $J^a{}_m := K^{ab}{}_{mn}\nabla_b u^n,\ \dot{u}^b := u^a \nabla_a u^b$. Multiplying Eq. (3) by u_a, we have

$$\lambda = c_4 \dot{u}^2 + u^a \nabla_m J^m_{\ a}\ . \tag{4}$$

Varying the action with respect to the metric, we have

$$G_{ab} = \nabla_m \left[J^m{}_{(a} u_{b)} - J_{(a}{}^m u_{b)} + J_{(ab)} u^m \right] + c_1 \left(\nabla_a u_m \nabla_b u^m - \nabla_m u_a \nabla^m u_b \right) + c_4 \dot{u}_a \dot{u}_b + \lambda u_a u_b - \frac{1}{2} g_{ab} \mathcal{L}_{\mathrm{u}}\ ,$$

[1]E-mail:tamaki@gravity.phys.waseda.ac.jp
[2]E-mail:umpei@phys.huji.ac.il

where $\mathcal{L}_{\rm u} := K^{ab}{}_{cd}\nabla_a u^c \nabla_b u^d$.

If we assume the weak field and slow-motion limits in EA theory [3], we have to take Newton's gravitational constant as $G_{\rm N} = \left(1 - \frac{c_1+c_4}{2}\right)^{-1} G$, to reproduce Newtonian gravity correctly. For all the PPN parameters to coincide with those in GR, we have

$$c_2 = \frac{-2c_1^2 - c_1c_3 + c_3^2}{3c_1} \ , \quad c_4 = -\frac{c_3^2}{c_1} \ . \tag{5}$$

From the maximum mass of neutron stars $\sim 2M_\odot$, we have $c_1 + c_4 \leq 0.5 \sim 1.6$ [7]. In [9], the sound modes are analyzed by expanding the metric and the Aether around the Minkowski metric. For these sound velocities to be equal to or larger than the photon velocity, or, to ensure stability against linear perturbation in Minkowski (or FRW) background and linearized energy positivity, we have [9, 10, 11]

$$0 < c_+ < 1 \ , \quad 0 < c_- := c_1 - c_3 < \frac{c_+}{3(1-c_+)} \ . \tag{6}$$

Radiation damping was also analyzed in [12], which almost restricts c_+ as a function of c_- based on the observation of, say, B1913+16.

3 Analysis in a single-null coordinate system

Our purpose in investigating black holes in EA theory is not to give a further restriction but to understand generic features of vector-tensor theories under the condition that weak gravity tests are satisfied. From this point of view, we take the following strategy. (i) We assume (5) since the constraints by the solar experiments are severe. (ii) We assume (6). Otherwise, a naked singularity appears outside the event horizon in general. Constraints from neutron stars and from radiation damping are related to strong gravity tests at least partially. For the above reasons, we do not impose these constraints. Thus, we have two theoretical parameters (c_+, c_-) with the condition (6).

We write a static and spherically symmetric line element in a single null coordinate system as,

$$ds^2 = -N(r)dv^2 + 2B(r)dvdr + r^2 d\Omega^2 \ . \tag{7}$$

In this coordinate, the vector field takes the form of $u = a(r)\partial_v + b(r)\partial_r$. $b(r) \neq 0$ means that the Aether is not aligned with the timelike Killing field, which is inevitable because of the event horizon. From Eq. (3), $-Na^2 + 2Bab = -1$. We can eliminate λ with Eq. (4). Then, we obtain basic equations, which can be written schematically as

$$N' = f_1(B, N, a, a') \ , \quad B' = f_2(B, N, a, a') \ , \quad a'' = f_3(B, N, a, a') \ , \tag{8}$$

where the prime denotes the derivative with respect to r.

The boundary condition at the horizon $r_{\rm h}$ is $N(r_{\rm h}) = 0$. We set $B(r_{\rm h}) = 1$. We can also set $r_{\rm h} = 1$ since there is no scale in the present theory. In this sense, it is assumed that the area coordinate r is normalized by the horizon radius below. If we use a rescaling freedom of v as $dv' = B(\infty)dv$, the asymptotic form of the metric is written as $ds^2 = -\frac{N(\infty)}{B(\infty)^2}dv'^2 + 2dv'dr + r^2d\Omega^2$. Thus, the boundary condition at spatial infinity for the asymptotic flatness is $N(\infty) = B(\infty)^2$. We should require $b(\infty) = 0$, for the Aether to be aligned with the timelike Killing field. Then, we have $a(\infty) = -B(\infty)^{-1}$. We can determine the pair of $a_{\rm h} := a(r_{\rm h})$ and $a'_{\rm h} := a'(r_{\rm h})$ as shooting parameters, one of which is fixed by $a(\infty) = -B(\infty)^{-1}$. Thus, there remains one freedom. Fixing this freedom is done as follows. Even in the spherically symmetric case, there is a spin-0 mode. The freedom mentioned above is fixed by the requirement that the regularity at the spin-0 horizon which is inside the event horizon.

However, since the asymptotic observer is insensitive to the regularity at the spin-0 horizon, we permit the singularity at the spin-0 horizon. For this reason, we leave one freedom. In concrete terms, we obtain $a_{\rm h}$ iteratively for some $a'_{\rm h}$, which is regarded as a free parameter.

4 Properties of solutions

We show several asymptotically flat solutions in Figs. 1 (a) and (c) for $c_+ = 0.4$ and $c_- = 0.1$. Figure 1 (a) shows that we can determine an $a_{\rm h}$ that satisfies the asymptotic condition for various values of $a'_{\rm h}$. Figure 1 (c) shows a "mass" function. If we define the mass function $m(r)$ by $m(r) := \frac{r}{2G}\left(1 - \frac{N}{B^2}\right)$, we can interpret $m(\infty)$ as ADM mass $M_{\rm ADM}$. As we can see, $m(r)$ monotonically decreases. This is not surprising since energy conditions are not necessarily satisfied in EA theory [11].

Since Figs. 1 show that the deviation from the Schwarzschild black hole is largest for the smallest value of $a'_{\rm h}$, it is natural to ask whether or not there is a lower limit $a'_{\rm h,crit}$ below which there is no regular solution. We show the relation $a'_{\rm h}$ and $M_{\rm ADM}$ for various values of c_+ and c_- in Fig. 2 (a). Typically, $M_{\rm ADM}$ is smaller than that of a Schwarzschild black hole by about 10%, which is consistent with the result in [5]. For $a'_{\rm h} < a'_{\rm h,crit}$, we cannot find an appropriate value of $a_{\rm h}$. $a'_{\rm h,crit}$ depends on c_+ and c_-. As $a'_{\rm h}$ approaches $a'_{\rm h,crit}$, $dM_{\rm ADM}/da'_{\rm h}$ tends to diverge.

We consider the possibility of distinguishing black holes in EA theory from Schwarzschild black hole by observation. In Ref. [7], the innermost stable circular orbit (ISCO) for neutron stars in EA theory was analyzed. The result is that the deviation from the Schwarzschild black hole is at most several percent. But this is not necessarily the case in the present situation, as shown below. The differences occur since we have the freedom parameterized by $a'_{\rm h}$ and the Aether is not static. These facts will be important if we consider observations such as Constellation-X, which tracks the motion of individual elements near black holes. We show the dependence of $r_{\rm ISCO}$ (normalized by $r_{\rm h}$) on $a'_{\rm h}$ in Fig. 2 (b). Notice that $r_{\rm ISCO} = 3$ for the Schwarzschild black hole. Therefore, the difference is nearly 10% for $a'_{\rm h} \simeq a'_{\rm h,crit}$.

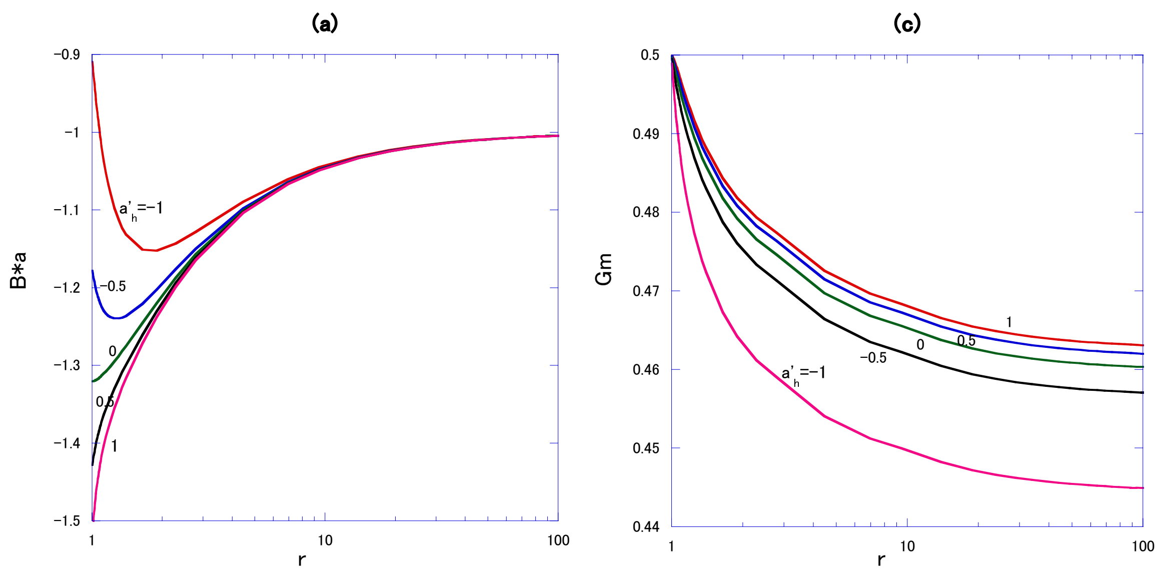

Figure 1: Field configurations for $c_+ = 0.4$ and $c_- = 0.1$.

5 Discussion

We have reanalyzed black hole solutions in EA theory while assuming that all the PPN parameters are the same as those for GR, resulting in two theoretical parameters c_+ and c_-. As another difference, we do not assume regularity at the spin-0 horizon since this is inside the event horizon. Interestingly, we find $a'_{\rm h,crit}$ below which there is no regular black hole solution. Near $a'_{\rm h,crit}$, the deviation of black hole mass $M_{\rm ADM}$ and ISCO $r_{\rm ISCO}$ from those for the Schwarzschild black hole become large.

These results are instructive for other cases. If we consider the case with rotation, freedom of the vector field is added. Then, it also contributes the kinetic term of the vector field, enhancing the differences

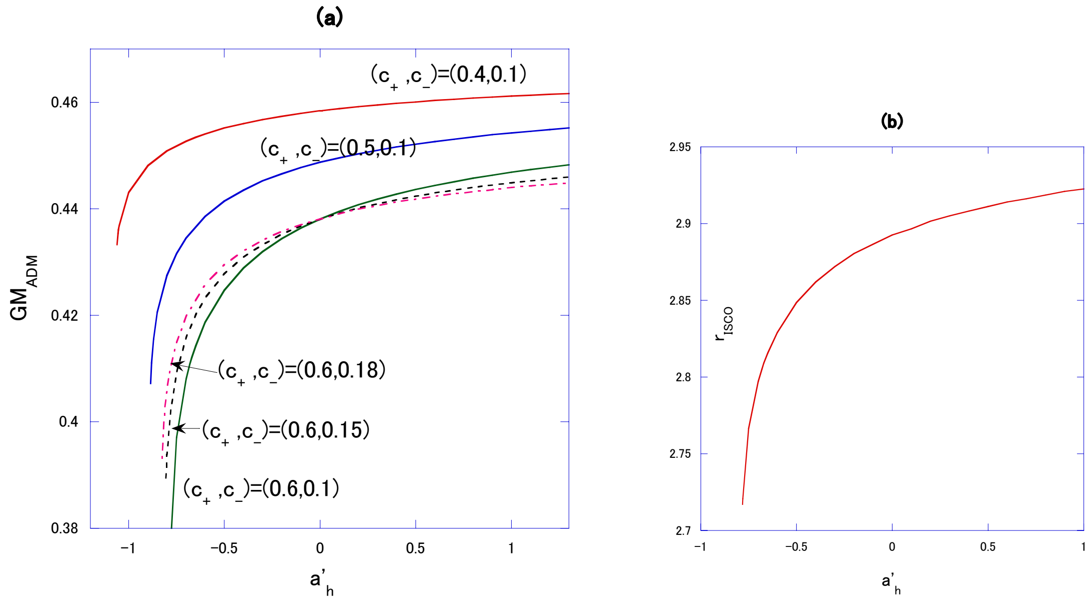

Figure 2: (a) $a'_{\rm h}$ v.s. $GM_{\rm ADM}$ and (b) $a'_{\rm h}$ v.s. $r_{\rm ISCO}$.

from the vacuum solution. This would also be true in other vector-tensor theories. For this reason, it is important to consider rotational black holes in vector-tensor theories, if we are to constrain them.

References

[1] J. D. Bekenstein, Phys. Rev. D **70**, 083509 (2004); *ibid.,* 069901 (E) (2005).

[2] T. Jacobson and D. Mattingly, Phys. Rev. D **64**, 024028 (2001).

[3] B. Z. Foster and T. Jacobson, Phys. Rev. D **73**, 064015 (2006).

[4] C. Eling and T. Jacobson, Class. Quant. Grav. **23**, 5625 (2006).

[5] C. Eling and T. Jacobson, Class. Quant. Grav. **23**, 5643 (2006).

[6] R. A. Konoplya and A. Zhidenko, Phys. Lett. B **644**, 186 (2007).

[7] C. Eling, T. Jacobson, and M. C. Miller, Phys. Rev. D **76**, 042003 (2007).

[8] T. Tamaki and U. Miyamoto, arXiv: 0709.1011 [gr-qc], to appear in Physical Review D.

[9] T. Jacobson and D. Mattingly, Phys. Rev. D **70**, 024003 (2004).

[10] J. W. Elliott, G. D. Moore, and H. Stoica, JHEP **0508**, 066 (2005).

[11] C. Eling, Phys. Rev. D **73**, 084026 (2006).

[12] B. Z. Foster, Phys. Rev. D **73**, 104012 (2006); Erratum *ibid.*, **75**, 129904 (2007).

Characterization of chaotic motions of a charged particle in Kerr black hole magnetosphere

Hiroko Koyama [1] and Masaaki Takahashi [2]

[1] *Department of Physics, Nagoya University, Nagoya 464–8602, Japan*
[2] *Department of Physics and Astronomy, Aichi University of Education, Kariya, Aichi 448–8542, Japan*

Abstract

We study the properties of chaos in the motions of a charged test particle confined in a dipole magnetic field around a Kerr black hole. We characterize the chaos using the power spectrum of the time series of the particle's position. We find that the pattern of the power spectrum shows not only white noise but also $1/f$ fluctuation, depending on the values of the system parameters (the black hole's spin, the strength of the magnetic field, the total energy, and the total angular momentum). So we succeed in classifying the chaotic motions into the two distinct types. One is $1/f$, and the other is white noise. Based on this classification, we obtain "phase diagram" for the properties of the chaos. This phase diagram enables us to guess the black hole's spin and the strength of the magnetic field by observing the dynamics of the charged particle, even if the motion is chaotic.

1 Introduction

Black hole and accretion disk system, like as a central engine of AGN, compact X-ray sources and GRB, is astrophysically important, and has been investigated by many authors. Observationally, we can obtain X-ray spectrum and time variability data, and near future we may see black hole shadow. We are interested in such magnetic phenomena near a black hole, and our motivation is to understand property of magnetosphere near a black hole. So we assume global magnetic fields in black-hole geometry. The problem is how to get peculiar informations about the black hole and the surrounding magnetic fields.

Now we go back to a basic subject that motions of a charged test particle in black hole magnetosphere. Firstly we consider test-particle motions around a Kerr black hole. In this system, number of spacetime dimension is 4, and number of constants of motion is also 4. That is, rest mass, energy, angular momentum, and Carter constant [1]. Then this system is integrable, and the particle's orbits are regular. Next, we consider charged-particle motions in the dipole magnetic field around a Kerr black hole [2]. In this system, number of spacetime dimension is 4, but number of constants of motion is 3. That is, rest mass, energy, and angular momentum. The separation of variable has not been found, and this system can show nonintegrability [3]. So the particle motions in this system can be chaotic and complicated. In this way, nature is filled with phenomena that exhibit chaotic behavior.

In roughly speaking, motions of a charged particle in dipole magnetic field near Kerr black hole can be explained as following [3]. A charged particle can be trapped in the doughnut-like shaped zones which is similar to Van Allen belt in Earh's magnetic field. The particle motions are combination of gyration, bouncing and drifting. The particle gyrates around the magnetic field line, oscillates in the poloidal plane along the magnetic field line, and drifts in the toroidal direction. Chaotic sea in the Poincare maps have been confirmed [4].

Having found the existence of chaotic motions, we should now characterize and quantify the chaos to clarify the effect of the black-hole spin and the magnetic field. Then, in this paper, we look for statistical laws in the chaotic motions in the dipole magnetic field around a Kerr black hole to classify the chaos. Indeed, we can hardly learn anything about the chaos if we judge it only from the randomness of the distribution of the points in Poincaré maps or the positiveness of the Lyapunov exponents. Not a few people believe that chaotic system is simply random and completely unpredictable. Of course, we cannot predict the time evolution of the state of the test particle exactly, when its system is chaotic. However,

[1] E-mail:hiroko@allegro.phys.nagoya-u.ac.jp
[2] E-mail:takahasi@phyas.aichi-edu.ac.jp

even in such cases, we can frequently find some statistical laws which are proper to the system. One possible measure of chaos is the power spectrum of the time series. In our previous paper [5], we have succeeded to classify the chaos in the motions of a spinning test particle around Schwarzschild black hole, using the power spectrum of the time series of the particle's position. We have found out that the pattern of the power spectra are divided into two distinct types depending on the system parameters (spin and angular momentum) [5]. One is $1/f$-type fluctuations and the other is white noise. In this paper, we apply this method to characterize chaos in the motions of a charged test particle confined in the dipole magnetic field around a Kerr black hole. Our goal is to clarify the effect of the spin of the black hole and the magnetic field into the chaos in the particle's motions.

Our strategy to characterize the chaos in this paper is as follows. First, we introduce the power spectrum of the time series of z components of the particle's position. Then we characterize the properties of the chaos in the charged-particle motions in the dipole magnetic field in Kerr spacetime, using the pattern of the power spectrum. It is found that the pattern of the power spectrum can be classified as $1/f$ or white noise. That is, we succeed in classifying the chaotic motions into two distinct types. Based on this classification, we plot phase diagrams for properties of the chaos.

2 Equations for a charged particle around a black hole

We solve the motion of a charged test particle in a dipole magnetic field around a Kerr black hole. The metric is written by the Boyer-Lindquist coordinates (t, r, θ, ϕ) with $c = G = 1$, and the non-zero components of the contravariant metric $g^{\mu\nu}$ are given by

$$g^{tt} = \frac{A}{\Delta\Sigma}, \quad g^{t\phi} = \frac{2Mar}{\Delta\Sigma}, \quad g^{\phi\phi} = -\frac{1-2Mr/\Sigma}{\Delta\sin^2\theta}, \quad g^{rr} = -\frac{\Delta}{\Sigma}, \quad g^{\theta\theta} = -\frac{1}{\Sigma}, \tag{1}$$

where $\Delta \equiv r^2 - 2Mr + a^2$, $\Sigma \equiv r^2 + a^2\cos^2\theta$, and $A \equiv (r^2+a^2)^2 - \Delta a^2 \sin^2\theta$. M is mass of the black hole, and a is the spin parameter. The Hamiltonian for the charged particle is

$$H = \frac{1}{2} g^{\mu\nu} (\pi_\mu - qA_\mu)(\pi_\nu - qA_\nu), \tag{2}$$

where π_μ is the canonical momentum, q is charge, and A_μ is the 4-potential of the electromagnetic field. The equations of motion are given by the Hamilton's equations,

$$\frac{dx^\mu}{d\lambda} = \frac{\partial H(x^\nu, \pi_\nu)}{\partial \pi_\nu}, \qquad \frac{d\pi^\mu}{d\lambda} = -\frac{\partial H(x^\nu, \pi_\nu)}{\partial x_\nu}. \tag{3}$$

The 4-momentum of a charged particle are given by

$$p^\mu \equiv \frac{dx^\mu}{d\lambda} = g^{\mu\nu}(\pi_\nu - qA_\nu). \tag{4}$$

The magnetic field configuration is assumed by dipole magnetic field [2], which is a solution of vacuum Maxwell equations in Kerr geometry. The non-zero components of A_μ are given by

$$A_t = \frac{-3\mu}{2\gamma^2\Sigma}\left\{ \left[r(r-M) + (a^2 - Mr)\cos^2\theta\right] \frac{1}{2\gamma} \ln\left(\frac{r-r_-}{r-r_+}\right) - (r - M\cos^2\theta)\right\}, \tag{5}$$

$$\begin{aligned} A_\phi = & \frac{-3\mu\sin^2\theta}{4\gamma^2\Sigma}\Big\{(r-M)a^2\cos^2\theta + r(r^2+Mr+2a^2) \\ & - \left[r(r^3 - 2Ma^2 + a^2 r) + \Delta a^2\cos^2\theta\right] \frac{1}{2\gamma}\ln\left(\frac{r-r_-}{r-r_+}\right)\Big\}, \end{aligned} \tag{6}$$

where μ is a dipole moment, $\gamma \equiv \sqrt{M^2 - a^2}$ and $r_\pm \equiv M \pm \gamma$.

The rest mass of the charged particle, m, is defined by $m^2 \equiv -p_\mu p^\mu$. m is constant. In addition, from the stationary and axial symmetry of both the electromagnetic field and the spacetime geometry, energy and angular momentum, $E \equiv \pi_t = p_t + qA_t$ and $L \equiv -\pi_\phi = -(p_\phi + qA_\phi)$, respectively, are also constants of motion. That is, number of constants of motion is 3. On the other hand, number of spacetime dimension is 4. Then, the particle's orbits in this system can be chaotic. We solve Eqs. (3) by the Runge-Kutta method numerically.

3 Phase diagram for the properties of chaos

In this section, we characterize the chaos in the charged particle motions in dipole magnetic field around Kerr black hole. Here we analyze the time series of the particle position. In order to that, first, we introduce the power spectrum. The power spectrum of the time series of z components of the particle's position, $P_z(\omega)$, is defined by

$$P_z(\omega) = \left| \frac{1}{T} \int_0^T z(t) e^{i\omega t} dt \right|^2 . \tag{7}$$

We test the pattern of the power spectrum $P_z(\omega)$ for various grid points in the parameter space, and show the results in Figs. 1 and 2. Here we define the parameter Q as $Q \equiv 3q\mu/(4M^2 m)$. The value of L/M is fixed to -7.

In Fig. 1 we test the pattern of the power spectrum $P_z(\omega)$ of the chaotic orbits for grid points in two-dimensional $(a/M, E/m)$ configuration. The value of Q is fixed to -30 in Fig. 1 . In the region where the symbols ($\bigcirc$) are marked the power spectrum $P_z(\omega)$ shows $1/f$-type spectrum. On the other hand, in the region where symbols ($\Box$) are marked, the power spectrum $P_z(\omega)$ shows white noise. At the points where the symbols ($\times$) are marked, the orbits are not chaotic but regular.

In Fig. 2 we test the pattern of the power spectrum $P_z(\omega)$ for grid points in two-dimensional $(a/M, Q)$ configuration. At the points where the symbols ($\bigcirc$) are marked, the $1/f$-type power spectrum is observed. At the points where the symbols (Δ) are marked, the $1/f$-type power spectra are observed for low energy, and the white-noise power spectra are observed for high energy. At the points where the symbols ($+$) are marked, the orbit apparently behaves regular for low energy, and the white-noise power spectra are observed for high energy.

Figs. 1 and 2 can be considered as "phase diagrams" for the properties of chaos. These phase diagrams illustrate the effect of the black-hole spin and the strength of the magnetic field. When the black hole is slowly rotating, or when the magnetic field is not weak, the pattern of the power spectrum $P_z(\omega)$ of the chaotic orbits shows $1/f$ fluctuation for low energy, and shows white noise for high energy. On the other hand, when the black hole is rapidly rotating and the magnetic field is weak, we cannot observe such $1/f$ fluctuations. The particle's orbits are regular for low energy, and $P_z(\omega)$ of the chaotic orbits shows white noise for high energy. These phase diagrams (Figs. 1, 2) enables us in principle to guess the black hole's spin and the strength of the magnetic field, even if the particle's motion is chaotic.

4 Summary

In this paper we have investigated the properties of chaos in the motions of a charged particle in dipole magnetic field around a Kerr black hole. We have characterized the chaos using the power spectrum of the time series of z components of the test particle's position, $P_z(\omega)$. We have found that the pattern of the power spectrum $P_z(\omega)$ can be divided into distinct 2 types, $1/f$ and white noise, depending on the system parameters (black hole's spin and magnetic field). Based on this classification, we have obtained "phase diagrams" for the property of chaos (Figs. 1, 2). These phase diagrams illustrate the effect of the black-hole spin and the strength of the magnetic field. The chaos we found in this system is not always merely random. Using the various properties of chaos, we have presented new possibility to estimate black hole's spin and magnetic field.

References

[1] B. Carter, Phys. Rev. **174**, 1559 (1968).

[2] J. A. Petterson, Phys. Rev. **D 12**, 2218 (1975).

[3] A. R. Prassana and R. K. Varma, Pramana **8**, 229 (1977).

[4] Y. Nakamura and T. Ishizuka, Astrophysics and Space Science **210**, 105 (1993)

[5] H. Koyama, K. Kiuchi and T. Konishi, Phys. Rev. **D 76**, 064031 (2007).

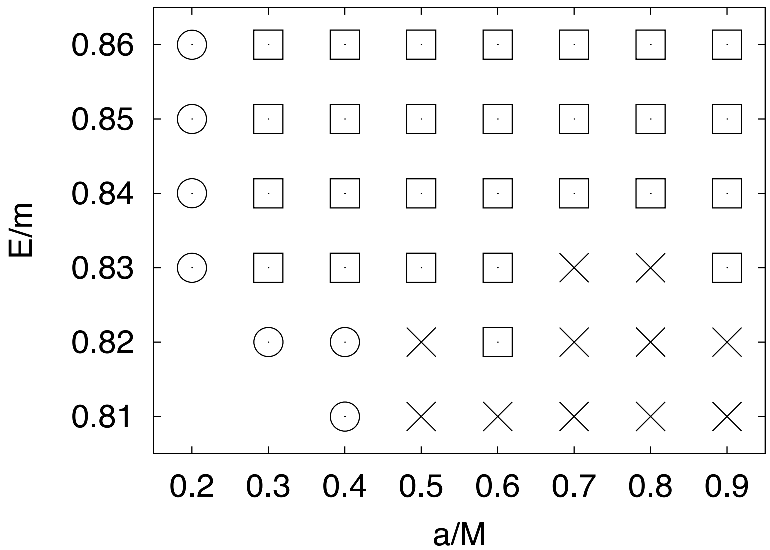

Figure 1: The phase diagram for the chaotic orbits. The patterns of the power spectrum for the chaotic orbits at grid points in two-dimensional $(a/M, E/m)$ configuration are tested. Here we set $Q = -30$ and $L/M = -7$. At the points where the symbols ($\bigcirc$) are marked, the $1/f$-type power spectra are observed. At the points where the symbols ($\Box$) are marked, the white-noise power spectra are observed. At the points where the symbols ($\times$) are marked, the orbits are regular (not chaotic).

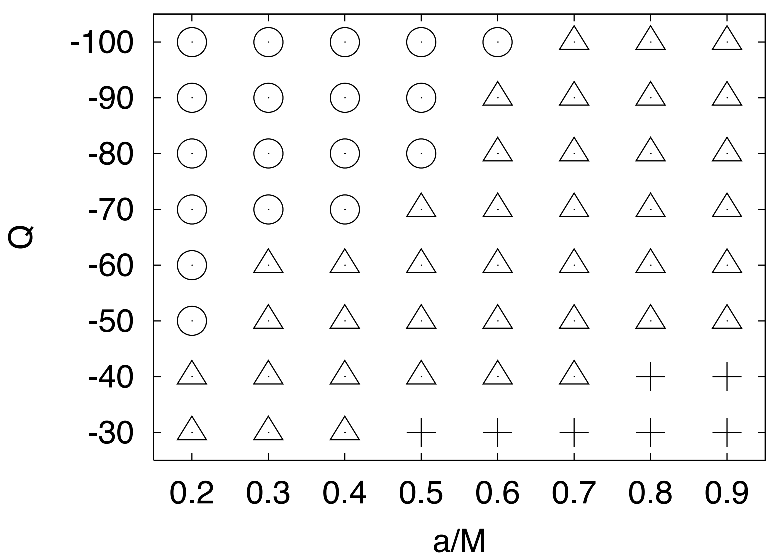

Figure 2: The phase diagram for the chaotic orbits. The patterns of the power spectrum for the chaotic orbits at grid points in two-dimensional $(a/M, Q)$ configuration are tested. Here we set $L/M = -7$. At the points where the symbols ($\bigcirc$) are marked, the $1/f$-type power spectrum is observed. At the points where the symbols (Δ) are marked, the $1/f$-type power spectra are observed for low energy, and the white-noise power spectra are observed for high energy. At the points where the symbols ($+$) are marked, the orbits are regular (not chaotic) for low energy, and the white-noise power spectra are observed for high energy.

Particle creation in a resonant microwave cavity?

Y. Kido† , H. Hatano†, S. Matsuki†, W. Naylor†[1] , T. Nishimura† and K. Yamamoto⋆

†*Department of Physics, Ritsumeikan University, Kusatsu, Shiga, 525-8577, Japan*
⋆*Department of Nuclear Engineering, Kyoto University, Kyoto 606–8501, Japan*

Abstract

Parametric photon creation via the so called dynamical Casimir effect is calculated numerically. We consider a model where a three-dimensional resonant cavity is bisected by a semiconductor diaphragm, which is irradiated by a pulse laser with frequency of the GHz order. Our preliminary results show that the photon number density depends on where the diaphragm is placed with the midpoint giving the largest contribution.

1 Introduction

In the pursuit of an experimental verification of the dynamical Casimir effect (DCE), the problem arises of how to oscillate a cavity wall with an extremely high frequency of the GHz or THz order? A particularly nice idea was by Yablonovitch [1], also see references in [2], who proposed an optical excitation of valence electrons of a semiconductor into the conduction band by a pulse laser, which makes the semiconductor metallic. The metallized semiconductor wall reflects electromagnetic waves and thus the semiconductor diaphragm (SCD) acts like an oscillating cavity wall. Quite recently, experimental schemes to detect DCE photons have been proposed using a semiconductor wall irradiated by a pulse laser [3].

From a theoretical standpoint there have been been some works on the *SCD idea* [2, 4, 5]. However, in [5] the prerequisite guaranteeing a perturbative treatment is not satisfied when the SCD is placed far from the cavity wall and a numerical approach should be used, e.g. [6]. Also, recently the work of Dodonov & Dodonov [7] discussed some possible problems with the *SCD idea*, relating to that fact that the dielectric constant of the semiconductor has a large positive imaginary part in the conducting (irradiated) state, which therefore leads to dissipative effects. A possible resolution to this problem was advocated in [8] by applying a single mode phenomenological dissipation model. The purpose of this work is to discuss how the location of the SCD affects the number of created photons assuming the SCD is a perfect conductor when irradiated (unitary evolution). Furthermore, we find that when the SCD is not attached to one of the cavity walls, such as at the midpoint, then the single mode approach used in [8] should somehow be generalized to multimode coupling.

2 Model for TE Modes

We evaluate numerically the number density for TE photons for an SCD placed in an aluminum cavity with dimensions $L_x \times L_y \times L_z (L_x = L_y \equiv L = 5$ cm, $L_z = 2L)$ which is bisected by an n-type semiconductor diaphragm (SCD) placed at a position d from the left wall along the z-axis (the exact details of the experimental design & detection will be presented elsewhere [9]). Electromagnetic waves in a vacuum can be conveniently decoupled into two scalar functions (or scalar Hertz potentials as they are commonly known) ψ_E and ψ_M instead of the usual scalar & vector potential $(\phi, \mathbf{A})$, e.g. see [10]. This allows us to find solutions for each respective scalar Klein-Gordon equation:

$$[\nabla^2 - \frac{1}{c^2}\frac{\partial^2}{\partial t^2}]\psi_E(x, y, z, t) = V(t)\delta(z - d)\psi_E(x, y, z, t) \tag{1}$$

where the subscript E will be used to denote the TE mode. Similarly to the work of [4, 5], we model the SCD by a Dirac delta function, $\delta(z-d)$ with potential $V(t) = 4\pi\rho_e(t)\Delta z e^2/m^* c^2$; where ρ_e is the density of conduction electrons, Δz is the effective thickness of the SCD for laser absorption, e is the electronic charge and m^* the effective mass of the conduction electrons in the SCD with $m^* = 0.07m_0$ (m_0 being

[1]naylor@se.ritsumei.ac.jp

the electron rest mass and c, the velocity of light). Estimating a pulse laser power of around 100 J/pulse then we find $\rho_e \Delta z \cong 1 \times 10^{13}$ cm^{-2}, where we have assumed a donor density of 10^{18} atoms cm^{-3} and an energy interval of 10 meV between the conduction band minimum and donor level (at a temperature of 1 K). Thus one obtains the following maximum and minimum values for $V(t)$ of $V_{max} = 500$ cm^{-1} and $V_0 \approx 0$ cm^{-1}.

In the following we shall assume that the period of the laser pulse is set to $T = 149.07$ ps, which corresponds to a frequency of about three GHz for the TE fundamental modes: $(1, 0, 1)$ & $(0, 1, 1)$ respectively. The overall shape of $V(t)$ is assumed to asymmetric because the SCD excitation and recombination times are expected to differ [7]. We use a profile for $V(t)$ of the form of one Gaussian of half-width $\sigma_1 = 4$ ps going from V_0 to $V_{\max}$ where saturation at the maximum lasts for $t_{sat} = 7$ ps with the second Gaussian with $\sigma_2 = 11$ ps going back down to V_0 . We assume the pulse is offset by 30 ps. In practice these times can be measured experimentally and for example lifetimes of the order of 10 ps may be achievable. In order to avoid strong dissipation effects in the SCD we have also set the saturation time to a short time $t_{sat} = 7$ ps.

The scalar function ψ_E represents the longitudinal component of the magnetic field $\mathbf{B}_z$ and satisfies Dirichlet boundary conditions (BCs) on the longitudinal boundary and Neumann BCs on the transverse boundaries. Thus, the solution for the TE mode takes the form

$$\psi_E(\mathbf{x}, t) = \begin{cases} \sqrt{\frac{2}{L_x}} \cos\left(\frac{\pi m_x x}{L_x}\right) \sqrt{\frac{2}{L_z}} \cos\left(\frac{\pi m_y y}{L_y}\right) \times A_m^E \sqrt{\frac{1}{d}} \sin\left(k_m z\right) & 0 < z < d \\ \sqrt{\frac{2}{L_x}} \cos\left(\frac{\pi m_x x}{L_x}\right) \sqrt{\frac{2}{L_z}} \cos\left(\frac{\pi m_y y}{L_y}\right) \times B_m^E \sqrt{\frac{1}{L_z - d}} \sin\left(k_m (L_z - z)\right) & d < z < L_z \end{cases}, \tag{2}$$

where m_x and m_y are integers $(0, 1, 2, 3, \ldots)$ with $m_x = m_y \neq 0$ and m (dropping subscript z) denotes the eigenvalues of the function $k_m(t)$ in the z-direction A_m^E is a normalization constant satisfying

$$(\psi_n, \psi_n)_E = \left(1 - \frac{\sin(2dk_n)}{2dk_n}\right)(A_n^E)^2 + \left(\frac{\sin(2k_n(L_z - d))}{2k_n(d - L_z)} - 1\right)(B_n^E)^2 = 1\,. \tag{3}$$

The SCD δ-function in the wave equation leads to a discontinuity in the spatial derivative at $z = d$, while the field itself is continuous:

$$\psi_I(z = d, t) = \psi_{II}(z = L_z - d, t) \tag{4}$$

$$\frac{\partial}{\partial z}\psi_I(z = d, t) - \frac{\partial}{\partial z}\psi_{II}(z = L_z - d, t) = -V(t)\psi(z = d, t) \tag{5}$$

From the above relations, we obtain the following continuity and eigenvalue relations for the TE mode:

$$\frac{A_m^E}{B_m^E} = \sqrt{\frac{d}{L_z - d}} \frac{\sin(k_m(L_z - z))}{\sin(k_m d)} \qquad\qquad \frac{\sin(k_m L_z)}{\sin(k_m[L_z - d])\sin(k_m d)} = -V(t)L_z\,. \tag{6}$$

In this work we solve for the eigenvalues $k_m(t)$ exactly.

3 Photon Number Density

The second quantization of the equations of motion using the instantaneous basis approach leads to a set of infinitely coupled equations [11]. The TE field is quantized as $\psi_E(\mathbf{x}, t) = \sum_m C_m \left[a_m u_m(\mathbf{x}, t) + a_m^\dagger u_m^*(\mathbf{x}, t)\right]$ with the standard harmonic oscillator solution $u_m(\mathbf{x}, t) = e^{-i\omega_m^0 t}/(\sqrt{2\omega_m^0})\, \psi_m(\mathbf{x}, 0)$ for $t < 0$, before irradiation and the instantaneous basis $u_s(\mathbf{x}, t \geq 0) = \sum_m P_m^{(s)}(t)\psi_m(\mathbf{x}, t)$ for $t \geq 0$ while irradiated. On substituting this expression into the wave equation (1) we obtain, after using orthonormality,

$$\ddot{P}_n^{(s)} + \omega_n^2(t) P_n^{(s)} = -\sum_m^\infty \left[\left(2\dot{P}_m^{(s)}\dot{k}_m + P_m^{(s)}\ddot{k}_m\right) g_{mn}^{\mathrm{A}} + P_m^{(s)}\dot{k}_m^2 g_{mn}^{\mathrm{B}}\right], \tag{7}$$

where

$$g_{mn}^{\mathrm{A}} = \frac{\delta_{m_x n_x}\delta_{m_y n_y}}{(\psi_n, \psi_n)} \left(\frac{\partial \psi_m}{\partial k_m}, \psi_n\right) \qquad\qquad g_{mn}^{\mathrm{B}} = \frac{\delta_{m_x n_x}\delta_{m_y n_y}}{(\psi_n, \psi_n)} \left(\frac{\partial^2 \psi_m}{\partial^2 k_m}, \psi_n\right)\,. \tag{8}$$

The g^A_{mn} and g^B_{mn} are very complicated functions and would require numerical integration in general (we have verified numerically that $g^A_{nn} = 0$ in all cases). However, for special cases (such as at the midpoint and for $d = L_z/3$) they can be integrated exactly to give a complicated function of $k_n(t)$. The wave number at a given instant of time is

$$\omega_n^2(t) = k_n^2(t) + \left(\frac{n_x \pi}{L_x}\right)^2 + \left(\frac{n_y \pi}{L_y}\right)^2 \qquad \omega_m(0) = \omega_m^0 \,. \tag{9}$$

and imposing continuity of u_n and $\dot{u}_n$ at $t = 0$ leads to the following initial conditions: $P^{(s)}_m(0) = 1/\sqrt{2\omega^0_m}$ and $\dot{P}^{(s)}_m(0) = -i\sqrt{\omega^0_m/2}$.

As has been well discussed in the literature [12] the number density, N_m, in a particular mode m is[2]

$$N_m = \frac{1}{C_m^2} \sum_n C_n^2 |\beta_{mn}|^2 \qquad C_m^2 = 8\pi / \left[\left(\frac{\pi m_x}{L_x}\right)^2 + \left(\frac{\pi m_y}{L_y}\right)^2\right] \tag{10}$$

where C_m is a TE normalization [10] and β_{mn} is a Bogolubov coefficient [12]. These can be calculated by choosing the solution in $u_m(t)$ for time $t \geq 0$ as the *out* basis states and use the continuity conditions valid for $t < 0$ for the *in* basis states. A straightforward calculation leads to

$$\beta_{mn}(t) = \sqrt{\frac{\omega_m(t)}{2}} \left(P^{(n)}_m(t) - \frac{i}{\omega_m(t)} \left[\dot{P}^{(n)}_m(t) + \sum_\ell g^A_{\ell m}(t) P^{(n)}_\ell(t) \right] \right) , \tag{11}$$

with α_{mn} given by the complex conjugate. The choice of normalization in equation (11) is defined to satisfy the continuity conditions, which implies $\alpha_{mn}(0) = \delta_{mn}$ and $\beta_{mn}(0) = 0$. By solving equation (7) numerically we can find $\beta_{mn}(t)$ and hence the photon number density via equation (10).

4 Results & Discussion

There are various approaches to solve the set of equations (7), e.g. [6], and what we try here is to just solve the equations directly in MATHEMATICA. It may be worth mentioning that the larger the power of the pulse laser the more pulses which can fit into a given carrier wave pulse. In our case we expect the carrier wave pulse to be about 5000 ps long and thus the fundamental TE mode would contain about 33 pulses. However, due to limitations with our code we can only integrate the equations up to 1000 ps, about 7 pulses. In the numerics we went up to a given cutoff m_{max} in equation (7) such that the results converged, which we checked by verifying that the unitarity constraint, $\sum_n(|\alpha_{mn}|^2 - |\beta_{mn}|^2) = 1$, [12] is satisfied to a given accuracy, see Figure 1. For the midpoint this was at $m_{max} = 17$ while that for $d/L_z = 1/3$ was at $m_{max} = 10$.

A further point is that due to the $\delta_{m_x n_x}$, $\delta_{m_y n_y}$ terms in g^A_{mn} and g^B_{mn} we only consider the coupling of the modes in the z-direction to the $(1, 0, 1)$ mode: with $(1, 0, n_z)$. The equations effectively become equivalent to those of a one-dimensional *massive* scalar field in a cavity with Dirichlet BCs [6], where the effective mass acts as a damping term. Thus, although there are some limitations with the code (larger the cutoff m_{max} the slower the code), these results at the very least give an upper bound on the number of photons produced for 1000 ps.

The results are presented in Figure 1 and show that the largest amount of photon production occurs for the SCD placed at the midpoint (at least as compared to the case $d/L_z = 1/3$ for 1000 ps). Also our numerics show that assuming single mode coupling leads to an over-prediction in the number of photons produced, which is simply because we must include the damping terms coming from the effective scalar field mass (though there are cases where the effective damping is negligible, see [6]).

We are now currently writing code in FORTRAN to deal with the limitations of the integration of equation (7) over time, the cutoff m_{max} (which must be increased as we go to larger times) and the fact that the values for the g^A_{mn} and g^B_{mn} also require numerical integration in general. However, although the results presented here have their limitations, if the results are converging then we should be able to partially extraploate themto larger times.

[2]The method of detection relies on a Rydberg atom beam which can detect individual photons of single frequency [9].

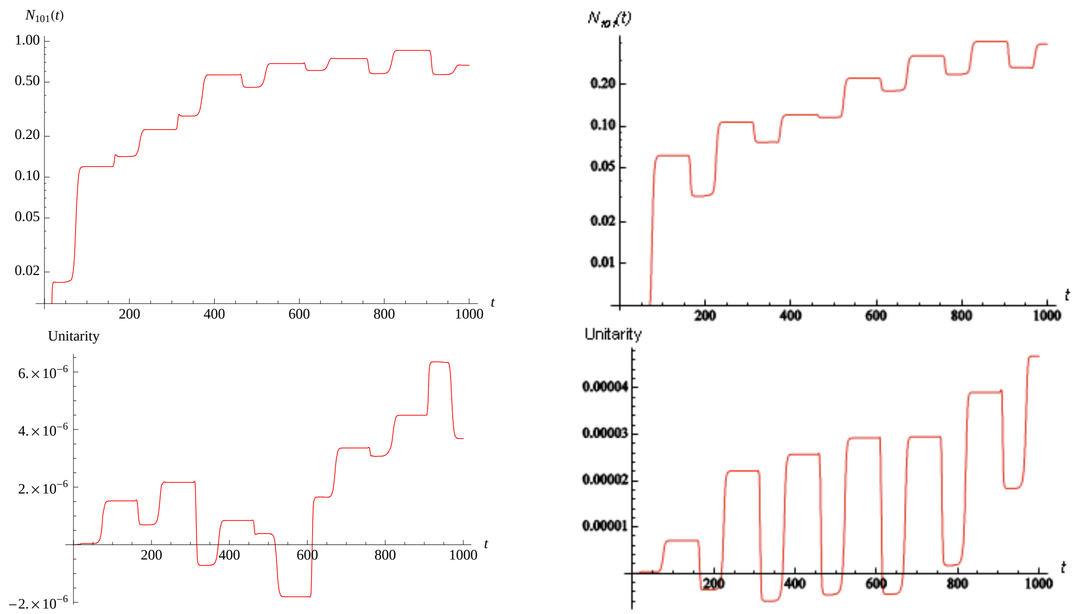

Figure 1: Top: the number of photons produced in the $(1,0,1)$ fundamental mode against time. Bottom: the unitarity constraint $\sum_n (|\alpha_{mn}|^2 - |\beta_{mn}|^2) = 1$. Left & right panels are for the SCD at the midpoint and $d/L_z = 1/3$ respectively.

References

[1] E. Yablonovitch, Phys. Rev. Lett. **62**, 1742 (1989).

[2] A. V. Dodonov and V. V. Dodonov, J. Opt. B: Quantum Semiclass. Opt. **7**, S47 (2005).

[3] C. Braggio, G. Bressi, G. Carugno, C.D. Noce, G. Galeazzi, A. Lombardi, A. Palmieri, G. Ruoso, and D. Zanello, Europhys. Lett. **70**, 754 (2005).

[4] G. Barton and A. Calogeracos, Anals of Phys. **238**, 227 (1995).

[5] M. Crocce, D.A.R. Dalvit, F.C. Lombardo, and F.D. Mazzitelli, Phys. Rev. A 70, 033811 (2004).

[6] M. Ruser, Phys. Rev. A **73**, 043811 (2006) [arXiv:quant-ph/0509030].

[7] V. V. Dodonov and A. V. Dodonov, J. Phys. A: Math. Gen. **39**, 6271 (2006); *ibid.* S749.

[8] V. V. Dodonov, J. Opt. B: Quantum Semiclass. Opt. **7**, S445 (2005) .

[9] S. Matsuki, H. Hatano, Y. Kido, T. Nishimura, W. Naylor, and K. Yamamoto, submitted to Europhys. Lett.

[10] M. Crocce, D.A.R. Dalvit, F.C. Lombardo, and F.D. Mazzitelli, J. Opt. B: Quantum Semiclass. Opt. **7**, S32 (2006).

[11] C. K. Law, Phys. Rev. A **51**, 2537 (1995).

[12] N. D. Birrell and P. C. W. Davies, Quantum Fields In Curved Space (Cambridge University Press, UK, 1982).

Unsuppressed creation of excited child universes

Stefano Ansoldi[†1], Eduardo I. Guendelman[‡2] and Idan Shilon[‡3]

[†]*Department of Physics, Kyoto University, Kitashirakawa, Sakyo, Kyoto 606–8502, Japan and International Center for Relativistic Astrophysics (ICRA), Italy*

[‡]*Department of Physics, Ben-Gurion University, Beer-Sheva 84105, Israel*

Abstract

We study a special model able to describe child universe formation by using a sphere of strings separating two domains of spacetime (the exterior one of the Schwarzschild type). We show that no energy barrier for the process exists and we discuss consequences and possible refinements of the model.

In general relativity the dynamics of spacetime is very rich and often we have to face situations which seem counterintuitive if interpreted with a Newtonian mind. This is also the case when considering what are known as *child universes* [8, 7]. Child universes (or *vacuum bubbles* [13, 14, 12, 15, 32, 26, 31, 25, 29]) are regions of spacetime that expand up to very large size without displacing the surrounding space (*parent space*), which is often modelled using Schwarzschild spacetime (non-asymptotically flat generalizations have also been considered [1, 2]). The fact that the expanding child universe does not (and, actually, cannot) displace the parent space, is assured by the pressure gradient, which is always pointing from the parent space toward the child universe. Nevertheless the bubble *can actually have* another way to expand, thanks to the structure of the maximally extended manifold. Indeed, if wormholes can be realized, then the child universe can *make its own space* on the *other* side of the wormhole throat (where *other* means, with respect to the one in which an observer in the parent space is living): as the child universe grows, the wormhole will be increasingly thinned, until its throat will collapse and the child universe will continue its expansion finally disconnecting from the parent spacetime.

The above picture has been a preferred model for inflationary bubbles. Referring to the literature [22, 23, 6, 8, 16, 18, 17] for details, often a model with three parameters is used: these are the energy density inside the vacuum bubble, Λ, a parameter describing the matter content of the bubble surface[4] , σ_p, and the total mass-energy of the parent spacetime, M. Depending on their values child universes can be formed or not and there are two reasons why a generic choice might not give birth to a child universe. The first one is that there can be no solution which is small enough at earlier times and big enough at later ones, as when, for instance, there is a potential barrier separating small bubble configurations from large ones (this is often the case). The second one is, instead, related to the geometrodynamics of the problem, since it can happen that a wormhole is not created. To have a child universe both the above "environmental" conditions must be favorable (although the first one can be relaxed using quantum tunnelling under the potential barrier [16, 18, 17]: this does not substantially modify the main results of the following discussion). It then turns out that, in the existing models of *classical* child universe creation, these conditions are fulfilled only provided M exceeds a critical value $M_{\rm cr}$. It is thus interesting to ask if this is a necessary condition. That there may be a negative answer to this question can be conjectured by considering appropriate limits of well known models [8], which are characterized by $p = 2$, i.e. in which the surface of the bubble has a constant surface energy density σ_2 and the familiar equation of state (surface energy density) = −(pressure) holds. More precisely, we are interested in the limits

[1]E-mail:ansoldi@dimi.uniud.it

[2]E-mail:guendel@bgu.ac.il

[3]silon@bgu.ac.il

[4]The notation which we are going to use is such that in the symbol σ_p the subscript p remembers that the total mass energy of the vacuum bubble surface is proportional to $\sigma_p R^p$. For instance, in the case of pressureless dust $p = 0$ and σ_0 is the total mass energy of the system; a matter which obeys the equation of state (surface energy density) = −(pressure), will instead correspond to $p = 2$, so that the corresponding constant surface energy density will be σ_2, and so on. In this contribution we will also be interested in the case of a string gas living on the bubble surface, in which case $p = 1$ and the corresponding parameter will be denoted, accordingly, as σ_1.

in which the volume energy density Λ and/or the surface energy density σ_2 become very large; it has, indeed, been proved that in this cases $M_{\rm cr}$ can be made very small [19].

We will briefly review this argument. When we consider the models parametrized by Λ, M and σ_2, all the relevant quantities depend only on the following dimensionless parameters

$$a = \frac{2M}{(3/\Lambda)^{1/2}}, \quad b = \frac{12\pi\sigma_2}{\Lambda}$$

provided we measure the radius of the child universe in units of the square root of the inverse cosmological constant

$$x = \frac{r}{(3/\Lambda)^{1/2}}.$$

In particular the potential of the effective one dimensional problem that describes the radial motion is given by

$$V(x) = -\frac{a^2 + 2a(b^2-1)x^3 - 4b^2x^4 + (1+b^2)^2x^6}{4b^2x^4}.$$

This potential tends to $-\infty$ when, both, $x \to 0^+$ and $x \to +\infty$, so it will have at least one maximum point; it is, in fact, possible to show that it has exactly one maximum point, located at $x_{\rm max}$, defined as

$$x^3_{\rm max} = \frac{a}{2}Z(b), \quad \text{where} \quad Z(b) = \frac{b^2 - 1 + (9 + 14b^2 + 9b^4)^{1/2}}{(b^2+1)^2}.$$

The value of the potential at the maximum, $V(x_{\rm max})$, is given by

$$V(x_{\rm max}) = -\frac{N(a,b)}{D(a,b)}, \quad \text{where} \quad D(a,b) = 4bx^2_{\rm max} \quad \text{and} \quad N(a,b) = a^{4/3}W(b)$$

with

$$W(a;b) = a^{2/3}\left[1 + (b^2-1)Z(b) - (b^2+1)^2Z^2(b)/4\right] - 2^{2/3}b^2Z^{4/3}(b).$$

Since $D(a,b) \geq 0$, it turns out that the condition $V(x_{\rm max}) \geq 0$ is satisfied if $W(a;b) \leq 0$, i.e. if

$$a \leq a_{\rm cr.} = 2\left[\frac{b^2Z^{4/3}(b)}{1 + (b^2-1)Z(b) + (b^2+1)^2Z^2(b)/4}\right]^{3/2}.$$

The value of M corresponding to $a_{\rm cr.}$,

$$M_{\rm cr.} = \left(\frac{3}{\Lambda}\right)^{1/2}\left[\frac{b^2Z^{4/3}(b)}{1 + (b^2-1)Z(b) + (b^2+1)^2Z^2(b)/4}\right]^{3/2}$$

(where we remember that b is an expression containing both Λ and σ_2), is the critical mass of the system. Following [19] we now observe that:

1. in the case in which Λ is very large (mathematically $\Lambda \to +\infty$) and σ_2 is kept fixed, we have $b \to 0$; correspondingly $Z(b) \to 2$ and we see that quite generally $M_{\rm cr.} \to 0$;

2. when σ_2 is very large (i.e in the limit $\sigma_2 \to +\infty$) but Λ is kept fixed, we have $b \to \infty$; nevertheless, again $Z(b)$ is bounded in the limit and, actually, $Z(b) \to 0$ as $4b^{-2}$, so that $M_{\rm cr.} \to \text{const.} \times b^{-1}$, so that, again, $M_{\rm cr.} \to 0$.

Thus we see that[5] when the child universe is characterized by a very high volume/surface energy density the critical mass above which the creation process can happen becomes very small. Even if we were interested in the more elaborated tunnelling process, it turns out that the upper bound for M, close to

[5] It is straightforward to verify that, as expected, if both σ_2 and Λ are very large, the above conclusion is not altered; indeed, when $\sigma_2 \to +\infty$ and $\Lambda \to +\infty$, if one of the two parameters scales faster than the other, we trivially recover the already discussed cases. Otherwise, i.e. when they scale in the same way $\sigma_2 \sim \Lambda$, b is a constant as $Z(b)$, so that $M_{\rm cr.} \to \text{const.} \times \Lambda^{-1/2} \to 0$.

which a limited amount of tunnelling is required, becomes smaller and smaller. This seems to indicate that the presence of a critical mass is not a necessary feature in the child universe creation process.

To support this conjecture, recently, another *minimal* realization was found [4]. This new model corresponds to a situation in which $\Lambda = 0$ and $p = 1$, so that σ_1 describes a gas of strings [11, 27, 3, 10]. In this case, if $\sigma_1 > 2/G$ (G is the gravitational constant) child universes can be created for arbitrary M; in other words, if the string content of the surface of the child universe is transplanckian, creation can again happen at an arbitrary small value of M, i.e. the critical mass threshold is completely absent. As an additional result, this model shows that creation can take place out of *almost empty space*, since the only matter-energy content of the spacetime is the string gas on the surface of the bubble which is the newly formed child universe (the exterior Schwarzschild and interior Minkowski regions are, obviously, empty). It appears that this essential model can be generalized without affecting the conclusions. In particular it is possible i) to add a non zero vacuum energy Λ in the interior of the child universe and/or ii) to also add a standard surface energy density σ_2 (as required by conventional field theoretical models of the child universe formation process) and/or iii) to consider the effect of magnetic monopoles in appropriate configurations [20, 28, 33, 9, 30]: in all these cases the possibility of creating the child universe without the existence of a critical mass threshold, or with a critical mass threshold $M_{\mathrm{cr.}}$ which can be arbitrarily small as the energy density of the child universe is increased, remains [5].

The crucial point of the above discussion is that it supports the idea that child universe creation is more likely to happen when the energy density of the child universe becomes bigger and bigger: in field theoretical realizations of child universe creation, the energy density in spacetime is related to the vacuum expectation value of a scalar field; the higher its energy density the more excited the state (false vacuum). In this sense child universes with a higher energy density are more excited than child universes with a lower energy density and following our discussion above, it seems that the creation of more and more excited child universes is more and more likely. In this sense, the above results support the idea that *transplanckian* child universe creation can be unsuppressed.

Since the classical process might be affected by the presence of singularities, it may be interesting to consider what happens if we would like to try to avoid them by using quantum tunnelling. In this case we welcome the existence of a potential barrier, through which we may be able to tunnel from a nonsingular bounded solution into an infinitely expanding bounce one, thereby allowing for a late evolution of the vacuum bubble that resembles the evolution of the present universe while starting from a less troubled initial configuration. We thus now that, in this case, a mass threshold $M_{\mathrm{cr.}}$ will be, indeed, present. We also know that to have a potential barrier, we will need to have $0 < M < M_{\mathrm{cr.}}$. On the other hand as the energy density of the newly formed child universe becomes bigger and bigger we also know that $M_{\mathrm{cr.}}$ becomes smaller and smaller. This will likely make the value of the action for the tunnelling trajectory also smaller, i.e. give a higher probability for the tunnelling process to actually take place. When the tunnelling occurs in the ambient spacetime a black hole is left, with mass M. Since this mass must be smaller than the critical mass, we see that the more the child universe is excited, the smaller the mass of the formed black hole will be. Thus, always from the point of view of the ambient spacetime, smaller mass black holes, which more rapidly evaporate, are more likely to be associated to the bay universe formation process, which seems highly consistent from the point of view of the ambient spacetime.

In the above picture, it is suggestive to consider child universes with high energy density as models for ultraviolet excitations in quantum gravity. In this sense, the higher the energy density of such an excitation, the higher the probability that it will disappear from our universe and be realized as a child universe, leaving a small mass, rapidly evaporating black hole behind. In this sense, unsuppressed child universe creation might, in fact, significantly soften ultraviolet problems in quantum gravity, since super heavy states arising in the spectrum of the theory or in the interaction picture could be removed, being realized as causally disconnected child universes. The evaporating black hole will radiate back in the ambient space a flux of *renormalized* energy, while the child universe evolves independently and causally disconnected (at least at the classical level). In this sense child universe might stabilize our spacetime against ultraviolet catastrophe. The same process will, of course, also be relevant in connection with the vacuum of the theory: in an *unsuppressed production framework* condensation processes are likely to occur and, maybe, help to address the cosmological constant problem. Another potentially relevant application is in connection with unitarity and information loss [21], since states "eaten up" in the unsuppressed creation process, would then evolve in a region of spacetime causally disconnected from the one in which they were before. Last, but not least, it could be interesting to analyze various aspects of the child universe formation process in the framework of analog models of gravity [24], where an experimental contact with the signature of unsuppressed child universe creation might be found and provide an invaluable guidance in identifying this process in (and/or at the very beginning of) our universe. Some of these ideas will be presented elsewhere [5].

Acknowledgements

EIG would like to thank the Department of Physics of Osaka City University for partial support. The work of SA is supported by a long–term invitation fellowship of the Japan Society for the Promotion of Science (JSPS). SA would like to thank the Department of Physics of the University of Kyoto for additional support.

References

[1] A. Aguirre and M. C. Johnson. *Phys. Rev. D*, 72:103525, 2005.
[2] A. Aguirre and M. C. Johnson. *Phys. Rev. D*, 73:123529, 2006.
[3] S. Alexander, R. H. Brandenberger, and D. Easson. *Phys. Rev. D*, 62:103509, 2000.
[4] S. Ansoldi and E. I. Guendelman. arXiv:0706.1233 [gr-qc], 2007.
[5] S. Ansoldi, E. I. Guendelman, and I. Shilon. In preparation, 2007.
[6] C. Barrabes and W. Israel. *Phys. Rev. D*, 43:1129, 1991.
[7] V. A. Berezin, V. A. Kuzmin, and I. I. Tkachev. *Phys. Rev. D*, 36:2919, 1987.
[8] S. K. Blau, E. I. Guendelman, and A. H. Guth. *Phys. Rev. D*, 35:1747, 1987.
[9] A. Borde, M. Trodden, and T. Vachaspati. *Phys. Rev. D*, 59:043513, 1999.
[10] R. Brandenberger, D. A. Easson, and D. Kimberly. *Nucl. Phys.*, B623:421, 2002.
[11] R. H. Brandenberger and C. Vafa. *Nucl. Phys.*, B316:391, 1989.
[12] J. C. G. Callan and S. Coleman. *Phys. Rev. D*, 16:1762, 1977.
[13] S. Coleman. *Phys. Rev. D*, 15:2929, 1977.
[14] S. Coleman. *Phys. Rev. D*, 16:1248, 1977: *errata.*
[15] S. Coleman and F. D. Luccia. *Phys. Rev. D*, 21:3305, 1980.
[16] E. Farhi, A. H. Guth, and J. Guven. *Nucl. Phys.*, B339:417, 1990.
[17] W. Fischler, D. Morgan,, and J. Polchinski. *Phys. Rev. D*, 42:4042, 1990.
[18] W. Fischler, D. Morgan, and J. Polchinski. *Phys. Rev. D*, 41:2638, 1990.
[19] E. I. Guendelman. gr-qc/0703105, 2007.
[20] E. I. Guendelman and A. Rabinowitz. *Phys. Rev. D*, 44:3152, 1991.
[21] S. W. Hawking. *Phys. Lett. B*, 195:337, 1987.
[22] W. Israel. *Nuovo Cimento*, B44:1, 1966.
[23] W. Israel. *Nuovo Cimento*, B48:463, 1967: *errata.*
[24] T. Jacobson and T. Koike. In *Workshop on Analog Models for General Relativity*, 2000.
[25] H. Kodama, M. Sasaki, and K. Sato. *Progr. Theor. Phys.*, 68:1979, 1982.
[26] H. Kodama, M. Sasaki, K. Sato, and K. I. Maeda. *Progr. Theor. Phys.*, 66:2052, 1981.
[27] E. W. Kolb. *Astroph. J.*, 344:543, 1989.
[28] A. Linde. *Phys. Lett. B*, 327:208, 1994.
[29] K. I. Maeda, K. Sato, M. Sasaki, and H. Kodama. *Phys. Lett. B*, 108:98, 1982.
[30] N. Sakai, K. I. Nakao, H. Ishihara, and M. Kobayashi. *Phys. Rev. D*, 74:024026, 2006.
[31] K. Sato. *Progr. Theor. Phys.*, 66:2287, 1981.
[32] K. Sato, M. Sasaki, H. Kodama, and K. I. Maeda. *Progr. Theor. Phys.*, 65:1443, 1981.
[33] A. Vilenkin. *Phys. Rev. Lett.*, 72:3137, 1994.

Topology change in causal quantum gravity

J. Ambjørn[1,2], R. Loll[2], W. Watabiki[3], W. Westra[4] and S. Zohren[5]

[1] *The Niels Bohr Institute, Copenhagen University, Blegdamsvej 17, DK-2100 Copenhagen Ø, Denmark*
[2] *Theoretical Physics Institute, Utrecht University, Leuvenlaan 4, NL-3584 CE Utrecht, The Netherlands*
[3] *Department of Physics, Tokyo Institute of Technology, Oh-okayama, Meguro, Tokyo 152-8551, Japan*
[4] *Department of Physics, University of Iceland, Dunhaga 3, 107 Reykjavik, Iceland*
[5] *Blackett Laboratory, Imperial College, London SW7 2AZ, U.K. and*
Department of Physics, Ochanomizu University, Otsuka, Bunkyo-ku, Tokyo 112-8610, Japan

Abstract

The role of topology change in a fundamental theory of quantum gravity is still a matter of debate. However, when regarding string theory as two-dimensional quantum gravity, topological fluctuations are essential. Here we present a third quantization of two-dimensional surfaces based on the method of causal dynamical triangulation (CDT). Formally, our construction is similar to the $c = 0$ non-critical string field theory developed by Ishibashi, Kawai and others, but physically it is quite distinct. Unlike in non-critical string theory the topology change of spatial slices is well controlled and regulated by Newton's constant.

1 Causal quantum gravity, topology change and Euclidean quantum gravity

Why do we study two-dimensional quantum gravity? Firstly, one can test quantisation procedures for gravity in a simple setting. Secondly, it has long been known that string theory can be viewed as two-dimensional quantum gravity coupled to matter fields. This particular view of string theory spawned the development of the dynamical triangulation (DT) approach to quantum gravity. This method is particularly powerful in two dimensions, since exact nonperturbative solutions can be obtained by loop equations or matrix models.

In the nineties the DT approach was invoked in an attempt to nonperturbatively define four-dimensional quantum gravity through computer simulations [1]. The results were not satisfactory however since no suitable semiclassical limit was found.

To improve this state of affairs the method of *causal* dynamical triangulation (CDT) was developed [2]. Contrary to the aforementioned applications of DT, CDT incorporates some essential Lorentzian features. Recent computer simulations indicate that in four dimensions CDT does lead to a sensible classical limit [3], unlike in earlier attempts employing DT.

To better understand the relation between the Euclidean (DT) and the causal (CDT) approach we study a generalisation of the 2d CDT model [4, 5]. Let us start with a discussion of the original 2d CDT model as introduced in [2].

A natural amplitude in CDT is the so-called proper-time propagator. This amplitude is computed by a functional integral over all "causal" geometries with topology $S^1 \times [0, 1]$. It computes the transition amplitude between an initial and a final boundary, where all points on the initial boundary are separated a geodesic distance t from the final boundary. Here the term causal geometry refers to Euclidean geometries that can be obtained from Lorentzian geometries through a Wick rotation defined in the discrete formalism of CDT. This restriction requires spatial sections of the geometries to be a single S^1 and not change as a function of time. Formally, the proper-time propagator is given by the following equation

$$G_\lambda(x, y; t) = \int \mathcal{D}[g_{\mu\nu}]\, e^{-S[g_{\mu\nu}]}, \quad S[g_{\mu\nu}] = \lambda \int \mathrm{d}^2\xi \sqrt{\det g_{\mu\nu}(\xi)} + x \oint \mathrm{d}l_1 + y \oint \mathrm{d}l_2, \tag{1}$$

where λ is the cosmological constant, x and y are the boundary cosmological constants and $g_{\mu\nu}$ is the causal world sheet metric. By taking the continuum limit of a discrete iteration equation it can be shown that the proper-time propagator satisfies the equation

$$\frac{\partial}{\partial t} G_\lambda(x,y;t) = -\frac{\partial}{\partial x}\Big[(x^2-\lambda)G_\lambda(x,y;t)\Big], \tag{2}$$

which can be solved in a straightforward manner to obtain $G_\lambda(x,y;t)$. For some purposes it can be more convenient to study correlators $G_\lambda(l_1,l_2;t)$ where the lengths of the boundaries are fixed rather than the boundary cosmological constants. Since the lengths of the boundaries are conjugate to the corresponding boundary cosmological constants, the different propagators are related by Laplace transformations,

$$G_\lambda(x,y;t) = \int_0^\infty \mathrm{d}l_2 \int_0^\infty \mathrm{d}l_1\; G_\lambda(l_1,l_2;t)\; \mathrm{e}^{-xl_1-yl_2}. \tag{3}$$

Strictly speaking it is not possible to define a disc function for a Lorentzian theory of two-dimensional quantum gravity, assuming that the disc boundary represents an instance of constant time. The reason is that it is impossible to cover the disc with an everywhere nondegenerate Lorentzian metric. This is however possible if one excises one point. Consequently one can define the CDT disc function by the ensemble of punctured discs which is given by

$$W_\lambda(x) = \int_0^\infty \mathrm{d}t\; G_\lambda(x,l_2=0;t) = \frac{1}{x+\sqrt{\lambda}}. \tag{4}$$

Starting from the discrete setup one can now also include the possibility of the *spatial* topology to change as a function of proper time t keeping the *space-time* topology fixed to be $S_1\times[0,1]$. In [2] it was shown that the corresponding propagator is given by the partial differential equation

$$a^\varepsilon \frac{\partial}{\partial t} G_{\lambda,g}(x,y;t) = -\frac{\partial}{\partial x}\Big[\Big(a(x^2-\lambda)+2g\,a^{\eta-1}W_{\lambda,g}(x)\Big)G_{\lambda,g}(x,y;t)\Big]. \tag{5}$$

Here a is a ultraviolet cutoff, η and ε are the scaling exponents of the regularized disc function and time respectively, and g is a coupling constant assigned to each splitting of the spatial universe. In [2] it was shown that if the coupling constant does not scale, there are only two possible scaling relations:

$$\begin{array}{lllll}
(i) & W_{reg} & \underset{a\to 0}{\longrightarrow} & a^\eta\, W_\lambda(x), & \eta<0, \\
 & t_{reg} & \underset{a\to 0}{\longrightarrow} & t/a^\varepsilon, & \varepsilon=1, \\
(ii) & W_{reg} & \underset{a\to 0}{\longrightarrow} & \text{const.} + a^\eta\, W_\lambda(x), & \eta=3/2 \\
 & t_{reg} & \underset{a\to 0}{\longrightarrow} & t/a^\varepsilon, & \varepsilon=1/2.
\end{array}$$

The first possibility (i) corresponds to the scaling of causal quantum gravity for $\eta=-1$. Inserting this scaling relation into (5) implies that g must be set to zero and one recovers (2) in which no spatial topology changes are allowed.

For the scaling (ii) one recovers 2d Euclidean quantum gravity as defined through Liouville theory or matrix models. In this case the kinetic term is subdominant and the dynamics is purely governed by the splitting of spatial universes, i.e.

$$\frac{\partial}{\partial t} G^e_\lambda(x,y;t) = -\frac{\partial}{\partial x}\Big[2g\,W^e_{\lambda,g}(x)G^e_\lambda(x,y;t)\Big]. \tag{6}$$

It is possible to show that in this continuum limit there is a baby universe at every point in the quantum geometry. One can see this by contracting the final boundary of the propagator. After contraction the propagator reduces to the disc function with a marked point that can be located anywhere in the bulk, i.e.

$$\frac{\partial W^e_{\lambda,g}(x)}{\partial\lambda} = \int_0^\infty \mathrm{d}t\; G^e_{\lambda,g}(x,l_2=0;t). \tag{7}$$

Inserting this into (6) and absorbing the dimensionless factor $2g$ in the cosmological constant, one obtains the disc function of 2d Euclidean quantum gravity

$$W^e_\lambda(x) = \left(x-\frac{1}{2}\sqrt{\lambda}\right)\sqrt{x+\sqrt{\lambda}}. \tag{8}$$

2 Taming the topology changes

In the previous section we showed how starting from 2d CDT one can obtain 2d Euclidean quantum gravity when allowing for spatial topology changes. Under the scaling relations (*i*) and (*ii*) discussed above, there was only the possibility of either zero or infinite numbers of spatial topology changes. However, in [4] it was shown that there exists a unique renormalization of the coupling constant that leads to a well defined double scaling limit

$$g = g_s a^3. \tag{9}$$

In this scaling limit spatial topology changes are included in a controlled manner. The partial differential equation for the propagator then reads

$$\frac{\partial}{\partial t} G_{\lambda,g_s}(x,y;t) = -\frac{\partial}{\partial x}\Big[\Big((x^2-\lambda)+2g_s\, W_{\lambda,g_s}(x)\Big)G_{\lambda,g_s}(x,y;t)\Big]. \tag{10}$$

Interestingly, the model described by (10) can be solved to all orders in the coupling constant [4]. In particular, one obtains for the disc function [4] that

$$W_{\lambda,g_s}(x) = \frac{-(x^2-\lambda)+(x-\alpha)\sqrt{(x+\alpha)^2-2g_s/\alpha}}{2\,g_s}, \quad \alpha = u\sqrt{\lambda}, \quad u^3 - u + \frac{g_s}{\lambda^{3/2}} = 0. \tag{11}$$

For $g_s = 0$ one recovers the disc function of the pure CDT model without any spatial topology changes, however, as shown in [4], it is not possible to obtain the disc function of Euclidean quantum gravity as an analytic continuation in g_s.

It is interesting to give a gravitational interpretation to the coupling constant g_s. As was mentioned above, the disc function of a Lorentzian theory of 2d quantum gravity needs one point of the manifold to be excised. Since each baby universe that splits off is essentially a disc function, a surface with N baby universes contains N punctures. Because of the Gauss-Bonnet theorem each puncture is associated with a factor of one inverse Newton constant $1/G_N$. Hence, we can make the identification $g_0(a)=e^{-1/G_N(a)}$, where $G_N(a)$ denotes the "bare" gravitational coupling constant. One can introduce a *renormalized* gravitational coupling constant by

$$\frac{1}{G_N^{ren}} = \frac{1}{G_N(a)} + \frac{3}{2}\ln \lambda a^2, \tag{12}$$

which leads to the identification $e^{1/G_N^{ren}} = g_s/\lambda^{3/2}$. The corresponding scaling limit of 2d Euclidean quantum gravity reads

$$\frac{1}{G_N^{ren}} = \frac{1}{G_N(a)} + \frac{5}{4}\ln \lambda a^2. \tag{13}$$

3 A string field theory for causal and Euclidean quantum gravity

In string field theories (SFT) one defines operators that can create and annihilate strings. From the $2d$ quantum gravity point of view we thus have a third quantization of gravity, where one-dimensional universes can be created and annihilated. Such a formalism was developed in [6] for non-critical strings, i.e. 2d Euclidean quantum gravity and recently in [5] as a third quantization for CDT reproducing the results of the previous section.

The starting point is the assumption of a vacuum from which universes can be created. We denote this state by $|0\rangle$ and define creation and annihilation operators:

$$[\Psi(l),\Psi^\dagger(l')] = l\delta(l-l'), \quad \Psi(l)|0\rangle = \langle 0|\Psi^\dagger(l) = 0. \tag{14}$$

The Hamiltonian for the CDT SFT is given by [5]

$$\begin{aligned}\hat{H} = \hat{H}_0 - g_s \int \mathrm{d}l_1 \int \mathrm{d}l_2 \Psi^\dagger(l_1)\Psi^\dagger(l_2)\Psi(l_1+l_2)\\ - \alpha g_s \int \mathrm{d}l_1 \int \mathrm{d}l_2 \Psi^\dagger(l_1+l_2)\Psi(l_2)\Psi(l_1) - \int \frac{dl}{l}\,\rho(l)\Psi(l),\end{aligned} \tag{15}$$

The first term is the "second-quantized" Hamiltonian of the pure CDT model,

$$\hat{H}_0 = \int \frac{dl}{l}\ \Psi^\dagger(l) H_0(l) \Psi(l), \quad H_0(l) = -l\frac{\partial^2}{\partial l^2} + \lambda l. \tag{16}$$

The third term corresponds to the splitting of strings with the assigned coupling g_s and the fourth term to the joining of strings. The last term, the tadpole, is responsible for the termination of a string into the vacuum and is simply given by $\rho(l) = \delta(l)$, meaning that only strings of length zero can be terminated.

The disc function of the model can be written in the string field theory language as follows,

$$W_{\lambda,g_s}(l) = \lim_{t\to\infty} W_{\lambda,g_s}(l,t) = \lim_{t\to\infty} \langle 0|\, \mathrm{e}^{-t\hat{H}} \Psi^\dagger(l)|0\rangle. \tag{17}$$

In SFT one derives the amplitudes by solving the so-called Dyson-Schwinger (DS) equations,

$$0 = \lim_{t\to\infty} \frac{\partial}{\partial t} W_{\lambda,g_s}(l,t) = \lim_{t\to\infty} \langle 0| e^{-t\hat{H}} [\hat{H}, \Psi^\dagger(l)]|0\rangle. \tag{18}$$

These equations express the fact that the solution should be slowly varying in time for $t \to \infty$. In the limit where the joining of strings is forbidden ($\alpha \to 0$), the DS equation (18) leads to a closed equation for the disc function,

$$\frac{\partial}{\partial x}\big((x^2 - \lambda)W_{\lambda,g_s}(x) + g_s W^2_{\lambda,g_s}(x)\big) = 1. \tag{19}$$

The solution of equation (19) is again given by (11). This shows that the diagrammatic techniques of [4] are equivalent to the string field theory techniques of [5]. For finite α the DS equations become considerably more complicated as they cannot be written in closed form. To evaluate the higher-genus disc functions, say, one also requires knowledge of the higher-loop correlators.

4 Discussion

In this contribution we recalled that the loop-loop correlator used in $c = 0$ non-critical string theory can be obtained by extending the formalism of CDT by allowing the topology of spatial slices to fluctuate. In the non-critical string theory these spatial topology fluctuations dominate the dynamics completely. It was seen that by introducing a coupling constant and a suitable double-scaling limit one can obtain a $2d$ quantum gravity theory where the changes of spatial topology are well controlled [4]. The amplitudes of this theory have been computed to all orders in the coupling constant. Evaluation can be done both by diagrammatic techniques [4] or by a string field theory [5]. Within the string field theory it is in principle possible to compute diagrams of arbitrary space-time topology. When introducing the merging process of strings in the Hamiltonian, one can iteratively solve the corresponding Dyson-Schwinger equations.

Acknowledgments: J.A., R.L. W.W. and S.Z. acknowledge support by ENRAGE (European Network on Random Geometry), a Marie Curie Research Training Network in the European Community's Sixth Framework Programme, network contract MRTN-CT-2004-005616. R.L. acknowledges support by the Netherlands Organisation for Scientific Research (NWO) under their VICI program. S.Z. thanks Professor A. Sugamoto for discussion and the JSPS Short Term Award Program for financial support.

References

[1] S. Catterall, R. Renken and J. B. Kogut, Phys. Lett. B **416** (1998) 274 [arXiv:hep-lat/9709007].

[2] J. Ambjørn and R. Loll, Nucl. Phys. B **536** (1998) 407 [arXiv:hep-th/9805108].

[3] J. Ambjørn, J. Jurkiewicz and R. Loll, Phys. Rev. D **72** (2005) 064014 [arXiv:hep-th/0505154], Phys. Rev. Lett. **95** (2005) 171301 [arXiv:hep-th/0505113], Phys. Lett. B **607** (2005) 205-213 [arXiv:hep-th/0411152], Phys. Rev. Lett. **93** (2004) 131301 [arXiv:hep-th/0404156].

[4] J. Ambjørn, R. Loll, W. Westra and S. Zohren, JHEP **0712** (2007) 017 [arXiv:0709.2784 [gr-qc]].

[5] J. Ambjørn, R. Loll, Y. Watabiki, W. Westra, and S. Zohren, *preprint* Jan 2008.

[6] N. Ishibashi and H. Kawai, Phys. Lett. B **314** (1993) 190 [arXiv:hep-th/9307045].

Black hole entropy from spin-network

Tomo Tanaka[1], Takashi Tamaki[2]

[1,2] *Department of Physics, Waseda University, Tokyo 169–8555, Japan*

Abstract

We calculate the black hole entropy in loop quantum gravity considering the general area spectrum. Although its spectrum has a complex expression, we obtained that black hole entropy is proportional to its area as in previous works which used the simplified area formula. This confirms the idea that black hole entropy is obtained by counting the degrees of freedom of the spin-network.

1 Introduction

Black hole thermodynamics is one of the most exciting arenas for those investigating quantum gravity. Recently, the origin of black hole entropy is interpreted by Loop Quantum Gravity(LQG), which has background independent formulation. The spin-network has played a key role in the development of this theory [1]. Basic ingredients of the spin-network are edges. Edges are expressed by lines lebeled by $j = 0$, $1/2$, 1, $3/2$, ... reflecting the SU(2) nature of the gauge group. A vertex is an intersection between edges. For three edges having spin j_1, j_2, and j_3 that merges at an arbitrary vertex, we have

$$j_1 + j_2 + j_3 \in N \ , \tag{1}$$

$$j_i \leq j_j + j_k, \quad (i, j, k \ \text{ different from each other.}) \tag{2}$$

to garantee the gauge invariance of the spin-network.

Using this formalism, general expressions for the spectrum of the area and the volume operators can be derived [2, 3]. For example, the area spectrum A is

$$A = 4\pi\gamma \sum \sqrt{2j_i^u(j_i^u + 1) + 2j_i^d(j_i^d + 1) - j_i^t(j_i^t + 1)} \ , \tag{3}$$

where γ is the Immirzi parameter related to an ambiguity in the choice of canonically conjugate variables [4]. The sum is added up all intersections between a surface and edges. Here, the indices u, d, and t means edges above, below, and tangential to the surface, respectively (We can determine which side is above or below arbitrarily).

In [5], it was proposed that black hole entropy is obtained by counting the number of freedom in j when we fix the horizon area where simplified area formula

$$A = 8\pi\gamma \sum \sqrt{j_i(j_i + 1)} \ , \tag{4}$$

is used. This is obtained using the assumption that there is no edges tangential to the horizon, i.e., $j_i^t = 0$. Then, by using (2), we obtain $j_i^u = j_i^d := j_i$. This idea has been elaborated in [6] (ABCK framework) which is explained in Sec.2. This takes into account the quantum geometrical states based on the isolated horizon proposal. In concrete, [6] divides the Hilbert space H into the isolated horizon Hilbert space H_{IH} and the Hilbert space outside the horizon H_Σ and write H as the direct product as $H = H_{IH} \otimes H_\Sigma$. They count the freedom related to H_{IH} where (4) is also used. The standard procedure is to impose the Bekenstein-Hawking entropy-area law for large black holes in order to fix the value of γ.

The value of γ obtained in [6] has been corrected in [7, 8] which gives $\gamma = 0.237\cdots$. It is also discused that j should also be an independent freedom since it makes the area eigenvalue [9–12]. It is also important that whether or not using (4) is verified in the ABCK framework. Thiemann in [13] used

[1] E-mail:tomo@gravity.phys.waseda.ac.jp

[2] E-mail:tamaki@gravity.phys.waseda.ac.jp

the boundary condition that there is no other side of the horizon, i.e., $j_i^d = 0$. Then, by using (2), we obtain $j_i^u = j_i^t := j_i$ which gives

$$A = 4\pi\gamma \sum \sqrt{j_i(j_i+1)} \ . \tag{5}$$

Based on this proposal, the number counting has been performed in [14] which gives $\gamma = 0.323\cdots$.

However, the fundamental problem is that we should not but use classical conditions to divide H into H_{IH} and H_Σ. It is natural that we describe all the space-time by only using the spin-network. In this case, we should consider (3) which is also pointed out in [15]. Then, it is quite difficult to take into account the condition as a black hole. Is there anything we can do ?

Fortunately, the value of γ in [6] is qualitatively same as that infered in [5] which count the j freedom without taking into acconut the black hole condition. For this reason, counting the j freedom using (3) would be meaningful. In particular, it is important to clarify whether or not black hole entropy is proportional to its area. Otherwise, we might doubt the idea that black hole entropy is obtained by counting the degrees of freedom of the spin-network.

This paper is organized as follows. In section 2, we summarize and reconsider the framework [6] that is necessary in counting the number of states of black holes. In section 3, we determine the number of states. In section 4, we summarize our results.

2 ABCK framework

We briefly introduce and consider the ABCK framework in [6]. One usually considers the event horizon, which is determined after the complete evolution of spacetime, when one describes black hole thermodynamics. Thus, it would be too restrictive to establish a thermodynamical situation in which the system is isolated. To explore this idea appropriately, the isolated horizon(IH) is defined in the ABCK framework. The main difficulty in defining IH is to establish the surface gravity or black hole thermodynamics when, in general, there is no global Killing field. For details, see [16]. Because of the requirement at IH, we can reduce the $SU(2)$ connection to the $U(1)$ connection. Using the curvature F_{ab} of the $U(1)$ connection, we can express the boundary condition between IH and the bulk as

$$F_{ab} = -\frac{2\pi\gamma}{A}\underline{\Sigma}^i_{ab} r_i, \tag{6}$$

where A is the area of IH. Σ^i_{ab} is related to a triad density E^a_i as

$$E^a_i = \gamma\eta^{abc}\Sigma_{bci}, \tag{7}$$

where η^{abc} is the Levi-Civita 3-form density. $\underline{\sum}^i_{ab} r_i$ is its pull back to IH and r_i is unit normal. (6) plays an important role in determining the condition (iv) below.

Usually, we consider the Hilbert space using the spin-network in LQG. When there is IH, we decompose the Hilbert space as the tensor product of that in IH H_{IH} and that in the bulk H_Σ, i.e., $H = H_{IH} \otimes H_\Sigma$.

First, we consider H_Σ. Using edges having spin $(j_1, j_2, \cdots, j_n)$ which pierce IH, we can write H_Σ as the orthogonal sum

$$H_\Sigma = \bigotimes_{j_i, m_i} H_\Sigma^{j_i, m_i}, \tag{8}$$

where m_i takes the value $-j_i, -j_i+1, \cdots, j_i-1, j_i$. This is related to the flux operator eigenvalue $e_{s'}^{m_i}$ that is normal to IH (s' is the part of IH that has only one intersection between the edge with spin j_i.)

$$e_{s'}^{m_i} = 8\pi\gamma m_i. \tag{9}$$

The area operator eigenvalue A_j is obtained by operating the area operator $\hat{A}$ to the IH wave function Ψ_{IH} and that of the bulk Ψ_Σ as $\hat{A}\Psi_{IH}\Psi_\Sigma = A_j\Psi_{IH}\Psi_\Sigma$. Then, it is natural to adopt (5). In this case, A_j should satisfy

$$\text{(i)} \qquad A_j = 4\pi\gamma\Sigma_i\sqrt{j_i(j_j+1)} \le A. \tag{10}$$

Here, though we consider A not an interval $[A-\delta A, A+\delta A]$, this does not affect the final results. Because of the expression (19), $S := \ln W := \ln(\frac{dN}{dA}\delta A)$ is equal to $\ln N$ for $A \to \infty$.

Next, we consider H_{IH}. We have, in general, difficulty in constructing H_{IH}. However, if we fix the horizon area A as

$$A = 4\pi\gamma k, \tag{11}$$

where k is a natural number, which is called the level of the Chern-Simons theory, we can construct H_{IH} using a function which is invariant under the diffeomorphism and the Z_k gauge transformation, i.e., a 'quantized' U(1) gauge transformation. In addition to this condition, it is required that

$$\text{(ii)} \qquad \text{we should fix an ordering}(j_1, j_2, \cdots, j_n). \tag{12}$$

At IH, we do not consider the scalar constraint, since the lapse function disappears. As a result, H_{IH} is written as an orthogonal sum similar to (8) by eigenstates Ψ_b of the holonomy operator $\hat{h}_i$, i.e.,

$$\widehat{h_i}\Psi_b = e^{\frac{2\pi i b_i}{k}}\Psi_b. \tag{13}$$

From the quantum Gauss-Bonnet theorem that guarantees that IH is S^2, we require

$$\text{(iii)} \qquad \sum_{i=1}^{n} b_i = 0 \quad mod\ k. \tag{14}$$

Finally, we should consider the quantization of the boundary condition between IH and the bulk (6). Since only the exponential version $exp(i\hat{F})$ is welldefined on H_{IH}, we consider

$$\left(exp(i\hat{F}) \otimes 1\right)\Psi = \left(1 \otimes exp(-i\frac{2\pi\gamma}{A}\underline{\Sigma}\cdot r)\right)\Psi, \tag{15}$$

where Ψ expresses the state in $H_{IH} \otimes H_\Sigma$. From this, we have

$$\text{(iv)} \qquad b_i = -2m_i \quad mod\ k. \tag{16}$$

All we need to consider in number counting is (i)–(iv).

3 Consideration of the general area spectrum

For the case we use (4) or (5), it is known that the only condition which affects the number of freedom is (i) if we take the large area limit $A \to \infty$. Here, we assume that this holds even if we use (3). Then conditon (i) is replaced by (i)'.

$$\text{(i)}' \qquad A_j = 4\pi\gamma\sum\sqrt{2j_i^u(j_i^u+1) + 2j_i^d(j_i^d+1) - j_i^t(j_i^t+1)} \le A. \tag{17}$$

We denote the number of states about j as $N(A)$. Then, we obtain the recursion relation

$$N(A) = \sum_{n=1}^{\infty}\left[\sum_{s=1}^{n}\sum_{t=s}^{n} 2(n+1)N(A-x) + \sum_{s=0}^{0}\sum_{t=0}^{n}(n+1)N(A-x)\right], \tag{18}$$

where x in this formula is $\frac{1}{2}\sqrt{2n+n^2+s^2-t(t+1)}$. If we assume the relation

$$N(A) = Ce^{\frac{A\gamma_M}{4\gamma}}, \tag{19}$$

where C is a constant, we obtain

$$1 = \sum_{n=1}^{\infty}\left[\sum_{s=1}^{n}\sum_{t=s}^{n} 2(n+1)\exp(-2\pi\gamma_M x) + \sum_{s=0}^{0}\sum_{t=0}^{n}(n+1)\exp(-2\pi\gamma_M x)\right] \tag{20}$$

by plugging (19) into (18) and taking the limit $A \to \infty$. Then we require $S = A/4$, we have $\gamma = \gamma_M = 0.7847\cdots$ which is larger compared with that of previous work [7–14].

4 Conclusion

In this paper, we considered the general area formula to derive the number of states of black holes. It is surprising that we obtained the black hole entropy proportional to the horizon area even in this case. This suggests the validity that black hole entropy is obtained by counting the degrees of freedom of the spin-network. By taking into account the horizon condition should be elaborated in future.

References

[1] C. Rovelli and L. Smolin, Phys. Rev. D **52**, 5743 (1995).

[2] C. Rovelli and L. Smolin, Nucl. Phys. B **442**, 593 (1995); Erratum, *ibid.*, **456**, 753 (1995).

[3] A. Ashtekar and J. Lewandowski, Class. Quantum Grav. **14**, A55 (1997).

[4] G. Immirzi, Nucl. Phys. Proc. Suppl. B **57**, 65 (1997).

[5] C. Rovelli, Phys. Rev. Lett. **77**, 3288 (1996).

[6] Ashtekar A, Baez J, Corichi A and Krasnov K, Phys. Rev. Lett. **80**, 904 (1998); Ashtekar A, Baez J and Krasnov K 2000 Adv. Theor. Math. Phys. **4**, 1 (2000).

[7] M. Domagala and J. Lewandowski, Class. Quant. Grav. **21**, 5233 (2004).

[8] K. A. Meissner, Class. Quant. Grav. **21**, 5245 (2004).

[9] A. Alekseev, A. P. Polychronakos, and M. Smedback, Phys. Lett. B **574**, 296 (2003); A. P. Polychronakos, Phys. Rev. D **69**, 044010 (2004).

[10] I.B. Khriplovich, gr-qc/0409031; gr-qc/0411109.

[11] A. Ghosh and P. Mitra, Phys. Lett. B **616**, 114 (2005); Ind. J. Mod. Phys. **80**, 867 (2006); Phys. Rev. D **74**, 064026 (2006).

[12] T. Tamaki and H. Nomura, Phys. Rev. D **72**, 107501 (2005).

[13] T.Thiemann, gr-qc/0110034.

[14] T. Tamaki, Class. Quant. Grav. **24**, 3837 (2007).

[15] M. H. Ansari, gr-qc/0603121; Nucl. Phys. B **783**, 179 (2007).

[16] A. Ashtekar, A. Corichi, and K. Krasnov, Adv. Theor. Math. Phys. **3**, 419 (1999).

Evidence for the Stability of 5-dimensional Myers-Perry Black Holes with Equal Angular Momenta

Keiju Murata[1] and Jiro Soda[2]

[1,2]*Department of Physics, Kyoto University, Kyoto 606-8501, Japan*
[2]*Kavli Institute for Theoretical Physics, Zhong Guan Cun East Street 55, Beijing 100080, P.R. China*

Abstract

We study the stability of 5-dimensional Myers-Perry black holes with equal angular momenta. Using the symmetry of these black hole spacetimes, $U(2)$, we derive master equations for a part of the metric perturbations relevant to the stability. The stability is shown for these modes. Our result gives a strong evidence for the stability of Myers-Perry black holes.

1 Introduction

It is important to study the stability of Myers-Perry black holes [1], which are the higher dimensional generalization of Kerr black holes. The stability of higher dimensional Schwarzschild black holes has been proved in [2, 3]. In the case of rotating black holes, the stability analysis becomes difficult because of the difficulty of separation of variables in perturbation equations. However, it is possible to analyze the stability of Myers-Perry black holes with equal angular momenta. In the case of odd dimensions higher than five, equations for the special modes can be reduced to single ordinary differential equations [4]. There, the stability of Myers-Perry black holes for these modes is shown. In five dimensions, the stability of Myers-Perry black holes for the most symmetric mode has been shown [5]. In our previous work, we have developed a method to analyze the stability of five dimensional Myers-Perry black holes with equal angular momenta by focusing on the spacetime symmetry $U(2)$ [6]. The same method has been proved to be useful for the stability analysis of other $U(2)$ symmetric black holes [7]. In this paper, making use of this formalism, we will study the stability of 5-dimensional Myers-Perry black holes with equal angular momenta.

2 Background spacetime and its perturbations

The metric of 5-dimensional Myers-Perry black hole with equal angular momenta is given by

$$ds^2 = -dt^2 + \frac{dr^2}{G(r)} + \frac{r^2}{4}\{(\sigma^1)^2 + (\sigma^2)^2 + (\sigma^3)^2\} + \frac{2\mu}{r^2}\left(dt + \frac{a}{2}\sigma^3\right)^2 , \tag{1}$$

$$G(r) = 1 - \frac{2\mu}{r^2} + \frac{2\mu a^2}{r^4} . \tag{2}$$

Here, we have defined the invariant forms σ^a $(a = 1, 2, 3)$ of $SU(2)$ as

$$\sigma^1 = -\sin\psi d\theta + \cos\psi \sin\theta d\phi , \quad \sigma^2 = \cos\psi d\theta + \sin\psi \sin\theta d\phi , \quad \sigma^3 = d\psi + \cos\theta d\phi , \tag{3}$$

where $0 \le \theta < \pi$, $0 \le \phi < 2\pi$, $0 \le \psi < 4\pi$. It is easy to check the relation $d\sigma^a = 1/2\epsilon^{abc}\sigma^b \wedge \sigma^c$. Because σ^a are invariant under $SU(2)$ group, the spacetime (1) has $SU(2)$ symmetry. From the metric (1), we can also read off the additional $U(1)$ symmetry, which keeps the part of the metric, $\sigma_1^2 + \sigma_2^2$ invariant. Thus, the symmetry of 5-dimensional degenerate Myers-Perry black hole becomes $SU(2) \times U(1) \simeq U(2)$.

The horizon $r = r_+$ is located at $G(r_+) = 0$ and it is given by $r_+^2 = \mu + \sqrt{\mu(\mu - 2a^2)}$. There exists the horizon for the parameter range

$$a^2 \le \mu/2 \equiv a_{\max}^2 . \tag{4}$$

[1]E-mail:murata@tap.scphys.kyoto-u.ac.jp
[2]E-mail:jiro@tap.scphys.kyoto-u.ac.jp

The angular velocity of horizon is given by $\Omega_H = a/r_+^2$.

To study the stability of this spacetime, we perturb the metric as $g_{\mu\nu} \to g_{\mu\nu} + h_{\mu\nu}$. From Einstein equation, we get the partial differential equations for metric perturbation $h_{\mu\nu}(t, r, \theta, \phi, \psi)$. This partial differential equation can be reduced to ordinary differential equations by mode decomposition. Because the Myers-Perry spacetime (1) has the $U(2)$ symmetry, the perturbation equation can be separated by irreducible representations of $U(2)$. The irreducible representations are called Wigner functions denoted by $D^J_{KM}(\theta, \phi, \psi)$, where J, K, M are integers satisfying $|K|, |M| \le J$. They are defined by

$$L^2 D^J_{KM} = J(J+1) D^J_{KM} \ , \quad L_z D^J_{KM} = M D^J_{KM} \ , \quad W D^J_{KM} = K D^J_{KM} \ , \tag{5}$$

where L_α ($\alpha = x, y, z$) and W are generators of $SU(2)$ and $U(1)$ respectively. We can also construct vector and tensor types of irreducible representations of $U(2)$. Those are denoted as D^{JKM}_i and D^{JKM}_{ij}, where $i = \theta, \phi, \psi$. D^{JKM}_i is defined for $|K| \le J+1, |M| \le J$ and D^{JKM}_{ij} is defined for $|K| \le J+2, |M| \le J$. Making use of these mode functions, we can separate the perturbation equations and get ordinary differential equations labelled by J, K, M. Because of $SU(2) \times U(1)$ symmetry, each eigen mode is decoupled from others. In general, there are many physical degrees of freedom for each (J, K, M). However, we see that only one physical degree of freedom is contained in $(J = 0, M = 0, K = 0, 1)$ and $(J, M, K = J + 2)$ modes, respectively. We will study the stability of the Myers-Perry black holes for these modes.

3 Stability Analysis

3.1 $(J = 0, M = 0, K = 0)$ mode

First, we consider the $(J = 0, M = 0, K = 0)$ mode. The stability for this mode has been already shown in [5]. However, we will show the stability again using our formalism. For this mode, we get the Schrödinger type master equation,

$$-\frac{d^2\Phi_0}{dr_*^2} + V_0(r)\Phi_0 = \omega^2\Phi_0 \ , \quad dr_* = \frac{(r^4 + 2\mu a^2)^{1/4}}{r^2 G(r)} dr \ , \tag{6}$$

where

$$\begin{aligned} V_0(r) = \frac{G(r)}{4(3r^4 + 2\mu a^2)^2 (r^4 + 2\mu a^2)^3 r^2} \big[& 315 r^{20} + 162\mu r^{18} + 2430\mu a^2 r^{16} + 1392\mu^2 a^2 r^{14} + 5400\mu^2 a^4 r^{12} \\ & + 5808\mu^3 a^4 r^{10} + 2608\mu^3 a^6 r^8 + 6080\mu^4 a^6 r^6 - 2064\mu^4 a^8 r^4 + 32\mu^5 a^8 r^2 - 160\mu^5 a^{10} \big] \ , \end{aligned} \tag{7}$$

The typical form of potential is shown in Figure.1. We have verified the positivity of the potential. This proves the stability of Myers-Perry black hole for this mode.

3.2 $(J = 0, M = 0, K = 1)$ and $(J, M, K = J + 2)$ modes

In this subsection, we consider $(J = 0, M = 0, K = 1)$ and $(J, M, K = J + 2)$ modes. The master equations for these modes can be written as

$$-\frac{d^2\Phi_K}{dr_*^2} + V_K(r)\Phi_K = [\omega - 2K\Omega_K(r)]^2 \Phi_K \ , \tag{8}$$

where $K = 1, J + 2$. Here, $\Omega_K(r)$ and $V_K(r)$ are defined by

$$\begin{aligned} \Omega_1(r) &= \frac{2\mu a}{r^4 + 2\mu a^2} \left(1 - \frac{a^2 r^4 (5r^4 + 6\mu a^2) G(r)}{4(r^{10} + 2\mu a^2 r^6 + \mu^2 a^6)} \right) \ , \\ \Omega_{J+2}(r) &= \frac{2\mu a}{r^4 + 2\mu a^2} \ . \end{aligned} \tag{9}$$

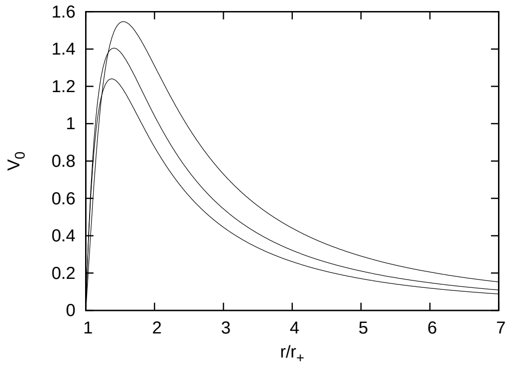

Figure 1: Typical profiles for the potential $V_0(r)$ are depicted. We used the normalization $\mu = 1$. From the bottom to the top, each curve represents the potential for $a/a_{\max} = 0.1, 0.8, 0.99$. We see the positivity of these potentials.

The potential functions are given by

$$
\begin{aligned}
V_1(r) &= \frac{G(r)}{4r^2(r^4+2\mu a^2)^3(r^{10}+2\mu a^2 r^6+\mu^2 a^6)^2}[35r^{32}+18\mu r^{30}+310\mu a^2 r^{28}+160\mu^2 a^2 r^{26} \\
&\quad +1192\mu^2 a^4 r^{24}+2\mu^2 a^4(152\mu-75a^2)r^{22}+3068\mu^3 a^6 r^{20}-64\mu^3 a^6(2\mu+15a^2)r^{18} \\
&\quad +5208\mu^4 a^8 r^{16}-16\mu^4 a^8(30\mu+133a^2)r^{14}+3\mu^4 a^{10}(1424\mu+5a^2)r^{12}-1654\mu^5 a^{12} r^{10} \\
&\quad +2\mu^5 a^{12}(432\mu+25a^2)r^8-168\mu^6 a^{14} r^6+68\mu^6 a^{16} r^4-24\mu^7 a^{16} r^2+56\mu^7 a^{18}] \ , \\
V_{J+2}(r) &= \frac{G(r)}{4r^2(r^4+2\mu a^2)^3}[(4J+7)(4J+5)r^{12}+18\mu r^{10}+2\mu a^2(16J^2+32J+5)r^8 \\
&\quad -40\mu^2 a^2 r^6-4\mu^2 a^4(16J+35)r^4+8\mu^3 a^4 r^2-40\mu^3 a^6] \ .
\end{aligned}
\tag{10}
$$

For $K = 1$ and $K = J + 2$, Eq. (8) gives a master equation for $(J = 0, M = 0, K = 1)$ mode and $(J, M, K = J + 2)$ modes, respectively.

Because the master equation (8) is not a Schrödinger form, we cannot show the stability of black holes for these modes from the potential form of V_K. Therefore, we have to resort to the numerical analysis. We use the strategy adopted to show the stability of Kerr black holes [4, 8]. We start from the assumption that this Myers-Perry black holes are stable for sufficiently small rotation parameter a. This is a reasonable assumption because higher dimensional Schwarzschild black holes are stable [2]. From this assumption, there are only solutions with $\operatorname{Im}\omega < 0$ for small a, i.e., quasinormal modes. However, if there is an instability for large a, the imaginary part of some mode becomes positive, $\operatorname{Im}\omega > 0$, as a becomes large. It means that one of quasinormal modes must cross the real axis in the complex ω plane for some a. Therefore, if the black hole is unstable for large a, there is some critical value $a = a_{\rm crit}$ for which there exists a mode with real ω whose boundary condition is the same as that of quasinormal modes. We will search for such a value $a_{\rm crit}$ numerically.

For the purpose of searching for $a_{\rm crit}$, we assume that ω is real. The boundary condition we adopt is

$$
\Phi_K \to e^{-i(\omega-2K\Omega_H)r_*} \quad (r \to r_+) \ , \qquad \Phi_K \to Z_{\rm out} e^{i\omega r_*} + Z_{\rm in} e^{-i\omega r_*} \quad (r \to \infty) \ . \tag{11}
$$

From the constancy of Wronskian for Φ_K and $Z_{\rm in} = 0$, we can get the inequality,

$$
0 \le \omega \le 2K\Omega_H \ . \tag{12}
$$

This is the region we should search for.

We integrate the master equation (8) from $r = r_+$ to $r = \infty$ numerically. We adopt ingoing boundary condition at the horizon and, at $r = \infty$, we check the ratio of amplitudes of outgoing mode and ingoing mode, $Z(\omega, a) = |Z_{\rm out}|^2/|Z_{\rm in}|^2$. This ratio can be calculated for each ω and a in the domain defined by

Eq. (4) and (12). If $Z_{\rm in} = 0$ at $r = \infty$ for some ω and a, the function $Z(\omega, a)$ will diverge. It is a signal of instability. We plot $Z_{\rm max}(a)$ in Figure. 2, which is a maximum value of $Z(\omega, a)$ for fixed a. From these figures, we see that $Z_{\rm max}(a)$ does not diverge for $a^2 < \mu/2$. Therefore, we conclude that Myers-Perry black holes are stable for these modes.

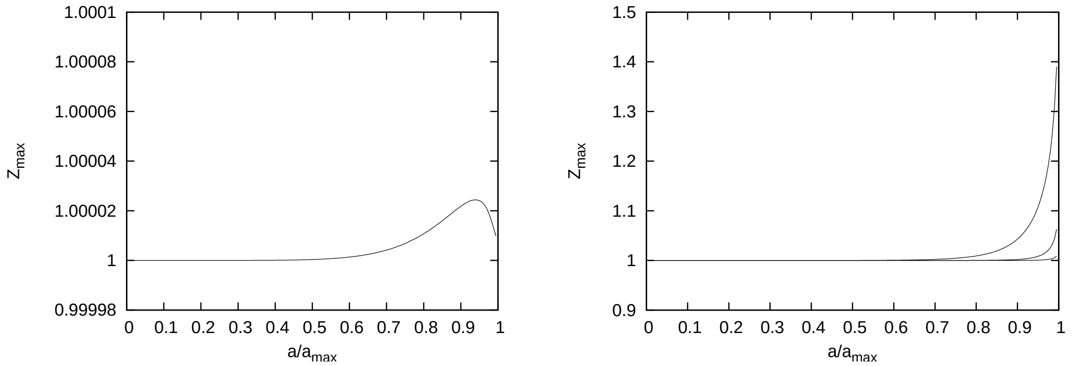

Figure 2: Functions $Z_{\rm max}(a)$ are plotted. The left and right figures are for $(J = 0, M = 0, K = 1)$ mode and $(J, M, K = J + 2)$ modes, respectively. In the right figure, we have plotted $Z_{\rm max}$ for $J = 0, 1, 2$ from the top to the bottom. We see that these do not diverge for $a < a_{\rm max}$.

4 Conclusion

We have studied the stability of 5-dimensional Myers-Perry black holes with equal angular momenta. We have obtained the master equations for the relevant modes to the stability analysis and shown the stability of Myers-Perry black holes for these modes. Strictly speaking, we have not shown the stability of Myers-Perry black holes completely, because we have analyzed the restricted modes. Empirically, however, the instability appears in the lower modes. For example, the Gregory-Laflamme instability appears in a s-wave. Therefore, our result for $(J = 0, M = 0, K = 0, 1, 2)$ modes gives a strong evidence for the stability of Myers-Perry black holes.

This work is supported in part by JSPS Grant-in-Aid for Scientific Research, No.193715 (K.M.), No. 18540262 (J.S.) and also by the 21COE program “Center for Diversity and Universality in Physics,” Kyoto University.

References

[1] R. C. Myers and M. J. Perry, Annals Phys. **172**, 304 (1986).

[2] A. Ishibashi and H. Kodama, Prog. Theor. Phys. **110**, 901 (2003) [arXiv:hep-th/0305185].

[3] R. A. Konoplya and A. Zhidenko, Nucl. Phys. B **777**, 182 (2007) [arXiv:hep-th/0703231].

[4] H. K. Kunduri, J. Lucietti and H. S. Reall, Phys. Rev. D **74**, 084021 (2006) [arXiv:hep-th/0606076].

[5] P. Bizon, T. Chmaj, G. W. Gibbons and C. N. Pope, Class. Quant. Grav. **24**, 4751 (2007) [arXiv:hep-th/0701190].

[6] K. Murata and J. Soda, arXiv:0710.0221 [hep-th].

[7] M. Kimura, K. Murata, H. Ishihara and J. Soda, arXiv:0712.4202 [hep-th].

[8] W. H. Press, S. A. Teukolsky, Astrophys. J. **185**, 649 (1973)

Black Rings on Eguchi-Hanson Space

Shinya Tomizawa[1], Hideki Ishihara[2], Masashi Kimura[3] and Ken Matsuno[4]

Department of Mathematics and Physics, Graduate School of Science, Osaka City University, 3-3-138 Sugimoto, Sumiyoshi, Osaka 558-8585, Japan

Abstract

We construct new supersymmetric black ring solutions on the Eguchi-Hanson base space as solutions of five-dimensional minimal supergravity. The solutions have the same two angular momentum components and the asymptotic structure on timeslices is asymptotically locally Euclidean. The S^1-direction of the black ring is along the equator on a S^2-bolt on the Eguchi-Hanson space. We also investigate the limit to a black hole, which describes the BMPV black hole with the topology of the lens space $L(2;1) = S^3/\mathbb{Z}_2$.

1 Introduction and Conclutions

A lot of physicists are also specially attracted with black hole solutions with asymptotically Euclidean time slices since they would be a good idealization in the situation such that we can ignore the tension of the brane and the curvature radius of the bulk, or the size of extra dimensions. However, from more realistic view point, we need not impose the asymptotic Euclidean condition toward the extra dimensions. In fact, higher dimensional black holes admit a variety of asymptotic structures: Kaluza-Klein black hole solutions [1, 2] have the spatial infinity with compact extra dimensions; Black hole solutions on the Eguchi-Hanson space [3] have the spatial infinity of topologically various lens spaces $L(2n; 1) = S^3/\mathbb{Z}_{2n}$ (n:natural number). Since the latter black hole spacetimes are asymptotically locally Euclidean, we cannot locally distinguish these asymptotic structure. In spacetimes with such asymptotic structures, furthermore, black holes have the structures considerably different from the black hole with the asymptotically Euclidean structure. For instance, the Kaluza-Klein black holes [1, 2] and the black holes on the Eguchi-Hanson space [3] can have the horizon of lens spaces in addition to S^3.

As solutions in five-dimensional Einstein-Maxwell theory with a positive cosmological constant, black hole solutions on Taub-NUT space [4] and Eguchi-Hason space [5] were also constructed by the present authors. These multi-black hole solutions describe the non-trivial coalescence of black holes, which is brought about by the non-trivial asymptotic structure. In the reference [5], we investigated how the coalescence of five-dimensional two black holes depends on the asymptotic structure of spacetime and compared with the five-dimensional Kastor-Traschen solution. Namely, two black holes with the topology of S^3 coalesce into a single black hole with the topology of the lens space $L(2; 1) = S^3/\mathbb{Z}_2$, while in the Kastor-Traschen solution, two black holes with the topology of S^3 coalesce into a single black hole with the topology of S^3. The difference helps us know what kind of asymptotic structure we live in the world with. In general, the toplogy of the spatial infinity and the spatial toplogy of a black hole horizon are very related to the number of nuts in the space because the toplogy of the closed surface surrounding n nuts is homeomorphic to the lens space $S^3/\mathbb{Z}_n$. (There is a single nut on the four-dimensional Euclid space, while the Eguchi-Hanson space has two nuts on the S^2-bolt.) Hence in a spacetime with n nuts, the spatial infinity also has the toplogical structure of the lens space $S^3/\mathbb{Z}_n$. If in such a spacetime there is no nut outside the black hole horizon, the spatial cross section of the horizon is homeomorphic to the spatial infinity. Therefore, since in both the Kastor-Traschen solutions and the our solutions in Ref.[5], there is no nut outside the horizons at the late time, the toplogies of the black holes after the coalescenses become S^3 and $S^3/\mathbb{Z}_2$, respectively. In the context of Kaluza-Klein theory and string theory, nuts also appear as monopoles in the effective four-dimesional theory. Therefore, it is impotrant to study what

[1]E-mail:tomizawa@sci.osaka-cu.ac.jp
[2]E-mail:ishihara@sci.osaka-cu.ac.jp
[3]E-mail:mkimura@sci.osaka-cu.ac.jp
[4]E-mail:matsuno@sci.osaka-cu.ac.jp

happens in the exsitence of nuts, in particular, it is an interesting issue and gives us some suggestions to investigate the possible topology of an event horizon. This is why we need to study a black object solution with such non-trivial asymptotic structure.

Our end is to construct new supersymmetric stationary black ring solutions on the Eguchi-Hanson space which has asymptotically locally Euclidean timeslices as solutions of five-dimensional minimal supergravity [6]. The black ring has two equal angular momentum components in two orthogonal planes. Interestingly, the S^1-direction of the black ring must be along the equator on a S^2-bolt since, otherwise, a Dirac-Misner string would arise near the nuts on the S^2-bolt.

2 Black ring solutions

The construction of our solutions [6] is essentially based on the program to classification of solutions in the five-dimensional minimal supergravity [7]. From the requirement of the absence of Dirac-Misner strings and asymptotic condition, we obtain the following metric and the gauge potential

$$\begin{aligned} ds^2 &= -H^{-2}\left[dt+\omega_0\left(\frac{a}{8}d\psi+\varphi_\phi d\phi\right)+\tilde{\omega}_\phi d\phi\right]^2 \\ &\quad +H\left[H_k(dr^2+r^2d\Omega^2_{S^2})+H_k^{-1}\left(\frac{a}{8}d\psi+\varphi_\phi d\phi\right)^2\right], \end{aligned} \tag{1}$$

$$\boldsymbol{A}=\frac{\sqrt{3}}{2}\left[H^{-1}\left(dt+\omega_0\left(\frac{a}{8}d\psi+\varphi_\phi d\phi\right)+\tilde{\omega}_\phi d\phi\right)-H_k^{-1}\frac{k_1}{r}\left(\frac{a}{8}d\psi+\varphi_\phi d\phi\right)+k_1\cos\theta\right], \tag{2}$$

respectively, where $d\Omega^2_{S^2}=d\theta^2+\sin^2\theta d\phi^2$. The coordinates r,ψ,ϕ,θ run the ranges

$$r>0,\ 0\le\psi\le 4\pi,\ 0\le\phi\le 2\pi,\ 0\le\theta\le\pi. \tag{3}$$

The five functions $H_k, H, \omega_0, \tilde{\omega}_\phi$ and φ_ϕ are given by

$$H_k=\frac{a}{8}\left(\frac{1}{\Delta_a}+\frac{1}{\Delta_{-a}}\right), \tag{4}$$

$$H=1+\frac{l_1}{r}+\frac{8k_1^2\Delta_a\Delta_{-a}}{ar^2(\Delta_a+\Delta_{-a})}, \tag{5}$$

$$\omega_0=2k_1\left(-\frac{3}{a}+\frac{3}{r}+\frac{6(l_1+r)\Delta_a\Delta_{-a}}{ar^2(\Delta_a+\Delta_{-a})}+\frac{32k_1^2\Delta_a^2\Delta_{-a}^2}{a^2r^3(\Delta_a+\Delta_{-a})^2}\right), \tag{6}$$

$$\tilde{\omega}_\phi = \frac{3k_1}{4\Delta_a\Delta_{-a}}[(r+a)(\Delta_{-a}-\Delta_a)+((r+a)(\Delta_{-a}+\Delta_a)-2\Delta_{-a}\Delta_a)\cos\theta], \tag{7}$$

$$\varphi_\phi=\frac{a}{8}\left(\frac{a(\Delta_{-a}-\Delta_a)+r(\Delta_a+\Delta_{-a})\cos\theta}{\Delta_a\Delta_{-a}}\right), \tag{8}$$

where $\Delta_{\pm a}=\sqrt{r^2\pm 2ar+a^2}$ and $r=|\boldsymbol{r}|$ ($\boldsymbol{r}$ denotes the position vector on a three-dimensional Euclid space). It is noted that our solutions have three independent parameters l_1, k_1 and a, where k_1 and l_1 are related to the dipole charge q of the black ring and the total electric charge Q_e by $k_1=-q/2$ and $al_1=4G_5Q_e/(\sqrt{3}\pi)-q^2$, and a is the radius of the S^2-bolt on the Eguchi-Hanson space. Furthermore, we impose the following conditions on these parameters

$$k_1<0,\quad l_1>-4k_1. \tag{9}$$

These are the conditions for the absence of closed timelike curves everywhere outside the event horizon.

3 Properties

3.1 Asymptotic structure

Let us introduce a new coordinate defined by $\tilde{r}^2 := ar$. Then the asymptotic form of the metric for $r \to \infty$ becomes

$$\begin{aligned} ds^2 \simeq & \left(-1 + \frac{2(4k_1^2 + l_1 a)}{\tilde{r}^2}\right) dt^2 \\ & - \frac{k_1(3a^2 + 8k_1^2 + 3al_1)\cos\theta}{\tilde{r}^2} dt d\phi - \frac{k_1(3a^2 + 8k_1^2 + 3al_1)}{2\tilde{r}^2} dt d\psi \\ & + d\tilde{r}^2 + \frac{\tilde{r}^2}{4}\left[\left(\frac{d\psi}{2} + \cos\theta d\phi\right)^2 + d\theta^2 + \sin^2\theta d\phi^2\right], \end{aligned} \tag{10}$$

which means that the spatial infinity is topologically the lens space $L(2;1) = S^3/\mathbb{Z}_2$. The asymptotic form of the metric on $t =$constant surfaces resembles the four-dimensional Euclid space, but they differ from each other in the topology of $r =$ constant surfaces on timeslices. We can regard S^3 and the lens space $L(2;1) = \mathrm{S}^3/\mathbb{Z}_2$ as S^1 bundle over S^2. The difference between these metric appears in the term of $d\psi$ in (10). If $d\psi/2$ in Eq.(10) is replaced by $d\psi$, the topology of $r =$ constant surfaces is S^3, i.e., the timeslices is asymptotically Euclidean. Furthermore, we introduce new angular variables $\tilde{\phi} = (2\phi + \psi)/4$, $\tilde{\psi} = (-2\phi + \psi)/4$ and $\Theta = \theta/2$. The ADM mass and angular momentums of our solutions can be computed as

$$\mathcal{M}_{\mathrm{ADM}} = \frac{\sqrt{3}}{2}|Q_e| = \frac{3\pi}{8G_5}(4k_1^2 + al_1), \tag{11}$$

$$J_{\tilde{\phi}} = J_{\tilde{\psi}} = -\frac{\pi}{4G_5}k_1(a^2 + 8k_1^2 + 3al_1). \tag{12}$$

From the relationship between the mass and the electric charge, we see that the BPS inequality is saturated. It is worth noting that two angular momentums of our solutions are equal in contrast to the black ring solutions on a flat base space [8]. The property in that solutions have the same two angular momentum components is similar to that of the BMPV black hole solutions.

3.2 Near-horizon geometry

First, let us shift a origin of three-dimensional Euclid space so that $\Delta_{-a} \to r$, $\Delta_a \to \Delta_{2a}$ and $r \to \Delta_a$. Next, we introduce the coordinate $(x, y, \hat{\phi}, \hat{\psi})$ defined by

$$r = -a\frac{x+y}{x-y}, \quad \cos\theta = -1 + 2\frac{1-x^2}{y^2-x^2} = 1 - 2\frac{y^2-1}{y^2-x^2}, \tag{13}$$

$$\phi = \hat{\phi} - \hat{\psi}, \quad \psi = \hat{\phi} + \hat{\psi}. \tag{14}$$

As seen later, the horizon is located on $y = -\infty$. Furthermore, let us define a new coordinates (z, ζ) given by

$$z = -\frac{P}{y}, \quad x = \cos\zeta, \tag{15}$$

where P is a constant with dimension of length. The location of the event horizon corresponds to $z = 0$. To see the geometry in the neighborhood of the event horizon, we introduce the following coordinates $(v, \hat{\phi}', \hat{\psi}')$

$$dt = dv - \left(B_0 + \frac{B_1}{z} + \frac{B_2}{z^2}\right) dz, \tag{16}$$

$$d\hat{\phi} = d\hat{\phi}' - \left(C_0 + \frac{C_1}{z}\right) dz, \tag{17}$$

$$d\hat{\psi} = d\hat{\psi}' - \left(C_0 + \frac{C_1}{z}\right) dz, \tag{18}$$

where the constants B_2, C_1 and B_1 are chosen to cure the divergences $1/z$ in $g_{\hat{\psi}'z}$, $1/z^2$ and $1/z$ in g_{zz}, respectively. C_0 and B_0 are determined so that $g_{zz} = O(z)$ for $z \to 0$. Then, under the choice of these constants, the metric behaves as

$$\begin{aligned} ds^2 \quad &\simeq \quad \frac{a^2 C_1}{2k_1 P} dvdz - \frac{a[(48k_1^4 - 12ak_1^2 l_1 + al_1^3) + (-48k_1^4 + 3k_1^2 l_1^2)]\cos\zeta}{16k_1^2 P\sqrt{3l_1^2 - 48k_1^2}}(dzd\hat{\phi}' + dzd\hat{\psi}') \\ &+ \left(k_1^2 \sin^2\zeta + \frac{3(l_1^2 - 16k_1^2)a^2}{256k_1^2}\right)(d\hat{\phi}'^2 + d\hat{\psi}'^2) \\ &+2\left(-k_1^2 \sin^2\zeta + \frac{3(l_1^2 - 16k_1^2)a^2}{256k_1^2}\right) d\hat{\phi}' d\hat{\psi}' + k_1^2 d\zeta^2, \end{aligned} \tag{19}$$

for $z \to 0$. Since each component take the finite value, we see that $(v, \hat{\phi}', \hat{\psi}', z, \zeta)$ are good coordinates in the neighborhood of the event horizon. Hence, $z = 0$ corresponds to the Killing horizon since the Killing vector $\partial/\partial v$ becomes null there. For $z \to 0$, the induced metric on v, z =constant surfaces, i.e., the spatial cross section of the event horizon becomes

$$ds^2|_{\mathcal{H}} \simeq \frac{3(l_1^2 - 16k_1^2)a^2}{256k_1^2} d\phi_2^2 + k_1^2(d\zeta^2 + \sin^2\zeta d\phi_1^2), \tag{20}$$

where $\phi_1 := \hat{\phi}' - \hat{\psi}' = \hat{\phi} - \hat{\psi} = \phi$ and $\phi_2 := \hat{\phi}' + \hat{\psi}'$. It should be noted that $\partial/\partial\phi_2|_{z=0} = \partial/\partial\psi|_{z=0}$ and $0 \le \phi_1 \le 2\pi$. This implies that the spatial topology of the event horizon is $\mathrm{S}^1 \times \mathrm{S}^2$.

3.3 Black hole limit

Finally, we consider the limit of our black ring to the black hole. Setting $l_1 = \mu/a$ ($\mu > 0$: constants) and taking the limit of $a \to 0$ in our solution yields the following metic

$$\begin{aligned} ds^2 \quad &= \quad -\left(1 + \frac{4k_1^2 + \mu}{\tilde{r}^2}\right)^{-2} \left[dt + \frac{k_1(8k_1^2 + 3\mu)}{2\tilde{r}^2}\left(\frac{d\psi}{2} + \cos\theta d\phi\right)\right]^2 \\ &+ \left(1 + \frac{4k_1^2 + \mu}{\tilde{r}^2}\right)\left[d\tilde{r}^2 + \frac{\tilde{r}^2}{4} d\Omega_{\mathrm{S}^2}^2 + \frac{\tilde{r}^2}{4}\left(\frac{d\psi}{2} + \cos\theta d\phi\right)^2\right]. \end{aligned} \tag{21}$$

This is equal to the metric of the BMPV black hole solutions with the mass parameter $m = 4k_1^2 + \mu$ and the angular momentum parameter $j = k_1(8k_1^2 + \mu)$ except that $d\psi$ is replaced with $d\psi/2$. This difference means that they differ in the topology of $\tilde{r}$ = constat, i.e., while the BMPV black hole has a squashed S^3 horizon, the spatial topology of the black hole horizon in (21) is the squashed lens space $L(2;1) = \mathrm{S}^3/\mathbb{Z}_2$. If we do not set $l_1 = \mu/a$ and take the limit $a \to 0$, the metric coincides with that of the BMPV black hole with $j = m^{3/2}$, whose horizon topology is the squashed lens space $L(2;1) = \mathrm{S}^3/\mathbb{Z}_2$.

References

[1] H.Ishihara and K.Matsuno, Prog.Theor.Phys. **116**, 417 (2006).

[2] H. Ishihara, M. Kimura, K. Matsuno and S. Tomizawa, Class. Quant. Grav. **23**, 6919 (2006).

[3] H. Ishihara, M. Kimura, K. Matsuno and S. Tomizawa, Phys.Rev.D **74**, 047501 (2006).

[4] D.Ida, H. Ishihara, M. Kimura, K. Matsuno Y. Morisawa and S. Tomizawa, Class. Quant. Grav.**24**, 3141 (2007).

[5] H. Ishihara, M. Kimura and S. Tomizawa, Class. Quant. Grav. **23**, L89 (2006).

[6] S. Tomizawa, H. Ishihara, M. Kimura and K. Matsuno, Class. Quant. Grav. **24**, 5609 (2007).

[7] J. P. Gauntlett, J. B. Gutowski, C. M. Hull, S. Pakis and H. S. Reall, Class. Quant. Grav. **20**, 4587 (2003).

[8] H. Elvang, R. Emparan, D. Mateos and H. S. Reall Phys. Rev. Lett. **93**, 211302 (2004).

Topology Change of Event Horizon of Coalescing Black Holes on Eguchi-Hanson Space

[a]Masashi Kimura[1], [a]Hideki Ishihara[2], [a]Ken Matsuno[3], [a]Shinya Tomizawa[4] and [b]Chul-Moon Yoo[5]

[a]*Department of Physics, Graduate School of Science, Osaka City University Osaka 558-8585, Japan*

[b]*Yukawa Institute for Theoretical Physics, Kyoto University Kyoto 606-8502, Japan*

Abstract

We numerically study event horizon of coalescing black holes solution in five dimensions. Effects of a difference in space-time topology on the black hole coalescence process is discussed.

1 Introduction

Black hole coalescence is one of the most interesting issue in relativity, but to treat the coalescencing process is difficult in general. However, if mass and electric charge of each black hole are equal we can construct exact solutions which describe the coalescencing proseces driven by a positive cosmological constant.

In five dimensional case, the metric and gauge 1-form of Kastor-Traschen solution(5DKT)[1, 2] are given by

$$ds^2 = -H^{-2}dt^2 + He^{-\lambda t}\left[dx^2 + dy^2 + dz^2 + dw^2\right], \tag{1}$$

$$A = \pm\frac{\sqrt{3}}{2}H^{-1}dt \tag{2}$$

where

$$H = 1 + \frac{1}{e^{-\lambda t}}\left(\frac{m_1}{r_+^2} + \frac{m_2}{r_-^2}\right), \tag{3}$$

$$r_\pm = \sqrt{x^2 + y^2 + z^2 + (w \mp a)^2}. \tag{4}$$

Here $\lambda = 2\sqrt{\Lambda/3}$ and Λ is a positive cosmological constant. This solution describes that two black holes with the topology of S^3 coalesce into a single black hole with the topology of S^3.

Recently, coalescing black hole solution on Eguchi-Hanson space(CBEH)[3] were found as other exact solutions in five dimensions. The metric and gauge 1-form of this solution are given by

$$ds^2 = -H^{-2}dt^2 + He^{-\lambda t}\left[V^{-1}(dx^2 + dy^2 + dz^2) + V((a/8)d\psi + \omega)^2\right], \tag{5}$$

$$A = \pm\frac{\sqrt{3}}{2}H^{-1}dt, \tag{6}$$

where

$$H = 1 + \frac{1}{e^{-\lambda t}}\left(\frac{M_1}{R_+} + \frac{M_2}{R_-}\right), \tag{7}$$

$$V^{-1} = \frac{a/8}{R_+} + \frac{a/8}{R_-}, \tag{8}$$

$$\mathrm{rot}\ \omega = \mathrm{grad}\ V^{-1}, \tag{9}$$

$$R_\pm = \sqrt{x^2 + y^2 + (z \mp a)^2}. \tag{10}$$

[1]E-mail:mkimura@sci.osaka-cu.ac.jp
[2]E-mail:ishihara@sci.osaka-cu.ac.jp
[3]E-mail:matsuno@sci.osaka-cu.ac.jp
[4]E-mail:tomizawa@sci.osaka-cu.ac.jp
[5]E-mail:yoo@yukawa.kyoto-u.ac.jp

Here, we note that the square bracket in (5) is the metric of the Eguchi-Hanson space[4, 5] which has non-trivial asymptotic structure called lens space $L(2;1) = \mathrm{S}^3/\mathbb{Z}_2$.

This solution describes the physical process such that two black holes with the topology of S^3 coalesce into a single black hole with the topology of the lens space $L(2;1)$ due to the non-trivial asymptotic sturucrure[3]. To see this, we shall see the behaver of the metric at early time $\tau \to -\infty$ and at late time $\tau \to -0$ following the discussion of [3]. At early time $t \to -\infty$ and $R_i \to 0$, the metric behaves as

$$\begin{aligned} ds^2 \ &\simeq \ -\left(1+\frac{m_i}{e^{-\lambda t} r_i^2}\right)^{-2} dt^2 \\ &\quad + \left(1+\frac{m_i}{e^{-\lambda t} r_i^2}\right) e^{-\lambda t} \left[dr_i^2 + \frac{r_i^2}{4}\left(d\theta^2 + \sin^2\theta d\phi^2 + (d\psi + \cos\theta d\phi)^2 \right)\right], \end{aligned} \tag{11}$$

where we introduce a new radial coordinate $r_i^2 := R_i a/2$ and $m_i := M_i a/2$. This is the same form of the metric of five-dimensional Reissner-Nordström-de Sitter solution with mass parameter m_i written in the cosmological coordinate. Therefore, we can see that there are two black holes with the topology of S^3 at early time. On the other hand, at late time $t \to \infty$ and $R \to \infty$, the metric behaves as

$$\begin{aligned} ds^2 \ &\simeq \ -\left(1+\frac{2(m_1+m_2)}{r^2}\right)^{-2} dt^2 \\ &\quad + \left(1+\frac{2(m_1+m_2)}{e^{-\lambda t} r^2}\right) \left[dr^2 + \frac{e^{-\lambda t} r^2}{4}\left(d\theta^2 + \sin^2\theta d\phi^2 + \left(\frac{d\psi}{2} + \cos\theta d\phi\right)^2 \right)\right], \end{aligned} \tag{12}$$

where we introduce the new radial coordinate $r^2 := aR$. This resembles the metric of the five-dimensional Reissner-Nordström-de Sitter solution with mass equal to $2(m_1+m_2)$ but the topology of horizon is lens space $L(2;1)$. Therefore, we can see the solution (5) describes the process such that two black holes with S^3 at the early time coalesce into a single black hole with lens space $L(2;1)$ at late time.

However, since in this discussion we only compared the behavor of the metric at early time and that of late time, it is not clarified how two black holes with S^3 coalesce into a single black hole with lens space $L(2;1)$. So, in the following sections, we numerically investigate the event horizon of the solution (5) and make clear the process of the coalesecnce.

2 Event Horizons of Coalescing Black Holes in Five Dimensions

Event horizon is the boudary of the causal past of I^+ and we can caluculate the event horizon numerically by solving null geodesics backward from the future to the past.

For 5DKT case, we plot the coordinate values $\tau := e^{-\lambda t},\ w,\ x$ of the event horizon in Fig.1. Note that it is sufficient that we only plot the x coordinate out of x, y, z coordinates because of the SO(3) symmetry in (x, y, z) space. From Fig.1 we can see that the contact point of black holes for 5DKT is given by $\tau = \text{const.}, x = y = z = w = 0$ then the topology of this point is a point.

On the other hand, for CBEH case, we plot the coordinate values $\tau := e^{-\lambda t},\ z,\ x$ of the event horizon in Fig.2. Note that it is sufficient that we only plot the x coordinete out of x, y coordinates because of the SO(2) symmetry in (x, y) space, and we omit the ψ direction which is S^1 in Fig.2 because ∂_ψ is a Killing vector. From Fig.2 we can see that the contact point of black hole coalescence for CBEH is given by $\tau = \text{const.}, x = y = z = 0$.

Here considering the fact that the S^1 direction is omitted in Fig.2, the topology of contact point of black hole coalescence for CBEH is not a point but S^1. This is the specific difference in topology changing process S^3 into lens space $L(2;1)$.

3 Change of Time Slices

As discussed in [6, 7], the coalescence of black holes is characterized invariantly by the structure of crease set, where crease set is a set of end points of null geodesics on the event horizon and the event horizon

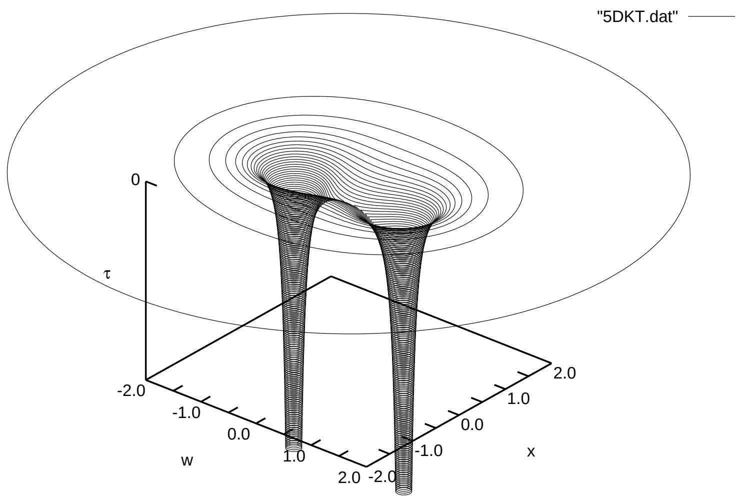

Figure 1: Event horizon of five dimensional Kastor-Traschen solution. $(m_1 = m_2 = 1, a = 1, \lambda = 1/(2\sqrt{2}))$

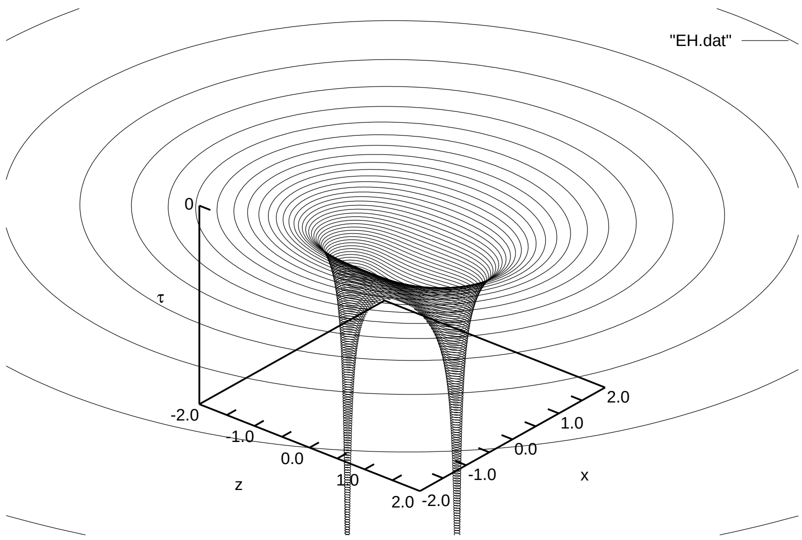

Figure 2: Event horizon of coalescing black holes on Eguchi-Hanson space. $(M_1 = M_2 = 2, a = 1, \lambda = 1/(2\sqrt{2}))$

is indifferentiable on these points. The intermediate evolution of black hole coalescence depends on the choise of time slice in general.

For the 5DKT case, the crease set is given by $\tau = \tau(w), x = y = z = 0, -a < w < a$, then the topology of crease set is R^1. On the other hand, for the CBEH case, the crease set is given by $\tau = \tau(z), x = y = 0, -a < t < a$, then the topology of the crease set is $R^1 \times S^1$, where S^1 is generated by ∂_ψ. Clearly, the dimension of crease sets of 5DTK and CBEH are different.

To see the difference of intermediate evolutions explicitely, we consider another time slice, $\tau' =$const., shown in Fig.3 for the both 5DKT and CBEH cases. For simplicity, we assume the spatial symmetry is

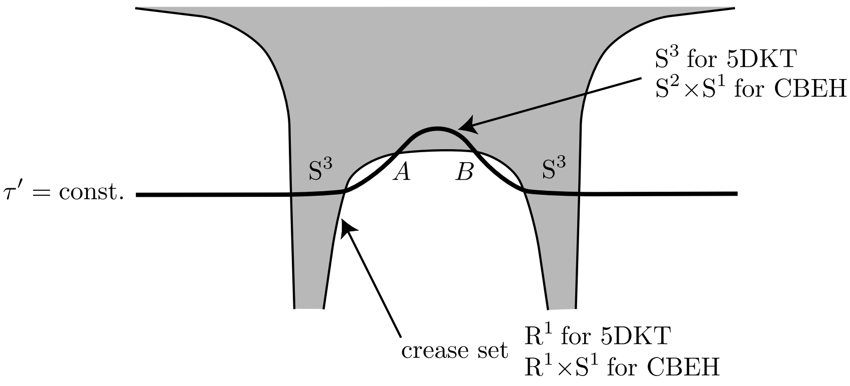

Figure 3: Schematic figure of the side view of the event horizon of 5DKT and CBEH. A time slice $\tau' = \tau'(\tau, z)$. is depicted.

the same as τ =const. surface. The central part of the intersection of τ' = const. surface and the event horizon makes a three-dimensional closed surface. This is the event horizon at τ' =const. surface.

In the case of 5DKT, because of the existence of SO(3) symmetry in (x, y, z) space, where the points A and B in Fig.3 are fixed points, the closed surface is topologically S^3. Then, the intermediate object is a black hole with the S^3 horizon. For more general time slice, a number of black holes with S^3 horizons can appear in the 5DKT case.

In contrast, in the case of CBEH, because of SO(2) symmetry in (x, y) space, where A and B are fixed points, and the existence of S^1, which is supressed in Fig.3, the intersection of τ' =const. surface and the event horizon is topologically $S^2 \times S^1$. Then a black ring $S^2 \times S^1$ is formed in the time slice τ' = const. during coalescence of two black holes in CBEH case. This is due to the defferences of the structure of crease set.

References

[1] D. Kastor and J. Traschen, Phys. Rev. D **47**, 5370 (1993).

[2] L.A.J. London, Nucl. Phys. B **424**, 709 (1995).

[3] H. Ishihara, M. Kimura and S. Tomizawa, Class. Quant. Grav. **23**, L89 (2006)

[4] T. Eguchi and A.J. Hanson, Phys. Lett. **74B**, 249 (1978).

[5] H. Ishihara, M. Kimura, K. Matsuno and S. Tomizawa, Phys. Rev. D **74**, 047501 (2006).

[6] M. Siino, Phys.Rev.D **58**, 104016, (1998).

[7] M. Siino, Prog.Theor.Phys. **99**, 1, (1998).

See also the report by C. Yoo in this volume.

Gravitational energy in higher dimensions
— Asymptotically flat case[1] —

Akihiro Ishibashi[2]

Cosmophysics Group, IPNS, KEK, Tsukuba, 305-0801 Japan

Abstract

We propose a higher (even spacetime) dimensional generalization of the Bondi energy within the framework of conformal infinity and Hamiltonian formalizm, employing the Gaussian null conformal gauge as a natural global specification which admits compact, spherical cross-sections of null infinity. Our Bondi energy expression takes a universal form in arbitrary (even spacetime) dimensions greater than or equal to four.

1 Introduction

There is considerable theoretical interest in gravitational theories in higher dimensions, and it is therefore important to define a precise notion of the total energy of an isolated gravitational system in higher dimensions. Such a notion may be given by generalizing to higher dimensions the notion of asymptotic flatness and associated energy of the ADM-type [1] and Bondi-type [2]. In particular, the latter type energy—if generalized to higher dimensions—may be used to probe extra dimensions with gravitational radiation.

An attempt to define a higher dimensional Bondi energy has previously been made by S. Hollands and the present author [3], employing a particular gauge condition—the *Minkowskian conformal gauge*—which requires a conformal background geometry to be locally, exactly Minkowskian in some neighborhood of conformal null infinity $\mathscr{I}$. This gauge is convenient for writing down some key geometrical quantities in terms of (unphysical conformal) curvature tensor since it simplifies relevant computations to certain extent. However, this gauge—which can be taken, at least, locally—is not globally well-defined in the sense that under that gauge condition, cross-sections of conformal null infinity $\mathscr{I}$ become anisotropic and, actually, non-compact; they are sphere with a single point removed and hence do not naturally reflect the topology of $\mathscr{I}$. For the purpose of computing the Bondi-energy in general, asymptotically flat radiative spacetimes and obtaining physical consequences, it would be much preferable that the Bondi-energy is defined under gauge conditions that can be taken *globally* in a neighborhood of $\mathscr{I}$ so that the Bondi-energy is evaluated on a *compact* cross-section of $\mathscr{I}$.

The purpose of this article is to introduce briefly the main results of the paper [4], in which a higher dimensional Bondi energy is re-formulated by employing the *Gaussian null conformal gauge*, which admits a *global specification of background structure with compact, spherical cross-sections of* $\mathscr{I}$, in contrast to the case of the Minkowskian conformal gauge [3].

2 Main results

2.1 Asymptotic flatness at null infinity and Gaussian null conformal gauge

Let $(\tilde{M}, \tilde{g}_{ab})$ and $(\bar{M}, \bar{g}_{ab})$ be an unphysical conformal spacetime and background geometry associated with a physical spacetime, (M, g_{ab}). The two fictitious metrics, $\tilde{g}_{ab}$ and $\bar{g}_{ab}$, are related to the physical metric, g_{ab}, and the Minkowski metric, η_{ab}, via a smooth *conformal factor*, Ω, as $\tilde{g}_{ab} = \Omega^2 g_{ab}$ and $\bar{g}_{ab} = \Omega^2 \eta_{ab}$ so that one can attach a *boundary* $\mathscr{I}$ at $\Omega = 0$ to M such that there exists an open neighborhood of $\mathscr{I}$ in $\tilde{M} = M \cup \mathscr{I}$ which is diffeomorphic to an open subset of the manifold $\bar{M}$, and $\mathscr{I}$ is mapped to a subset of the boundary of $\bar{M}$. (See [3] for more details.) We assume that $\mathscr{I}$ be

[1] KEK-Cosmo-5 KEK/TH/1215

[2] E-mail: akihiro.ishibashi@kek.jp

topologically $\mathbb{R} \times S^{d-2}$ so that it is consistent with the notion of a (higher dimensional version of) *weakly asymptotically simple* spacetime.

Following the standard procedure (see, e.g., Appendix A of [5]), we can construct a coordinate system $x^\mu = (u, \Omega, x^A)$ with $A = 1, \ldots, d-2$ on a (sufficiently small open) neighborhood, $\mathcal{O}$, of an arbitrary point of $\mathscr{I}$ in $\tilde{M}$ such that in $\mathcal{O}$, the unphysical metric takes the following form,

$$\mathrm{d}\tilde{s}^2 = \tilde{g}_{\mu\nu}\mathrm{d}x^\mu \mathrm{d}x^\nu = \tilde{\alpha}\mathrm{d}u^2 + 2\mathrm{d}u\mathrm{d}\Omega + 2\tilde{\beta}_A \mathrm{d}u\mathrm{d}x^A + \tilde{\gamma}_{AB}\mathrm{d}x^A\mathrm{d}x^B \,, \tag{1}$$

where u parametrizes a congruence of null generators of $\mathscr{I} \cap \mathcal{O}$ with $(\partial/\partial u)^a$ being a tangent vector field of the congruence, and where Ω, chosen to be $\Omega = 0$ on $\mathscr{I} \cap \mathcal{O}$, is an affine parameter of null geodesics which are orthogonal to each $(u, \Omega) = const.$ surfaces $B(u, \Omega)$ in $\mathcal{O}$ and transverse to $\mathscr{I} \cap \mathcal{O}$ so that $\tilde{g}_{ab}(\partial/\partial\Omega)^a(\partial/\partial u)^b = 1$, and where $\tilde{\alpha}$, $\tilde{\beta}_A$, $\tilde{\gamma}_{AB}$ are smooth functions with $\tilde{\alpha} = 0 = \tilde{\beta}_A$ on $\mathscr{I} \cap \mathcal{O}$. Note that $x^A = (x^1, \ldots, x^{d-2})$ may be regarded as local coordinates on $B(u, \Omega)$ and also that $\tilde{\gamma}_{AB}$ is a Riemaniann $(d-2)$-metric, which does not necessarily coincide with the induced metric on $B(u, \Omega)$ when $\Omega \neq 0$. The chart, $(\mathcal{O}, x^\mu)$, is called the *Gaussian null coordinate system* with respect to the null hypersurface $\mathscr{I} \cap \mathcal{O}$.

It is, a priori, not obvious when one can construct a Gaussian null coordinate system that covers the entire $\mathscr{I}$ so that, in particular, the set of $B(u) = B(u, \Omega = 0)$ becomes a *global* foliation of $\mathscr{I}$; each $B(u)$ is, in general, an open subset of global cross-sections of $\mathscr{I}$ and one may need to patch together more than one coordinate chart to cover the whole $\mathscr{I}$. However, when, for example, a null hypersurface is ruled by some Killing vector field which generates a one-parameter group of isometries, one can construct, by patching together local results, essentially a global Gaussian null coordinate system that covers the null hypersurface (see e.g., [6]). Although asymptotically flat spacetimes we are concerned with do not necessarily have a Killing symmetry, they do admit asymptotic symmetries, ξ^a, which are tangent to $\mathscr{I}$ and play a similar role of a Killing symmetry on $\mathscr{I}$. Therefore there seems to be no obstruction in assuming that one always be able to construct a desired, global Gaussian null coordinate system in some neighborhood $\mathcal{O}$ of $\mathscr{I}$ in $\tilde{M}$ such that $B(u)$ appropriately foliate $\mathscr{I}$ as global cross-sections of $\mathscr{I}$ with topology $B(u) \approx S^{d-2}$, reflecting $\mathscr{I} \approx \mathbb{R} \times S^{d-2}$.

For our background geometry $(\bar{M}, \bar{g}_{ab})$, the above coordinate system $(\mathcal{O}, x^\mu)$ yields

$$\bar{\alpha} = -\Omega^2 \,, \quad \bar{\beta}_A = 0 \,, \quad \bar{\gamma}_{AB} = \sigma_{AB} \,, \tag{2}$$

with σ_{AB} being the metric of $(d-2)$-dimensional unit round sphere, and covers $\mathscr{I} = \partial\bar{M}$ globally. We shall view σ_{AB} as a *global specification of cross-sections of* $\mathscr{I}$. In the following we call the gauge choice, eqs. (1) and (2), the *Gaussian null conformal gauge*.

A general, stable definition of asymptotic flatness at $\mathscr{I}$ in higher dimensions ($d > 4$ and even) has been given in [3], which arrived at via stability analysis of conformal null infinity against linear gravitational perturbations. In terms of the Gaussian null conformal gauge, the flatness (fall off at $\mathscr{I}$) conditions given in [3] are rewritten as

$$\begin{aligned}
&\tilde{\gamma}_{AB} = \sigma_{AB} + O(\Omega^{(d-2)/2}) \,, \quad \tilde{\gamma}^{AB}\frac{\partial}{\partial u}\tilde{\gamma}_{AB} = O(\Omega^{d/2}) \,, \ \tilde{\gamma}^{AB}\frac{\partial}{\partial\Omega}\tilde{\gamma}_{AB} = O(\Omega^{(d-2)/2}) \\
&\tilde{\beta}_A \,, \ \tilde{\beta}^A = O(\Omega^{d/2}) \,, \quad \tilde{\alpha} = -\Omega^2 + O(\Omega^{(d+2)/2}) \,.
\end{aligned} \tag{3}$$

(Note that the fall off conditions for $d = 4$ differ from the above ones [4]. See also [7].)

2.2 Bondi energy in Gaussian null conformal gauge

Once boundary conditions for asymptotic flatness are established, one can introduce the notion of asymptotic symmetries and then define conserved quantities associated with the (infinitesimal) symmetries ξ^a. (See [4] for details of our definition of asymptotic symmetries at null infinity in higher dimensions.) A general strategy for defining conserved quantities associated with symmetries that preserve given boundary conditions has been developed by Wald and Zoupas [8]. We apply the formula of Wald and Zoupas to asymptotically flat, vacuum solutions to Einstein's equations. For this purpose, we introduce

$$\tilde{S}_{ab} \equiv \frac{2}{d-2}\tilde{R}_{ab} - \frac{1}{(d-1)(d-2)}\tilde{R}\tilde{g}_{ab} \,, \tag{4}$$

where $\tilde{R}_{ab}$ is the Ricci tensor with respect to $\tilde{g}_{ab}$. We note here that the Minkowskian conformal gauge requires the background geometry to be exactly flat in a neighborhood of $\mathscr{I}$ and thus yields

$$\tilde{S}_{ab} = O(\Omega^{(d-4)/2}) \,, \tag{5}$$

while the Gaussian conformal gauge yields

$$\tilde{S}_{uu} = \Omega^2 + O(\Omega^{d/2}) \,, \quad \tilde{S}_{u\Omega} = -1 + O(\Omega^{(d-2)/2}) \,, \quad \tilde{S}_{uA} = O(\Omega^{d/2}) \,, \quad \tilde{S}_{\Omega A}, \tilde{S}_{AB} = O(\Omega^{(d-4)/2}) \,. \tag{6}$$

We define a higher dimensional news tensor under the Gaussian null conformal gauge by

$$N_{ab} \equiv \zeta^* \left(\Omega^{-(d-4)/2} q^m{}_a q^n{}_b \tilde{S}_{mn} \right) - \Omega^{-(d-4)/2} \sigma_{ab} \,, \tag{7}$$

where $q_{ab} \equiv \tilde{g}_{ab} - 2\tilde{\ell}_{(a}\tilde{n}_{b)}$ with $\tilde{\ell}_a = (\mathrm{d}u)_a$ and $\tilde{n}_a = (\mathrm{d}\Omega)_a$ and ζ^* denotes the pull back to $\mathscr{I}$. This is a global definition as it involves the $(d-2)$-dimensional round-sphere metric σ_{ab}, which specifies a background structure at $\mathscr{I}$ and looks a natural higher dimensional generalization of the news tensor, $N_{ab} = \zeta^*(\tilde{S}_{ab}) - \rho_{ab}$, in 4-dimensions, given by Geroch [9]. (In 4-dimensional case, the global specification, ρ_{ab}, is defined by equation (33) in [9] and can be taken such that $\rho_{ab} = \sigma_{ab}$ [8].) Note that the previous definition of the news tensor under the Minkowskian conformal gauge (eq. (61) of [3]) does not include σ_{ab}.

We now introduce the following vector field associated with asymptotic time-translations $\xi^a = \tau\tilde{n}^a$ (with $\tau = const.$ on $\mathscr{I}$),

$$P^a[\xi] \equiv \frac{1}{8(d-3)\pi G} \left(\Omega^{-(d-4)/2} \xi^{[a} q^{b]d} N_{de} q^{ce} C^f{}_{bc} \tilde{\ell}_f - \Omega^{-(d-3)} \tilde{C}^{abcd} \xi_b \tilde{\ell}_c n_d \right) \,, \tag{8}$$

where $C^c{}_{ab}$ denotes the connection defined by, $(\tilde{\nabla}_a - \bar{\nabla}_a)\omega_b = C^c{}_{ab}\omega_c$, for an arbitrary 1-form ω_c and $\tilde{C}_{abcd}$ the Weyl curvature tensor with respect to $\tilde{g}_{ab}$. Note that in 4-dimensions, the above formula, eq. (8), agrees with the known, 4-dimensional Bondi energy-momentum integrand. We now state our main results in the following theorem.

Theorem: Consider an even-dimensional $d \geqslant 4$ vacuum spacetime (M, g_{ab}) which is asymptotically flat at null infinity $\mathscr{I}$, satisfying the boundary conditions, eq. (3) (for $d = 4$, see [4]). Let $\mathcal{O} \subset \tilde{M}$ be a neighborhood of $\mathscr{I}$ in which the Gaussian null conformal gauge eq. (1), can be taken. In $\mathcal{O}$, the divergence, $\tilde{\nabla}_a P^a$, of P^a introduced by eq. (8) smoothly extends to $\mathscr{I}$ and solves

$$\tilde{\nabla}_a P^a = -\frac{\tau}{32\pi G} N^{ab} N_{ab} + O(\Omega) \,. \tag{9}$$

Proof is given in [4]. Then, following the Wald-Zoupas formula, we find the charge associated with the asymptotic symmetry $\xi^a = \tau\tilde{n}^a$,

$$\mathcal{H}_\xi = \int_B {}^{(d-2)}\tilde{\epsilon}\; P^a \tilde{\ell}_a \,, \tag{10}$$

with ${}^{(d-2)}\tilde{\epsilon}$ being a natural volume element on a closed $(d-2)$-surface B on $\mathscr{I}$ induced from $\tilde{g}_{ab}$. (See [4] for details.) We propose to take the charge $\mathcal{H}_\xi$ defined above with P^a given by eq. (8) as a natural higher dimensional generalization of the Bondi-energy.

It should be noted that although the divergence $\tilde{\nabla}_a P^a$—whose integral over a segment of $\mathscr{I}$ gives rise to a flux formula—is well-defined, the limit to $\mathscr{I}$ of P^a itself does not appear to exist under our boundary conditions. This, however, does not necessarily imply that the *integral* of $P^a\tilde{\ell}_a$ over a compact cross-section B of $\mathscr{I}$ also would be singular for general, asymptotically flat radiative spacetimes. Attempts to justify P^a given by eq. (8) as the legitimate Bondi energy-momentum integrand are made [4] by discussing the case in which an asymptotically flat, radiative spacetime has a stationary region in some neighborhood of spatial infinity i^0, and also by considering gravitational perturbations off of Minkowski spacetime. Therefore, although we have not yet fully justify the regularity of P^a for generic case, in full non-linear theory, we would like to make the following conjecture.

Conjecture: For any asymptotically flat (at null infinity $\mathscr{I}$) spacetime and any cross-section B of $\mathscr{I}$, the integral of $P^a\tilde{\ell}_a$ given by eq. (8) over a $(d-2)$-closed surface S in $\mathcal{O}$ always has a well-defined limit as S approaches B, and the limit is independent of how S approaches B, so that the integral, eq. (10), is well-defined.

We should keep in mind that the vector P^a has degrees of freedom in the addition of a vector field of the form $\tilde{\nabla}_b X^{ab}$ with X^{ab} being an arbitrary anti-symmetric tensor field on $\tilde{M}$; $P'^a = P^a + \tilde{\nabla}_b X^{ab}$ also solves eq. (9) if P^a does. A relevant question is then whether there exists a P'^a for which $P'^a\tilde{\ell}_a$ smoothly extends to $\mathscr{I}$ and yields an equivalent formula for the higher dimensional Bondi-energy. This problem is left open for future work. Also, more work on non-linear analysis of asymptotic flatness conditions need to be done.

Acknowledgements

I am greatly indebted to Bob Wald for many useful discussions and valuable comments. I have also benefited greatly from discussions with Stefan Hollands. This work was mostly done at Enrico Fermi Institute, The University of Chicago, supported in part by NSF grant no PHY 04-56619 to the University of Chicago.

References

[1] R. Arnowitt, S. Deser, and C.W. Misner, “Canonical variables for general relativity” Phys. Rev. **117**, 1595 (1960)

[2] H. Bondi, M.G.J. van der Burg, and A.W.K. Metzner, “Gravitational Waves in General Relativity. VII. Waves from Axi-Symmetric Isolated Systems” Proc. R. Soc. London, Ser. A **269**, 21 (1962)

[3] S. Hollands and A. Ishibashi, “Asymptotic flatness and Bondi energy in higher dimensional gravity” J. Math. Phys. **46** 022503, 2005

[4] A. Ishibashi, “Higher Dimensional Bondi Energy with a Globally Specified Background Structure” Preprint: KEK-Cosmo-3, KEK/TH/1213, Archives: 0712.4348 [gr-qc]

[5] H. Friedrich, I. Racz, and R.M. Wald, Commun. Math. Phys. **204**, 691 (1999)

[6] S. Hollands, A. Ishibashi, and R.M. Wald, “A Higher dimensional stationary rotating black hole must be axisymmetric” Commun. Math. Phys. **271**, 699 (2007)

[7] R. Geroch and B.C. Xanthopoulos, “Asymptotic simplicity is stable” J. Math. Phys. **19**, 714 (1978)

[8] R.M. Wald and A. Zoupas, “General definition of “conserved quantities” in general relativity and other theories of gravity” Phys. Rev. D **61**, 084027 (2000)

[9] R. Geroch, in *Asymptotic Structure of Spacetime*, edited by F. Esposito and L. Witten (Plenum, New York, 1977)

Fermion evaporation of a black hole off a tense brane
Proceedings for the JGRG17 international conference Nagoya, Japan, December 2007

H. T. Cho[1], A. S. Cornell[2], Jason Doukas[3], Wade Naylor[4]

[1] *Department of Physics, Tamkang University, Tamsui, Taipei, Taiwan, Republic of China*
[2] *Université Lyon 1, Institut de Physique Nucléaire de Lyon, France*
[3] *School of Physics, University of Melbourne, Parkville, Victoria 3010, Australia*
[4] *Department of Physics, Ritsumeikan University, Kusatsu, Shiga 525-8577, Japan*

Abstract

Using the WKBJ approximation we obtain numerical plots of the power emission spectrum for the evaporation of massless bulk Dirac fermions from six dimensional black holes off a tense 3-brane with codimension two. We also present the multiplicity factors for eigenvalues of the deficit four sphere and show that these reduce to the usual case in the tenseless limit.

1 Introduction

One of the most distinct predictions of large extra-dimensional models [1] is the production of black holes (BHs) at particle accelerators such as the LHC [2]. In these models the standard model (SM) fields are restricted to motion along a 3-brane in the extra dimensions, while the gravitational field can propagate isotropically. By readjusting the fundamental cut-off scale one can simultaneously resolve the gauge-hierarchy problem and give some explanation for the observed weakness of gravity relative to the other forces. Recently, a metric describing a BH located on a 3-brane with finite tension, embedded in locally flat 6-dimensional (6D) spacetime was discovered [7]. Before this, no exact solution that incorporated brane tension was known and the effect of brane tension on the observational signatures of mini BHs was largely ignored.

While early incarnations of large extra dimensional models assumed that only gravitational fields existed in the space off the brane (known as the *bulk*), over time more elaborate scenarios were devised that required other bulk fields. Split fermion models [3] are examples of this kind. In split fermion models proton decay inducing operators can be suppressed while simultaneously giving the correct SM mass hierarchies. The result is achieved by using a kink configuration of a bulk scalar field to localise quarks and leptons and the left- and right- chiral components of the fermion fields to different locations in the higher dimension(s). In supersymmetric versions of this idea the scalars that localise the bulk fields will also have bulk fermionic superpartners.

Having a larger number of degrees of freedom propagating in the bulk would lower the probability of witnessing a BH event at the LHC i.e., evaporation into bulk modes would reduce the amount radiation seen from the brane thereby lowering the chance of identifying a BH event [5]. Regardless of which model you prefer, there is clearly an imperative to determine precisely how bulk modes effect the Hawking emission spectrum so that in the event that a mini BH is observed the correct extra dimensional model may be able to be inferred.

In what follows we study the effect of brane tension on the BH emission spectrum of massless bulk fermions. The analogous emission rates for scalar, gauge boson and graviton bulk fields were calculated in [8], however as we will be using the WKBJ approximation our treatment differs somewhat to theirs.

[1] htcho"at"mail.tku.edu.tw
[2] cornell@ipnl.in2p3.fr
[3] j.doukas"at"physics.unimelb.edu.au
[4] naylor"at"se.ritsumei.ac.jp
[5] While the missing energy may be some evidence for extra dimensions it would not conclusively identify a BH event.

The metric for a black hole residing on a tensional 3-brane embedded in a six-dimensional spacetime is [7, 9]:

$$\mathrm{d}s^2 = -f(r)dt^2 + \frac{dr^2}{f(r)} + r^2 d\Omega_4^2 \ , \qquad f(r) = 1 - \left(\frac{r_H}{r}\right)^3 \tag{1}$$

where the radius of the horizon is given by

$$r_H = \left(\frac{\mu}{b}\right)^{1/3} \qquad\qquad \mu \equiv \frac{M_{BH}}{4\pi^2 M_*^4} \tag{2}$$

and M_{BH} is the mass of the black hole. The parameter b is a measure of the conical deviation from a perfect sphere and has the following angle element:

$$d\Omega_4^2 = d\theta_3^2 + \sin^2\theta_3 \left(d\theta_2^2 + \sin^2\theta_2 \left(d\theta_1^2 + b^2 \sin^2\theta_1 d\phi^2\right)\right), \qquad 0 < b \leq 1. \tag{3}$$

For $b = 1$ this is the line element of the unit sphere S^4 and corresponds to zero brane tension. In the case of non-vanishing brane tension the parameter $b < 1$ is a measure of the deficit angle about an axis parallel to the 3-brane in the angular direction ϕ, such that the canonically normalized angle $\phi' = \phi/b$ runs over the interval $[0, 2\pi/b]$. It can be expressed in term of the brane tension λ as:

$$b = 1 - \frac{\lambda}{4\pi M_*^4} \ , \tag{4}$$

where M_* is the fundamental Planck constant of six-dimensional gravity. As can be seen the tension of the brane ($b \to 0$) increases the radius of the horizon.

The Dirac operator on this metric is solved by use of the conformal transformation:

$$g_{\mu\nu} \quad \to \quad \overline{g}_{\mu\nu} = \Omega^2 g_{\mu\nu}, \tag{5}$$

$$\psi \quad \to \quad \overline{\psi} = \Omega^{-5/2}\psi, \tag{6}$$

$$\gamma^\mu \nabla_\mu \psi \quad \to \quad \Omega^{7/2}\overline{\gamma}^\mu \overline{\nabla}_\mu \overline{\psi}, \tag{7}$$

where $\Omega = 1/r$, the metric in equation (1) then separates into a $t - r$ part and a deficit 4-sphere part:

$$d\overline{s}^2 = \frac{1}{r^2}\left(-f(r)dt^2 + \frac{1}{f(r)}dr^2\right) + d\Omega_4^2. \tag{8}$$

The massless Dirac equation, $\overline{\gamma}^\mu \overline{\nabla}_\mu \overline{\psi} = 0$, can then be written:

$$\left[\left(\overline{\gamma}^t \overline{\nabla}_t + \overline{\gamma}^r \overline{\nabla}_r\right) \otimes 1\right] \overline{\psi} + \left[\overline{\gamma}^5 \otimes \left(\overline{\gamma}^a \overline{\nabla}_a\right)_{S_4}\right] \overline{\psi} = 0, \tag{9}$$

where $(\overline{\gamma}^5)^2 = 1$ and $\overline{\psi} = r^{5/2}\psi$. Note that from this point on we shall change our notation by omitting the bars.

The eigenvalues, κ, for the eigenspinors of the deficit 4-sphere,

$$\left(\gamma^a \nabla_a\right)_{S_4} \chi_l^{(\pm)} = \pm i\kappa \chi_l^{(\pm)}, \tag{10}$$

where found in [10] and are given by

$$\kappa(n, m) = n + 2 + |m|\left(\frac{1}{b} - 1\right), \tag{11}$$

where $n = 0, 1, 2, \ldots$ and $m = \pm 1/2, \pm 3/2, \ldots, \pm(n + 1/2)$. After a little algebra [10], the radial part of the Dirac equation reduces to a Schrödinger-like equation in the tortoise coordinate r_*:

$$\left(-\frac{d^2}{dr_*^2} + V_1\right) G = E^2 G \ , \tag{12}$$

where $dr = f(r)dr_*$, and the potential is given by $V_1(r) = \kappa^2 \frac{f}{r^2} + \kappa f \frac{d}{dr}\left[\frac{\sqrt{f}}{r}\right]$.

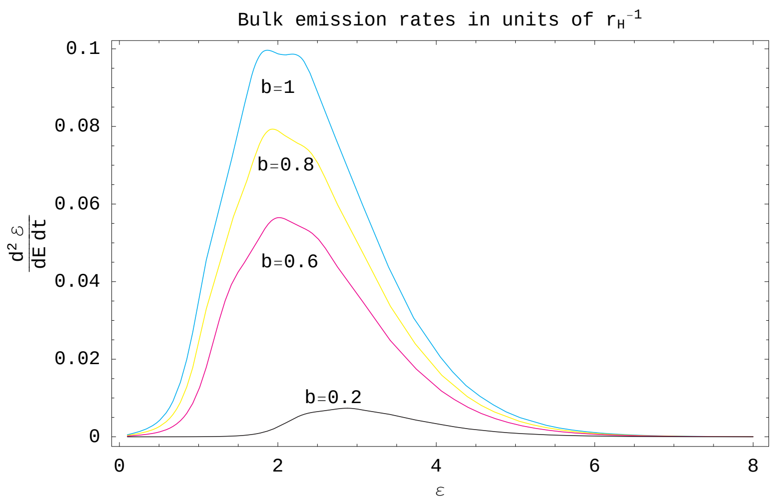

Figure 1: We display the results of third order WKBJ, which show the variation of the Hawking radiation spectrum with brane tension. Increasing brane tension (decreasing b), while holding r_H and M_* fixed, results in a reduction of the emitted power.

2 Absorption probability and emission rates

When the BH perturbation equation takes the Schrödinger form as in equation (12) an adapted form of the WKBJ method [5] can be employed to find the absorption probability. The absorption probability is written:

$$|\mathcal{A}_\kappa(E)|^2 = \frac{1}{1+e^{2S(E)}} \quad , \tag{13}$$

where $S(E)$ is calculated to third order in [10, 5]. In our case it will be convenient to make a change of variables to $x = Er$ [4]. This leads to the following form of the potential:

$$Q(x_*) = 1 - \kappa^2 \frac{f}{x^2} - \kappa f \frac{d}{dx}\left[\frac{\sqrt{f}}{x}\right] , \qquad f(x) = 1 - \left(\frac{\varepsilon}{x}\right)^{d-3} , \tag{14}$$

where $E^2 Q(x_*) = E^2 - V_1$, and $\varepsilon = r_H E$. As such, the Schrödinger equation (12) becomes:

$$\left(\frac{d^2}{dx_*^2} + Q\right) G = 0 \ . \tag{15}$$

The emission rate for a massless fermion from a BH is related to the cross-section by a d^5k dimensional momentum integral times a fermionic thermal temperature distribution:

$$\frac{d\mathcal{E}}{dt} = \sum_{\lambda,E} \sigma_{\lambda,E} \frac{E}{e^{\frac{E}{T_H}}+1} \frac{d^5k}{(2\pi)^5} \quad , \tag{16}$$

where T_H is the Hawking temperature, $\sigma_{\lambda,E}$ are the greybody factors and the sum is a generic sum over all angular momentum and momentum variables. The greybody factor can be related to the absorption probability by considering the results of reference [6]:

$$\sigma_{\lambda,E} = \frac{1}{2\Omega_4}\left(\frac{2\pi}{E}\right)^4 \sum_\kappa D_\kappa |\mathcal{A}_\kappa(E)|^2 \ . \tag{17}$$

The degeneracy, D_κ, of eigenspinors for the deficit four sphere is found to be:

$$\begin{aligned} D_\kappa(n,|m|) &= \sum_{n_2=|m|-1/2}^{n} 2 \sum_{n_1=|m|-1/2}^{n_2} 2, \\ &= 2\left(n-|m|+\frac{5}{2}\right)\left(n-|m|+\frac{3}{2}\right) . \end{aligned} \tag{18}$$

Summing over $|m|$ reproduces to the degeneracy calculated in [11] for the regular four sphere:

$$\begin{aligned} D_4(n) &= \sum_{|m|=1/2,\ldots,n+1/2} 2\left(n-|m|+\frac{5}{2}\right)\left(n-|m|+\frac{3}{2}\right), \\ &= \frac{2}{3}(n+1)(n+2)(n+3), \end{aligned} \tag{19}$$

Given that $\int d^5k = \int \Omega_4 E^4 dE$, and using the fact that the Hawking temperature is $T_H = 5/(4\pi r_H)$, we obtain:

$$\frac{d^2\mathcal{E}}{dEdt} = \frac{1}{\pi r_H}\sum_{\kappa>0}\frac{\varepsilon}{e^{\frac{4\pi\varepsilon}{5}}+1}D_\kappa|\mathcal{A}_\kappa(\varepsilon)|^2 \ . \tag{20}$$

3 Results and Conclusion

The power emission for various values of the tension parameter b are overlaid in figure 1. In plotting the graphs as a function of epsilon we have implicitly assumed that the horizon radius is fixed, i.e., $\epsilon = Er_H$. Since $r_H = (\frac{\mu}{b})^{1/3}$ depends on b, the ratio $\frac{\mu}{b}$ is also fixed, this can be done, see equation (2), by fixing the fundamental scale, M_*, and changing the mass of the black hole proportionally with b.

We find that for increased tension ($b \to 0$) the emitted power due to Hawking radiation is reduced. These results are consistent with the those made for the integer representations of the Poincare group in [8], and completes a missing piece of the picture of emission from BHs off tense branes in being the first time that the power emission spectrum from massless spin 1/2 fields has been calculated.

References

[1] N. Arkani-Hamed, S. Dimopoulos and G. R. Dvali, Phys. Lett. B **429**, 263 (1998); I. Antoniadis, N. Arkani-Hamed, S. Dimopoulos and G. R. Dvali, Phys. Lett. B **436**, 257 (1998) [arXiv:hep-ph/9804398].

[2] P. C. Argyres, S. Dimopoulos and J. March-Russell, Phys. Lett. B **441**, 96 (1998); S. Dimopoulos and G. Landsberg, Phys. Rev. Lett. **87**, 161602 (2001); S. B. Giddings and S. D. Thomas, Phys. Rev. D **65**, 056010 (2002); R. Casadio and B. Harms, Int. J. Mod. Phys. A **17**, 4635 (2002) [arXiv:hep-th/0110255].

[3] N. Arkani-Hamed and M. Schmaltz, Phys. Rev. D **61**, 033005 (2000); N. Arkani-Hamed, Y. Grossman and M. Schmaltz, Phys. Rev. D **61**, 115004 (2000); T. Han, G. D. Kribs and B. McElrath, Phys. Rev. Lett. **90**, 031601 (2003); D. C. Dai, G. D. Starkman and D. Stojkovic, Phys. Rev. D **73**, 104037 (2006) [arXiv:hep-ph/0605085].

[4] A. S. Cornell, W. Naylor and M. Sasaki, JHEP **0602** (2006) 012 [arXiv:hep-th/0510009].

[5] C. M. Will and J. W. Guinn, Phys. Rev. A **37** (1988) 3674; S. Iyer and C. M. Will, Phys. Rev. D **35** (1987) 3621. ; S. Iyer, Phys. Rev. D **35** (1987) 3632.

[6] V. Cardoso, M. Cavaglia and L. Gualtieri, JHEP **0602**, 021 (2006) [arXiv:hep-th/0512116].

[7] N. Kaloper and D. Kiley, JHEP **0603** (2006) 077 [arXiv:hep-th/0601110].

[8] D. C. Dai, N. Kaloper, G. D. Starkman and D. Stojkovic, [arXiv:hep-th/0611184];

[9] S. Chen, B. Wang and R. K. Su, Phys. Lett. B **647** (2007) 282 [arXiv:hep-th/0701209]. U. A. al-Binni and G. Siopsis, arXiv:0708.3363 [hep-th].

[10] H. T. Cho, A. S. Cornell, J. Doukas and W. Naylor, Phys. Rev. D **75** (2007) 104005 [arXiv:hep-th/0701193]; ; H. T. Cho, A. S. Cornell, J. Doukas and W. Naylor, arXiv:0709.1661 [hep-th]. ; H. T. Cho, A. S. Cornell, J. Doukas and W. Naylor, arXiv:0710.5267 [hep-th].

[11] R. Camporesi and A. Higuchi, J. Geom. Phys. **20** (1996) 1 [arXiv:gr-qc/9505009].

Self-similar cosmological solutions with dark energy

Tomohiro Harada[1]

Department of Physics, Rikkyo University, Toshima, Tokyo 171-8501, Japan

Abstract

Based on the asymptotic analysis of ordinary differential equations, we classify all spherically symmetric self-similar solutions to the Einstein equations which are asymptotically Friedmann at large distances and contain a perfect fluid with equation of state $p = (\gamma - 1)\rho$ with $0 < \gamma < 2/3$. The expansion of the Friedmann universe is accelerated in this range of the parameter due to anti-gravity. For asymptotically Friedmann solutions, we find eight classes of possible asymptotic behaviours. In particular, we find that there are asymptotically quasi-static and quasi-Kantowski-Sachs solutions which are analytically extendible. This opens up the possibility of physically interesting cosmological solutions, in which any physical scale increases in proportion to time. We study these solutions numerically and consider their physical interpretation. In particular, we consider whether there are physically realistic self-similar solutions in which a primordial black hole is attached to an exact or asymptotically Friedmann model. This would correspond to the black hole growing at the same rate as the universe. In fact, there are genuinely asymptotically Friedmann solutions containing a black hole. This suggests that black holes in cosmological models with dark energy can grow as fast as the cosmological horizon. We also find self-similar cosmological wormhole and white hole solutions.

1 Introduction

There are accumulating observational evidences supporting that our Universe is on an accelerated expanding phase at present epoch. Assuming the Einstein equation with homogeneity and isotropy, we lead to the violation of the strong energy condition. This is often referred to as "anti-gravity" because the violation of the strong energy condition implies repulsive force in terms of the Raychaudhuri equation. We do not know what causes the cosmic acceleration at all. However, the phenomenological analysis of the observational data implies that more than 70 % of energy in our Universe is in the matter field which causes the cosmic acceleration, which is called dark energy. The simplest candidate for dark energy is the cosmological constant, which can be described by a perfect fluid with the equation of state $p = -\rho$. However, this needs incredibly fine tuning by one part in 10^{120}. To relax this problem, one can consider a matter field, whose energy density was higher in the early universe. Such a matter field can be parameterised by a perfect fluid with the equation of state $p = w\rho$, where $w < -1/3$ should hold to violate the strong energy condition. Here, we consider a perfect fluid $p = (\gamma - 1)\rho$, where γ is a constant and $0 < \gamma < 2/3$.

It is usually assumed that black holes are stationary and asymptotically flat with an event horizon in vacuum, which are uniquely described by the Kerr solution. However, black holes in our Universe cannot be stationary or asymptotically flat or in vacuum. We now study black holes in an expanding universe, which are called cosmological black holes. Little is known about the properties of cosmological black holes in contrast to stationary, asymptotically flat and vacuum black holes. In general, it is difficult even to define the notion of black holes in the cosmological context. The notion of future outer trapping horizons probably provides the most general and physical definition of black holes. In our case, we assume a flat Friedmann universe where a black hole is embedded and then define a future event horizon due to the existence of future null infinity.

[1]E-mail:harada@rikkyo.ac.jp

2 Self-similar black holes in a flat Friedmann universe

To study black holes embedded into a flat Friedmann universe, self-similar solutions can play crucial roles [2, 3]. Remember that since the Minkowski spacetime is static, one can have static black holes which are asymptotically flat. Analogously, since the power-law flat Friedmann solution is self-similar, one might have self-similar black holes which are asymptotically Friedmann. Self-similar black holes grow as fast as the Hubble length. We can covariantly define self-similar spacetimes by the existence of homothetic Killing vector. For spherically symmetric spacetimes, this condition results in the following metric form:

$$ds^2 = -e^{2\Phi(z)}dt^2 + e^{2\Psi(z)}dr^2 + r^2S^2(z)(d\theta^2 + \sin^2\theta d\phi^2), \tag{1}$$

where $z = r/t$. A hypersurface on which z =const is called a similarity surface. A null similarity surface is called a similarity horizon. Similarity horizons are analogous to Killing horizons for static spacetimes and can be identified with event horizons. To see the causal structure, we define a velovity function $V \equiv |z|e^{\Psi-\Phi}$. If $(V-1)$ is zero, positive and negative, the similarity surface is null, spacelike and timelike, respectively. The Einstein equation reduces to a set of ordinary differential equations. See Ref. [1] for self-similar solutions in general relativity in more general context.

Since we adopt a perfect fluid with the equation of state $p = (\gamma - 1)\rho$ for $0 < \gamma < 2/3$, we have no critical point in the ordinary differential equations except for $z = \pm 0, \pm\infty$. We need very careful treatment to get the physical insight into the solutions of the ordinary differential equations. All details are described in [4, 5]. In the following we only quote some of the results.

3 Analytical result

There are two exact solutions in this self-similar system. One is the Friedmann solution and the other is the Kantowski-Sachs solution. Although the static solution is possible in the positive pressure case, it is not in the negative pressure case.

Table 1: Asymptotic behaviours. The abbreviations are the following: Q=Quasi, F=Friedmann, S=Static, KS=Kantowski-Sachs, CV=Constant-Velocity, PMS=Positive-Mass Singular, NMS=Negative-Mass Singular

Name	z	#param	Extension	Structure	Distance
F	± 0	1	n/a	Spacelike	∞
QF	± 0	1	n/a	Spacelike	∞
QF	$\pm\infty$	1	n/a	Timelike	0
QS	$\pm\infty$	2	$t = \pm 0$	Spacelike	∞
QKS	$\pm\infty$	2	$r = \pm\infty$	Timelike	Intermediate
CV	$\pm\infty$	1	n/a	Timelike	∞
PMS	z_*	2	n/a	Spacelike	0
NMS	z_*	2	n/a	Timelike	0

We also find various asymptotic behaviours. They are summarised in Table I. Note that, in our coordinates, $z = 0$ and $z = \infty$ correspond to infinity and regular centre for the Friedmann solution, respectively. There are solutions which are asymptotic to the exact solutions. There are also solutions of which the asymptotic form is similar to the exact solutions but the coefficients are different even at the lowest order. We add a term "quasi" to the name of the exact solutions to describe such asymptotic behaviours. Note that asymptotically quasi-static and quasi-Kantowski-Sachs solutions are analytically extendible beyond $z = \pm\infty$.

4 Numerical result

We also integrate the ordinary differential equations numerically. We set the initial condition to be an asymptotically Friedmann form for small z, which are parameterised by one parameter. We numerically integrate the equations and extend it beyond $z = \infty$ into the negative z region if the solution is asymptotically quasi-static or quasi-Kantowski-Sachs.

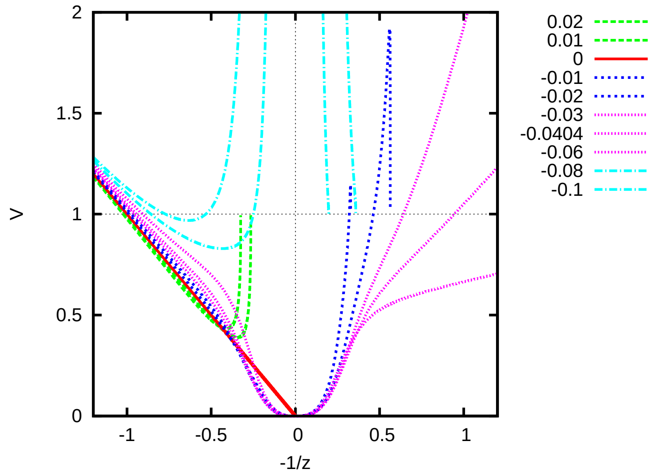

Figure 1: Velocity function. There are shown naked singularity solutions (0.02, 0.01), the flat Friedmann solution (0), black hole solutions (-0.01, -0.02), wormhole solutions (-0.03, -0.0404, -0.06) and white hole solutions (-0.08, -0.1).

Figure 1 shows the behaviours of V for the numerical solutions. The horizontal axis denotes $-1/z$, while the vertical axis denotes V. Each curve is labelled by the value for the parameter. The behaviour of V determines whether a similarity horizon is null, spacelike or timelike. Moreover, to determine the causal structure of the numerical solutions for $z = \pm 0, \pm\infty$, the result of the asymptotic analysis is essentially considered. We have found a variety of solutions, including naked singularities, black holes, wormholes and white holes.

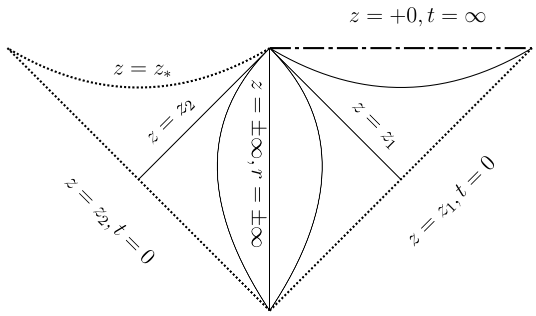

Figure 2: Cosmological black hole solution

Then, we have found interesting solutions, which describes a black hole in an accelerated expanding universe. The Penrose diagram for this solution is shown in Fig. 2. There are a one-parameter family of such solutions, implying that such solutions will not require fine-tuning of the initial data. This result shows that black holes can grow self-similarly in an accelerated expanding universe filled with the present model for dark matter. These solutions are actually parameterised by the physical radius of the black hole event horizon normalised by the Hubble length. It is interesting to note that there is an upper bound $\simeq 0.7$ on this normalised black hole radius.

Table 2: Classification of the numerical solutions. A_0 parameterises asymptotically Friedmann solutions and hence does the numerical solutions obtained here. $\alpha_1 \simeq -0.0253$, $\alpha_2 \simeq -0.0404$, $\alpha_3 \simeq -0.0780$ and $\alpha_4 \simeq -0.108$ for the choice of the gauge constants $a_0 = b_0 = 1$. The abbreviations are SH=similarity horizons and TH=trapping horizons.

A_0	Spacetime	Asymptote	# SH	# TH
	Naked singularity	F-NMS	1	1
0	Friedmann universe	F	1	1
	Black hole	F-QKS-PMS	2	2
α_1	Black hole	F-QKS-PMS	2	1 (d)
	Wormhole	F-QKS-QF	2	0
α_2	Wormhole	F-QKS-F	2	0
	Wormhole	F-QKS-QF	2	0
α_3	–	–	–	–
	White hole	F-QS-PMS	2	0
α_4	White hole	F-QS-PMS	1(d)	0
	White hole	F-QS-PMS	0	0

We have also found a one-parameter family of wormhole solutions. These solutions connect a flat Friedmann universe and a distinct (quasi-) Friedmann universe with a throat of nonzero finite radius. It should be noted that the throat is not traversable, which is consistent with Hayward's theorem on the violation of null energy condition for traversable dynamical wormholes [6]. The numerical solutions are summarised in Table II.

5 Summary

We study self-similar solutions with a perfect fluid with the equation of state $p = (\gamma - 1)\rho$ as a model for dark energy. There are two exact solutions, the flat Friedmann solution and the Kantowski-Sachs solutions. There are eight possible asymptotic behaviours, among which quasi-Kantowski-Sachs and quasi-static solutions are extendible beyond $z = \infty$. We have numerically integrated the field equations from the asymptotically Friedmann solution at very small z. Then, we have found a one-parameter family of black hole solutions, which implies effective accretion onto black holes in the accelerating universe. We have also found naked singularity solutions, wormhole solutions and white hole solutions which all are asymptotically Friedmann at spatial and null infinity. The present suggests that black holes in cosmological models with dark energy can grow as fast as the cosmological horizon. This relates to the issue of whether supermassive black holes in galactic nuclei could be generated by accretion of quintessence onto primordial black holes. See Ref. [4, 5] for details.

References

[1] B. J. Carr and A. A. Coley, Class. Quant. Grav. **16**, R31 (1999).

[2] Y. B. Zeldovich and I. D. Novikov, Sov. Astronomy, **10**, 602 (1967).

[3] B. J. Carr and S. W. Hawking, Mon. Not. R. astr. Soc. **168**, 399 (1974).

[4] T. Harada, H. Maeda and B. J. Carr, Phys. Rev. D**77**, 024022 (2008).

[5] H. Maeda, T. Harada and B. J. Carr, Phys. Rev. D**77**, 024023 (2008).

[6] S. A. Hayward, Int. J. Mod. Phys. D**8**, 373 (1999).

Classical black hole evaporation conjecture and floating black holes

Takahiro Tanaka[1]

Department of Physics, Kyoto University, Kyoto 606-8502, Japan

Abstract

In Randall-Sundrum single-brane (RS-II) model, it was conjectured that there is no static large black hole localized on the brane. The conjecture is based on adS/CFT correspondence. Here we consider the phase diagram of black objects in the models extended from the RS-II model to see if we can falsify this conjecture. We find that there is a scenario for the phase diagram consistent with the classical black hole evaporation conjecture. The proposed scenario indicates the existence of a rich variety of the families of black objects.

1 Introduction

Current candidates for the fundamental theory of particle physics such as string theory or M-theory are all defined as a theory in higher dimension. To obtain an appropriate 4-dimensional effective theory starting with such higher-dimensional models, a certain dimensional reduction needs to be assumed. One well-known scheme of dimensional reduction is the Kaluza-Klein compactification, in which the size of the extra-dimensions is supposed to be very small so as not to excite the modes having momentum in the direction of the extra-dimensions. This scheme seems to work well as a mechanism to shield the effect of extra dimensions. This Kaluza-Klein scheme, however, is not a unique possible scheme for dimensional reduction. Recently, the braneworld scenario has been attracting a lot of attention as an alternative possibility[1]. The essential feature of the braneworld scenario distinct from the ordinary Kaluza-Klein compactification is that the matter fields of the standard model are supposed to be localized on the brane, while the graviton can propagate in a higher-dimensional bulk spacetime. Owing to the assumption that the ordinary matter fields are localized on the brane the braneworld models can be consistent with the particle physics experiments even if the length scale of the extra dimension is not extremely small.

In the course of studies on braneworld, a different type of scenario was proposed by Randall and Sundrum (RS)[2, 3]. In their second model (RS-II), the gravity is effectively localized due to the warped compactification even though the extension of the extra dimension is infinite. So far any results observationally distinguishable from the 4D general relativity have not been reported if the bulk curvature scale is small enough.

However, in RS-II model no stable large black hole solution localized on the brane is known. We proposed a conjecture that such a large localized black hole solution does not exist [4, 5]. Once gravitational collapse occurs on the brane, the collapsed object will form something like a black hole, but the conjecture tells that it should eventually evaporate within the classical dynamics. In the dual CFT picture this evaporation can be interpreted as back-reaction due to the Hawking radiation [6].

2 Can the phase diagram be consistent with classical black hole evaporation?

In the previous studies [8, 9], small black hole solutions localized on the brane have been constructed numerically, but the numerical construction of solutions becomes more and more difficult as the horizon size increases. Our interpretation of this numerical results is that localized black hole solutions exist if and only if their size is small compared with the bulk curvature scale, ℓ.

[1]E-mail:tama@scphys.kyoto-u.ac.jp

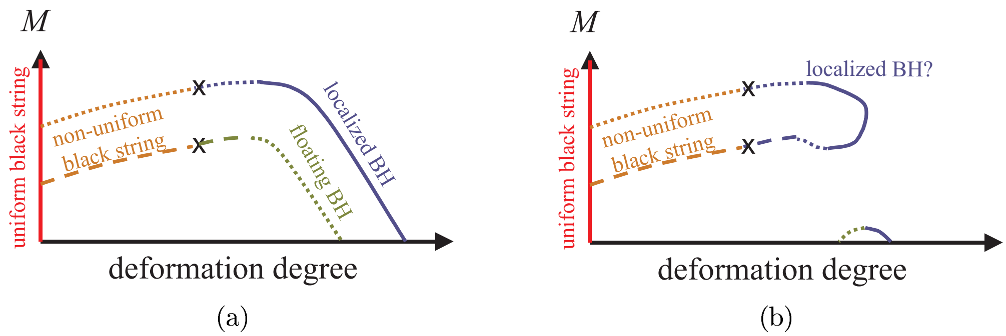

Figure 1: Phase diagram of black objects in the (a) un-warped and (b) warped two-brane models. Dashed curves represent unstable sequences.

The phase diagram of the black objects in RS-II model has not been clarified yet, but the diagram in the usual Kaluza-Klein compactification (un-warped two-brane model) has been established [10, 11, 12]. These two models are continuously connected with each other in the space of model-specifying parameters, the bulk curvature length ℓ and the brane separation d. As we change these parameters, the phase diagram of the black objects will also change continuously. Then, there must be a consistent scenario for the phase diagram in which only small black hole solutions are allowed in the RS-II model. Our basic assumption is that, when the model-specifying parameters are continuously varied, a sequence of solutions should also change continuously. We propose a consistent scenario of the diagram, assuming that the classical black hole evaporation conjecture is correct.

Here we begin with discussing the phase diagram of black objects in two-brane model with un-warped bulk. The phase diagram is summarized in Fig. 1(a). The horizontal axis represents the degree of deformation from the uniform black string. The non-uniform black string branch starts at the GL instability point. At some point, the sequence of non-uniform black string solutions continues to that of localized black hole solutions. In the same plot, we have also shown another curve corresponding to the sequence starting at the second GL instability point. In the un-warped case the black hole on the second branch is floating in the bulk on the black hole branch.

The question is how this diagram is modified once we introduce the warp in the bulk. We point out that the floating black hole in the un-warped case cannot stay apart from the UV brane when ℓ gets smaller. The gravity between the UV (IR) brane, which has positive tension, and a particle floating in the bulk is repulsive (attractive). To have a static configuration, the only way to compensate this repulsive (attractive) force from the UV (IR) brane is the self-gravity caused by the mirror images of the particle on the other side of the branes. However, the attractive self-gravity acceleration is at most inverse of the black hole size. While the repulsive force from the brane is almost constant of $O(\ell^{-1})$ independently of the location of the black hole. Thus a black hole whose size is larger than ℓ cannot float in the bulk and the black hole necessarily touches the UV brane.

If the topology of the phase diagram is preserved, there must be, at least, two black hole solutions localized on the UV brane for a large horizon radius ($\gtrsim \ell$). We think that the co-existence of two branches of localized black holes looks quite unlikely. Our standpoint is to assume that the classical black hole evaporation conjecture is correct. Then, the phase diagram should be modified probably as shown in Fig. 1(b). The absence of a large black hole is explained by the reconnection between two branches.

3 Extension to the detuned brane tension

Our current discussion can be extended to more general cases by considering de-tuned brane tension [13]. First we consider the case that the deviation from the Randall-Sundrum condition is small. We introduce a parameter

$$\delta\sigma \equiv (6/\kappa_5\ell) - \sigma > 0,$$

where σ is the tension of the UV brane. Here we consider the large separation limit ($d \to \infty$) for simplicity. In order to describe the unperturbed solution with a detuned brane, it is convenient to use the coordinates

$$ds^2 = dy^2 + \ell^2 \cosh^2(y/\ell) ds^2_{adS_4},$$

where $ds^2_{adS_4}$ is the metric of four-dimensional anti-de Sitter (adS) space with unit curvature. The brane is on a y =constant surface, and the value of y on the brane, y_b, is determined by the condition $\kappa_5\sigma = -(6/\ell)\tanh(y/\ell)$. The limit corresponding to the RS-II model is obtained by setting $\sigma = 6/\ell$ ($y_b \to -\infty$). When $\delta\sigma$ is small, we have $\delta\sigma \approx (12/\kappa_5\ell)e^{2y_b/\ell}$. The very outstanding feature for $\delta\sigma \neq 0$ is that the warp factor $\ell^2\cosh^2(y/\ell)$ is not monotonic but has a minimum at $y = 0$. When $\delta\sigma$ is sufficiently small, $-y_b$ is very large. Hence, significant deviation from the exact RS limit arises only in the region distant from the UV brane ($y \gtrsim 0$).

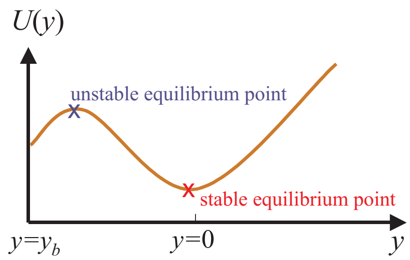

Figure 2: Effective potential for a small particle in the bulk in detuned-tension model with adS brane.

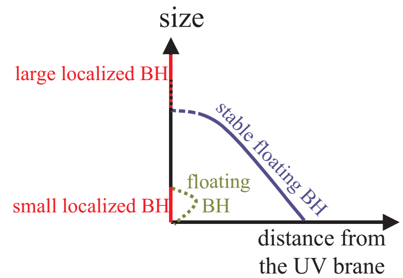

Figure 3: Phase diagram of black objects in detuned-tension model with adS brane.

Let us consider a small black hole floating in the bulk. Since the acceleration of a static test particle is given by $a = (\log\sqrt{g_{00}})_{,y}$, the effective gravitational potential (without self-gravity) becomes $U_{eff} = \log(g_{00}) = \log(\ell\cosh(y/\ell))$. The effective potential after taking into account the self-gravity will be modified as shown in Fig. 2. From this plot, we expect that there are two floating black hole solutions when the size is small. The one close to the UV brane is unstable, while the other close to $y = 0$ is stable. When $\delta\sigma$ is small, the stable floating black hole is very far from the UV brane. In the limit $\delta\sigma \to 0$, this black hole is infinitely far. As a result, this sequence of solutions disappears from the phase diagram of the RS-II model. The distance from the UV brane to the unstable equilibrium point will not be sensitive to the small change of σ. Hence, this branch is smoothly connected to the diagram shown in Fig. 1(b).

In order to draw the phase diagram in the regime $0 < \delta\sigma \ll 1/\kappa_5\ell$, it will be important to know how the branch of stable floating black holes extends to a larger size. It will be easy to imagine that this sequence also touches the UV brane when the area of the five dimensional horizon becomes sufficiently large. Again adS/CFT correspondence provides us with a method for estimating the critical size at which the floating black hole touches the UV brane.

In the asymptotically flat case we cannot construct a static quantum black hole solution due to the quantum back-reaction [14]. In this case the back-reaction is too strong to keep the asymptotic spacetime structure unchanged. However, it is not the case in asymptotically adS spacetime [15, 16]. In asymptotically adS spacetime the temperature of CFT infinitely redshift at infinity. Therefore the back-reaction is effectively shut off at the adS curvature length scale. When the black hole is small, this redshift effect is not significant. But, as the size becomes large, the picture changes dramatically. It is therefore expected that there is a minimum size of large static black holes in adS space. We quote the results from Ref. [15]. Substituting the effective number of species $\approx \ell^2/\kappa_4$ that the dictionary of the adS/CFT correspondence tells, we find that the back reaction becomes important when $M < \sqrt{\ell L}/\kappa_4$. This result suggests that the sequence of four dimensional large localized black holes with a small value of $\delta\sigma$ starts with $\kappa_4 M \approx \sqrt{\ell L}$. Ref. [15] also states that the configuration with $\kappa_4 M \lesssim (\ell^2 L^3)^{1/5}$ is unstable.

In the five dimensional picture the above statement means that the sequence of stable floating black holes should touch the UV brane when the size of the black hole is as large as $\sqrt{\ell L}$. Thus, the phase diagram in this regime will become like Fig. 3.

Let us further reduce the brane tension. When $\sigma \approx 0$, y_b is close to 0. In the most of region in the bulk, the repulsive force from the UV brane is screened by the attractive nature of the bulk negative cosmological constant. As a result, a test particle feels net repulsive force from the brane only in the limited small region near the brane. Thus, only a small black hole which can fit within this tiny region can float in the bulk.

In the limit $\sigma \to 0$ the floating branches are not allowed at all. The size of the horizon measured on the brane at the transition point becomes zero in this limit. As a result, one sequence of black hole solutions localized on the brane remains. In this limit, this sequence of solution is nothing but adS-Schwarzschild solution cut by a tensionless brane placed on the equatorial plane. It is already proven that there is no branching point (= solution with a zero mode) along this sequence [17]. This fact is completely in harmony with our phase diagram. More detailed discussions are found in Ref. [18].

The author thanks R. Emparan, N. Kaloper and N. Tanahashi for valuable conversation. This work is partially supported by Monbukagakusho Grant-in-Aid for Scientific Research Nos. 17340075 and 19540285, and also in part by the 21st Century COE "Center for Diversity and Universality in Physics" at Kyoto university, from the Ministry of Education, Culture, Sports, Science and Technology of Japan.

References

[1] N. Arkani-Hamed, S. Dimopoulos and G. Dvali, Phys. Lett. B **429**, 263 (1998);
I. Antoniadis, N. Arkani-Hamed, S. Dimopoulos and G. Dvali, Phys. Lett. B **436**, 257 (1998).

[2] L. Randall and R. Sundrum, Phys. Rev. Lett. **83**, 3370 (1999).

[3] L. Randall and R. Sundrum, Phys. Rev. Lett. **83**, 4690 (1999).

[4] T. Tanaka, Prog. Theor. Phys. Suppl. **148**, 307 (2003).

[5] R. Emparan, A. Fabbri and N. Kaloper, JHEP **0208**, 043 (2002).

[6] J. M. Maldacena, Adv. Theor. Math. Phys. **2**, 231 (1998) [Int. J. Theor. Phys. **38**, 1113 (1999)].

[7] T. Tanaka, arXiv:gr-qc/0402068.

[8] H. Kudoh, T. Tanaka and T. Nakamura, Phys. Rev. D **68**, 024035 (2003).

[9] H. Kudoh, Prog. Theor. Phys. **110**, 1059 (2004).

[10] E. Sorkin, B. Kol and T. Piran, Phys. Rev. D **69**, 064032 (2004).

[11] B. Kol, Phys. Rept. **422**, 119 (2006).

[12] H. Kudoh and T. Wiseman, Phys. Rev. Lett. **94**, 161102 (2005).

[13] A. Karch and L. Randall, JHEP **0105**, 008 (2001).

[14] A. Fabbri, S. Farese, J. Navarro-Salas, G. J. Olmo and H. Sanchis-Alepuz, Phys. Rev. D **73**, 104023 (2006).

[15] S. W. Hawking and D. N. Page, Commun. Math. Phys. **87**, 577 (1983).

[16] C. Galfard, C. Germani and A. Ishibashi, Phys. Rev. D **73**, 064014 (2006).

[17] H. Kodama, Prog. Theor. Phys. **112**, 249 (2004).

[18] T. Tanaka, arXiv:0709.3674 [gr-qc].

Second-order power spectra of CMB anisotropies due to primordial random perturbations in flat cosmological models

Kenji Tomita[1]

Yukawa Institute for Theoretical Physics, Kyoto University, Kyoto 606–8502, Japan

Abstract

Second-order power spectra of Cosmic Microwave Background (CMB) anisotropies due to random primordial perturbations are studied, based on the relativistic second-order theory of perturbations in flat cosmological models and on the second-order formula of CMB anisotropies. The second-order density perturbations are small, compared with the first-order ones. The second-order power spectra of CMB anisotropies, however, are not small at all, compared with the first-order power spectra, because at the early stage the first-order integrated Sachs-Wolfe effect is very small and the second-order integrated Sachs-Wolfe effect may be dominant over the first-order ones. So their characteristic behaviors may be measured through the future precise observation and bring useful informations on the structure and evolution of our universe in the future.

1 Introduction

In most studies of Cosmic Microwave Background (CMB) anisotropies, the comparison between observed and theoretical quantities have so far been done, assuming the linear approximation for cosmological perturbations. The present state of our universe is, however, locally complicated and associated with nonlinear behavior on various scales, and so the observed quantities of CMB anisotropies may include some effects caused by various primordial perturbations through nonlinear process.

In recent years we studied these nonlinear effects of inhomogeneities on CMB anisotropies, based on the relativistic second-order theory of cosmological perturbations, which we have recently derived[1], and on the second-order formula of CMB anisotropies[2]. We studied the second-order effects of local large-scale inhomogeneities on CMB anisotropies, paying attention to the interaction between them and primordial perturbations[3, 4, 5, 6, 7].

In the present work we study the **nonlinear effect** of only **primordial random perturbations** on CMB anisotropies and derive the power spectra. The second-order density perturbations are small, compared with the first-order ones. The **second-order power spectra of CMB anisotropies, however, are not small at all**, compared with the first-order power spectra, because at the early stage the first-order integrated Sachs-Wolfe effect is very small and **the second-order integrated Sachs-Wolfe effect may be dominant over the first-order ones**. Their characteristic behaviors may be measured through the future precise observation and bring useful informations on the structure and evolution of our universe in the future. In §2, we derive the temperature fluctuations corresponding to simple density perturbations of top-hat type, and show their dependence on Ω_0 and z. In §3, we treat second-order power spectra due to primordial random perturbations.

2 Temperature fluctuations in a simple model of top-hat type

First we consider a first-order spherical density perturbation with the top-hat type and the corresponding second-order perturbation. In this case the potential function F is related to the density perturbation $\delta_1 \rho/\rho$ as $\delta_1 \rho/\rho \propto -\Delta F$, which has the form shown in Fig.1. Here it is assumed that the radius in the perturbed spherical region is much smaller than the cosmic horizon scale and its center is at an epoch with redshift z.

[1] E-mail:tomita@yukawa.kyoto-u.ac.jp

Figure 1: The matter density contrast for a top-hat type spherical lump.

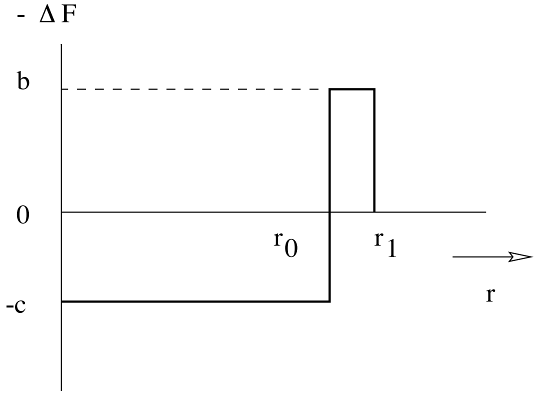

Figure 3: The change in the first-order and second order temperature fluctuations with redshift z for a light path passing through the center in the Λ dominated model. The solid and dotted curves denote 0.05 $(\delta_2\, T/T)_{int}(z)/(\delta_2\, T/T)_{int}(0)$ and $(\delta_1\, T/T)_{int}(z)/(\delta_1\, T/T)_{int}(0)$, respectively.

Figure 2: The change in the first-order and second order temperature fluctuations with Ω_0 for a light path passing through the center in the nonzero-Λ models, where we assume the redshift $z = 0.035$, the density perturbation $\epsilon_{mc} = 0.3$ and $r_0 = 0.1/(a'/a)$, $r_1 = 1.05 r_0$. The solid and dotted curves denote $(\delta_2\, T/T)_{int}(z)$ and $(\delta_1\, T/T)_{int}(z)$, respectively.

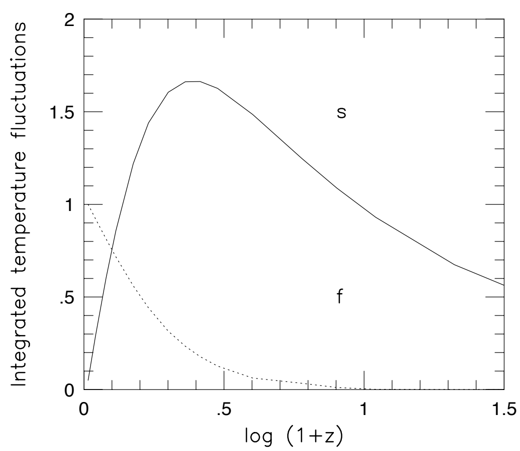

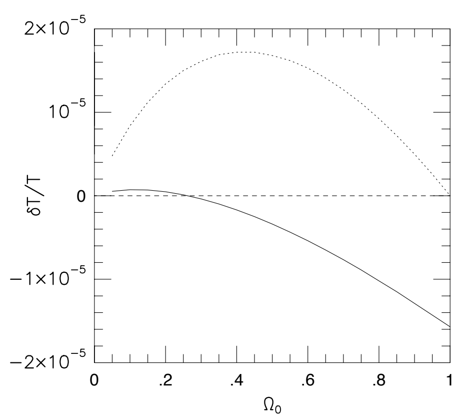

Next we consider first-order and second-order CMB temperature fluctuations caused by the above density perturbations through the Sachs-Wolfe effect, and derive the Ω_0 dependence of the amplitudes of temperature fluctuations at the present epoch (shown in Fig.2). From this you can see that for $\Omega_0 \approx 1$ the first-order temperature fluctuation is nearly zero but the corresponding second-order temperature fluctuation is not small. It should be noticed that the density parameter $\Omega(z)$ at epochs with redshift z increases with z. For $z \gg 1$, $\Omega(z) \approx 1$. The change in the first-order and second-order temperature fluctuations with redshift z are shown in Fig.3. We can see a characteristic peak in the second-order fluctuations, while the first-order fluctuations decrease monotonically with the increase of z. The details are shown in our paper[8]. **So at the early stage with large z, the second-order temperature fluctuation is relatively important, compared with the first-order one.**

3 Second-order power spectra of temperature fluctuations caused by the primordial random density perturbations

We consider primordial scalar perturbations with F defined by

$$F = \int d\mathbf{k}\alpha(\mathbf{k})e^{i\mathbf{kx}}, \tag{1}$$

where the spatial average for $\alpha(\mathbf{k})$ is given by

$$\langle \alpha(\mathbf{k})\alpha(\bar{\mathbf{k}})\rangle = (2\pi)^{-2}\mathcal{P}_F(\mathbf{k})\delta(\mathbf{k}+\bar{\mathbf{k}}), \tag{2}$$

with

$$\mathcal{P}_F(\mathbf{k}) = \mathcal{P}_{F0}k^{-3}(k/k_0)^{n-1}T_s^2(k), \tag{3}$$

where $T_s(k)$ is the matter transfer function and $\mathcal{P}_{F0}$ is the normalization constant.

Then the **first-order temperature perturbations** are

$$\underset{1}{\delta} T/T \equiv \Theta_P = -\frac{1}{2}\int d\mathbf{k}\alpha(\mathbf{k})\int_{\lambda_o}^{\lambda_e} d\lambda P'(\eta)(k\mu)^2 e^{i\mathbf{kx}}, \tag{4}$$

where $P(\eta)$ is the growth factor of density paertubations, $\mathbf{x} = r\mathbf{e}, \mathbf{kx} = kr\mu, \mu \equiv \cos\theta_k$ and θ_k is the angle between the wave vector k^i and a unit vector e^i.

In order to derive the power spectra, we take the statistical average $\langle\rangle$ for the primordial perturbations, and $\langle(\delta T/T)^2\rangle$ is expressed for the first-order anisotropies as

$$\langle(\underset{1}{\delta} T/T)^2\rangle = \langle(\Theta_P)^2\rangle = (T_0)^{-2}\sum_l \frac{2l+1}{4\pi}C_l. \tag{5}$$

The power spectra C_l are

$$C_l = (T_0)^2\int dkk^2\mathcal{P}_F(k)|\mathcal{H}_P^{(l)}(k)|^2, \tag{6}$$

where T_0 is the present CMB temperature and the expressions for $\mathcal{H}_P^{(l)}(k)$ are omitted here.

For the two directions with unit vectores $\mathbf{e}_1$ and $\mathbf{e}_2$, we have the correlation

$$(T_0)^2\langle\Theta_P(\mathbf{e}_1)\Theta_P(\mathbf{e}_2)\rangle = \sum_l \frac{2l+1}{4\pi}C_lP_l(\cos\beta). \tag{7}$$

where the product $\mathbf{e}_1\mathbf{e}_2$ is equal to $\cos\beta$.

For the **second-order temperature anisotropies**, we obtain

$$\begin{aligned}\underset{2}{\delta} T/T \quad &= \quad \int\int d\mathbf{k}d\bar{\mathbf{k}}\alpha(\mathbf{k})\alpha(\bar{\mathbf{k}})\Big\{\frac{1}{8}\int_{\lambda_o}^{\lambda_e}\int_{\lambda_o}^{\lambda_e} d\lambda d\bar{\lambda}P'(\lambda)P'(\bar{\lambda})(k_e\bar{k}_e)^2 e^{i(\mathbf{kx}+\bar{\mathbf{k}}\bar{\mathbf{x}})}\\ &+ \quad \int_{\lambda_o}^{\lambda_e} d\lambda\Big[\frac{1}{8}P'(\lambda)\Big(3k_e\bar{k}_e + 2(k_e)^2 - \frac{1}{2}\mathbf{k}\bar{\mathbf{k}}\Big)\end{aligned}$$

$$
\begin{aligned}
&+ \quad \frac{1}{56} P(\lambda) P'(\lambda) \left(19 k_e \bar{k}_e \mathbf{k}\bar{\mathbf{k}} - 26 (k_e \bar{k}_e)^2 - 3(\mathbf{k}\bar{\mathbf{k}})^2 + 3k^2 (\bar{k})^2\right) \\
&+ \quad \frac{1}{112} Q'(\lambda)(k_e + \bar{k}_e)^2 \left(k^2 \bar{k}^2 - (\mathbf{k}\bar{\mathbf{k}})^2\right)/(\mathbf{k}+\bar{\mathbf{k}})^2 \Big] e^{i(\mathbf{k}+\bar{\mathbf{k}})\mathbf{x}} \\
&+ \quad \frac{1}{4} \int_{\lambda_o}^{\lambda_e} d\lambda \Big[P''(\lambda) \int_{\lambda_o}^{\lambda} d\bar{\lambda} P(\bar{\lambda})(k_e \bar{k}_e)^2 \Big] e^{i(\mathbf{k}\mathbf{x}+\bar{\mathbf{k}}\bar{\mathbf{x}})} \Big\}, \qquad (8)
\end{aligned}
$$

where $k_e = \mathbf{ke}$, $P'(\lambda) \equiv dP(\lambda)/d\lambda$, and $P'(\bar{\lambda}) \equiv dP(\bar{\lambda})/d\bar{\lambda}$. Here temperature fluctuations due to emitter's and observer's motions were neglected, because we pay attentions to the Sachs-Wolfe effect after the recombination epoch. It is found from the above equation that the average $\langle \delta_2 T/T \rangle$ does not vanish in contrast to the vanishing first-order one ($\langle \delta_1 T/T \rangle$).

The total average of $(\delta T/T)^2$ is expressed as

$$
\begin{aligned}
\langle (\delta T/T)^2 \rangle &= \langle (\underset{1}{\delta} T/T)^2 \rangle + (\langle \underset{2}{\delta} T/T \rangle)^2 + \langle (\underset{2}{\delta} T/T - \langle \underset{2}{\delta} T/T \rangle)^2 \rangle \\
&= \langle \Theta_p^2 \rangle + (\langle \underset{2}{\delta} T/T \rangle)^2 + \langle \Theta_{pp}^2 \rangle, \qquad (9)
\end{aligned}
$$

where $\Theta_{pp} \equiv \delta_2 T/T - \langle \delta_2 T/T \rangle$.

Now let us make a reduction of $\langle \Theta_{pp}^2 \rangle$. It is expressed as

$$
\langle \Theta_{pp}^2 \rangle = \langle \Big(\underset{2}{\delta} T/T(\alpha(\mathbf{k})\alpha(\bar{\mathbf{k}})) - \langle \underset{2}{\delta} T/T \rangle \Big) \Big(\underset{2}{\delta} T/T(\alpha(\bar{\bar{\mathbf{k}}})\alpha(\bar{\bar{\bar{\mathbf{k}}}})) - \langle \underset{2}{\delta} T/T \rangle \Big) \rangle, \qquad (10)
$$

where $\delta_2 T/T(\alpha(\mathbf{k})\alpha(\bar{\mathbf{k}}))$ is given by Eq.(8) and $\delta_2 T/T(\alpha(\bar{\bar{\mathbf{k}}})\alpha(\bar{\bar{\bar{\mathbf{k}}}}))$ is obtained from Eq.(8) by replacing $\mathbf{k}, \bar{\mathbf{k}}$ by $\bar{\bar{\mathbf{k}}}$, $\bar{\bar{\bar{\mathbf{k}}}}$.

Then the correlation reduces to

$$
(T_0)^2 \langle \Theta_{pp}(\mathbf{e}_1) \Theta_{pp}(\mathbf{e}_2) \rangle = \sum_n \frac{2n+1}{4\pi} C_n^{(2)} P_n(\cos\beta), \qquad (11)
$$

where

$$
C_n^{(2)} = \frac{4\pi}{2n+1} (T_0)^2 \sum_{l,l'} \Big(B_{ll'}^{I} + B_{ll'}^{II} + B_{ll'}^{III} \Big) b_{ll'n}, \qquad (12)
$$

where the expressions for $B_{ll'}^{I}$, $B_{ll'}^{II}$, $B_{ll'}^{III}$ are shown in a recent paper[9].

The formulas for $\langle \delta_2 T/T \rangle$, $\langle (\Theta_{pp})^2 \rangle$ and $\langle \Theta_{pp}(\mathbf{e}_1) \Theta_{pp}(\mathbf{e}_2) \rangle$ are our new result which will be useful to derive the second-order power spectra.

The author thanks K.T. Inoue for helpful discussions.

References

[1] K. Tomita, Phys. Rev. **D71**, 083504 (2005).

[2] S. Mollerach and S. Matarrese, Phys. Rev. **D56**, 4494 (1997).

[3] K. Tomita, Phys. Rev. **D72**, 043526 (2005).

[4] K. Tomita, Phys. Rev. **D72**, 103506 (2005).

[5] K. Tomita, Phys. Rev. **D73**, 029901(E) (2006).

[6] K.T. Inoue and J. Silk, Astrophys. J. **648**, 23 (2006).

[7] K.T. Inoue and J. Silk, Astrophys. J. **664**, 650 (2007).

[8] K. Tomita and K.T. Inoue, astro-ph/0712.1291.

[9] K. Tomita, astro-ph/0712.2511.

Inclusion of the first-order vector- and tensor-modes in the second-order gauge-invariant cosmological perturbation theory

Kouji Nakamura[1]

Department of Astronomical Science, the Graduate University for Advanced Studies, Mitaka 181-8588, Japan

Abstract

Gauge-invariant treatments of the second-order cosmological perturbation in a four dimensional homogeneous isotropic universe are formulated without any gauge fixing. We have derived the Einstein equations in the case of the single perfect fluid without ignoring any modes. These equations imply that any types of mode-coupling arise due to the second-order effects of the Einstein equations.

The second-order general relativistic cosmological perturbation theory has very wide physical motivation. In particular, the first order approximation of our universe from a homogeneous isotropic one is revealed by the recent observations of Cosmic Microwave Background (CMB) by Wilkinson Microwave Anisotropy Probe[1], which suggests that the fluctuations of our universe are adiabatic and Gaussian at least in the first order approximation. One of the next theoretical researches is to clarify the accuracy of this result through the non-Gaussianity, or non-adiabaticity, and so on. To carry out this, it is necessary to discuss the second-order cosmological perturbations.

However, general relativistic perturbation theory requires delicate treatments of "gauges" and this situation becomes clearer by the general arguments of perturbation theories. Therefore, it is worthwhile to formulate the higher-order gauge-invariant perturbation theory from general point of view. According to this motivation, we proposed the general framework of the second-order gauge-invariant perturbation theory on a generic background spacetime[2]. This general framework was applied to cosmological perturbation theory[3] and all components of the second-order perturbation of the Einstein equation were derived in gauge invariant manner. The derived second-order Einstein equations are quite similar to the equations for the first-order one but there are source terms which consist of the quadratic terms of the linear-order perturbations.

In this article, we show the extension of the formulation in Refs. [3] to include the first-order vector- and tensor-modes in the source terms of the second-order Einstein equation, which were ignored in Refs. [3].

As emphasized in Refs.[2, 3], in any perturbation theory, we always treat two spacetime manifolds. One is a physical spacetime $\mathcal{M}_\lambda$ and the other is the background spacetime $\mathcal{M}_0$. In this article, the background spacetime $\mathcal{M}_0$ is the Friedmann-Robertson-Walker universe filled with a perfect fluid whose metric is given by

$$g_{ab} = a^2(\eta)\left(-(d\eta)_a(d\eta)_b + \gamma_{ij}(dx^i)_a(dx^j)_b\right), \tag{1}$$

where γ_{ij} is the metric on maximally symmetric three space. The physical variable Q on the physical spacetime is pulled back to ${}_{\mathcal{X}}Q$ on the background spacetime by an appropriate gauge choice $\mathcal{X}$ which is an point-identification map from $\mathcal{M}_0$ to $\mathcal{M}_\lambda$. The gauge transformation rules for the pulled-back variable ${}_{\mathcal{X}}Q$, which is expanded as ${}_{\mathcal{X}}Q_\lambda = Q_0 + \lambda {}^{(1)}_{\mathcal{X}}Q + \frac{1}{2}\lambda^2 {}^{(2)}_{\mathcal{X}}Q$, are given by

$${}^{(1)}_{\mathcal{Y}}Q - {}^{(1)}_{\mathcal{X}}Q = \pounds_{\xi_{(1)}}Q_0, \quad {}^{(2)}_{\mathcal{Y}}Q - {}^{(2)}_{\mathcal{X}}Q = 2\pounds_{\xi_{(1)}}{}^{(1)}_{\mathcal{X}}Q + \left\{\pounds_{\xi_{(2)}} + \pounds^2_{\xi_{(1)}}\right\}Q_0, \tag{2}$$

where $\mathcal{X}$ and $\mathcal{Y}$ represent two different gauge choices, $\xi^a_{(1)}$ and $\xi^a_{(2)}$ are generators of the first- and the second-order gauge transformations, respectively. The metric $\bar{g}_{ab}$ on the physical spacetime $\mathcal{M}_\lambda$ is also expanded as $\bar{g}_{ab} = g_{ab} + \lambda h_{ab} + \frac{\lambda^2}{2}l_{ab}$ under a gauge choice. Inspecting gauge transformation rules (2), the first-order metric perturbation h_{ab} is decomposed as $h_{ab} =: \mathcal{H}_{ab} + \pounds_X g_{ab}$, where $\mathcal{H}_{ab}$ and X_a

[1]E-mail:kouchan@th.nao.ac.jp

are transformed as ${}_{\mathcal{Y}}\mathcal{H}_{ab} - {}_{\mathcal{X}}\mathcal{H}_{ab} = 0$, and ${}_{\mathcal{Y}}X_a - {}_{\mathcal{X}}X_a = \xi_{(1)a}$ under the gauge transformation (2), respectively[3]. The gauge invariant part $\mathcal{H}_{ab}$ of h_{ab} is given in the form

$$\mathcal{H}_{ab} = -2a^2 \overset{(1)}{\Phi} (d\eta)_a(d\eta)_b + 2a^2 \overset{(1)}{\nu_i} (d\eta)_{(a}(dx^i)_{b)} + a^2 \left(-2 \overset{(1)}{\Psi} \gamma_{ij} + \overset{(1)}{\chi_{ij}}\right) (dx^i)_a(dx^j)_b, \quad (3)$$

where $D^i \overset{(1)}{\nu_i} = \overset{(1)}{\chi}_{[ij]} = \overset{(1)}{\chi^i}_i = D^i \overset{(1)}{\chi_{ij}} = 0$ and $D^i := \gamma^{ij} D_j$ is the covariant derivative associate with the metric γ_{ij}. In the cosmological perturbations[5], $\{\overset{(1)}{\Phi}, \overset{(1)}{\Psi}\}$, $\overset{(1)}{\nu_i}$, and $\overset{(1)}{\chi_{ij}}$ are called the scalar-, vector-, and tensor-modes, respectively. We have to note that we used the existence of the Green functions $\Delta^{-1} =: (D^iD_i)^{-1}$, $(\Delta + 2K)^{-1}$, and $(\Delta + 3K)^{-1}$ to accomplish the above decomposition of h_{ab}.

As shown in Ref.[2], through the above variables X_a and h_{ab}, the second order metric perturbation l_{ab} is decomposed as $l_{ab} =: \mathcal{L}_{ab} + 2\pounds_X h_{ab} + \left(\pounds_Y - \pounds_X^2\right) g_{ab}$ The variables $\mathcal{L}_{ab}$ and Y^a are the gauge invariant and variant parts of l_{ab}, respectively. The vector field Y_a is transformed as ${}_{\mathcal{Y}}Y_a - {}_{\mathcal{X}}Y_a = \xi^a_{(2)} + [\xi_{(1)}, X]^a$ under the gauge transformations (2). The components of $\mathcal{L}_{ab}$ are given by

$$\mathcal{L}_{ab} = -2a^2 \overset{(2)}{\Phi} (d\eta)_a(d\eta)_b + 2a^2 \overset{(2)}{\nu_i} (d\eta)_{(a}(dx^i)_{b)} + a^2 \left(-2 \overset{(2)}{\Psi} \gamma_{ij} + \overset{(2)}{\chi_{ij}}\right) (dx^i)_a(dx^j)_b, \quad (4)$$

where $D^i \overset{(2)}{\nu_i} = \overset{(2)}{\chi}_{[ij]} = \overset{(2)}{\chi^i}_i = D^i \overset{(2)}{\chi_{ij}} = 0$. As shown in Ref.[2], by using the above variables X_a and Y_a, we can find the gauge invariant variables for the perturbations of an arbitrary field as

$${}^{(1)}\mathcal{Q} := {}^{(1)}Q - \pounds_X Q_0,, \quad {}^{(2)}\mathcal{Q} := {}^{(2)}Q - 2\pounds_X {}^{(1)}Q - \left\{\pounds_Y - \pounds_X^2\right\} Q_0. \quad (5)$$

As the matter contents, in this article, we consider a perfect fluid whose energy-momentum tensor is given by $\bar{T}_a{}^b = (\bar{\epsilon} + \bar{p})\, \bar{u}_a\bar{u}^b + \bar{p}\delta_a{}^b$. We expand these fluid components $\bar{\epsilon}$, $\bar{p}$, and $\bar{u}_a$ as

$$\bar{\epsilon} = \epsilon + \lambda \overset{(1)}{\epsilon} + \frac{1}{2}\lambda^2 \overset{(2)}{\epsilon}, \quad \bar{p} = p + \lambda \overset{(1)}{p} + \frac{1}{2}\lambda^2 \overset{(2)}{p}, \quad \bar{u}_a = u_a + \lambda \overset{(1)}{u}_a + \frac{1}{2}\lambda^2 \overset{(2)}{u}_a\, p. \quad (6)$$

Following the definitions (5), we easily obtain the corresponding gauge invariant variables for these perturbations of the fluid components:

$$\overset{(1)}{\mathcal{E}} := \overset{(1)}{\epsilon} - \pounds_X\epsilon, \quad \overset{(1)}{\mathcal{P}} := \overset{(1)}{p} - \pounds_X p, \quad \overset{(1)}{\mathcal{U}_a} := \overset{(1)}{(u_a)} - \pounds_X u_a, \quad \overset{(2)}{\mathcal{E}} := \overset{(2)}{\epsilon} - 2\pounds_X \overset{(1)}{\epsilon} - \left\{\pounds_Y - \pounds_X^2\right\}\epsilon,$$

$$\overset{(2)}{\mathcal{P}} := \overset{(2)}{p} - 2\pounds_X \overset{(1)}{p} - \left\{\pounds_Y - \pounds_X^2\right\} p, \quad \overset{(2)}{\mathcal{U}_a} := \overset{(2)}{(u_a)} - 2\pounds_X \overset{(1)}{u_a} - \left\{\pounds_Y - \pounds_X^2\right\} u_a.$$

Through $\bar{g}^{ab}\bar{u}_a\bar{u}_b = g^{ab}u_au_b = -1$, the components of $\overset{(1)}{\mathcal{U}_a}$ and $\overset{(2)}{\mathcal{U}_a}$ are given by

$$\overset{(1)}{\mathcal{U}_a} = -a \overset{(1)}{\Phi} (d\eta)_a + a \left(D_i \overset{(1)}{v} + \overset{(1)}{\mathcal{V}_i}\right) (dx^i)_a, \quad \overset{(2)}{\mathcal{U}_a} = \overset{(2)}{\mathcal{U}_\eta} (d\eta)_a + a \left(D_i \overset{(2)}{v} + \overset{(2)}{\mathcal{V}_i}\right) (dx^i)_a, \quad (7)$$

$$\overset{(2)}{\mathcal{U}_\eta} := a \left\{\left(\overset{(1)}{\Phi}\right)^2 - \overset{(2)}{\Phi} - \left(D_i \overset{(1)}{v} + \overset{(1)}{\mathcal{V}_i} - \overset{(1)}{\nu_i}\right)\left(D^i \overset{(1)}{v} + \overset{(1)}{\mathcal{V}^i} - \overset{(1)}{\nu^i}\right)\right\} \quad (8)$$

where $D^i \overset{(1)}{\mathcal{V}_i} = D^i \overset{(2)}{\mathcal{V}_i} = 0$.

We also expand the Einstein tensor as $\bar{G}_a{}^b = G_a{}^b + \lambda {}^{(1)}G_a{}^b + \frac{1}{2}\lambda^2 {}^{(2)}G_a{}^b$. From the decomposition of the first- and the second-order metric perturbation into gauge-invariant parts and gauge-variant parts, each order perturbation of the Einstein tensor is given by

$${}^{(1)}G_a{}^b = {}^{(1)}\mathcal{G}_a{}^b[\mathcal{H}] + \pounds_X G_a{}^b, \quad {}^{(2)}G_a{}^b = {}^{(1)}\mathcal{G}_a{}^b[\mathcal{L}] + {}^{(2)}\mathcal{G}_a{}^b[\mathcal{H},\mathcal{H}] + 2\pounds_X {}^{(1)}G_a{}^b + \left\{\pounds_Y - \pounds_X^2\right\} G_a{}^b \quad (9)$$

as expected from Eqs. (5). Here, ${}^{(1)}\mathcal{G}_a{}^b[\mathcal{H}]$ and ${}^{(1)}\mathcal{G}_a{}^b[\mathcal{L}] + {}^{(2)}\mathcal{G}_a{}^b[\mathcal{H},\mathcal{H}]$ are gauge invariant parts of the first- and the second- order perturbations of the Einstein tensor, respectively. On the other hand, the energy momentum tensor of the perfect fluid is also expanded as $\bar{T}_a{}^b = T_a{}^b + \lambda^{(1)}T_a{}^b + \frac{1}{2}\lambda^{2(2)}T_a{}^b$ and ${}^{(1)}T_a{}^b$ and ${}^{(2)}T_a{}^b$ are also given in the form

$$ {}^{(1)}T_a{}^b = {}^{(1)}\mathcal{T}_a{}^b + \pounds_X T_a{}^b, \quad {}^{(2)}T_a{}^b = {}^{(2)}\mathcal{T}_a{}^b + 2\pounds_X {}^{(1)}T_a{}^b + \left\{\pounds_Y - \pounds_X^2\right\} T_a{}^b \tag{10} $$

through the definitions (7) of the gauge invariant variables of the fluid components. Here, ${}^{(1)}\mathcal{T}_a{}^b$ and ${}^{(2)}\mathcal{T}_a{}^b$ are gauge invariant part of the first- and the second-order perturbations of the energy momentum tensor, respectively. Then, the first- and the second-order perturbations of the Einstein equation are necessarily given in term of gauge invariant variables:

$$ {}^{(1)}\mathcal{G}_a{}^b[\mathcal{H}] = 8\pi G {}^{(1)}\mathcal{T}_a{}^b, \quad {}^{(1)}\mathcal{G}_a{}^b[\mathcal{L}] + {}^{(2)}\mathcal{G}_a{}^b[\mathcal{H},\mathcal{H}] = 8\pi G \ {}^{(2)}\mathcal{T}_a{}^b. \tag{11} $$

In the single perfect fluid case, the traceless scalar part of the spatial component of the first equation in Eq.(11) yields $\overset{(1)}{\Psi} = \overset{(1)}{\Phi}$ due to the absence of the anisotropic stress in the first order perturbation of the energy momentum tensor and the other components of Eq. (11) give well-known equations[5]. We show the expression of the second-order perturbations of the Einstein equation after imposing these first-order perturbations of the Einstein equations. Though we have derived all components of the second equation in Eq. (11), we only show their scalar parts of it for simplicity:

$$ \begin{aligned} 4\pi G a^2 \overset{(2)}{\mathcal{E}} &= \left(-3\mathcal{H}\partial_\eta + \Delta + 3K - 3\mathcal{H}^2\right) \overset{(2)}{\Phi} - \Gamma_0 + \frac{3}{2}\left(\Delta^{-1}D^iD_j\Gamma_i{}^j - \frac{1}{3}\Gamma_k{}^k\right) \\ &\quad - \frac{9}{2}\mathcal{H}\partial_\eta(\Delta+3K)^{-1}\left(\Delta^{-1}D^iD_j\Gamma_i{}^j - \frac{1}{3}\Gamma_k{}^k\right), \end{aligned} \tag{12} $$

$$ \begin{aligned} 8\pi G a^2(\epsilon+p)D_i \overset{(2)}{v} &= -2\partial_\eta D_i \overset{(2)}{\Phi} - 2\mathcal{H}D_i \overset{(2)}{\Phi} + D_i\Delta^{-1}D^k\Gamma_k \\ &\quad - 3\partial_\eta D_i (\Delta+3K)^{-1}\left(\Delta^{-1}D^iD_j\Gamma_i{}^j - \frac{1}{3}\Gamma_k{}^k\right), \end{aligned} \tag{13} $$

$$ \begin{aligned} 4\pi G a^2 \overset{(2)}{\mathcal{P}} &= \left(\partial_\eta^2 + 3\mathcal{H}\partial_\eta - K + 2\partial_\eta\mathcal{H} + \mathcal{H}^2\right) \overset{(2)}{\Phi} - \frac{1}{2}\Delta^{-1}D^iD_j\Gamma_i{}^j \\ &\quad + \frac{3}{2}\left(\partial_\eta^2 + 2\mathcal{H}\partial_\eta\right)(\Delta+3K)^{-1}\left(\Delta^{-1}D^iD_j\Gamma_i{}^j - \frac{1}{3}\Gamma_k{}^k\right), \end{aligned} \tag{14} $$

$$ \overset{(2)}{\Psi} - \overset{(2)}{\Phi} = \frac{3}{2}(\Delta+3K)^{-1}\left(\Delta^{-1}D^iD_j\Gamma_i{}^j - \frac{1}{3}\Gamma_k{}^k\right). \tag{15} $$

where $\mathcal{H} := \partial_\eta a/a$. Γ_0, Γ_i and Γ_{ij} in Eqs. (12)-(15) are defined by

$$ \begin{aligned} \Gamma_0 \;:=\;& +8\pi G a^2(\epsilon+p) D_i \overset{(1)}{v} D^i \overset{(1)}{v} - 3D_k \overset{(1)}{\Phi} D^k \overset{(1)}{\Phi} - 8 \overset{(1)}{\Phi} \Delta \overset{(1)}{\Phi} - 3\left(\partial_\eta \overset{(1)}{\Phi}\right)^2 - 12\left(K+\mathcal{H}^2\right)\left(\overset{(1)}{\Phi}\right)^2 \\ & - 4\left(\partial_\eta D_i \overset{(1)}{\Phi} + \mathcal{H} D_i \overset{(1)}{\Phi}\right) \overset{(1)}{\mathcal{V}^i} - 2\mathcal{H} D_k \overset{(1)}{\Phi} \overset{(1)}{\nu^k} + 8\pi G a^2(\epsilon+p) \overset{(1)}{\mathcal{V}_i}\overset{(1)}{\mathcal{V}^i} + \frac{1}{2} D_k \overset{(1)}{\nu_l} D^{(k} \overset{(1)}{\nu^{l)}} + 3\mathcal{H}^2 \overset{(1)}{\nu^k}\overset{(1)}{\nu_k} \\ & + D_l D_k \overset{(1)}{\Phi} \overset{(1)}{\chi^{lk}} - 2\mathcal{H} D^k \overset{(1)}{\nu^l} \overset{(1)}{\chi_{kl}} - \frac{1}{2} D^k \overset{(1)}{\nu^l} \partial_\eta \overset{(1)}{\chi_{lk}} \\ & + \frac{1}{8}\partial_\eta \overset{(1)}{\chi_{lk}} \partial_\eta \overset{(1)}{\chi^{kl}} + \mathcal{H} \overset{(1)}{\chi_{kl}} \partial_\eta \overset{(1)}{\chi^{lk}} - \frac{1}{8} D_k \overset{(1)}{\chi_{lm}} D^k \overset{(1)}{\chi^{ml}} + \frac{1}{2} D_k \overset{(1)}{\chi_{lm}} D^{[l} \overset{(1)}{\chi^{k]m}} - \frac{1}{2} \overset{(1)}{\chi^{lm}} (\Delta - K) \overset{(1)}{\chi_{lm}}, \\ \Gamma_i \;:=\;& -16\pi G a^2\left(\overset{(1)}{\mathcal{E}} + \overset{(1)}{\mathcal{P}}\right) D_i \overset{(1)}{v} + 12\mathcal{H} \overset{(1)}{\Phi} D_i \overset{(1)}{\Phi} - 4 \overset{(1)}{\Phi} \partial_\eta D_i \overset{(1)}{\Phi} - 4\partial_\eta \overset{(1)}{\Phi} D_i \overset{(1)}{\Phi} \\ & - 16\pi G a^2\left(\overset{(1)}{\mathcal{E}} + \overset{(1)}{\mathcal{P}}\right) \overset{(1)}{\mathcal{V}_i} - 2D^j \overset{(1)}{\Phi} D_i \overset{(1)}{\nu_j} + 2D_iD^j \overset{(1)}{\Phi}\overset{(1)}{\nu_j} + 2\Delta \overset{(1)}{\Phi}\overset{(1)}{\nu_i} + \overset{(1)}{\Phi} \Delta \overset{(1)}{\nu_i} + 2K \overset{(1)}{\Phi}\overset{(1)}{\nu_i} \\ & - 4\mathcal{H} \overset{(1)}{\nu^j} D_i \overset{(1)}{\nu_j} + 2D^j \overset{(1)}{\Phi} \partial_\eta \overset{(1)}{\chi_{ji}} - 2\partial_\eta D^j \overset{(1)}{\Psi}\overset{(1)}{\chi_{ij}} \\ & + 2D_kD_{[i} \overset{(1)}{\nu_{m]}}\overset{(1)}{\chi^{km}} + 2D^{[k} \overset{(1)}{\nu^{j]}} D_j \overset{(1)}{\chi_{ki}} + 2K \overset{(1)}{\nu^j}\overset{(1)}{\chi_{ij}} - \overset{(1)}{\nu^j} \Delta \overset{(1)}{\chi_{ji}} - \frac{1}{2}\partial_\eta \overset{(1)}{\chi^{jk}} D_i \overset{(1)}{\chi_{kj}} + 2 \overset{(1)}{\chi^{kj}} \partial_\eta D_{[j} \overset{(1)}{\chi_{i]k}}, \end{aligned} \tag{16} $$

$$
\begin{aligned}
\Gamma_{ij} \;:=\; & 16\pi G a^2 (\epsilon + p) D_i \overset{(1)}{v} D_j \overset{(1)}{v} - 4 D_i \overset{(1)}{\Phi} D_j \overset{(1)}{\Phi} - 8 \overset{(1)}{\Phi} D_i D_j \overset{(1)}{\Phi} \\
& + \left\{ 6 D_k \overset{(1)}{\Phi} D^k \overset{(1)}{\Phi} + 8 \overset{(1)}{\Phi} \Delta \overset{(1)}{\Phi} + 2 \left(\partial_\eta \overset{(1)}{\Phi} \right)^2 + 16 \mathcal{H} \overset{(1)}{\Phi} \partial_\eta \overset{(1)}{\Phi} + 8 \left(2\partial_\eta \mathcal{H} + K + \mathcal{H}^2 \right) \left(\overset{(1)}{\Phi} \right)^2 \right\} \gamma_{ij} \\
& + 32\pi G a^2 (\epsilon + p) D_{(i} \overset{(1)}{v} \overset{(1)}{\mathcal{V}}_{j)} - 4 \partial_\eta \overset{(1)}{\Phi} D_{(i} \overset{(1)}{\nu}_{j)} + 4 \partial_\eta D_{(i} \overset{(1)}{\Phi} \overset{(1)}{\nu}_{j)} + \left(4 \partial_\eta D_k \overset{(1)}{\Phi} \overset{(1)}{\nu}{}^k + 4 \mathcal{H} D_k \overset{(1)}{\Phi} \overset{(1)}{\nu}{}^k \right) \gamma_{ij} \\
& + 16\pi G a^2 (\epsilon + p) \overset{(1)}{\mathcal{V}}_i \overset{(1)}{\mathcal{V}}_j - 2 \overset{(1)}{\nu}{}^k D_k D_{(i} \overset{(1)}{\nu}_{j)} + 2 \overset{(1)}{\nu}_k D_i D_j \overset{(1)}{\nu}{}^k + D_i \overset{(1)}{\nu}{}^k D_j \overset{(1)}{\nu}_k + D^k \overset{(1)}{\nu}_i D_k \overset{(1)}{\nu}_j \\
& + \left(- D_k \overset{(1)}{\nu}_l D^{[k} \overset{(1)}{\nu}{}^{l]} - D_k \overset{(1)}{\nu}_l D^k \overset{(1)}{\nu}{}^l - 2 \overset{(1)}{\nu}_k \Delta \overset{(1)}{\nu}{}^k - 4 \partial_\eta \mathcal{H} \overset{(1)}{\nu}_k \overset{(1)}{\nu}{}^k + 6 \mathcal{H}^2 \overset{(1)}{\nu}_k \overset{(1)}{\nu}{}^k \right) \gamma_{ij} \\
& - 4 \mathcal{H} \partial_\eta \overset{(1)}{\Phi} \overset{(1)}{\chi}_{ij} - 2 \partial_\eta^2 \overset{(1)}{\Phi} \overset{(1)}{\chi}_{ij} - 4 D^k \overset{(1)}{\Phi} D_{(i} \overset{(1)}{\chi}_{j)k} + 4 D^k \overset{(1)}{\Phi} D_k \overset{(1)}{\chi}_{ij} - 8 K \overset{(1)}{\Phi} \overset{(1)}{\chi}_{ij} + 4 \overset{(1)}{\Phi} \Delta \overset{(1)}{\chi}_{ij} \\
& - 4 D^k D_{(i} \overset{(1)}{\Phi} \overset{(1)}{\chi}_{j)k} + 2 \Delta \overset{(1)}{\Phi} \overset{(1)}{\chi}_{ij} + 2 D_l D_k \overset{(1)}{\Phi} \overset{(1)}{\chi}{}^{lk} \gamma_{ij} \\
& - 2 D^k \overset{(1)}{\nu}_{(i} \partial_\eta \overset{(1)}{\chi}_{j)k} - 2 \overset{(1)}{\nu}{}^k \partial_\eta D_{(i} \overset{(1)}{\chi}_{j)k} + 2 \overset{(1)}{\nu}{}^k \partial_\eta D_k \overset{(1)}{\chi}_{ij} + D^k \overset{(1)}{\nu}{}^l \partial_\eta \overset{(1)}{\chi}_{lk} \gamma_{ij} \\
& + \partial_\eta \overset{(1)}{\chi}_{ik} \partial_\eta \overset{(1)}{\chi}_j{}^k + 2 D_{[l} \overset{(1)}{\chi}_{k]i} D^k \overset{(1)}{\chi}_j{}^l - \frac{1}{2} D_j \overset{(1)}{\chi}_{lk} D_i \overset{(1)}{\chi}{}^{lk} - \overset{(1)}{\chi}{}^{lm} D_i D_j \overset{(1)}{\chi}_{ml} + 2 \overset{(1)}{\chi}{}^{lm} D_l D_{(i} \overset{(1)}{\chi}_{j)m} \\
& - \overset{(1)}{\chi}{}^{lm} D_m D_l \overset{(1)}{\chi}_{ij} + \left(- \frac{3}{4} \partial_\eta \overset{(1)}{\chi}_{lk} \partial_\eta \overset{(1)}{\chi}{}^{kl} + \frac{3}{4} D_k \overset{(1)}{\chi}_{lm} D^k \overset{(1)}{\chi}{}^{ml} - \frac{1}{2} D_k \overset{(1)}{\chi}_{lm} D^l \overset{(1)}{\chi}{}^{mk} + K \overset{(1)}{\chi}_{lm} \overset{(1)}{\chi}{}^{lm} \right) \gamma_{ij},
\end{aligned}
$$

and $\Gamma_i{}^j := \gamma^{jk}\Gamma_{ik}$. These equations (12)-(15) coincide with the equations derived in Refs.[3] except for the definition of the source terms Γ_0, Γ_i, and Γ_{ij}. Further, as shown in Refs.[3], the equations (12) and (15) are reduced to the single equation for $\overset{(2)}{\Phi}$. We also derived the similar equations in the case where the matter content of the universe is a single scalar field[4].

In summary, we have extended our formulation without ignoring the first-order vector- and tensor-modes. As the result, these equations imply that any types of mode-coupling arise due to the second-order effects of the Einstein equations, in principle. In some inflationary scenario, the tensor mode are also generated by the quantum fluctuations. This extension will be useful to clarify the evolution of the second order perturbation in the existence of the first-order tensor-mode. Further, to apply this formulation to clarify the non-linear effects in CMB physics[6], we have to extend our formulation to multi-field system and to the Einstein-Boltzmann system. These extensions will be one of our future works.

References

[1] C.L. Bennett et al., Astrophys. J. Suppl. Ser. **148**, (2003), 1.

[2] K. Nakamura, Prog. Theor. Phys. **110** (2003), 723; K. Nakamura, Prog. Theor. Phys. **113** (2005), 481.

[3] K. Nakamura, Phys. Rev. D **74** (2006), 101301(R); K. Nakamura, Prog. Theor. Phys. **117** (2007), 17.

[4] K. Nakamura, in preparation.

[5] J. M. Bardeen, Phys. Rev. D **22** (1980), 1882; H. Kodama and M. Sasaki, Prog. Theor. Phys. Suppl. No.78, 1 (1984); V. F. Mukhanov, H. A. Feldman and R. H. Brandenberger, Phys. Rep. **215**, 203 (1992).

[6] N. Bartolo, S. Matarrese and A. Riotto, JCAP **0401**, 003 (2004); N. Bartolo, S. Matarrese and A. Riotto, Phys. Rev. Lett. **93** (2004), 231301; N. Bartolo, E. Komatsu, S. Matarrese and A. Riotto, Phys. Rept. **402**, 103 (2004); N. Bartolo, S. Matarrese, and A. Riotto, arXiv:astro-ph/0512481.

CMB Anisotropy Generated by Nonlinear Structures
— Effect of Λ —

Nobuyuki Sakai[1] and Kaiki Taro Inoue[2]

[1]*Department of Education, Yamagata University, Yamagata 990-8560, Japan*
[2]*Department of Science and Engineering, Kinki University, Higashi-Osaka 577-8502, Japan*

Abstract

We study the cosmic microwave background (CMB) anisotropy generated by nonlinear structures in a flat universe with a cosmological constant. We model a spherical compensated void/lump by a family of Lemaitre-Tolman-Bondi spacetimes, and numerically solve the null geodesic equations together with the Einstein equations. We find that voids redshift CMB photons regardless of Ω (or z), while lumps blueshift CMB photons if Ω (or z) is small. Those nonlinear structures could be observed as cold/hot spots in the CMB sky map.

1 Introduction

Recently it has been argued [1, 2] that the anomalies of the cosmic microwave background (CMB) such as octopole planarity and the alignment between quadrupole and octopole components [3], anomalously cold spots on angular scales $\sim 10^\circ$ [4], and asymmetry in the large-angle power between opposite hemispheres [5] could be explained by the Rees-Sciama (RS) effect [6] of nonlinear large-scale structures.

To test such a conjecture, we study the RS effect due to nonlinear structures in a flat universe with a cosmological constant Λ. We model a spherical compensated void/lump by a family of Lemaitre-Tolman-Bondi (LTB) spacetimes, and numerically solve the null geodesic equations together with the Einstein equations. In the literature [7] the CMB signature of voids/lumps has been extensively studied, using LTB spacetimes; however, $\Lambda = 0$ has been assumed in all the papers. In this paper, we consider large voids/lumps ($>$ 100Mpc) in a flat universe with $\Lambda > 0$, as suggested by recent observations.

2 Model and Basic Equations

Consider a family of spherically symmetric spacetimes with dust and a cosmological constant. Their general solutions are represented by the LTB metric,

$$ds^2 = -dt^2 + \frac{R'^2(t,r)}{1+f(r)}dr^2 + R^2(t,r)(d\theta^2 + \sin^2\theta d\varphi^2), \tag{1}$$

which satisfies the Einstein equations,

$$\dot{R}^2 = \frac{2Gm(r)}{R} + \frac{\Lambda}{3}R^2 + f(r), \quad \rho(t,r) = \frac{m'(r)}{4\pi R^2 R'}, \tag{2}$$

where $' \equiv \partial/\partial r$ and $\dot{} \equiv \partial/\partial t$. ρ is energy density of matter, and $m(r)$ and $f(r)$ are arbitrary functions, which should be fixed by initial conditions.

Our model of a void/lump is composed of three regions: the outer flat Friedmann-Robertson-Walker (FRW) spacetime ($r > r_+$), the inner open FRW spacetime ($r < r_-$) and the intermediate shell region ($r_- < r < r_+$). Hereafter we denote quantities in $r > r_+$ and in $r < r_-$ by subscripts + and −,

[1]E-mail:nsakai@e.yamagata-u.ac.jp
[2]E-mail:kinoue@phys.kindai.ac.jp

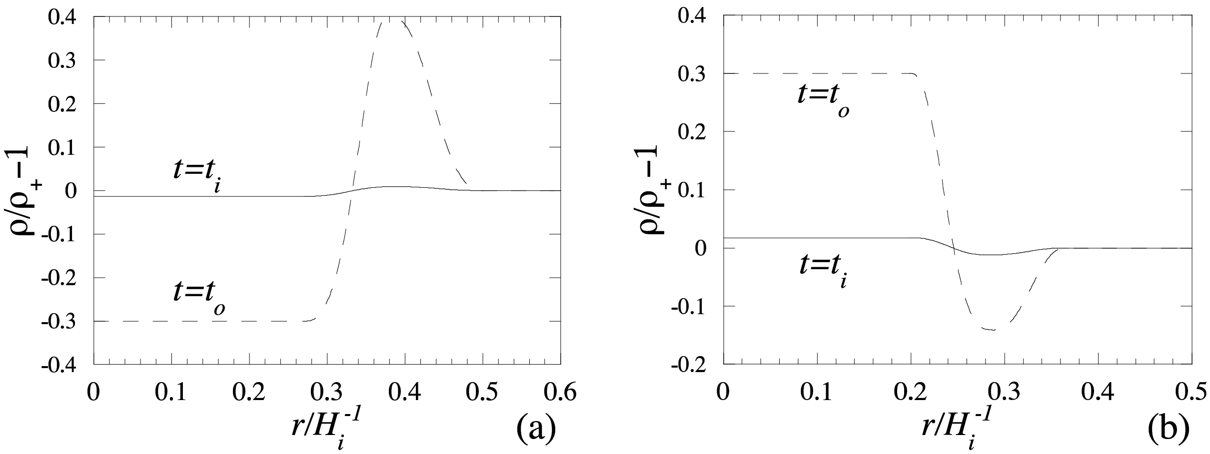

Figure 1: Examples of initial and evolved profiles of $\rho(t,r)$. (a) and (b) represent a void ($\delta < 0$) and a lump ($\delta > 0$), respectively.

respectively. At the initial time $t = t_i$ we give small perturbations on ρ in such a way that $\rho_-(t_i) = \rho_+(t_i)(1+\delta_i)$ with $\delta_i \ll 1$ and in the shell,

$$\rho(t_i, r) = \begin{cases} \rho_- & \text{for} \quad r \le r_-, \\ \dfrac{\rho_c - \rho_-}{16}(3X_-^5 - 10X_-^3 + 15X_- + 8) + \rho_- & \text{for} \quad r_- \le r \le r_c, \\ \dfrac{\rho_+ - \rho_c}{16}(3X_+^5 - 10X_+^3 + 15X_+ + 8) + \rho_c & \text{for} \quad r_c \le r \le r_+, \\ \rho_+ & \text{for} \quad r \ge r_+, \end{cases} \tag{3}$$

$$\text{where} \quad r_c \equiv \frac{r_+ + r_-}{2}, \quad w \equiv \frac{r_+ - r_-}{2}, \quad X_\pm \equiv \frac{r - r_c \mp w/2}{w/2}, \tag{4}$$

and $\rho_c \equiv \rho(r_c)$ is determined by the boundary condition at $r = r_+$. Examples of initial and evolved configurations of $\rho(t,r)$ are shown in Fig. 1.

As for initial values of $H(t,r) \equiv \dot{R}/R$, we assume $H(t_i, r) = H_+(t_i) = H_-(t_i)$. We fix the gauge of the radial coordinate as $r = R(t_i, r)$. In this model there are four dimensionless parameters,

$$\Omega \equiv \frac{8\pi G\rho_+}{3H_+^2}, \quad \delta \equiv \frac{\rho_-}{\rho_+} - 1, \quad \frac{R(r_c)}{H_+^{-1}}, \quad \frac{w}{r_c}, \tag{5}$$

which should be fixed at a certain time.

Let us consider a photon which passes the center, $r = 0$. The geodesic equations with the metric (1) are given by

$$\frac{dt}{d\lambda} = k^t, \quad \frac{dr}{d\lambda} = k^r, \quad k^\theta = k^\varphi = 0, \quad k^r = \epsilon\frac{\sqrt{1+f}}{R'}k^t, \quad \epsilon \equiv \mathrm{sign}\left(\frac{dr}{dt}\right), \tag{6}$$

$$\frac{dk^t}{d\lambda} = -\frac{\dot{g_{rr}}}{2}(k^r)^2, \quad \frac{d}{d\lambda}(g_{rr}k^r) = \frac{{g_{rr}}'}{2}(k^r)^2, \quad g_{rr} \equiv \frac{(R')^2}{1+f} \tag{7}$$

By numerical integration of the null geodesic equations (6) and (7) together with the Einstein equation (2), we evaluate temperature fluctuations,

$$\frac{\Delta T}{T} = \frac{k^t}{k^t_+} - 1, \tag{8}$$

where k^μ_+ is the null vector of another photon which passes the homogeneous region, and given by $k^t_+ \propto 1/a_+$.

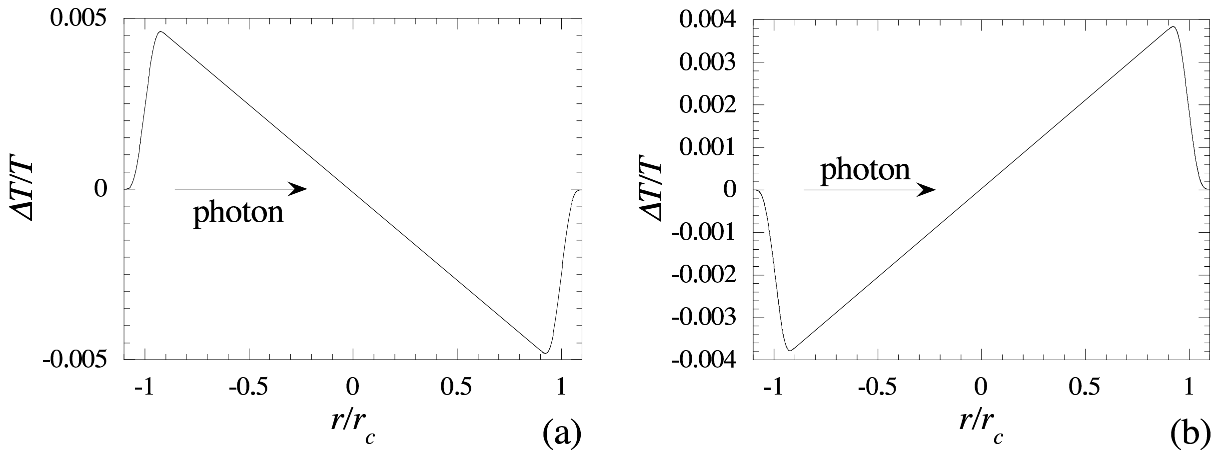

Figure 2: Temperature fluctuations of photons passing through a void (a) and a lump (b). We put $\delta_o = \mp 0.3$, $\Omega_o = 0.24$, $R_o(r_c) = 0.1 H_o^{-1}$ and $w/r_c = 0.1$. The arrow indicates the traveling direction of a photon.

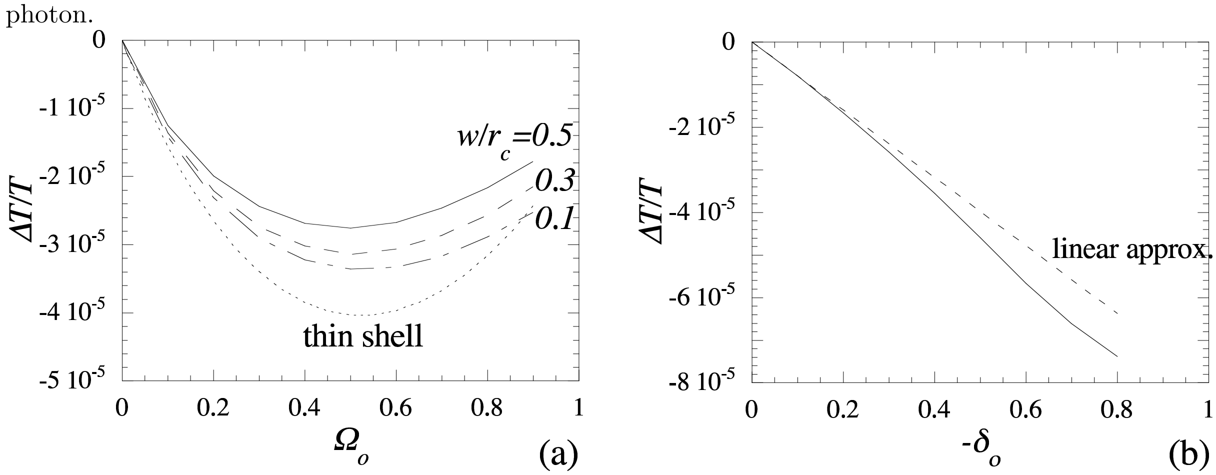

Figure 3: Temperature fluctuations for a large void with $R_o(r_c) = 0.1 H_o^{-1}$. (a) shows $\Delta T/T$ versus Ω_o with $\delta_o = -0.3$. The dotted line indicated by "thin shell" shows $\Delta T/T$ for the thin-shell model [2]. (b) shows $\Delta T/T$ versus δ_o with $\Omega_o = 0.24$ and $w/r_c = 0.3$ The dashed line indicated by "linear approx." shows a linear extrapolation from the values for $|\delta_o| \leq 0.1$.

3 Results and Discussions

Figure 2 shows temperature fluctuations of photons passing through a void/lump. The subscript o denotes quantities at the time t_o when a photon comes out of a void/lump. Although $\Delta T/T$ temporarily becomes $\sim 10^{-3}$, it finally reduces to $\sim 10^{-5}$ because of mass compensation of a void/lump.

In what follows we discuss only the eventual values of $\Delta T/T$ measured outside a void/lump. Figure 3 shows $\Delta T/T$ for a large void. (a) indicates how $\Delta T/T$ depends on Ω_o and the width of the shell w/r_c. We find our result is consistent with that for the thin-shell model [2], and that $\Delta T/T$ decreases as w/r_c increases. (b) shows that the nonlinear effects enhance $\Delta T/T$.

In Fig. 4 we plot $\Delta T/T$ for a large lump. According to Martínez-González and Silk [8], lumps redshift CMB photons in the Einstein-de Sitter universe ($\Omega = 1,\ \Lambda = 0$), just like voids. In contrast, we find in (a) that lumps blueshift CMB photons in low-Ω universes. That is, large lumps at high-z and at low-z have opposite effects on the CMB anisotropy. We also see that our result is consistent with that for the top-hat model calculated by the second-order perturbation [9]. (b) shows that the nonlinear effects reduce $\Delta T/T$, in contrast to those for a void.

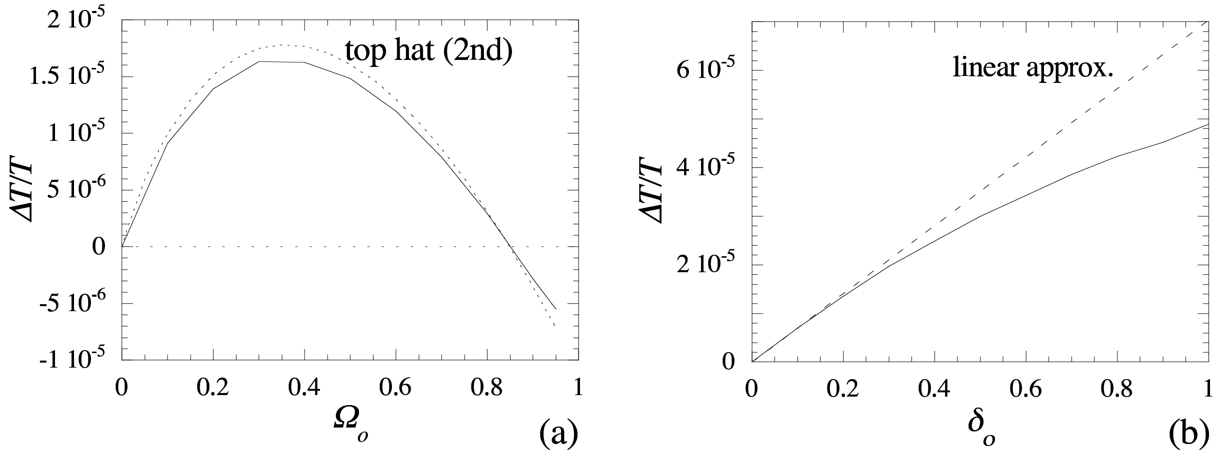

Figure 4: Temperature fluctuations for a large lump. (a) shows $\Delta T/T$ versus Ω_o with $\delta_o = 0.3$, $R_o(r_c) = 0.09H_o^{-1}$ and $w/r_c = 0.1$. The dotted line indicated by "top hat (2nd)" shows $\Delta T/T$ for the top-hat model calculated by the second-order perturbation [9]. (b) shows $\Delta T/T$ versus δ_o with $\Omega_o = 0.24$, $R_o(r_c) = 0.1H_o^{-1}$ and $w/r_c = 0.2$.

Our results indicate that, if quasi-linear ($|\delta| \sim 0.3$) and extra-large ($R \sim 0.1H^{-1}$) voids/lumps exist, they could be observed as cold/hot spots in the CMB sky map. Furthermore, with such observations we could estimate the quantity of dark matter in voids.

Acknowledgements. The numerical computations of this work were carried out at the Yukawa Institute Computer Facility. This work was supported in part by JSPS Grant-in-Aid for Scientific Research (C) No. 18540248 and for Young Scientists (B) No. 17740159.

References

[1] A.Cooray and N. Seto, J. Cosmol. Astropart. CAP, **12**, 004 (2005); K. Tomita, Phys. Rev. D **71**, 083504 (2005); *ibid.* **72**, 043526; *ibid.* **72**, 103506; K.T. Inoue and J. Silk, Astrophys. J. **648**, 23 (2006).

[2] K.T. Inoue and J. Silk, Astrophys. J. **664**, 650 (2007).

[3] M. Tegmark, A. de Oliveira-Costa, and A.J.S. Hamilton, Phys. Rev. D **68**, 123523 (2003); A. de Oliveira-Costa, M. Tegmark, M. Zaldarriaga, and A. Hamilton, *ibid.* **69**, 063516 (2004).

[4] P. Vielva, E. Martínez-González, R.B. Barreiro, J.L. Sanz, and L. Cayon, 2004, Astrophys. J. **609**, 22 (2004); M. Cruz, E. Martínez-González, P. Vielva, and L. Cayon MNRAS **356**, 29 (2005).

[5] H.K. Eriksen, F.K. Hansen, A.J. Banday, K.M. Goński, and P.B. Lilje, Astrophys. J. **605**, 14 (2004); F.K. Hansen, A. Balbi, A.J. Banday, K.M. Goński, MNRAS **354**, 905 (2004).

[6] M.J. Rees and D.W. Sciama, Nature **217**, 511 (1968).

[7] M. Panek, Astrophys. J. **388**, 225 (1992); J.V. Arnau, M.J. Fullana, L. Monreal, and D. Sáez, *ibid.* **402**, 359 (1993); M.J. Fullana, J.V. Arnau, and D. Sáez, MNRAS **280**, 1181 (1996); S.L. Vadas, S. L., *ibid.* **299**, 285 (1998).

[8] E. Martínez-González and J. Silk, MNRAS **247**, 478 (1990).

[9] K. Tomita and K.T. Inoue, arXiv:0712.1291 (astro-ph).

Wave scattering in the black hole magnetosphere

Kohei Onda[1], Eiji Mitsuda[2], and Akira Tomimatsu[3]

Department of Physics, Graduate School of Science, Nagoya University, Nagoya 464–8602, Japan

Abstract

Low-frequency disturbances in a stationary and axisymmetric force-free black hole magnetosphere is studied. We investigate time-dependent axisymmetric linear perturbations on the split-monopole magnetic field around the slowly rotating black hole. Imposing boundary conditions on the event horizon and the outer light surface, we obtain the specific solution representing waves from vertical direction to be scattered and absorbed by the black hole. Then, the global energy transport in this process is investigated.

1 Introduction

The rotating black hole surrounded by a magnetosphere is believed to be an important energy source in astrophysical systems. Blandford & Znajek developed general theory of stationary and axisymmetric black hole magnetospheres in the strong magnetic field limit (so called *force-free* limit). They also demonstrated the possibility that rotational energy of the black hole can be extracted through the electromagnetic process[1]. This Blandford-Znajek effect is believed to be a plausible process for powering jets in active galactic nuclei and gamma-ray bursts.

Though most of foregoing works on this subject were concerned with stationary configurations, recent general relativistic magnetohydrodynamic simulations have been able to remove this restriction. Some works investigated time evolution of a magnetized torus surrounding the Kerr black hole and found the realizable structure of the magnetic field developed by accretion flows (e.g. [2]). Most important results in these simulations is that, in polar regions, the rate-time structure of the magnetic field corresponds to the stationary field found in [1] and these Poynting-dominated jets are consistent with being powered by the Blandford-Znajek effect. In this sense, some perturbation analysis around this stationary configurations would be also important to clarify effects brought by disturbances. Especially, there are important issues such as wave propagation or stability of stationary and axisymmetric configurations.

One can see importance of wave propagation analysis in clarifying the physical differences between magnetohydrodynamic wave modes; the Alfvén mode and the fast magnetosonic mode. In connection with this, Uchida investigated linear perturbations in the force-free, stationary and axisymmetric black hole magnetospheres[3]. He considered the high-frequency limit and derived the local dispersion relations in order to investigate properties of each mode; such as way of wave propagation or possibility of super-radiant scattering. On the other hand, one can also see importance of wave propagation analysis in investigation of the global energy and angular momentum transport in the black hole magnetospheres. This involves wave scattering and is an interesting issue as an extension from the vacuum to the non-vacuum case. The purpose of this paper lies in this direction.

For this purpose, we consider axisymmetric linear perturbations in the typical stationary and axisymmetric force-free black hole magnetosphere. Though the high-frequency limit is crucial for separating perturbations into two modes and for general analysis without detailed knowledge of the unperturbed configurations, we prefer the low-frequency limit. This is because we assume the generation of external disturbances in electromagnetic fields and would like to estimate the energy and angular momentum transport from the large distance to the black hole; this involves knowledge about global evolution of waves and that can not be obtained in the high-frequency limit. Moreover, analysis of low-frequency waves might be important in connection with the eigenvalue problems. Especially, it is known that the kink instability of the magnetic field is a prior non-axisymmetric mode which work on low-frequency

[1]E-mail:nambu@gravity.phys.nagoya-u.ac.jp
[2]E-mail:emitsuda@gravity.phys.nagoya-u.ac.jp
[3]E-mail:atomi@gravity.phys.nagoya-u.ac.jp

waves[4] and it may suppress the Blandford-Znajek mechanism. In this sense, though we only treat axisymmetric waves as a first step, the extension of this work to non-axisymmetric case is also important.

2 Axisymmetric force-free field in the Kerr space-time

The force-free black hole magnetosphere is determined by Maxwell's equations and the force-free conditions;

$$F^{\mu\nu}{}_{;\nu} = 4\pi j^{\mu}, \quad F_{[\mu\nu;\lambda]} = 0, \quad F_{\mu\nu} j^{\nu} = 0. \tag{1}$$

Here, since the gravitational field induced by the electromagnetic field and plasma around the black hole is weak, we assume the background geometry of the magnetosphere is described by the Kerr metric and use the Boyer-Lindquist coordinates. For non-stationary and axisymmetric fields, (1) reduce to the eight equations (B10)–(B17) given in [5] and we follow this notation. These equations determine eight quantities; the toroidal component of the vector potential A_ϕ, the toroidal magnetic field $B_{\rm T}$, the current j^μ and ψ_θ, ψ_r. Measured by a ZAMO, $-\psi_r$, $-\sqrt{\Delta}\psi_\theta$ are r and θ components of the electric field. Here, as usual, $\Delta \equiv r^2 - 2Mr + a^2$, M and a is the mass and specific angular momentum of the black hole.

Especially for stationary fields, the force-free black hole magnetosphere is characterized by two functions of A_ϕ, $\Omega_{\rm F}(A_\phi)$ interpreted as the electromagnetic angular velocity and $B_{\rm T}(A_\phi)$. In the slow rotation limit of the black hole, the split-monopole solution was derived in [1]. We only note here that A_ϕ is given by the form $A_\phi = -C\cos\theta + C\Omega_{\rm F}^2 \mathscr{A}(r)\sin^2\theta\cos\theta + \mathcal{O}(a/M)^4$, where $\mathscr{A}(r)$ is regular on the event horizon and $\Omega_{\rm F}$ is related to the angular velocity of the black hole as $\Omega_{\rm F} = \Omega_{\rm H}/2$. We use this solution as the background fields. The reason for this choice comes from mathematical simplicity. Moreover, recent simulations suggest that this solution is consistent with the simulation in the polar region[2].

In the black hole magnetospheres, unlike in the vacuum case, some singular surfaces of magnetohydrodynamic flows exist. In case of the force-free limit, there are two singular surfaces which are called light surfaces and coincident with the singular surfaces of Alfvén waves. For the split-monopole magnetic field around the slowly rotating black hole, one of them degenerates to the event horizon. The other is in the large distance and defined by $r\Omega_{\rm F}\sin\theta \simeq 1$ (*light cylinder*). In this work, we assume the generation of electromagnetic disturbances outside the light cylinder and treat accretion of low-frequency waves into the black hole. For this purpose, we would set the split-monopole fields as the unperturbed fields because it is valid to the distance well beyond the light cylinder. On the other hand, for perturbed fields, we have to demand the regularity of the fields as the boundary condition on the light cylinder (and on the event horizon). This causes difficulty of global analysis of the black hole magnetospheres.

3 Linear perturbations in force-free black hole magnetospheres

For above eight quantities f, we consider axisymmetric linear perturbations δf on the background split-monopole fields $f_{\rm B}$ as $f = f_{\rm B} + \delta f$ and derive equations for δf. Because we are interested in the disturbances exited within the timescale of rotational period of the black hole, we assume frequency of wave ω as $\omega \lesssim \Omega_{\rm F}(=\Omega_{\rm H}/2)$. To manage the difficulty of the treatment of the light cylinder, we follow the following procedure in the investigation of perturbed fields. To begin with, though we focus on accretion of waves from the large distance toward the black hole, we first solve the perturbation equations around the black hole with the slow rotation approximation of it. In this approximation, we can regard $M\Omega_{\rm F}$ as a small parameter and neglect higher order terms of it. Though, even in this case, $r\Omega_{\rm F}$ could be large in the large distance and this treatment is valid only for $r \ll 1/\Omega_{\rm F}$. Then, we extend these solutions to the larger distance in the flat space-time approximation. This treatment is justified by the fact that the overlap region $M \ll r \ll 1/\Omega_{\rm F}$ exists in this case. This procedure has the advantage that we can separate "effect of the black hole" and "effect of the light cylinder" because we need not care the light cylinder for $r \ll 1/\Omega_{\rm F}$. In this way, we can investigate behavior of waves come from the large distance toward the black hole. In the following, we only show the solution δA_ϕ and omit the other seven quantities. Moreover, by the symmetry, we only consider the region $0 \le \theta < \pi/2$.

3.1 Accretion of waves into the black hole

Now, using the slow rotation approximation, we expand perturbations as $\delta f = \sum_{n=\mathcal{N}}^{\infty}(a/M)^n \delta f_{(n)} e^{-i\omega(t+r_*)}$. Here, r_* is defined by $\mathrm{d}r_*/\mathrm{d}r = (r^2+a^2)/\Delta$ and $\mathcal{N}$ determines the dependence of a/M in the leading order. To begin with, we determine $\mathcal{N}$ for each perturbation. In view of the force-free equations $\delta F_{\mu\nu} j^\nu + F_{\mu\nu}\delta j^\nu = 0$, a natural choice is to follow the background field. As a result, in the determinations of $\mathcal{N}$, we follow the background except for δA_ϕ and choose $\mathcal{N}=2$ for δA_ϕ. Of course this choice is not unique one, this is also favorable for the boundary conditions on the pole $\theta=0$. Then, requiring the ingoing wave condition and the regularity of the electromagnetic fields on the event horizon as the boundary condition, we obtain a solution

$$\delta A_\phi = -2\delta C\left[\Omega_{\mathrm{F}}^2\left(r^2+\frac{4M}{3}r+\frac{28M^2}{9}\right)\sin^2\theta\cos\theta + O(a/M)^3\right]e^{-i\omega(t+r_*)}, \tag{2}$$

where δC is a constant representing the intensity of disturbances and $\delta C/C$ must be small enough to neglect non-linear terms. As mentioned above, this solution is valid only for $r \ll 1/\Omega_{\mathrm{F}}$.

3.2 Wave inflow in the distant region

Now, we consider perturbations in the far region $M \ll r$ with the flat space-time approximation. In this region, we can neglect $\mathscr{A}(r)$ and obtain the single equation for δA_ϕ;

$$\begin{aligned}\left[\varrho^2-\frac{1}{\sin^2\theta}\right]\delta A_{\phi,\varrho\varrho\varrho}-\left[i\sigma\varrho^2-4\varrho+\frac{i\sigma}{\sin^2\theta}\right]\delta A_{\phi,\varrho\varrho}+\left[\sigma^2\varrho^2-4i\sigma\varrho+2-\frac{\sigma^2}{\sin^2\theta}+\hat{L}_2(\theta)-\frac{1}{\varrho^2}\hat{L}_1(\theta)\right]\delta A_{\phi,\varrho}\\ -\left[i\sigma^3\varrho^2+2i\sigma+\frac{i\sigma^3}{\sin^2\theta}+i\sigma\hat{L}_2(\theta)+\left(\frac{i\sigma}{\varrho^2}-\frac{2}{\varrho^3}\right)\hat{L}_1(\theta)\right]\delta A_\phi \simeq 0.\end{aligned} \tag{3}$$

Here, we have defined $\hat{L}_1(\theta) \equiv \csc\theta\partial/\partial\theta\,(\csc\theta\partial/\partial\theta)$, $\hat{L}_2(\theta) \equiv (\partial/\partial\theta + 3\cot\theta)\,(\partial/\partial\theta - 2\cot\theta)$, $\varrho \equiv r\Omega_{\mathrm{F}}$ and $\sigma \equiv \omega/\Omega_F$. Though δA_ϕ has the θ-dependence of $\sin^2\theta\cos\theta$ in the region $\varrho \ll 1$, we can find that some other θ-dependence arises as ϱ glows and the light cylinder becomes a singular surface for this equation. This causes difficulty of analysis in the magnetospheres and we can not assume a specific separation of variables in the distant region any more.

To handle this difficulty, we consider a expansion

$$\delta A_\phi = \sum_{n=1}^{\infty} a_n(\varrho)\sin^{2n}\theta\cos\theta\; e^{-i\omega(t+r)}. \tag{4}$$

Then demanding each coefficient of $\sin^{2l}\theta\cos\theta$ to be zero, (3) reduces to recurrence equations for $a_n(\varrho)$. For example, the relation between $a_1(\varrho)$ and $a_2(\varrho)$ is

$$a_2 = -\frac{1}{8}\varrho^2 a_{1,\varrho\varrho} + \frac{i}{4}\sigma\varrho^2 a_{1,\varrho} + \frac{3}{4}a_1 + \delta C\varrho^2, \tag{5}$$

where we have integrated the equation. Other recurrence equations relate $a_{l+2}(\varrho)$ to $a_{l+1}(\varrho)$ and $a_l(\varrho)$, where l represents positive integers. To solve these equation, we would impose two boundary conditions. Of course, one of them is the matching boundary condition of the solution in the overlap region $M \ll r \ll 1/\Omega_{\mathrm{F}}$. Namely, in this overlap region, we assume $a_{l+1}(\varrho) = \mathcal{O}(\varrho^3)$ and obtain the approximate solution of (5) as $a_1(\varrho) = -2\delta C\varrho^2 + \mathcal{O}(\varrho^3)$ which connects with (2). One the other hand, the other boundary condition should be imposed on the light cylinder. We can show that (3) intrinsically contains solutions which can not pass the light cylinder from the outside of it. Because the light cylinder is the critical surface for ingoing Alfvén waves, these solutions might represent ingoing Alfvén waves and we require the absence of these waves.

In this manner, $a_l(\varrho)$ can be uniquely determined in principle. However, we have no idea to separate out going terms from ingoing ones, we restrict our treatment for low frequency limit $\sigma \ll 1$ in the following. To this end, regarding δA_ϕ as functions of $\sigma\varrho$ and θ, we rewrite (3) with $\sigma\varrho$ and take the limit $\sigma \to 0$

(Though σ is small, we keep $\sigma\varrho$ to treat disturbances in the large distance.). To this end, we obtain the equation of δA_ϕ in this limit;

$$\left[\frac{\partial^2}{\partial\varrho^2}+\frac{2}{\varrho}\frac{\partial}{\partial\varrho}+\sigma^2\left(1-\frac{2i\sigma}{\varrho}\right)+\frac{1}{\varrho^2}\hat{L}_2(\theta)\right]\delta A_\phi=0. \tag{6}$$

Again, if we consider the expansion (4) and impose the boundary conditions we can determine δA_ϕ. Moreover, in this low-frequency limit, we can pick out the pure outgoing wave part $\delta A_\phi^{(out)}$ in it;

$$\delta A_\phi^{(out)}=-\frac{\delta C}{\sigma^2}\left[S(\theta)+\frac{3i}{\sigma\varrho}\sin^2\theta\right]e^{i(\sigma\varrho-\omega t)}, \tag{7}$$

where $S(\theta)\equiv[17\sin^2\theta-8-8\csc^2\theta+(12+8\csc^2\theta)\cos\theta+12\sin^2\theta\log\{(1+\cos\theta)/2\}]/10$. On the other hand, the ingoing wave part $\delta A_\phi^{(in)}$ is more complex and we only derive the approximate form of it for $\sigma\varrho=r\omega\gg1$;

$$\delta A_\phi^{(in)}=-\frac{8i\delta C}{\sigma^2}\left[\sigma\varrho(1-\cos\theta)+\mathcal{O}(\sigma\varrho)^0\right]e^{-i(\sigma\varrho\cos\theta+\omega t)}. \tag{8}$$

As a result our solution represents the scattering of waves coming from vertical directions.

4 Global energy transport

Because we have found the perturbations of the electromagnetic fields $\delta F_{\mu\nu}$, we can investigate the global energy and angular momentum transport. Here, we only show the energy transport. Because the first order energy-momentum tensor vanishes after they have been averaged over periods, we consider the time-averaged second order energy-momentum tensor and introduce the time-averaged conserved energy flux as usual; $\mathscr{E}^\mu=-\left[\delta F^{\lambda\mu}\delta F_{\lambda t}-\delta^\mu{}_t\delta F^{\lambda\tau}\delta F_{\lambda\tau}/4\right]/(4\pi)$. To begin with, we consider the energy inflow in the large distance. Because we know the ingoing wave parts of $\delta F_{\mu\nu}$ for the region $r\gg1/\omega$ (e.g.(8)) and they come from vertical directions, we integrate the energy flux of ingoing wave parts on $z\equiv r\cos\theta=constant$ plane of radius $w\equiv r\sin\theta$ in this region. Then the net energy inflow can be obtained as $E_{(in)}\simeq-2\int2\pi w\mathscr{E}^z_{(in)}dw\simeq4\delta C^2\Omega_{\rm F}^6(r\sin\theta)^4$. Next, let us consider the scattered energy flow. Because the scattered waves propagate along radial dirrections (see (7)), we integrate the energy flux brought by them on the sphere of radius r. Then the net energy outflow can be obtained as $E_{(out)}\simeq2\int_0^{\pi/2}2\pi r^2\sin\theta\mathscr{E}^r_{(out)}d\theta\simeq\delta C^2\Omega_{\rm F}^6/(3\omega^4)$. Finally, the net energy inflow into the black hole is given by $E_{(BH)}\simeq\delta C^2\Omega_{\rm F}^2/3$. Because we have regarded ω and r as $\omega\ll1/\Omega_{\rm F}$ and $r\gg1/\omega$ to derive (8), the relation $E_{(BH)}\ll E_{(out)}\ll E_{(in)}$ must be satisfied. Then most of the energy inflow $E_{(in)}$ is stored in the disc ($\theta=\pi/2$). As a summary, let us pay attention the ratios,

$$E_{(BH)}/E_{(out)}\sim(\omega/\Omega_{\rm F})^4,\quad E_{(BH)}/E_{(in)}\sim(r\Omega_{\rm F}\sin\theta)^{-4},\quad E_{(out)}/E_{(in)}\sim(r\omega\sin\theta)^{-4}. \tag{9}$$

All of them are independent of the mass M. The first ratio is consistent with the well-known result in case of vacuum; higher frequency waves are absorbed by the black hole better than lower ones. Moreover, it shows that the energy given to the black hole is brought by energy inflow beyond the light cylinder radius rather than the black hole radius. This is because, even though waves come from vertical directions far from the black hole, they are scattered by the non-vacuum fields and collimated into radial directions. In fact, the first and second ratios depend on the parameter of the unperturbed fields $\Omega_{\rm F}$. Though, it is interesting that the third ratio does not depend on it.

References

[1] R. D. Blandford and R. L. Znajek, MNRAS, **179**, 433 (1977)

[2] J. C. McKinney, MNRAS, **368**, 1561 (2006)

[3] T. Uchida, MNRAS, **286**, 931 (1997a), MNRAS, **291**, 125 (1997b)

[4] A. Tomimatsu, T. Matsuoka and M. Takahashi, Phys. Rev. D **64**, 123003 (2001)

[5] A. Levinson, ApJ, **608**, 411 (2004)

Stability of global vertex solution in higher-dimensional spacetime

Takashi Torii[1]

[1] *General Education of Science, Osaka Institute of Technology, Omiya, Asahi-ku, Osaka 535-8585*

Abstract

It is well known that higher-dimensional black objects with translational invariance are unstable, which is called Gregory-Laflamme instability. There is a question if this instability is eliminated by adding a scalar hair to the black objects. For the first step, we investigate a regular topological string solution and its stability in the 5-dimensional Einstein-Higgs system. Linear analysis shows that the string solution is stable against non-uniform perturbations.

1 Introduction

In higher-dimensional spacetime there is variety of black objects such as a black string, a black ring, and black branes aside from a black hole. The black string and black branes have translational invariance along one or some spatial direction(s). It is shown that these objects are unstable against the non-uniform perturbation, which is known as Gregory-Laflamme instability[1]. What is their final state? This is a question which attracted much attention in the last decade. Analysis beyond perturbation is necessary to answer this question. The numerical approach is the only method, and static solutions with nontrivial horizon geometry were constructed in 6-dimensional spacetime[2]. They are candidates for the final state. There are, however, other candidates. For instance, the horizon is pinched and continues to shrinks with infinite time[3].

Dynamical stability is the one of the aspects of the system. Thermodynamical stability is another aspect. It was proposed that dynamical stability is strongly related to thermodynamical stability, which is called Gubser-Mitra conjecture[4]. It states that for systems with a translational symmetry and an infinite extent dynamical Gregory-Laflamme instability arises precisely when the system is thermodynamically unstable. There are a lot of examples which support Gubser-Mitra conjecture in vacuum and electro-vacuum systems.

The black object has an event horizon, and we do not know what matters were distributed before the gravitational collapse. It is natural, however, to assume that the initial object has the same translational symmetry as the black objects. Topological defects such as a vertex (sting) and a domain wall are regular objects with the symmetry. Besides, they have the different type of stability, i.e., topological stability. Although perturbative analysis of dynamical stability shows local stability, topological stability indicates global stability in flat spacetime. When gravity is taken into account, global stability is not guaranteed. An event horizon may be formed in the middle of the transition to the "globally stable solution". Then all the energy density may be swallowed into the event horizon, and a vacuum black object remains.

In 4-dimensional spacetime, a static black hole solution with a scalar hair was discovered[5]. It is called a monopole black hole. Although its field configuration of far region is similar to the global monopole, the monopole black hole has an event horizon around the center. In 5-dimensional spacetime, a black string solution with the analogous scalar hair exists. Then what happens if a non-uniform perturbation is added to it? Which win, dynamical instability or topological stability? In this paper we investigate stability of the regular global string solution in 5-dimensional spacetime as the first step, because the above question is almost trivial if the global string is unstable against non-uniform perturbation.

The organization of this paper is as follows. In the next section, we construct the global string solution in 5-dimenion. In Sec. 3, we perform a perturbative analysis and give a result.

[1]E-mail: torii@ge.oit.ac.jp

2 Global String

We consider a real triplet scalar field Φ^a ($a = 1, 2, 3$) which has spontaneously broken internal $O(3)$ symmetry, and minimally couples to gravity. The action is

$$S = \int dx^5 \sqrt{-g} \left[\frac{R}{16\pi G} - \frac{1}{2}\partial_\mu \Phi^a \partial^\mu \Phi^a - \frac{\lambda}{4}(\Phi^a\Phi^a - v^2)^2 \right], \tag{1}$$

where R is the Ricci scalar of 5-dimensional spacetime. λ and v are the self-coupling constant and the vacuum expectation value (VEV) of the scalar field, respectively.

We shall assume that spacetime is static and has translational invariance along one of the spatial direction. The metric form is

$$ds^2 = -f(r)e^{-2\delta(r)}dt^2 + \frac{1}{f(r)}dr^2 + r^2(d\theta^2 + \sin^2\theta d\phi^2) + w(r)dz^2. \tag{2}$$

Basic equations becomes simpler by adopting function $z(r)$ defined by $g_{ww} = e^{z(r)}$. However, since the function $w(r)$ is useful when $g_{zz} \to 0$, we use $w(r)$.

The scalar field is assumed to have unit winding number and so-called hedge-hog configuration,

$$\Phi^a = h(r)\frac{x^a}{r}, \tag{3}$$

where x^a ($a = 1, 2, 3$) are the Cartesian coordinates for the fixed z.

There are two physical parameters λ and v in this system. By scaling the variables as

$$\bar{x}^\mu = v\sqrt{\lambda}x^\mu, \qquad \bar{\Phi}^a = \frac{\Phi}{v}, \tag{4}$$

the action can be rewritten as

$$\bar{S} = \int d^5x\sqrt{-g}\left[\frac{\bar{R}}{16\pi v^2} - \frac{1}{2}\partial_\mu\bar{\Phi}^a\partial^\mu\bar{\Phi}^a - \frac{1}{4}\left(\bar{\Phi}^2 - 1\right)^2\right], \tag{5}$$

In this formula, the coupling constant λ is scaled out. The VEV appears only in the denominator of curvature term and affects the system only when self-gravity is taken into account.

The basic equations are

$$\frac{f'}{r} + \frac{w'f'}{4w} + \frac{w''f}{2w} - \frac{1}{r^2} + \frac{fw'}{rw} + \frac{f}{r^2} - \frac{w'^2 f}{4w^2} = -2\pi v^2(h^2-1)^2 - 4\pi v^2 f h'^2 - \frac{8\pi v^2 h^2}{r^2}, \tag{6}$$

$$\frac{w''}{2w} - \frac{w'^2}{4w^2} + \frac{2\delta'}{r} + \frac{w'\delta'}{2w} = -8\pi v^2 h'^2, \tag{7}$$

$$\frac{1}{r^2}\left(f - 1 + rf' - rf\delta'\right) - \frac{fw'}{2rw} + \frac{w'^2 f}{4w^2} - \frac{w'f'}{2w} + \frac{fw'\delta'}{2w} - \frac{w''f}{2w} = -8\pi v^2\frac{h^2}{r^2}, \tag{8}$$

$$h'f' + h''f - h'f\delta' + \frac{2h'f}{r} - \frac{2h}{r^2} + \frac{h'fw'}{2w} - (h^2-1)h = 0, \tag{9}$$

where a prime denotes a derivative with respect to the radial coordinate. We have omitted the bar of the variables.

Basic equations are solved with suitable boundary conditions. Putting the regularity condition at the axis $r = 0$, we will obtain the self-gravitating global vertex solution. The variables are expanded as

$$f(r) = 1 - \frac{2\pi v^2}{9}(1 + 18{h_1}^2)r^2 + \dots, \qquad w(r) = w_0\left(1 - \frac{4\pi v^2}{9}r^2 + \dots\right),$$

$$\delta(r) = \delta_0 + \frac{\pi v^2}{9}(1 - 18{h_1}^2)r^2 + \dots, \qquad h(r) = h_1 r - \frac{h_1}{10}\left[1 - \frac{2\pi v^2}{9}(7 + 54{h_1}^2)\right]r^3 + \dots.$$

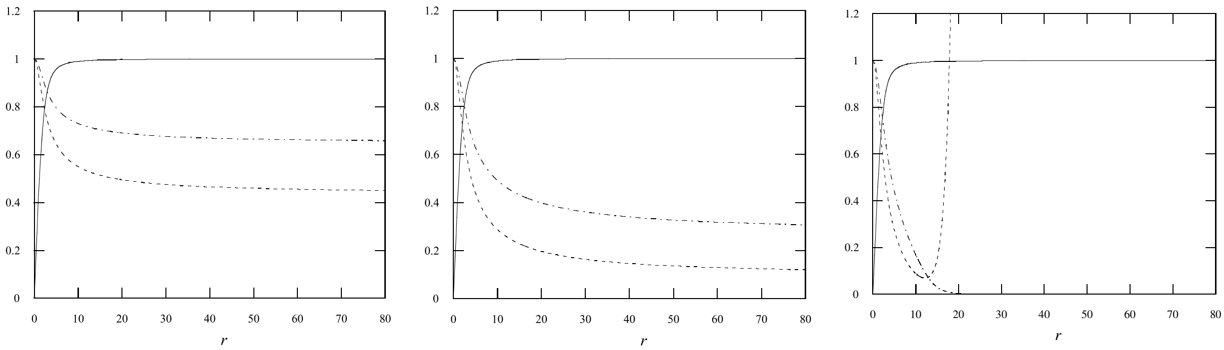

Figure 1: The field configurations of the static global string in 5-dimensional spacetime (left: $v = 0.15$, center: $v = 0.19$, right: $v = 0.20$). The solid, the dashed, and the dot-dashed lines show the field variables h, f, and w, respectively.

δ_0 and w_0 are not determined by the regularity condition. However, we can assume $\delta_0 = 1$ and $w_0 = 1$ without loss of generality because of scaling of the coordinates t and z. Therefore, the free parameter is just h_1.

At infinity $r \to \infty$, the variables are expanded as

$$f(x) = 1 - 8\pi v^2 + f_1 x + \left[\frac{1}{4}w_1^2(1 - 8\pi v^2) - \frac{1}{4}w_1 f_1 - \frac{40}{3}\pi v^2\right]x^2 + \cdots ,$$
$$w(x) = w_\infty\left(1 + w_1 x + \frac{1}{2}w_2 x^2 + \cdots\right), \qquad \delta(x) = \delta_\infty + \frac{w_1}{2}x + \frac{1}{8}(3w_2^2 - 2w_1^2)x^2 + \cdots ,$$
$$h(x) = 1 - x^2 - \frac{3 - 16\pi v^2}{2}x^4 + \cdots .$$

where $x := 1/r$, and

$$w_2 = \left[\frac{1}{8\pi v^2 - 1}\left(\frac{32\pi v^2}{3} + f_1 w_1\right) + w_1^2\right].$$

w_∞ and δ_∞ are determined by solving the basic equations from the axis to infinity. The solution is characterized by the boundary values f_1 and w_1. f_1 corresponds to the mass observed at infinity $r \to \infty$. w_1 has following physical meaning. Since there is the translational invariance along the z axis, the spacetime can be reduced to a 4-dimensional system by Kaluza-Klein dimensional reduction. Then the metric function $w(r)$ becomes a dilaton field. w_1 is related to the scalar charge of this dilaton field.

The first step to obtain the static solution is choosing a value of h_1 at the axis. And secondary, we integrate numerically the basic equations from the axis to $r \to \infty$. The field variables diverge at finite r in the most cases, and hence, the value of h_1 should be tuned to satisfy the boundary condition at infinity by iterative method. In this sense, h_1 is a shooting parameter.

Fig. 1 shows the field configurations of the static global string in 5-dimensional spacetime. For the large VEV ($v \approx 0.20$), the metric function w vanishes and the numerical calculation stops at finite r.

3 Stability analysis

In this section, we analyze stability of the global string solution obtained in the previous section. The metric is perturbed as

$$g_{\mu\nu}(t, x^a) = \bar{g}_{\mu\nu}(x^a) + h_{\mu\nu}(t, x^a), \tag{10}$$

where $\bar{g}_{\mu\nu}(x^a)$ is the static solution and $h_{\mu\nu}(t, x^a)$ is perturbation function. Here, we define a new variable by

$$\psi_{\mu\nu} = h_{\mu\nu} - \frac{1}{2}\bar{g}_{\mu\nu}h, \tag{11}$$

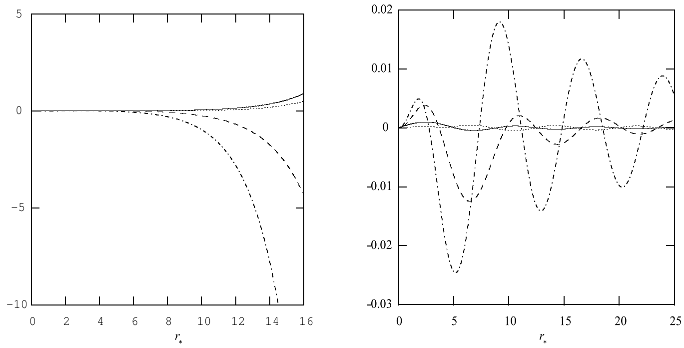

Figure 2: The configuration of the perturbation functions (left: $v = 0.15$, $k = 0.5$, $\sigma = 0$, right: $v = 0.15$, $k = 0.5$, $\sigma = 1.0$). The solid, the dotted, the dashed and the dot-dashed lines show the field variables η, N, L, and z, respectively.

where $h = h_\lambda{}^\lambda$, and adopt the gauge condition $\psi_\mu{}^\lambda{}_{;\lambda} = 0$. The perturbation of the scalar field is

$$\Phi^a(t, x^a) = \bar{\Phi}(x^a) + \delta\Phi^a(t, x^a), \tag{12}$$

where $\bar{\phi}(x^a)$ is the static solution.

We assume that perturbation does not depend on θ and ϕ and adopt the metric perturbation as

$$\psi_{\mu\nu} = e^{i(\sigma t + kw)} \begin{pmatrix} -fe^{-2\delta}N & iS_{tr} & 0 & 0 & S_{tz} \\ iS_{tr} & f^{-1}L & 0 & 0 & iS_{rz} \\ 0 & 0 & r^2T & 0 & 0 \\ 0 & 0 & 0 & r^2T\sin^2\theta & 0 \\ S_{tz} & iS_{rz} & 0 & 0 & wS_{zz} \end{pmatrix}, \tag{13}$$

where the functions N, L, T, S_{tr}, S_{rz}, S_{tz}, S_{zz} are the functions of r. The perturbation of the scalar field is assumed as

$$\delta\Phi^a = \eta(r)\frac{x^a}{r}. \tag{14}$$

The perturbation equations are obtained by substituting these ansätze. They are, however, tedious and we do not show them here explicitly.

The perturbation equations are integrated with the regular boundary condition at the axis. If there are bound states with $\sigma^2 < 0$, the perturbation grows exponentially with time, and the solution is found out to be unstable. By our analysis, however, we cannot find such modes. Configurations of the perturbation functions with $\sigma^2 = 0$ are shown in Fig. 2. In case where unstable modes exist, the perturbation functions with $\sigma^2 = 0$ usually have extremum points and nodes. But we cannot find them in Fig. 2. These facts imply that the static global solutions are stable against the perturbation assumed above. All the details will be reported elsewhere[6].

References

[1] R. Gregory and R. Laflamme, Phys. Rev. Lett. **70**, 2837 (1993); R. Gregory and R. Laflamme, Nucl. Phys. B **428**, 399 (1994).

[2] H. Kudoh and T. Wiseman, Phys. Rev. Lett. **94**, 161102 (2005) [arXiv:hep-th/0409111].

[3] G. T. Horowitz and K. Maeda, "Inhomogeneous near-extremal black branes," Phys. Rev. D **65**, 104028 (2002) [arXiv:hep-th/0201241].

[4] S. S. Gubser and I. Mitra, arXiv:hep-th/0009126; S. S. Gubser and I. Mitra, JHEP **0108**, 018 (2001).

[5] S. L. Liebling, Phys. Rev. D**61**, 024030 (1999).

[6] T. Torii and H. Watabe, in preparation.

Induced Gravity in Deconstructed Space at Finite Temperature
— Self-consistent Einstein Universe —

Nahomi Kan[1] and Kiyoshi Shiraishi[2]

[1] *Yamaguchi Junior College, 1346–2 Daidou, Hofu-shi, Yamaguchi 747–1232, Japan*
[2] *Yamaguchi University, 1677–1 Yoshida, Yamaguchi-shi, Yamaguchi 753–8512, Japan*

Abstract

We study self-consistent cosmological solutions for an Einstein Universe in a graph-based induced gravity model. The graph-based field theory has been proposed by the present authors to generalize dimensional deconstruction. In this paper, we consider self-consistent Einstein equations for a "graph theory space". Especially, we demonstrate specific results for cycle graphs.

1 Pre-history

1.1 Induced Gravity

Induced Gravity or Emergent Gravity has been studied by many authors. The idea of induced gravity is, "Gravity emerges from the quantum effect of matter fields." The one-loop effective action can be expressed as the form:

$$-\frac{1}{2}\int\frac{dt}{t}\sum_i \mathrm{Tr}\exp\left[-(-\nabla^2+M_i^2)t\right]. \tag{1}$$

In curved D-dimensional spacetime, the trace part including the D-dimensional Laplacian becomes

$$\mathrm{Tr}\exp\left[-(-\nabla^2)t\right]=\frac{\sqrt{|\det\ g_{\mu\nu}|}}{(4\pi)^{D/2}}t^{-D/2}(a_0+a_1t+\cdots), \tag{2}$$

where the coefficients depend on the background fields. In four-dimensional spacetime, the coefficients are $a_0=1$ and $a_1=R/6$ for a minimal scalar field, $a_0=-4$ and $a_1=R/3$ for a Dirac field, $a_0=3$ and $a_1=-R/2$ for a massive vector field, where R is the scalar curvature.

In Kaluza-Klein (KK) theories, inducing Einstein-Hilbert term were also studied [1]. In Dimensional Deconstruction (see the next subsection), we also have constructed models of induced gravity based on a graph [2].

1.2 Dimensional Deconstruction

Dimensional Deconstruction (DD) [3] is equivalent to a higher-dimensional theory with discretized extra dimensions at a low energy scale. The Lagrangian density for vector fields is

$$\mathcal{L}=-\frac{1}{2g^2}\sum_{k=1}^{N}\mathrm{tr}F_{\mu\nu k}^2+\sum_{k=1}^{N}\mathrm{tr}\left|D_\mu U_{k,k+1}\right|^2, \tag{3}$$

where $F_k^{\mu\nu}=\partial^\mu A_k^\nu-\partial^\nu A_k^\mu-i[A_k^\mu,A_k^\nu]$ is the field strength of $U(m)_k$ and $\mu,\nu=0,1,2,3$, while g is the gauge coupling constant. We should read $A_{N+k}^\mu=A_k^\mu$, *etc.* $U_{k,k+1}$, called a link field, is transformed as

$$U_{k,k+1}\to L_kU_{k,k+1}L_{k+1}^\dagger\ ,\quad L_k\in U(m)_k, \tag{4}$$

under $U(m)_k$. The covariant derivative is defind as $D^\mu U_{k,k+1}\equiv\partial^\mu U_{k,k+1}-iA_k^\mu U_{k,k+1}+iU_{k,k+1}A_{k+1}^\mu$.

[1] E-mail:kan@yamaguchi-jc.ac.jp
[2] E-mail:shiraish@sci.yamaguchi-u.ac.jp

We may use a "moose" or "quiver" diagram to describe this theory. In such a diagram, gauge groups are represented by open circles, and link fields by single directed lines attached to these circles. Open circles and single directed lines are sometimes called sites and links. The geometry built up from sites, links, and faces is sometimes called "theory space". These geometrical objects are identified as gauge groups, fields and potentials in the action. The moose diagram characterizing the transformation (4) is an N-sided polygon.

We assume that the absolute value of each link field $|U_{k,k+1}|$ has the same value, f. Then $U_{k,k+1}$ is expressed as

$$U_{k,k+1} = f \exp(i\chi_k/f) \ . \tag{5}$$

The $U_{k,k+1}$ kinetic terms go over to a mass-matrix for the gauge fields. The gauge boson $(mass)^2$ matrix for $N = 5$ is

$$g^2 f^2 \begin{pmatrix} 2 & -1 & 0 & 0 & -1 \\ -1 & 2 & -1 & 0 & 0 \\ 0 & -1 & 2 & -1 & 0 \\ 0 & 0 & -1 & 2 & -1 \\ -1 & 0 & 0 & -1 & 2 \end{pmatrix} \ . \tag{6}$$

We obtain the gauge boson mass spectrum:

$$M_p^2 = 4g^2 f^2 \sin^2\left(\frac{\pi p}{N}\right), \qquad p \in \mathbf{Z} \ , \tag{7}$$

by diagonalizing (6).

For $|p| \ll N$, the masses become

$$M_p \simeq \frac{2\pi|p|}{r} \ , \tag{8}$$

where $r \equiv Nb$ and $b \equiv 1/gf$. This is precisely the Kaluza-Klein spectrum for a five-dimensional gauge boson compactified on a circle of circumference r.

1.3 Spectral Graph Theory

In general, the theory space does not necessarily have a continuum limit. Sites can be complicatedly connected by links. Such a connection is a *graph*. We identify the theory space as a graph consisting of vertices and edges, which correspond to sites and links, respectively. Therefore, DD can be generalized to field theory on a graph [4].

A graph G consists of a *vertex* set $V(G) \neq \emptyset$ and an *edge* set $E(G) \subseteq V(G) \times V(G)$, where an edge is an unordered pair of distinct vertices of G. The *degree* of a vertex v, denoted by $deg(v)$, is the number of edges incident with v.

There are various matrices that are naturally associated with a graph. The *graph Laplacian* (or *combinatorical Laplacian*) $\Delta(G)$ is defined by

$$(\Delta)_{vv'} = \begin{cases} deg(v) & \text{if } v = v' \\ -1 & \text{if } v \text{ is adjacent to } v' \\ 0 & \text{otherwise} \end{cases} \ . \tag{9}$$

For example, we consider a *cycle* graph, which is equivalent to a moose diagram. The cycle graph with p vertices is denoted by C_p. For C_5, the Laplacian matrix takes the form:

$$\Delta(C_5) = \begin{pmatrix} 2 & -1 & 0 & 0 & -1 \\ -1 & 2 & -1 & 0 & 0 \\ 0 & -1 & 2 & -1 & 0 \\ 0 & 0 & -1 & 2 & -1 \\ -1 & 0 & 0 & -1 & 2 \end{pmatrix} \ . \tag{10}$$

Up to the dimensionful coefficient $g^2 f^2$, this matrix is identified with the gauge boson $(mass)^2$ matrix (6). We find, indeed, any theory space can be associated with the graph and the $(mass)^2$ matrix for a field on a graph can be expressed by the graph Laplacian owing to the Green's theorem for a graph.

2 Our story thus far

We have constructed models of induced gravity by using several graphs [2]. With the help of knowledge of spectral graph theory, we can easily find that the UV divergent terms concern the graph Laplacian in DD or theory on a graph. Therefore, the UV divergences can be controlled by the graph Laplacian and we can construct the models of one-loop finite induced gravity from a graph.

In the model [2], the one-loop finite Newton's constant is induced and the positive-definite cosmological constant can also be obtained.

3 Self-consistent Einstein Universe ($T \times S^3$)

The metric of the static Einstein Universe [5][6] is given by

$$ds^2 = -dt^2 + a^2 \left[d\chi^2 + \sin^2 \chi (d\theta^2 + \sin^2 \theta d\phi^2) \right], \tag{11}$$

where a is the scale factor and $0 \le \chi \le \pi$, $0 \le \theta \le \pi$ and $0 \le \phi \le 2\pi$. At finite temperature T, the one-loop effective action is regarded as free energy $F(a, \beta)$ and the Einstein equation becomes

$$\frac{\partial(\beta F)}{\partial \beta} = \frac{\partial(\beta F)}{\partial a} = 0, \tag{12}$$

where $\beta \equiv 1/T$. In this paper, we study self-consistent Einstein Universe in theory on a graph. In our models, four-dimensional fields are on cycle graphs. The first model is that scalar fields are on 8 $C_{N/2}$, $U(1)$ vector fields on 4 C_N and Dirac fermions on 2 $C_{N/2}$ + 3 C_N. The second model is that scalar fields are on 16 $C_{N/4}$ + 2 $C_{N/2}$, vector fields on 5 C_N and Dirac fermions on 4 $C_{N/4}$ + 3 C_N + 2 $C_{N/2}$. In each model, Newton's constant and the cosmological constant are calculable and are not given by hand.

4 Results

We exhibit βF for the first model in Fig. 1 and for the second in Fig. 2, for large N. The horizontal axis indicates the scale factor a, while the vertical one indicates the inverse of temperature T. The scale of each axis is in the unit of N/f. In the first model, the cosmological constant is zero and the solution can be found at the maximum of βF, corresponding to be in Casimir regime [5]. In the second model, the solution in Casimir regime and the solution in Planck regime [5] are found.

5 Summary and Prospects

We have studied self-consistent Einstein Universe in the graph theory space. The solutions can be systematically obtained with the help of the graph structure.

As the future works, we should investigate the possibility of obtaining the small cosmological constant and the large Plank scale in a model that scalar fields are on 4 $G_{(1)}$, vector fields on 4 $G_{(2)}$ and Dirac fermions on $G_{(1)}$ + 3 $G_{(2)}$, while $\#V(G_{(1)}) = \#V(G_{(2)})$. We also should investigate the model with the time-dependent scale factor, $a(t)$.

In the present analysis, we have constructed models by using cycle graphs, but we are also interested in the model of general graphs. For a k-regular graph, the trace formula [7] is useful if we have a single mass scale. Field theory on *weighted* graphs, which might correspond to warped spaces in the continuous limit or not, is also interesting. A quasi-continuous mass spectrum is conceivable and dynamics of graphs such as Hosotani mechanism is also thinkable.

We expect that the knowledge of spectral graph theory produces useful results on deconstructed theories and open up another possibilities of gravity models.

Acknowledgements

I would like to thank T. Hanada for useful comments, and also the organizers of JGRG17.

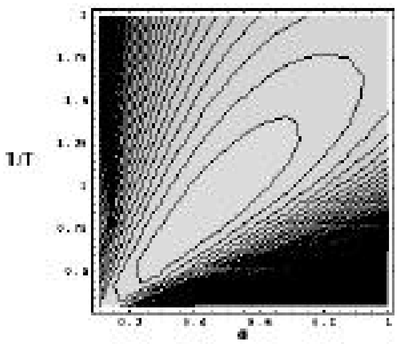

Figure 1: A contour plot of βF in the first model, in which scalars on 8 $C_{N/2}$, vectors on 4 C_N and Dirac fermions on 2 $C_{N/2}$+ 3 C_N. A solution of the Einstein equation can be found at the maximum point.

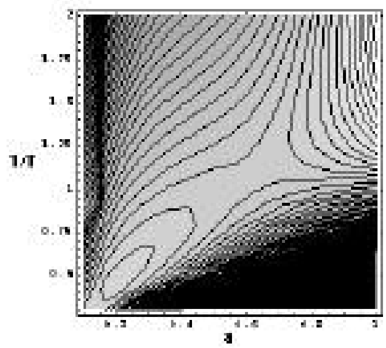

Figure 2: A contour plot of βF in the second model, in which scalars on 16 $C_{N/4}$+2 $C_{N/2}$, vectors on $5C_N$ and Dirac fermions on 4 $C_{N/4} + 3C_N + 2\,C_{N/2}$. Two solutions of the Einstein equation can be found at the maximum and at the saddle point.

References

[1] D. J. Toms, Phys. Lett. **B129** (1983) 31.

[2] Nahomi Kan and Kiyoshi Shiraishi, Prog. Theor. Phys. **111** (2004) 745.

[3] N. Arkani-Hamed, A. G. Cohen and H. Georgi, Phys. Rev. Lett. **86** (2001) 4757; C. T. Hill, S. Pokorski and J. Wang, Phys. Rev. **D64** (2001) 105005.

[4] Nahomi Kan and Kiyoshi Shiraishi, J. Math. Phys. **46** (2005) 112301.

[5] M. B. Altaie and J. S. Dowker, Phys. Rev. **D18** (1978) 3557; M. B. Altaie, Phys. Rev. **D65** (2001) 044028; M. B. Altaie, Class. Quantum Grav. **20** (2003) 331; M. B. Altaie and M. R. Setare, Phys. Rev. **D67** (2003) 044018; T. Inagaki, K. Ishikawa and T. Muta, Prog. Theor. Phys. **96** (1996) 847.

[6] J. S. Dowker, Phys. Rev. **D29** (1984) 2773; J. S. Dowker, Class. Quantum Grav. **1** (1984) 359; J. S. Dowker and I. H. Jermyn, Class. Quantum Grav. **7** (1990) 965; I. H. Jermyn, Phys. Rev. **D45** (1992) 3678.

[7] V. Ejov et al., J. Math. Anal. Appl. **333** (2007) 236; P. Mnev, Commun. Math. Phys. **274** (2007) 233.

Normal Modes of Scalar Fields in BTZ Black Hole Spacetime

Maiko Kuwata[1], Masakatsu Kenmoku [2] and Kazuyasu Shigemoto[3]

[1,2] *Department of Physics, Nara Women's University, Nara 630–8506, Japan*
[3] *Tezukayama University, Nara 631–8501, Japan*

Abstract

Study of BTZ black hole spacetime becomes important and interesting recently. We obtained all the normal models and eigenfunctions for the scalar fields in (2+1) BTZ black hole spacetime. We impose Dirichlet boundary condition at infinity and Dirichlet or Neumann boundary condition at horizon. We studied the effect by negative cosmological constant and the effects by rotation extensively.

1 Scalar field in BTZ spacetime

This section is preparation of definitions and notations in the following sections. For the negative cosmological constant ($\Lambda = -1/\ell^2$) in (2+1) dimension, the Black Hole metric is obtained by Banados, Teitelboim and Zanelli (BTZ) [1]:

$$\begin{aligned} ds^2 &= g_{tt}dt^2 + g_{\phi\phi}d\phi^2 + 2g_{t\phi}dtd\phi + g_{rr}dr^2 \\ g_{tt} &= M - \frac{r^2}{\ell^2}\ , \ \ g_{t\phi} = -\frac{J}{2}\ , \ \ g_{\phi\phi} = r^2\ , \ \ g_{rr} = \left(-M + \frac{J^2}{4r^2} + \frac{r^2}{\ell^2}\right)^{-1}\ , \end{aligned}$$

where M and J are mass and angular momentum of black hole respectively. Outside and inside horizon are defined by:

$$r_\pm^2 = \frac{M\ell^2}{2}\left(1 \pm \sqrt{1 - \frac{J^2}{M^2\ell^2}}\right)\ . \tag{1}$$

The action of complex scalar field $\Phi(x)$ of mass μ is

$$I_{\mathsf{scalar}} = -\int dtdrd\phi(-g)^{1/2}(g^{\mu\nu}\partial_\mu\Phi^*(x)\partial_\nu\Phi(x) + \frac{\mu}{\ell^2}\Phi^*(x)\Phi(x))\ . \tag{2}$$

The scalar field is written in the form of separation of variables $\Phi = \mathrm{e}^{-\mathrm{i}\omega t + \mathrm{i}m\phi}R(r)$ with frequency ω and azimuthal angular momentum m. Then the equation for radial wave function $R(z)$ is obtained :

$$\left(g_{rr}\left(\omega - \frac{J}{2r^2}m\right)^2 - \frac{m^2}{r^2} + \frac{1}{r}\partial_r\frac{r}{g_{rr}}\partial_r - \frac{\mu}{\ell^2}\right)R(r) = 0\ . \tag{3}$$

Introducing variable $z = (r^2 - r_+^2)/(r^2 - r_-^2)$ and function $F(z) = z^{i\alpha}(1-z)^{-\beta}R(z)$, the Hypergeometric differential equation is obtained :

$$z(1-z)\frac{\mathrm{d}^2F}{\mathrm{d}z^2} + (c - (1+a+b)z)\frac{\mathrm{d}F}{\mathrm{d}z} - abF = 0\ . \tag{4}$$

The parameters a, b, c are defined :

$$a = \beta - i\frac{\ell^2}{2(r_+ + r_-)}\left(\omega + \frac{m}{\ell}\right)\ , \ b = \beta - i\frac{\ell^2}{2(r_+ - r_-)}\left(\omega - \frac{m}{\ell}\right)\ , \ c = 1 - 2i\alpha\ , \tag{5}$$

[1] kuwata@asuka.phys.nara-wu.ac.jp
[2] kenmoku@asuka.phys.nara-wu.ac.jp
[3] shigemot@tezukayama-u.ac.jp

$$\alpha = \frac{\ell^2 r_+}{2(r_+^2 - r_-^2)}(\omega - \Omega_{\mathsf{H}} m) \ , \quad \beta = \frac{1-(1+\mu)^{1/2}}{2} \ , \tag{6}$$

where $\Omega_{\mathsf{H}} = J/2r_+^2$ is angular velocity at horizon. General solution of Hypergeometric differential equation is expressed by linear combination of two independent solutions at horizon or infinity.

2 Eigenstate problem of scalar field

We set up Dirichlet boundary condition of eigenstate problem for normal modes at infinity because BTZ solution is asymptotic AdS spacetime:

$$R_\infty = \frac{z^{-i\alpha}(1-z)^{\beta}(1-z)^{c-a-b}}{\Gamma(c-a-b+1)} F(c-a, c-b, c-a-b+1; 1-z) \ . \tag{7}$$

This solution is also expressed near horizon as outgoing wave and incoming wave to black hole as:

$$R_\infty \ = \ \frac{\Gamma(1-c)}{\Gamma(1-a)\Gamma(1-b)} R_{r_+,\mathsf{in}} + \frac{\Gamma(c-1)}{\Gamma(c-a)\Gamma(c-b)} R_{r_+,\mathsf{out}} \ .$$

where ingoing wave is expressed: $R_{r_+,\mathsf{in}} = z^{-i\alpha}(1-z)^{\beta} F(a,b,c;z)$ and outgoing wave is $R_{r_+,\mathsf{out}} = z^{i\alpha}(1-z)^{\beta} F(1+b-c, 1+a-c, 2-c; z)$. Eigenvalue equations for normal modes are obtained for each boundary condition:

(i) Eigenvalue equation for Dirichlet boundary condition:

$$(\omega - \Omega_{\mathsf{H}} m) r_{*,\mathsf{H}} + \gamma_0(\omega) = -\pi \left(n + \frac{1}{2} \right) \quad \text{for} \quad n = 0, 1, 2, \cdots \ , \tag{8}$$

(ii) Eigenvalue equation for Neumann boundary condition:

$$(\omega - \Omega_{\mathsf{H}} m) r_{*,\mathsf{H}} + \gamma_0(\omega) = -\pi n \quad \text{for} \quad n = 0, 1, 2, \cdots \ , \tag{9}$$

where the phase function $\gamma_0(\omega)$ is defined :

$$\gamma_0(\omega) = \frac{\ell^2 r_+(\omega - \Omega_{\mathsf{H}} m)}{2(r_+^2 - r_-^2)} \log \left(\frac{4r_+^2}{r_+^2 - r_-^2} \right) + \arg \left(\frac{\Gamma(c-1)}{\Gamma(c-a)\Gamma(c-b)} \right) \ . \tag{10}$$

The number n labels each quantum state and the horizon expressed by tortoise coordinate with regularlization parameter ϵ is: $r_{*,\mathsf{H}} \simeq \ell^2 r_+ \log(\epsilon/2r_+)/2(r_+^2 - r_-^2)$.

Square of absolute value of eigenfunction at horizon with respect to frequency ω is shown in Figure 1, where the zeros correspond to normal frequencies ω for Dirichlet boundary condition. In this report, only Dirichlet boundary condition is considered. Square of absolute values of eigenfunction with respect to radial coordinate r for lowest two state $(n = 0, 1)$ are shown in Fig. 2. The sets of eigenvalue (ω, m) for each fixed n in case without rotation $(J = 0)$ form convex curves due to the negative cosmological constant effects shown in left hand side of Fig. 3. Curves become flat for the case that ℓ is set to larger value 2ℓ and M to $4M$ shown in the right hand side of Fig. 3. The rotation effects to the eigenvalue $(\omega,\ m)$ are shown in Fig. 4. Eigenvalues $(\omega,\ m)$ rotate corresponding to the angler velocity Ω_{H} for the cases of $J = 0.2$ (Fig. 4) compared with the cases of $J = 0$ (Fig. 3).

3 Summary

(1) The set of eigenvalues (ω, m) forms curved lines in (ω, m) plane for fixed n. The coefficient to ω is invariant but the coefficient to m decrease as $1/\lambda$ in parameters a, b and c under the scalar transformation : $\ell \to \lambda\ell, \quad M \to \lambda^2 M, \quad (0 \le \lambda)$. Therefore the slope of eigenvalue becomes more flat for more small cosmological constant $(\ell \to \lambda\ell)$.

(2) Eigenvalues (ω, m) rotate corresponding to the angular velocity Ω_{H}. Then the allowed region of $0 < \omega$ for $J = 0$ becomes $0 < \omega - \Omega_{\mathsf{H}} m$ for $J \neq 0$.

The eignvalues for normal modes relate the super-radiant problem [2, 3] and statistical mechanics of scalar fields around BTZ black hole [4].

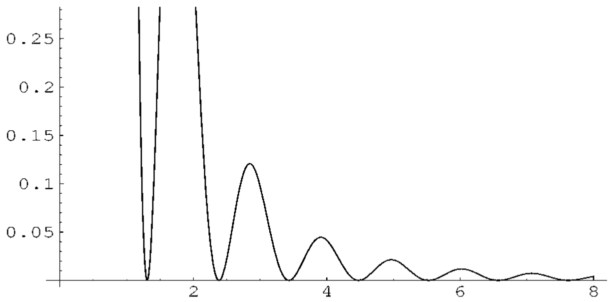

Figure 1: Square of absolute value of eigenfunction with frequency

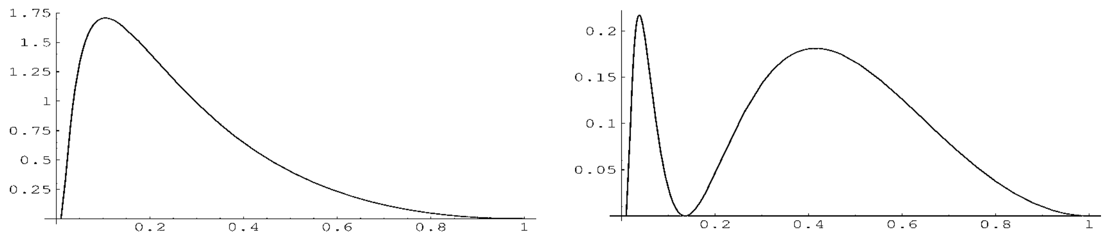

Figure 2: Square of absolute value of eigenfunctions with radial coordinate for n=0,1

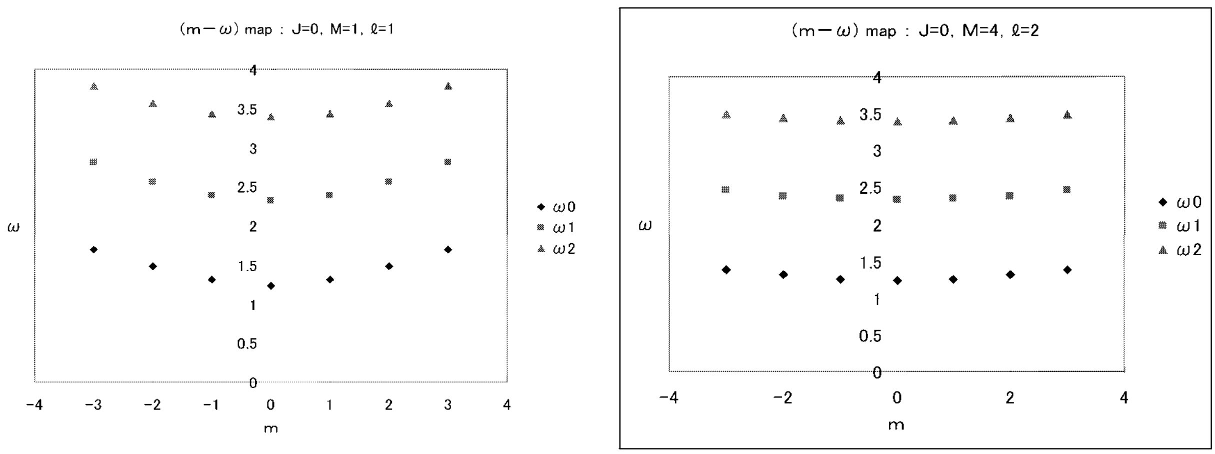

Figure 3: Eigenvalue map in (m, ω) plane without rotation

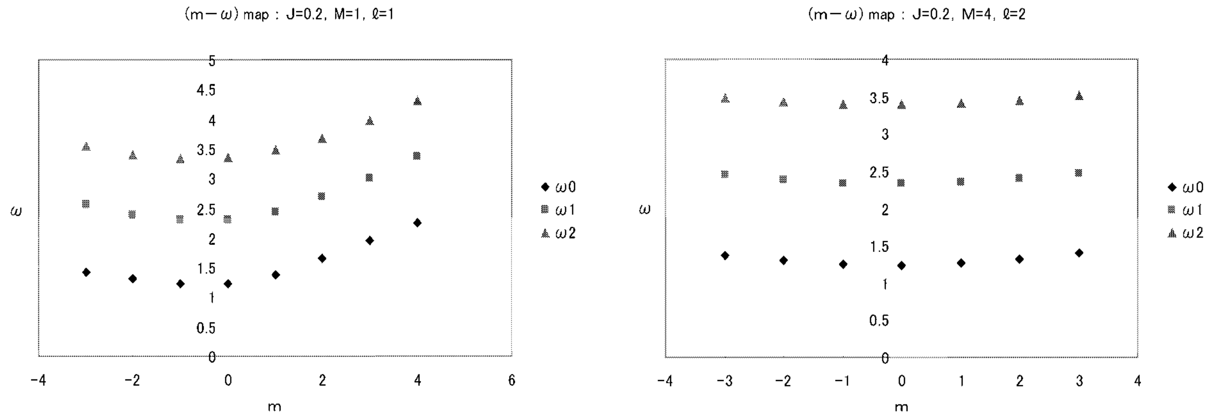

Figure 4: Eigenvalue map in (m, ω) plane with rotation

References

[1] M. Bañados, C. Teitelboim and J. Zanelli, Phys. Rev. Lett. 69 (1992) 1849.

[2] I. Ichinose and Y. Satoh, Nucl. Phys. 447 (1995) 340.

[3] J. Ho and G. Kang, Phys. Lett. B445 (1998) 27.

[4] M. Kenmoku, M. Kuwata and K. Shigemoto, arXive:0801.2044.

Coalescence of Rotating Black Holes on Eguchi-Hanson space

Ken Matsuno[1], Hideki Ishihara[2], Masashi Kimura[3] and Shinya Tomizawa[4]

Department of Mathematics and Physics, Graduate School of Science, Osaka City University, 3-3-138 Sugimoto, Sumiyoshi-ku, Osaka 558-8585, Japan

Abstract

We obtain new charged rotating multi-black hole solutions on the Eguchi-Hanson space in the five-dimensional Einstein-Maxwell system with a Chern-Simons term and a positive cosmological constant. In the two-black holes case, these solutions describe the coalescence of two rotating black holes with the horizon topologies of S^3 into a single rotating black hole with the horizon topology of the lens space $L(2;1) = S^3/\mathbb{Z}_2$. We discuss the differences in the horizon areas between our solutions and the two-centered Klemm-Sabra solutions which describe the coalescence of two rotating black holes with the horizon topologies of S^3 into a single rotating black hole with the horizon topology of S^3.

1 Solutions

We construct new multi-black hole solutions on the Eguchi-Hanson base space in the five-dimensional Einstein-Maxwell system with a Chern-Simons term and a positive cosmological constant $\Lambda > 0$ [1]. The metric and the gauge potential 1-form are given by

$$ds^2 = -H^{-2}\left[d\tau + \alpha V^{-1}(d\zeta + \omega)\right]^2 + H ds^2_{\mathrm{EH}}, \tag{1}$$

$$ds^2_{\mathrm{EH}} = V^{-1}\left(dr^2 + r^2 d\Omega^2_{S^2}\right) + V(d\zeta + \omega)^2, \tag{2}$$

$$\boldsymbol{A} = \frac{\sqrt{3}}{2}H^{-1}\left[d\tau + \alpha V^{-1}(d\zeta + \omega)\right], \tag{3}$$

where $H,\ V^{-1}$ and $\boldsymbol{\omega}$ are given by

$$H = \lambda\tau + \frac{M_1}{|\boldsymbol{r} - \boldsymbol{r}_1|} + \frac{M_2}{|\boldsymbol{r} - \boldsymbol{r}_2|}, \quad V^{-1} = \frac{N}{|\boldsymbol{r} - \boldsymbol{r}_1|} + \frac{N}{|\boldsymbol{r} - \boldsymbol{r}_2|}, \quad \boldsymbol{\omega} = N\left(\frac{z - z_1}{|\boldsymbol{r} - \boldsymbol{r}_1|} + \frac{z - z_2}{|\boldsymbol{r} - \boldsymbol{r}_2|}\right)d\phi, \tag{4}$$

with the constants $M_1,\ M_2,\ N,\ \alpha$ and $\lambda = \pm 2\sqrt{\Lambda/3}$. $d\Omega^2_{S^2} = d\theta^2 + \sin^2\theta d\phi^2$ denotes the metric of the unit two-sphere. The coordinates run the range of $-\infty < \tau < \infty,\ 0 \le r < \infty,\ 0 \le \theta \le \pi,\ 0 \le \phi \le 2\pi$ and $0 \le \zeta \le 4\pi N$. The equation (2) denotes the metric of the Eguchi-Hanson space in the Gibbons-Hawking coordinate. $\boldsymbol{r}_i = (x_i,\ y_i,\ z_i)$ $(i = 1,\ 2)$ denote the position vectors of the i-th nut singularity characterized by N on the three-dimensional flat space. The functions H and V^{-1} are the harmonics on the three-dimensional flat space. The 1-form $\boldsymbol{\omega}$ is determined by the equation $\nabla \times \boldsymbol{\omega} = \nabla V^{-1}$.

For the appearance of the first term in H, the solution (1) is dynamical, i.e., it admits no timelike Killing vector field. The parameter α in the metric (1) is an additional parameter to the solution in [2]. If $\alpha = 0$ then the solution (1) describes the coalescence of two non-rotating black holes on the Eguchi-Hanson space [2]. Here and after, we restrict ourselves to considering the contracting phase with $\lambda = -2\sqrt{\Lambda/3} < 0$ and the range of time $\tau = (-\infty,\ 0)$.

We focus on the regions of the neighborhood of $\boldsymbol{r} = \boldsymbol{r}_i$ $(i = 1,\ 2)$ and the asymptotic region $r \simeq \infty$ in the solution (1). In the neighborhood of $\boldsymbol{r} = \boldsymbol{r}_i$, the above metric (1) approaches to that of the Klemm-Sabra solution [3]. Similarly, in the asymptotic region $r \simeq \infty$, the local geometry of the metric (1) can be regarded as that of the Klemm-Sabra solution. So, we review the physical properties of the Klemm-Sabra solution.

[1]E-mail: matsuno@sci.osaka-cu.ac.jp
[2]E-mail: ishihara@sci.osaka-cu.ac.jp
[3]E-mail: mkimura@sci.osaka-cu.ac.jp
[4]E-mail: tomizawa@sci.osaka-cu.ac.jp

2 Review of Klemm-Sabra Solution

We review here properties of the Klemm-Sabra solution [3], which is the BMPV black hole [4] with a cosmological constant. The metric and the gauge potential 1-form in the cosmological coordinates $(\tau,\ R)$ are given by

$$\begin{aligned} ds^2 &= -\left(\lambda\tau + \frac{m}{R^2}\right)^{-2}\left[d\tau + \frac{j}{2R^2}\left(d\psi + \cos\theta d\phi\right)\right]^2 + \left(\lambda\tau + \frac{m}{R^2}\right)\left[dR^2 + \frac{R^2}{4}\left\{d\Omega^2_{S^2} + (d\psi + \cos\theta d\phi)^2\right\}\right], \quad (5)\\ \boldsymbol{A} &= \frac{\sqrt{3}}{2}\left(\lambda\tau + \frac{m}{R^2}\right)^{-1}\left[d\tau + \frac{j}{2R^2}\left(d\psi + \cos\theta d\phi\right)\right], \quad (6)\end{aligned}$$

where m and j are constants which specify the mass and the angular momentum, and $0 \le \psi \le 4\pi$.

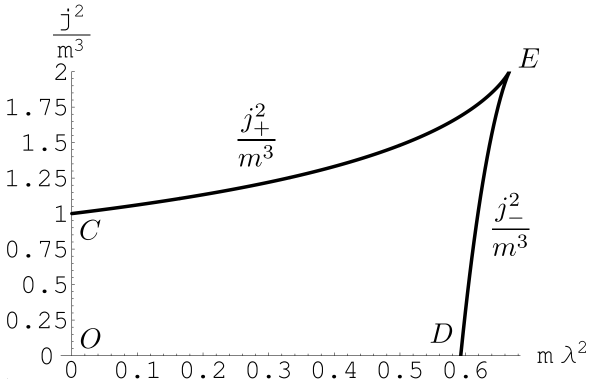

Figure 1: This figure shows the region of parameters such that the solutions have no naked singularity.

The curvature singularity exists at $\lambda\tau R^2 = -m$. One obtains the expansions $\theta_\pm$ of the outgoing and ingoing null geodesics for the τ = const. and R = const. surface as $\theta_\pm = \lambda \pm 2x\left[(x+m)^3 - j^2\right]^{-1/2}$, where we introduced a coordinate $x = \lambda\tau R^2$. Thus, the horizon occur at x such that

$$\lambda^2\left[(x+m)^3 - j^2\right] - 4x^2 = 0. \quad (7)$$

The equation (7) has three real roots $x_-,\ x_+,\ x_c$ ($x_- \le 0 \le x_+ \le x_c$), where $x_-,\ x_+,\ x_c$ correspond to the inner horizon, the black hole horizon and the cosmological horizon, respectively, if the mass parameter m and the angular momentum parameter j satisfies the following conditions,

$$0 \le m\lambda^2 \le \frac{2}{3}, \quad j_-^2(m) \le j^2 \le j_+^2(m), \quad (8)$$

where $j_\pm^2(m) = 4\left[9m\lambda^2(8-3m\lambda^2) - 32 \pm 8\sqrt{2}(2-3m\lambda^2)^{3/2}\right]\Big/\left(27\lambda^6\right)$. In the case of $j = j_+$, the black hole horizon x_+ coincides with the inner horizon x_-, and in the case of $j = j_-$, the black hole horizon x_+ coincides with the cosmological horizon x_c. The naked singularity appears if m and j are out of the ranges (8). We draw the region of $(m,\ j)$ satisfying the condition (8) in FIG.1. Next, we focus on the conditions for the absence of closed timelike curves (CTCs) outside the black hole horizon $x_+(m,\ j)$. These CTCs occur if and only if the two dimensional $(\psi,\ \phi)$ part of the metric (5), namely, g_{2D} has a negative eigenvalue. In this case, it is sufficient to show $g_{\psi\psi} > 0$ and $\det g_{2D} > 0$ on the horizon x_+ for the absence of CTCs. Actually, we see that

$$g_{\psi\psi} = \left[\frac{x_+}{\lambda(x_+ + m)}\right]^2 > 0, \quad \det g_{2D} = \frac{x_+^2\sin^2\theta}{4\lambda^2(x_+ + m)} > 0,$$

for $x_+ > 0$ and $m > 0$. Fortunately, we obtain the regular black hole solutions with parameters $(m,\ j)$ satisfying the condition (8) which have no CTC outside the black hole horizon.

3 Coalescence of Rotating Black Holes

Asymptotic Behaviors at Early Time and Late Time First, we investigate the asymptotic behaviors of the metric (1) in the neighborhood of $\boldsymbol{r} = \boldsymbol{r}_i$ $(i = 1,\ 2)$. In this region, the metric (1) takes the form of

$$ds^2 \simeq -\left(\lambda\tau + \frac{m_i}{\tilde{r}^2}\right)^{-2}\left[d\tau + \frac{j}{2\tilde{r}^2}\left(d\psi + \cos\theta d\phi\right)\right]^2 + \left(\lambda\tau + \frac{m_i}{\tilde{r}^2}\right)\left[d\tilde{r}^2 + \frac{\tilde{r}^2}{4}\left\{d\Omega^2_{S^2} + (d\psi + \cos\theta d\phi)^2\right\}\right], \quad (9)$$

where we introduced the coordinates $\tilde{r}^2 = 4Nr,\ \psi = \zeta/N,\ m_i = 4NM_i$ and $j = 8\alpha N^3$. This metric is equal to that of the Klemm-Sabra solutions (5) with the mass parameters m_i and the angular momentum parameter j. This solution (9) admits three horizons at $x = x_\pm,\ x_c$, in the coordinate $x = \lambda\tau\tilde{r}^2$. At the early time $\tau \simeq -\infty$, sufficiently small squashed S^3 centered at $\boldsymbol{r} = \boldsymbol{r}_i$ are always outer trapped since there are solutions for $\theta_+ = 0$ at $\tilde{r}^2 = x_+(m_i, j)/(\lambda\tau)$. Because there is an apparent horizon in the neighborhood of each point source $\boldsymbol{r} = \boldsymbol{r}_i$ $(i = 1, 2)$, we can find two rotating black holes with the horizon topology S^3 at the early time.

Next, we focus on the asymptotic region of the solution (1), $r \simeq \infty$. We assume the separation of two black holes $|\boldsymbol{r}_1 - \boldsymbol{r}_2|$ is much smaller than r. In this region, the metric (1) behaves as

$$
\begin{aligned}
ds^2 \simeq & -\left[\lambda\tau + \frac{2(m_1+m_2)}{\rho^2}\right]^{-2}\left[d\tau + \frac{8j}{2\rho^2}\left(\frac{d\psi}{2} + \cos\theta d\phi\right)\right]^2 \\
& + \left[\lambda\tau + \frac{2(m_1+m_2)}{\rho^2}\right]\left[d\rho^2 + \frac{\rho^2}{4}\left\{d\Omega^2_{S^2} + \left(\frac{d\psi}{2} + \cos\theta d\phi\right)^2\right\}\right],
\end{aligned}
\tag{10}
$$

where we introduced the coordinates $\rho^2 = 8Nr$, $\psi = \zeta/N$ and the parameters $m_i = 4NM_i$ and $j = 8\alpha N^3$, as same as in (9). This metric (10) resembles that of the Klemm-Sabra solution (5) with the mass parameter $2(m_1+m_2)$ and angular momentum parameter $8j$. Like the Klemm-Sabra solution (5), at the late time $\tau \simeq 0$, a sufficiently large squashed S^3 becomes outer trapped, since $\theta_+ = 0$ at $\rho^2 = x_+(2(m_1+m_2), 8j)/(\lambda\tau)$, which give an approximately large sphere. However, we see this solution (10) differs from the Klemm-Sabra solution (5) in the following point; each $\rho =$ const. surface in the $\tau =$ const. hypersurface of the metric (10) denotes topologically the lens space $S^3/\mathbb{Z}_2$, while in the Klemm-Sabra solution (5), it is diffeomorphic to S^3. The difference between these metrics appears in (9) and (10): the term $d\psi$ in the S^3 metric (9) is replaced by the term $d\psi/2$ in the $S^3/\mathbb{Z}_2$ metric (10). Therefore, at the late time $\tau \simeq 0$, the topology of the outer trapped surface is the lens space $S^3/\mathbb{Z}_2$.

Hence, we find that the solution (1) describes the dynamical evolution such that two rotating black holes with the spatial topologies of S^3 coalesce and convert into a single rotating black hole with the spatial topology of the lens space $S^3/\mathbb{Z}_2$. At the early time, there are two rotating black holes specified by (m_1, j) and (m_2, j), and at the late time, there is a single rotating black hole specified by $(2(m_1+m_2), j)$. Here and after, we call such relations "mapping rule".

Typical Processes We restrict ourselves to the solution (1) with the same mass parameters $m = m_1 = m_2$.

According to the "mapping rule" of our solutions (1), the dimensionless parameters $m\lambda^2$ and j^2/m^3 are mapped as $(m\lambda^2, j^2/m^3) \to \left(4m\lambda^2, j^2/m^3\right)$ (see FIG.2). Any solutions lying in the region $ODEC$ describe regular initial condition such that there exist two isolated apparent horizons. In contrast, according to the "mapping rule" of our solution (1), any solutions lying in the region $OAFC$ describe a single rotating black hole with the $S^3/\mathbb{Z}_2$ horizon at the late time. So, any solutions lying in the region $OABC$ describe a coalescence of two rotating black holes. There are four types of regions, namely, $OABC$, $ADEB$, CBF and outside of $DEBFC$. These regions correspond to the four kinds of process. The dashed arrows represent typical processes. The process $d \to d'$ describes the situation such that two rotating black holes with the S^3 horizon coalesce and convert into a single rotating black hole with the $S^3/\mathbb{Z}_2$ horizon. The arrow $e \to e'$ describes the situation such that there are two isolated apparent horizons at the early time, and there exist a naked singularity at the late time. The process $f \to f'$ describes the situation such that there is not an apparent horizon but CTCs at the early time, while at the late time, there exist a single rotating black hole with the $S^3/\mathbb{Z}_2$ horizon and there is no CTC outside the horizon.

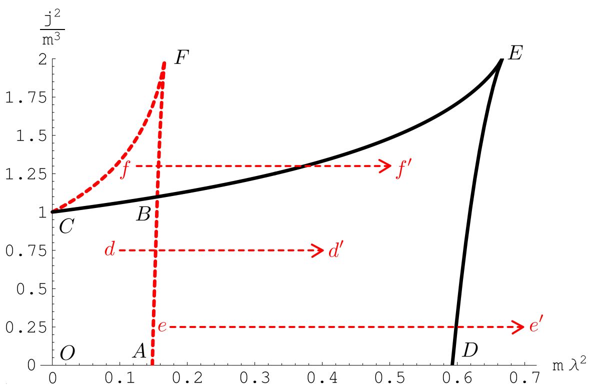

Figure 2: This figure shows typical processes described by our solutions (1).

Comparison of Horizon Areas We compare the area of a single rotating black hole formed by the coalescence of two rotating black holes at the late time. We assume that each black hole in our solution (1) has the same mass, angular momentum and horizon area as that in the two-centered Klemm-Sabra solution at the early time. In this case, the "mapping rule" for the two-centered Klemm-Sabra solution becomes as follows: At the early time, there are two rotating black holes specified by $(m,\ j)$ and $(m,\ j)$. At the late time, there is a single rotating black hole specified by $(2m,\ 2j)$. The total horizon areas in the two-centered Klemm-Sabra solutions and our solutions at the early time, $A^{(e)}_{\rm Flat}$ and $A^{(e)}_{\rm EH}$, are given by

$$A^{(e)}_{\rm Flat} = A^{(e)}_{\rm EH} = 2 \times \frac{2}{\lambda} x_+(m,\ j) A_{S^3}, \tag{11}$$

where A_{S^3} denotes the area of the unit S^3. On the other hand, according to the "mapping rules" of both solutions, the horizon areas at the late time, $A^{(l)}_{\rm Flat}$ and $A^{(l)}_{\rm EH}$, are given by

$$A^{(l)}_{\rm Flat} = \frac{2}{\lambda} x_+(2m,\ 2j) A_{S^3}, \quad A^{(l)}_{\rm EH} = \frac{2}{\lambda} x_+(4m,\ 8j) \frac{A_{S^3}}{2}, \tag{12}$$

respectively. Note the factor $1/2$ in $A^{(l)}_{\rm EH}$ reflects the fact that the black hole at the late time after coalescence of two black holes is topologically the lens space $S^3/\mathbb{Z}_2$.

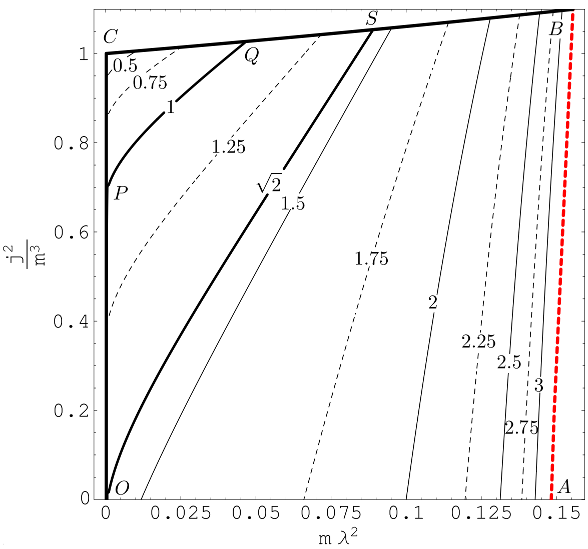

Figure 3: This figure shows the dependence of the ratio $A^{(l)}_{\rm EH}\big/A^{(l)}_{\rm Flat}$ on $m\lambda^2$ (horizontal axis) and j^2/m^3 (vertical axis). The curves in this figure denote $A^{(l)}_{\rm EH}\big/A^{(l)}_{\rm Flat}$ = const.

In turn, to clarify the differences in the ratio of the horizon areas of the two-centered Klemm-Sabra solution to that of our solution, we consider the ratio $A^{(l)}_{\rm EH}\big/A^{(l)}_{\rm Flat}$. FIG.3 shows the dependence of $A^{(l)}_{\rm EH}\big/A^{(l)}_{\rm Flat}$ on $(m\lambda^2,\ \ j^2/m^3)$. The behavior of $A^{(l)}_{\rm EH}\big/A^{(l)}_{\rm Flat}$ along the boundary OA corresponds to the $j = 0$ case which was discussed in [2]. In the non-rotating case, the ratio always satisfies $\sqrt{2} < A^{(l)}_{\rm EH}\big/A^{(l)}_{\rm Flat} < 4$. However in the rotating case there is the case such that $0 < A^{(l)}_{\rm EH}\big/A^{(l)}_{\rm Flat} < \sqrt{2}$ in the region OSC in FIG.3.

Both solutions in this paper describe the coalescence of black holes by virtue of a positive cosmological constant. Nevertheless, in $\lambda \to 0$ limit our results would suggest some information about the coalescence of two rotating supersymmetric black holes on the flat space (BMPV solutions) and on the Eguchi-Hanson space. Therefore, let us discuss the limit $\lambda \to 0$. Two rotating supersymmetric black holes characterized by the parameters (m, j) with a total horizon area $A^{(e)}$ coalesce into a single rotating supersymmetric black hole with a horizon area $A^{(l)}_{\rm Flat} = \sqrt{(2m^3 - j^2)/(m^3 - j^2)} A^{(e)}_{\rm Flat}$ on the flat space, while on the Eguchi-Hanson space $A^{(l)}_{\rm EH} = 2A^{(e)}_{\rm EH}$, which is independent of parameters (m, j). In the FIG.3, the behavior of $A^{(l)}_{\rm EH}\big/A^{(l)}_{\rm Flat}$ along the boundary OC corresponds to that in this $\lambda \to 0$ limit. For the large angular momentum, i.e., $2/3 < j^2/m^3 < 1$, the area of black hole horizon after the coalescence on the Eguchi-Hanson space is smaller than that on the flat space, i.e., $0 < A^{(l)}_{\rm EH}\big/A^{(l)}_{\rm Flat} < 1$.

References

[1] K. Matsuno, H. Ishihara, M. Kimura and S. Tomizawa, Phys. Rev. D **76**, 104037 (2007).

[2] H. Ishihara, M. Kimura and S. Tomizawa, Class. Quant. Grav. **23**, L89 (2006).

[3] D. Klemm and W.A. Sabra, Phys. Lett. B **503**, 147 (2001).

[4] J.C. Breckenridge, R.C. Myers, A.W. Peet and C. Vafa, Phys. Lett. B **391**, 93 (1997).

Gravitational time delays along multiple light paths as a probe of physics beyond Einstein gravity

Hideki Asada[1]

Faculty of Science and Technology, Hirosaki University, Hirosaki 036-8561, Japan

Abstract

The gravitational time delay of light is reexamined, allowing for various models of modified gravity. We clarify the dependence of the time delay (and induced frequency shift) on modified gravity models and investigate how to distinguish those models, when light propagates in static spherically symmetric spacetimes.

1 Introduction

Recent observations such as the magnitude-redshift relation of type Ia supernovae (SNIa) and the cosmic microwave background (CMB) anisotropy by WMAP strongly suggest a certain modification, in whatever form, in the standard cosmological model. We are forced to add a new component into the energy-momentum tensor in the Einstein equation or modify the theory of general relativity itself. Indeed, there have been a lot of proposals motivated by, for instance, scalar tensor theories, string theories, higher dimensional scenarios and quantum gravity. Therefore, it is of great importance to observationally test these models.

The theory of general relativity has passed "classical" tests, such as the deflection of light, the perihelion shift of Mercury and the Shapiro time delay, and also a systematic test using the remarkable binary pulsar "PSR 1913+16" [1]. In the twentieth century, these tests proved that the Einstein's theory is correct with a similar accuracy of 0.1%.

Since the time delay effect along a light path in the gravitational field was first noticed in 1964 by Shapiro [2], this effect has successfully tested the Einstein's theory [3]. A significant improvement was reported in 2003 from Doppler tracking of the Cassini spacecraft on its way to the Saturn, with $\gamma - 1 = (2.1 \pm 2.3) \times 10^{-5}$ [4]. Here, γ is one of parameters in the parameterized post-Newtonian (PPN) formulation of gravity [1]. The sensitivity in the Cassini experiment approaches the level at which, theoretically, deviations $10^{-6} - 10^{-7}$ are expected in some cosmological models [5, 6]. Therefore, it is important to investigate the Shapiro time delay with such a high accuracy.

Here, we discuss the dependence of the time delay (and induced frequency shift) on modified gravity models and investigate how to distinguish those models by using the Shapiro time delay [7]. An important point in this paper is that we allow for various modified gravity theories beyond the scope of the PPN formulation. Introducing a new energy or length scale (e.g. extra dimension scale) may make changes in functional forms of the gravitational field. Thus it is worthwhile to investigate how to probe such a modified functional form, by using the light propagation in the solar system. Throughout this paper, we take the units of $G = c = 1$.

2 Shapiro Time Delay

Let us assume that the electromagnetic fields propagate in four-dimensional spacetimes (even if the whole spacetime is higher dimensional). Thus photon paths follow null geodesics (as the geometrical optics approximation of Maxwell equation).

We shall consider a static spherically symmetric spacetime, in which light propagates, expressed as

$$ds^2 = -A(r)dt^2 + B(r)dr^2 + r^2 d\Omega^2, \tag{1}$$

[1]E-mail:asada@phys.hirosaki-u.ac.jp

where r and $d\Omega^2$ denote the circumference radius and the metric of the unit 2-sphere, respectively. The functions $A(r)$ and $B(r)$ depend on gravity theories.

The time lapse along a photon path is obtained as

$$t(r, r_0) = \int_{r_0}^{r} \frac{dr}{b} \sqrt{\frac{B(r)}{A(r)}} \frac{1}{\sqrt{\frac{A(r_0)}{r_0^2} - \frac{A(r)}{r^2}}}, \tag{2}$$

where b and r_0 denote the impact parameter and the closest point, respectively. Their relation is $b^2 = r_0^2/A(r_0)$.

For practical calculations, we keep only the leading term at a few AU in the corrections. Namely, $A(r)$ and $B(r)$ are approximated as

$$\begin{aligned} A(r) &\approx 1 - \frac{2M}{r} + A_m r^m, & (3)\\ B(r) &\approx 1 + \frac{2M}{r} + B_n r^n, & (4) \end{aligned}$$

where M denotes the mass of the central body.

Examples of modified gravity theories are as follows. (1) $n = 1/2$, $A_n = -2B_n = -2\sqrt{M/r_c^2}$ for DGP model with r_c that is the extra scale within which gravity becomes five dimensional [8]. (2) $n = 3/2$, $A_n = (2/3)m_g^2\sqrt{2M/13}$ and $B_n = -m_g^2\sqrt{2M/13}$ with graviton mass m_g for one of massive gravity models [9, 10]. (3) $n = 2$, $A_n = -B_n = -\Lambda/3$ for the Schwarzschild-de Sitter spacetime, that is, general relativity with the cosmological constant Λ as a possible candidate for the dark energy, though this is not a manifest modification of gravity.

Up to the linear order, the extra contribution to time delay due to modified gravity is

$$\begin{aligned} \delta t &= r_0^{n+1} \left(\int_1^{R_E} + \int_1^{R_R} \right) dR \\ &\quad \times \left(-A_n \frac{R^{n+3} - 2R^{n+1} + R}{(R^2 - 1)^{3/2}} + B_n \frac{R^{n+1}}{\sqrt{R^2 - 1}} \right), \end{aligned} \tag{5}$$

where we define $R \equiv r/r_0$.

It is convenient to use the relative change in the frequency, which is caused by the gravitational time delay. This frequency shift is defined as $y = -d(\Delta T)/dt$.

The general relativistic contribution is expressed as [1]

$$y_{GR} = 4\frac{M}{b}\frac{db}{dt}. \tag{6}$$

For $n \neq 1$, the extra frequency shift becomes

$$\delta y = -\frac{A_n + B_n}{n - 1} \{ r_E^{n-1} + r_R^{n-1} - (n+1) r_0^{n-1} \} b \frac{db}{dt}, \tag{7}$$

while we obtain $\delta y = -(A_n + B_n)[\ln(r_E r_R/r_0^2) - 1] b db/dt$ for $n = 1$.

Here, we make an order-of-magnitude estimate of the frequency shift. First, we obtain $y_{GR} \sim 10^{-9}(M/M_\odot)(r_\odot/b)(\dot{b}/v_E)$, where the dot denotes the time derivative, and v_E is the orbital velocity of Earth ($\sim$ 30 km/s).

For a receiver at $r_R > r_E$, the extra frequency shift is

$$\begin{aligned} \delta y &\sim (A_n + B_n) r_R^n \frac{b}{r_R} \frac{db}{dt} \\ &\sim 10^{-17} \left(\frac{10\text{AU}}{r_\odot} \right)^n \left(\frac{(A_n + B_n) r_\odot^n}{10^{-10}} \right) \left(\frac{r_R}{10\text{AU}} \right)^{n-1} \left(\frac{b}{r_\odot} \right) \left(\frac{db/dt}{v_E} \right), \end{aligned} \tag{8}$$

where $10\text{AU}/r_\odot \sim 2 \times 10^3$. The larger the index of n, the longer the delay δy.

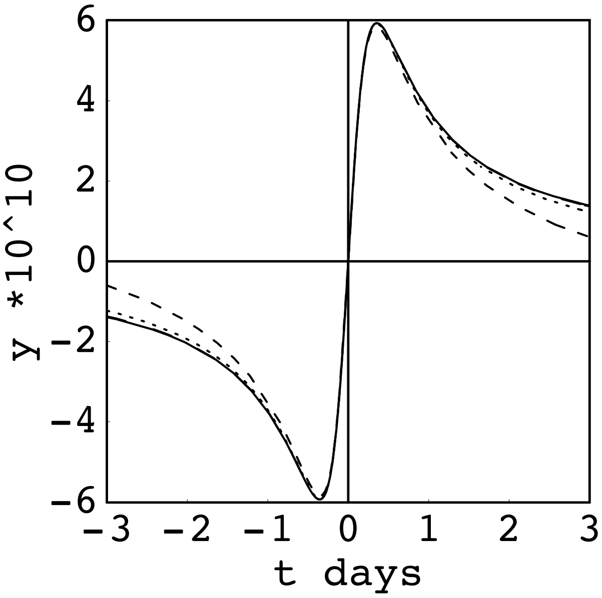

Figure 1: Dependence of the frequency shift on the distance r_R and the index n. The long dashed, short dashed and dotted curves denote the frequency shift for $(n, r_R) = (3/2, 10\mathrm{AU})$, $(n, r_R) = (2, 10\mathrm{AU})$, $(n, r_R) = (2, 1\mathrm{AU})$, respectively. The long dashed curve for $n = 3/2$ and $r_R = 10$ AU is overlapped with the solid curve denoting the general relativistic case. Here, we assume $(A_n + B_n)r_\odot^n = 3 \times 10^{-11}$.

Figure 1 shows that an extra distortion due to δy would appear especially in the tail parts of $y - t$ curves. One can distinguish modified gravity models, which are characterized by various values of n, A_n, B_n, from observations using receivers at very different distances from Sun, as shown by Fig. 1.

Figure 2 shows the dependence of δy on n and $A_n + B_n$. Hence, one can put a constraint on n and $A_n + B_n$ from δy observed.

3 Multiple Paths

We consider three light paths, for which the impact parameters of the photon paths are almost the same (several times of the solar radius) for convenience sake. The locations of the receivers are denoted as r_{R1}, r_{R2} and r_{R3}, where the subscripts from 1 to 3 denote each light path. We assume that r_E is constant in time for simplicity. It is a straightforward task to take account of the eccentricity of the Earth orbit and a difference between the impact parameters.

We make use of a difference such as $y_2 - y_1$ and $y_3 - y_1$, in order to cancel out general relativistic parts. We find

$$y_2 - y_1 = \frac{A_n + B_n}{n-1}(r_{R1}^{n-1} - r_{R2}^{n-1})b\frac{db}{dt}. \tag{9}$$

It should be noted that $y_2 - y_1$ is proportional to $A_n + B_n$. Hence, the following ratio depends only on n as

$$\frac{y_3 - y_1}{y_2 - y_1} = \frac{r_{R1}^{n-1} - r_{R3}^{n-1}}{r_{R1}^{n-1} - r_{R2}^{n-1}}. \tag{10}$$

Thereby, one can determine the index n. Next, one obtains $A_n + B_n$ by substituting the determined n into Eq. (9).

4 Conclusion

In summary, we have clarified the dependence of the gravitational time delay on modified gravity models [7]. For neighboring light rays, the time delays become almost the same so that one can hardly distinguish

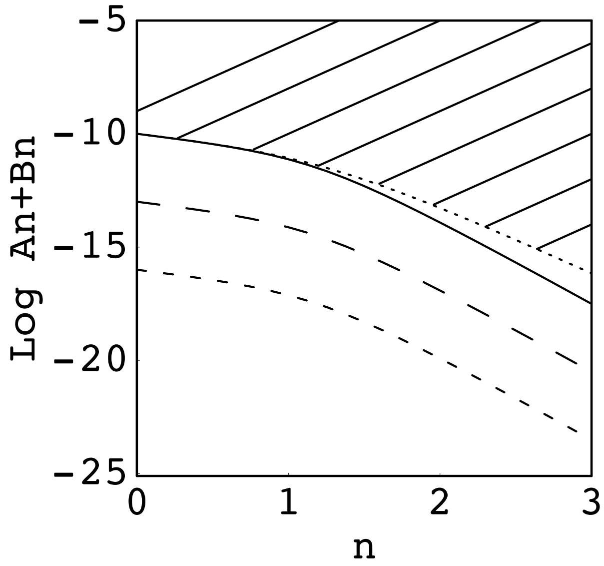

Figure 2: Contours of δy on the n - $|A_n + B_n| r_\odot^n$ plane. The solid, long-dashed and short-dashed curves correspond to $\delta y = 10^{-14}, 10^{-17}, 10^{-20}$, respectively, where we assume $r_E = 1$ AU, $r_R = 40$ AU, $b \sim r_\odot$ and $db/dt \sim v_E$. The limit due to the current technology is $\delta y \sim 10^{-17}$. The shaded region above the dotted curve ($\delta y = 10^{-14}$ for $r_R = 8.43$ AU) has been excluded by the Cassini experiment.

models of gravity. This implies that we should prepare receivers at very different distances from Sun.

Furthermore, b becomes the same order of r_E, r_R for future space-borne laser interferometric detectors such as LISA, DECIGO and especially ASTROD [11]. Namely, r_R and b change with time. Therefore, the sophisticated experiments by space-borne laser interferometric detectors, which are originally designed to detect time-dependent part of gravity, *i.e.* gravitational waves, could probe also a time-independent part of gravity at the relative level ofΔ $y \sim \Delta\nu/\nu \sim \Delta L/L < 10^{-20}$.

References

[1] C. M. Will, *Theory and experiment in gravitational physics* (Cambridge Univ. Press, Cambridge, 1993).

[2] I. I. Shapiro, Phys. Rev. Lett. **13**, 789 (1964).

[3] C. M. Will, Living Rev. Relativity 9, 3 (2006), http://relativity.livingreviews.org/Articles/lrr-2006-3.

[4] B. Bertotti, L. Iess and P. Tortora, Nature, **425**, 374 (2003).

[5] T. Damour and A. M. Polyakov, Nucl. Phys. B **423**, 532 (1994).

[6] T. Damour, F. Piazza and G. Veneziano, Phys. Rev. D **66**, 046007 (2002).

[7] H. Asada, arXiv:0710.0477 [gr-qc]

[8] G. R. Dvali, G. Gabadadze and M. Porrati, Phys. Lett. B **485**, 208 (2000).

[9] A. I. Vainshtein, Phys. Lett. B **39**, 393 (1972).

[10] T. Damour, I. I. Kogan and A. Papazoglou, Phys. Rev. D **67**, 064009 (2003).

[11] W. T. Ni *et al.*, J. Phys. **32**, 154 (2006).

Does Astronomical Unit increase?:
Cosmological Expansion and Solar System Dynamics

Hideyoshi ARAKIDA[1]

[1] *School of Education, Waseda University, Tokyo 169-8050, JAPAN*

Abstract

Based on Robertson-McVittie metric, we re-examined whether the cosmological expansion causes the increasing of Astronomical Unit (of length) reported by Krasinsky and Brumberg (2004). We investigated the influence of cosmological expansion on the motion of test particle in this spacetime. We found the cosmological expansion affects these three aspects however they are negligible small. Therefore we confirmed that the cosmological expansion does not give an explanation of the observed $d\mathrm{AU}/dt$.

1 Introduction

Recent years, the accuracy of the positional observations of celestial bodies in the solar system is drastically improved and this improvement is in progress. For example, the planetary radar measurement achieves the observational accuracy of the distance within a few 100 [m], the spacecraft ranging a few [m] and the lunar laser ranging a few [cm]. Using such a accurate observational data, the various astronomical constants are derived. Especially the astronomical unit of length (hereafter abbreviated as AU) is currently determined within the accuracy of 0.1 [m] or 12 digits level as $1\mathrm{AU} = 1.49597870696.0 \times 10^{11} \pm 0.1$ [m]. [1] AU is one of the fundamental and important astronomical constants which gives the relation of two units of length; the AU of astronomical system of units and the meter of SI ones. Then AU, as the astronomical constant, fundamentally must be the time-independent. However thees days, Krasinsky and Brumberg [2] reported that from the analysis of the data of planetary radar (Mercury, Venus and Mars) and the martian spacecraft ranging (Viking I/II, Mars Pathfinder, Mariner 9, Mars Global Surveyor, and Mars Odyssey), AU increases monotonically with respect to meter as $d\mathrm{AU}/dt = 15 \pm 4$ [m/cent]. This value is about 100 times larger than the recent determination error of AU, ~ 0.1 [m]. The similar variation of AU is also corroborated by Standish and Pitjeva. [3]

The observable quantity of the planetary radar and the spacecraft ranging is the round-trip time of light/signal. Then the positive $d\mathrm{AU}/dt$ means the lengthening of light/signal path between Earth and objective planet/spacecraft with the time because of the principle of the constancy of the speed of light.

Krasinsky and Brumberg investigated the possibility that the cosmological expansion prolongs the light/signal path and causes the increasing of AU. From the Einstein equation they derived the approximate cosmological model which is regarded as FLRW universe including the gravity of the single central body, and studied not only the planetary motion around Sun but also the light/signal propagation and time scale transformation between the coordinate time t and proper time τ of the atomic clocks on Earth. They found there appear comparatively large effects due to the cosmological expansion, but the contribution on the planetary motion is completely cancelled out by that on the time scale transformation relating with the light/signal propagation. Therefore they concluded the cosmological expansion does not give an explanation of positive $d\mathrm{AU}/dt$. So far, the problem "the cosmological expansion affects the gravitationally bound local system or not" has sometimes awakened the interest and been investigated by many authors. [4, 5, 6, 7, 8, 9, 10, 11, 12, 13, 14, 15, 16, 17] However they took into account the effect on the planetary motion only and the contributions on light/signal propagation and the time scale transformation were not made consideration.

In order to verify whether the cosmological expansion induces the detectable traces in the solar system and provides an explanation of $d\mathrm{AU}/dt$, we will re-examine its contributions on the planetary motion, the light/signal propagation, and the time scale transformation by means of Robertson-McVittie solution.

[1] E-mail:arakida@edu.waseda.ac.jp

2 Motion of Test Particle in Robertson-McVittie Spacetime

Robertson-McVittie metric is given by, [18, 4]

$$ds^2 = -\left(\frac{1-\frac{GM}{2c^2ra(t)}}{1+\frac{GM}{2c^2ra(t)}}\right)^2 c^2dt^2 + \left(1+\frac{GM}{2c^2ra(t)}\right)^4 a^2(t)(dr^2 + r^2d\theta^2 + r^2\sin^2\theta d\phi^2), \tag{1}$$

where G is the gravitational constant, M is the mass of central body, c is the speed of light in vacuum, and $a(t)$ is a scale factor. We impose two transformations, [18, 5]

$$R = a(t)r\left(1+\frac{GM}{2c^2ra(t)}\right)^2, \quad cT = ct + \frac{H_0}{c}\int \frac{RdR}{\left(1-\frac{2GM}{c^2R}-\frac{H_0^2}{c^2}R^2\right)\sqrt{1-\frac{2GM}{c^2R}}}, \tag{2}$$

where the Hubble constant $H(t)$ is supposed to be that at present, $H_0 = (h_0/3.08)\times 10^{-17}$ [1/s], $h_0 = 0.7$ since it is considered to be constant in the order of 100 [yr]. Using (2) and limiting the planar motion in the equatorial plane $\theta = \pi/2$, we obtain,

$$ds^2 = -\left(1-\frac{2GM}{c^2r}-\frac{H_0^2}{c^2}r^2\right)c^2dt^2 + \left(1+\frac{2GM}{c^2r}+\frac{H_0^2}{c^2}r^2\right)dr^2 + r^2d\phi^2, \tag{3}$$

here we expanded the coefficient of dr^2 and replaced $T \to t$ and $R \to r$, respectively.

First, let us examine the planetary motion in Robertson-McVittie spacetime. The equations of motion of $r,\ \phi$ become, neglecting $\mathcal{O}(GM/c^4, H_0^2/c^2)$ and the higher order terms,

$$\frac{d^2r}{dt^2} - r\left(\frac{d\phi}{dt}\right)^2 + \frac{GM}{r^2} = \frac{GM}{c^2}\left[\frac{2GM}{r^3}+\frac{3}{r^2}\left(\frac{dr}{dt}\right)^2 - 2\left(\frac{d\phi}{dt}\right)^2\right] + H_0^2 r \tag{4}$$

$$\frac{d}{dt}\left(r^2\frac{d\phi}{dt}\right) = \frac{2GM}{c^2}\frac{dr}{dt}\frac{d\phi}{dt}. \tag{5}$$

In order to extract the dominant contributions due to cosmological expansion, we restrict ourselves here to the quasi-Newtonian equations of motion,

$$\frac{d^2r}{dt^2} - r\left(\frac{d\phi}{dt}\right)^2 + \frac{GM}{r^2} = H_0^2 r, \quad r^2\frac{d\phi}{dt} = \text{constant}. \tag{6}$$

Further we suppose the planetary orbit is initially circular one, $r_0 = 1.5\times 10^{11}$ [m]. The mean motion n is written by,

$$n \simeq n_0 + \delta n, \quad \delta n = -n_0\frac{r_0^3H_0^2}{2GM} \sim 1.0\times 10^{-28} \ \text{[rad/s]}, \tag{7}$$

where $n_0 = \sqrt{GM/r_0^3} \sim 2.0\times 10^{-7}$ [rad/s]. From (7) the variation of longitude ϕ is evaluated in 100 [yr] as,

$$\delta\phi = \delta n(t-t_0) \sim -3.5\times 10^{-18} \ \text{[rad]}. \tag{8}$$

The orbital period of planet becomes,

$$T = \frac{2\pi}{n} \simeq T_0 + \delta T, \quad \delta T = T_0\frac{r_0^3H_0^2}{2GM} \sim 7\times 10^{-26}, \tag{9}$$

here $T_0 = 2\pi/n_0$. Putting $r = r_0 + \delta r$ and inserting into (6), it yields,

$$\delta r = \frac{r_0^4H_0^2}{GM}\left(1+\frac{r_0^3H_0^2}{GM}\right) \sim 2.0\times 10^{-11} \ \text{[m]}. \tag{10}$$

Rounding up the results, the estimated orbital variations $\delta r, \delta\phi$ and change of orbital period δT are much smaller than the observed $d\text{AU}/dt = 15$ [m/cent] and the measurement limit of light/signal propagation, that is, the relative error of atomic clocks on Earth, $\sim 10^{-8}$ [s]. Therefore the effect of cosmological expansion on the planetary motion does not induce the observed increasing of AU.

The observable quantity of the planetary radar and the spacecraft ranging is the round-trip time of light/signal. Hence it is important to deal with the light propagation in Robertson-McVittie spacetime. So that, we derive the extra time delay due to the cosmological expansion. The world line of light/signal is the null geodesic, $ds^2 = 0$, then it results,

$$\begin{aligned} t(r, r_0) &= t_{1\mathrm{PN}}(r, r_0) + t_{\mathrm{Cosmo}}(r, r_0) &(11)\\ t_{1\mathrm{PN}}(r, r_0) &= \frac{1}{c}\sqrt{r^2 - r_0^2} + \frac{2GM}{c^3}\ln\left(\frac{r + \sqrt{r^2 - r_0^2}}{r_0}\right) + \frac{GM}{c^3}\sqrt{\frac{r - r_0}{r + r_0}} &(12)\\ t_{\mathrm{Cosmo}}(r, r_0) &= \frac{H_0^2}{6c^3}\sqrt{r^2 - r_0^2}\left(2r^2 - r_0^2\right), &(13) \end{aligned}$$

here $t_{1\mathrm{PN}}$ is the Shapiro's time delay in 1st post-Newtonian approximation, and t_{Cosmo} is the extra one caused by the cosmological expansion. If we assume Earth E and objective planet/spacecraft R are almost at rest during the round-trip of light/signal, the round-trip time $\mathcal{T}$ becomes,

$$\mathcal{T} = \mathcal{T}_{1\mathrm{PN}} + \mathcal{T}_{\mathrm{Cosmo}} = 2[t(r_E, r_0) + t(r_R, r_0)]. \tag{14}$$

and the time delay produced by the cosmological expansion is,

$$\mathcal{T}_{\mathrm{Cosmo}} = \frac{H_0^2}{3c^3}\left[\sqrt{r_E^2 - r_0^2}\left(2r_E^2 - r_0^2\right) + \sqrt{r_R^2 - r_0^2}\left(2r_R^2 - r_0^2\right)\right]. \tag{15}$$

The measurement of round-trip time is actually carried out by the atomic clocks on Earth moving around Sun, which ticks the proper time τ. Therefore, we must convert $\mathcal{T}$ into the proper time scale. It is sufficient to consider the quasi-Newtonian approximation,

$$\frac{d\tau}{dt} = 1 - \frac{GM}{c^2 r} - \frac{v^2}{2c^2} - \frac{H_0^2}{2c^2}r^2. \tag{16}$$

Taking the orbital radius, r_E and the orbital velocity, v_E of Earth, the round-trip time $\bar{\mathcal{T}}$ measured in proper time scale is given by,

$$\bar{\mathcal{T}} = \left(1 - \frac{GM}{c^2 r_E} - \frac{v_E^2}{2c^2} - \frac{H_0^2}{2c^2}r_E^2.\right)\mathcal{T}. \tag{17}$$

Making use of (14), the contribution of cosmological expansion, $\bar{\mathcal{T}}_{\mathrm{Cosmo}}$ is,

$$\bar{\mathcal{T}}_{\mathrm{Cosmo}} = \frac{H_0^2}{c^3}\left\{\frac{1}{3}\left[\sqrt{r_E^2 - r_0^2}\left(2r_E^2 - r_0^2\right) + \sqrt{r_R^2 - r_0^2}\left(2r_R^2 - r_0^2\right)\right] - r_E^2\left(\sqrt{r_E^2 - r_0^2} - \sqrt{r_R^2 - r_0^2}\right)\right\}. \tag{18}$$

Roughly estimating, $\bar{\mathcal{T}}_{\mathrm{Cosmo}}$ has the order $\bar{\mathcal{T}}_{\mathrm{Cosmo}} \sim H_0^2 r_E^3/c^3 \sim 6.5 \times 10^{-28}$ [s]. Since the present internal error of the atomic clocks on Earth is about 10^{-9} [s], therefore the $\bar{\mathcal{T}}_{\mathrm{Cosmo}}$ is much smaller than the current measurement limit.

Conversely, the time transformation from the proper time to the coordinate one is needed when obtaining the position/velocity of planet/spacecraft at certain proper time τ on Earth. To this end, we integrate (16) assuming Earth moving along the circular orbit $r_E = 1.5 \times 10^{11}$ [m]. Then the difference between coordinate time and proper one due to the cosmological expansion is in the order of 100 [yr],

$$\tau_{\mathrm{Cosmo}} = -\frac{H_0^2 r_E^2}{2c^2}\int_{t_0}^{t} dt = -\frac{H_0^2 r_E^2}{2c^2}(t - t_0) \sim -4.1 \times 10^{-20} \text{ [s]}, \tag{19}$$

which is much smaller than the relative error of atomic clocks on Earth 10^{-9} [s] and then $c\tau_{\mathrm{Cosmo}} \sim 10^{-12}$ [m] that is also much smaller than the observed $d\mathrm{AU}/dt$.

3 Conclusions

We re-examined whether the cosmological expansion explains the observed increasing of AU. As the cosmological model, we adopted Robertson-McVittie metric which is regarded as FLRW universe including the gravitation of single point mass, and then analyzed the motion of test particle in this spacetime; the planetary motion, the light/signal propagation and the time scale transformation between the coordinate time and the proper one. We found the cosmological expansion affects these dynamical and kinematical aspects, however the estimated corrections are much smaller than the observed $d\mathrm{AU}/dt$ and the measuring limit, namely the internal error of atomic clocks on Earth, 10^{-9} [s]. In consequence, we confirmed the cosmological expansion does not provide a explanation of the increasing of AU.

In order to investigate the influence of cosmological expansion on the gravitationally bound system, the metric must be fundamentally the function of the time. But our metric (3) expresses the completely static gravitational field. Therefore, it is important to examine the motion of test particle in the time-dependent gravitational field. This subject will be investigated at some future time.

References

[1] E. V. Pitjeva, Solar System Research, **39** (2005), 176

[2] G. A. Krasinsky and V. A. Brumberg, Celest. Mech. Dyn. Astrn., **90** (2004), 267

[3] E. M. Standish, Proc. IAU Colloq., **196** (2005), 163

[4] G. C. McVittie, MNRAS, **93** (1933), 325

[5] G. Järnefelt, Ann. Acad. Soc. Sci. Fennicae, **A45** (1940a), 3

[6] G. Järnefelt, Arkiv Matem. Astron. Fys,, **27** (1940b), 1

[7] G. Järnefelt, Ann. Acad. Soc. Sci. Fennicae, **A45** (1942), 12

[8] A. Einstein and E. G. Straus, Rev. Mod. Phys., **17** (1945), 120

[9] A. Einstein and E. G. Straus, Rev. Mod. Phys., **18** (1946), 148

[10] E. Schücking, Zeitschrift für Physik, **137** (1954), 595

[11] P. D. Noerdlinger and V. Petrosian, Astrophys. J., **168** (1971), 1

[12] R. Gautreau, Phys. Rev. D, **29** (1984), 198

[13] F. I. Cooperstock, V. Faraoni, and D. N. Vollick, Astrophys. J., **503** (1998), 61

[14] M. Carrera and D. Giulini, arXiv:gr-qc/0602098, (2005)

[15] M. Sereno and P. Jetzer, Phys. Rev. D, **75** (2007), 4031

[16] V. Faraoni and A. Jacques, Phys. Rev. D, **76** (2007), 3510

[17] B. Mashhoon, N. Mobed and D. Singh, Class. Quant. Grav., **24** (2007), 5031

[18] H. P. Robertson, Phil. Mag., **7** (1928), 845

[19] B. C. Nolan, Class. Quant. Grav., **16** (1999), 1227

[20] B. C. Nolan, Class. Quant. Grav., **16** (1999), 3183

Dynamical solution of supergravity

Pierre Binetruy[1], Misao Sasaki[2], Kunihito Uzawa[3]

[1] *Astroparticule et Cosmologie (UMR 7164), Universite Paris 7, F-75205 Paris Cedex 13, France*
[2] *Yukawa Institute for Theoretical Physics, Kyoto University, Kyoto 606–8502, Japan*
[3] *Yukawa Institute for Theoretical Physics, Kyoto University, Kyoto 606–8502, Japan, Graduate School of Science and Technology Kwansei Gakuin University, Sanda 669-1337, Japan*

Abstract

We present a class of dynamical solutions for an intersecting D4-D8 brane system in ten-dimensional type IIA supergravity. The dynamical solutions reduces to a static warped $\mathrm{AdS}_6 \times \mathrm{S}^4$ geometry in a certain spacetime region. We also consider lower-dimensional effective theories for the warped compactification of general p-brane system. It is found that an effective $p+1$-dimensional description is not possible in general due to the entanglement of the transverse coordinates and the $p+1$-dimensional coordinates in the metric components. Then we discuss cosmological solutions. We find a solution that behaves like a Kasner-type cosmological solution at $\tau \to \infty$, while it reduces to a warped static solution at $\tau \to 0$, where τ is the cosmic time.

1 Introduction

Recently studies on dynamical solutions of supergravity have been a topic of great interest. Conventionally time dependent solutions of higher dimensional supergravity are discussed in the context of lower dimensional effective theories after compactifying the internal space. However, it is unclear how far this effective low-dimensional description is valid. Thus it is much more desirable to discuss the four-dimensional cosmology in terms of the dynamics of the original higher-dimensional theory. This is particularly true in string cosmology in which the behavior of the early universe is to be understood in the light of string theory. Indeed, it was pointed out that the four-dimensional effective theory for warped compactification of ten-dimensional type IIB supergravity allows solutions that cannot be obtained from solutions in the original higher-dimensional theories [1].

In the present work, we consider dynamical solutions for intersecting D4-D8 brane systems in the ten-dimensional type IIA supergravity model[2]. In § 2, we first consider p-brane systems in D-dimensions and derive a class of dynamical solutions under a certain metric ansatz. In § 3, focusing on intersecting D4-D8 brane systems in the ten-dimensional type IIA supergravity, we extend the metric ansatz used in the previous section to intersecting branes and obtain a class of dynamical solutions. Then further specializing the form of the metric, we consider a cosmological solution. Interestingly, this solution is found to approach a warped static solution as $\tau \to 0$ and a Kasner type anisotropic solution as $\tau \to \infty$, where τ is the cosmic time. Finally we conclude in § 4.

2 Dynamical p-brane solutions

We consider a gravitational theory with the metric g_{MN}, dilaton ϕ, and an anti-symmetric tensor field of rank $(p+2)$ in D dimensions. This corresponds to a p-brane system in string theory. The most general action for the p-brane system in the Einstein frame can be written as

$$S = \frac{1}{2\kappa^2} \int \left(R * \mathbf{1}_D - \frac{1}{2} d\phi \wedge * d\phi - \frac{1}{2} e^{-c\phi} F_{(p+2)} \wedge * F_{(p+2)} \right), \tag{2.1}$$

[1] E-mail:Pierre.Binetruy@apc.univ-paris7.fr
[2] E-mail:misao@yukawa.kyoto-u.ac.jp
[3] E-mail:uzawa@ksc.kwansei.ac.jp

where κ^2 is the D-dimensional gravitational constant, $*$ is the Hodge dual operator in the D-dimensional spacetime, and c is a constant given by $c^2 = 4 - 2(p+1)(D-p-3)(D-2)^{-1}$. The expectation values of fermionic fields are assumed to be zero.

To solve the field equations, we assume the D-dimensional metric in the form

$$ds^2 = h^a(x,y) q_{\mu\nu} dx^\mu dx^\nu + h^b(x,y) u_{ij} dy^i dy^j, \tag{2.2}$$

where $q_{\mu\nu}$ is a $(p+1)$-dimensional metric which depends only on the $(p+1)$-dimensional coordinates x^μ, and u_{ij} is the $(D-p-1)$-dimensional metric which depends only on the $(D-p-1)$-dimensional coordinates y^i. The parameters a and b are given by $a = -(D-p-3)(D-2)^{-1}$, $b = (p+1)(D-2)^{-1}$.

Furthermore, we assume that the scalar field ϕ and the gauge field strength $F_{(p+2)}$ are given by

$$e^\phi = h^{-c/2}, \qquad F_{(p+2)} = \sqrt{-q}\, d(h^{-1}) \wedge dx^0 \wedge dx^1 \wedge \cdots \wedge dx^p. \tag{2.3}$$

Here, q is the determinant of the metric $q_{\mu\nu}$. Let us first consider the Einstein equations. Using the assumptions (2.2) and (2.3), the Einstein equations are given by

$$hR_{\mu\nu}(\mathrm{X}) - D_\mu D_\nu h - \frac{a}{2} q_{\mu\nu} \left(\triangle_{\mathrm{X}} h + h^{-1} \triangle_{\mathrm{Y}} h\right) = 0, \quad R_{ij}(\mathrm{Y}) - \frac{b}{2} u_{ij} \left(\triangle_{\mathrm{X}} h + h^{-1} \triangle_{\mathrm{Y}} h\right) = 0, \quad \partial_\mu \partial_i h = 0, \tag{2.4}$$

where D_μ is the covariant derivative with respective to the metric $q_{\mu\nu}$, $\triangle_{\mathrm{X}}$ and $\triangle_{\mathrm{Y}}$ are the Laplace operators on the space of X and the space Y, and $R_{\mu\nu}(\mathrm{X})$ and $R_{ij}(\mathrm{Y})$ are the Ricci tensors of the metrics $q_{\mu\nu}$ and u_{ij}, respectively. From the third equation of (2.4), the warp factor h must be in the form $h(x,y) = h_0(x) + h_1(y)$. Let us next consider the gauge field. Under the assumption (2.3), we find $dF_{(p+2)} = 0$. Thus, the Bianchi identity is automatically satisfied. Also the equation of motion for the gauge field becomes $d\left[e^{-c\phi} * F_{(p+2)}\right] = 0$. Hence, the gauge field equation is automatically satisfied under the assumption (2.3).

Let us consider the scalar field equation. Substituting the forms of the scalar and the gauge field (2.3), and the warp factor $h(x,y) = h_0(x) + h_1(y)$ into the equation of motion for the scalar field, we obtain

$$ch^{-b}\left(\triangle_{\mathrm{X}} h_0 + h^{-1} \triangle_{\mathrm{Y}} h_1\right) = 0. \tag{2.5}$$

Thus, unless the parameter c is zero, the warp factor h should satisfy the equations $\triangle_{\mathrm{X}} h_0 = 0$ and $\triangle_{\mathrm{Y}} h_1 = 0$. If $F_{(p+2)} \neq 0$, the function h_1 is non-trivial. In this case, the Einstein equations reduce to

$$R_{\mu\nu}(\mathrm{X}) = 0, \qquad R_{ij}(\mathrm{Y}) = 0, \qquad D_\mu D_\nu h_0 = 0. \tag{2.6}$$

On the other hand, if $F_{(p+2)} = 0$, the function h_1 becomes trivial. Namely the internal space is no longer warped [1].

Here we mention an important fact about the nature of the dynamical solutions described in the above. In general, we regard the $(p+1)$-dimensional spacetime to contain our four-dimensional universe while the remaining space is assumed to be compact and sufficiently small in size. Then one would usually think that an effective $(p+1)$-dimensional description of the theory should be possible at low energies. However, solutions of the field equations have the property that they are genuinely D-dimensional in the sense that one can never neglect the dependence on Y, say of h. This is clear from an inspection of Eqs. (2.4). In particular, the second equation involves the Laplacian of h with respect to the space X. Hence the equations determining the internal space Y cannot be determined independently from the geometry of the space X. The origin of this property is due to the existence of a non-trivial gauge field strength which forces the function h to be a linear combination of a function of x^μ and a function of y^i, instead of a product of these two types of functions as conventionally assumed. This fact is in sharp contrast with the case when one is allowed to integrate out the internal space to obtain an effective lower dimensional theory.

Finally we comment on the exceptional case of $c = 0$, which happens when $(D,p) = (10,3)$, $(11,5)$, $(11,2)$. The scalar field becomes constant because of the ansatz (2.3), and the scalar field equation is automatically satisfied. Then, the Einstein equations become

$$R_{\mu\nu}(\mathrm{X}) = 0, \qquad R_{ij}(\mathrm{Y}) = \frac{b}{2}(p+1)\lambda u_{ij}(\mathrm{Y}), \qquad D_\mu D_\nu h_0 = \lambda q_{\mu\nu}(\mathrm{X}), \tag{2.7}$$

where λ is a constant. As seen from these equations, the internal space Y is not necessarily Ricci flat, and the function h_0 becomes more complicated. For example, when the metric $q_{\mu\nu}$ is Minkowski, h_0 is no longer linear in the coordinates x^μ but quadratic in them [3].

3 Dynamical solutions for D4-D8 brane system

Now we consider dynamical solutions for the D4-D8 brane system which appears in the ten-dimensional type IIA supergravity. The bosonic action of D4-D8 brane system in the Einstein frame is given by

$$S = \frac{1}{2\kappa^2}\int\left(R*\mathbf{1} - \frac{1}{2}d\phi\wedge *d\phi - \frac{1}{2\cdot 4!}e^{\phi/2}F_{(4)}\wedge *F_{(4)} - \frac{1}{2}e^{5\phi/2}m^2 *\mathbf{1}\right). \tag{3.1}$$

In the following, we look for a solution whose spacetime metric has the form

$$ds^2 = h^{1/12}(z)\left[h_4^{-3/8}(x,r,z)q_{\mu\nu}dx^\mu dx^\nu + h_4^{5/8}(x,r,z)\left(dr^2 + r^2 u_{ij}dy^i dy^j + dz^2\right)\right], \tag{3.2}$$

where $q_{\mu\nu}$ is the five-dimensional metric depending only on the coordinates x^μ of X_5, and u_{ij} is the three-dimensional metric depending only on the coordinates y^i of Y_3. As for the scalar field and the 4-form field strength, we adopt the following assumptions

$$e^\phi = h^{-5/6}h_4^{-1/4}, \quad F_{(4)} = e^{-\phi/2} *\left[\sqrt{-q}\,d(h_4^{-1})\wedge\, dx^0\wedge dx^1\wedge dx^2\wedge dx^3\wedge dx^4\right]. \tag{3.3}$$

Let us first consider the Einstein equations. Under the assumptions (3.2) and (3.3), the Einstein equations give $h_4(x,y,z) = H_0(x) + H_1(r,z)$. Let us next consider the gauge field $F_{(4)}$. Under the assumptions (3.2) and (3.3), the Bianchi identity $dF_{(4)} = 0$ gives

$$\partial_r^2 h_4 + (3/r)\partial_r h_4 + \partial_z^2 h_4 + (1/3)\partial_z \ln h\,\partial_z h_4 = 0\,, \quad \partial_\mu\partial_r h_4 = 0\,, \quad \partial_\mu\partial_z h_4 = 0\,. \tag{3.4}$$

The last two equations are consistent with the result $h_4(x,y,z) = H_0(x)+H_1(r,z)$. Then the first equation (3.4) becomes

$$\partial_r^2 H_1 + (3/r)\partial_r H_1 + \partial_z^2 H_1 + (1/3)\partial_z \ln h\,\partial_z H_1 = 0\,. \tag{3.5}$$

The gauge field equation $d(e^{\phi/2} * F_{(4)}) = 0$ is automatically satisfied under the assumption (3.3) and the form of h_4 given by $h_4(x,y,z) = H_0(x) + H_1(r,z)$.

Next we consider the scalar field equation. Substituting the assumptions for the metric (3.2), the scalar and gauge fields (3.3), and the form of $h_4(x,y,z) = H_0(x) + H_1(r,z)$ into the scalar field equation, we find

$$\triangle_{\mathrm{X}_5} H_0 + (5/4)\left[(4/9)(\partial_z \ln h)^2 + (2/3)h^{-1}\partial_z^2 h - m^2 h^{-2}\right] = 0\,, \tag{3.6}$$

where $\triangle_{\mathrm{X}_5}$ is the Laplace operator on the space X_5, and we used the equation (3.5).

Inserting Eqs. (3.5) and (3.6) into the Einstein equations, we find for non-trivial H_1,

$$R_{\mu\nu}(\mathrm{X}_5) = 0, \quad R_{ij}(\mathrm{Y}_3) = 2u_{ij}, \quad D_\mu D_\nu H_0 = 0\,, \quad \triangle_{\mathrm{X}_5} H_0 = 0\,, \quad 4\left(\partial_z h\right)^2/9 - m^2 = 0\,, \quad \partial_z^2 h = 0\,, \tag{3.7}$$

where $R_{\mu\nu}(\mathrm{X}_5)$, $R_{ij}(\mathrm{Y}_3)$ are the Ricci tensors of the metric $q_{\mu\nu}$ and u_{ij}, respectively, D_μ is the covariant derivative with respective to the metric $q_{\mu\nu}$. The last two equations of (3.7) is immediately solved to give $h(z) = 3m(z-z_0)/2$, where z_0 is an integration constant (corresponding to the position of the D8-brane). Below we set $z_0 = 0$ without loss of generality. Then (3.5) gives the solution $H_1(r,z) = c_1(r^2+z^2)^{-5/3}+c_2$, where c_1 and c_2 are constant parameters.

Let us investigate the geometrical properties of the D4-D8 brane system. As a particular solution to the 3-dimensional metric u_{ij} which satisfies the second equation of (3.7), we take the space Y_3 to be a three-dimensional sphere S^3. Then if we make a change of coordinates, $z = \tilde{r}\sin\alpha$, $r = \tilde{r}\cos\alpha$ $(0 \le \alpha \le \pi/2)$, the metric reads

$$ds^2 = h^{1/12}\left[h_4^{-3/8}q_{\mu\nu}dx^\mu dx^\nu + h_4^{5/8}(d\tilde{r}^2 + \tilde{r}^2 d\Omega_4^2)\right], \tag{3.8}$$

where $d\Omega_4^2 = d\alpha^2 + \cos^2\alpha d\Omega_3^2$, $h_4(x,\tilde{r}) = H_0(x) + c_1\tilde{r}^{-10/3}$, $h(\tilde{r},\alpha) = (3m/2)\tilde{r}\sin\alpha$. Here $d\Omega_3^2$ and $d\Omega_4^2$ denote the line elements of the three-dimensional sphere S^3 and the four-dimensional sphere S^4, respectively.

Now we further define a new coordinate U by $\tilde{r}^2 = U^3$. In the case $q_{\mu\nu}$ is the five-dimensional Minkowski metric $\eta_{\mu\nu}$, the ten-dimensional metric in the limit $U \to 0$ reduced to a warped $\mathrm{AdS}_6 \times \mathrm{S}^4$ space [2].

Let us consider the case $q_{\mu\nu} = \eta_{\mu\nu}$ in more detail. In this case, the solution for the warp factors h_4 and h can be obtained explicitly as $h_4(t,\tilde{r}) = \beta t + H_1(\tilde{r})$, $h(\tilde{r},\alpha) = (3m/2)\tilde{r}\sin\alpha$, where $H_1(\tilde{r}) = c_1\tilde{r}^{-10/3}$, and β is a constant parameter.

If we introduce a new time coordinate τ by $\tau/\tau_0 = (\beta t)^{13/16}$, $\beta\tau_0 = 16/13$, the ten-dimensional metric is given by

$$\begin{aligned} ds^2 &= h^{1/12}\left(1+(\tau/\tau_0)^{-16/13}H_1\right)^{-3/8}\Big[\left(-d\tau^2 + (\tau/\tau_0)^{-6/13}\delta_{ab}dx^a dx^b\right) \\ &\quad + \left(1+(\tau/\tau_0)^{-16/13}H_1\right)(\tau/\tau_0)^{10/13}\left(d\tilde{r}^2 + \tilde{r}^2 d\Omega_4^2\right)\Big], \end{aligned} \tag{3.9}$$

where the metric δ_{ab} is the spatial part of the five-dimensional Minkowski metric $\eta_{\mu\nu}$. If we set $H_1 = 0$, the scale factor of the four-dimensional space is proportional to $\tau^{-6/13}$, while that for the remaining five-dimensional space is proportional to $\tau^{10/13}$. Thus in the limit when the terms with H_1 are negligible, which is realized in the limit $\tau \to \infty$, we have a cosmological solution. Although this cosmological solution is by no means realistic, it is interesting to note that this cosmological solution is asymptotically static in the past $\tau \to 0$.

4 Conclusion

In this work, we investigated dynamical solutions of higher-dimensional supergravity models. We found a class of time-dependent solutions for an intersecting D4-D8 brane system. These solutions were obtained by replacing a constant A in the warp factor $h = A + h_1(y)$ of a supersymmetric solution by a function $h_0(x)$ of the coordinates x^μ [3], where the coordinates y^i would describe the internal space and x^μ would describe our universe if the spatial dimensions of our universe were four instead of three. In the D4-D8 brane solution, the geometry was found to approach a warped static $\mathrm{AdS}_6 \times \mathrm{S}^4$ in a certain region of the spacetime.

In particular, we found an interesting solution which is warped and static as $\tau \to 0$ but approaches a Kasner-type solution as $\tau \to \infty$, where τ is the cosmic time. Although the solution itself is by no means realistic, its interesting behavior suggests a possibility that the universe was originally in a static state of warped compactification and began to evolve toward a universe with a Kaluza-Klein compactified internal space.

Conventionally one would expect an effective theory description in lower dimensions to be valid at low energies. However, as clearly the case of the cosmological solution mentioned above, the solutions we found have the property that they are genuinely D-dimensional in the sense that one can never neglect the dependence on y^i, say of h. Thus our result indicates that we have to be careful when we use a four-dimensional effective theory to analyse the moduli stabilisation problem and the cosmological problems in the framework of warped compactification of supergravity or M-theory.

References

[1] H. Kodama and K. Uzawa, JHEP **0603** (2006) 053 [arXiv:hep-th/0512104].

[2] P. Binetruy, M. Sasaki and K. Uzawa, arXiv:0712.3615 [hep-th].

[3] H. Kodama and K. Uzawa, JHEP **0507** (2005) 061 [arXiv:hep-th/0504193].

Uniqueness of Pomeransky-Sen'kov black ring solution as boundary value problem

Yoshiyuki Morisawa[1], Shinya Tomizawa[2] and Yukinori Yasui[2]

[1]*Faculty of Liberal Arts and Sciences, Osaka University of Economics and Law, Yao City, Osaka 581-8511, Japan*

[2]*Department of Mathematics and Physics, Graduate School of Science, Osaka City University, 3-3-138 Sugimoto, Sumiyoshi, Osaka 558-8585, Japan*

Abstract

We study the boundary value problem for asymptotically flat stationary black ring solutions to the five-dimensional vacuum Einstein equations. Assuming the existence of two additional commuting axial Killing vector fields and the horizon topology of $\mathrm{S}^1 \times \mathrm{S}^2$, we show that the only asymptotically flat black ring solution with a regular horizon and without conical singularity is the Pomeransky-Sen'kov black ring solution.

1 Introduction

In recent years, studies of black holes in higher dimensions have attracted much attention in the context of string theory and the brane world scenario. In fact, it has been predicted that higher-dimensional black holes would be produced in a future linear collider. Such physical phenomena are expected not only to give us a piece of evidence for the existence of extra dimensions but also to help us to draw some information toward quantum gravity. Studies on stationary black hole solutions are important since we may detect the Hawking radiation after the formation of stationary black holes in a collider.

A striking feature of asymptotically flat stationary black hole solutions in five dimensions is that they admit event horizons with non-spherical topologies in contrast to four dimensions. For instance, the topology of the event horizon in higher dimensions cannot be uniquely determined [1, 2, 3] in contrast to four-dimensional ones, which is restricted only to the two sphere [4, 5]. In five dimensions, however, the possible geometric types of the horizon topology are S^3 and $\mathrm{S}^1 \times \mathrm{S}^2$ [1], and in dimensions higher than five, more complicated [2, 3]. The black ring solutions with the horizon topology $\mathrm{S}^1 \times \mathrm{S}^2$, which rotate along the S^1 direction, were found by Emparan and Reall as solutions to the five-dimensional vacuum Einstein equations [6]. This is the first example of black hole solution with non-spherical topology. In addition to the black ring solution, the rotating black hole solution with S^3 horizon topology had been already found by Myers and Perry [7]. Remarkably, within some range of the parameters, there are one black hole and two black rings with the same values of the mass and the angular momentum, which means the violation of the uniqueness known in four dimensions. Subsequently, other black ring solutions were found. The black ring solutions with a rotating two sphere were found by Mishima and Iguchi [8], and moreover, one with two angular momenta was constructed by Pomeransky and Sen'kov [9] by using the inverse scattering method [10, 11, 12, 13, 14, 15, 16, 17, 18, 19, 20, 21].

For the asymptotically flat, static solutions of higher-dimensional vacuum Einstein equations, the Schwarzschild-Tangherlini solution [22] is the unique solution [23], and moreover, which is stable against linear perturbations [24]. It has been shown that the five-dimensional Myers-Perry solution is unique if the topology is restricted to S^3 and the spacetime admits three commuting Killing vectors [25]. Hence it is natural to ask whether the Pomeransky-Sen'kov black ring solution is also unique under the assumptions of the existence of three commuting Killing vector field and the horizon topology of $\mathrm{S}^1 \times \mathrm{S}^2$. As mentioned above, however, there are two different black ring solutions for the same mass and the same angular momenta. Therefore, we must add some additional information to consider the boundary value problem for black ring solutions. One of the examples is the *rod structure* introduced by Harmark [26]. By introducing the rod structure, Hollands and Yazadjiev [27] applied the discussion in Ref. [25] to the case of non-spherical horizon topology and showed that two asymptotically flat and five-dimensional black hole solutions with the same topology, the same mass, the same angular momenta and the same rod structure are isometric to each other.

2 General Black Ring

The metric of general black ring solution, which in general has a conical singularity, is given by

$$\begin{aligned} ds^2 &= -\frac{H(y,x)}{H(x,y)}(dt+\Omega)^2 - \frac{F(x,y)}{H(y,x)}d\phi^2 - 2\frac{J(x,y)}{H(y,x)}d\phi d\psi + \frac{F(y,x)}{H(y,x)}d\psi^2 \\ &\quad + \frac{2k^2 H(x,y)}{(x-y)^2(1-\nu)^2}\left(\frac{dx^2}{G(x)} - \frac{dy^2}{G(y)}\right), \end{aligned} \tag{1}$$

where the C-metric coordinates x, y run the ranges of $-1 \le x \le 1$ and $(-\lambda + \sqrt{\lambda^2 - 4\nu})/2 \le y < \infty$ or $-\infty < y \le -1$, respectively. The solution has parameters satisfying the inequalities $0 \le \nu < 1$, $2\sqrt{\nu} \le \lambda < 1+\nu$, $k > 0$ and $c \le b < 1$ with $c = \sqrt{\lambda^2 - 4\nu}/(1-\nu)$. The function G appearing in the metric is defined as $G(x) = (1-x^2)(1+\lambda x+\nu x^2)$. Since the other functions H, J, F and the one-form Ω have considerably complicated forms, we do not write it here. The explicit expressions of them are given in the full version of this article [28]. As shown there, this solution has the four independent parameters since there are the seven parameters $\lambda, \nu, q, \alpha, b, c, k$ and the three relations between them. Under the choice of the parameters $b = 2c/(1+c^2)$, which is the condition for a conical singularity inside the black ring to vanish, the metric reduces to that of the Pomeransky-Sen'kov black ring solution [9].

3 Conclusions

Since there are two black ring solutions with different shapes for the same mass and the same angular momenta [6, 9], we must introduce some additional geometrical information in order to consider the uniqueness of black rings as the boundary value problem. By introducing the rod structure [26], Hollands and Yazadjiev applied the discussion in Ref. [25] to the case of non-spherical horizon topology and showed the following theorem in Ref. [27].

Theorem 1 *Consider two stationary, asymptotically flat, vacuum black objects spacetimes of the five-dimensions with commuting two axial Killing vector fields and a timelike Killing vector field. Then, if both solutions have the same topology, the same rod structure and the values of the mass M and angular momenta J_1, J_2, they are isometric.*

However, even if we restrict the horizon topology to $S^1 \times S^2$, this theorem does not imply that the Pomeransky-Sen'kov black ring solution is the only *conical-free* black ring solution within the class of these solutions since there may exist another *conical-free* black ring solution with the same mass and two angular momenta and different rod structure data. Our purpose in this article is to prove the uniqueness of the Pomeransky-Sen'kov black ring solution by showing that the black rings with the rod structures different from that of the Pomeransky-Sen'kov black ring solution have conical singularities. Our proof is composed of two steps: First, we show the existence of asymptotically flat black ring solution with conical singularities and without curvature singularities such that they coincides with the Pomeransky-Sen'kov black ring solution under the condition of no conical singularity; next, once these black ring solution is given, using the theorem 1 obtained by Hollands and Yazadjiev, we can show the uniqueness of the black ring solution (1) in this class of the solutions admitting three mutually commuting Killing vector fields, i.e., a timelike Killing vector field and two axial Killing vector fields. However, we should note the following point. If we apply the Hollands-Yazadjiev's theorem to this black ring solution (1), it seems to be specified by the asymptotic charges M, J_ϕ, J_ψ and the additional parameters z_1, z_2, z_3 appearing in the rod data, although all of these six parameters are not independent. In fact, the only four parameters M, J_ϕ, J_ψ and c are independent, where $M, J_I (I = \phi, \psi)$ denote the mass and angular momenta, respectively, and the constant c has the geometrical meaning of the ratio of the radius of S^2 to the radius of S^1. In terms of these parameters, we obtain the following result:

Corollary 1 *Consider asymptotically flat black ring solutions to the five-dimensional vacuum Einstein equations admitting three commuting Killing vector fields, i.e., two axial Killing vector fields and a timelike Killing vector field. Then, in this class of solutions, the only solution with the horizon topology of $S^1 \times S^2$ is the black ring solution (1) specified by a mass M, two angular momenta J_ϕ, J_ψ and the ratio c of the radius of S^2 to the radius of S^1.*

In particular, if we impose that the black ring solutions do not admit a conical singularity, we obtain the main result in this article:

Theorem 2 *The only asymptotically flat, five-dimensional black ring solution with commuting two axial Killing vector fields and a timelike Killing vector field and without a conical singularity is the Pomeransky-Sen'kov solution.*

References

[1] M. l. Cai and G. J. Galloway, Class. Quant. Grav. **18**, 2707 (2001).

[2] C. Helfgott, Y. Oz and Y. Yanay, JHEP **0602**, 025 (2006).

[3] G. J. Galloway and R. Schoen, Commun. Math. Phys. **266**, 571 (2006).

[4] S. W. Hawking, Commun. Math. Phys. **25**, 152 (1972).

[5] S. W. Hawking and G. F. R. Ellis, *The large scale structure of space-time* (Cambridge University Press, 1973).

[6] R. Emparan and H. S. Reall, Phys. Rev. Lett. **88**, 101101 (2002).

[7] R. C. Myers and M. J. Perry, Annals Phys. **172**, 304 (1986).

[8] T. Mishima and H. Iguchi, Phys. Rev. D **73**, 044030 (2006).

[9] A. A. Pomeransky and R. A. Sen'kov, arXiv:hep-th/0612005.

[10] V. A. Belinsky and V. E. Zakharov, Sov. Phys. JETP **48**, 985 (1978);
V. A. Belinsky and V. E. Sakharov, Sov. Phys. JETP **50**, 1 (1979).

[11] V. A. Belinski and E. Verdaguer, *Gravitational Solitons*, (Cambridge University Press, 2001).

[12] S. Tomizawa, Y. Morisawa and Y. Yasui, Phys. Rev. D **73**, 064009 (2006).

[13] S. Tomizawa and M. Nozawa, Phys. Rev. D **73**, 124034 (2006).

[14] S. Tomizawa, H. Iguchi and T. Mishima, Phys. Rev. D **74**, 104004 (2006).

[15] S. Tomizawa, H. Iguchi and T. Mishima, arXiv:hep-th/0702207.

[16] H. Iguchi, T. Mishima and S. Tomizawa, Phys. Rev. D **76**, 124019 (2007).

[17] A. A. Pomeransky, Phys. Rev. D **73**, 044004 (2006).

[18] T. Koikawa, Prog. Theor. Phys. **114**, 793 (2005).

[19] T. Azuma and T. Koikawa, Prog. Theor. Phys. **116**, 319 (2006).

[20] H. Iguchi and T. Mishima, Phys. Rev. D **73**, 121501 (2006).

[21] J. Castejon-Amenedo and V. S. Manko, Phys. Rev. D **41**, 2018 (1990).

[22] F. R. Tangherlini, Nuovo Cim. **27**, 636 (1963).

[23] G. W. Gibbons, D. Ida and T. Shiromizu, Prog. Theor. Phys. Suppl. **148**, 284 (2003);
G. W. Gibbons, D. Ida and T. Shiromizu, Phys. Rev. Lett. **89**, 041101 (2002).

[24] A. Ishibashi and H. Kodama, Prog. Theor. Phys. **110**, 901 (2003).

[25] Y. Morisawa and D. Ida, Phys. Rev. D **69**, 124005 (2004).

[26] T. Harmark, Phys. Rev. D **70**, 124002 (2004);
T. Harmark and P. Olesen, Phys. Rev. D **72**, 124017 (2005).

[27] S. Hollands and S. Yazadjiev, arXiv:0707.2775 [gr-qc].

[28] Y. Morisawa, S. Tomizawa and Y. Yasui, arXiv:0710.4600 [hep-th].

Multi graviton theory in vierbein formalism

Teruki Hanada,[1] Kazuhiko Shinoda[2] and Kiyoshi Shiraishi[3]

Graduate School of Science and Engineering, Yamaguchi University, Yoshida, Yamaguchi-shi, Yamaguchi 753–8512, Japan

Abstract

Recently, multi-graviton theory on a simple closed circuit graph corresponding to the S^1 compactification of the Kaluza-Klein (KK) theory has been considered. In the present paper, we extend this theory to that on a general graph and study what modes of particles are included. Furthermore, we generalize it in a possible non-linear theory based on the vierbein formalism and study cosmological solutions.

1 Introduction

Both astronomical and cosmological data seem to require the presence of yet directly undetected dark matter and dark energy in the universe. The necessity for these mysterious components occurs at distances where the gravitational interaction is not understood sufficiently. This suspicious coincidence inspires a search for modifications of the general relativity at large distances.

It is important for understanding cosmology and unification to study massive and multi-graviton theory. In the linear theory, gravitons have a Fierz-Pauli (FP) type mass [1]. But there is an ambiguity in its nonlinear generalization. We study thus far the linear multi-graviton theory on a circle corresponding to S^1 compactification of KK theory with dimensional deconstruction [2]. This model is an extended version of Hamamoto's model [4].

In this article, we construct the FP Lagrangian on a general graph and investigate what modes of particles are included. Furthermore, we extend it to a nonlinear theory based on the vierbein formalism.

2 FP on a graph

We consider the matrix representation of the graph theory.[4] A graph G is a pair of V and E, where V is a set of vertices while E is a set of edges. An edge connects two vertices; two vertices located at the ends of an edge e are denoted as $o(e)$ and $t(e)$. Then, we introduce two matrices, an incidence matrix and a graph Laplacian, associated with a specific graph. The incidence matrix represents the condition of connection or structure of a graph, and the graph Laplacian Δ can be obtained by EE^T. By use of these matrices, a quadratic form of vectors $a^T\Delta a(= a^T EE^T a)$ can be written as a sum of $(a_i - a_j)^2$. If all a_i $(i = 1, 2, \ldots, \#V)$, components of a, take the same value, $E^T a = 0$ and then $\Delta a = 0$.

So, we consider the Lagrangian for a massive graviton $h^v_{\mu\nu}$ on each vertex with the Stueckelberg vector field A^e_μ on each edge and a scalar field ϕ^v on each vertex:

$$L_m = L_0 - \frac{m^2}{2}\sum_{v\in V}\left[h^{v\mu\nu}(EE^T h_{\mu\nu})^v - h^v(EE^T h)^v\right] \\ -2\sum_{v\in V}\left[m(EA_\mu)^v + \partial_\mu\phi^v\right]\left(\partial_\nu h^{v\mu\nu} - \partial^\mu h^v\right) - \frac{1}{2}\sum_{e\in E}\left(\partial_\mu A^e_\nu - \partial_\nu A^e_\mu\right)^2,$$

where L_0 is the linearized Einstein-Hilbert Lagrangian:

$$L_0 = \sum_{v\in V}\left[-\frac{1}{2}\partial_\lambda h^v_{\mu\nu}\partial^\lambda h^{v\mu\nu} + \partial_\lambda h^{v\lambda}{}_\mu\partial_\nu h^{v\nu\mu} - \partial_\mu h^{v\mu\nu}\partial_\nu h^v - \frac{1}{2}\partial_\lambda h^v\partial^\lambda h^v\right],$$

[1] E-mail : k004wa@yamaguchi-u.ac.jp
[2] E-mail : k009vc@yamaguchi-u.ac.jp
[3] E-mail : shiraish@yamaguchi-u.ac.jp
[4] Please see [3] for a review of application of graph theory to field theory.

and $h^v \equiv \eta^{\mu\nu} h^v_{\mu\nu}$.

This action is invariant under the following transformations:

$$h^v_{\mu\nu} \to h^v_{\mu\nu} + \partial_\mu \xi^v_\nu + \partial_\nu \xi^v_\mu, \quad A^e_\mu \to A^e_\mu + m(E^T \xi_\mu)^e - \partial_\mu \zeta^e, \quad \phi^v \to \phi^v + m(E\zeta)^v,$$

where ξ^v and ζ^e are parameters on each vertex and each edge respectively.

Suppose the following gauge fixing terms:

$$L_{gf} = -\sum_{v\in V} \Big[\partial_\nu h^{v\mu\nu} - \frac{1}{2}\partial^\mu h^v - m(EA^\mu)^v - \partial^\mu \phi^v\Big]^2 - \sum_{e\in E} \Big[\partial_\mu A^{e\mu} - \frac{m}{2}(E^T h)^e - m(E^T\phi)^e\Big]^2,$$

then, the gauge-fixed Lagrangian becomes

$$L_m + L_{gf} = \frac{1}{2} H^{\mu\nu}(\partial^2 - m^2 EE^T)\Big(H_{\mu\nu} - \frac{1}{2}H\eta_{\mu\nu}\Big) + A^\mu(\partial^2 - m^2 E^T E)A_\mu + 3\phi(\partial^2 - m^2 EE^T)\phi,$$

where $H_{\mu\nu} = h_{\mu\nu} + \phi\eta_{\mu\nu}$. Here the indices v and e, and the notion of sum over them are omitted.

3 Dimensional deconstruction

It is assumed that we put fields on vertices or a edges. An idea that there are four dimensional fields on the sites (vertices) and links (edges), dimensional deconstruction, is introduced by Arkani-Hamed *et al.* [5, 6]. In this scheme, the square of mass matrix is proportional to the Laplacian of the associated graph.

In the case of a cycle graph (a 'closed circuit') with N sites (C_N), when N becomes large, the model on the graph corresponds with the five-dimensional theory with S^1 compactification. In other words, the mass scale of the model f over N correspond to the inverse of the compactification radius:

$$M_\ell^2 = 4f^2(\sin \pi\ell/N)^2 \quad \to \quad M_\ell^2 = (2\pi\ell/L)^2, \qquad (f/N \to 1/L)\,.$$

For a cycle graph, the linear graviton model presented in the previous section coincides with the model proposed in [2]. The model is a most general linear graviton theory on a generic graph.

4 Multi graviton theory on a general graph

For this model, we investigate what modes of particles are contained. Although any graph is valid for the model, here we consider two examples, a cycle graph C_N and a path graph P_N. In the case of the cycle graph C_N ($\#V = N$, $\#E = N$), $N-1$ massive spin two's, a massless spin two, $N-1$ massive vectors, a massless vector, $N-1$ massive scalars, and a massless scalar seem to be included, as seen from the gauge-fixed Lagrangian. The mass spectra of different spin fields are the same, up to zero modes. This is due to the fact that eigenvalues of EE^T and ones of E^TE are the same except for zero eigenvalues.

However, $N-1$ massive spin two, a massless spin two, a massless vector, and a massless scalar are left physically, because massive vectors and massive scalars are absorbed by massive spin two fields to form massive gravitons with five degrees of freedom each.

Similarly, in the case of the path graph P_N ($\#V = N$, $\#E = N-1$), $N-1$ massive spin two's, a massless spin two, and a massless scalar is left physically, the massless vector mode is absent.

The limits of N to infinity in the cases of C_N and P_N realize the KK theory with S^1 and S^1/Z_2 compactification, respectively.

5 Nonlinear generalization

Now we will consider a nonlinear extension of the linear theory. Following Nibbelink *et al.* [7, 8], we introduce a useful 'tool':

$$\langle ABCD\rangle \equiv -\varepsilon_{abcd}\varepsilon^{\mu\nu\rho\sigma} A^a_\mu B^b_\nu C^c_\rho D^d_\sigma,$$

where ε is the totally antisymmetric tensor. Using this expression, we have the Einstein-Hilbert term replacing A and B by vierbeins and C and D by the curvature 2-form. In addition, because fourth power of vierbein in the angle bracket is equal to the determinant of vierbeins ($\langle eeee\rangle = \langle e^4\rangle = |e|$), this expression means that the Einstein-Hilbert term and the cosmological term have the same structure.

We now assume that the following term is assigned for each edge of a graph:

$$\langle (e_1e_1 - e_2e_2)^2\rangle,$$

where e_1 and e_2 are vierbeins at two ends of one edge. Note that this term has a reflection symmetry $e \leftrightarrow -e$ at each vertex and an exchange symmetry $e_1 \leftrightarrow e_2$ at each edge.

In the weak field limit, *i.e.* $e_1 = \eta + f_1$, $e_2 = \eta + f_2$,

$$\langle (e_1e_1 - e_2e_2)^2\rangle = 8\left(([f_1] - [f_2])^2 - \left[(f_1 - f_2)^2\right]\right) + O(f^3)\,,$$

where η is the Minkowski metric, and $[f] = \mathrm{tr} f$ for notational simplicity. This quadratic term corresponds to FP mass term.[5]

On the other hand, the Einstein-Hilbert term $\frac{1}{2}|e|R$ contains the kinetic terms of a graviton in the lowest order up to the total derivative:

$$\frac{1}{2}|e|R = -\frac{1}{2}\partial_\lambda f_{\mu\nu}\partial^\lambda f^{\mu\nu} + \partial_\lambda f^\lambda_{\ \mu}\partial_\nu f^{\nu\mu} - \partial_\mu f^{\mu\nu}\partial_\nu f - \frac{1}{2}\partial_\lambda f\partial^\lambda f + O(f^3)\,,$$

and $\frac{1}{2}R$ contains the following terms in the first order:

$$\frac{1}{2}R = -\partial^\lambda\partial_\lambda f + \partial_\mu\partial_\nu f^{\mu\nu} + O(f^2)\,.$$

In the case of a tree graph (a graph with no closed circuit—the path graph P_N is a tree graph, for example), we have the nonlinear Lagrangian of multi-graviton theory without higher derivertive and non-local terms,

$$L_M = \frac{1}{2}\exp\Phi\sum_{v\in V}|e^v|\,R^v + M^2\sum_{e\in E}\left\langle\left(e_{o(e)}e_{o(e)} - e_{t(e)}e_{t(e)}\right)^2\right\rangle,$$

where $M^2 \equiv m^2/16$. The scalar zero-mode field Φ can be identified as $\phi_1 = \phi_2 = \cdots = \Phi$.

6 Cosmological solution

We will derive a cosmological solution of our model on a tree graph with N vertices. We assume $L = L_M + L_\Lambda$, where

$$L_\Lambda = \exp(a\Phi)\sum_{v\in V}|e^v|\,\Lambda^v\,.$$

Here, L_Λ represents the simplest effects of matters and a is a coupling constant. Suppose that each metric is homogeneous, isotropic, and flat, *i.e.*

$$ds_k^2 = -B_k^2(t)dt^2 + A_k^2(t)d\vec{x}^2\,.$$

Moreover, if we assume

$$A_k(t) = \alpha_k A(t),\quad B_k(t) = \alpha_k,\quad \frac{\dot{A}}{A} = H\,,$$

and $\Lambda_1 = \Lambda_2 = \cdots = \Lambda_N = \Lambda = \lambda_{(\ell)}M^2$, we obtain the following solution;

$$\alpha_k^2 = \frac{3H^2}{\Lambda}\left(1 + \sqrt{2}\frac{\sqrt{2-a}}{\sqrt{a}}v_k^{(\ell)}\right),\qquad \left(\frac{4}{3} < a < 2\right),\qquad \Phi \equiv 0,$$

where $\{\lambda_{(\ell)}, v_k^{(\ell)}\}$ are the nonzero eigenvalues and the components of eigenvectors. Note that this 'synchronized' solution is not a general solution but a special one.

Interestingly enough, in the case of the path graph, we have other solutions of Randall-Sundrum type by tuning the value of Λ_1 and Λ_N.

[5] It is known that the asymmetric part of f can be omitted [9].

7 Summary and prospects

We have studied the simple theory of multi-graviton, and have shown a cosmological solution. We should investigate more plausible solution for classical as well as quantum cosmology, including usual matter.

To this end, we should study the graviton coupling to various matter fields. At the same time, we expect that the Higgs-like mechanism on gravity might be developed by pursuing complicated, non-minimal interactions with matters. Incorporating SUSY (SUGRA) is also of much interest.

Permitting higher-derivative terms and non-local terms in the action will bring more possibilities to the completion of nonlinearity and be worth studying still.

From the mathematical point of view, it is interesting to construct models with the use of generic graphs, such as weighted graphs, fractals, and so on.

Acknowledgements

The authors would like to thank N. Kan for useful comments, and also the organizers of JGRG17.

References

[1] M. Fierz and W. Pauli, Proc. Roy. Soc. Lond. **A173** (1939) 211.

[2] N. Kan and K. Shiraishi, Class. Quant. Grav. **20** (2003) 4965, gr-qc/0212113.

[3] N. Kan and K. Shiraishi, J. Math. Phys. **46** (2005) 112301.

[4] S. Hamamoto, Prog. Theor. Phys. **97** (1997) 327, hep-th/9611141.

[5] N. Arkani-Hamed, A. G. Cohen and H. Georgi, Phys. Rev. Lett. **86** (2001) 4757; Phys. Lett. **B513** (2001) 232.

[6] C. T. Hill, S. Pokorski and J. Wang, Phys. Rev. **D64** (2001) 105005.

[7] S. G. Nibbelink, M. Peloso and M. Sexton, Eur. Phys. J. **C51** (2007) 741, hep-th/0610196.

[8] S. G. Nibbelink and M. Peloso, Class. Quant. Grav. **22** (2005) 1313, hep-th/0411184.

[9] C. Bizdadea et al., JHEP **02** (2005) 016; C. Bizdadea et al., Eur. Phys. J. **C48** (2006) 265.

Dilatonic Charged Domain-like Universe of Arbitrary Dimensions

Takuya Maki[1] and Kiyoshi Shiraishi[2]

[1] *Japan Women's College of Physical Education, Setagaya, Tokyo 157-8565, Japan*
[2] *Faculty of Science, Yamaguchi University,*
Yoshida, Yamaguchi-shi, Yamaguchi 753-8512, Japan

Abstract

Dilatonic domain-like space-time is investigated in arbitrary D-dimensions. We find a class of the static solutions depend only on a space-like co-ordinate for Einstein-dilaton theory with the cosmological constant and with the Maxwell field. The space-time can be interpreted as dilatonic $D-1$ dimensional domain-like universe.

1 Introduction

In the present report, dilatonic domain-like space-time is investigated in arbitrary D-dimensions. We find a class of the static solutions depend only on a space-like co-ordinate for Einstein-Dilaton theory with the cosmological constant and with the Maxwell field. The space-time can be interpreted as dilatonic $D-1$ dimensional domain-like universe.
First we shall find static domain-like solutions of the action:

$$S = \int dx^{N+1}\sqrt{-g}\left\{R - \frac{4}{N-1}(\partial\phi)^2 - e^{4b\phi/(N-1)}\Lambda\right\}, \tag{1}$$

where R is the scalar curvature and Λ is the cosmological constant. The scalar ϕ is the dilaton field. The constant b represents the dilaton coupling constant to Λ as a general free parameter in this framework.
We consider the metric given by

$$ds^2 = -e^{\rho_0}dt^2 + e^{\rho_1}dz^2 + \sum_{i=2}^{N} e^{\rho_i}dx_i^2, \tag{2}$$

where t is a time-like co-ordinate while z and x_i are space-like co-ordinates.
In order to find the static space-time solutions that depend only on a space-like co-ordinate, we suppose that all the components of the metric depend only on z.
Furthermore we choose the following ansatz:

$$\rho_1 = \rho_0 + \sum_{i=2}^{N}\rho_i\,. \tag{3}$$

Defining a variable $\psi_1(z)$ as

$$\psi_1 := \rho_0 + \sum_{i=2}^{N}\rho_i + 4b\phi/(N-1), \tag{4}$$

the field equations can be obtained as the following simple form:

$$\ddot{\rho}_\mu = -\frac{4}{N-1}\Lambda e^{\psi_1}, \quad \ddot{\phi} = \frac{b}{2}\Lambda e^{\psi_1} \tag{5}$$

---
[1] E-mail: maki@jwcpe.ac.jp
[2] E-mail: shiraish@sci.yamaguchi-u.ac.jp

and we obtain the equation of motion for the variable ψ_1 as

$$\ddot{\psi}_1 = \frac{2(b^2 - N)}{N-1}\Lambda e^{\psi_1}. \tag{6}$$

where $i, j, k = 2, 3, \cdots, N$ and $\mu, \nu = 0, 2, 3, \cdots, N$, and the dot denotes the derivative with respect to z. Also we obtain the Hamiltonian constraint

$$\frac{1}{2}\sum_{\nu\neq\mu}\sum_{\mu}\dot{\rho}_\mu\dot{\rho}_\nu = -\frac{8}{N-1}\dot{\phi}^2 - 2\Lambda e^{\psi_1}. \tag{7}$$

Eq.(6) is the Liouville equation for ψ_1 when $b \neq 2$ and can be analytically soloved:

$$e^{\psi_1} \;=\; \left(\frac{2c_1(N-1)}{\mid (b^2-N)\Lambda \mid}\right) \Big/ \left(e^{\sqrt{c_1/2}(z-z_{01})} - \varepsilon e^{-\sqrt{c_1/2}(z-z_{01})}\right)^2, \tag{8}$$

where c_1 and z_{01} are integration constants and the symbol ε denotes the signature of $(b^2 - N)\Lambda$, *i.e.* when $(b^2 - N)\Lambda > 0$, $\varepsilon = +1$ and then $-\infty < c_1 < \infty$, while $(b^2 - N)\Lambda < 0$ corresponds $\varepsilon = -1$ and $0 < c_1 < \infty$.
Substituting this solution into the *r.h.s.* of Eq.(5), one can obtain the general solutions:

$$\rho_1 \;=\; \left(\frac{2N}{(b^2-N)}\right)\ln\left(e^{\sqrt{c_1/2}(z-z_{01})} - \varepsilon e^{-\sqrt{c_1/2}(z-z_{01})}\right) + d_1 z + d_1', \tag{9}$$

$$\rho_\mu \;=\; \left(\frac{2}{(b^2-N)}\right)\ln\left(e^{\sqrt{c_1/2}(z-z_{01})} - \varepsilon e^{-\sqrt{c_1/2}(z-z_{01})}\right) + d_\mu z + d_\mu', \tag{10}$$

$$\phi \;=\; \left(\frac{b(N-1)}{2(b^2-N)}\right)\ln\left(e^{\sqrt{c_1/2}(z-z_{01})} - \varepsilon e^{-\sqrt{c_1/2}(z-z_{01})}\right) + d_\phi z + d_\phi', \tag{11}$$

where d_μ, d_μ' $(\mu = 0, 2, 3, \cdots, N)$, d_ϕ and d_ϕ' are the integration constants which satisfy

$$d_1 = \sum_\mu d_\mu = -\frac{4b}{N-1}d_\phi, \qquad d_1' = \sum_\mu d_\mu' = \ln\frac{2c_1(N-1)}{\mid (b^2-N)\Lambda \mid}. \tag{12}$$

The Hamiltonian constraint (7) gives the relation among the constants of integration:

$$\frac{c(N-1)}{2(N-b^2)} = \frac{4(b^2-N+1)}{(N-1)^2}d_\phi^2 - \frac{1}{4}\sum_\mu d_\mu^2. \tag{13}$$

One can interpret z as a 'radius' co-ordinate and another space-like co-ordinate, for example x_2, as 'angle'. Planer dilatonic domain-like brane Universe has also been studied in [3].

2 Charged Dilatonic Domain-like Universe

We shall study the static one-parameter solutions of Einsetin-dilaton-Maxwell theory with non-zero cosmological constant:

$$S = \int dx^{N+1}\sqrt{-g}\left\{R - \frac{4}{N-1}\left(\partial\phi\right)^2 - e^{-4a\phi/(N-1)}F^2 - e^{4b\phi/(N-1)}\Lambda\right\}. \tag{14}$$

Using the variable ψ's the field equations can be written by

$$\ddot{\psi}_\mu \;=\; 4\sum_\alpha \eta^{\mu\alpha}q_\alpha q_\mu e^{\psi_\mu} + \frac{4(a^2-1)}{N-1}\sum_{\alpha,\beta}\eta^{\alpha\beta}q_\alpha q_\beta e^{\psi_\alpha} + \frac{2(ab-1)}{N-1}\Lambda e^{\psi_1}, \tag{15}$$

$$\ddot{\psi}_1 \;=\; \frac{4(ab-1)}{N-1}\sum_{\mu,\nu}\eta^{\mu\nu}q_\mu q_\nu e^{\psi_\mu} + \frac{2(b^2-N)}{N-1}\Lambda e^{\psi_1}, \tag{16}$$

$$\ddot{\phi} \;=\; a\sum_{\mu,\nu}\eta^{\mu\nu}q_\mu q_\nu e^{\psi_\mu} + \frac{b}{2}\Lambda e^{\psi_1}, \tag{17}$$

where $\eta^{\mu\nu} = diag.(-1, +1, +1, ..., +1)$ and $q_\mu = (q_e, q_{mj})$ are the constants of integration with respect to the Maxwell field:

$$F_{1\mu} = \dot{A}_\mu = q_\mu e^{\psi_\mu}. \tag{18}$$

Then the Hamiltonian constraint is

$$\frac{1}{2}\sum_{\nu\neq\mu}\sum_{\mu}\dot{\rho}_\mu\dot{\rho}_\nu = \frac{-8}{N-1}\dot{\phi}^2 - 4\sum_{\alpha,\beta}\eta^{\alpha\beta}q_\alpha q_\beta e^{\psi_\alpha} - 2\Lambda e^{\psi_1}. \tag{19}$$

(1) electric solutions with vanishing cosmological constant
In this case, *i.e.* $q_\mu = (q_e, 0, 0, \cdot\cdot\cdot, 0)$ and $\Lambda = 0$, the field equations are

$$\begin{aligned}
\ddot{\psi}_0 &= -4\left(1 + \frac{a^2-1}{N-1}\right)q_e^2 e^{\psi_0}, \quad \ddot{\psi}_j = -4\left(\frac{a^2-1}{N-1}\right)q_e^2 e^{\psi_0}, && (20)\\
\ddot{\rho}_0 &= -4\left(1 - \frac{1}{N-1}\right)q_e^2 e^{\psi_0} \qquad \ddot{\rho}_j = \frac{4}{N-1}q_e^2 e^{\psi_0}, && (21)\\
\ddot{\phi} &= -a q_e^2 e^{\psi_0}, && (22)\\
F_{10} &= \dot{A}_0 = q_e e^{\psi_0}. && (23)
\end{aligned}$$

One can integrate these equations and obtain the 'electric solutions':

$$\begin{aligned}
\rho_0 &= \frac{2(N-2)}{N+a^2-2}\ln\cosh\sqrt{\frac{c_1}{2}}(z - z_{01}) + d_0 z + d_0', && (24)\\
\rho_1 &= \frac{2(2N-3)}{N+a^2-2}\ln\cosh\sqrt{\frac{c_1}{2}}(z - z_{01}) + d_1 z + d_1', && (25)\\
\rho_i &= \frac{2}{N+a^2-2}\ln\cosh\sqrt{\frac{c_1}{2}}(z - z_{01}) + d_i z + d_i', && (26)\\
\phi &= \frac{-a(N-1)}{N+a^2-2}\ln\cosh\sqrt{\frac{c_1}{2}}(z - z_{01}) + d_\phi + d_\phi', && (27)\\
F_{10} &= .\frac{(c/4q_e)(N-1)}{N+a^2-2}\frac{1}{\cosh^2\sqrt{\frac{c_1}{2}}(z - z_{01})}. && (28)
\end{aligned}$$

(2) magnetic solutions
The magnetic solutions can also be obtained by 'duality' transformation.

(3) the case of a finite cosmological constant
We focus only on electric solutions for $a = b = 1$ (low energy string case). The equation of motion can be written by

$$\begin{aligned}
\ddot{\psi}_0 &= -4q_e^2 e^{\psi_0}, \quad \ddot{\psi}_1 = -2\Lambda e^{\psi_1}, \quad \ddot{\psi}_j = 0, && (29)\\
\ddot{\phi} &= -q_e^2 e^{\psi_0} + \frac{1}{2}\Lambda e^{\psi_1}, && (30)\\
F_{10} &= q_e e^{\psi_0}. && (31)
\end{aligned}$$

The solutions are

$$\begin{aligned}
\rho_0 &= \frac{2(N-2)}{N-1}\ln\cosh\sqrt{\frac{c_1}{2}}(z - z_{01}) && (32)\\
&\quad + \frac{2\varepsilon}{N-1}\frac{\Lambda}{|\Lambda|}\ln\left(e^{\sqrt{c_1/2}(z-z_{01})} - \varepsilon e^{-\sqrt{c_1/2}(z-z_{01})}\right) + d_0 z + d_0', && (33)\\
\rho_1 &= \frac{2(2N-3)}{N-1}\ln\cosh\sqrt{\frac{c_1}{2}}(z - z_{01}) && (34)
\end{aligned}$$

$$
\begin{aligned}
& +\frac{2\varepsilon N}{N-1}\ln\left(e^{\sqrt{c_1/2}(z-z_{01})}-\varepsilon e^{-\sqrt{c_1/2}(z-z_{01})}\right)+d_1 z+d_1'\,, && (35)\\
\rho_i \;=\; & \frac{2}{N-1}\ln\cosh\sqrt{\frac{c_1}{2}}(z-z_{01}) && (36)\\
& +\frac{2\varepsilon}{N-1}\frac{\Lambda}{\mid\Lambda\mid}\ln\left(e^{\sqrt{c_1/2}(z-z_{01})}-\varepsilon e^{-\sqrt{c_1/2}(z-z_{01})}\right)+d_i z+d_i'\,, && (37)\\
\phi \;=\; & \frac{-1}{2}\ln\cosh\sqrt{\frac{c_1}{2}}(z-z_{01}) && (38)\\
& -\frac{\varepsilon}{2}\frac{\Lambda}{\mid\Lambda\mid}\ln\left(e^{\sqrt{c_1/2}(z-z_{01})}-\varepsilon e^{-\sqrt{c_1/2}(z-z_{01})}\right)+d_\phi+d_\phi'\,, && (39)\\
F_{10} \;=\; & \frac{c}{4q_e}\frac{1}{\cosh^2\sqrt{\frac{c_1}{2}}(z-z_{01})}\,, && (40)
\end{aligned}
$$

where $\varepsilon=+1$ for $\Lambda<0$, while $\varepsilon=-1$ for $\Lambda>0$.

3 Summary

We investigate the domain-like solution of dilaton gravity with cosmological constant and with the Maxwell field in arbitrary dimensions. We find the prescription to obtain a classs of the exact static domain-like solutions and describe these solutions. By means of these solutions, we can study the physical properties and applications to cosmology. Also the manifold consisted of these solutions needs to be investigated.

References

[1] N. Arkani-Hamed, S. Dimpooulos and G.Dvali, *Phys. Lett.* **B429** (1998) 263.

[2] L. Randall and R. Sundrum, *Phys. Rev. Lett.* **83** (1999) 3370.

[3] C. Charmousis, *Class. Quant. Grav.* **19** (2002) 83.

A new criterion for the final fate of gravitational collapse

Hayato Kawakami[1], Eiji Mitsuda[2], Yasusada Nambu[3] and Akira Tomimatsu[4]

Department of Physics, Nagoya University, Nagoya 464–8602, Japan

Abstract

We investigate the final fate of spherical dust collapse by using the orthonormal frame formalism with the Hubble normalized variables and the separable volume gauge, which is usually used for analyzing cosmological dynamics. As a result, we find that the final fate of spherical dust collapse is characterized by the quantity concerned with the energy density in this formalism. We discuss the final fate of spherical perfect fluid collapse with a barotropic equation of state and conjecture a criterion for the final fate of spherical gravitational collapse.

1 Introduction

The final fate of gravitational collapse is one of important issues in general relativity. According to the singularity theorem, a singularity is formed in the generic gravitational collapse of a massive star. However, it does not state the feature of the singularity. Also, there is the cosmic censorship conjecture, which states that a naked singularity is not formed in physically reasonable gravitational collapse. However, the proof of this conjecture has not existed. Moreover, there are many counterexamples to this conjecture. If a naked singularity is formed in gravitational collapse, it is interesting because an extreme strong gravity region can be observed. Therefore, it is important to understand whether or not the solutions of Einstein equation with a naked singularity are physically reasonable and it will be helpful to investigate the final fate of specific gravitational collapse.

So far, various solutions which describe gravitational collapse have been studied and some solutions with a naked singularity have been found [1]. Generally, the nakedness of the singularity formed in gravitational collapse is understood by investigating whether or not future directed non-spacelike geodesics coming out of the singularity exist. However, there is not a well-defined criterion for the nakedness of a singularity based on the physical quantities characterizing a spacetime and a matter although some researchers have investigated the relation between the final fate of gravitational collapse and the quantities [2,3]. Such a criterion should help us understand the intrinsic difference between the black hole formation and the naked singularity formation.

In this paper, We investigate the final fate of spherical dust collapse by using the orthonormal frame formalism with the Hubble normalized variables and the separable volume gauge, which is usually used for analyzing the asymptotic behavior of cosmological dynamics. As a result, we find that the final fate of spherical dust collapse is characterized by the quantity concerned with the energy density in this formalism. We discuss the final fate of perfect fluid collapse with the equation of state $\tilde{p} = (\gamma - 1)\tilde{\mu}$ in this formalism and get the two sufficient conditions, the one for the naked singularity formation of the perfect fluid collapse and the other for that the behavior of the spacetime of the perfect fluid collapse is self-similar. Based on these results, we conjecture a criterion for the final fate of spherical gravitational collapse.

2 Orthonormal frame formalism for spherical gravitational collapse

We apply the orthonormal frame formalism with the Hubble normalized variables and the separable volume gauge to spherical gravitational collapse of a perfect fluid with a barotropic equation of state.

[1]E-mail:kawakami@gravity.phys.nagoya-u.ac.jp
[2]E-mail:emitsuda@gravity.phys.nagoya-u.ac.jp
[3]E-mail:nambu@gravity.phys.nagoya-u.ac.jp
[4]E-mail:atomi@gravity.phys.nagoya-u.ac.jp

This formalism is usually used for analyzing the asymptotic behavior of cosmological dynamics [4]. Here a spacetime is described in terms of a coordinate system (t, x^i) and an orthonormal frame $(\mathbf{e}_{\hat{0}}, \mathbf{e}_{\hat{\alpha}})$ where the index i and the index $\hat{\alpha}$ describe the spatial components. It is assumed that $\mathbf{e}_{\hat{0}}$ is hypersurface orthogonal and the frame relates to the coordinate by the form $\mathbf{e}_{\hat{0}} = N^{-1}(\partial_t - N^i\partial_i)$ and $\mathbf{e}_{\hat{\alpha}} = e_{\hat{\alpha}}{}^i\partial_i$, where N is the lapse function and N^i is the shift vector. The basic variables in this formalism are the orthonormal frame vector components, the commutation functions associated with the frame and the matter variables which are normalized by dividing by the Hubble scalar $H = \Theta/3$, where Θ is the expansion rate of the temporal frame $\mathbf{e}_0$. The stress-energy tensor of a perfect fluid and the equation of state are as follows:

$$T_{\hat{a}\hat{b}} = \tilde{\mu}\tilde{u}_{\hat{a}}\tilde{u}_{\hat{b}} + \tilde{p}(\tilde{u}_{\hat{a}}\tilde{u}_{\hat{b}} + \eta_{\hat{a}\hat{b}}), \qquad \tilde{p} = (\gamma - 1)\tilde{\mu}, \tag{1}$$

where $\tilde{u}_a$, $\tilde{\mu}$ and $\tilde{p}$ are the 4-velocity of the fluid, the energy density and the pressure. We choose the separable volume gauge, which is the gauge so that the lapse function N is equal to H^{-1} and the shift vector N^i is equal to 0. For the case of spherical symmetry, the variables are $E_{\hat{\alpha}}{}^{\alpha}$, $A^{\hat{r}}$, $r^{\hat{r}}$, $\Sigma^{\hat{r}\hat{r}}$, Ω and $v^{\hat{r}}$. $E_{\hat{\alpha}}{}^{\alpha}$ are the frame vector components normalized by H, which are $E_{\hat{r}}{}^{r}$ and $E_{\hat{\theta}}{}^{\theta}$ in the case of spherical symmetry. $A^{\hat{r}}$ is the quantity obtained from the commutation function and normalized by H. $r^{\hat{r}}$ is the spatial Hubble gradient defined by $r^{\hat{r}} \equiv -E_{\hat{r}}{}^{r}\partial_r \ln H$. $\Sigma^{\hat{r}\hat{r}}$ is the shear rate of $\mathbf{e}_0$ normalized by H. Ω and $v^{\hat{r}}$ are defined by

$$\Omega \equiv \frac{[1 + (\gamma - 1)(v_{\hat{a}}v^{\hat{a}})]\tilde{\mu}}{3H^2[1 - (v_{\hat{a}}v^{\hat{a}})]}, \quad \tilde{u}^{\hat{a}} \equiv \frac{1}{\sqrt{1 - (v_{\hat{a}}v^{\hat{a}})}}(u^{\hat{a}} + v^{\hat{a}}), \tag{2}$$

where $u^{\hat{a}} \equiv e_{\hat{0}}{}^{\hat{a}}$. The evolution equations and the constraints in the case of prefect fluid spherical gravitational collapse are as follows:
Evolution equations:

$$\partial_t E_{\hat{r}}{}^{r} = -(q - \Sigma^{\hat{r}\hat{r}})E_{\hat{r}}{}^{r}, \tag{3}$$

$$\partial_t E_{\hat{\theta}}{}^{\theta} = -(q + \frac{1}{2}\Sigma^{\hat{r}\hat{r}})E_{\hat{\theta}}{}^{\theta}, \tag{4}$$

$$\partial_t A^{\hat{r}} = -(q - \Sigma^{\hat{r}\hat{r}})A^{\hat{r}} - \frac{1}{2}E_{\hat{r}}{}^{r}\partial_r\Sigma^{\hat{r}\hat{r}}, \tag{5}$$

$$\partial_t r^{\hat{r}} = -(q - \Sigma^{\hat{r}\hat{r}})r^{\hat{r}} - E_{\hat{r}}{}^{r}\partial_r q, \tag{6}$$

$$\partial_t\Sigma^{\hat{r}\hat{r}} = -(q-2)\Sigma^{\hat{r}\hat{r}} + \frac{2}{3}E_{\hat{r}}{}^{r}\partial_r A^{\hat{r}} - \frac{2}{3}E_{\hat{r}}{}^{r}\partial_r r^{\hat{r}} - \frac{4}{3}r^{\hat{r}}A^{\hat{r}} - \frac{2}{3}(E_{\hat{\theta}}{}^{\theta})^2 - 2\gamma G_+{}^{-1}\Omega(v^{\hat{r}})^2, \tag{7}$$

$$\begin{aligned}\partial_t\Omega = -(2q-1)\Omega + 3G_+{}^{-1}\Big[\gamma - 1 + \Big(1 - \frac{2}{3}\gamma\Big)(v^{\hat{r}})^2\Big]\Omega + E_{\hat{r}}{}^{r}\partial_r(\gamma G_+{}^{-1}\Omega v^{\hat{r}}) \\ -2\gamma G_+{}^{-1}\Omega v^{\hat{r}}A^{\hat{r}} + \gamma G_+{}^{-1}\Omega(v^{\hat{r}})^2\Sigma^{\hat{r}\hat{r}},\end{aligned} \tag{8}$$

$$\partial_t v^{\hat{r}} = \frac{G_+}{\gamma G_-\Omega}\Big(G_+[\partial_t(\gamma G_+{}^{-1}\Omega v^{\hat{r}}) + 2(q+1)\gamma G_+{}^{-1}\Omega v^{\hat{r}}] - \gamma v^{\hat{r}}(\partial_t\Omega + 2(q+1)\Omega)\Big). \tag{9}$$

Constraints:

$$1 + \frac{1}{3}(2E_{\hat{r}}{}^{r}\partial_r A^{\hat{r}} - 2r^{\hat{r}}A^{\hat{r}} - 3(A^{\hat{r}})^2 + (E_{\hat{\theta}}{}^{\theta})^2) - \frac{1}{4}(\Sigma^{\hat{r}\hat{r}})^2 - \Omega = 0, \tag{10}$$

$$E_{\hat{r}}{}^{r}\partial_r\Sigma^{\hat{r}\hat{r}} + 2r^{\hat{r}} - \Sigma^{\hat{r}\hat{r}}r^{\hat{r}} - 3A^{\hat{r}}\Sigma^{\hat{r}\hat{r}} + 3\gamma G_+{}^{-1}\Omega v^{\hat{r}} = 0, \tag{11}$$

$$E_{\hat{r}}{}^{r}\partial_r E_{\hat{\theta}}{}^{\theta} - (A^{\hat{r}} + r^{\hat{r}})E_{\hat{\theta}}{}^{\theta} = 0, \tag{12}$$

where

$$q = \frac{1}{2}(\Sigma^{\hat{r}\hat{r}})^2 - \frac{1}{3}E_{\hat{r}}{}^{r}\partial_r r^{\hat{r}} + \frac{2}{3}r^{\hat{r}}A^{\hat{r}} + \frac{1}{2}\Big[1 + 3G_+{}^{-1}[\gamma - 1 + \Big(1 - \frac{2}{3}\gamma\Big)(v^{\hat{r}})^2]\Big]\Omega, \tag{13}$$

$$G_{\pm} = 1 \pm (\gamma - 1)(v_{\hat{a}}v^{\hat{a}}). \tag{14}$$

Base on Ref. [5], suppose that $q - \Sigma^{\hat{r}\hat{r}} > 0$ and $q + \frac{1}{2}\Sigma^{\hat{r}\hat{r}} > 0$. Then we find that $E_{\hat{r}}{}^{r}$ and $E_{\hat{\theta}}{}^{\theta}$ exponentially decrease from Eqs. (3) and (4) as t increases. The terms containing $E_{\hat{r}}{}^{r}$ or $E_{\hat{\theta}}{}^{\theta}$ become negligible. From Eqs. (5) and (6), $r^{\hat{r}}$ and $A^{\hat{r}}$ exponentially decrease as well. From Eqs. (8), (9) and (10), $v^{\hat{r}}$ becomes negligible as t increases. Then it follows that there are two possibilities: (i) $\Sigma^{\hat{r}\hat{r}} \neq 0$ and $\Omega = 0$ or (ii) $\Sigma^{\hat{r}\hat{r}} = 0$ and $\Omega = 1$. In the case (i), the spacetime looks like Schwarzschild inner spacetime in vacuum and seems that the singularity is not naked. In the case (ii), the spacetime looks like flat Friedmann spacetime and also seems that the singularity is not naked. Although the fact that the singularity is not naked is not proved, this suggests the possibility of the criterion for the nakedness of singularity, that is, the singularity seems to be judged by the behavior of q, $\Sigma^{\hat{r}\hat{r}}$ and Ω. In the next section, we investigate the behavior of q, $\Sigma^{\hat{r}\hat{r}}$ and Ω of the LTB spacetime.

3 LTB solution marginally bound collapse

We consider inhomogeneous dust spherical gravitational collapse. It is described by the LTB solution. Although the solution has two free functions $F(\rho)$ and $f(\rho)$, here we consider marginally bound collapse, $f = 0$. For comoving coordinate, the metric and the stress-energy tensor are

$$ds^2 = -dT^2 + (\partial_\rho R)^2 d\rho^2 + R^2 d\Omega^2, \tag{15}$$

$$R(T, \rho) = \rho \left(1 - \frac{3}{2}\sqrt{\frac{F(\rho)}{\rho^3}}T\right)^{\frac{2}{3}}, \tag{16}$$

$$T_{ab} = \tilde{\mu}\tilde{u}_a\tilde{u}_b, \quad \tilde{p} = 0. \tag{17}$$

where $d\Omega^2 = d\theta^2 + \sin^2\theta d\phi^2$. $F(\rho)$ is concerned with initial density distribution $\tilde{\mu}_0(\rho) \equiv \tilde{\mu}(0, \rho)$ by $F(\rho) = \int \tilde{\mu}_0(\rho)\rho^2 d\rho$. The behavior of $F(\rho)$ near $\rho = 0$ relates to the nakedness of the singularity at $\rho = 0$. We assume that $F(\rho)$ can be expanded in a power series near $\rho = 0$ as follows:

$$F(\rho) = F_0\rho^3 + F_n\rho^{n+3} + O(\rho^{n+4}), \tag{18}$$

where $n > 0$. We assume the initial density to decrease outwards from the center, hence the first non-vanishing derivative of the density has a negative sign, i.e., $F_n < 0$. Then, if $F_1 < 0$, the singularity is naked. If $F_1 = 0, F_2 < 0$, the singularity is naked. If $F_1 = F_2 = 0, F_3 < 0$, the singularity is naked if $F_3 < -(26 + 15\sqrt{3})F_0^{5/2}/2 \equiv F_c$ and the singularity is not naked if $F_3 > F_c$. If $F_1 = F_2 = F_3 = 0, F_n < 0$ ($n \geq 4$), the singularity is not naked. When we say that the singularity is naked, we mean that it is locally naked at least. These results are obtained by investigating whether or not future directed non-spacelike geodesics coming out of the singularity exist [6].

To evaluate q, $\Sigma^{\hat{r}\hat{r}}$ and Ω for the LTB solution in the coordinate with the separable volume gauge, we consider the coordinate transformation between the comoving coordinate and this coordinate. The coordinate transformation near $\rho = 0$ can be written as

$$T \simeq \frac{2}{3\sqrt{F_0}}(1 - \eta_n(r)e^{-t}), \quad \rho \simeq \xi_n(r)e^{-\alpha t}. \tag{19}$$

These are the leading term of the coordinate transformation near $\rho = 0$. $\eta_n(r)$ and $\xi_n(r)$ depend on n, where n denotes the first nonvanishing F_n of $F(\rho)$ expanded near $\rho = 0$, and we don't explicitly write them here. α depends on n and it is $3/(3 + 2n)$ if $n < 3$ and it is $1/3$ if $n \geq 3$.

For the coordinate with the separable volume gauge, the leading behavior of the metric near $t \to \infty$ can be written as

$$ds^2 \simeq -I_n^2(r)dt^2e^{-2t} + J_n^2(r)e^{-2t}dr^2 + R_n^2(r)e^{-2t}d\Omega^2. \tag{20}$$

$I_n(r)$, $J_n(r)$ and $R_n(r)$ depend on n and we don't explicitly write them here. However, the time dependence does not depend on n. After some calculations by using the metric, we find that q and $\Sigma^{\hat{r}\hat{r}}$ become 0 at $t \to \infty$ for all n and Ω become as follows:

$$\Omega \to \left\{ \begin{array}{ll} 0 & (n \leq 2) \\ \Omega_\infty(r, F_3) & (n = 3) \\ \frac{4}{9} & (n \geq 4) \end{array} \right. . \tag{21}$$

n	Ω	Self-similarity	Nakedness
$n \leq 2$	0	No	Naked
$n = 3$	$\Omega_\infty(r, F_3)$	Yes	$\Omega_{min} < \Omega_c$, Naked
			$\Omega_{min} > \Omega_c$, Not naked
$n \geq 4$	4/9	Yes	Not naked

Table 1: The behaior of LTB solution near $t \to \infty$ in the separable volume gauge.

For $n = 3$, $\Omega_\infty(r, F_3)$ has Ω_{min}, which is the minimum value of Ω_∞, to each F_3 and Ω_{min} decreases as F_3 decreases. Considering the result noted above, it follows that the singularity is naked if $\Omega_{min} < \Omega_c$, which the minimum value of Ω_∞ to F_c, and the singularity is not naked if $\Omega_{min} > \Omega_c$.

To investigate another behavior of the metric (20), we introduce the self-similarity of a spacetime. Self-similarity is defined in terms of the homothetic vector X^a which satisfies $\mathcal{L}_{\vec{X}} g_{ab} = 2g_{ab}$, where $\mathcal{L}_{\vec{X}}$ denotes the Lie derivative with respect to X^a [7]. We find that the spacetime described by the metric (20) has the X^a so that $X^t = -1, X^r = X^\theta = X^\phi = 0$. Also, the form of the metric (20) can be obtained from q, $\Sigma^{\hat{r}\hat{r}} = 0$ for the perfect fluid. Therefore, considering the matter, if q, $\Sigma^{\hat{r}\hat{r}} = 0$ and $\Omega \neq 0$, a spacetime is self-similar and if q, $\Sigma^{\hat{r}\hat{r}} = 0$ and $\Omega = 0$, a spacetime is not self-similar. That is, the LTB spacetime with the separable volume gauge for $n \geq 3$ is self-similar at $t \to \infty$ and q, $\Sigma^{\hat{r}\hat{r}} = 0$ and $\Omega \neq 0$ are the sufficient condition for that the behavior of a spacetime with a perfect fluid with the barotropic equation of state is self-similar.

4 Summary and Discussion

We investigated the final fate of spherical dust collapse by using the orthonormal frame formalism with the Hubble normalized variables and the separable volume gauge. The results are summarized in Table 1. We found that the final fate of spherical dust collapse is characterized by Ω_{min}, which is the minimum value of Ω at $t \to \infty$ in this formalism. That is, Ω_{min} is the criterion for the final fate of spherical dust collapse. Also, we found that the behavior of the LTB solution for $n \geq 3$ in the coordinate with the separable volume gauge is self-similar at $t \to \infty$ and that q, $\Sigma^{\hat{r}\hat{r}} = 0$ and $\Omega \neq 0$ are the sufficient condition for that the behavior of a spcetime with a perfect fluid with the barotropic equation of state is self-similar.

We noted that the evolution equations and constraints of the orthonormal frame formalism for perfect fluid spherical collapse with $\tilde{p} = (\gamma - 1)\tilde{\mu}$ are the same as the ones for dust spherical collapse only if q, $\Sigma^{\hat{r}\hat{r}} = 0$ and $\Omega = 0$. It means that q, $\Sigma^{\hat{r}\hat{r}} = 0$ and $\Omega = 0$ are the sufficient condition for the naked singularity formation of the perfect fluid collapse because the dust collapse in the case that q, $\Sigma^{\hat{r}\hat{r}} = 0$ and $\Omega = 0$ at $t \to \infty$ forms the naked singularity. On the basis of these results, we conjecture that the final fate of the perfect fluid collapse is characterized by Ω as well as the dust collapse.

References

[1] T. Harada, H. Iguchi and K. Nakao, Prog. Theor. Phys. **107**, 449 (2002).

[2] P. S. Joshi, R. Goswami and N. Dadhich, Phys. Rev. D **70**, 087502 (2004).

[3] R. Goswami and P. S. Joshi, Class. Quantum Grav. **19**, 5229 (2002).

[4] C. Uggla, H. van Elst, J. Wainwright and G. F. R. Ellis, Phys. Rev. D **68**, 103502 (2003).

[5] J. Curtis and D. Garfinkle, Phys. Rev. D **72**, 064003 (2005).

[6] T. P. Singh and P. S. Joshi, Class. Quantum Grav. **13**, 559 (1996).

[7] M. E. Cahill and A. H. Taub, Commun. Math. Phys. **21**, 1 (1971).

Charged Rotating Kaluza-Klein Black Holes in Five Dimensions

Toshiharu Nakagawa[1] , Hideki Ishihara[2] , Ken Matsuno[3] and Shinya Tomizawa[4]

Depertment of Mathematics and Physics, Graduate School of Science, Osaka City University, 3-3-138 Sugimoto, Sumiyoshi, Osaka 558-8585, Japan

Abstract

We construct a new charged rotating Kaluza-Klein black hole solution in the five-dimensional Einstein-Maxwell theory with a Chern-Simon term. The features of the solutions are also investigated. The spacetime is asymptotically locally flat, i.e., it asymptotes to a twisted S^1 bundle over the four-dimensional Minkowski spacetime. The solution describe a non-BPS black hole rotating in the direction of the extra dimension. The solutions have the limits to the supersymmetric black hole solutions, a new extreme non-BPS black hole solutions.

1 Introduction

In the context of string theory, the five-dimensional Einstein-Maxwell theory with a Chern-Simon term gathers much attention since it is the bosonic sector of the minimal supergravity. Supersymmetric (BPS) black hole solutions to the five-dimensional Einstein-Maxwell equations with a Chern-Simon term have been found by various authors. Based on the classification of the five-dimensional supersymmetric solutions by Gauntlett.et.al. [1], they have been constructed on hyper-Kähler base spaces, especially, the Gibbons-Hawking base space. The first asymptotically flat supersymmetric black hole solution, BMPV (Breckenridge-Myers-Peet-Vafa) solution, was constructed on the four-dimensional Euclid space [2]. A supersymmetric black hole solution with a compactified extra dimension on the Euclidean self-dual Taub-NUT base space was constructed by Gaiotto.et.al [3]. It was extended to multi-black hole solution with the same asymptotic structure [4].

In addition to the BPS solutions, the non-BPS black hole solutions have also been studied by several authors. Cvetic et.al. [5] found a non-extremal, charged and rotating black hole solution with asymptotic flatness. We consider the case of vanishing cosmological constant. In the specified limits, the solution reduces to the known solutions: the same angular momenta case of the Myers-Perry black hole solution [6], and the supersymmetric BMPV black hole solution [2].

Exact solutions of non-BPS Kaluza-Klein black hole solutions are found in neutral case [7, 8] and charged case [9]. These solutions have a non-trivial asymptotic structure, i.e., they asymptotically approach a twisted S^1 bundle over the four-dimensional Minkowski spacetime. The horizons are deformed due to this non-trivial asymptotic structure and have a shape of a squashed S^3, where S^3 is regarded as a twisted bundle over a S^2 base space. The ratio of the radius S^2 to that of S^1 is always larger than one.

Wang proposed that a kind of Kaluza-Klein black hole solutions can be generated by the '*squashing transformation*' from black holes with asymptotic flatness [10]. In fact, he regenerated the five-dimensional Kaluza-Klein black hole solution found by Dobiasch and Maison [7, 8] from the five-dimensional Myers-Perry black hole solution with two equal angular momenta.

Using the squashing transformation, we construct a new non-BPS rotating charged Kaluza-Klein black hole solutions in the five-dimensional Einstein-Maxwell theory with a Chern-Simon term.

2 Solution

In the metric of squashing Kaluza-Klein black hole in ref. [9], a function of radial coordinate $k(r)$, which describes the squashing of the horizons, appeares. Wang pointed out that the function $k(r)$ would give a

[1]E-mail:tosiharu@sci.osaka-cu.ac.jp
[2]E-mail:ishihara@sci.osaka-cu.ac.jp
[3]E-mail:matsuno@sci.osaka-cu.ac.jp
[4]E-mail:tomizawa@sci.osaka-cu.ac.jp

transformation from asymptotically flat solutions to Kaluza-Klein type solutions. He call this *squashing transformation*.

Applying the squashing transformation to the non-BPS charged rotating black hole solution found by Cvetic et.al. [5], we construct a new charged, rotating Kaluza-Klein black hole solution to the five-dimensional Einstein-Maxwell theory with a Chern-Simon term. The metric and the gauge potential of the solution are given by

$$ds^2 = -\frac{w(r)}{h(r)}dt^2 + k(r)^2\frac{dr^2}{w(r)} + \frac{r^2}{4}\left[k(r)(\sigma_1^2+\sigma_2^2) + h(r)(f(r)dt+\sigma_3)^2\right], \tag{1}$$

and

$$A = \frac{\sqrt{3}q}{2r^2}\left(dt - \frac{a}{2}\sigma_3\right), \tag{2}$$

respectively, where the metric functions $w(r), h(r), f(r)$ and $k(r)$ are defined as

$$w(r) = \frac{(r^2+q)^2 - 2(m+q)(r^2-a^2)}{r^4}, \tag{3}$$

$$h(r) = 1 - \frac{a^2q^2}{r^6} + \frac{2a^2(m+q)}{r^4}, \tag{4}$$

$$f(r) = -\frac{2a}{r^2h(r)}\left(\frac{2m+q}{r^2} - \frac{q^2}{r^4}\right), \tag{5}$$

$$k(r) = \frac{(r_\infty^2+q)^2 - 2(m+q)(r_\infty^2-a^2)}{(r_\infty^2-r^2)^2}, \tag{6}$$

and the left-invariant 1-forms on S^3 are given by

$$\sigma_1 = \cos\psi d\theta + \sin\psi\sin\theta d\phi, \tag{7}$$

$$\sigma_2 = -\sin\psi d\theta + \cos\psi\sin\theta d\phi, \tag{8}$$

$$\sigma_3 = d\psi + \cos\theta d\phi. \tag{9}$$

The coordinates r, θ, ϕ and ψ run the ranges of $0 < r < r_\infty$, $0 \le \theta < \pi$, $0 \le \phi < 2\pi$, $0 \le \psi < 4\pi$, respectively. In the case of $k(r) = 1$, i.e., $r_\infty \to \infty$, the metric coincides with that of the Cvetic et.al.'s solution without a cosmological constant. We assume that the parameters a, m, q, and r_∞ appearing in the solutions satisfy the inequalities

$$m > 0, \tag{10}$$

$$q^2 + 2(m+q)a^2 > 0, \tag{11}$$

$$(r_\infty^2+q)^2 - 2(m+q)(r_\infty^2-a^2) > 0, \tag{12}$$

$$(m+q)(m-q-2a^2) > 0, \tag{13}$$

$$m+q > 0,. \tag{14}$$

The inequalities (10)-(13) are the conditions for the existence of two horizons, and the condition (14) is the requirement for the absence of closed timelike curves outside the outer horizon. Figure1 shows the region of the parameters.

3 Features of the solutions

3.1 Asymptotic form

In the coordinate system $(t, r, \theta, \phi, \psi)$, the metric diverges at $r = r_\infty$ but we see that this is an apparent singularity and corresponds to the spatial infinity. To confirm this, introduce a new coordinate defined as

$$\rho = \rho_0\frac{r^2}{r_\infty^2 - r^2} \tag{15}$$

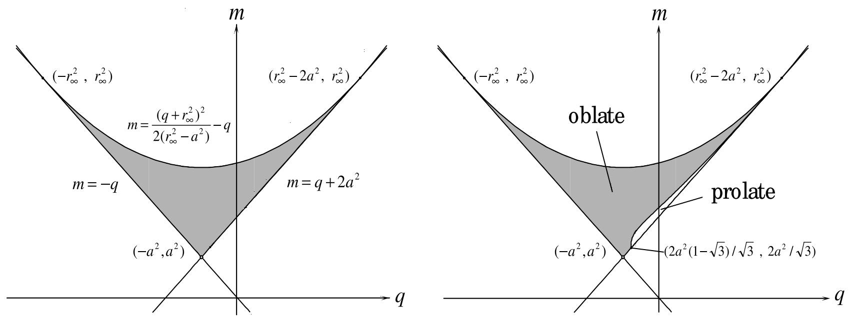

Figure 1: Region of the parameters in the (q, m)-plane and the aspect ratio of the outer horizon.

where the constant ρ_0 is given by

$$\rho_0^2 = \frac{(r_\infty^2 + q)^2 - 2(m+q)(r_\infty^2 - a^2)}{4r_\infty^2}. \tag{16}$$

This new radial coordinate ρ runs from 0 into ∞. For $\rho \to \infty$, which corresponds to the limit of $r \to r_\infty$, the metric behaves as

$$ds^2 \simeq -d\tilde{t}^2 + d\rho^2 + \rho^2(d\theta^2 + \sin^2\theta d\phi^2) + \frac{r_\infty^6 - a^2(q^2 - 2(m+q)r_\infty^2)}{4r_\infty^4}(d\tilde{\psi} + \cos\theta d\phi)^2 \tag{17}$$

in the rest frame $(\tilde{t}, \rho, \theta, \phi, \tilde{\psi})$.

The spacetime is asymptotically locally flat, i.e., the asymptotic form of the metric is a twisted S^1 bundle over four-dimensional Minkowski spacetime.

3.2 Geometry of horizon

The solution within the region of the parameters in Figure1 has two horizons, an event horizon at $r = r_+$ and an inner horizon at $r = r_-$,which are determined by the equation $w(r) = 0$. The horizons are deformed and have a shape of a squashed S^3.

The shape of the horizon, especially, the aspect ratio of S^2 base space to the S^1 fiber, which characterize the squashing of S^3 is denoted by $k(r_+)/h(r_+)$. In the case of $k(r_+)/h(r_+) > 1$, the event horizon is called *oblate*, where the radius of S^2 larger than that of S^1. In the case of $k(r_+)/h(r_+) < 1$, the event horizon is called *prolate*, where the radius of S^2 smaller than that of S^1. Figure1 shows the oblate region and the prolate region in the (m, q)-plane. At the boundary of two regions, the ratio is $k(r_+)/h(r_+) = 1$, where the horizon becomes a round S^3. Thus unlike the static solution [9], the horizon admits a prolate shape in addition to a round S^3.

3.3 Ergo region

In the region of parameters (10)-(14) and the boundary of (13), an ergo surface is always located at $r = r_e(r_+ < r_e < r_\infty)$ satisfying $g_{\tilde{t}\tilde{t}}(r) = 0$.

4 Various limits

In the limit of $r_\infty \to \infty$ with the other parameters fixed, where the size of an extra dimension becomes infinite, the function $k(r)$ takes the limit of $k(r) \to 1$. Then the metric coincides with that of the asymptotically flat solutions obtained by Cvetic. et.al. [5].

In the limit of $q \to 0$, the solution coincides with the one obtained by Gibbons et.al. [7, 8]. And the case of $a \to 0$ corresponds to the metric of the static non-BPS Kaluza-Klein black hole solution with a squashed horizon obtained by two of authors [9].

Taking the limit of $m \to -q$, two horizons degenerate and the solution coincides with the metric of the supersymmetric black hole solutions with a compactified extra dimension on the Euclidean self-dual Taub-NUT space in Ref [3]. In the case of $m \to q + 2a^2$, two horizons degenerate, although this is not a BPS solution.

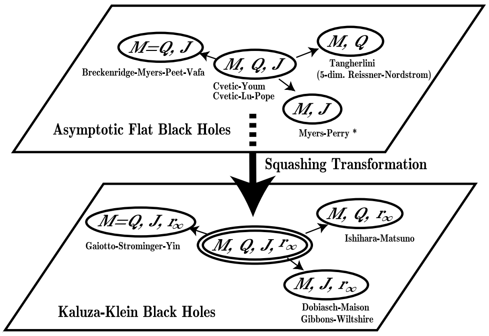

Figure 2: Various limits

5 Summary

We have constructed a new rotating charged Kaluza-Klein black hole solution in the five-dimensional Einstein-Maxwell theory with a Chern-Simon term. The spacetime is asymptotically locally flat, i.e., a twisted S^1 bundle over the four-dimensional Minkowski spacetime. This solution has four parameters, the mass, the angular momenta in the direction of an extra dimension, the electric charge and the size of the extra dimension. The solution describes the physical situation such that in general a non-BPS black hole is boosted in the direction of the extra dimension. The solution has the limits to the supersymmetric black hole solution and a new extreme non-BPS black hole solutions.

References

[1] J.P. Gauntlett, J.B. Gutowski, C.M. Hull, S. Pakis and H.S. Reall, Class. Quant. Grav. **20**, 4587 (2003).

[2] J.C. Breckenridge, R.C. Myers, A.W. Peet and C. Vafa, Phys. Lett. B **391**, 93 (1997).

[3] D. Gaiotto, A. Strominger and X. Yin, JHEP **0602**, 024 (2006).

[4] H. Ishihara, M. Kimura, K. Matsuno and S. Tomizawa, Class. Quant. Grav. **23**, 6919 (2006).

[5] M. Cvetic and D. Youm, Nucl. Phys. B **476**, 118 (1996).
M. Cvetic, H. Lu and C.N. Pope, Phys. Lett B **598**, 273 (2004).

[6] R.C. Myers and M.J. Perry, Annals Phys. **172**, 304 (1986).

[7] P. Dobiasch and D. Maison, Gen. Rel. Grav. **14**, 231 (1982).

[8] G.W. Gibbons and D.L. Wiltshire, Ann. Phys. **167**, 201 (1986).

[9] H. Ishihara and K. Matsuno, Prog. Theor. Phys. **116**, 417 (2006).

[10] T. Wang, Nucl. Phys. B, **756**, 86 (2006).

$N + 1$ formalism in Einstein-Gauss-Bonnet gravity

Takashi Torii[1] and Hisa-aki Shinkai[2]

[1] *General Education of Science, Osaka Institute of Technology, Omiya, Asahi-ku, Osaka 535-8585*
[2] *Dept. of Information Systems, Osaka Institute of Technology, Kitayama, Hirakata, Osaka 573-0196*

Abstract

With the aim of numerical investigations of spacetime dynamics in higher curvature models, we present the basic equations of the Einstein-Gauss-Bonnet gravity theory. We show $(N + 1)$-dimensional version of the ADM decomposition including Gauss-Bonnet terms, and also show conformally-transformed constraint equations for obtaining an initial data.

1 Introduction

One of the most surprising achievements in studies of general relativity (GR) is the singularity theorems established by Hawking and Penrose in 1960s. It states that the spacetime singularities inevitably occur (or occurred) under natural conditions within the framework of GR. This fact implies that GR cannot describe whole of the spacetime structure, and GR itself is incomplete as a physics theory since an appearance of singularity makes the future unpredictable.

One of the remedy of this paradox is the cosmic censorship conjecture proposed by Penrose. The conjecture states that any singularity is hidden inside an event horizon in the process of gravitational collapse, and is causally disconnected from our side of spacetime. However, it is also true that this censorship does not essentially solve the break-down of GR at the singularity, and also that the initial singularity at the birth of the universe, which is the consequence of the standard Big-Bang scenario, can not be resolved. Therefore, we expect that the true fundamental theory will resolve this problematic singularity treatment.

Up to now, several quantum theories of gravity have been proposed. Among them superstring/M-theory, formulated in higher dimensional spacetime, is the most promising candidate. We are still far from understanding the non-perturbative aspects of the theory, but perturbative treatments of string effects to classical gravity theory begin revealing new features of the spacetime.

One of the typical string effects can be seen in a series of studies of cosmological models, which is called string cosmology [1] or pre-Big-Bang scenario [2]. Although these analysis show that the singularity problem has not been resolved yet, there are some cosmological solutions which do not start from an initial singularity.

Another attractive proposal is the brane-world model of the Universe [3]; a picture that we live on a four-dimensional timelike hypersurface embedded in higher-dimensional bulk spacetime. Since the fundamental scale of the brane-world model could be around TeV scale, the model is thought to be tested using the large hadron collider (LHC) by monitoring the creations and evaporations of tiny black holes[4].

Along to such a theoretical developments, we are planning to promote a direct numerical approach to investigate non-linear dynamics in higher-dimensional and/or higher curvature gravitational models both for singularity structure and cosmological models. This article is the first step; we rewrite the fundamental equations into a suitable form for future numerical treatments.

The standard numerical approach is to treat the spacetime as a Cauchy problem. We therefore apply the ADM formalism of GR for the $(N + 1)$-dimensional Einstein-Gauss-Bonnet gravity theory. The Gauss-Bonnet terms are the next leading order of the α'-expansion of type IIB superstring theory, where α' is the inverse string tension [5], so that the first model to be investigated. In §2.1, we show that the set of equations are divided into two constraints and evolution equations along to the standard procedure. In §2.2, we present the conformal approach to solve the constraints which shall be used for preparing an initial data. All the details will be reported elsewhere[6].

[1] E-mail: torii@ge.oit.ac.jp
[2] E-mail: shinkai@is.oit.ac.jp

2 Equations in Einstein-Gauss-Bonnet gravity

2.1 Equations to solve

We consider $(N+1)$-dimensional spacetime $(\mathcal{M}, g_{\mu\nu})$ which is described by the Einstein-Gauss-Bonnet action: *

$$\begin{aligned} S &= \int_{\mathcal{M}} d^{N+1}X\sqrt{-g}\left[\frac{1}{2\kappa^2}\left(\mathcal{R}-2\Lambda+\alpha_{GB}\mathcal{L}_{GB}\right)+\mathcal{L}_{\rm matter}\right], &(1)\\ &\text{with } \mathcal{L}_{GB} = \mathcal{R}^2-4\mathcal{R}_{\mu\nu}\mathcal{R}^{\mu\nu}+\mathcal{R}_{\mu\nu\rho\sigma}\mathcal{R}^{\mu\nu\rho\sigma}, &(2)\end{aligned}$$

where κ^2 is the $(N+1)$-dimensional gravitational constant, $\mathcal{R}$, $\mathcal{R}_{\mu\nu}$, $\mathcal{R}_{\mu\nu\rho\sigma}$ and $\mathcal{L}_{\rm matter}$ are the $(N+1)$-dimensional scalar curvature, Ricci tensor, Riemann curvature and the matter Lagrangian, respectively.

The action (1) gives the gravitational equation as

$$\mathcal{G}_{\mu\nu}+\alpha_{GB}\mathcal{H}_{\mu\nu}=\kappa^2\,\mathcal{T}_{\mu\nu}\,, \tag{3}$$

$$\begin{aligned} \text{where}\quad \mathcal{G}_{\mu\nu} &= \mathcal{R}_{\mu\nu}-\frac{1}{2}g_{\mu\nu}\mathcal{R}+\Lambda g_{\mu\nu}, &(4)\\ \mathcal{H}_{\mu\nu} &= 2\left[\mathcal{R}\mathcal{R}_{\mu\nu}-2\mathcal{R}_{\mu\alpha}\mathcal{R}^{\alpha}{}_{\nu}-2\mathcal{R}^{\alpha\beta}\mathcal{R}_{\mu\alpha\nu\beta}+\mathcal{R}_{\mu}{}^{\alpha\beta\gamma}\mathcal{R}_{\nu\alpha\beta\gamma}\right]-\frac{1}{2}g_{\mu\nu}\mathcal{L}_{GB}, &(5)\\ \text{and}\quad \mathcal{T}_{\mu\nu} &= -2\frac{\delta\mathcal{L}_{\rm matter}}{\delta g^{\mu\nu}}+g_{\mu\nu}\mathcal{L}_{\rm matter}. &(6)\end{aligned}$$

We define the projection operator to N-dimensional (spacelike or timelike) hypersurface, Σ, $\perp_{\mu\nu}=g_{\mu\nu}-\varepsilon n_\mu n_\nu$, where n_μ is the unit-normal vector to Σ with $n_\mu n^\mu=\varepsilon$, with which we define n_μ is timelike (if $\varepsilon=-1$) or spacelike (if $\varepsilon=1$). Σ is spacelike (timelike) if n_μ is timelike (spacelike). We define the induced N-dimensional metric γ_{ij} as $\gamma_{ij}=\perp_{ij}$, and the extrinsic curvature K_{ij} as $K_{ij}=-\perp^{\alpha}_{i}\perp^{\beta}_{j}\nabla_\alpha n_\beta$.

The projections of the gravitational equation can be the following three:

$$\begin{aligned} \left(\mathcal{G}_{\mu\nu}+\alpha_{GB}\mathcal{H}_{\mu\nu}\right)n^\mu\,n^\nu &= \kappa^2\,T_{\mu\nu}\,n^\mu\,n^\nu =: \kappa^2\rho_H, &(7)\\ \left(\mathcal{G}_{\mu\nu}+\alpha_{GB}\mathcal{H}_{\mu\nu}\right)n^\mu\perp^{\nu}_{\rho} &= \kappa^2\,T_{\mu\nu}\,n^\mu\perp^{\nu}_{\rho} =: -\kappa^2 J_\rho, &(8)\\ \left(\mathcal{G}_{\mu\nu}+\alpha_{GB}\mathcal{H}_{\mu\nu}\right)\perp^{\mu}_{\rho}\perp^{\nu}_{\sigma} &= \kappa^2\,T_{\mu\nu}\perp^{\mu}_{\rho}\perp^{\nu}_{\sigma} =: \kappa^2 S_{\rho\sigma}, &(9)\end{aligned}$$

where we defined $T_{\mu\nu}=\rho_H n_\mu n_\nu+J_\mu n_\nu+J_\nu n_\mu+S_{\mu\nu}$, which gives $T=-\rho_H+S^{\ell}{}_{\ell}$.

Following the standard procedure of the ADM formulation, we find the equations, eq. (7)-(9), correspond to (a) the Hamiltonian constraint equation:

$$M+\alpha_{GB}\big(M^2-4M_{ab}M^{ab}+M_{abcd}M^{abcd}\big)=-2\varepsilon\kappa^2\mathcal{T}_{\mu\nu}n^\mu n^\nu\,, \tag{10}$$

(b) the momentum constraint equation:

$$N_i+2\alpha_{GB}\left(MN_i-2M_i{}^aN_a+2M^{ab}N_{iab}-M_i{}^{cab}N_{abc}\right)=-\kappa^2\mathcal{T}_{\mu\nu}n^\mu\gamma^{\nu}{}_{i}\,, \tag{11}$$

and (c) the evolution equations for γ_{ij}:

$$\begin{aligned} &M_{ij}-\frac{1}{2}M\gamma_{ij}-\varepsilon\big(-K_{ia}K^{a}_{j}+\gamma_{ij}K_{ab}K^{ab}-\pounds_n K_{ij}+\gamma_{ij}\gamma^{ab}\pounds_n K_{ab}\big)\\ &\quad+2\alpha_{GB}\Big[H_{ij}+\varepsilon\big(M\pounds_n K_{ij}-2M_i{}^a\pounds_n K_{aj}-2M_j{}^a\pounds_n K_{ai}-W_{ij}{}^{ab}\pounds_n K_{ab}\big)\Big]=\kappa^2\mathcal{T}_{\mu\nu}\gamma^{\mu}_{i}\gamma^{\nu}{}_{j}\,,\end{aligned} \tag{12}$$

respectively, where

$$\begin{aligned} M_{ijkl} &= R_{ijkl}-\varepsilon(K_{ik}K_{jl}-K_{il}K_{jk}), &(13)\\ N_{ijk} &= D_iK_{jk}-D_jK_{ik}, &(14)\end{aligned}$$

*The Greek indices move $1,\cdots,N+1$, while the Latin indices move $1,\cdots,N$.

$$
\begin{aligned}
H_{ij} &= MM_{ij} - 2(M_{ia}M^a_{\ j} + M^{ab}M_{iajb}) + M_{iabc}M_j^{\ abc} \\
&\quad -2\varepsilon\Big[-K_{ab}K^{ab}M_{ij} - \frac{1}{2}MK_{ia}K^a_{\ j} + K_{ia}K^a_{\ b}M^b_{\ j} + K_{ja}K^a_{\ b}M^b_{\ i} + K^{ac}K_c^{\ b}M_{iajb} \\
&\qquad +N_iN_j - N^a(N_{aij} + N_{aji}) - \frac{1}{2}N_{abi}N^{ab}_{\ \ j} - N_{iab}N_j^{\ ab}\Big] \\
&\quad -\frac{1}{4}\gamma_{ij}\big[M^2 - 4M_{ab}M^{ab} + M_{abcd}M^{abcd}\big] \\
&\quad -\varepsilon\gamma_{ij}\big[K_{ab}K^{ab}M - 2M_{ab}K^{ac}K_c^{\ b} - 2N_aN^a + N_{abc}N^{abc}\big], \qquad (15) \\
W_{ij}^{\ \ kl} &= M\gamma_{ij}\gamma^{kl} - 2M_{ij}\gamma^{kl} - 2\gamma_{ij}M^{kl} + 2M_{iajb}\gamma^{ak}\gamma^{bl}\,, \qquad (16)
\end{aligned}
$$

and these contracted variables; $M_{ij} = \gamma^{ab}M_{iajb}$, $M = \gamma^{ab}M_{ab}$, and $N_i = \gamma^{ab}N_{aib}$. Note that the terms of $\pounds_n K_{\mu\nu}$ appear only in the linear form. This is due to the quali-linear property of the Gauss-Bonnet gravity.

2.2 Conformal Approach to solve the Constraints

In order to prepare an initial data for numerical evolution, we have to solve two constraints, (10) and (11). The standard approach [7] is to apply conformal transformation between the initial trial metric $\hat{\gamma}_{ij}$ and the solution γ_{ij}, as

$$\gamma_{ij} = \psi^{2m}\hat{\gamma}_{ij}, \qquad (17)$$

and solve for ψ. (We generalized the power to $2m$ here.) For N-dimensional spacetime, Ricci scalar is transformed as

$$\tilde{R} = \psi^{-2m}R - 2(N-1)(\Delta\psi)\psi^{-2m-1} - (N-1)\big[2-(N-2)m\big]m(\nabla\psi)^2\psi^{-2m-2},$$

from which we specify $m = 2/(N-2)$ for simplifying the equation.

Regarding to the extrinsic curvature, we decompose K_{ij} into its trace part, $K = \gamma^{ij}K_{ij}$, and traceless part, $A_{ij} = K_{ij} - \frac{1}{N}\gamma_{ij}K$, and assume the conformal transformation as

$$A_{ij} = \psi^{\ell}\hat{A}_{ij}. \qquad (18)$$

The conformal transformation of the divergence D_jA^{ij} becomes

$$D_jA^{ij} = \psi^{-4m+\ell}\hat{D}_j\hat{A}^{ij} + \psi^{-4m+\ell-1}\big[\ell + m(N-2)\big]\hat{A}^{ij}\hat{D}_j\psi, \qquad (19)$$

which indicates to set $\ell = -m(N-2) = -2$ for simplifying the equation.

We introduce the longitudinal part of $\hat{A}^{ij}$, $\hat{A}^{ij}_L = \hat{A}^{ij} - \hat{A}^{ij}_{TT}$, where $\hat{D}_j\hat{A}^{ij}_{TT} = 0$, and express $\hat{A}^{ij}_L$ with a vector potential $\hat{A}^{ij}_L = \hat{D}^iW^j + \hat{D}^jW^i - \frac{2}{N}\hat{\gamma}^{ij}\hat{D}_kW^k$.

We also assume the conformal transformation of matter terms as $\rho = \psi^{-n}\hat{\rho}$ and $J^i = \psi^{-4m+\ell}\hat{J}^i$, and assume $K = \hat{K}$, then two constraints, (10) and (11), can be written as

$$
\begin{aligned}
4\frac{N-1}{N-2}\hat{\Delta}\psi &= \hat{R}\psi - (\hat{A}_{ij}\hat{A}^{ij})\psi^{(-3N+2)/(N-2)} + \left[\frac{N-1}{N}K^2 - 2\Lambda - 16\pi G\hat{\rho}\psi^{-n}\right]\psi^{(N+2)/(N-2)} \\
&\quad +\alpha_{GB}\left(M^2 - 4M_{ab}M^{ab} + M_{abcd}M^{abcd}\right)\psi^{(N+2)/(N-2)} \qquad (20)
\end{aligned}
$$

and

$$
\begin{aligned}
\hat{\Delta}W^i + \frac{N-2}{N}\hat{D}^i\hat{D}_kW^k + \hat{R}^i_{\ k}W^k &= \frac{N-1}{N}\psi^{2N/(N-2)}\hat{D}^i\hat{K} + 8\pi G\hat{J}^i \\
&\quad -2\alpha_{GB}\left(MN^i - 2M^{ia}N_a + 2M^{ab}N^i_{\ ab} - M^{iabc}N_{bca}\right). \qquad (21)
\end{aligned}
$$

Note that we do not transformed Gauss-Bonnet terms in these expression, since they produce higher-power terms in ψ. Therefore we have to proceed iterative schemes for solving both (20) and (21) updating the trial metric as $\hat{\gamma}_{ij}|_{\rm new} = \psi_{\rm old}^{4N/(N-2)}\hat{\gamma}_{ij}|_{\rm old}$. Although there is no proof to guarantee the existence of a solution in such a system, our numerical code obtains converged solutions. We will report details elsewhere.

2.3 Evolution equations

The Einstein evolution equation in general N-dimensional ADM version is presented in [8]. With the Gauss-Bonnet terms, the evolution equation, (12), cannot be expressed explicitly for each $\pounds_n K_{ij}$. That is, eq. (12) is rewritten as

$$
\begin{aligned}
&(1+2\alpha_{GB}M)\pounds_n K_{ij} - (h_{ij}h^{ab} + 2\alpha_{GB}W_{ij}{}^{ab})\pounds_n K_{ab} - 8\alpha_{GB}M_{(i}{}^{a}\pounds_n K_{|a|j)} \\
&\quad = -\varepsilon\left(M_{ij} - \frac{1}{2}Mh_{ij}\right) - K_{ia}K^{a}{}_{j} + h_{ij}K_{ab}K^{ab} + \varepsilon\kappa^2 \mathcal{T}_{\mu\nu}h^{\mu}{}_{i}h^{\nu}{}_{j} - 2\varepsilon\alpha_{GB}H_{ij}\,, \qquad (22)
\end{aligned}
$$

and the second and third terms in RHS include the mixing terms between $\pounds_n K_{ij}$. Therefore, in an actual simulation, we have to evolve γ_{ij} and K_{ij} in each step simultaneously using a matrix form of (22) like

$$
\begin{pmatrix} \pounds_n\gamma_{11} \\ \pounds_n\gamma_{12} \\ \pounds_n\gamma_{13} \\ \vdots \\ \pounds_n K_{11} \\ \pounds_n K_{12} \\ \pounds_n K_{13} \\ \vdots \end{pmatrix}
=
\begin{pmatrix} O & O \\ & \\ O & \text{Mixing} \end{pmatrix}
\begin{pmatrix} \pounds_n\gamma_{11} \\ \pounds_n\gamma_{12} \\ \pounds_n\gamma_{13} \\ \vdots \\ \pounds_n K_{11} \\ \pounds_n K_{12} \\ \pounds_n K_{13} \\ \vdots \end{pmatrix}
+
\begin{pmatrix} K_{11} \\ K_{12} \\ K_{13} \\ \vdots \\ \\ \text{Source} \\ \\ \end{pmatrix}.
$$

We are now developing our numerical code and hope to present some results elsewhere near future.

References

[1] H. Ishihara, Phys. Lett. B **179**, 217 (1986),
A. A. Starobinsky, Phys. Lett. B **91**, 99 (1980); K. Maeda, Phys. Lett. B **166**, 59 (1986);
J. R. Ellis, N. Kaloper, K. A. Olive and J. Yokoyama, Phys. Rev. D **59**, 103503 (1999).
H. Yajima, K. Maeda, and H. Okubo, Phys. Rev. D **62**, 024020 (2000).

[2] M. Gasperini and G. Veneziano, Phys. Rep. **373**, 1 (2003);

[3] N. Arkani-Hamed, S. Dimopoulos, and G. Dvali, Phys. Lett. B **429**, 263 (1998);
I. Antoniadis, N. Arkani-Hamed, S. Dimopoulos, and G. Dvali, Phys. Lett. B **436**, 257 (1998).
L. Randall and R. Sundrum, Phys. Rev. Lett. **83**, 3370 (1999); **83**, 4690 (1999).

[4] S. Dimopoulos and G. Landsberg, Phys. Rev. Lett. **87** (2001) 161602;
A. Chamblin and G.C. Nayak, Phys. Rev. D **66** (2002) 091901;
S. B. Giddings and S. Thomas, Phys. Rev. D **65** (2002) 056010.

[5] D. J. Gross and E. Witten, Nucl. Phys. **B277**, 1 (1986);
D. J. Gross and J. H. Sloan, Nucl. Phys. **B291**, 41 (1987);

[6] T. Torii and H. Shinkai, in preparation.

[7] N. ÓMurchadha, J.W. York,Jr., Phys. Rev. **D10**, 428 (1974)

[8] H. Shinkai and G. Yoneda, Gen. Rel. Grav. **36**, 1931 (2004)

Weakly nonlinear evolution of the baryon acoustic oscillations

Hidenori Nomura[1] and Kazuhiro Yamaoto[2]

Graduate School of Sciences, Hiroshima University, Higashi-Hiroshima 739–8526, Japan

Abstract

We examine the effect of the quasi-nonlinear gravitational clustering on the baryon acoustic oscillation (BAO) feature in the matter power spectrum. In particular, we investigate the damping nature of the BAO feature, which is extracted from the matter power spectrum, based on the third order perturbation theory. We construct a fitting formula of the BAO feature in an analytic way. We also investigate a future feasibility of constraing the cosmological parameters through the weakly nonlinear evolution of the BAO.

1 Introduction

Baryon acoustic oscillations (BAO) imprinted in the galaxy power spectrum has recently attracted remarkable attention as a cosmological standard ruler to constrain the equation of state of dark energy. The BAO signature has been detected in the 2dFGRS and the SDSS galaxy samples, and the feasibility of constraining the dark energy parameter is demonstrated. Furthermore, future BAO survey projects are discussed to explore the origin of the dark energy [1].

Although the BAO signature is called as the cosmological standard ruler, for a precise confrontation of the theoretical predictions with observation, we need clarify uncertainities such as gravitational nonlinear evolution of the matter fluctuations, redshift-space distortions of the observed cosmological objects and the galaxy bias effect, because these effects might yield some systematics when comparing the observed power spectrum with the theoretical predictions.

We examine one of these uncertainties about the nonlinear correction due to the gravitational clustering. This effect cause the shift of peaks and troughs and suppression of the amplitude of the BAO feature. In this work, we focus on the damping nature of the BAO due to the nonlinear gravitational clustering as shown by figure 1.

2 Damping nature of the BAO

To investigate the effect of the nonlinear gravitational clustering, in present work, we employ the perturbative approach of the matter fluctuations. Based on the third order perturbation theory [2], the second order matter power spectrum can be given by

$$P(k,z) = D_+^2(z)P_{lin}(k) + D_+^4(z)P_2(k), \tag{1}$$

where $P_{lin}(k)$ is the linear power spectrum given by

$$P_{lin}(k)\delta^{(3)}(\boldsymbol{k}+\boldsymbol{k}') = \langle \delta_1(\boldsymbol{k})\delta_1(\boldsymbol{k}')\rangle, \tag{2}$$

$D_+(z)$ is the linear growth rate, and $P_2(k)$ is the second order contribution to the spectrum, which can be conventionally expressed as follows;

$$P_2(k) = P_{22}(k) + 2P_{13}(k). \tag{3}$$

Taking the 4-point correlations of $\delta_1(\boldsymbol{k})$ into consideration, we can obtain the explicit form of $P_{22}(k)$ expressed as the integral of the square of the linear power spectrum,

$$P_{22}(k) = 2\int d^3q P_{lin}(q)P_{lin}\left(|\boldsymbol{k}-\boldsymbol{q}|\right)\left[F_2^{(s)}(\boldsymbol{q},\boldsymbol{k}-\boldsymbol{q})\right]^2. \tag{4}$$

[1]E-mail:hide@theo.phys.sci.hiroshima-u.ac.jp
[2]E-mail:kazuhiro@hiroshima-u.ac.jp

On the other hand, $P_{13}(k)$ has the form slightly different with $P_{22}(k)$,

$$2P_{13}(k) = 6P_{lin}(k) \int d^3q P_{lin}(q) F_3^{(s)}(\boldsymbol{q}, -\boldsymbol{q}, \boldsymbol{k}). \tag{5}$$

Here we follow the definition of $F_2^{(s)}$ and $F_3^{(s)}$ given by [2].

We will examine the damping nature of the BAO signature due to the nonlinear gravitational clustering. The oscillation signature in the matter power spectrum can be extracted as follows:

$$B(k,z) \equiv \frac{P(k,z)}{\tilde{P}(k,z)} - 1. \tag{6}$$

where $P(k,z)$ is the matter power spectrum including the BAO signature, but $\tilde{P}(k,z)$ is the matter power spectrum without the BAO, which is calculated using the no-wiggle transfer function by [3]. Hereafter, the quantity with the 'tilde' implies to be computed using the no-wiggle transfer function. With the use of the formula of the second order power spectra we have

$$B(k,z) = \frac{P_{lin}(k) + D_+^2(z)P_2(k)}{\tilde{P}_{lin}(k) + D_+^2(z)\tilde{P}_2(k)} - 1. \tag{7}$$

First, we adopt the approximation,

$$P_2(k) \simeq \tilde{P}_{22}(k) + 2P_{13}(k). \tag{8}$$

Namely, $P_{22}(k)$ in (1) is replace with $\tilde{P}_{22}(k)$. The validity of this approximation is demonstrated in Figure 2. The validity of this approximation comes from the fact that the mode-couplings of different Fourier modes decreases the coherent BAO signature.

On the other hand, $P_{13}(k)$ can not be simply replaced with $\tilde{P}_{13}(k)$. However, careful consideration leads to an expression for $\tilde{P}_{13}(k)$. First, we define

$$B_{lin}(k) \equiv \frac{P_{lin}(k)}{\tilde{P}_{lin}(k)} - 1, \tag{9}$$

which corresponds (7), but within the linear theory of density fluctuations. With this definition, we obtain

$$2P_{13}(k) \simeq 2\left[1 + B_{lin}(k)\right]\tilde{P}_{13}(k). \tag{10}$$

Substituting (10) into (8), $P_2(k)$ is written as

$$P_2(k) = \tilde{P}_2(k) + 2B_{lin}(k)\tilde{P}_{13}(k). \tag{11}$$

Then, from (7), we obtain

$$B(k,z) = \frac{1 + D_+^2(z)\dfrac{2\tilde{P}_{13}(k)}{\tilde{P}_{lin}(k)}}{1 + D_+^2(z)\dfrac{\tilde{P}_2(k)}{\tilde{P}_{lin}(k)}} B_{lin}(k), \tag{12}$$

This formula indicates how the BAO signature is modified as the gravitational clustering evolves, which is expressed by the BAO signature in the linear theory multiplied by the correction determined by the no-wiggle quantities and the growth factor.

The second term of the denominator in (12) is smaller than unity as far as the perturbation theory is valid. Accordingly, expanding it and taking the terms up to the second order of $D_+(z)$, we obtain

$$B(k,z) = \left[1 - D_+^2(z)\frac{\tilde{P}_{22}(k)}{\tilde{P}_{lin}(k)}\right] B_{lin}(k). \tag{13}$$

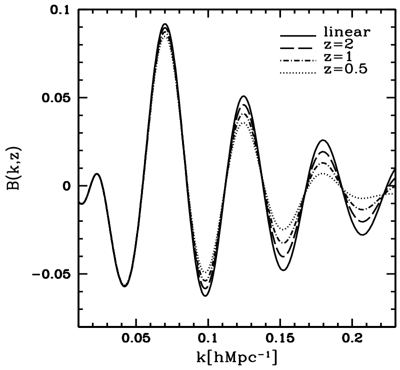

Figure 1: BAO feature extracted from the matter power spectrum including the second order contributions for several redshifts. The cosmological parameters adopted are same as Figure 1.

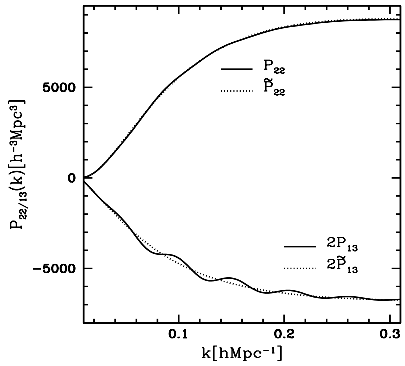

Figure 2: Typical behavior of the second order contributions to the linear spectrum. The cosmological parameters adoped are $h = 0.73$, $\Omega_m = 0.24$, $\Omega_b = 0.042$, $n_s = 0.96$ and $\sigma_8 = 0.76$.

From a detailed analysis of $\tilde{P}_{22}(k)/\tilde{P}_{lin}(k)$ as a function of k, we find that the following fitting formula works well,

$$B(k,z) = \left[1 - \sigma_8^2 D_+^2(z)\left(\frac{k}{k_n}\right)^2\left(1-\frac{\gamma}{k}\right)\right] B_{lin}(k), \tag{14}$$

where σ_8 is the rms matter density fluctuation averaged over the sphere with the radius of $8h^{-1}$Mpc, k_n and γ are the constant parameters which depend on Ω_m and Ω_b as

$$k_n = -0.536(\Omega_m + 0.326)(\Omega_b - 0.416) \ \ h\text{Mpc}^{-1}, \tag{15}$$
$$\gamma = -2.75(\Omega_m - 0.114)(\Omega_b - 0.122) \ \ h\text{Mpc}^{-1}. \tag{16}$$

Though these dependency might have to be investigated more carefully, but the validity is guaranteed in the following narrow range: $0.22 < \Omega_m < 0.26$, $0.040 < \Omega_b < 0.042$. Figure 3 shows an example to show the agreement of the fitting formula with the second order power spectrum. The relative error is about less than 10 % for the range of the wave number $k \lesssim 0.19$ hMpc^{-1} .

3 A feasibility of constraining the cosmological parameters

The nonlinear correction derived in the previous section describes how the BAO are damped depending on the values of Ω_m, Ω_b and $\sigma_8 D_+(z)$. This suggests that these cosmological parameters may be able to constrain through the nonlinear evolution of the BAO. For this investigation, we consider the constraints on Ω_m and σ_8 for example. Here our fiducial model we adopted is $\Omega_m = 0.24$, $\sigma_8 = 0.76$, $\Omega_b = 0.042$, $h = 0.73$ and $n_s = 0.96$.

The error of the galaxy power spectrum depends on its amplitude. The clustering bias and the redshift-space distortions contribute the amplitude of the power spectrum and the error in measuring $B(k,z)$. For our modeling the galaxy power spectrum, we assume the scale-independent bias model [4], and incorporate the redshift-space distortion within the linear theory, for simplicity. In addition, we assume the variance of the error in measuring the BAO signature can be estimated by

$$\triangle B^2(k) = \frac{\triangle P^2(k,z)}{[\tilde{P}^{(s)}(k,z)]^2}, \tag{17}$$

where $\triangle P(k,z)$ is the variance of the power spectrum, which can be estimated by the formula adopted by [5], and $\tilde{P}^{(s)}(k,z)$ is the power spectrum in redshift space.

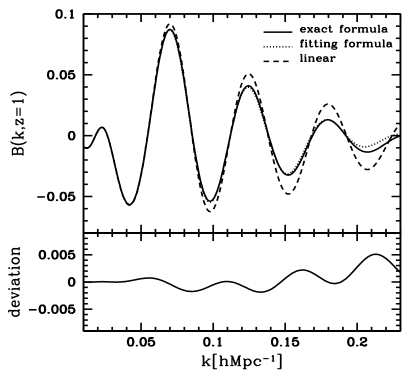

Figure 3: Top panel: The BAO calculated by the exact formula (7) and our fitting formula are plotted. Bottom panel: The deviation of the dashed line(fitting) from the solid line(exact) is plotted.

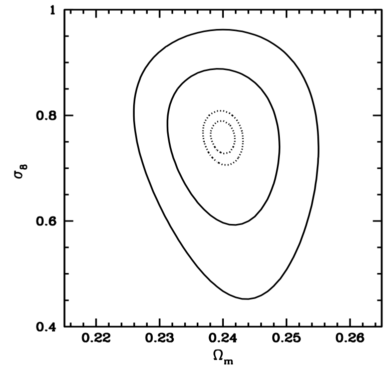

Figure 4: Constraints on Ω_m and σ_8. The solid line and the dotted line corresponds to $\triangle A = 2000\mathrm{deg}^2$ and $\triangle A = 4\pi$ respectively. Inner circle and outer circle indicate 1σ and 2σ confidence level respectively.

With the above expected error, we generate the power spectrum based on a Monte Calro simulation and assess the χ^2 defined by

$$\chi^2 = \sum_i \frac{\left[B(k_i,z)^{th} - B(k_i,z)^{obs}\right]^2}{\triangle B^2(k_i,z)}, \tag{18}$$

where $B(k_i,z)^{th}$ is the theoretical one at the wavenumber $k_i = \triangle k(i-0.5)$, for $i = 4, 5, \cdots, 19$. Here we specify a bin of the Fourier space, $\triangle k = 0.01h\mathrm{Mpc}^{-1}$, and consider the range of $0.03 < k < 0.19$, where the validiy of our formula in the previous section is guaranteed. $B(k_i,z)^{obs}$ is the observational one obtained through a Monte Carlo simulation.

Figure 4 shows the 1 sigma (inner solid curve) and the 2 sigma (outer solid curve) contours of $\triangle\chi^2$ in the Ω_m and σ_8 plane, where we assume the galaxy redshift samples provided a forthcoming experiment, WFMOS, which contains 2.1×10^6 galaxies, over $2000\mathrm{deg}^2$, at $0.5 < z < 1.3$. The dotted curves show the 1 sigma (inner) and the 2 sigma (outer) contours when assuming the survey area $\Delta A = 4\pi$.

4 Summary

In this work, we examined the damping nature of the BAO signature in the matter power spectrum due to the nonlinear gravitational clustering. First, we found an analytic expression for the damping behavior of the BAO signature. On the basis of the result, we constructed a fitting formula for the damping behavior in the weakly nonlinear regime. Furthermore, based on the simple numerical simulation, we found how Ω_m and σ_8 can be constrained through the weakly nonlinear evolution of the BAO.

References

[1] Bassett B A, Nichol R C, Eisenstein D J, the WFMOS Feasibility Study Dark Energy Team, arXiv:astro-ph/0510272

[2] Jain B, & Bertschinger E, 1994, ApJ, 431, 495

[3] Eisenstein, D. J., & Hu, W. 1998, ApJ, 496, 605

[4] Fry, J. N. 1996, ApJ, 461, L65

[5] Yamamoto K, et al., 2007, Phys. Rev. D, 76, 023504

Stationary solutions of black hole - bubble sequence in Kaluza-Klein theory

Hideo Iguchi[1], Takashi Mishima[1] and Shinya Tomizawa[2]

[1] *Laboratory of Physics, College of Science and Technology, Nihon University, Narashinodai, Funabashi, Chiba 274-8501, Japan*
[2] *Department of Mathematics and Physics, Graduate School of Science, Osaka City University, 3-3-138 Sugimoto, Sumiyoshi, Osaka 558-8585, Japan*

Abstract

We construct exact stationary solutions of black hole – bubble sequence in the five dimensional Kaluza-Klein (KK) theory by using solitonic solution generating techniques. The solution describes two stationary black holes with topology S^3 on a Kaluza-Klein bubble and has a momentum component. There are two different solutions. One is boosted black holes on KK bubble. This solution describes rotating black holes on KK bubble in the local point of view. It however has an ADM linear momentum. Therefore we call it boosted black holes on KK bubble. Only one black hole has non-zero Komar angular momentum which is equal to the ADM linear momentum. The rotation of black hole with no intrinsic spin is a consequence of frame-dragging effect. The other is a solution of rotating black holes on KK bubble . This solution has an ADM angular momentum as an asymptotic charge. The Komar angular momentum of one black hole is positive and the other is negative. The sum of Komar angular momenta is equal to the ADM angular momentum. The angular velocities of the black holes have the same sign because of the frame-dragging effect of dominant black hole.

1 Introduction

Kaluza-Klein (KK) theory is the five dimensional theory of gravity which unifies Einstein's four-dimensional theory of gravity and Maxwell's electromagnetic theory. The spacetime is asymptotically the product of the four-dimensional Minkowski spacetime $\mathcal{M}^{3,1}$ and a circle S^1. The extra dimension with S^1 is compactified too small for us to observe it. This type of compactification of the extra dimensions are also extended to the supergravity theories and the superstrings. The studies on black holes in the KK theory have attracted much attention since they admit much richer structures than asymptotically flat higher dimensional black holes. Recently, we obtained the new five-dimensional vacuum solutions of stationary black holes on the KK bubble [1, 2]. This solution is the extension of the static solution found by Elvang and Horowitz [3]. In the following, we briefly explain the solutions and describe several important features of them.

2 Boosted black holes on KK bubble

2.1 solutions

At first we briefly present the boosted black holes solution. We start from the following form of a seed static metric

$$ds^2 = e^{-T^{(0)}}\left[-e^{S^{(0)}}(dt)^2 + e^{-S^{(0)}}\rho^2(d\phi)^2 + e^{2\gamma^{(0)}-S^{(0)}}\left(d\rho^2+dz^2\right)\right] + e^{2T^{(0)}}(d\psi)^2, \tag{1}$$

with seed functions

$$\begin{aligned} S^{(0)} &= U_{\lambda\sigma} - \tilde{U}_{\eta_1\sigma} + 2\tilde{U}_{\eta_2\sigma} = -\tilde{U}_{\lambda\sigma} - \tilde{U}_{\eta_1\sigma} + 2\tilde{U}_{\eta_2\sigma} + \ln\rho \qquad (2)\\ T^{(0)} &= U_{\lambda\sigma} + \tilde{U}_{\eta_1\sigma} = -\tilde{U}_{\lambda\sigma} + \tilde{U}_{\eta_1\sigma} + \ln\rho, \qquad (3)\end{aligned}$$

where we assume $\eta_1 < \eta_2 < -1 < \lambda < 1$ and $\sigma > 0$. The function U_d is defined as $U_d := \frac{1}{2}\ln[\,R_d - (z-d)\,]$ and the function $\tilde{U}_d$ is defined as $\tilde{U}_d := \frac{1}{2}\ln[\,R_d + (z-d)\,]$ where $R_d := \sqrt{\rho^2 + (z-d)^2}$. Here we take the coordinate ϕ as a Kaluza-Klein compactified direction. The solitonic solution has two event horizons at $\eta_1\sigma \le z \le \eta_2\sigma$ and $-\sigma \le z \le \lambda\sigma$ and a Kaluza-Klein bubble at $\eta_2\sigma \le z \le -\sigma$, where the Kaluza-Klein circles shrink to zero. The metric of the solitonic solution can be written in the following form

$$ds^2 = e^{-T}\left[-e^{S}(dt-\omega d\phi)^2 + e^{-S}\rho^2(d\phi)^2 + e^{2\gamma - S}\left(d\rho^2 + dz^2\right)\right] + e^{2T}(d\psi)^2. \tag{4}$$

The function T is derived from the seed functions

$$T = -\tilde{U}_{\lambda\sigma} + \tilde{U}_{\eta_1\sigma} + \ln\rho. \tag{5}$$

The other metric functions for the five-dimensional metric (4) are obtained as

$$e^{S} = e^{S^{(0)}}\frac{A}{B}, \tag{6}$$

$$\omega = 2\sigma e^{-S^{(0)}}\frac{C}{A} - C_1, \tag{7}$$

$$e^{2\gamma} = C_2(x^2-1)^{-1}Ae^{2\gamma'}, \tag{8}$$

where C_1 and C_2 are constants and A, B and C are given by

$$\begin{aligned}
A &= \frac{1}{(2\sigma)^2}\left\{\left(e^{2\tilde{U}_{-\sigma}} + e^{2U_\sigma}\right)\left(e^{2\tilde{U}_\sigma} + e^{2U_{-\sigma}}\right)(1+ab)^2 - \left(e^{2\tilde{U}_{-\sigma}} - e^{2\tilde{U}_\sigma}\right)\left(e^{2U_\sigma} - e^{2U_{-\sigma}}\right)(b-a)^2\right\},\\
B &= \frac{1}{(2\sigma)^2}\left\{\left[\left(e^{2\tilde{U}_{-\sigma}} + e^{2U_\sigma}\right) + \left(e^{2\tilde{U}_\sigma} + e^{2U_{-\sigma}}\right)ab\right]^2 + \left[\left(e^{2\tilde{U}_{-\sigma}} - e^{2\tilde{U}_\sigma}\right)a - \left(e^{2U_\sigma} - e^{2U_{-\sigma}}\right)b\right]^2\right\},\\
C &= \frac{1}{(2\sigma)^3}\left\{\left(e^{2\tilde{U}_{-\sigma}} + e^{2U_\sigma}\right)\left(e^{2\tilde{U}_\sigma} + e^{2U_{-\sigma}}\right)(1+ab)\left(\left(e^{2U_\sigma} - e^{2U_{-\sigma}}\right)b - \left(e^{2\tilde{U}_{-\sigma}} - e^{2\tilde{U}_\sigma}\right)a\right)\right.\\
&\quad\left. + \left(e^{2\tilde{U}_{-\sigma}} - e^{2\tilde{U}_\sigma}\right)\left(e^{2U_\sigma} - e^{2U_{-\sigma}}\right)(b-a)\left(\left(e^{2\tilde{U}_{-\sigma}} + e^{2U_\sigma}\right) - \left(e^{2\tilde{U}_\sigma} + e^{2U_{-\sigma}}\right)ab\right)\right\}.
\end{aligned}$$

The functions a and b, which are auxiliary potential to obtain the new Ernst potential by the transformation, are given by

$$a = \alpha\sqrt{\frac{(e^{2\tilde{U}_{-\sigma}} + e^{2U_\sigma})(e^{2U_\sigma} - e^{2U_{-\sigma}})}{(e^{2\tilde{U}_\sigma} + e^{2U_{-\sigma}})(e^{2\tilde{U}_{-\sigma}} - e^{2\tilde{U}_\sigma})}\frac{e^{\tilde{U}_{\lambda\sigma}}}{e^{2U_\sigma} + e^{2\tilde{U}_{\lambda\sigma}}}\frac{e^{\tilde{U}_{\eta_1\sigma}}}{e^{2U_\sigma} + e^{2\tilde{U}_{\eta_1\sigma}}}\left(\frac{e^{2U_\sigma} + e^{2\tilde{U}_{\eta_2\sigma}}}{e^{\tilde{U}_{\eta_2\sigma}}}\right)^2}, \tag{9}$$

$$b = \beta\sqrt{\frac{(e^{2\tilde{U}_{-\sigma}} + e^{2U_\sigma})(e^{2\tilde{U}_{-\sigma}} - e^{2\tilde{U}_\sigma})}{(e^{2\tilde{U}_\sigma} + e^{2U_{-\sigma}})(e^{2U_\sigma} - e^{2U_{-\sigma}})}\frac{e^{2U_{-\sigma}} + e^{2\tilde{U}_{\lambda\sigma}}}{e^{\tilde{U}_{\lambda\sigma}}}\frac{e^{2U_{-\sigma}} + e^{2\tilde{U}_{\eta_1\sigma}}}{e^{\tilde{U}_{\eta_1\sigma}}}\left(\frac{e^{\tilde{U}_{\eta_2\sigma}}}{e^{2U_{-\sigma}} + e^{2\tilde{U}_{\eta_2\sigma}}}\right)^2}. \tag{10}$$

In addition the function γ' is obtained as

$$\begin{aligned}
\gamma' &= \gamma'_{\sigma,\sigma} + \gamma'_{-\sigma,-\sigma} + \gamma'_{\lambda\sigma,\lambda\sigma} + \gamma'_{\eta_1\sigma,\eta_1\sigma} + \gamma'_{\eta_2\sigma,\eta_2\sigma}\\
&\quad -2\gamma'_{\sigma,-\sigma} - \gamma'_{\sigma,\lambda\sigma} - \gamma'_{\sigma,\eta_1\sigma} + 2\gamma'_{\sigma,\eta_2\sigma} + \gamma'_{-\sigma,\lambda\sigma} + \gamma'_{-\sigma,\eta_1\sigma} - 2\gamma'_{-\sigma,\eta_2\sigma}\\
&\quad -\gamma'_{\lambda\sigma,\eta_1\sigma} - \gamma'_{\lambda\sigma,\eta_2\sigma} - \gamma'_{\eta_1\sigma,\eta_2\sigma}\\
&\quad +\tilde{U}_\sigma - \tilde{U}_{-\sigma} - 2\tilde{U}_{\lambda\sigma} + \tilde{U}_{\eta_1\sigma} + \tilde{U}_{\eta_2\sigma} + \ln\rho,
\end{aligned} \tag{11}$$

where

$$\gamma'_{cd} = \frac{1}{2}\tilde{U}_c + \frac{1}{2}\tilde{U}_d - \frac{1}{4}\ln[R_cR_d + (z-c)(z-d) + \rho^2]. \tag{12}$$

The constants C_1 and C_2 are chosen as follows

$$C_1 = 0, \quad C_2 = \frac{1}{(1+\alpha\beta)^2}, \tag{13}$$

to avoid the global boost of the spacetime and to set the period of ψ to 2π, respectively. Also the integration constants α and β should be decided as

$$\alpha^2 = \frac{(1-\lambda)(1-\eta_1)}{(1-\eta_2)^2}, \quad \beta = 0, \tag{14}$$

to remove the singularity at $z = \sigma$ on z-axis and closed timelike curves around the bubble, respectively. In order to avoid conical singularity for $z \in [\eta_2\sigma, -\sigma]$ and $\rho = 0$, ϕ has the periodicity of

$$\frac{\Delta\phi}{2\pi} = 2\sigma\frac{\eta_2+1}{\eta_2-1}\sqrt{\frac{(\lambda-\eta_1)(\lambda-\eta_2)(\eta_1-1)}{\eta_1+1}}. \tag{15}$$

2.2 properties

The asymptotic structure of the solution is the S^1 bundle over the four-dimensional Minkowski spacetime. Two black holes have the topological structure of S^3 and the bubble is topologically $S^1 \times R$. The solution describes the physical situation such that two black holes have the boost velocity of the same direction, even though the black holes are considered as the rotating S^3 black holes for the local observer near the horizon. The ADM mass and the linear momentum of the solution are obtained as

$$M_{ADM} = \frac{(\lambda - 2\eta_1 + \eta_2 + 2)\sigma}{4}\Delta\phi, \quad P = -\frac{\alpha\sigma}{2}\Delta\phi. \tag{16}$$

We obtain the Komar angular momenta of left and right black holes as

$$J_{\text{Komar},1} = 0, \quad J_{\text{Komar},2} = -\frac{\alpha\sigma}{2}\Delta\phi, \tag{17}$$

respectively. The left black hole has no intrinsic rotation. The Komar angular momentum of right black hole is exactly same as the linear momentum of the spacetime. We conclude that one of the two black holes has intrinsic rotation and the other rotates by the effect of the gravitational frame-dragging. In the static case, it coincides with the solution found by Elvang and Horowitz. In the small black holes limit, one black hole approaches an extremal black hole and the other approaches the round S^3 sphere. No matter how large the size of the horizons increase, the black holes cannot merge each other if the size of the KK circle is fixed. To construct the single boosted black string from the solution, we have to redefine the size of the KK circle after the limit of $\eta_2 \to -1$. It cannot be expected that the boosted black hole spontaneously breaks down to the boosted black holes on KK bubble from the comparison of areas between the black holes on KK bubble and the black string for the same asymptotic charges.

3 Rotating black holes on KK bubble

3.1 solutions

The solution of rotating black holes on KK bubble is obtained by the similar procedure of boosted black holes in the previous section. Here we only give the functions $S^{(0)}, T^{(0)}, a, b, \gamma'$ and the constants C_1, C_2, α, β.

$$S^{(0)} = \tilde{U}_{\lambda\sigma} - 2\tilde{U}_{\eta_1\sigma} + \tilde{U}_{\eta_2\sigma}, \quad T^{(0)} = \tilde{U}_{\lambda\sigma} - \tilde{U}_{\eta_2\sigma}. \tag{18}$$

The functions a and b are given by

$$a = \alpha\cdot\frac{e^{2U_\sigma}+e^{2\tilde{U}_{\lambda\sigma}}}{e^{\tilde{U}_{\lambda\sigma}}}\cdot\frac{e^{2U_\sigma}+e^{2\tilde{U}_{\eta_2\sigma}}}{e^{\tilde{U}_{\eta_2\sigma}}}\cdot\left(\frac{e^{\tilde{U}_{\eta_1\sigma}}}{e^{2U_\sigma}+e^{2\tilde{U}_{\eta_1\sigma}}}\right)^2, \tag{19}$$

$$b = \beta\cdot\frac{e^{\tilde{U}_{\lambda\sigma}}}{e^{2U_{-\sigma}}+e^{2\tilde{U}_{\lambda\sigma}}}\cdot\frac{e^{\tilde{U}_{\eta_2\sigma}}}{e^{2U_{-\sigma}}+e^{2\tilde{U}_{\eta_2\sigma}}}\cdot\left(\frac{e^{2U_{-\sigma}}+e^{2\tilde{U}_{\eta_1\sigma}}}{e^{\tilde{U}_{\eta_1\sigma}}}\right)^2. \tag{20}$$

In addition the function γ' is obtained as

$$\begin{aligned}\gamma' \;=\;& \gamma'_{\sigma,\sigma}+\gamma'_{-\sigma,-\sigma}+\gamma'_{\lambda\sigma,\lambda\sigma}+\gamma'_{\eta_1\sigma,\eta_1\sigma}+\gamma'_{\eta_2\sigma,\eta_2\sigma}\\ &-2\gamma'_{\sigma,-\sigma}+\gamma'_{\sigma,\lambda\sigma}-2\gamma'_{\sigma,\eta_1\sigma}+\gamma'_{\sigma,\eta_2\sigma}-\gamma'_{-\sigma,\lambda\sigma}+2\gamma'_{-\sigma,\eta_1\sigma}-\gamma'_{-\sigma,\eta_2\sigma}\\ &-\gamma'_{\lambda\sigma,\eta_1\sigma}-\gamma'_{\lambda\sigma,\eta_2\sigma}-\gamma'_{\eta_1\sigma,\eta_2\sigma}.\end{aligned} \tag{21}$$

The constants C_1 and C_2 are chosen as follows

$$C_1=-\frac{2\sigma(\alpha-\beta)}{1+\alpha\beta},\quad C_2=\frac{1}{(1+\alpha\beta)^2},\quad \alpha+\beta=0. \tag{22}$$

To avoid a singular behavior of $g_{\phi\phi}$ on the ϕ-axis, we also need to impose the following condition on β

$$\beta^2=-\frac{(\lambda+1)(1+\eta_2)}{(1+\eta_1)^2}. \tag{23}$$

The KK compactified direction is ψ with the periodicity $\Delta\psi$,

$$\frac{\Delta\psi}{2\pi} \;=\; 2\sigma\frac{(\eta_1+1)((\eta_1-1)^2+(\lambda+1)(\eta_2-1))}{(\eta_1-1)((\eta_1+1)^2+(\lambda+1)(\eta_2+1))}\sqrt{\frac{(\lambda-\eta_1)(\lambda-\eta_2)(\eta_2+1)}{\eta_2-1}}. \tag{24}$$

The solution has two event horizons at $\eta_1\sigma\le z\le\eta_2\sigma$ and $\lambda\le z\le\sigma$ and a Kaluza-Klein bubble at $\eta_2\sigma\le z\le\lambda\sigma$.

3.2 properties

The solution describes the physical situation such that two black holes have the angular velocity of the same direction and the bubble plays a role in holding two black holes. In the static case, it coincides with the solution found by Elvang and Horowitz. The ADM mass of the solution is computed as

$$M_{ADM}=\frac{\sigma(4-2\eta_1+\eta_2+\lambda+\beta^2(4+2\eta_1-\eta_2-\lambda))}{4(1-\beta^2)}\Delta\psi. \tag{25}$$

The nonzero component of the angular momentum becomes

$$J=-\frac{\beta\sigma^2(2-2\eta_1+\eta_2+\lambda+\beta^2(2+2\eta_1-\eta_2-\lambda))}{(1-\beta^2)^2}\Delta\psi. \tag{26}$$

It should be noted that the ADM mass is non-negative when $\beta^2<1$. The two black holes have inverse intrinsic spin each other

$$J_{\mathrm{Komar},1}=\frac{\sigma^2\beta}{(1-\beta^2)^2}\frac{(\eta_2-\eta_1)^2((1+\lambda)(1+\eta_2)-(1-\eta_1^2))^2}{(1+\eta_1)^2(1+\eta_2)((1+\lambda)(1-\eta_2)-(1-\eta_1)^2)}\Delta\psi, \tag{27}$$

$$J_{\mathrm{Komar},2}=-\frac{\sigma^2\beta}{(1-\beta^2)^2}\frac{((1-\lambda)(1+\eta_2)-(1+\eta_1)^2)((1-\lambda^2)(1-\eta_2^2)-(1-\eta_1^2)^2)}{(1+\eta_1)^2(1+\eta_2)((1+\lambda)(1-\eta_2)-(1-\eta_1)^2)}\Delta\psi, \tag{28}$$

even though the angular velocities are same sign. This feature is attributed to the gravitational frame-dragging of the faster black hole. We have also compared the entropy of two black holes on a bubble with a rotating black string with the same mass and the same angular momentum. Like the static solution [3] and the boosted black hole solutions on a bubble [1], we cannot expect that a black string spontaneously generates a Kaluza-Klein bubble and it splits the horizon with the topology $S^1\times S^2$ into two black holes with the topology S^3.

References

[1] H. Iguchi, T. Mishima and S. Tomizawa, Phys. Rev. D **76**, 124019 (2007) [arXiv:0705.2520 [hep-th]].

[2] S. Tomizawa, H. Iguchi and T. Mishima, arXiv:hep-th/0702207.

[3] H. Elvang and G. T. Horowitz, Phys. Rev. D **67**, 044015 (2003) [arXiv:hep-th/0210303].

New method to integrate 2+1 wave equations with Dirac's delta functions as sources

Hiroyuki Nakano[1] and Carlos O. Lousto[2]

[1,2] *Center for Computational Relativity and Gravitation, School of Mathematical Sciences, Rochester Institute of Technology, Rochester, New York 14623, USA*

Abstract

Gravitational perturbations in a Kerr black hole background can not be decomposed into simple tensor harmonics in the time domain. Here, we make the mode decomposition only in the azimuthal direction and discuss the resulting (2+1)-dimensional Klein-Gordon differential equation for scalar perturbations with a two dimensional Dirac's δ-function as a source representing a point particle orbiting a much larger black hole. To make this equation amenable for numerical integrations we explicitly remove analytically the singular behavior of the source and compute a global effective source for the corresponding waveform.

1 Introduction

One of the main source targets of LISA is the gravitational waves generated by the inspiral of compact objects into massive black holes. For these Extreme Mass Ratio Inspirals (EMRI) we use the black hole perturbation approach to compute waveforms, where the compact object is approximated by a point particle orbiting a massive Kerr black hole. In order to obtain the precise theoretical gravitational waveform, we need to solve the self-force problem and problems in the second order perturbations [1].

In this paper, we focus on one aspect of the self-force problem, specifically to derive the retarded field of a point source. As a first step, we consider the Klein-Gordon equation in the Schwarzschild spacetime, but do not decompose it into spherical harmonics, in order to model perturbations in the more generic Kerr background. Recently, Barack and Golbourn [2] have discussed this equation in (2+1)-dimensions as derived by the mode decomposition in the azimuthal direction. Another treatment is proposed here to deal with this problem globally. We also note that there is a method to use a narrow Gaussian rather than a Dirac δ-function [3]. It is, however, difficult to ascertain the error introduced by smearing the particle and if this is accurate enough for self force computations.

2 Formulation

When we calculate the $(2+1)$-dimensional (D) equation derived from the $4D$ Klein-Gordon equation by the azimuthal mode decomposition, the resulting equation is not exactly same as the $(2+1)D$ wave equation. By transforming the scalar field, we can obtain an equation which includes the $(2+1)D$ d'Alambertian and a remainder. Then, we remove the $2D$ δ-function in the source term.

In order to do so, we consider the Schwarzschild metric in the isotropic coordinates,

$$ds^2 \;=\; -(2\rho - M)^2/(2\rho + M)^2 dt^2 + (1 + M/(2\rho))^4 \left(d\rho^2 + \rho^2 \left(d\theta^2 + \sin^2\theta d\phi^2\right)\right) . \tag{1}$$

This radial coordinate is related to that of the Schwarzschild, r, as $\rho = \left(r - M + \sqrt{r^2 - 2Mr}\right)/2$. In the above coordinates, the Klein-Gordon equation with a point source becomes

$$\left[-\frac{(2\,\rho + M)^2}{(2\,\rho - M)^2}\partial_t^2 + \frac{16\rho^4}{(2\,\rho + M)^4}\partial_\rho^2 + \frac{128\rho^5}{(2\,\rho - M)\,(2\,\rho + M)^5}\partial_\rho + \frac{16\rho^2}{(2\,\rho + M)^4}\left(\partial_\theta^2 + \cot\theta\partial_\theta + \frac{1}{\sin^2\theta}\partial_\phi^2\right)\right]$$
$$\times\psi(t,\rho,\theta,\phi) = -q\int_{-\infty}^{\infty} d\tau \frac{64\rho^4\delta(t - t_z(\tau))\delta(\rho - \rho_z(\tau))\delta(\theta - \theta_z(\tau))\delta(\phi - \phi_z(\tau))}{(2\rho - M)(2\rho + M)^5 \sin\theta} . \tag{2}$$

[1] E-mail:hxnsma1@rit.edu

[2] E-mail:colsma@rit.edu

Here, we use the azimuthal mode decomposition, $\psi(t,r,\theta,\phi) = \sum_{m=-\infty}^{\infty} \psi_m(t,\rho,\theta)e^{im\phi}$, and transform the field ψ_m as $\psi_m = 2\sqrt{\rho/[(2\,\rho+M)\,(2\,\rho-M)\sin\theta]}\,\chi_m$. Then, χ_m satisfies the following equation.

$$\left[-\frac{1}{16}\frac{(2\rho+M)^6}{(2\rho-M)^2\rho^4}\partial_t^2 + \partial_\rho^2 + \frac{1}{\rho}\partial_\rho + \frac{1}{\rho^2}\left(\partial_\theta^2 - \frac{1}{\sin^2\theta}\left(m^2 - \frac{1}{4}\frac{(4\rho^2+M^2)^2 - 16\rho M\cos^2\theta}{(2\rho+M)^2(2\rho-M)^2}\right)\right)\right]$$
$$\times\chi_m(t,\rho,\theta) = -q\int_{-\infty}^{\infty} d\tau \frac{2\,\delta(t-t_z(\tau))\delta(\rho-\rho_z(\tau))\delta(\theta-\theta_z(\tau))}{\sqrt{(2\rho-M)(2\rho+M)\rho\sin\theta}}e^{-im\phi_z(\tau)}\,. \quad (3)$$

Next, we use a new time coordinate which is defined by $T = \int^t dt\,4\,(2\rho_z(t)-M)\rho_z(t)^2/(2\rho_z(t)+M)^3$, where ρ_z is obtained by solving a geodesic equation. Using this, we derive an equation which can be divided into the $(2+1)D$ d'Alambertian of the flat case $\Box^{(2+1)}$ and a remainder.

$$\begin{aligned}
\mathcal{L}_m\,\chi_m(T,\rho,\theta) &= \left(\Box^{(2+1)} + \mathcal{L}_m^{rem}\right)\chi_m(T,\rho,\theta) = S_m(T,\rho,\theta)\,; \\
\Box^{(2+1)} &= -\partial_T^2 + \partial_\rho^2 + (1/\rho)\partial_\rho + (1/\rho^2)\partial_\theta^2\,, \\
\mathcal{L}_m^{rem} &= \left(1 - \frac{(2\rho_z(T)-M)^2\rho_z(T)^4(2\rho+M)^6}{(2\rho_z(T)+M)^6(2\rho-M)^2\rho^4}\right)\partial_T^2 \\
&\quad - \frac{2(4\rho_z(T)-M)(2\rho_z(T)-M)(2\rho+M)^6\rho_z(T)^3 M}{(2\rho_z(T)+M)^7(2\rho-M)^2\rho^4}\left(\frac{d\rho_z(T)}{dT}\right)\partial_T \\
&\quad - \frac{1}{\rho^2\sin^2\theta}\left(m^2 - \frac{1}{4}\frac{(4\rho^2+M^2)^2 - 16\rho M\cos^2\theta}{(2\rho+M)^2(2\rho-M)^2}\right)\,, \\
S_m(T,\rho,\theta) &= -q\int_{-\infty}^{\infty} d\tau \frac{2\,\delta(t(T)-t_z(\tau))\delta(\rho-\rho_z(\tau))\delta(\theta-\theta_z(\tau))}{\sqrt{(2\rho-M)(2\rho+M)\rho\sin\theta}}e^{-im\phi_z(\tau)}\,.
\end{aligned} \quad (4)$$

To remove the δ-function in the source term, we set

$$\chi_m(T,r,\theta) = \chi_m^S(T,r,\theta) + \chi_m^{rem}(T,r,\theta)\,, \quad (5)$$

where we define the new functions, χ_m^S and χ_m^{rem} as calculated from

$$\Box^{(2+1)}\chi_m^S(T,r,\theta) = S_m(T,r,\theta)\,; \quad \mathcal{L}_m\,\chi_m^{rem}(T,r,\theta) = -\mathcal{L}_m^{rem}\chi_m^S(T,r,\theta) = S_m^{(eff)}(T,\rho,\theta)\,. \quad (6)$$

This decomposition of χ_m does not have any physical-meaning, i.e., χ_m^S is not identified as the singular part to be removed in the self-force calculation. Note that $\mathcal{L}_m^{rem}$ includes a second-order derivative. But, since the factor of ∂_T^2 is zero at the particle location, the singular behavior of the effective source $S_m^{(eff)}$ weakens. The derivation of the singular field χ_m^S can be performed through the Green function,

$$G(T,\mathbf{x};T',\mathbf{x}') = \theta((T-T') - |\mathbf{x}-\mathbf{x}'|)/\left(2\pi\sqrt{(T-T')^2 - |\mathbf{x}-\mathbf{x}'|^2}\right)\,, \quad (7)$$

where $|\mathbf{x}-\mathbf{x}'| = (\rho^2 + {\rho'}^2 - 2\,\rho\,\rho'\cos(\theta-\theta'))^{1/2}$ and χ_m^S is calculated by the following integral

$$\chi_m^S(T,\rho,\theta) = \int dT'\rho' d\rho' d\theta'\,G(T,\mathbf{x};T',\mathbf{x}')S_m(T',\rho',\theta')\,. \quad (8)$$

3 Circular Orbit Case

We consider a particle in circular orbit, $z^\alpha(\tau) = \{u^t\tau,\, r_0,\, \pi/2,\, u^\phi\tau\}$, where $u^t = \sqrt{r_0/(r_0-3M)}$ and $u^\phi = \sqrt{M/[r_0^2(r_0-3M)]}$. Here, we focus on the $m \neq 0$ modes; the $m = 0$ mode can be dealt with by the same treatment.

3.1 Singular field

First, the relationship between the new time coordinate T and the Schwarzschild time t is obtained analytically as $T = 4\,(2\rho_0 - M)\rho_0^2/(2\rho_0+M)^3\,t$ where $\rho_0 = 1/2(r_0 - M + \sqrt{r_0^2 - 2Mr_0})$. Note that in general, for non circular orbits, we need a numerical integration to derive this relationship. From Eq. (8), the singular field is derived as

$$\chi_m^S(t,r,\theta) \;=\; \frac{i}{4}\frac{2\sqrt{\rho_0}}{u^t\sqrt{(2\rho_0+M)(2\rho_0-M)}}H_0^{(1)}\left(\frac{(2\rho_0+M)^3}{4\,(2\rho_0-M)\rho_0^2}m\Omega|\mathbf{x}-\mathbf{x_z}|\right)e^{-im\Omega t}\,, \tag{9}$$

where $\Omega = u^\phi/u^t$ and the spatial difference is given by $|\mathbf{x}-\mathbf{x_z}| = \sqrt{\rho^2+\rho_0^2-2\,\rho\,\rho_0\sin\theta}$ and $H_0^{(1)}$ is the Hankel function. The local behavior of the above solution near the particle location is obtained as

$$\chi_m^S(t,r,\theta) \sim \chi_m^{SL}(t,r,\theta) = -\frac{1}{2\pi}\frac{2\sqrt{\rho_0}}{u^t\sqrt{(2\rho_0+M)(2\rho_0-M)}}\ln\left(\frac{(2\rho_0+M)^3}{4\,(2\rho_0-M)\rho_0^2}m\Omega|\mathbf{x}-\mathbf{x_z}|\right)e^{-im\Omega t}\,. \tag{10}$$

Therefore, $S_m^{(eff)}(t,\rho,\theta)$ shown by the dashed green curve in Fig. 1, is singular at the particle location. In order to perform the numerical integration with higher accuracy, it is convenient to regularize the source term to be at least C^0 at the particle location.

3.2 Local behavior

When we write the singular field as $\chi_m^S = \chi_m^{SL} + \hat{\chi}_m^S$, $\hat{\chi}_m^S$ is finite at the particle location. Then, the effective source in Eq. (6) becomes

$$\begin{aligned}
S_m^{(eff)}(t,\rho,\theta) \;=\; & -\frac{1}{2\pi}\frac{2\sqrt{\rho_0}}{u^t\sqrt{(2\rho_0+M)(2\rho_0-M)}}\ln\left(\frac{(2\rho_0+M)^3}{4\,(2\rho_0-M)\rho_0^2}m\Omega|\mathbf{x}-\mathbf{x_z}|\right)e^{-im\Omega t} \\
& \times\Bigg(-\frac{1}{\rho^2\sin^2\theta}\left(m^2-\frac{1}{4}\frac{(4\rho^2+M^2)^2-16\rho M\cos^2\theta}{(2\rho+M)^2(2\rho-M)^2}\right) \\
& \quad -(m\Omega)^2\left(\frac{(2\rho_0+M)^6}{(2\rho_0-M)^2\rho_0^4}-\frac{(2\rho+M)^6}{(2\rho-M)^2\rho^4}\right)\Bigg) - \mathcal{L}_m^{rem}\hat{\chi}_m^S(t,r,\theta)\,,
\end{aligned} \tag{11}$$

Note that the third line of the R.H.S. is at least C^0 at the location of the particle.

To remove the logarithmic divergence in the source, we introduce

$$\begin{aligned}
\chi_m^{rem,S}(t,\rho,\theta) \;=\; & -\frac{1}{16}|\mathbf{x}-\mathbf{x_z}|^2\ln\left(\frac{(2\rho_0+M)^3}{4\,(2\rho_0-M)\rho_0^2}m\Omega|\mathbf{x}-\mathbf{x_z}|\right){\rho_0}^{19/2}\,(2\,\rho-M)^3\,e^{-im\Omega\,t} \\
& \times\frac{64\,m^2\rho^4-32\,m^2\rho^2M^2+4\,m^2M^4+16\,\cos^2\theta\rho^2M^2-(4\rho^2+M^2)^2}{\pi u^t\,(2\,\rho_0+M)^{5/2}\,(2\,\rho_0-M)^{11/2}\,\rho^{11}\sin^2\theta}\,.
\end{aligned} \tag{12}$$

Using this regularization function, we obtain a source $S_m^{reg,I}$ for the function $\chi_m^{rem} - \chi_m^{rem,S}$ as

$$S_m^{reg,I}(t,\rho,\theta) \;=\; S_m^{(eff)}(t,\rho,\theta) - \mathcal{L}_m\chi_m^{rem,S}(t,\rho,\theta)\,. \tag{13}$$

The local behavior of $S_m^{reg,I}$, which is shown by the solid green curve in Fig. 1 (b), is an "$x\ln|x|$ for $x\to 0$" type, i.e., C^0 around the particle location.

3.3 Boundary behaviors

We now focus on the behaviors of the source term at the two boundaries, i.e at the horizon of the large hole and spatial infinity. The source for a final regularized function χ_m^{reg} must go like $O(\rho^{-2})$ for $\rho\to\infty$ in the case of the $m=0$ mode and $O(\rho^{-3/2})$ for the $m\neq 0$ mode because of integrability conditions. More precisely, the source for the regularized function of ψ_m derived by numerical calculations has a factor $\sim 1/\rho^{1/2}$. For $\rho\to M/2$, the source should be zero, i.e., the behavior should be a power of $(\rho - M/2)$ greater than 1/2. To regularize the source at the boundaries, we note that the source contribution from $\chi_m^{rem,S}$ is well behaved. This means that the ill behaviors of the source arise from χ_m^S. Therefore, it is convenient to use asymptotic behaviors of χ_m^S (and some correction factor) for regularization.

First, for the regularization near the horizon, we use the regularization function χ_m^h which is too long to be shown here. Then, the source for the function $\chi_m^{rem} - \chi_m^{rem,S} - \chi_m^h$ becomes

$$S_m^{reg,h}(t,\rho,\theta) = S_m^{reg,I}(t,\rho,\theta) - \mathcal{L}_m \chi_m^h(t,\rho,\theta)\,, \tag{14}$$

This $S_m^{reg,h}$ is shown by the solid black curve in Fig. 1 and behaves as $O(\rho^{-1/2})$ for large ρ. To regularize it, we use the regularization function,

$$\begin{aligned}\chi_m^\infty(t,\rho,\theta) &= -\sqrt{2}\,i\,\frac{\rho_0^{3/2}}{(2\,\rho_0+M)^2\,u^t\,\sqrt{\pi}\,\sqrt{m\,\Omega\,\rho}\,\rho^7}\,e^{(-i\,m\,\Omega\,t)}\left(\rho-\frac{M}{2}\right)^3(\rho^2+\rho_0^2-2\,\rho_0\,\rho\,\sin\theta)^2 \\ &\quad\times\exp\left(\frac{1}{4}i\,\frac{(2\,\rho_0+M)^3\,m\,\Omega\,\sqrt{\rho^2+\rho_0^2-2\,\rho_0\,\rho\,\sin\theta}}{(2\,\rho_0-M)\,\rho_0^2}-\frac{\pi}{4}i\right).\end{aligned} \tag{15}$$

The final source for the regularized function $\chi_m^{reg} = \chi_m^{rem} - \chi_m^{rem,S} - \chi_m^h - \chi_m^\infty$ becomes

$$S_m^{reg,f}(t,\rho,\theta) = S_m^{reg,h}(t,\rho,\theta) - \mathcal{L}_m \chi_m^\infty(t,\rho,\theta)\,, \tag{16}$$

which is used in the numerical calculation. This $S_m^{reg,f}$ is shown by the dashed black curve in Fig. 1, and behaves like $O(\rho^{-3/2}) \times$ (an oscillation factor with respect to ρ) for large ρ.

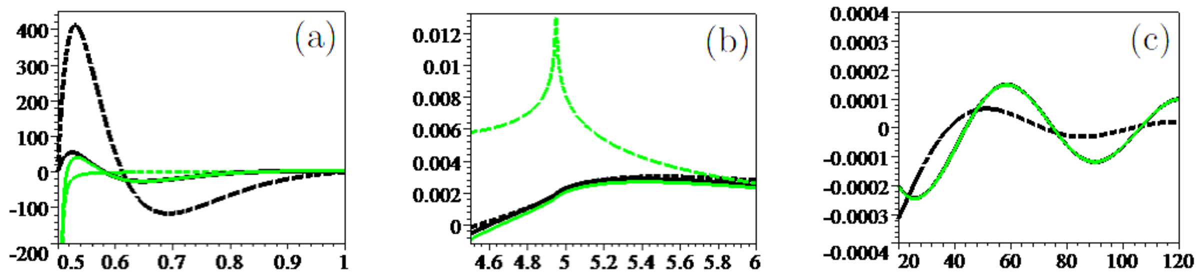

Figure 1: Plot for the $m=1$ mode of S_m with respect to ρ. $S_1^{(eff)}$, $S_1^{reg,I}$, $S_1^{reg,h}$ and $S_1^{reg,f}$ are shown by the dashed green, solid green, solid black and dashed black curve, respectively.

4 Discussion

In this paper, we obtained the regularized effective source which is C^0 at the location of the particle, and $O(\rho - M/2)$ near the horizon. The behavior at infinity is $O(\rho^{-3/2}) \times$ (an oscillation factor with respect to ρ) which allows straightforward numerical integration.

When we consider the extension of this formulation to the Kerr background case, we can also extract a similar differential operator to that of Eq. (4). In the case of gravitational perturbations, we have ten field equations for the linear perturbation in the Lorenz gauge. (See [4].) The same treatment discussed in this paper is applicable to those equations.

Acknowledgments

We would like to thank N. Sago and H. Tagoshi for useful discussions.

References

[1] H. Nakano and C. O. Lousto, arXiv:gr-qc/0701039.

[2] L. Barack and D. A. Golbourn, Phys. Rev. D **76**, 044020 (2007).

[3] R. Lopez-Aleman, G. Khanna and J. Pullin, Class. Quant. Grav. **20**, 3259 (2003).

[4] L. Barack and C. O. Lousto, Phys. Rev. D **72**, 104026 (2005).

Dynamics of strings in the space-time

Tatsuhiko Koike[1], Hiroshi Kozaki[2] and Hideki Ishihara[3]

[1]*Department of Physics, Keio University, Yokohama 223–8522 Japan*
[2]*Department of Applied Chemistry and Biotechnology, Niigata Institute of Technology, Kashiwazaki, Niigata 945–1195 Japan*
[3]*Department of Mathematics and Physics, School of Science, Osaka City University, Osaka 558–8585 Japan*

Abstract

The equation of motion of an extended object in spacetime reduces to an ordinary differential equation if there is cohomogeneity-one symmetry, which allows one to obtain exact solutions. We present a general method for solving the motion of cohomogeneity-one strings. With applications in higher-dimensional cosmology in mind, we give an explicit solution in the five-dimensional anti-de Sitter space.

1 Introduction

Existence and dynamics of extended objects play important roles in various stages in cosmology. Examples of extended objects include topological defects, such as strings and membranes, and the Universe as a whole which is embedded in a higher-dimensional spacetime in the context of the brane-world universe model [1].

The trajectory of an extended object forms a hypersurface in the spacetime which is described by a partial differential equation (PDE) such as the Nambu-Goto equation. Because the dynamics is more complicated than that of a particle, one usually cannot obtain general solutions. One way to find exact solutions is to assume symmetry. The simplest solutions to such a PDE are homogeneous ones, in which case the problem reduces to a set of algebraic equations. However, the solutions do not have much variety and the dynamics is trivial.

One may expect that if we assume "less" homogeneity, the equation still remains tractable and the solutions have enough variety to include nontrivial configurations and dynamics of physical interest. The cohomogeneity-one objects give such a class, which helps us to understand the basic properties of the extended objects and serves as a base camp to explore their general dynamics. For a string, stationarity is a special case of the cohomogeneity one condition. Some stationary configurations of the Nambu-Goto strings are obtained in the Schwarzchild spacetime [2]. Even in the Minkowski space, many nontrivial cohomogeneity-one solutions of the string were recently found [3, 4]. A cohomogeneity-one object is defined, roughly speaking, as the one whose world sheet is homogeneous except in one direction. Then any covariant PDE governing such an object reduces to an ordinary differential equation (ODE), which can easily be solved analytically, or at least, numerically. A solution represents the dynamics of a spatially homogeneous object, or the nontrivial configuration of a stationary object, depending on the homogeneous "direction" is spacelike or timelike. The case of null homogeneous "direction" should also give new intriguing models.

In this paper, we treat dynamics of a string in spacetime. For Nambu-Goto strings, we give a general procedure to solve the trajectory, which can be easily applied to other PDEs. We choose the spacetime to be the five-dimensional anti-de Sitter space AdS^5, which is to meet the recent interest in higher-dimensional cosmology including the brane-world universe model, and in string theory. Among the cohomogeneity-one strings which have been completely classified in [5], we chosse one type and demonstrate the procedure giving an explicit solution.

[1]E-mail:koike@phys.keio.ac.jp
[2]kozaki@adm.niit.ac.jp
[3]ishihara@sci.osaka-cu.ac.jp

2 General treatment of cohomogeneity-one strings

In this section, we develop a general procedure of classifying cohomogeneity-one objects and solving their dynamics in an arbitrary spacetime (M, g). Let us start with the definition of the cohomogeneity-one objects. We say that a m-dimensional hypersurface S in M is of *cohomogeneity one* if it is foliated by $(m-1)$-dimensional submanifolds S_σ labeled by a real number σ and there is a subgroup K of G which preserves the foliation and acts transitively on S_σ. In particular, the hypersurfaces S_σ's are embedded homogeneously in M. A cohomogeneity-one object has a world sheet which is a cohomogeneity-one hypersurface. In this paper, we focus on the case that the extended objects are strings, so that $m = 2$, and K is a one-parameter group $(\phi_\tau)_{\tau\in\mathbb{R}}$ of isometries (Fig. 1).

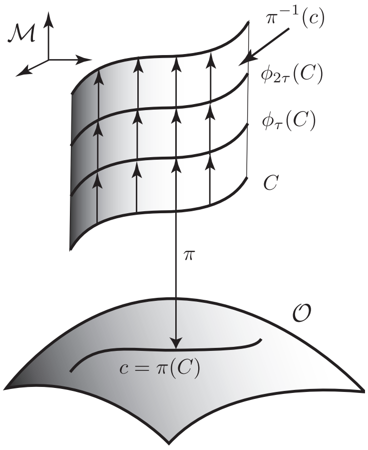

Figure 1: To solve a trajectory of the cohomogeneity-one string is to find a curve C in M which projects to a geodesic c on O.

Let us show a formalism to solve the dynamics and the configuration of the cohomogeneity-one strings. We assume the motion is governed by the Nambu-Goto action. The orbit space for K is defined by $O := M/K$, i.e., by identifying all the points on each Killing orbit in M. The submanifolds S_σ mentioned above are the preimages $\pi^{-1}(x)$ of a point $x \in O$. One can endow O with a metric h so that the projection $\pi : (M, g) \to (O, h)$ is an orthogonal projection, or more precisely, a Riemannian submersion. The metric h is given by $h_{ab} := g_{ab} - \xi_a\xi_b/f$, where $f := \xi^a\xi_a$. This metric has the Euclidean signature if the Killing vector ξ is timelike, i.e., if $f < 0$, and the Lorentzian signature if ξ is spacelike, i.e., if $f > 0$. Carrying out the integration along ξ, one obtains

$$S = \int_c \sqrt{-f h_{ab} dx^a dx^b}, \tag{1}$$

where c is a curve on O. Thus the problem of the string reduces to finding geodesics on the orbit space O with the metric $-fh$. For convenience, we adopt a modified action

$$S = \int_c d\sigma \left(-\frac{1}{\alpha} f h_{ab} \dot{x}^a \dot{x}^b + \alpha \right), \tag{2}$$

where an overdot denotes the differentiation by σ. The action (2) derives the same geodesic equations as (1) and retains the invariance under reparametrization of σ. The function α is the norm of the tangent vector.

The two-dimensional world sheet of the string is the preimage $\pi^{-1}(c)$ of the geodesic c on $(O, -fh)$. Sometimes it is more convenient to find a curve C on M, a *lift* curve, such that its projection $\pi(C)$ is a geodesic on $(O, -fh)$ (Fig. 1). The Hopf string in Sec. 3 is such an example. In the case, the trajectory of the string is given by

$$S = \pi^{-1}(\pi(C)) = \{\phi_\tau(C(\sigma));\ (\tau,\sigma) \in \mathbb{R}^2\}. \tag{3}$$

Note that the last expression in (3) is purely written with objects in M. The trajectory S can also be viewed as a foliation by mutually isometric curves $\phi_\tau \circ C$ labeled by τ.

3 The Hopf string

Hereafter in this paper, we assume that the spacetime (M, g) is the five-dimensional anti-de Sitter space AdS^5, or its universal cover $\widetilde{AdS^5}$. The former space has closed timelike curves which in the latter space are "opened up" to infinite nonclosed curves. The latter is usually more suitable when we discuss cosmology, but we will not distinguish them strictly in the following. The space AdS^5 is most easily expressed as a pseudo-sphere

$$\overline{\psi}\psi = -1 \tag{4}$$

in the pseudo-Euclidean space $E^{4,2}$ whose metric is $dS^2 = l^2 d\overline{\psi} d\psi$, where we have employed complex coordinates $\psi := (\psi^0, \psi^1, \psi^2)^T \in \mathbb{C}^3$, and have defined $\overline{\psi} := \psi^\dagger \zeta$ and $\zeta := \mathrm{diag}[-1, 1, 1]$. The all possible types of cohomogeneity-one strings in AdS^5 are classified in [5].

Let us choose one of the types in [5] and find the trajectory for the Nambu-Goto string. This example also shows that working with the lift curves as explained in Sec. 2 can make the calculations and geometric interpretation of the trajectory simple and transparent.

We shall say that a *Hopf string* is a cohomogeneity-one string which is homogeneous under the change of the overall phase in the complex coordinates ψ:

$$\psi \mapsto e^{i\tau}\psi, \tau \quad \in \mathbb{R}. \tag{5}$$

This isometry is the simultaneous rotations in the st, xy, and zw planes. The Killing vector field ξ is proportional to $L + J_{xy} + J_{zw}$ and falls into Type $(1, 1, 1, 1|0)$ with the condition $a = b = c$. The Killing orbit is timelike and is closed in AdS^5. The closedness is because AdS^5 itself has closed timelike curves. In the universal cover $\widetilde{AdS^5}$, the Killing orbits are not closed. The solution represents a stationary string.

Let us solve the configuration of the Hopf string, assuming that it obeys the Nambu-Goto equation. Because ξ is timelike, the orbit space (O, h) is a Riemannian manifold. A special feature of ξ is that its squared norm is a constant, which we set $f = -1$, so that the the metric $-fh$ to determine the configuration of the string equals the metric h on the orbit space O. Thus our task is nothing but solving geodesics on (O, h).

The metric h on O is written as $h = l^2 d\overline{\psi}(1 + \psi\overline{\psi})d\psi$, with the constraint (4), where $-\psi\overline{\psi}$ is the normal projection along ψ. This is the Fubini-Study metric except that we started with an indefinite scalar product $\zeta = \mathrm{diag}[-1, 1, 1]$ in (4) and in $E^{4,2}$, while the usual Fubini-Study metric is defined by means of a positive definite scalar product. We shall also call h as the Fubini-Study metric and denote the Riemannian manifold (O, h) by $\mathbb{C}P^2_-$. The fibration $\mathbb{C}P^2_- \simeq AdS^5/U(1)$ is the generalization of the Hopf fibration to the case of indefinite scalar product. Thus the problem of finding Nambu-Goto strings has reduced to solving geodesics on $\mathbb{C}P^2_-$. From the argument in Sec. 2, our action (2) for the Hopf string should be

$$S = \int_c d\sigma \left(\frac{1}{\alpha}\dot{\overline{\psi}}(1 + \psi\overline{\psi})\dot{\psi} + \alpha + \mu(1 + \overline{\psi}\psi) \right), \tag{6}$$

where μ is a Lagrange multiplier. This is the action for geodesics on O written in terms of the coordinates ψ in AdS, or in $E^{4,2}$. In fact, the action (6) has a $U(1)$ gauge degree of freedom and is invariant under the local phase change $\psi(\sigma) \mapsto e^{i\theta(\sigma)}\psi(\sigma)$, if $\psi(\sigma)$ satisfies the constraint $\overline{\psi}\psi = -1$.

The Euler-Lagrange equations are the constraint (4) and

$$\dot{\overline{\psi}}(1 + \psi\overline{\psi})\dot{\psi} = \alpha^2, \quad -\left(\frac{1}{\alpha}(1 + \psi\overline{\psi})\dot{\psi}\right)^{\bullet} + \frac{1}{\alpha}\dot{\overline{\psi}}\psi\dot{\psi} + \mu\psi = 0. \tag{7}$$

Multiplying $\overline{\psi}$ on the second equation from the left and using the constraint (4), one obtains an equation which merely determines μ. On the other hand, the time derivative of (4) implies that $\overline{\psi}\dot{\psi}$ is pure imaginary. This value can be changed by the gauge transformation $\psi \mapsto e^{i\theta(\sigma)}\psi(\sigma)$. Thus we can always choose the gauge such that $\overline{\psi}\dot{\psi} = 0$. With the choice $\alpha \equiv 1$, one can write the geodesic equation, after some calculation, in a particularly simple form:

$$\ddot{\psi} = \psi. \tag{8}$$

One can immediately solve the equation to obtain

$$\psi(\sigma) = A\cosh\sigma + B\sinh\sigma, \tag{9}$$

$$\overline{A}A = -1, \quad \overline{A}B = 0, \quad \overline{B}B = 1, \tag{10}$$

where $A, B \in \mathbb{C}^3$. The projection $\pi \circ C$ of the curves $C : \sigma \mapsto \psi(\sigma)$ expressed by (9) are geodesics on O. The geodesics on the four-dimensional manifold O should contain seven independent real constants: the initial position and the direction of the initial velocity. One sees that $\pi \circ C$ actually contains seven independent real constants because we have twelve real constants, four constraints (10) and one redundancy, i.e., the phase of $\psi(0)$.

We note that the curve (9) is a *horizontal geodesic* on AdS^5. where, a curve C on M is said horizontal if it is orthogonal, with respect to g, to the fiber $\pi^{-1}(\pi\circ C(\sigma))$ at each point $C(\sigma)$. What is special for the Hopf string is that one can always choose a lift—the horizontal lift in this case— of any given geodesic on the orbit space $(O, -fh)$ such that it also is a geodesic on the spacetime AdS^5. A horizontal geodesic C is the intersection of AdS^5 and a two-dimensional plane through the origin in $E^{4,2}$ which corresponds to the great circle in the case of positive definite metric. Thus the hyperbolic curve (9) is unique up to isometry, for any choice of A and B. Furthermore, C is a Killing orbit on AdS^5. From (3), (5) and (9), the explicit form for the trajectory of the Hopf string is given by

$$\psi(\tau,\sigma) = e^{i\tau}(A\cosh\sigma + B\sinh\sigma), \tag{11}$$

with the condition (10).

4 Conclusion

The cohomogeneity-one symmetry reduces the partial differential equation governing the dynamics of an extended object in the spacetime M to an ordinary differential equation. Assuming that the string obeys the Nambu-Goto equation in AdS^5, we have solved the world sheet of one of the strings, which we call the Hopf string, in the classification. The problem has reduced to find geodesics on the orbit space. By using a technique similar to the one used in quntum information theory and working on the lift curves in M, we have obtained a solution which describes the trajectories of the Hopf string.

References

[1] L. Randall and R. Sundrum, Phys. Rev. Lett. **83**, (1999) 3370.

[2] V. P. Frolov, V. Skarzhinsky, A. Zelnikov and O. Heinrich, Phys. Lett. B **224**, 255 (1989). V. P. Frolov, S. Hendy and J. P. De Villiers, Class. Quant. Grav. **14**, 1099 (1997).

[3] K. Ogawa, H.Ishihara, H. Kozaki, H. Nakano, and I. Tanaka, "Gravitational radiation from stationary rotating cosmic strings", *Proceeding of 15th JGRG workshop*, ed. by T.Shiromizu et al. (Tokyo, 2005) 159.

[4] H. Ishihara and H. Kozaki, Phys. Rev. **D72**, 061701(R) (2005).

[5] T. Koike, H. Kozaki and H. Ishihara, JGRG16.

Gravitino dark matter from decaying thermal relics in RS type brane world [1]

Nobuchika Okada⋆ and Osamu Seto†

⋆ *Theory Division, KEK, 1-1 Oho, Tsukuba 305-0801, Japan,*
† *Instituto de Física Teórica UAM/CSIC, Universidad Autónoma de Madrid, Madrid 28049, Spain*

Abstract

We investigate the superWIMP scenario with gravitino as the lightest supersymmetric particle (LSP) in the context of brane world cosmology. Brane world cosmological effects dramatically enhance the relic density of the slepton or sneutrino NLSP, so that the NLSP with mass of order 100 GeV can provide the correct abundance of gravitino dark matter through its decay. We find that with an appropriate five dimensional Planck mass, this scenario can be realized consistently with the constraints from Big Bang Nucleosynthesis (BBN) for both NLSP candidates of slepton and sneutrino.

1 Introduction

The weakly interacting massive particle (WIMP) is the attractive dark matter candidate. The most interesting feature of the WIMP dark matter is that it can be thermal relics with its abundance

$$\Omega_{DM} h^2 \simeq 1 \times 10^9 \frac{(m_{DM}/T_f)\mathrm{GeV}^{-1}}{\sqrt{g_*} M_{Pl} \langle \sigma v \rangle} =_{\mathrm{typically}} \mathcal{O}(10^{-2} - 1), \tag{1}$$

where m_{DM} is the mass of dark matter particle, T_f is the freeze out temperature, g_* is the effective total number of relativistic degrees of freedom, $M_{Pl} = 1.2 \times 10^{19}$ GeV is the Planck mass, and $\langle \sigma v \rangle$ is the thermal averaged product of the annihilation cross section and the relative velocity [1]. This relic abundance is essentially determined by only its annihilation cross section, and does not depend on the detail thermal history before $T \gtrsim T_f$. This predictability and definiteness is fascinating.

There is another interesting possibility for the candidate of dark matter with highly suppressed interactions. Even though it cannot be in thermal equilibrium, this type of dark matter can have the appealing feature in its abundance. This is the superWIMP scenario, where the superWIMP dark matter is produced through the late decay of a long-lived WIMP [2, 3] and its abundance is given the characteristic form

$$\Omega_{DM} h^2 = \frac{m_{DM}}{m_X} \Omega_X h^2, \tag{2}$$

where $\Omega_X h^2$ is given by Eq. (1) if X were stable. The representative superWIMP candidate is gravitino [3].

The superWIMP scenario is an interesting possibility, however, it is not so easy to consistently realize the scenario with Big Bang Nucleosynthesis (BBN). If the NLSP decays after BBN, its energetic daughters of the SM particles would destroy light nuclei and spoil the success of the standard BBN predictions. When the NLSP is neutralino or stau (or slepton in general), this scenario is very hard for gravitino LSP [4, 5, 6]. On the other hand, the sneutrino NLSP has rather mild constraints from BBN compared with the others [6]. Nevertheless the sneutrino NLSP has not been appealing within this framework, because the thermal relic abundance $\Omega_{\tilde{\nu}} h^2$ is, as well known, too small to be suitable in Eq. (2) [7].

Of course, one may remember that the gravitino LSP can be produced through scattering and decay processes of particles in thermal plasma (thermal production) and its abundance is given as $\Omega^{\mathrm{TP}} h^2 \sim 0.27 \left(T_R/10^{10}\ \mathrm{GeV}\right) \left(100\ \mathrm{GeV}/m_{3/2}\right)$ where T_R is the reheating temperature after inflation [8] and $m_{3/2}$ is the gravitino mass. If this contributions dominant, some parameter region in a model is free from the BBN constraints. However, this scenario may not be appealing, because the gravitino dark matter can not inherit the WIMP thermal relic density Eq. (1) there.

[1] Presented by O. Seto.

We consider the superWIMP scenario with the gravitino LSP in the brane world cosmology [9] based on the Randall-Sundrum II model [10] and find that this scenario can be realized consistently with the successful predictions of BBN [11].

2 Brane world cosmology

In the RS II model [10], our four dimensional universe is realized on the 3-brane with a positive tension located at the ultraviolet (UV) boundary of a five dimensional Anti de-Sitter spacetime. In this setup, the Friedmann equation for a spatially flat spacetime is given by

$$H^2 = \frac{8\pi G}{3}\rho\left(1+\frac{\rho}{\rho_0}\right), \tag{3}$$

where $\rho_0 = 96\pi G M_5^6$ with M_5 being the five dimensional Planck mass. Here the four dimensional cosmological constant has been tuned to be zero, and the negligible dark radiation has been omitted [12]. The second term proportional to ρ^2 is a new ingredient in the brane world cosmology and leads to a non-standard expansion law of the early Universe. In the following, we call a temperature T_t defined as $\rho(T_t) = \frac{\pi^2}{30} g_* T_t^4 \equiv \rho_0$ "transition temperature". This modification of the expansion law $H^2 \propto \rho^2$ at a high temperature ($T > T_t$) leads to some drastic changes in the thermal relic abundance of dark matter [13, 14]. Needless to say, until the onset of BBN, the standard expansion law, $H^2 \propto \rho$, has to be recovered. This requirement leads to the model-independent constraint on the transition temperature as $T_t \gtrsim 1$ MeV or equivalently $M_5 \gtrsim 8.8$ TeV [9].

To be precise, we here specify our setup. We discuss a supersymmetric dark matter scenario, and our model should be a supersymmetric version of the Randall-Sundrum brane world model [15]. Since the Einstein's equation belongs to the bosonic part in supergravity, the cosmological solution of Eq. (3) remains the same. Although gravitino is a bulk field, we can, as a good approximation, regard it as a field residing on the UV brane as in the previous works [16] because the zero-mode gravitino is localized around the UV brane as the same as the zero-mode graviton is. We assume the cancellation of the four dimensional cosmological constant by some mechanism different from that discussed in the original paper [10], such a situation can be realized in dilatonic brane world models [17]. As the result, we do not seriously refer constraints from the gravitational law in sub millimeter range, $T_t \gtrsim 1.3$ TeV or equivalently $M_5 \gtrsim 1.1 \times 10^8$ GeV, these values are strongly depends on the four dimensional cosmological constant cancellation mechanism. Therefore, we take only the BBN bound into account to keep our discussion general. Moreover, we do not specify the supersymmetry breaking mechanism and its mediation to the visible sector, so that we treat the NLSP mass of $\mathcal{O}(100\text{ GeV})$ and the gravitino mass as a free parameter.

3 Gravitino abundance from enhanced relic density

As has been pointed out in Ref. [13], the relic density of dark matter can be enhanced in brane world cosmology when the five dimensional Planck mass M_5 is low enough. Applying this effect to abundance of NLSPs, we calculate the relic density of the gravitino LSP produced by the decay of the NLSP at late time. The enhancement can be seen by taking the ratio of the relic energy density of dark matter in the brane world cosmology ($\Omega_{(b)}$) to the one in the standard cosmology ($\Omega_{(s)}$)

$$\frac{\Omega_{(b)}}{\Omega_{(s)}} \simeq 0.54\left(\frac{x_t}{x_{d(s)}}\right), \tag{4}$$

for S-wave annihilation [13]. Here x_t is defined as $x_t \equiv m/T_t$ and $x_{d(s)}$ denotes the freeze out temperature in the standard cosmology. Note that the relic abundance in the brane world cosmology is characterized by the transition temperature rather than the decoupling temperature. Thus, the enhacement is sizable for a low transition temperature, $T_t < T_f$. In the following analysis, we assume such a low transition temperature. Then, one should notice the gravitino production from thermal plasma is negligible, as has been pointed out in Ref. [16].

3.1 slepton (stau) NLSP

First, let us consider the case of the slepton NLSP. Using Eqs. (4) and the slepton thermal relic density in the the standard cosmology [18], we obtain

$$m_{\tilde{l}} Y_{\tilde{l}(b)} \simeq 4 \times 10^{-10} [\mathrm{GeV}] \times \left(\frac{m_{\tilde{l}}}{100\ \mathrm{GeV}}\right)^2 \left(\frac{23}{x_{d(s)}}\right) \left(\frac{x_t}{1700}\right), \tag{5}$$

$$\Omega_{3/2} h^2 = \frac{m_{3/2}}{m_{\tilde{l}}} \Omega_{\tilde{l}(b)} h^2 \simeq 0.1 \times \left(\frac{m_{3/2}}{m_{\tilde{l}}}\right) \left(\frac{m_{\tilde{l}}}{100\ \mathrm{GeV}}\right)^2 \left(\frac{23}{x_{d(s)}}\right) \left(\frac{x_t}{1700}\right). \tag{6}$$

Detailed BBN constraint analysis for the stau NLSP case has been done and the results are summarized in Fig. 2 and 3 for $m_{\tilde{\tau}_R} = 100$ GeV and 300 GeV, in Ref. [5] . For $m_{\tilde{\tau}_R} = 100$ GeV, the region, which is consistent with BBN and provides a suitable amount of the gravitino relic density via the stau NLSP decay, can be read off as

$$(m_{\tilde{\tau}_R} Y_{\tilde{\tau}_R}, m_{3/2}) \simeq (10^{-6}\,\mathrm{GeV},\ 10\,\mathrm{MeV}). \tag{7}$$

In order to realize this allowed region, Eq. (6) indicates $T_t \simeq 24$ keV, but this contradicts against $T_t \gtrsim 1$ MeV. For $m_{\tilde{\tau}_R} = 300$ GeV, the allowed region appears in

$$m_{\tilde{\tau}_R} Y_{\tilde{\tau}_R} \gtrsim 2 \times 10^{-7}\,\mathrm{GeV}, \quad m_{3/2} \lesssim 0.6\,\mathrm{GeV}. \tag{8}$$

This region can be realized for $T_t \lesssim 3.2$ MeV (or equivalently $M_5 \lesssim 19$ TeV).

It has been discussed that problems of CDM at a small scale, such as "missing satellite problem" [19] and "cusp problem" [20], can be solved with appropriate large velocity dispersion of the superWIMP [21]. On the other hand, too large velocity dispersion, which exceeds the damping scale $\gtrsim 1$ Mpc, is constrained from Lyman alpha clouds. In the above allowed region of our case with Eq. (8), the typical damping scale is found to be $\mathcal{O}(1\ \mathrm{Mpc})$. Thus, our scenario is in fact marginally possible.

3.2 sneutrino NLSP

Together with Eqs. (2), (4) and the sneutrino thermal relic abundance in the the standard cosmology [7], we find, in the brane world cosmology,

$$m_{\tilde{\nu}} Y_{\tilde{\nu}(b)} \simeq 4 \times 10^{-10}\ [\mathrm{GeV}] \times \left(\frac{m_{\tilde{\nu}}}{100\ \mathrm{GeV}}\right)^2 \left(\frac{23}{x_{d(s)}}\right) \left(\frac{x_t}{2100}\right), \tag{9}$$

$$\Omega_{3/2} h^2 = \frac{m_{3/2}}{m_{\tilde{\nu}}} \Omega_{\tilde{\nu}} h^2 \simeq 0.1 \times \left(\frac{m_{3/2}}{m_{\tilde{\nu}}}\right) \left(\frac{m_{\tilde{\nu}}}{100\ \mathrm{GeV}}\right)^2 \left(\frac{23}{x_{d(s)}}\right) \left(\frac{x_t}{2100}\right). \tag{10}$$

The BBN constraints for the sneutrino LSP have been analyzed in detail and the results are summarized in Fig. 5 for $m_{\tilde{\nu}} = 300$ GeV in Ref. [6] . The allowed region can be read off as

$$\begin{array}{rcl} \text{(i)} & m_{\tilde{\nu}} Y_{\tilde{\nu}(b)} \gtrsim 2 \times 10^{-6}\,\mathrm{GeV}, & m_{3/2} \lesssim 0.06\,\mathrm{GeV}, \\ \text{(ii)} & m_{\tilde{\nu}} Y_{\tilde{\nu}(b)} \simeq 2 \times 10^{-7}\,\mathrm{GeV}, & m_{3/2} \simeq 0.3\,\mathrm{GeV}, \\ \text{(iii)} & 4 \times 10^{-10}\,\mathrm{GeV} \lesssim m_{\tilde{\nu}} Y_{\tilde{\nu}(b)} \lesssim 7 \times 10^{-10}\,\mathrm{GeV}, & 300\ \mathrm{GeV} > m_{3/2} \gtrsim 150\,\mathrm{GeV}. \end{array}$$

The region (i) is not consistent with $T_t \gtrsim 1$ MeV. The point (ii) is marginally acceptable as in the case of the stau NLSP. Finally, the region (iii) is typical for the sneutrino NLSP case, because such a region is never viable for other NLSP cases.

4 Conclusion and discussions

We have shown that gravitino superWIMP dark matter produced by the decay of thermal relic stau or sneutrino NLSP is viable in brane world cosmology. Even if the NLSP mass is around 100 GeV, the brane world cosmological effects can dramatically enhance its thermal relic density enough to yield the correct abundance for the gravitino dark matter through the NLSP decay with a suitable five dimensional Planck mass. Especially, sneutrino would be an interesting choice of NLSP, because it is a rather harmless mother particle than others like neutralino or slepton. The long-lived NLSP in this scenario is also interesting at future collider experiments such as the Large Hadron Collider and the International Linear Collider [22].

Acknowledgments

The work of N.O. is supported in part by the Grant-in-Aid for Scientific Research from the Ministry of Education, Science and Culture of Japan, (No. 18740170). The work of O.S. is supported by the MEC project FPA 2004-02015 and the Comunidad de Madrid project HEPHACOS (No. P-ESP-00346).

References

[1] See, e.g., E. W. Kolb, and M. S. Turner, *The Early Universe*, Addison-Wesley (1990).

[2] L. Covi, J. E. Kim and L. Roszkowski, Phys. Rev. Lett. **82**, 4180 (1999).

[3] J. L. Feng, A. Rajaraman and F. Takayama, Phys. Rev. Lett. **91**, 011302 (2003).

[4] See, e.g., J. L. Feng, S. f. Su and F. Takayama, Phys. Rev. D **70**, 063514 (2004) and Phys. Rev. D **70**, 075019 (2004); D. G. Cerdeno, K. Y. Choi, K. Jedamzik, L. Roszkowski and R. Ruiz de Austri, JCAP **0606**, 005 (2006); M. Kawasaki, K. Kohri and T. Moroi, Phys. Lett. B **649**, 436 (2007).

[5] M. Kawasaki, K. Kohri and T. Moroi, Phys. Lett. B **649**, 436 (2007).

[6] T. Kanzaki, M. Kawasaki, K. Kohri and T. Moroi, Phys. Rev. D **75**, 025011 (2007).

[7] T. Falk, K. A. Olive and M. Srednicki, Phys. Lett. B **339**, 248 (1994).

[8] M. Bolz, W. Buchmuller and M. Plumacher, Phys. Lett. B **443**, 209 (1998).

[9] For a review, see, e.g., D. Langlois, Prog. Theor. Phys. Suppl. **148**, 181 (2003).

[10] L. Randall and R. Sundrum, Phys. Rev. Lett. **83**, 4690 (1999).

[11] N. Okada and O. Seto, arXiv:0710.0449 [hep-ph].

[12] T. Shiromizu, K. i. Maeda and M. Sasaki, Phys. Rev. D **62**, 024012 (2000); P. Binetruy, C. Deffayet and D. Langlois, Nucl. Phys. B **565**, 269 (2000); D. Ida, JHEP **0009**, 014 (2000).

[13] N. Okada and O. Seto, Phys. Rev. D **70**, 083531 (2004).

[14] T. Nihei, N. Okada and O. Seto, Phys. Rev. D **71**, 063535 (2005) and Phys. Rev. D **73**, 063518 (2006).

[15] T. Gherghetta and A. Pomarol, Nucl. Phys. B **586**, 141 (2000); R. Altendorfer, J. Bagger and D. Nemeschansky, Phys. Rev. D **63**, 125025 (2001); A. Falkowski, Z. Lalak and S. Pokorski, Phys. Lett. B **491**, 172 (2000); M. Zucker, Phys. Rev. D **64**, 024024 (2001); T. Kugo and K. Ohashi, Prog. Theor. Phys. **108**, 203 (2002).

[16] N. Okada and O. Seto, Phys. Rev. D **71**, 023517 (2005).

[17] K. i. Maeda and D. Wands, Phys. Rev. D **62**, 124009 (2000).

[18] T. Asaka, K. Hamaguchi and K. Suzuki, Phys. Lett. B **490**, 136 (2000).

[19] A. A. Klypin, A. V. Kravtsov, O. Valenzuela and F. Prada, Astrophys. J. **522**, 82 (1999); B. Moore, *et al.*, Astrophys. J. **524**, L19 (1999); A. R. Zentner and J. S. Bullock, Astrophys. J. **598**, 49 (2003).

[20] B. Moore, Nature **370**, 629 (1994); R. A. Flores and J. R. Primack, Astrophys. J. **427**, L1 (1994); W. J. G. de Blok and S. S. McGaugh, Mon. Not. Roy. Astron. Soc. **290**, 533 (1997); A. R. Zentner and J. S. Bullock, Phys. Rev. D **66**, 043003 (2002).

[21] J. A. R. Cembranos, J. L. Feng, A. Rajaraman and F. Takayama, Phys. Rev. Lett. **95**, 181301 (2005); M. Kaplinghat, Phys. Rev. D **72**, 063510 (2005); J. Hisano, K. T. Inoue and T. Takahashi, Phys. Lett. B **643**, 141 (2006).

[22] W. Buchmuller, K. Hamaguchi, M. Ratz and T. Yanagida, Phys. Lett. B **588**, 90 (2004); J. L. Feng, A. Rajaraman and F. Takayama, Int. J. Mod. Phys. D **13**, 2355 (2004).

Adiabatic evolution of orbital parameters in the black hole spacetime

Ryuichi Fujita[1], Wataru Hikida[2] and Hideyuki Tagoshi[3]

[1,2,3] *Department of Earth and Space Science, Graduate School of Science, Osaka University, Toyonaka, Osaka 560-0043, Japan*

Abstract

We develop an efficient numerical code to compute gravitational waves radiated by a particle orbiting around a Kerr black hole. We estimate the accuracy of our code by checking the spherical symmetry of Schwarzshild black hole such that energy flux radiated by a point particle is invariant for its inclination angles from the equatorial plane of black hole. We find that the accuracy of our code is limited by truncation of ℓ-mode, degree of the spin-weighted spheroidal harmonics. Then, we also evaluate gravitational wave flux in the case of Kerr black hole and the adiabatic evolution of particle's orbit duo to the emission of gravitational waves. The accuracy of our code is sufficient for constructing templates for LISA data analysis. Future work is to evaluate gravitational waves including effects of adiabatic evolution of particle's orbit and to search for efficient templates for LISA data analysis.

1 Introduction

Gravitational wave from an extreme mass ratio inspiral (EMRI) is one of the most promising sources for the Laser Interferometer Space Antenna (LISA). If we can detect and observe gravitational waves from such binary system, we can obtain physical information such as distance to the source, masses of binary, spin of the black hole, geometry of black hole spacetime and so on. In order to obtain these information, we have to achieve the phase accuracy of theoretical gravitational wave forms within one radian over the total cycle of wave, $\sim 10^5$. Therefore, in order to obtain information of source, we have to achieve accuracy of gravitational waves better than $\sim 10^{-5}$.

The dynamics of EMRI is accurately modeled as a point particle of small mass moving around a Kerr black hole and we estimate gravitational waves from EMRI by black hole perturbation method. The basic equation of black hole perturbation is the Teukolsky equation [1]. For rather simple orbits of a particle, there are many works which estimate gravitational waves with sufficient accuracy to construct LISA templates. Recently, Drasco and Hughes evaluated gravitational waves for general geodesic orbits [2]. But many problems are still unsolved for general geodesic orbits. For example, accuracy is at most 10^{-3} which is not sufficient for LISA templates, change rate of the Carter constant is computed by invalid approximation and change rates of orbital parameters of a particle are not evaluated.

2 Our numerical methods and results

We evaluate gravitational waves from EMRI by solving the Teukolsky equation which is the basic equation of the black hole perturbation theory. We solve the Teukolsky equation by the Green function method. In this work, we compute the homogeneous solutions of the Teukolsky equation using formalism developed by Mano, Suzuki and Takasugi(MST) [3]. In numerical application of MST method, we use the method which is developed by Fujita and Tagoshi [4, 5]. The source term of the Teukolsky equation depends on the orbits of a point particle. The geodesic equation is completely characterized by three constants of motion such as the energy $\mathcal{E}$, the z-component of the angular momentum $\mathcal{L}_z$ and the Carter constant per unit mass $\mathcal{C}$. Although the orbits of a particle is very complicated, we can introduce the orbital

[1] E-mail:draone@vega.ess.sci.osaka-u.ac.jp
[2] E-mail:hikida@vega.ess.sci.osaka-u.ac.jp
[3] E-mail:tagoshi@vega.ess.sci.osaka-u.ac.jp

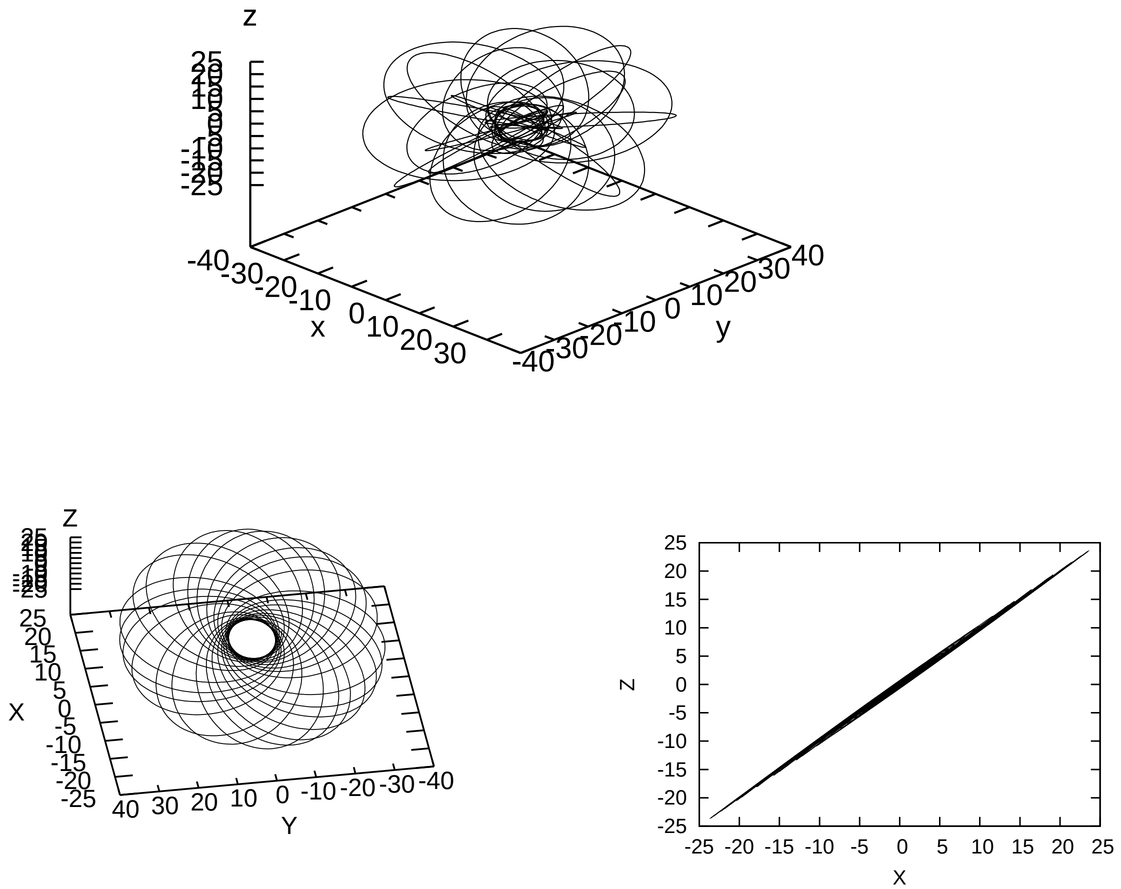

Figure 1: Plots the orbits for a generic geodesic orbit, which has eccentricity $e = 0.7$, semi-latus rectum $p = 10M$ and inclination angle $\theta_{\rm inc} = 45°$. The black hole's spin is set to $a = 0.9M$. The upper figure is expressed by Cartesian coordinate system. While, the lower figures are expressed by co-rotational one, which cancel out the precession of orbital plane.

parameters such as eccentricity e, a semi-latus rectum p and inclination angle $\theta_{\rm inc}$ (Fig. 1). The details of our method will be described in our paper [6].

In this section, we check accuracy of our code using the spherical symmetry of Schwarzshild black hole in Tab. 1 and evaluate the rate of change of constants of motion of a particle in the case of the Kerr black hole in Tab. 2. Once the rate of change of constants of motion of a particle are computed, we can evaluate evolution of orbital parameters of a point particle (Fig. 2).

In Tab. 1, we check that the energy flux radiated to the infinity is independent of inclination angle in the case of Schwarzshild black hole. Then, we find that relative error of our code may be almost the same as the accuracy of truncation of ℓ-mode, degree of the spin-weighted spheroidal harmonics.

In Tab. 2, we compute the rate of change of three constants of motion in the case of Kerr black hole. We use the same orbital parameters as those used by Drasco and Hughes in Ref. [2]. Our results are consistent with their ones, except for the rates of change of the Carter consistent, $\langle d\mathcal{C}/dt \rangle$. This is because they computed $\langle d\mathcal{C}/dt \rangle$ using incorrect approximation such that the inclination angle does not change. Therefore, this is the first calculation that evaluates the rate of change of the Carter constant without any approximation.

In Fig. 2, we show adiabatic evolution of orbital parameters of a point particle due to the emission of

a/M	p/M	e	$\theta_{\rm inc}$	$\langle d\mathcal{E}/dt\rangle^{\infty}$	Relative error
0	10	0.1	0	$6.31752474714\times10^{-5}$	$[10^{-11}]$
0	10	0.1	20	$6.31752474711\times10^{-5}$	4.1×10^{-12}
0	10	0.1	45	$6.31752474687\times10^{-5}$	4.2×10^{-11}
0	10	0.1	70	$6.31752474699\times10^{-5}$	2.3×10^{-11}
0	10	0.5	0	$9.27335012129\times10^{-5}$	$[10^{-10}]$
0	10	0.5	20	$9.27335011989\times10^{-5}$	1.5×10^{-10}
0	10	0.5	45	$9.27335011942\times10^{-5}$	2.0×10^{-10}
0	10	0.5	70	$9.27335011362\times10^{-5}$	8.3×10^{-10}
0	10	0.7	0	$9.46979143586\times10^{-5}$	$[10^{-9}]$
0	10	0.7	20	$9.46979135472\times10^{-5}$	8.6×10^{-9}
0	10	0.7	45	$9.46979131618\times10^{-5}$	1.3×10^{-8}
0	10	0.7	70	$9.46979128748\times10^{-5}$	1.6×10^{-8}

Table 1: The energy flux of gravitational waves radiated by a particle around a Schwarzshild black hole. In this table, the orbital radius is $10M$. We compare the result for the equatorial plane case with the one for non-equatorial plane. Relative error in square brackets is an order of magnitude estimate for the fractional accuracy for the case of the equatorial plane, which is determined by truncating number of ℓ-mode. Here we set to $\ell_{\rm max}=20$. These results show that the accuracy of our code can be almost the same as the accuracy of truncation of ℓ-mode.

a/M	p/M	e	$\theta_{\rm inc}$	$\langle d\mathcal{E}/dt\rangle^{\infty}$	$\langle d\mathcal{L}_z/dt\rangle^{\infty}$	$\langle d\mathcal{C}/dt\rangle^{\infty}$
0.9	6	0.1	20°	$-5.873638000\times10^{-4}[10^{-8}]$	$-8.537278815\times10^{-3}$	$-5.240198485\times10^{-3}$
0.9	6	0.1	40°	$-6.183229400\times10^{-4}[10^{-8}]$	$-7.630994021\times10^{-3}$	$-2.022711360\times10^{-2}$
0.9	6	0.1	60°	$-6.833475260\times10^{-4}[10^{-8}]$	$-6.078295576\times10^{-3}$	$-4.321938503\times10^{-2}$
0.9	6	0.1	80°	$-8.057482365\times10^{-4}[10^{-8}]$	$-3.625850817\times10^{-3}$	$-7.184063984\times10^{-2}$
0.9	6	0.5	20°	$-7.989254232\times10^{-4}[10^{-6}]$	$-8.347502466\times10^{-3}$	$-4.947042936\times10^{-3}$
0.9	6	0.5	40°	$-8.743345386\times10^{-4}[10^{-6}]$	$-7.819404658\times10^{-3}$	$-1.989003098\times10^{-2}$
0.9	6	0.5	60°	$-1.058833575\times10^{-3}[10^{-6}]$	$-6.950634938\times10^{-3}$	$-4.656556303\times10^{-2}$
0.9	6	0.5	80°	$-1.676657675\times10^{-3}[10^{-6}]$	$-5.909338458\times10^{-3}$	$-1.017867814\times10^{-1}$
0.9	6	0.7	20°	$-7.731178913\times10^{-4}[10^{-6}]$	$-6.693013058\times10^{-3}$	$-3.886819966\times10^{-3}$
0.9	6	0.7	40°	$-8.751886316\times10^{-4}[10^{-6}]$	$-6.530519069\times10^{-3}$	$-1.624203273\times10^{-2}$
0.9	6	0.7	60°	$-1.146896675\times10^{-3}[10^{-6}]$	$-6.380243741\times10^{-3}$	$-4.146278305\times10^{-2}$
0.9	6	0.7	80°	$-2.718764108\times10^{-3}[10^{-5}]$	$-8.402286903\times10^{-3}$	$-1.341226528\times10^{-1}$

Table 2: Time-averaged rates of change of three constants of motion, energy $\langle d\mathcal{E}/dt\rangle^{\infty}$, angular momentum $\langle d\mathcal{L}_z/dt\rangle^{\infty}$ and the Carter constant $\langle d\mathcal{C}/dt\rangle^{\infty}$ due to gravitational wave radiated to infinity per unit mass in the case of some generic orbits. Each number in square brackets is an order of magnitude estimate for the fractional accuracy of the preceding number, which is determined by truncating number of ℓ-mode. Here we set to $\ell_{\rm max}=17$.

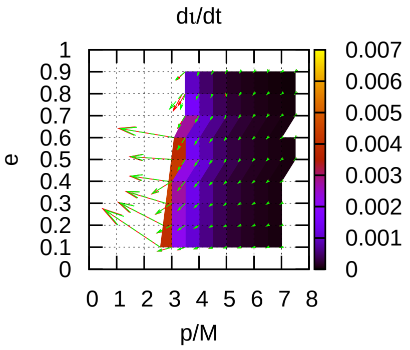

Figure 2: Adiabatic evolution of orbital parameters of a point particle due to the emission of gravitational waves. The black hole spin is $a/M = 0.9$ for left figure and $a/M = -0.9$ for right figure. The inclination angle is $\theta_{\rm inc} = 20°$ for both figures. We compute the evolution of orbital paramters outside the separatrix, which separates stable and unstable orbits. Each orbit corresponds to a point in the graph. $(M/\mu)(\dot{p}, M\dot{e})$ is expressed by a vector and $\dot{\theta}_{\rm inc}$ is expressed by color contor.

gravitational waves. We find that the semi-latus rectum always decreases. We also find that eccentricity decreases when the orbit is sufficiently far away from the separatrix and increases when the orbit is near the separatrix. We find that the inclination angle always increases when the black hole spin is positive and decreases when the spin is negative. The divergent behaviors of evolution of orbital parameters near the separatrix may represent the breakdown of adiabaticity.

3 Summary

In this paper, we develop an efficient numerical code to compute gravitational waves radiated by a particle orbiting around a Kerr black hole. We estimate the accuracy of our code by checking the spherical symmetry of the energy flux radiated from a Schwarzshild black hole spacetime. We find that the accuracy of our code is limited by truncation of ℓ-mode. We also evaluate gravitational waves in the case of a Kerr black hole and first compute the rate of change of the Carter constant with adiabatic approximation. Then, we evaluate the adiabatic evolution of orbital parameters duo to the emission of gravitational waves.

The accuracy of our code is sufficient for constructing templates for LISA data analysis. Future work is to evaluate gravitational waves including effects of adiabatic evolution of particle's orbit and to search for efficient templates for LISA data analysis.

References

[1] S. A. Teukolsky, Astrophys. J. **185** (1973), 635–647.

[2] S. Drasco and S. A. Hughes, Phys. Rev. D **69** (2005), 044015.

[3] S. Mano, H. Suzuki, and E. Takasugi, Prog. Theor. Phys. **95** (1996), 1079–1096.

[4] R. Fujita and H. Tagoshi, Prog. Theor. Phys. **112** (2004), 415–450.

[5] R. Fujita and H. Tagoshi, Prog. Theor. Phys. **113** (2005), 1165–1182.

[6] R. Fujita, H. Hikida and H. Tagoshi, in preparation.